

A 3D rendering of several cardboard boxes of various sizes and orientations, including a large open-top box, a smaller closed box, and a cylindrical box, set against a blue background.

CH-TRU Payload Appendices

Waste
Isolation
Pilot
Plant



**Revision 3
December 2012**

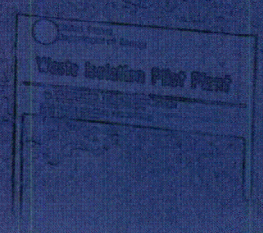


TABLE OF CONTENTS

1.0 INTRODUCTION

2.0 PAYLOAD QUALIFICATION METHODOLOGY

- 2.1 Logic for Payload Shipping Categories
- 2.2 Procedure for Determining Numeric Payload Shipping Category
- 2.3 Derivation of Decay Heat Limits
- 2.4 Mixing of Shipping Categories and Determination of the Flammability Index

3.0 GAS GENERATION METHODOLOGY

- 3.1 Radiolytic G Values for Waste Materials
- 3.2 Effective G Values for CH-TRU Waste Material Types
- 3.3 Use of Dose-Dependent G Values for CH-TRU Wastes
- 3.4 Shipping Period – General Case
- 3.5 Shipping Period – Close-Proximity Shipments
- 3.6 Shipping Period – Controlled Shipments
- 3.7 Aspiration of Unvented Payload Containers of CH-TRU Waste
- 3.8 Specification for Closure of Inner Confinement Layers
- 3.9 Determination of Steady-State VOC Concentrations from DACs
- 3.10 Determination of Flammable Gas/Volatile Organic Compound Concentrations by Measurement
- 3.11 Use of Filtered Bags as Confinement Layers for CH-TRU Wastes

4.0 PAYLOAD CONTAINER DESIGN BASIS EVALUATIONS

- 4.1 Description of Standard Pipe Overpack
- 4.2 Description of S100 Pipe Overpack
- 4.3 Description of S200 Pipe Overpack
- 4.4 Description of S300 Pipe Overpack
- 4.5 Description of Shielded Container
- 4.6 Description of Criticality Control Overpack

5.0 ASSESSMENT METHODS

- 5.1 Real-Time Radiography Procedures
- 5.2 DOE Assay Methods Used for Determination of Fissile Material Content and Decay Heat Values of CH-TRU Wastes
- 5.3 CH-TRU Waste Sampling Programs at DOE Sites

TABLE OF CONTENTS (Continued)**6.0 SUPPORTING EVALUATIONS**

- 6.1 Chemical Compatibility of Waste Forms
- 6.2 Free Halides in the CH-TRU Waste Payload – Source Term and Release Rate Estimates
- 6.3 Payload Compatibility with Butyl Rubber O-Ring Seals
- 6.4 Volatile Organic Compounds (VOC) in the CH-TRU Payload – Source Term and Release Rate Estimates
- 6.5 Biological Activity Assessment
- 6.6 Thermal Stability of Payload Materials at Transport Temperatures
- 6.7 Gas Release Assessment
- 6.8 Gas Release Testing
- 6.9 Temperature Dependence of Hydrogen Gas Generation and Release Rates
- 6.10 Effect on Decay Heat Limits of Overpacking Payload Containers
- 6.11 Shipment of Tritium-Contaminated Waste
- 6.12 Shipment of High-Wattage CH-TRU Waste
- 6.13 Shipment of CH-TRU Waste Packaging Configurations with Unvented Heat-Sealed Bag Layers
- 6.14 Test Category Measurement Methodology for Analytical Category Payload Containers Containing Puck Drums

1.0 INTRODUCTION

This document, the CH-TRU Payload Appendices, accompanies the Contact-Handled Transuranic Waste Authorized Methods for Payload Control (CH-TRAMPAC) and is provided as supplemental information pertaining to issues related to the transportation of contact-handled transuranic (CH-TRU) waste in the TRUPACT-II or HalfPACT. The CH-TRAMPAC contains all information, including requirements and methods of compliance, required for the qualification of a payload for transport in the TRUPACT-II or HalfPACT. The methodology and logic for the requirements are provided in this document, along with previously performed assessments and evaluations.

The information contained in this document is separated into specific sections, as follows:

- Payload Qualification Methodology (Section 2.0)
- Gas Generation Methodology (Section 3.0)
- Payload Container Design Basis Evaluations (Section 4.0)
- Assessment Methods (Section 5.0)
- Supporting Evaluations (Section 6.0).

This document supports both the TRUPACT-II and HalfPACT Safety Analysis Reports, as well as the CH-TRAMPAC document.

This page intentionally left blank

APPENDIX 2.1

LOGIC FOR PAYLOAD SHIPPING CATEGORIES

This page intentionally left blank.

2.1 Logic for Payload Shipping Categories

The contact-handled transuranic (CH-TRU) waste at the U.S. Department of Energy (DOE) sites has been classified into “payload shipping categories” to evaluate and ensure compliance with the gas generation requirements contained in the Contact-Handled Transuranic Waste Authorized Methods for Payload Control (CH-TRAMPAC). As shown in Appendices 6.1, 6.5, and 6.6 of the CH-TRU Payload Appendices, gas generation due to chemical, biological, and thermal mechanisms is insignificant during transport, and radiolysis is the primary mechanism for potential flammable gas generation.

A shipping category is defined by the following parameters:

- Chemical composition of the waste (waste type)
- Gas generation potential of the waste material type (quantified by the “G value” for hydrogen, which is the number of molecules of hydrogen generated per 100 electron volts (eV) of energy absorbed)
- Gas release resistance (type of payload container and type and maximum number of confinement layers used).

For any given payload container, the shipping category provides a basis to determine the gas generation potential of the contents and the resistance to gas release of the packaging configuration. This enables evaluation of compliance with the gas generation requirements.

Two payload shipping category notations are available. A shipping site may use either notation. Descriptions of the two notations are presented in the following sections.

2.1.1 Numeric Shipping Category Notation

The numeric shipping category notation is a ten-digit code:

XX YYYY ZZZZ

where,

- | | | |
|------|---|---|
| XX | = | The waste type, which indicates the chemical composition of the waste |
| YYYY | = | The G value, or gas generation potential, of the waste material type multiplied by 10^2 |
| ZZZZ | = | The resistance to hydrogen release of the packaging configuration multiplied by 10^4 . |

A description of each of the parameters follows.

Waste Type

Payloads are subdivided into four (4) waste types based on physical and chemical form as shown in Table 2.1-1. Table 2.1-1 also shows the shipping category notation denoting each waste type.

Table 2.1-1 — Summary of Payload Waste Types

Waste Type ^a	Waste Type ^b (XX)	Description and Examples
I	10	Solidified Aqueous or Homogeneous Inorganic Solids (<1 percent organics - not including packaging) <ul style="list-style-type: none"> - absorbed, adsorbed or solidified inorganic liquid - soils, solidified particulates, or sludges formed from precipitates - concreted inorganic particulate waste
II	20	Solid Inorganics <ul style="list-style-type: none"> - glass, metal, crucibles - other solid inorganics
III	30	Solid Organics <ul style="list-style-type: none"> - plastics (e.g., polyethylene, polyvinyl chloride) - cellulose (e.g., paper, cloth, wood) - cemented organic solids - other solid organics
IV	40	Solidified Organics <ul style="list-style-type: none"> - cemented or immobilized organic liquids and solids

^aPayload shipping category notation used until June 1999.

^bPayload shipping category notation initiated in June 1999.

Waste Material Type

The four waste types may be further subdivided into waste material types. The waste material types define the gas generation potential of the waste, and a listing of the chemicals/materials allowed in each waste material type is presented in Tables 4.3-1 through 4.3-8 of the CH-TRAMPAC. An effective bounding G value quantifying the gas generation potential of each waste material type is assigned based on the chemicals allowed. Dose-dependent G values are applicable to containers of CH-TRU waste materials of Waste Material Type II.1 and Waste Type III that meet a watt*year criteria of greater than 0.012, except for shielded container payload containers (see Appendix 3.3). The determination of bounding G values for each waste material type is described in Appendices 3.2 and 3.3 of the CH-TRU Payload Appendices. Table 2.1-2 presents the waste material types and their respective bounding G values, along with the shipping category notation denoting the bounding G value.

Table 2.1-2 — CH-TRU Waste Material Types and G Values

Waste Material Type	Typical Material Description ^a	G Value ^{b,c}	Numeric Shipping Category Notation (G Value x 10 ²) (YYYY)
I.1	Absorbed, adsorbed, or solidified inorganic liquid	1.6	0160
I.2	Soils, solidified particulates, or sludges formed from precipitation	1.3	0130
I.3	Concreted inorganic particulate waste	0.4	0040
II.1	Solid inorganic materials in plastic bags (watt*year ≤0.012)	1.7	0170
II.1	Solid inorganic materials in plastic bags (watt*year >0.012)	0.32	0032
II.2	Solid inorganic materials in metal cans	0	0000
II.3	Homogeneous solid inorganic materials with unbound absorbed ambient moisture (≤6% by weight) in metal cans	0.08	0008
III.1	Solid organic materials (watt*year ≤0.012)	3.4	0340
III.1	Solid organic materials (watt*year >0.012)	1.09	0109
III.2	Homogeneous mixed organic (10% by weight) and inorganic (90% by weight) materials in metal cans (watt*year ≤0.012)	0.34	0034
III.2	Homogeneous mixed organic (10% by weight) and inorganic (90% by weight) materials in metal cans (watt*year >0.012)	0.11	0011
III.3	Homogeneous mixed organic (10% by weight) and inorganic (90% by weight) materials in plastic bags (watt*year ≤0.012)	1.85	0185
III.3	Homogeneous mixed organic (10% by weight) and inorganic (90% by weight) materials in plastic bags (watt*year >0.012)	0.4	0040
IV.1	Solidified organics	Unknown (test)	9999

^aAppendix 3.3 of the CH-TRU Payload Appendices provides a complete discussion of watt*year criteria.

^bDose-dependent G values meeting the watt*year criteria (watt*year >0.012) cannot be used if absorbed, adsorbed, or solidified aqueous materials are present in the waste (see Appendix 3.3 of the CH-TRU Payload Appendices). Appendices 3.1 and 3.2 of the CH-TRU Payload Appendices provide a complete discussion of G values.

^cDose-dependent G values for waste meeting the watt*year criteria (watt*year >0.012) cannot be used for waste packaged in the shielded container payload container (see Appendix 3.3 of the CH-TRU Payload Appendices).

Total Resistance

The determination of the total resistance to gas release of a payload container requires a knowledge of the type and maximum number of layers of confinement used to package the waste. CH-TRU materials are typically placed in a payload container within multiple layers of plastic and/or metal cans that act as layers of confinement for radionuclides during waste handling operations. The payload safety analysis considers the layers of confinement as barriers that impede, but do not preclude, the release of gases from inside the layers of confinement (e.g., plastic bags or metal cans) to the outside of the payload container. Allowable closure methods for confinement layers are specified in Appendix 3.8 of the CH-TRU Payload Appendices. The plastic layers of confinement in payload containers are of three types—liner bags, inner bags, and filtered inner and liner bags. As described in Appendices 3.8, 6.7, and 6.13 of the CH-TRU Payload Appendices, the release rates for confinement layers have been quantified or presented as specifications. Any other type of confinement layer used at the sites shall be shown to be equivalent to one of these for purposes of minimum hydrogen release.

The numeric payload shipping category notation used to denote the total resistance to hydrogen release of the packaging configuration of a payload container is the sum of the resistances from all confinement layers (seconds/mole) multiplied by 10^{-4} , rounded up, and reported as four digits (ZZZZ). For example, the shipping category notation for a total resistance of 1,395,163 seconds/mole is "0140."

The shipping category assignment for a 55-gallon drum containing solid inorganic waste packaged within two filtered, plastic liner bag layers is:

20 0170 0140

where,

20	=	Waste Type II
0170	=	G value (1.7) of Waste Material Type II.1 ($\times 10^2$)
0140	=	Total resistance to hydrogen release ($\times 10^{-4}$) of two filtered liner bags, 55-gallon drum filter, rigid drum liner, and payload shipping configuration.

2.1.2 Alpha-numeric Shipping Category Notation

The alpha-numeric shipping category notation was based on the same parameters as the numeric notation, but conveyed the information through a different set of parameters. The alpha-numeric shipping category notation was based on the waste material type, the payload container type, and the type and number of confinement layers within a payload container. An example of the alpha-numeric shipping category notation is:

II.1A2af

where,

- II.1 = The waste material type (solid inorganics in plastic bags, see Table 2.1-2)
- A = The type of payload container (55-gallon drum, see Table 2.1-3)
- 2 = The number of confinement layers (2 bag layers, see Table 2.1-4)
- af = The type of confinement layers (filtered drum liner bags, see Table 2.1-4).

Table 2.1-3 — Alpha-numeric Shipping Category Notation for Payload Container Configurations

Notation	Description
A	55-gallon drums with materials in additional layers of confinement [such as rigid liner(s), bag(s), and can(s)] (includes 55-gallon drums overpacked in a TDOP)
B	Overpack of four 55-gallon drums in an SWB (SWB overpack)
C	SWB with materials in additional layers of confinement [such as bags(s) and can(s)]
D	Overpack of one experimental bin in an SWB
E	Overpack of one pipe component in a 55-gallon drum (standard pipe overpack)

Table 2.1-4 — Alpha-numeric Shipping Category Notation for Layers of Confinement in Payload Containers

Notation	Description
0	No closed bags around waste
1	Up to a maximum of 1 closed bag around waste
2	Up to a maximum of 2 closed layers of bags around waste
3	Up to a maximum of 3 closed layers of bags around waste
4	Up to a maximum of 4 closed layers of bags around waste
5	Up to a maximum of 5 closed layers of bags around waste
6	Up to a maximum of 6 closed layers of bags around waste
M	Metal container(s) as the innermost layer of confinement
a	For Waste Types II and III packaged in drums, denotes a minimum of 2 liner bags
b	For all waste types packaged in SWBs, denotes a minimum of 1 SWB liner bag
f	All layers of bags around waste are vented with a minimum of one filter vent
T	Payload container qualified for shipment under the test category (see Section 5.2 of the CH-TRAMPAC)

This page intentionally left blank.

APPENDIX 2.2

**PROCEDURE FOR DETERMINING NUMERIC
PAYLOAD SHIPPING CATEGORY**

This page intentionally left blank.

2.2 Procedure for Determining Numeric Payload Shipping Category

Completion of Tables 2.2-1 through 2.2-4, at the end of this appendix, constitutes the determination of the numeric payload shipping category.

2.2.1 Instructions for Completing Table 2.2-1: Numeric Payload Shipping Category Worksheet

For all of the tables, only the blank (unshaded) boxes need to be completed. Note that there are two separate columns for determining total resistance based on waste material type. Column 1 is used to calculate resistance factors for waste material types with G values based on water [waste material types with six-digit notations (XX YYYY) 10 0160, 10 0130, 10 0040, and 20 0008]. Column 2 is used to calculate resistance factors for all other waste material types. (Appendix 6.9 of the CH-TRU Payload Appendices describes the logic for using different resistances based on waste material type.)

Container ID

Record the container ID number in the space provided.

Waste Type

Record the two-digit waste type notation (XX) of the container from Table 2.1-1 of Appendix 2.1 of the CH-TRU Payload Appendices.

G Value

- From Table 2.1-2 of Appendix 2.1 of the CH-TRU Payload Appendices, determine the waste material type to which the container belongs.
- Record the G value for this waste material type from Table 2.1-2 of Appendix 2.1 of the CH-TRU Payload Appendices.
- Record the corresponding four-digit G value notation (YYYY) from Table 2.1-2 of Appendix 2.1 of the CH-TRU Payload Appendices.

Note: If the notation entered under Waste Type (XX) and G Value (YYYY) is 20 0000, the "Total Resistance Notation" to be entered at the bottom of Table 2.2-1 (ZZZZ) is always 0000, and the payload shipping category to be entered in the last row of Table 2.2-1 (XX YYYY ZZZZ) is 20 0000 0000. For Waste Material Type II.2 (20 0000), this completes the determination of the numeric payload shipping category, and the remainder of the instructions do not apply.

Total Resistance

For each packaging configuration, a unique resistance factor exists and is determined by totaling the individual resistance factors for the confinement layers, the payload container, and the load type. Instructions for completing this portion of the worksheet are as follows:

- Confinement Layers:

Packaging: Choose the layers of confinement that are applicable to the payload container. As specified in Appendix 3.8 of the CH-TRU Payload Appendices, if a confinement layer used for the payload container is not listed, but has been shown by testing or analysis to be equivalent to (i.e., hydrogen release rate equal to or greater than) one of the entries, choose the equivalent entry.

Type: Within each applicable layer of confinement, choose the closure type and calculate the “Total Resistance Factor” as shown below. If the confinement layer is filtered or if it is a rigid drum liner, the “Total Resistance Factor” for the layer is calculated using Table 2.2-2.

Number of Layers: Enter the number of layers of confinement for each type of internal packaging that is applicable to the payload container. Leave the space blank or enter zero (0) if it is not applicable.

Resistance Factor: Choose the “Resistance Factor” from either Column 1 or Column 2 that corresponds to the six-digit notation (XX YYYY) recorded above (see footnote “a” of Table 2.2-1). This is a numeric value associated with the resistance to hydrogen diffusion for each layer of confinement (resistance to hydrogen diffusion in seconds/mole divided by 100). The “Resistance Factor” for filtered or punctured confinement layers is calculated using Table 2.2-2.

Total Resistance Factor: Multiply the “Resistance Factor” by the “Number of Layers” of confinement for each applicable type of internal packaging. The total resistance factor for each confinement layer type is equal to the number of layers of confinement times the resistance factor (e.g., 2 twist-and-tape drum liner bags would have a total resistance factor of $2 \times 2,142 = 4,284$). Enter the “Total Resistance Factor” for each confinement layer type in the designated column on Table 2.2-1. Enter zero (0) or leave the space blank for confinement layers that are not applicable.

- Payload Container: The “Total Resistance Factor” for this section is calculated using Table 2.2-3.
- Load Type: The “Total Resistance Factor” for this section is calculated using Table 2.2-4.
- Total Resistance Factor Sum: Sum all the values in the “Total Resistance Factor” column and record on this line.
- Total Resistance Notation: Divide the “Total Resistance Factor Sum” by 100 and round up to the nearest whole number. Record “Total Resistance Notation” as four digits (ZZZZ) (e.g., for a total resistance factor sum of 13,954, $13,954 / 100 = 139.54$, rounded up to nearest whole number is 140, and reported as four digits, the total resistance notation is 0140).

The "Payload Shipping Category" on the worksheet is determined by combining the three components of the shipping category determined above. The shipping category is recorded as XX YYYY ZZZZ.

2.2.2 Instructions for Completing Table 2.2-2: Filtered/Punctured Confinement Layers Resistance Worksheet

Packaging/Type: Choose the layers of confinement that are applicable to the payload container.

Minimum Filter Hydrogen Diffusivity/Minimum Puncture Diameter: Choose the appropriate filter based on the minimum hydrogen diffusivity applicable to the filter. Section 2.5 of the Contact-Handled Transuranic Waste Authorized Methods for Payload Control (CH-TRAMPAC) lists the venting requirements for the payload container and confinement layers. Sites shall verify and document the use of filters with greater hydrogen diffusivity values in order to take credit for the associated decrease in total resistance per packaging configuration.

For the rigid drum liner, choose the value that matches the puncture diameter or filter diffusivity in the liner.

If the hydrogen diffusivity or puncture diameter of the confinement layer falls in between the numbers listed, select the lower value. For example, if a container has a rigid liner with a puncture diameter of 0.5 inch, select "0.375" Diameter Hole."

Number of Layers: Enter the number of layers of confinement for each type of internal packaging that is applicable to the payload container. Leave the space blank or enter zero (0) if it is not applicable.

Resistance Factor: Choose the "Resistance Factor" from either Column 1 or Column 2 that corresponds to the six-digit notation (XX YYYY) recorded on Table 2.2-1 (see footnote "a" of Table 2.2-2). This is a numeric value associated with the resistance to hydrogen diffusion for each layer of confinement.

Number of Filters/Punctures per Layer: Enter the number of filters in each confinement layer or the number of punctures in the rigid liner. If the number of filters on a given type of confinement layer varies from layer to layer, enter the minimum number of filter(s) that applies to all layers of that type. For example, if a payload container holds waste packaged in two filtered inner bag layers, one bag fitted with one filter, and one bag fitted with two filters, enter "1" for the "Number of Filters/Punctures."

Total Resistance Factor: The Total Resistance Factor for each layer is obtained as follows:

$$\frac{\text{Resistance Factor} * \text{Number of Layers}}{\text{Number of Filters/Punctures per Layer}}$$

If the calculated “Total Resistance Factor” is not a whole number, round up to the nearest whole number. Enter this number in the appropriate column in Table 2.2-2 and Table 2.2-1. Enter zero (0) or leave the space blank if it is not applicable.

2.2.3 Instructions for Completing Table 2.2-3: Payload Container Resistance Worksheet

Payload Container: Choose the payload container packaging configuration components that are applicable to the payload container (e.g., for a 55-gallon drum overpacked in a standard waste box (SWB), both 55-gallon drum and SWB overpack would be selected). For some overpacked configurations, overpacking does not impact the selection of the appropriate payload container. For example, for 55-gallon drums, the total resistance is not affected by overpacking in an SWB with filters having a total hydrogen diffusivity of 1.48×10^{-5} moles per second per mole fraction (m/s/mf) (equivalent to four filters each with a diffusivity of 3.7×10^{-6} m/s/mf) or greater or in a ten-drum overpack (TDOP). Therefore, only the Resistance Factor for the 55-gallon drum applies, and the resistance of the overpacking container is assigned a value of zero. See Appendix 6.10 of the CH-TRU Payload Appendices regarding the selection of Payload Containers for overpacked configurations.

Filter Type: Choose the filter type on the payload container (see Section 2.5 of the CH-TRAMPAC for minimum filter specifications). Choose the appropriate filter based on the minimum hydrogen diffusivity applicable to the filter. Section 2.5 of the CH-TRAMPAC lists the venting requirements for payload containers. Sites shall verify and document the use of filters with greater hydrogen diffusivity values in order to take credit for the associated decrease in total resistance per packaging configuration. If the minimum hydrogen diffusivity applicable to the filter falls in between the numbers listed, select the lower value. For example, if a 55-gallon drum filter has a minimum hydrogen diffusivity of 3.0×10^{-6} m/s/mf, select “ 1.9×10^{-6} m/s/mf Filter.”

Number of Filters on Payload Container: Enter the number of filters on each container. Section 2.5 of the CH-TRAMPAC specifies the minimum total hydrogen diffusivity required per container. The combination of filter diffusivity and number of filters must meet or exceed the minimum requirements of Section 2.5 of the CH-TRAMPAC. Leave the space blank or enter zero (0) if it is not applicable.

Resistance Factor: Choose the “Resistance Factor” from either Column 1 or Column 2 that corresponds to the six-digit notation (XX YYYY) recorded on Table 2.2-1 (see footnote “b” of Table 2.2-3). This is the numeric value associated with the resistance to hydrogen diffusion for each container.

Total Resistance Factor: Divide the “Resistance Factor” by the “Number of Filters on the Container” to obtain the “Total Resistance Factor.” If the calculated “Total Resistance Factor” is not a whole number, round up to the nearest whole number. Enter this number in the designated column on Tables 2.2-3 and 2.2-1. Enter zero (0) or leave the space blank if it is not applicable.

2.2.4 Instructions for Completing Table 2.2-4: Load Type Resistance Worksheet

Shipping Period: Choose the appropriate shipping period for the payload, as follows:

- 60 Days (General Case): All shipments that do not meet the criteria for the other shipping periods.
- 20 Days (Close-Proximity Shipment): For shipments to destinations within a radius of approximately 1,000 miles or less. For example, all shipments from the Los Alamos National Laboratory, the Rocky Flats Environmental Technology Site, and the Nevada Test Site to the Waste Isolation Pilot Plant meet this criterion, and a 20-day shipping period is applicable.
- 10 Days (Controlled Shipment): For all shipments that satisfy the administrative control requirements set forth in Appendix 3.6 of the CH-TRU Payload Appendices and Section 6.2.3 of the CH-TRAMPAC.

Payload Container: Choose the appropriate payload container for the load type. The load type describes how the payload container will be shipped with other payload containers in the TRUPACT-II or HalfPACT inner containment vessel; therefore, select only one load type. For some overpacked configurations, overpacking does not impact the selection of the appropriate Load Type. If a zero was entered in Table 2.2-3 for the overpacking payload container total resistance factor, select the load type for the container that is overpacked. For example, for 55-gallon drums, the total resistance and payload shipping category are not affected by overpacking in an SWB with filters having a total hydrogen diffusivity of 1.48×10^{-5} m/s/mf (equivalent to four filters each with a diffusivity of 3.7×10^{-6} m/s/mf) or greater. A zero should have been entered in Table 2.2-3 for the SWB in this configuration. Therefore, for this overpacked configuration, select the Load Type resistance for a payload of 55-gallon drums (Resistance Factor of 7,147). See Appendix 6.10 of the CH-TRU Payload Appendices regarding the use of equivalent Load Type resistance factors for overpacked configurations.

Resistance Factor: Choose the "Resistance Factor" for the load type.

Total Resistance Factor: Enter the chosen value in the "Total Resistance Factor" column. Enter zero (0) or leave the space blank for load types that are not applicable. Note: Only one value for Total Resistance Factor is entered in Table 2.2-4.

Table 2.2-1 — Numeric Payload Shipping Category Worksheet

Container ID Number:						
Two Digit Waste Type Notation (XX) from Table 2.1-1 of the CH-TRU Payload Appendices						
G Value for Waste Material Type from Table 2.1-2		Four Digit G Value Notation (YYYY) from Table 2.1-2				
Confinement Layers	Packaging	Type	Number of Layers	Resistance Factor (Use One Column Only) ^a		Total Resistance Factor ^b
				Column 1	Column 2	
	Inner Bag Layers	Filtered	From Table 2.2-2			
		Twist and Tape		23,989	17,922	
		Unvented Heat-Sealed Bag		c	115,741	
	Confinement Layers (e.g., Metal Can)	Slip-Top/Unsealed		0	0	
		Filtered	From Table 2.2-2			
	Liner Bag Layers	Filtered Drum Liner Bag	From Table 2.2-2			
		Twist and Tape Drum Liner Bag		2,142	2,142	
		Filtered SWB/Bin/TDOP Liner Bag	From Table 2.2-2			
Fold and Tape SWB/Bin/TDOP Liner Bag			1,257	1,257		
Rigid Drum Liner	Rigid Liner	From Table 2.2-2				
Choose Those That Apply	Payload Container	Pipe Component or Criticality Control Container		From Table 2.2-3		
		55-Gallon Drum or Pipe Overpack or Criticality Control Overpack		From Table 2.2-3		
		Shielded Container		From Table 2.2-3		
		85-Gallon Drum – Direct Load		From Table 2.2-3		
		100-Gallon Drum		From Table 2.2-3		
		Bin		From Table 2.2-3		
		85-Gallon Drum Overpack – One 55-Gallon Drum		From Table 2.2-3		
		SWB – Direct Load or Overpacking Bin		From Table 2.2-3		
		SWB Overpack – Four 55-Gallon Drums		From Table 2.2-3		
	Load Type	TDOP – Direct Load		From Table 2.2-3		
		55-Gallon Drums or Pipe Overpacks or Criticality Control Overpacks		From Table 2.2-4		
		Shielded Containers		From Table 2.2-4		
		85-Gallon Drums – Direct Load		From Table 2.2-4		
		100-Gallon Drums		From Table 2.2-4		
		SWBs – Direct Load or Overpacking Bin		From Table 2.2-4		
		SWB Overpacks Containing Up To Four 55-Gallon Drums per SWB, or 85-Gallon Drum Overpacks of 55-Gallon Drums		From Table 2.2-4		
	TDOP – Direct Load		From Table 2.2-4			
	Total Resistance Factor Sum					
Divide Total Resistance Factor Sum by 100 and Round Up to Whole Number					÷ 100	
Total Resistance Notation (ZZZZ) Report as Four Digits If Waste Material Type II.2 (20 0000), enter 0000.						
Payload Shipping Category (XX YYYY ZZZZ)						

- a Use Column 1 for the following six-digit notations (XX YYYY): 10 0160, 10 0130, 10 0040, and 20 0008. Use Column 2 for all other six-digit notations.
- b Multiply the “Number of Layers” by the appropriate “Resistance Factor” to obtain the “Total Resistance Factor.”
- c A resistance factor has not been established for this confinement layer with these waste material types (Column 1).

Table 2.2-2 — Filtered/Punctured Confinement Layers Resistance Worksheet

Packaging/Type	Minimum Filter Hydrogen Diffusivity/Minimum Puncture Diameter	Number of Layers	Resistance Factor ^a (Use One Column Only)		Number of Filters/Punctures per Layer	Total Resistance Factor ^b
			Column 1	Column 2		
Inner Bag Layers: Filtered ^c	1.075 x 10 ⁻⁵ m/s/mf Filter		1,290	931		
	2.150 x 10 ⁻⁵ m/s/mf Filter		645	466		
	5.375 x 10 ⁻⁵ m/s/mf Filter		258	187		
	2.688 x 10 ⁻⁴ m/s/mf Filter		52	38		
	1.075 x 10 ⁻³ m/s/mf Filter		13	10		
Confinement Layer (e.g., Metal Can or Rigid Liner): Filtered	1.9 x 10 ⁻⁶ m/s/mf Filter		7,294	5,264		
	3.7 x 10 ⁻⁶ m/s/mf Filter		3,746	2,703		
	7.4 x 10 ⁻⁶ m/s/mf Filter		1,873	1,352		
	1.85 x 10 ⁻⁵ m/s/mf Filter		750	541		
	9.25 x 10 ⁻⁵ m/s/mf Filter		150	109		
	3.7 x 10 ⁻⁴ m/s/mf Filter		38	28		
Liner Bag Layers: Filtered Drum Liner Bag ^c	1.075 x 10 ⁻⁵ m/s/mf Filter		933	673		
	2.150 x 10 ⁻⁵ m/s/mf Filter		542	391		
	5.375 x 10 ⁻⁵ m/s/mf Filter		240	173		
	2.688 x 10 ⁻⁴ m/s/mf Filter		51	37		
	1.075 x 10 ⁻³ m/s/mf Filter		13	10		
Liner Bag Layers: Filtered SWB/Bin/TDOP Liner Bag ^c	1.075 x 10 ⁻⁵ m/s/mf Filter		764	551		
	2.150 x 10 ⁻⁵ m/s/mf Filter		480	347		
	5.375 x 10 ⁻⁵ m/s/mf Filter		227	164		
	2.688 x 10 ⁻⁴ m/s/mf Filter		51	37		
	1.075 x 10 ⁻³ m/s/mf Filter		13	10		
Rigid Drum Liner:	0.3" Diameter Hole		197	197		
	0.375" Diameter Hole		126	126		
	0.75" Diameter Hole		32	32		
	1" Diameter Hole		18	18		
	2" Diameter Hole		5	5		

- a Use Column 1 for the following six-digit notations (XX YYYY): 10 0160, 10 0130, 10 0040, and 20 0008. Use Column 2 for all other six-digit notations.
 - b Multiply the "Number of Layers" by the appropriate "Resistance Factor" and divide by the "Number of Filters/Punctures per Layer" to obtain the "Total Resistance Factor."
 - c No credit allowed for filter if waste is directly packaged in a filtered bag and there is potential for contact of the filter with water (see Appendix 3.11 of the CH-TRU Payload Appendices).
- m/s/mf = Moles/second/mole fraction.

Table 2.2-3 — Payload Container Resistance Worksheet^a

Payload Container	Filter Type	Number of Filters on Payload Container	Resistance Factor ^b (Use One Column Only)		Total Resistance Factor ^c
			Column 1	Column 2	
Pipe Component or Criticality Control Container (Must also select Pipe Overpack or Criticality Control Overpack, respectively)	1.9 x 10 ⁻⁶ m/s/mf Filter	1	7,294	5,264	
	3.7 x 10 ⁻⁶ m/s/mf Filter	1	3,746	2,703	
	7.4 x 10 ⁻⁶ m/s/mf Filter	1	1,873	1,352	
	1.85 x 10 ⁻⁵ m/s/mf Filter	1	750	541	
	9.25 x 10 ⁻⁵ m/s/mf Filter	1	150	109	
	3.7 x 10 ⁻⁴ m/s/mf Filter	1	38	28	
55-Gallon Drum or Pipe Overpack or Criticality Control Overpack	1.9 x 10 ⁻⁶ m/s/mf Filter		7,294	5,264	
	3.7 x 10 ⁻⁶ m/s/mf Filter		3,746	2,703	
	7.4 x 10 ⁻⁶ m/s/mf Filter		1,873	1,352	
	1.85 x 10 ⁻⁵ m/s/mf Filter		750	541	
	9.25 x 10 ⁻⁵ m/s/mf Filter		150	109	
	3.7 x 10 ⁻⁴ m/s/mf Filter		38	28	
Shielded Container (Must also select filtered confinement layer on Table 2.2-2 for inner 30-gallon drum)	3.7 x 10 ⁻⁶ m/s/mf Filter		3,746	2,703	
	7.4 x 10 ⁻⁶ m/s/mf Filter		1,873	1,352	
	1.85 x 10 ⁻⁵ m/s/mf Filter		750	541	
	9.25 x 10 ⁻⁵ m/s/mf Filter		150	109	
	3.7 x 10 ⁻⁴ m/s/mf Filter		38	28	
85-Gallon Drum Direct load	3.7 x 10 ⁻⁶ m/s/mf Filter		3,746	2,703	
	7.4 x 10 ⁻⁶ m/s/mf Filter		1,873	1,352	
	1.85 x 10 ⁻⁵ m/s/mf Filter		750	541	
	9.25 x 10 ⁻⁵ m/s/mf Filter		150	109	
	3.7 x 10 ⁻⁴ m/s/mf Filter		38	28	
100-Gallon Drum	3.7 x 10 ⁻⁶ m/s/mf Filter		3,746	2,703	
	7.4 x 10 ⁻⁶ m/s/mf Filter		1,873	1,352	
	1.85 x 10 ⁻⁵ m/s/mf Filter		750	541	
	9.25 x 10 ⁻⁵ m/s/mf Filter		150	109	
	3.7 x 10 ⁻⁴ m/s/mf Filter		38	28	

Payload Container	Filter Type	Number of Filters on Payload Container	Resistance Factor ^b (Use One Column Only)		Total Resistance Factor ^c
			Column 1	Column 2	
Bin (Must also select SWB)	3.7 x 10 ⁻⁶ m/s/mf Filter		3,746	2,703	
	7.4 x 10 ⁻⁶ m/s/mf Filter		1,873	1,352	
	1.85 x 10 ⁻⁵ m/s/mf Filter		750	541	
	9.25 x 10 ⁻⁵ m/s/mf Filter		150	109	
	3.7 x 10 ⁻⁴ m/s/mf Filter		38	28	
85-Gallon-Drum Overpack Containing One 55-Gallon Drum (Must also select 55-Gallon Drum)	3.7 x 10 ⁻⁶ m/s/mf Filter		7,490	5,406	
	7.4 x 10 ⁻⁶ m/s/mf Filter		3,746	2,703	
	1.85 x 10 ⁻⁵ m/s/mf Filter		1,499	1,082	
	9.25 x 10 ⁻⁵ m/s/mf Filter		300	217	
	3.7 x 10 ⁻⁴ m/s/mf Filter		75	55	
SWB Direct load or overpacking one bin	3.7 x 10 ⁻⁶ m/s/mf Filter		3,746	2,703	
	7.4 x 10 ⁻⁶ m/s/mf Filter		1,873	1,352	
	1.85 x 10 ⁻⁵ m/s/mf Filter		750	541	
	9.25 x 10 ⁻⁵ m/s/mf Filter		150	109	
	3.7 x 10 ⁻⁴ m/s/mf Filter		38	28	
SWB Overpack Containing Up to Four 55-Gallon Drums (Must also select 55-Gallon Drum) ^d	3.7 x 10 ⁻⁶ m/s/mf Filter		14,980	10,812	
	7.4 x 10 ⁻⁶ m/s/mf Filter		7,490	5,406	
	1.85 x 10 ⁻⁵ m/s/mf Filter		2,998	2,164	0
	9.25 x 10 ⁻⁵ m/s/mf Filter		600	434	0
	3.7 x 10 ⁻⁴ m/s/mf Filter		150	110	0
TDOP Direct load	3.7 x 10 ⁻⁶ m/s/mf Filter		3,746	2,703	
	7.4 x 10 ⁻⁶ m/s/mf Filter		1,873	1,352	
	1.85 x 10 ⁻⁵ m/s/mf Filter		750	541	
	9.25 x 10 ⁻⁵ m/s/mf Filter		150	109	
	3.7 x 10 ⁻⁴ m/s/mf Filter		38	28	

- a See Appendix 6.10 of the CH-TRU Payload Appendices regarding the selection of payload containers for overpacked configurations.
 - b Use Column 1 for the following six-digit notations (XX YYYY): 10 0160, 10 0130, 10 0040, and 20 0008. Use Column 2 for all other six-digit notations.
 - c Divide the appropriate "Resistance Factor" by the "Number of Filters on Payload Container" to obtain the "Total Resistance Factor."
 - d If total resistance factor of an SWB overpacking up to four 55-gallon drums is ≤3745 (if using Column 1) or ≤2703 (if using Column 2), the total resistance of the SWB layer can be assigned a value of zero pursuant to Appendix 6.10 of the CH-TRU Payload Appendices.
- m/s/mf = Moles/second/mole fraction.

Table 2.2-4 — Load Type Resistance Worksheet^a

Shipping Period ^a	Payload Container ^b	Resistance Factor	Total Resistance Factor
60 Days (General Case)	55-Gallon Drum	7,147	
	Shielded Container	1,787	
	85-Gallon Drum	4,795	
	100-Gallon Drum	2,764	
	SWB – Direct Load	1,430	
	SWB Overpack	5,718	
	TDOP – Direct Load	980	
20 Days (Close-Proximity Shipment)	55-Gallon Drum	2,383	
	Shielded Container	596	
	85-Gallon Drum	1,599	
	100-Gallon Drum	922	
	SWB – Direct Load	477	
	SWB Overpack	1,906	
	TDOP – Direct Load	327	
10 Days (Controlled Shipment)^c	55-Gallon Drum	1,192	
	Shielded Container	298	
	85-Gallon Drum	800	
	100-Gallon Drum	461	
	SWB – Direct Load	239	
	SWB Overpack	953	
	TDOP – Direct Load	164	

^aSee Appendices 3.4, 3.5, and 3.6 of the CH-TRU Payload Appendices regarding the selection of a shipping period.

^bSee Appendix 6.10 of the CH-TRU Payload Appendices regarding the use of equivalent Load Type factors for overpacked configurations.

^cThe 10-day shipping period may be used only if the requirements for controlled shipment are met as described in Appendix 3.6 of the CH-TRU Payload Appendices and Section 6.2.3 of the CH-TRAMPAC.

APPENDIX 2.3

DERIVATION OF DECAY HEAT LIMITS

This page intentionally left blank.

2.3 Derivation of Decay Heat Limits

The purpose of this appendix is to provide the logic and mathematical analysis used to arrive at the maximum decay heats for each payload shipping category when all payload containers in a payload belong to the same shipping category and a complete payload is shipped.

Appendix 6.12 of the CH-TRU Payload Appendices describes the derivation of decay heat limits for Content Codes LA 154 and SQ 154 and establishes associated conditions for compliance. Due to the similarities of the TRUPACT-II and HalfPACT packagings (with respect to void volume per payload container and all other variables such as shipment time), decay heat limits per payload container are determined using conservative values and are independent of the packaging (e.g., void volumes per payload container are slightly higher for the HalfPACT, but decay heat limits are calculated using the TRUPACT-II void volumes). Appendix 2.4 of the CH-TRU Payload Appendices presents the methodology for arriving at allowable flammable gas generation limits when dunnage containers are used and/or mixing of shipping categories is used in a payload.

When the logic and mathematical analysis requires the variable of shipment time, the conservative value of 60 days is utilized. For close-proximity shipments and controlled shipments, conservative values of 20 days and 10 days may be assumed, as described in Appendices 3.5 and 3.6, respectively, of the CH-TRU Payload Appendices.

At steady state, the flow rate of hydrogen across each of the confinement layers is equal to the same value and to the hydrogen generation rate. The maximum hydrogen concentration in a payload container vented per Section 2.5 of the Contact-Handled Transuranic Waste Authorized Methods for Payload Control (CH-TRAMPAC) is reached at steady state. That is, a filter vented container with a hydrogen generation source has increasing concentrations of hydrogen with time until steady state conditions are reached. For the purpose of these calculations, it has been assumed that all payload containers are at steady state at the start of transport. As described in Section 5.3 of the CH-TRAMPAC, all payload containers generated in an unvented condition are required to be aspirated to ensure steady-state conditions prior to transport.

The temperature dependence of decay heat limits is discussed in Appendix 6.9 of the CH-TRU Payload Appendices. As shown in that appendix, for Waste Material Type II.1 and Waste Type III, minimum values for the decay heat limits are obtained by using the hydrogen generation and release rates at an ambient temperature of 70°F. For Waste Type I and Waste Material Type II.3, the lowest values for the decay heat limits are obtained by using the hydrogen generation and release rates at the minimum operating temperature of -20°F.

Once the payload containers are sealed inside the TRUPACT-II or HalfPACT inner containment vessel (ICV), concentrations of hydrogen in the different layers increase due to the accumulation of hydrogen in the ICV cavity. Some of the hydrogen generated during the transport period would accumulate in the payload containers, with the remainder being released into the cavity. For the purpose of these calculations, the mole fraction of hydrogen in a bag layer is set equal to the steady state value plus the mole fraction of hydrogen that has accumulated in the cavity. The ICV cavity mole fraction of hydrogen is obtained by assuming that all of the hydrogen generated

is released into the ICV cavity. The maximum hydrogen concentration in the innermost layer is then limited to less than or equal to five (5) volume percent at the end of the shipping period by suitably choosing the gas generation rates. The maximum number of moles of hydrogen that can accumulate in the ICV cavity is:

$$N_{\text{gen}} = (\text{CG})(n_{\text{gen}})(t) \quad (1)$$

Where:

- N_{gen} = total moles of hydrogen generated
- CG = hydrogen gas generation rate per innermost layer of confinement (moles/sec)
- n_{gen} = number of hydrogen generators (55-gallon drums, standard pipe overpacks, S100 pipe overpacks, S200 pipe overpacks, S300 pipe overpacks, criticality control overpacks, 85-gallon drums, 100-gallon drums, SWBs, TDOPs) (see Table 2.4-1 of Appendix 2.4 of the CH-TRU Payload Appendices)
- t = shipping period duration (e.g., 60 days).

The maximum mole fraction of hydrogen in the TRUPACT-II or HalfPACT ICV cavity is then equal to:

$$X_{\text{fh}} = (N_{\text{gen}}/N_{\text{tg}}) = \{N_{\text{gen}}/[P(V_{\text{void}})/RT]\} \quad (2)$$

Where:

- X_{fh} = maximum mole fraction of hydrogen in the ICV cavity
- N_{tg} = total moles of gas inside the ICV cavity
- P = pressure inside the TRUPACT-II or HalfPACT, assumed to be constant at 1 atm (760 mm Hg), because the amount of gas generated is much less than the total amount of air originally in the cavity
- V_{void} = void volume inside the ICV cavity (liters)
- R = gas constant = 62.361 mm Hg-liter/mole-K
- T = absolute temperature of air in the ICV cavity at the time of closure = 70°F = 294K.

The gas generation rate per innermost confinement layer that will yield a maximum hydrogen concentration of five (5) volume percent is then computed as the following:

$$X_{\text{inner}} = X_{\text{th}} + (CG)(R_{\text{eff}}) \quad (3)$$

Where:

X_{inner} = mole fraction of hydrogen in innermost confinement layer (a value of 0.05 has been used for this parameter since this is the maximum permissible concentration)

R_{eff} = the effective resistance to the release of hydrogen (sec/mole).

The effective resistance is computed by summing the individual confinement layer resistances. The resistance of a layer is equal to the reciprocal of the release rate from that layer. After substituting equations (1) and (2) into (3) and solving for the gas generation rate the following results:

$$CG = (X_{\text{inner}}) / \{R_{\text{eff}} + [(t)(n_{\text{gen}})/N_{\text{tg}}]\} \quad (4)$$

where all terms are as defined previously. The decay heat per innermost confinement layer is then computed as:

$$Q_i = [(CG)(N_A)/(G \text{ molecules}/100\text{eV})][1.602(10)^{-19} \text{ watt-sec/eV}] \quad (5)$$

Where:

Q_i = decay heat per innermost confinement layer (watts)

N_A = Avogadro's number = $6.023(10)^{23}$ molecules/mole

G = G_{eff} (flam gas) = effective G value for flammable gas (molecules of hydrogen formed/100 electron volts [eV] emitted energy).

The logic for arriving at the input parameters is detailed in Appendix 6.7 of the CH-TRU Payload Appendices.

As an example, the decay heat limit per innermost confinement layer will be computed for shipping category I.1A2 (or 10 0160 0190).

The effective resistance is the sum of the following resistances (see Appendix 6.8 of the CH-TRU Payload Appendices for a derivation of the resistances):

- There are two liner bags, thus the combined resistance is twice the resistance of one liner bag, $2 \times 214,133$ sec/mole or 428,266 sec/mole.
- Resistance of the drum liner, which is 19,646 sec/mole, and
- Resistance of the drum filter, which is 729,327 sec/mole.

The effective resistance, R_{eff} , is therefore 1,177,239 sec/mole.

Assuming an atmospheric pressure of 760 mm Hg, a TRUPACT-II ICV cavity void volume of 2,450 liters (for 14 drums/TRUPACT-II) and a temperature of 70°F (294K), the total moles of gas inside the TRUPACT-II Package ICV cavity is computed using the ideal gas law,

$$\begin{aligned} N_{\text{tg}} &= (P)(V_{\text{void}})/RT = (760 \text{ mm Hg}) (2,450 \text{ liters}) / [(62.361 \text{ mm Hg} \cdot \text{liter/mole} \cdot \text{K}) \\ &\quad (294\text{K})] \\ &= 101.56 \text{ moles} \end{aligned}$$

There will be 14 drums of shipping category I.1A2 (10 0160 0190) inside a TRUPACT-II package so that the number of gas generators, $n_{\text{gen}} = 14$.

The hydrogen gas generation rate per the innermost confinement layer may then be computed using equation (4) assuming a maximum five (5) volume percent concentration at the end of sixty days.

$$\begin{aligned} \text{CG} &= (0.05)/\{1,177,239 \text{ sec/mole} \\ &\quad + [(60 \text{ days})(86,400 \text{ sec/day})(14)/(101.56 \text{ moles})]\} \\ &= 2.643(10)^{-8} \text{ mole/sec} \end{aligned}$$

[Note: The ratio of number of generators to total moles for a HalfPACT is 7/76.52 moles, which results in a slightly higher CG. Therefore, use of the TRUPACT-II CG value for the HalfPACT is conservative.]

For shipping category I.1A2 (10 0160 0190), the effective G (flam gas) value is 1.60. Therefore, the decay heat limit per innermost confinement layer, Q_i , through equation (5) is:

$$\begin{aligned} Q_i &= [2.643(10)^{-8} \text{ mole/sec}][6.023(10)^{23} \text{ molecules/mole}] \\ &\quad \times [1.602(10)^{-19} \text{ watt-sec/eV}]/[1.6 \text{ molecules/100 eV}] \\ &= 0.1594 \text{ watt} \end{aligned}$$

The methodology used for deriving the decay heat limit described above applies to the derivation of decay heat limits for all shipping categories under the alpha-numeric notation system (see Appendix 2.1 of the CH-TRU Payload Appendices). The methodology used for calculating the decay heat limits for numeric shipping categories is simplified and conservative to provide a direct correlation between shipping category and decay heat limits. Both methodologies produce decay heat limits that limit the concentration of hydrogen gas within any layer of confinement to less than or equal to 5% by volume.

For numeric shipping categories that do not have a corresponding alpha-numeric shipping category notation, the decay heat limit calculation methodology follows. As described in Appendix 2.1 of the CH-TRU Payload Appendices, the last four digits of the numeric shipping category is a notation for the total resistance to hydrogen release. From equation (4) above, the

total resistance (R_T) can be defined as the combination of the effective resistance (R_{eff}), the resistance provided by the moles of gas in the void volume within the packaging (N_{tg}), the number of generators (n_{gen}), and the shipping period (t).

$$R_T = R_{eff} + [(t) (n_{gen}) / N_{tg}] \quad (6)$$

Substituting equation (6) into equation (4) yields:

$$CG = \frac{X_{inner}}{R_T}$$

Combining equations (4), (5), and (6), and solving for Q_i yields:

$$Q_i = \frac{(0.05 * 6.023 (10)^{23} \text{ molecules/mole} * 1.602 (10)^{-19} \text{ watt-sec/eV})}{(R_T \text{ sec/mole} * G \text{ value} / 100 \text{ eV})} \quad (7)$$

Simplifying and using the shipping category notation form of XX YYYY ZZZZ (described in Appendix 2.1 of the CH-TRU Payload Appendices) where YYYY represents the G value (multiplied by 100) and ZZZZ represents the total resistance, R_T , (divided by 10,000 and rounded up) yields:

$$CG = \frac{0.05}{(ZZZZ * 10,000) \text{ sec/mole}} \quad (8)$$

and

$$Q_i = \frac{(4824.42 \text{ molecules/mole} * \text{watt-sec/eV})}{(ZZZZ * YYYY) \text{ sec-molecules/mole-eV}} \quad (9)$$

For shipping category 10 0040 0160, substituting 0040 for YYYY and 0160 for ZZZZ yields:

$$CG = \frac{0.05}{(0160 * 10,000) \text{ sec/mole}} = 3.125E-08 \text{ mole/sec}$$

$$Q_i = \frac{4824.42 \text{ molecules/mole} * \text{watt-sec/eV}}{(0160 * 0040) \text{ sec-molecules/mole-eV}} = 0.7538 \text{ watts}$$

Because the total resistance, R_T , is rounded up to the nearest 10,000 sec/mole, the calculated decay heat limit using this simplified method is conservative. Decay heat limits for all other

numeric shipping categories that do not have a corresponding alpha-numeric shipping category are calculated from the shipping category notation using this simplified equation.

Because the decay heat limit cannot be directly calculated from the alpha-numeric payload shipping category notation, Table 2.3-1 presents the hydrogen gas generation rate limit and the decay heat limit for each alpha-numeric payload shipping category.

The parameters that are used in the calculations are described below.

<u>Parameter</u>	<u>Description</u>
Alpha-numeric Payload Shipping Category	Identifies payload shipping category using the alpha-numeric shipping category notation (form of the waste).
G Value (H ₂)	G _{eff} (flam gas)—Number of molecules of hydrogen produced per 100 eV of emitted energy. There is a characteristic effective G (flam gas) value associated with each waste material type as described in Appendix 3.2 of the CH-TRU Payload Appendices.
Number of Generators in ICV	n _{gen} —The number of generators inside the packaging ICV, e.g., in the case of SWB overpack in a TRUPACT-II, the number of generators is 8 (4 55-gallon drums per SWB) x (2 SWBs per TRUPACT-II ICV).
Number of Inner Bags	These are the small bags, such as those used to bag-out solid inorganics and organics. Only the leakage from the closure or filter has been used as the hydrogen release rate.
Number of Liner Bags	These are the large bags, such as those used to contain the solidified aqueous or homogeneous inorganic solids or that serve as drum liners for Waste Types II or III. Hydrogen release from both permeation through the bag material and diffusion through the closure or filter has been used in computing hydrogen release rates.
Total Number of Bags	Sum of the number of inner and liner bags.
Number of Containers in ICV	Number of payload containers inside the packaging ICV cavity.
Void Vol. in ICV Effective Resistance	Void volume inside the packaging ICV cavity (liters). Effective resistance to the release of hydrogen computed by summing the individual confinement layer resistances.

<u>Parameter</u>	<u>Description</u>
Gas Generation Rate	Gas generation rate per generator (CG), which is computed from input parameters via equation (4) for alpha-numeric shipping categories and equation (8) for numeric shipping categories.
Decay Heat Limit Per Generator (watts)	Decay heat limit per generator (watts), which is computed using equation (9) for numeric shipping categories and equation (5) for alpha-numeric shipping categories.
Numeric Payload Shipping Category	Identifies payload shipping category using the numeric shipping category notation (form of the waste).

Table 2.3-1 - List of Approved Alpha-numeric Shipping Categories, Maximum Allowable Hydrogen Gas Generation Rates, and Maximum Allowable Wattages

Numeric Payload Shipping Category	Alpha-numeric Payload Shipping Category	Maximum Allowable Hydrogen Gas Generation Rate (moles/sec)	Maximum Allowable Wattage (watts)
10 0040 0034	I.3C0	1.514E-07	3.6528
10 0040 0147	I.3A0	3.416E-08	0.8241
10 0040 0168	I.3A1	2.980E-08	0.7189
10 0040 0190	I.3A2	2.643E-08	0.6375
10 0040 0207	I.3B0	2.416E-08	0.5827
10 0040 0229	I.3B1	2.189E-08	0.5281
10 0040 0250	I.3B2	2.002E-08	0.4828
10 0040 0648	I.3A3	7.721E-09	0.1863
10 0040 0709	I.3B3	7.061E-09	0.1703
10 0040 0888	I.3A4	5.634E-09	0.1359
10 0040 0949	I.3B4	5.274E-09	0.1272
10 0130 0034	I.2C0	1.514E-07	1.1240
10 0130 0147	I.2A0	3.416E-08	0.2536
10 0130 0168	I.2A1	2.980E-08	0.2212
10 0130 0190	I.2A2	2.643E-08	0.1962
10 0130 0207	I.2B0	2.416E-08	0.1793
10 0130 0229	I.2B1	2.189E-08	0.1625
10 0130 0250	I.2B2	2.002E-08	0.1486
10 0130 0648	I.2A3	7.721E-09	0.0573
10 0130 0709	I.2B3	7.061E-09	0.0524
10 0130 0888	I.2A4	5.634E-09	0.0418
10 0130 0949	I.2B4	5.274E-09	0.0391
10 0160 0034	I.1C0	1.514E-07	0.9132
10 0160 0059	I.1C2	8.598E-08	0.5185
10 0160 0147	I.1A0	3.416E-08	0.2060
10 0160 0168	I.1A1	2.980E-08	0.1797
10 0160 0190	I.1A2	2.643E-08	0.1594
10 0160 0207	I.1B0	2.416E-08	0.1457

Table 2.3-1 - List of Approved Alpha-numeric Shipping Categories, Maximum Allowable Hydrogen Gas Generation Rates, and Maximum Allowable Wattages (Continued)

Numeric Payload Shipping Category	Alpha-numeric Payload Shipping Category	Maximum Allowable Hydrogen Gas Generation Rate (moles/sec)	Maximum Allowable Wattage (watts)
10 0160 0229	I.1B1	2.189E-08	0.1320
10 0160 0250	I.1B2	2.002E-08	0.1207
10 0160 0286	I.1C2b	1.751E-08	0.1056
10 0160 0648	I.1A3	7.721E-09	0.0466
10 0160 0709	I.1B3	7.061E-09	0.0426
20 0000 0000	II.2AM	NA	40.0000
20 0000 0000	II.2BM	NA	40.0000
20 0000 0000	II.2CM	NA	40.0000
20 0000 0000	II.2E0	NA	40.0000
20 0170 0028	II.1C0	1.798E-07	1.0206
20 0170 0034	II.1C1f	1.501E-07	0.8518
20 0170 0039	II.1C2f	1.288E-07	0.7309
20 0170 0041	II.1C1	1.238E-07	0.7029
20 0170 0043	II.1C2bf	1.173E-07	0.6659
20 0170 0049	II.1C3f	1.039E-07	0.5897
20 0170 0053	II.1C2	9.445E-08	0.5361
20 0170 0067	II.1D2	7.524E-08	0.4271
20 0170 0127	II.1A0	3.966E-08	0.2251
20 0170 0133	II.1A1f	3.765E-08	0.2137
20 0170 0140	II.1A2af	3.584E-08	0.2034
20 0170 0143	II.1A2f	3.519E-08	0.1997
20 0170 0148	II.1A1	3.391E-08	0.1924
20 0170 0152	II.1A3f	3.303E-08	0.1875
20 0170 0166	II.1B0	3.015E-08	0.1711
20 0170 0169	II.1A2a	2.961E-08	0.1680
20 0170 0188	II.1B1	2.670E-08	0.1516
20 0170 0209	II.1B2a	2.396E-08	0.1360
20 0170 0220	II.1C2b	2.277E-08	0.1292

Table 2.3-1 - List of Approved Alpha-numeric Shipping Categories, Maximum Allowable Hydrogen Gas Generation Rates, and Maximum Allowable Wattages (Continued)

Numeric Payload Shipping Category	Alpha-numeric Payload Shipping Category	Maximum Allowable Hydrogen Gas Generation Rate (moles/sec)	Maximum Allowable Wattage (watts)
20 0170 0233	II.1C3	2.154E-08	0.1222
20 0170 0327	II.1A2	1.531E-08	0.0869
20 0170 0367	II.1B2	1.364E-08	0.0774
20 0170 0412	II.1C4	1.215E-08	0.0690
20 0170 0506	II.1A3	9.883E-09	0.0561
20 0170 0546	II.1B3	9.163E-09	0.0520
20 0170 0686	II.1A4	7.298E-09	0.0414
20 0170 0725	II.1B4	6.898E-09	0.0392
20 0170 0865	II.1A5	5.785E-09	0.0328
20 0170 0905	II.1B5	5.530E-09	0.0314
20 0170 1044	II.1A6	4.791E-09	0.0272
20 0170 1084	II.1B6	4.616E-09	0.0262
30 0340 0028	III.1C0	1.798E-07	0.5103
30 0340 0034	III.1C1f	1.501E-07	0.4259
30 0340 0039	III.1C2f	1.288E-07	0.3655
30 0340 0041	III.1C1	1.238E-07	0.3515
30 0340 0043	III.1C2bf	1.173E-07	0.3329
30 0340 0049	III.1C3f	1.039E-07	0.2948
30 0340 0053	III.1C2	9.445E-08	0.2680
30 0340 0067	III.1D2	7.524E-08	0.2135
30 0340 0127	III.1A0	3.966E-08	0.1126
30 0340 0133	III.1A1f	3.765E-08	0.1069
30 0340 0140	III.1A2af	3.584E-08	0.1017
30 0340 0143	III.1A2f	3.519E-08	0.0999
30 0340 0148	III.1A1	3.391E-08	0.0962
30 0340 0152	III.1A3f	3.303E-08	0.0937
30 0340 0166	III.1B0	3.015E-08	0.0856
30 0340 0169	III.1A2a	2.961E-08	0.0840
30 0340 0188	III.1B1	2.670E-08	0.0758

Table 2.3-1 - List of Approved Alpha-numeric Shipping Categories, Maximum Allowable Hydrogen Gas Generation Rates, and Maximum Allowable Wattages (Concluded)

Numeric Payload Shipping Category	Alpha-numeric Payload Shipping Category	Maximum Allowable Hydrogen Gas Generation Rate (moles/sec)	Maximum Allowable Wattage (watts)
30 0340 0209	III.1B2a	2.396E-08	0.0680
30 0340 0220	III.1C2b	2.277E-08	0.0646
30 0340 0233	III.1C3	2.154E-08	0.0611
30 0340 0327	III.1A2	1.531E-08	0.0434
30 0340 0367	III.1B2	1.364E-08	0.0387
30 0340 0412	III.1C4	1.215E-08	0.0345
30 0340 0506	III.1A3	9.883E-09	0.0280
30 0340 0546	III.1B3	9.163E-09	0.0260
30 0340 0686	III.1A4	7.298E-09	0.0207
30 0340 0725	III.1B4	6.898E-09	0.0196
30 0340 0865	III.1A5	5.785E-09	0.0164
30 0340 0905	III.1B5	5.530E-09	0.0157
30 0340 1044	III.1A6	4.791E-09	0.0136
30 0340 1084	III.1B6	4.616E-09	0.0131
40 9999 0127	IV.1A0T	3.937E-08	7.0000
40 9999 0148	IV.1A1T	3.378E-08	7.0000
40 9999 0169	IV.1A2T	2.959E-08	7.0000
40 9999 0188	IV.1B1T	2.660E-08	7.0000
40 9999 0209	IV.1B2T	2.392E-08	7.0000
40 9999 0506	IV.1A3T	9.881E-09	7.0000
40 9999 0546	IV.1B3T	9.158E-09	7.0000

This page intentionally left blank.

APPENDIX 2.4

**MIXING OF SHIPPING CATEGORIES AND DETERMINATION OF
THE FLAMMABILITY INDEX**

This page intentionally left blank.

2.4 Mixing of Shipping Categories and Determination of the Flammability Index

The purpose of this appendix is to provide the logic and mathematical analysis for assembling a payload of containers with different shipping categories. An assembly of payload containers with different shipping categories is approved by ensuring that each payload container does not contain a flammable mixture of gases, while accounting for the properties of each of the other payload containers in the assembly, which may include dunnage containers. Each payload container is assessed through the calculation of the flammability index (FI) for the container, which accounts for the flammable properties of each container in the assembly. For each payload container, the FI is calculated as the ratio of the actual flammable gas generation rate to the allowable flammable gas generation rate limit multiplied by 50,000. Thus, the FI must be a non-negative number less than or equal to 50,000 for each payload container. The determination of allowable flammable gas generation rates takes into account the concentrations of flammable volatile organic compounds (VOCs) within the innermost layer of confinement, if present, and the void volume of dunnage containers. Unlimited mixing of shipping categories is allowed for direct loaded payload configurations, with the FIs calculated based on each payload container in the configuration. For overpacked payload configurations documented in this appendix, unlimited mixing of shipping categories is allowed pursuant to implementation of the methodology described in this appendix. For Content Codes LA 154 and SQ 154, mixing is only allowed within the content code as presented in Appendix 6.12 of the CH-TRU Payload Appendices.

At steady state, the flow of flammable gas across each of the confinement layers is equal to the flammable gas generation rate. The maximum flammable gas concentration in a payload container vented per Section 2.5 of the Contact-Handled Transuranic Waste Authorized Methods for Payload Control (CH-TRAMPAC) is reached at steady state. That is, a filtered container with a flammable gas generation source has increasing concentrations of hydrogen with time until steady-state conditions are reached. For the purpose of these calculations, it has been conservatively assumed that all payload containers are at steady state at the start of transport. As described in Section 5.3 of the CH-TRAMPAC, all payload containers generated in an unvented condition are required to be aspirated to ensure steady-state conditions prior to transport.

Once payload containers are sealed inside the packaging inner containment vessel (ICV), concentrations of flammable gas in the different layers increase due to the accumulation of flammable gas in the packaging ICV cavity. Some of the flammable gas generated during the transport period would accumulate in the innermost container and in the overpacking container (if present), with the remainder being released into the cavity. The packaging ICV cavity mole fraction of flammable gas is obtained by assuming that all of the flammable gas generated is instantaneously released into the packaging ICV cavity. The maximum concentration of flammable gas and flammable VOCs in the innermost layer is then limited to the mixture lower explosive limit (MLEL). The allowable flammable gas concentration (AFGC) is then calculated as the difference between the MLEL and the sum of the flammable VOC concentrations.

For analytical category payload containers or test category payload containers that have headspace concentrations of flammable VOCs less than or equal to 500 parts per million (ppm), the AFGC is equal to the MLEL of 0.05 mole fraction (i.e., 5 volume percent). For test category containers with headspace flammable VOC concentrations in excess of 500 ppm, the AFGC is calculated as the difference between the MLEL at the end of the 60-day shipping period and the innermost confinement layer sum of flammable VOC concentrations. For close-proximity shipments and controlled shipments, conservative values of 20 days and 10 days may be assumed, as described in Appendices 3.5 and 3.6, respectively, of the CH-TRU Payload Appendices.

The maximum number of moles of flammable gas that can accumulate in the packaging ICV cavity is:

$$N_{gen} = \sum_{i=1}^{n_{containers}} CG_i t \quad (1)$$

where,

N_{gen} = Total moles of flammable gas generated (mole).

CG_i = Flammable gas generation rate per innermost confinement layer of payload container "i" (mole/sec). When shipping categories are mixed in a single payload, this rate will be different for each payload container.

t = Shipping period duration (60 days or 5,184,000 seconds).

$n_{containers}$ = Number of generators in the payload (Table 2.4-1 lists the maximum number of generators based on the payload assembly configuration).

The maximum flammable gas mole fraction in the packaging ICV cavity is then equal to:

$$X_{fg} = \frac{N_{gen}}{N_{tg}} = \sum_{i=1}^{n_{containers}} \frac{CG_i t}{N_{tg}} \quad (2)$$

where,

X_{fg} = Maximum mole fraction of flammable gas in the packaging ICV cavity

N_{tg} = Total moles of gas inside the packaging ICV cavity that are equal to:

$$N_{tg} = \sum_{i=1}^{n_{containers}} CG_i t + \frac{PV_{void}}{RT} \quad (3)$$

Table 2.4-1 Parameter Values for Payload Assembly Configurations

Payload Assembly Configuration	Maximum Number of Flammable Gas Generators	Void Volume of Dunnage Payload Containers (liters)	V_{void} (liters)
Fourteen 55-Gallon Drums in TRUPACT-II Fourteen Standard Pipe Overpacks in TRUPACT-II Fourteen S100 Pipe Overpacks in TRUPACT-II Fourteen S200 Pipe Overpacks in TRUPACT-II Fourteen S300 Pipe Overpacks in TRUPACT-II Fourteen Criticality Control Overpacks in TRUPACT-II	14	208	2,450 + $n_{\text{dunnage}} * 208$
Seven 55-Gallon Drums in HalfPACT Seven Standard Pipe Overpacks in HalfPACT Seven S100 Pipe Overpacks in HalfPACT Seven S200 Pipe Overpacks in HalfPACT Seven S300 Pipe Overpacks in HalfPACT Seven Criticality Control Overpacks in HalfPACT	7	208	1,225 + $n_{\text{dunnage}} * 208$
Eight 85-Gallon Drums in TRUPACT-II	8	321	2,087 + $n_{\text{dunnage}} * 321$
Four 85-Gallon Drums in HalfPACT Four 85-Gallon Drum Overpacks in HalfPACT	4	321	1,043 + $n_{\text{dunnage}} * 321$
Six 100-Gallon Drums in TRUPACT-II	6	378	2,715 + $n_{\text{dunnage}} * 378$
Three 100-Gallon Drums in HalfPACT	3	378	1,357 + $n_{\text{dunnage}} * 378$
Three Shielded Containers in HalfPACT	3	157	2,100 + $n_{\text{dunnage}} * 157$
TDOP With Ten 55-Gallon Drums in TRUPACT-II	10 Actual + 4 assumed with most restrictive properties	208	2,450 + $n_{\text{dunnage}} * 208$
TDOP With Six 85-Gallon Drums in TRUPACT-II	6 Actual + 2 assumed with most restrictive properties	321	2,087 + $n_{\text{dunnage}} * 321$
TDOP With Six 85-Gallon Drum Overpacks in TRUPACT-II	See Two SWB Overpacks in TRUPACT-II		
Two SWBs in TRUPACT-II	2	1,750	1,750 or 3,500 with dunnage SWB

**Table 2.4-1 Parameter Values for Payload Assembly Configurations
(Continued)**

Payload Assembly Configuration	Maximum Number of Flammable Gas Generators	Void Volume of Dunnage Payload Containers (liters)	V_{void} (liters)
Two SWB Overpacks in TRUPACT-II	8	208	1,750 or 3,500 with dunnage SWB + $n_{\text{dunnage}} * 208$
One SWB in HalfPACT	1	No dunnage available	875
One SWB Overpack in HalfPACT	4	208	875 + $n_{\text{dunnage}} * 208$
One TDOP direct load in TRUPACT-II	1	No dunnage available	1,277

SWB = Standard waste box
 TDOP = Ten-drum overpack
 n_{dunnage} = Number of dunnage containers

where,

P = Pressure inside the package, conservatively assumed to be constant at 1 atmosphere (atm), because the amount of gas generated is much less than the total amount of air originally in the cavity

V_{void} = Void volume inside the packaging ICV cavity, which includes the void volume of appropriate dunnage containers (Table 2.4-1 lists appropriate values based on the payload assembly configuration)

R = Gas constant (0.082056 atm-liter/mole-K)

T = Absolute temperature of air originally in the cavity (294K).

It is assumed that the moles of flammable gas generated is much less than the moles of gas in the packaging ICV cavity at the time of package sealing:

$$\sum_{i=1}^{n_{\text{containers}}} CG_i t \ll \frac{PV_{\text{void}}}{RT} \quad (4)$$

Therefore, from equation (3),

$$N_{ig} \approx \frac{PV_{void}}{RT} \quad (5)$$

2.4.1 Derivation of Mass Balances for Payload Assembly Configurations

2.4.1.1 Drums, Drum Overpacks, Pipe Overpacks, Criticality Control Overpacks, or Shielded Containers Loaded in ICV

The flammable gas generation rate per innermost confinement layer that will yield a maximum flammable gas concentration equivalent to the AFGC, is then calculated for each payload container "i" as the following:

$$CG_i r_{eff,i} = AFGC_i - X_{fg} \quad (6)$$

where,

$AFGC_i$ = Allowable flammable gas concentration in innermost confinement layer of payload container "i"

$r_{eff,i}$ = The effective resistance to the release of hydrogen of payload container "i" (sec/mole).

The effective resistance is computed by summing the individual confinement layer resistances. The resistance of a layer is equal to the reciprocal of the release rate from that layer. Substituting X_{fg} from equation (2) into equation (6) and rearranging terms yields the following system of equations:

$$\left(r_{eff,1} + \frac{t}{N_{ig}} \right) CG_1 + \frac{t}{N_{ig}} CG_2 + \dots + \frac{t}{N_{ig}} CG_{n_{containers}} = AFGC_1$$

$$\frac{t}{N_{ig}} CG_1 + \left(r_{eff,2} + \frac{t}{N_{ig}} \right) CG_2 + \dots + \frac{t}{N_{ig}} CG_{n_{containers}} = AFGC_2$$

• • •
• • •
• • •

$$\frac{t}{N_{ig}}CG_1 + \frac{t}{N_{ig}}CG_2 + \dots + \left(r_{eff, n_{containers}} + \frac{t}{N_{ig}} \right) CG_{n_{containers}} = AFGC_{n_{containers}} \quad (7)$$

2.4.1.2 Ten-Drum Overpack With 55-Gallon Drums

The analyses presented in Appendix 6.10 of the CH-TRU Payload Appendices show that overpacking payload containers in a ten-drum overpack (TDOP) will not decrease the allowable decay heat limits, even when payload containers are allowed to remain overpacked in a TDOP for indefinite periods of time before transport inside a TRUPACT-II. For example, a 55-gallon drum that meets the decay heat limit for a 14-drum payload in a TRUPACT-II can also be shipped in a 10-drum configuration in a TDOP inside a TRUPACT-II. The overpacked configurations can be conservatively assigned the same decay heat limits as the equivalent configurations not using the TDOP. If 55-gallon drums or 85-gallon drum overpacks of different shipping categories are mixed within a TDOP, the mixing of shipping categories methodology for 14 55-gallon drums directly loaded in the ICV shall apply. For purposes of establishing allowable flammable gas generation rates, the payload will be assumed to consist of four additional drums that will be assigned the same packaging configuration as the most restrictive waste drum. These four drums will each be assigned the minimum AFGC value of the actual waste drums.

2.4.1.3 TDOP With 85-Gallon Drums/85-Gallon Drum Overpacks

As indicated above, the analyses presented in Appendix 6.10 of the CH-TRU Payload Appendices show that overpacking payload containers in a TDOP will not decrease the allowable decay heat limits, even when payload containers are allowed to remain overpacked in a TDOP for indefinite periods of time before transport inside a TRUPACT-II. The overpacked configurations can be conservatively assigned the same decay heat limits as the equivalent configurations not using the TDOP. If 85-gallon drums of different shipping categories are mixed within a TDOP, the mixing of shipping categories methodology for eight 85-gallon drums directly loaded in the ICV shall apply. As shown in Appendix 6.10, 85-gallon drum overpacks will be evaluated as eight 55-gallon drums overpacked in two SWBs with two filters using the methodology of Section 2.4.1.4. For purposes of establishing allowable flammable gas generation rates, the payload will be assumed to consist of two additional drums that will be assigned the same packaging configuration as the most restrictive waste drum. These two drums will each be assigned the minimum AFGC value of the actual waste drums.

2.4.1.4 Standard Waste Box Overpacks Loaded in ICV

The mass balances on hydrogen within a drum "i" and within the standard waste box (SWB) overpacking the n_{drums} number of waste drums may be expressed as:

Transient Mass Balance of Hydrogen in Drum "i"

$$\frac{PV_{ij}}{RT} \frac{dX_{ij}}{dt} = CG_{ij} - \frac{(X_{ij} - X_{SWBj})}{r_{effij}} \quad (8)$$

Transient Mass Balance on Hydrogen in SWB Overpack "j" Void

$$\frac{PV_{SWBj}}{RT} \frac{dX_{SWBj}}{dt} = \sum_{i=1}^{n_j} \frac{(X_{ij} - X_{SWBj})}{r_{eff,ij}} - \frac{(X_{SWBj} - X_{fg})}{r_{SWBj}} \quad (9)$$

where,

- V_{ij} = Void volume within the innermost confinement layer of drum "i" overpacked in SWB "j" (liters)
- V_{SWBj} = Void volume within an SWB overpack containing n_j drums of waste (liters)
- n_j = Number of waste drums inside SWB "j"
- X_{ij} = Mole fraction of flammable gas within innermost confinement layer of drum "i" overpacked in SWB "j" (dimensionless)
- X_{SWBj} = Mole fraction of flammable gas within SWB "j" void volume (dimensionless)
- X_{fg} = Mole fraction of flammable gas in the packaging ICV cavity (dimensionless)
- t = time (sec)
- CG_{ij} = Flammable gas generation rate per innermost confinement layer of drum "i" overpacked in SWB "j" (mole/sec)
- $r_{eff,ij}$ = The effective resistance to the release of hydrogen of drum "i" overpacked in SWB "j" (sec/mole)
- r_{SWBj} = The effective resistance to the release of hydrogen of the filters on SWB "j" (sec/mole).

Based on the pseudo steady-state assumption, the mass balance equations (equations (8) and (9)) are set to zero. The maximum concentration of flammable gas within the innermost confinement layer at the end of the transport period is set equal to the AFGC value:

$$X_{ij} = AFGC_{ij} \quad (10)$$

- $AFGC_{ij}$ = Allowable flammable gas concentration in innermost confinement layer of drum "i" in SWB "j".

Substitution of equation (10) into equations (8) and (9), which are both set to zero, and rearrangement of terms yields:

Pseudo Steady-State Mass Balance of Hydrogen in Drum "i"

$$CG_{ij} = \frac{AFGC_{ij} - X_{SWBj}}{r_{eff\ ij}} \quad (11)$$

Pseudo Steady-State Mass Balance on Hydrogen in SWB Overpack "j" Void

$$\sum_{i=1}^{n_j} \frac{AFGC_{ij} - X_{SWBj}}{r_{eff\ ij}} = \frac{X_{SWBj} - X_{fg}}{r_{SWBj}} \quad (12)$$

Rearranging equation (11) to express the SWB mole fraction in terms of drum "i" variables results in:

$$X_{SWBj} = AFGC_{ij} - CG_{ij}r_{eff\ ij} \quad (13)$$

Substitution of equation (13) in the left-hand side of equation (12) and substitution of equations (2) and (13) in the right-hand side of equation (12) results in the following system:

For j = 1 to n_{SWB}

For k = 1 to n_j

$$\sum_{i=1}^{n_j} CG_{ij} = \frac{AFGC_{kj} - CG_{kj}r_{eff\ kj} - \sum_{j=1}^{n_{SWB}} \sum_{i=1}^{n_j} \frac{CG_{ij}t}{N_{tg}}}{r_{SWB,j}} \quad (14)$$

Rearranging equation (14) results in the following system of equations that must be solved to obtain the allowable flammable gas generation rate limit for each drum "kj" (CG_{kj}):

For j = 1 to n_{SWB}

For k = 1 to n_j

$$r_{eff\ kj}CG_{kj} + r_{SWB,j} \sum_{i=1}^{n_j} CG_{ij} + \frac{t}{N_{tg}} \sum_{j=1}^{n_{SWB}} \sum_{i=1}^{n_j} CG_{ij} = AFGC_{kj} \quad (15)$$

2.4.2 Calculation of Allowable Flammable Gas Generation Rates

The systems of equations represented by equations (7) and (15) may be written in matrix form as:

$$A CG = b \quad (16)$$

where

- A = Matrix of gas generation rate coefficients (i.e., $r_{eff\ i}$, $r_{eff\ kj}$, $r_{SWB\ j}$, and t/N_{tg} terms)
- CG = Column vector of allowable gas generation rates
- b = Column vector of AFGCs within the innermost confinement layers. Thus, the elements of this vector are equal to the individual payload container AFGC values.

The solution for the unknown allowable flammable gas generation rate for each payload container is given as:

$$CG = A^{-1} b \quad (17)$$

where

- A^{-1} = Inverse of matrix A.

Dunnage containers and payload containers that have no flammable gas generation rate are excluded from the system of linear equations.

2.4.3 Calculation of the Flammability Index

The FI of each container is then calculated as:

$$FI_i = \frac{CG_{i,actual}}{CG_{i,allowable}} \times 50,000 \quad (18)$$

where

- FI_i = Flammability index of payload container "i"
- $CG_{i,actual}$ = Actual flammable gas generation of payload container "i" (mole/sec)
- $CG_{i,allowable}$ = Allowable flammable gas generation rate of payload container "i" (mole/sec).

For analytical category payload containers, the actual flammable gas generation rate is calculated as:

$$CG_{i,actual} = \frac{Q_i(G \text{ molecules}/100 \text{ eV})}{N_A(1.602(10)^{-19} \text{ watt} - \text{second} / \text{eV})} \quad (19)$$

where

- Q_i = Decay heat of payload container (watts)
- N_A = Avogadro's number = $6.0225(10)^{23}$ molecules/mole
- G = G_{eff} (flam gas) = effective G value for flammable gas (molecules of flammable gas formed/100 eV emitted energy).

For test category containers, the actual gas generation rate is obtained either through measurement of the flammable gas concentration and calculation of the rate through the AltMeth methodology (Appendix 3.10 of the CH-TRU Payload Appendices), or through testing pursuant to Section 5.2.5 of the CH-TRAMPAC. A payload is qualified for shipment only if the FI of each payload container is a non-negative number less than or equal to 50,000. If one or more containers fail the FI requirement, the payload shall be reconfigured until all containers satisfy this requirement. The FI determination can be performed either manually or by the use of a validated software package.

APPENDIX 3.1

RADIOLYTIC G VALUES FOR WASTE MATERIALS

This page intentionally left blank.

Table of Contents

3.1	Radiolytic G Values for Waste Materials.....	3.1-1
3.1.1	Introduction.....	3.1-1
3.1.2	Radiation Chemistry.....	3.1-2
3.1.2.1	Reactions of Radiation with Matter.....	3.1-3
3.1.2.2	Energy Transfer.....	3.1-4
3.1.2.3	Factors Affecting the Rate of Radiolytic Gas Generation (or Consumption) from a Material	3.1-6
3.1.3	Radiolysis of Liquids, Vapors, and Gases.....	3.1-17
3.1.3.1	Radiolysis of Saturated Hydrocarbons.....	3.1-18
3.1.3.2	Radiolysis of Unsaturated Hydrocarbons.....	3.1-19
3.1.3.3	Radiolysis of Aromatic Hydrocarbons.....	3.1-20
3.1.3.4	Radiolysis of Water.....	3.1-21
3.1.3.5	Radiolysis of Alcohols.....	3.1-24
3.1.3.6	Radiolysis of Ethers.....	3.1-24
3.1.3.7	Radiolysis of Aldehydes and Ketones.....	3.1-24
3.1.3.8	Radiolysis of Carboxylic Acids.....	3.1-27
3.1.3.9	Radiolysis of Esters.....	3.1-28
3.1.3.10	Radiolysis of Phosphate Esters.....	3.1-29
3.1.3.11	Radiolysis of Halogenated Hydrocarbons.....	3.1-30
3.1.3.12	Radiolysis of Organic Nitrogen Compounds.....	3.1-34
3.1.3.13	Radiolysis of Commercial Lubricants.....	3.1-36
3.1.3.14	Radiolysis of Gases.....	3.1-37
3.1.4	Radiolysis of Polymers.....	3.1-37
3.1.4.1	Radiolysis of Hydrocarbon Polymers Containing Only Saturated C-C Bonds.....	3.1-42
3.1.4.2	Radiolysis of Polymers Containing Alcohol Functional Groups.....	3.1-54
3.1.4.3	Radiolysis of Polymers Containing Ether Functional Groups.....	3.1-54
3.1.4.4	Radiolysis of Hydrocarbon Polymers Containing Unsaturated C-C Bonds.....	3.1-62
3.1.4.5	Radiolysis of Polymers Containing Ester Functional Groups.....	3.1-62
3.1.4.6	Radiolysis of Polymers with Aromatic Characteristics.....	3.1-64
3.1.4.7	Radiolysis of Polymers Containing Halogens.....	3.1-67
3.1.4.8	Radiolysis of Miscellaneous Polymers.....	3.1-80

Table of Contents (Concluded)

3.1.5	Radiolysis of Non-Polymer Solids	3.1-83
3.1.5.1	Radiolysis of Solidified Liquid Wastes.....	3.1-83
3.1.5.2	Radiolysis of Solid Organic Acids	3.1-88
3.1.5.3	Radiolysis of Asphalt	3.1-88
3.1.5.4	Radiolysis of Soil	3.1-88
3.1.5.5	Radiolysis of Dry, Solid Inorganic Materials.....	3.1-89
3.1.6	Comparison of Laboratory G Values With Effective G Values Measured for Drums of CH-TRU Wastes	3.1-89
3.1.6.1	Retrieved Drums of CH-TRU Wastes.....	3.1-90
3.1.6.2	Newly Generated Waste Experiments.....	3.1-91

List of Tables

Table 3.1-1 — Average Values of LET in Water Irradiated with Various Types of Radiation	3.1-7
Table 3.1-2 — G Values for Saturated Hydrocarbons.....	3.1-18
Table 3.1-3 — G Values for Three Unsaturated Hydrocarbons	3.1-20
Table 3.1-4 — Radiolysis Products and G Values for Liquid Cyclohexene	3.1-20
Table 3.1-5 — G Values for Several Aromatic Hydrocarbons.....	3.1-21
Table 3.1-6 — G Values for Water.....	3.1-22
Table 3.1-7 — G Values for Alcohols	3.1-25
Table 3.1-8 — G Values for Ethers in the Liquid Phase	3.1-26
Table 3.1-9 — G Values for Propionaldehyde	3.1-26
Table 3.1-10 — Effect of LET on the Gaseous Products of Acetone.....	3.1-26
Table 3.1-11 — G Values for Three Ketones	3.1-27
Table 3.1-12 — G Values for Carboxylic Acids (Liquids at Room Temperature)	3.1-28
Table 3.1-13 — G Values for Esters.....	3.1-28
Table 3.1-14 — G Values for Phosphate Esters	3.1-29
Table 3.1-15 — G Values for Carbon Tetrachloride	3.1-31
Table 3.1-16 — G Values for Aromatic Halides	3.1-32
Table 3.1-17 — G Values for Miscellaneous Organic Halogen Compounds.....	3.1-34
Table 3.1-18 — G Values for Liquid Organic Nitrogen Compounds	3.1-35
Table 3.1-19 — G Values for Many Commercial Lubricants	3.1-38
Table 3.1-20 — Radiation Resistance of Common Polymers that Predominantly Crosslink	3.1-39
Table 3.1-21 — Radiation Resistance of Common Polymers that are Borderline Between Predominant Crosslinking and Scission.....	3.1-40
Table 3.1-22 — Radiation Resistance of Common Polymers that Scission Predominantly	3.1-40
Table 3.1-23 — Expected Relative G(flam gas) Values for Polymers from G(flam gas) Values in Structurally Related Liquids	3.1-41
Table 3.1-24 — Summary of Maximum G Values for Polymers at Room Temperature	3.1-43
Table 3.1-25 — Summary of G Values for Hydrogen and Methane for Radiolysis of Polyethylene in a Vacuum	3.1-45
Table 3.1-26 — G Values for Polyethylene (Oxygen Depleted or Absent)	3.1-47
Table 3.1-27 — G Values for Polyethylene (Oxygen Present)	3.1-50
Table 3.1-28 — G Values for Polypropylene (Oxygen Absent)	3.1-52
Table 3.1-29 — G Values for Polypropylene (Oxygen Present).....	3.1-53
Table 3.1-30 — G Values for Cellulosic Materials (Oxygen Absent or Depleted).....	3.1-59
Table 3.1-31 — G Values for Cellulosic Materials (Oxygen Present).....	3.1-60
Table 3.1-32 — G Values for Polybutadiene (and Copolymers) and Polyisoprene.....	3.1-62
Table 3.1-33 — G Values for PMMA	3.1-64
Table 3.1-34 — G Values for Polyesters	3.1-66
Table 3.1-35 — G Values for Pure PVC (in Vacuum).....	3.1-72

List of Tables (Concluded)

Table 3.1-36 — G Values for Plasticized and/or Stabilized PVC (Oxygen Absent or Depleted).....	3.1-73
Table 3.1-37 — G Values for PVC (Oxygen Present).....	3.1-76
Table 3.1-38 — G Values for Polychloroprene.....	3.1-77
Table 3.1-39 — G Values for Hypalon ^R	3.1-78
Table 3.1-40 — G Values for PTFE (Oxygen Depleted or Absent).....	3.1-79
Table 3.1-41 — G Values for PTFE (Oxygen Present).....	3.1-79
Table 3.1-42 — G Values for Polyamides.....	3.1-81
Table 3.1-43 — G(gas) Values for Miscellaneous Commercial Plastics (Relative to Polyethylene).....	3.1-82
Table 3.1-44 — Data for RFETS Retrieved Waste Drums with $G(H_2)_{min} > 1.0$	3.1-92
Table 3.1-45 — Effective G Values for RFETS Newly-Generated Waste Drums.....	3.1-94
Table 3.1-46 — Effective G Values for LANL Newly-Generated Waste Drums.....	3.1-97

Figures

Figure 3.1-1 — Partial Pressures of Various Gases in a Drum of Newly-Generated Waste from RFP (Leaded Rubber Gloves).....	3.1-95
Figure 3.1-2 — Gas Yields vs. Time for LANL Drum BFB-116 (Leaded Rubber Gloves)..	3.1-98
Figure 3.1-3 — Gauge Pressure in Drum 122 vs. Time.....	3.1-100
Figure 3.1-4 — Moles of Gas Present in Drum 122 vs. Time.....	3.1-101
Figure 3.1-5 — $G(H_2)$ vs. Time for Drum 122.....	3.1-102

Attachments

- A Chemical Properties and Commercial Uses of Organic Materials
- B Absorption of Alpha Decay Energy Inside Particles of PuO_2

Glossary

adsorption	The adhesion in an extremely thin layer of molecules (such as gases, solutes, or liquids) to the surfaces of solid bodies or liquids with which they are in contact.
absorbed dose	The amount of energy absorbed from the radiation field per unit of mass of irradiated material.
activation energy	The energy, in excess over the ground state, that must be added to an atomic or molecular system to allow a particular process to take place.
adiabatic	Any change or process resulting in no heat loss or gain.
alcohol	A class of organic compounds derived from hydrocarbons, containing the hydroxyl group OH (general formula ROH). Phenols, a subgroup of alcohols, are derived from aromatic hydrocarbons.
aldehyde	Compounds of the general formula RCHO, where R is any aliphatic or aromatic group and the oxygen is attached via a double bond to the carbon chain.
aliphatic	Any of a class of organic compounds characterized by straight or branched chain structures. Aliphatic compounds may contain single, double, and/or triple carbon-carbon bonds.
alkane	Any of a class of aliphatic hydrocarbon compounds characterized by single carbon-carbon bonds.
alkene	Any of a class of unsaturated aliphatic hydrocarbon compounds characterized by at least one double carbon-carbon bond.
alkyd	A thermoplastic or thermoset synthetic resin used especially for protective coatings.
alkyl	An aliphatic hydrocarbon group that may be derived from an alkane by dropping one hydrogen from the formula, such as "methyl" (CH ₃).
alkyne	Any of a class of organic compounds containing at least one triple carbon-carbon bond.

alpha particle	A massive, positively charged particle (He^{++}) emitted by certain radioactive materials; particle energy depends on the parent material, and penetrating ability is limited.
amine	Any of a class of organic compounds that can be considered to be derived from ammonia by replacement of one or more hydrogen atoms with alkyl or aryl groups.
anaerobic	In the absence of oxygen.
antioxidant	An inhibitor, such as ascorbic acid, effective in preventing replacement of other elements by molecular oxygen.
aqueous solution	A solution that contains water as the dominant solvent.
aromatic	Any of a class of organic compounds characterized by closed ring structure and resonance stabilized (shifting/shared) unsaturation.
Arrhenius Equation	An equation relating the rate constant of a chemical reaction and the temperature at which the reaction is taking place: $k = A \exp(-E/RT)$ where A is a constant, k the rate constant, T the temperature in degrees Kelvin, R the gas constant, and E the activation energy of the reaction.
aryl	A compound whose molecules have the ring structure characterized by benzene; that is, six carbon atoms condensed into a planar ring.
beta particle	A particle emitted by certain radioactive materials. A negatively charged beta particle has the characteristics of an electron; a positively charged beta particle is called a positron.
bond dissociation energy	The required energy for complete separation of two atoms within a molecule.
carbonyl compound	A compound containing the carbonyl group, ($\text{C}=\text{O}$), such as aldehydes, carboxylic acids, esters, etc.
carboxyl	A univalent group ($-\text{COOH}$) typical of organic acids.
cellulosic	Any of the derivatives of cellulose, such as cellulose acetate.

chain reaction	A reaction that involves a series of steps, each of which generates a reactive substance that brings about the next step.
chemical reaction rate	The speed at which a change occurs when a substance (or substances) is (are) changed into one or more new substances.
contact-handled	Radioactively contaminated materials having a container surface dose rate of no more than 200 mrem/hr, which may be handled manually.
crosslink	A chemical bond formed between separate polymer elements; crosslinking may be intermolecular (between molecules) or intramolecular (between parts of the same molecule).
Curie	The basic unit of radioactivity; equal to 3.7×10^{10} disintegrations per second.
depolymerization	The decomposition of macromolecular compounds into relatively simple compounds.
diffusion	The spontaneous movement and scattering of atomic and molecular particles of liquids, gases, and solids.
diluent	An inert substance added to a material so that the concentration per unit volume of the material is decreased.
dose	See "absorbed dose."
dose rate	The rate at which energy is deposited in a material.
dose rate effect	An effect depending on the rate at which a material is irradiated.
elastomer	A natural or synthetic rubber that stretches to at least twice its original length and retracts rapidly to near its original length when released.
emulsifier	A surface-active agent (like a soap) that promotes the formation and stabilization of a solid-in-liquid or liquid-in-liquid suspension.
Envirostone [®]	A licensed (U. S. Gypsum) gypsum-based process used for the solidification of organic and low pH aqueous sludges.
ester	A compound formed from the bonding of an alcohol (including phenols) with an organic acid or organic acid derivative by the elimination of water.

ether	A compound formed by attaching two groups to an oxygen atom, of the form R-O-R'.
excitation	The process by which energy is supplied to electrons, atoms, or radicals, usually rendering them chemically more reactive.
free radical	An atom or group of atoms having at least one unpaired electron not involved in bond formation. Free radicals are highly reactive.
gamma rays	Electromagnetic radiation (photons) emitted from the nucleus of certain radioactive materials; gamma rays are more penetrating than particle radiation of comparable energy.
Gray (Gy)	The SI recommended unit of absorbed dose that represents an absorption by a specified material of 1×10^4 ergs/gram; 1 Gray = 100 rads.
G value	The number of molecules, radicals, crosslinks, etc., of a specified type formed or consumed per 100 electron volts (eV) of energy absorbed by a system; this value is also used to specify the number of reactions that occur per 100 eV absorbed.
half-life	The time required for a quantity of a specific radionuclide to decay to one-half of its original amount.
halogenated compound	A compound that contains a member of the halogen family (for example, fluorine, chlorine, bromine).
halogenation	A chemical process or reaction in which a halogen atom (F, Cl, Br, I, At) is introduced into a substance.
hydrocarbon	One of a very large group of chemical compounds composed only of carbon and hydrogen.
hydrolysis	Decomposition or alteration of a chemical substance by water. In aqueous solutions of electrolytes, the reaction of cations with water to produce a weak base or of anions with water to produce a weak acid.
inelastic collision	An encounter in which the total kinetic energy of the colliding particles is lower after the collision than before it.
inhibitor	A substance that slows down or stops a reaction.

ion	An electrically charged atom, radical, or molecule resulting from the addition or removal of electrons by any of a number of possible processes.
ionization	The process of ion formation.
ionizing radiation	Particles or photons that have sufficient energy to produce ionization directly by their passage through a substance.
irradiation	Exposure to radiation.
isomer	One of two or more chemical substances having the same elementary percentage composition and molecular weight but differing in structure and, therefore, usually differing in properties.
isotactic	Refers to crystalline polymers in which groups in the asymmetric carbon atoms have the same (rather than random) configuration in relation to the main chain.
ketone	Any of a class of organic compounds characterized by the presence of the carbonyl group, C=O, attached to two alkyl groups.
LET (Linear Energy Transfer)	The radiation energy lost per unit length of path through a material, usually expressed in kilo-electron volts (keV) per micron of path (or eV/nm). A higher value of LET indicates more effective ionization of the absorber.
monomer	A simple molecule that is a repeating structural unit within a polymer. It is capable of combining with a number of like or unlike molecules to form a polymer.
neutron	An uncharged elementary particle present in the nucleus of every atom heavier than hydrogen; neutrons are released during fission.
nitration	Introduction of an NO ₃ ⁻ group into an organic compound.
olefin	An alkene.
organic acid	A chemical compound with one or more carboxyl radicals (-COOH) in its structure.
outgas	The release of adsorbed or occluded gases or water vapor, usually as the result of heating or differences in vapor pressure.
oxidation	A chemical reaction in which a compound or radical loses electrons.

paraffin	An alkane.
permeation	The movement of atoms, molecules, or ions into or through a porous or permeable substance (such as a membrane).
pi orbital	A region in a molecule, formed by the overlap of atomic orbitals, in which there is a high probability of finding a "p" or "d" electron; two atomic p or d orbitals overlapping at right angles to the axis between the atoms' nuclei form a pi orbital with electron regions above and below the axis.
polyamide	The product of polymerization of an amino acid or the condensation of a polyamine with a polycarboxylic acid.
polymer	Any of a class of organic compounds characterized by repeating structural units (monomers).
polymerization	The process of bonding two or more monomers to produce a polymer.
rad	The traditional unit of absorbed radiation dose representing the absorption by a specified material of 100 ergs per gram of that material; 1 rad = 1.0E-2 Gray; 1 rad = 6.24E13 eV/g.
radiation	The emission and propagation of energy through matter or space; also, the energy so propagated; the term has been extended to particles, as well as electromagnetic radiation.
radical	A molecular fragment having one or more unpaired electrons (e.g., $\cdot\text{H}$ or $\cdot\text{CH}_3$). It may be charged or uncharged.
radical scavenger	A substance that readily combines with a radical.
radiolysis	Alteration of materials caused by irradiation.
range	The distance a given ionizing particle can penetrate into a given material before its energy drops to the point that the particle no longer ionizes the material.
repeat unit	See "monomer."
resin	Any of a class of solid or semisolid organic products of natural or synthetic origin with no definite melting point, generally of high molecular weight; most resins are polymers.

saturated hydrocarbon	A carbon-hydrogen compound containing no double or triple bonds.
saturated vapor pressure	The vapor pressure of a substance at its boiling point.
scission	The process by which chemical bonds are broken; also, the number of bonds broken by the process. Usually refers to breaks in the backbone of a polymer macromolecule.
spur	A small group of excited and ionized species associated with the track caused by passage of ionizing radiation. Consists of the molecules ionized directly, radicals, and secondary ionizations produced by electrons released in the primary ionization. A spur usually forms a side track from the path of the particle or ray.
steric hindrance	The prevention or retardation of chemical reaction caused by geometrical restrictions of neighboring groups on the same molecule.
synergistic effect	The effect on a material of two or more stresses applied simultaneously that is greater in magnitude than that resulting from the same stresses applied separately.
track	The path of gamma rays, x-rays, or charged particles through matter.
TRU nuclide	A nuclide with an atomic number greater than that of uranium (92). All transuranic nuclides are produced artificially and are radioactive.
TRU waste	Waste materials contaminated with alpha-emitting TRU nuclides with half-lives >20 years, in concentration >100 nCi/g of waste at the time of assay.
unsaturated hydrocarbon	One of a class of hydrocarbons that have at least one double or triple carbon-carbon bond. Such compounds are different from aromatic hydrocarbons.
vapor	A gas that exists at a temperature below the critical temperature and that can be liquefied by compression without lowering its temperature.
viscous	Having relatively high resistance to flow.
x-rays	Penetrating electromagnetic radiation, usually generated by decelerating high-velocity electrons through collision with a solid body or by inner-shell electron transitions for atoms with atomic number greater than 10.

Acronyms and Abbreviations

CH-TRU (wastes)	contact-handled transuranic wastes
e	accelerated electrons
E _a	activation energy
EPRI	Electric Power Research Institute
F	fraction of energy absorbed
FDA	Food and Drug Administration
HC	hydrocarbon
HDPE	high-density polyethylene
INEEL	Idaho National Engineering and Environmental Laboratory
LANL	Los Alamos National Laboratory
LDPE	low-density polyethylene
LET	linear energy transfer
ORNL	Oak Ridge National Laboratory
PET	polyethylene terephthalate
PMMA	polymethyl methacrylate
PTFE	polytetrafluoroethylene (Teflon)
PVC	polyvinyl chloride
RFETS	Rocky Flats Environmental Technology Site
SAR	Safety Analysis Report
SRS	Savannah River Site

Chemical Notation

CaCl ₂	calcium chloride
CaO	calcium oxide
Ca	calcium
C-C	carbon-carbon bond
C-Cl	carbon-chlorine bond
CCl ₃ F	trichlorofluoromethane
CCl ₄	carbon tetrachloride
C-F	carbon-fluorine bond
CF ₄	carbon tetrafluoride
C ₄ H ₈	butene
C ₄ H ₁₀	butane
C-H	carbon-hydrogen bond
CHCl ₃	chloroform
CH ₃	methyl group
CH ₄	methane
Cl ₂	chlorine
Cm-244	curium isotope with atomic mass of 244
CO	carbon monoxide
CO ₂	carbon dioxide
C ₃ H ₆	cyclopropane or propylene
C ₃ H ₈	propane
C ₂ H ₂	acetylene (or ethyne)
C ₂ H ₄	ethylene (or ethene)
C ₂ H ₆	ethane
Fe ₂ O ₃	iron (III) oxide (ferric oxide)
HCl	hydrogen chloride
He ⁺⁺	doubly charged helium ion. An alpha particle.
H ₂	Hydrogen
KCl	potassium chloride
MgCl ₂	magnesium chloride
MgO	magnesium oxide
NaCl	sodium chloride
Na ₂ O	sodium oxide
OH	hydroxyl group
O ₂	oxygen
Po	polonium
Pu-238	plutonium isotope with atomic mass of 238
Pu-239	plutonium isotope with atomic mass of 239
Pu(NO ₃) _x	plutonium nitrate
PuO ₂	plutonium dioxide
R, R'	any alkyl or aromatic group
SiO ₂	silicon dioxide
SO ₂	sulfur dioxide
Z	atomic number
Zn	zinc

G Value Notation

Notation	Interpretation - G Value for
G(C ₂)	all hydrocarbons with two carbon atoms
G(C ₃)	all hydrocarbons with three carbon atoms
G(C ₄)	all hydrocarbons with four carbon atoms
G(CH ₄)	methane
G(C ₂ H ₆)	ethane
G(H ₂)	hydrogen
G(S)	scission
G(gas)	all gas generated
G(water vapor)	water vapor
G(X)	crosslinking

Executive Summary

This document presents radiolytic G values for solids, liquids, vapors, and gases obtained from the technical literature. Experimental data are evaluated, and applicable maximum G values are determined for use in calculations of flammable gas concentration and total pressure for transport of contact-handled transuranic (CH-TRU) wastes. G values for organic solids are related to G values for structurally-related liquids. It is demonstrated that G values (for hydrogen and other flammable gases) for organic materials can be ranked according to the functional groups that determine most other chemical properties. This relationship allows G values for other organic solids to be estimated. Maximum G values obtained from laboratory-scale experiments are compared to effective G values measured for actual drums of CH-TRU wastes. For materials that are commonly present in the CH-TRU wastes, polyethylene has the highest value of $G(H_2)$ of 4.0. The maximum $G(H_2)$ value for water is 1.6.

This document is not meant to be a comprehensive summary of all radiolysis experiments that have measured gas generation. Instead, the literature has been searched for typical and upper bound G values, and for general characteristics that allow extrapolation to other materials for which no radiolysis experiments have been reported. Where possible, data obtained by various authors are discussed and compared. When authors disagree, an effort has been made to determine which data are valid and the reasons for the differences.

Factors affecting gas generation from the reactions of alpha, beta, neutron, or gamma radiation with matter are discussed. These factors include the linear energy transfer (LET) and range of the incident radiation; irradiation environment, including temperature, pressure, and gases present; absorbed dose and dose rate; specific composition of the material; and particle size and distribution of radioactive contaminants.

The controlling factor in the behavior of materials under irradiation, as under most other environmental influences, is the chemical structure. Chemical bonds are not broken randomly even though the excitation energy may exceed the bond dissociation energy. Energy may be transferred from the location on a molecule where it is absorbed to another chemical bond that is broken. Additives to improve physical or aging properties may affect changes produced by radiation.

For this reason, radiolysis can be discussed in terms of functional groups as can other chemical reactions. The functional group is the atom or group of atoms that defines the structure of a particular family of organic compounds, and, at the same time, determines their properties. A particular set of properties can be associated with a particular group wherever it is found.

G values for a given material may depend on the type of radiation absorbed by the material (LET effect). For several liquids, such as cyclohexane, benzene, water, and acetone, alpha radiolysis experiments yield higher G values than gamma radiolysis experiments. Similar effects may also occur in solids, such as polymers, but very few experiments have been conducted to determine LET effects in gas generation in solids. This is possibly due to the difficulty in measuring the absorbed dose in alpha radiolysis, where self-absorption of some of the alpha radiation emitted from particulate contamination occurs. G values measured using nonalpha radiation are the best

data available for many materials. These data are included in establishing maximum G values in a best faith effort to establish upper bound gas generation calculations for CH-TRU wastes.

Liquids that have G values for flammable gas greater than 4.0 are saturated hydrocarbons, alcohols, ethers, ketones, and organic acids. Liquids that have G values for flammable gases less than 4.0 include unsaturated hydrocarbons, aromatic hydrocarbons, water, esters, halogenated hydrocarbons, aromatic halides, and commercial lubricant oils. G values for liquid organic nitrogen compounds are low for those having aromatic characteristics or C-N triple bonds.

Common plastics and papers are composed of one or more base polymers and additives designed to increase flexibility, stability, or other properties. Organic functional groups found in common polymers include saturated C-C bonds, unsaturated C-C bonds, and alcohol, ether, and ester groups. Aromatic characteristics (resonant structures containing carbon and hydrogen or carbon and nitrogen atoms) greatly increase the stability of many polymers, and are commonly found in additives.

Saturated hydrocarbons produce hydrogen as the principal radiolysis gas. Small amounts of other hydrocarbons are formed. The maximum $G(H_2)$ value is 4.0 for polyethylene.

Polymers having ether functional groups generate gases that contain oxygen, even when irradiated in a vacuum. G values for cellulose and urea formaldehyde have been shown to be strongly dependent on the absorbed dose. For absorbed doses greater than 10 Mrad, the maximum value of $G(H_2)$ is 3.2 for cellulose. One of the polymers in this family (polyoxymethylene) generates other flammable gases that cause the $G(\text{flam gas})$ value to exceed 4.1, and another (polyvinyl formal) has a measured $G(\text{gas})$ that is 1.4 times the $G(\text{gas})$ value for polyethylene. For this reason, polyoxymethylene and polyvinyl formal are permitted in CH-TRU wastes only in trace amounts.

Polymers containing chlorine are stabilized to reduce the catalytic effect of HCl generated by radiolysis or thermal degradation. The strong effect of the plasticizers and stabilizers on the radiolysis of PVC is demonstrated by the differences in the composition of the radiolysis gas, which vary from 85% H_2 to 83% HCl to 70% CO_2 , depending on the specific polymer formulation and whether oxygen is present.

Radiolysis of adsorbed or absorbed liquids indicates that the sorbing medium can either be inert to radiation or can transfer energy to the sorbed liquid. Unless experimental data demonstrate that the binding medium is radiolytically inert (e.g., vermiculite), all of the radiation energy should be assumed to interact with the sorbed liquid. Nitrates present in solidified aqueous wastes significantly reduce $G(H_2)$ from the value for water, while increasing $G(O_2)$.

Very low G values have been observed from irradiation of water present as the hydrate in crystals. Water in the hydrates appears to exhibit the property of an "energy sink."

Gas generation experiments conducted on actual CH-TRU wastes are summarized. Typically, several different contaminated materials were present inside a given waste container. The results

are presented in terms of effective G values that include the effects of the different materials and self-absorption of some alpha decay energy by particulate contamination.

On the whole, the effective hydrogen G values for actual CH-TRU wastes are much lower than the maximum hydrogen G values for the waste forms that would be estimated based on the worst-case material. For drums of combustible wastes, the maximum $G(H_2)$ value determined in controlled experiments was 2.1 versus a possible value of 4.0 based on laboratory experiments. For drums of sludge, the maximum $G(H_2)$ value measured was 0.3 versus a possible value of 1.6 based on laboratory experiments. No explanation currently exists for high $G(H_2)$ values calculated from experiments conducted on solidified organic waste forms.

Gas pressure and composition data for retrieved drums of stored wastes are also discussed. Calculated G values for sealed retrieved drums provide only lower limits, because of uncertainties in the rates at which gases can permeate through the drum gaskets or diffuse through gaps between the gasket and the sealing surfaces. Typically, only the drum head space was sampled, and the concentrations of generated gases could have been higher inside the rigid liner and waste bags. Most of the lower limit G values were very low.

This page intentionally left blank

3.1 Radiolytic G Values for Waste Materials

3.1.1 Introduction

The purpose of this document is to establish maximum G values from the technical literature for production of gas (particularly hydrogen) from the radiolysis of materials in contact-handled transuranic (CH-TRU) wastes. These maximum G values are used in calculations of flammable gas concentrations and total pressure in safety analyses for transport of the wastes. In Section 3.1, the maximum G values obtained from laboratory-scale experiments are compared to G values calculated from gas generation experiments conducted on drums of actual CH-TRU wastes. The maximum G values typically are much larger than those obtained from actual wastes.

This document reports radiolysis data (including temperature dependence) for many types of materials, including the chemical families of organic compounds that are liquids (e.g., alcohols, aldehydes, and ketones); organic solvents; water; polymers; and commercial plastics, cellulose, and rubbers. Inorganic materials and commercial plastics, cellulose, and rubbers are the major constituents in CH-TRU wastes and packaging materials. Liquids may be major constituents (> 10 wt%) of solidified liquid wastes or minor or trace (≤ 1 wt%) constituents when they are absorbed on paper tissues or used as plasticizers in plastics and rubbers. For solid materials for which the G values are unknown, related organic solids or liquids are used to estimate bounding values. In order to provide a thorough discussion of this subject, G values are reported for some materials that are not known to be present in the CH-TRU wastes.

This document is not meant to be a comprehensive summary of all radiolysis experiments that have measured gas generation. Instead, the literature has been searched for typical and upper bound G values, and for general characteristics that allow extrapolation to other materials for which no radiolysis experiments have been reported. Where possible, data obtained by various authors are discussed and compared. When authors disagree, an effort has been made to determine which data are valid and the reasons for the differences. For example, discrepant data in the case of PVC appear to be largely caused by variations in material composition and not by experimental error.

Radiolysis data used in this report result from irradiation of materials by gamma, alpha, or other particles; accelerated electrons; or x-rays. For the CH-TRU wastes, alpha irradiation is the only significant contributor to gas generation. Chemists and materials scientists for many years have used gamma radiolysis as a tool to explore the stability of materials. As a result, many more materials have been studied by gamma than by alpha radiolysis. Many alpha radiolysis experiments were performed during the 1970s at the Los Alamos National Laboratory (LANL), the Savannah River Site (SRS), and the Rocky Flats Environmental Technology Site (RFETS) to measure radiolytic gas generation from common materials that appear in CH-TRU wastes [see Molecke (1979¹) and Blauvelt (1986²) for discussions of these experiments]. Some of these data have been reanalyzed in this report, and different conclusions are now drawn from these data.

¹ Molecke 1979. M. A. Molecke, "Gas Generation from Transuranic Waste Degradation: Data Summary and Interpretation," Sandia National Laboratories, SAND79-1245, December 1979.

² Blauvelt 1986. R. K. Blauvelt and R. J. Janowiecki, "General Strategy for Evaluating the Radiolytic Gas Generation Potential in Newly-Generated CH-TRU Waste," Monsanto Research Corporation, Mound Laboratory, MLM-MU-86-61-0013, January 1986.

G values for a given material may depend on the type of radiation absorbed by the material (known as an LET effect). For several liquids, such as cyclohexane, benzene, water, and acetone, alpha radiolysis experiments yield higher G values than gamma radiolysis experiments. Similar effects may also occur in solids, such as polymers, but very few experiments have been conducted to determine LET effects in gas generation in solids. This is possibly due to the difficulty in measuring the absorbed dose in alpha radiolysis, where self-absorption of some of the alpha radiation emitted from particulate contamination occurs. G values measured using nonalpha radiation are the best data available for many materials. These data are included in establishing maximum G values in a best-faith effort to establish upper bound gas generation calculations for CH-TRU wastes.

Section 3.1.2 of this document introduces basic concepts of radiation chemistry and factors that affect radiolytic gas generation or consumption. This forms the basis for discussions of the experimental data on radiolysis of liquids and vapors in Section 3.1.3, the radiolysis of polymers in Section 3.1.4, and the radiolysis of non-polymer solids in Section 3.1.5. Section 3.1.6 compares the laboratory G values measured for specific materials with rates of gas generation measured for actual drums of CH-TRU wastes. Attachment A describes the families of organic liquids and polymers, and shows the structures of many common polymers. Attachment B calculates the fraction of alpha decay energy escaping from a particle of PuO_2 as a function of particle radius. A glossary is provided that includes acronyms, abbreviations, chemical notation, and G value notation.

Major reviews of the radiation chemistry literature, such as An Introduction to Radiation Chemistry by J.W.T. Spinks; The Radiation Chemistry of Macromolecules edited by M. Dole; and Radiation Effects on Organic Materials edited by R.O. Bolt and J.G. Carroll, have been used extensively. When these references are cited, the original reports were not reviewed by this author.

3.1.2 Radiation Chemistry

Radiation chemistry is the study of the chemical effects produced in a system by the absorption of ionizing radiation. Included in this definition are the chemical effects produced by radiation (alpha and beta particles and gamma rays) and by electromagnetic radiation of short wavelength (x-rays). Photochemistry, on the other hand, deals with reactions of excited species unaccompanied by ionization.

This chapter discusses the factors affecting gas generation from the reactions of alpha, beta, gamma, or neutron radiation with matter. These factors include linear energy transfer (LET) and range of the incident radiation; irradiation environment including temperature, pressure, and atmosphere present; absorbed dose and dose rate; specific composition of the irradiated material; and particle size and distribution of radioactive contaminants.

3.1.2.1 Reactions of Radiation with Matter

The discussion that follows is based primarily on Spinks (1976³).

Absorption of energy from ionizing radiation results in the formation of tracks of excited and ionized species in matter. The incident radiation is not selective and may react with electrons of any atom or molecule lying along its track. Free radicals are produced by the dissociation of excited molecules and by ion reactions in or near the tracks of ionizing particles. Free radicals have one or more unpaired electrons available to form chemical bonds, but free radicals are generally uncharged. These free radicals are often more important in the chemical reactions that follow than are the primary species. Back reactions can combine two radicals to form a stable molecule. Radicals that do not undergo radical-radical reactions in the tracks diffuse into the bulk of the material and generally react there. Some of the more reactive radicals are H^+ , OH^- , Cl^+ , and CH_3^- . Stable radicals include NO, NO₂, and O₂. Nitric oxide and nitrogen dioxide both have a single unpaired electron. Oxygen has a triplet ground state and behaves in radical reactions as a diradical.³ Oxygen readily reacts with other free radicals and, if it is present, will almost invariably affect the radiation-induced reactions. Free radicals can also be produced by other processes, such as thermal degradation.

The species produced by ionizing radiation will, in general, be the same in a particular material regardless of the type or energy of the ionizing radiation. All ionizing radiation will, therefore, give rise to qualitatively similar chemical effects. With respect to gas generation, different types of ionizing radiation will generally produce the same gas species, though possibly in different amounts.

Alpha particles consist of two protons and two neutrons and, therefore, are the same as the nuclei of helium atoms and have a double positive charge. On passing through matter, alpha particles lose energy principally by inelastic collisions with electrons lying in their paths, leading to excitation and ionization (if the energy transmitted is high enough) of the atoms and molecules to which those electrons belong. Electrons liberated in the process also interact with other atoms and molecules of the material. An alpha particle loses only a small fraction of its energy per collision. As a consequence, alpha particles slow down gradually as the result of a large number of small energy losses and travel in a nearly straight path. The energy of an alpha particle decreases as the distance traveled increases. Because each of the alpha particles from a given radionuclide has the same initial energy, each will have about the same range in a given material. Alpha particles can also be produced in situ in a material by combining it with a compound of boron or lithium and irradiating the mixture with slow neutrons. Some radiolysis experiments have used this technique for producing alpha particles.

Beta particles are fast electrons emitted by radioactive nuclei. In contrast to alpha particles, the beta particles from a particular radioactive element are not all emitted with the same energy.³ Instead, the energies range from zero up to a maximum value that is characteristic of the element. On passing through matter, beta particles lose energy predominantly through inelastic collisions

³ Spinks 1976. J. W. T. Spinks and R. J. Woods, An Introduction to Radiation Chemistry, John Wiley & Sons, New York, 1976.

with electrons, in a similar manner to alpha particles. However, because the beta particle and the electron with which it collides have the same mass, the beta particle can lose up to half of its energy in a single collision and may be deflected through a large angle. As a result, even beta particles that start with the same energy may come to rest at widely separated points.

Gamma rays are electromagnetic radiation with wavelengths in the region of $3\text{E}-9$ to $3\text{E}-11$ cm. The gamma rays emitted by radionuclides are monoenergetic, but each decay may be to one of a small number of discrete energies. Low-energy gamma rays tend to lose most of their energy through a single interaction with an electron (the photoelectric effect). The entire energy is transferred to a single electron, which is then ejected from the atom. Photoelectric interactions are most probable for high-atomic-number materials and for low gamma energies. A fraction of the incident gamma rays is completely absorbed by the material, but the remainder are transmitted through the material with up to their full initial energy. For example, the number of low-energy-gamma photons transmitted through a sheet of absorbing material decreases exponentially as the thickness of the absorber increases.

For low-atomic-number materials and for gamma energies between 1 and 5 MeV in high-atomic-number materials, the Compton effect predominates. In the Compton effect, a gamma ray interacts with an electron, which may be loosely bound or free, so that the electron is accelerated and the gamma ray deflected with reduced energy. For example, Compton interactions in water predominate for gamma rays with energy from about 30 keV to 20 MeV.

Neutrons are uncharged nuclear particles with a mass of one mass unit (Spinks 1976³). Because they are uncharged, neutrons do not produce ionization directly in matter. However, the products of neutron interactions can produce ionization and give rise to radiation-induced chemical changes. The main ionizing species are protons or heavier positive ions, and the chemical effects of neutron irradiation are similar to those produced by beams of these positively charged particles.

3.1.2.2 Energy Transfer

Sometimes energy absorbed at one location on a large molecule appears to damage a more susceptible site elsewhere on the molecule. Thus, one type of bond may be broken more frequently than would be calculated from the statistical distribution of electrons.⁴ Another way of looking at this phenomenon is to compare the likelihood of a recombination reaction when a given kind of bond is broken. For example, by comparing the C-C and C-H bond energies in hydrocarbon polymers, one would think that cleavage of the main polymer chain is more probable than the splitting off of the hydrogen atoms. However, during irradiation of most polymers, processes caused by the cleavage of the C-H bonds predominate. A model used to explain this apparent contradiction is that simultaneous cleavages of the C-C and C-H bonds occur. In the case of polymers that primarily crosslink, a considerable fraction of the broken C-C

⁴ O'Donnell 1970. J. H. O'Donnell and D. F. Sangster, Principles of Radiation Chemistry, American Elsevier Publishing Company, Inc., New York, 1970.

bonds recombine, and as a result, the C-H bond cleavage processes predominate. In degradable polymers, a rapid recombination of the split ends of the chain is sterically hindered⁵.

The concept of energy transfer from the location on a molecule where energy is absorbed to the chemical bond that is broken is a key concept for understanding the effects of radiolysis. The major products of radiolysis are influenced by molecular structure⁶. Chemical bonds are not broken randomly even though the excitation energy may exceed the bond dissociation energy.

For this reason, radiolysis can be discussed in terms of functional groups as can other chemical reactions. The functional group is the atom or group of atoms that defines the structure of a particular family of organic compounds, and, at the same time, determines their properties⁷. A particular set of properties can be associated with a particular group wherever it is found. Functional groups in macromolecules also determine their chemical reactions. Sections 3.1.3 and 3.1.4 contain more detailed discussions of the functional groups.

Certain structures, such as aromatic rings (e.g., a benzene ring), seem to absorb ionizing energy and dissipate it as heat in the form of molecular vibrations. In this way, systems containing these structures undergo less decomposition than would be expected.⁴

When a homogeneous mixture of two compounds is irradiated, the yields of the different products often are generally directly proportional to the yields from the pure components and their relative proportions (by electron density) in the mixture. This behavior is found when each component degrades independently of another. However, some components of a mixture may transfer absorbed energy to other components. In a two-component mixture, the second component may be decomposed more readily, and the result is a higher product yield. On the other hand, if the second component is less readily decomposed, as with an aromatic compound, there may be correspondingly less decomposition and a lower product yield.⁴

During gamma irradiation of polymers filled with finely dispersed metals, the absorbed energy can distribute itself nonuniformly between the two components of the system. In rubbers containing heavy metals ($Z \geq 40$) in a free state or in the form of chemical compounds, the rate of radiation cross-linking has been observed to double. The energy absorbed by the polymeric component increases because of secondary electrons generated by gamma interactions with the metal.⁵ This effect is not expected to be significant for surface alpha irradiation of leaded rubber gloves because the lead is dispersed throughout the rubber material.

⁵ Makhlis 1975. F. A. Makhlis, Radiation Physics and Chemistry of Polymers, John Wiley & Sons, New York, 1975, translated from the Russian.

⁶ Hall 1963. K. L. Hall, et al., "Radiation Chemistry of Pure Compounds," in Radiation Effects on Organic Materials, Academic Press, New York, 1963, eds. R. O. Bolt and J. G. Carroll.

⁷ Morrison 1973. R. T. Morrison and R. N. Boyd, Organic Chemistry, Allyn and Bacon, Inc., Boston, 1973, 3rd edition.

3.1.2.3 Factors Affecting the Rate of Radiolytic Gas Generation (or Consumption) from a Material

The rate of radiolytic gas generation (or consumption) from a material depends on: (1) the G value for gas production (or consumption) for the given material and type of radiation, (2) the energy emitted from radioactive decay, and (3) the fraction of emitted energy absorbed by the material (F). G values also appear in the radiation chemistry literature for other products, such as the number of crosslinks or scissions, or the production of a non-gas substance. A G value may be positive (as in the generation of hydrogen or carbon dioxide) or negative (as in the depletion of oxygen). F depends on the nature of the emitted energy and the materials being irradiated. In the case of short-range radiation, F also will depend on the spatial distribution of radioactivity, especially when several different materials are present, such as in wastes.

The rate of radiolytic gas generation (n) in moles per second from a material is given by:

$$n = W \times \sum_i (F_i \times G_i) \times C$$

where

W = total decay heat (watts),

F_i = fraction of energy emitted that is of radiation type i and is absorbed by the material (range 0 to 1),

G_i = number of molecules of gas produced (or consumed) per 100 eV of energy absorbed from radiation type i, and

C = conversion constant

$$= (1 \text{ joule/W-sec}) \times (1\text{E}7 \text{ erg/joule}) \times (1 \text{ eV}/1.6\text{E-}12 \text{ erg}) \\ \times (1 \text{ g-mole}/6.02\text{E}23 \text{ molecules})$$

$$= 1.04\text{E-}5 \text{ (g-mole)(eV)/(molecule)(W-s)}$$

$$= 1.04\text{E-}7 \text{ (g-mole)(100 eV)/(molecule)(W-s)}$$

3.1.2.3.1 Factors Affecting the G Value

A number of factors influence the G value measured in an experiment. They include LET of the radiation, temperature, pressure, atmosphere in which irradiation occurs, total absorbed dose, and specific composition of the material.

3.1.2.3.1.1 Linear Energy Transfer (LET) Effect

Differences in G values for a material when irradiated by different types of radiation are ascribed to differences in the ways in which energy is lost in matter. Linear energy transfer (LET) is the linear rate of energy loss by an ionizing particle traveling through a material. An average LET

value is calculated by dividing the initial energy of a particle by its range in the material. Expressions that reflect the changing density of active species in particle tracks, such as specific ionization and LET, are useful in evaluating the overall chemical effect. Track effects of this sort have been thought to be more important in the case of liquids or solids, where the active species are hindered from moving apart by the proximity of other molecules, than in gases, where species can move apart with relative ease. In gases, the different types of radiation do not give the different yields of products that may be found in liquids or solids.

The linear energy transfer from alpha particles to irradiated materials follows the Bragg curve, which rises sharply from low energies to reach a peak at about 1 MeV, then falls off gradually at higher alpha particle energies. This behavior leads to an "end of track" effect, with higher LET than at the beginning of the track.⁸ Table 3.1-1 lists average LET values for irradiation of water.

Radiation-chemistry studies on LET effects in low-molecular-weight compounds have shown that the molecular product yields increase with increasing LET. Molecular products are generated in the spurs, before the reactive species can diffuse into the bulk of the system.⁹ The result is that $G(H_2)$ appears to increase with increasing LET, at least in liquids such as benzene, acetone, cyclohexane, and water (see Section 3.1.3 for details). These effects could also occur in solids. Unfortunately, similar experiments have not been uncovered in the radiation chemistry literature that measure G values of a solid material using different LET radiation at the same absorbed dose.

A characteristic feature of radiation with high LET is the sharp decrease in the effectiveness of protective additives (such as antioxidants) in the material being irradiated, particularly those that react with free radicals. The reason for this is the intense reactions of the radicals in the track.⁵

Table 3.1-1 — Average Values of LET in Water Irradiated with Various Types of Radiation

Radiation	Average LET (eV/nm)
Co-60 γ -rays	0.2
2-MeV electrons	0.2
200-kV x-rays	1.7
H-3 β -rays	4.7
50-kV x-rays	6.3
10 MeV H-1	8.3
10 MeV He-4	92
5.3 MeV α -particles (Po-210)	136
3 MeV He-4	180
65.7-MeV N-14 ions	553

Refs.: Spinks 1976³, Chapter 2 and Table 8.19.

⁸ Cember 1978. H. Cember, Introduction to Health Physics, Pergamon Press, New York, 1978.

⁹ Schnabel 1981. W. Schnabel, Polymer Degradation--Principles and Practical Applications, Macmillan Publishing Company, Inc., New York, 1981.

3.1.2.3.1.2 Temperature

Chemical reaction rates depend on temperature. The rate (k) of a chemical reaction can be expressed by: $k = A \exp(-B/T)$ where T is the absolute temperature, and A and B are constants. The equation can be written in the form $k = A \exp(-E_a/RT)$, generally known as the Arrhenius law. E_a is an activation energy, which will have different values for different chemical reactions. This law holds for elementary reactions but does not necessarily hold for successive reactions that may have different E_{as} .³ Also, the E_a can change when the reactions change, as at the melting point for crystalline materials.

In an Arrhenius plot, the log of the reaction rate versus the reciprocal temperature (degrees Kelvin), $\ln k$ vs. $1/T$, has a slope equal to $-E_a/R$. Arrhenius plots of G values versus $1/T$ for several materials are shown in Chapiro 1962¹⁰ and Jellinek 1978¹¹.

The activation energy (E_a) for G values for gas generation from most materials appears to be less than or equal to 3 kcal/g-mole, giving a weak temperature dependence compared to many other chemical reactions. E_a for PVC is about 3 kcal/g-mole, and E_a for polyethylene is about 0.8 kcal/g-mole (see Section 3.1.3.1.4). Alpha radiolysis data for cellulose are consistent with an E_a of 1-2 kcal/g-mole^{12,13} (see Section 3.1.3.1.4). The temperature dependence of $G(H_2)$ in liquid n-hexane and neopentane corresponds to an activation energy of about 3 kcal/g-mole.¹⁴

The relationship between the rate constants k_2 and k_1 at two different temperatures T_2 and T_1 is given by:

$$\ln(k_2/k_1) = (E_a/R)[(T_2-T_1)/(T_2 \times T_1)]$$

where R = ideal gas constant (1.99 cal/g-mole-K) and temperatures are in degrees Kelvin. For example, if the activation energy for gas produced by a material is equal to 1 kcal/g-mole, then the ratio of the $G(\text{gas})$ value at 55°C to the $G(\text{gas})$ value at 25°C would be:

$$\begin{aligned} G(55^\circ\text{C})/G(25^\circ\text{C}) &= \exp \{(1E3/1.99)[(328\text{ K} - 298\text{ K})/(328\text{ K} \times 298\text{ K})]\} \\ &= \exp \{(5.03E2)[30/(328)(298)]\} \end{aligned}$$

¹⁰ Chapiro 1962. A. Chapiro, Radiation Chemistry of Polymeric Systems, Interscience Publishers, New York, 1962.

¹¹ Jellinek 1978. H. H. G. Jellinek, Aspects of Degradation and Stabilization of Polymers, Elsevier Scientific Publishing Company, New York, 1978.

¹² Kosiewicz 1981. S. T. Kosiewicz, "Gas Generation from Organic Transuranic Wastes. I. Alpha Radiolysis at Atmospheric Pressure," Nuclear Technology 54, pp. 92-99, 1981.

¹³ Zerwekh 1979. A. Zerwekh, "Gas Generation from Radiolytic Attack of TRU-Contaminated Hydrogenous Waste," Los Alamos National Laboratory, LA-7674-MS, June 1979.

¹⁴ Bolt 1963. R. O. Bolt and J. G. Carroll, Radiation Effects on Organic Materials, Academic Press, New York, 1963.

$$= \exp(0.154)$$

$$= 1.17.$$

At -29 °C, the ratio $G(-29\text{ °C})/G(25\text{ °C})$ would be 0.69 for $E_a = 1$ kcal/g-mole. An activation energy of $E_a = 3$ kcal/g-mole, considered as the maximum value of E_a for materials present in the CH-TRU wastes, results in the following:

$$G(55\text{ °C})/G(25\text{ °C}) = \exp(3 \times 0.154) = \exp(0.462)$$

$$= 1.59.$$

For most polymers then, the radiolytic gas generation rate at 55°C should be no greater than approximately 1.6 times the gas generation rate at room temperature (25°C).

Rates and product yields from radiation-induced chemical reactions in many polymers are influenced by molecular mobility.^{9, 15} This explains why increases in temperature, leading to phase transitions or allowing specific intramolecular motions (such as rotations of side groups), frequently influence the G values. Increasing the temperature generally reduces the probability of radical recombinations⁹ and increases the diffusion rates of gas molecules, such as H_2 .

For polymers containing crystalline areas, the molecular mobility increases drastically above the crystalline melting temperature, with consequent changes radiation chemical yields.¹¹ For example, an abrupt increase in the activation energy occurs for both $G(X)$ (crosslinking between polymer molecules) and $G(S)$ (scission - breaking of the polymer molecule backbone) near the melting temperature. Large changes in the ratio $G(X)/G(S)$ are often observed at higher temperatures, which suggests changes in reaction mechanisms. For example, a ten-fold increase in $G(S)$ is observed in radiolysis of polystyrene when the temperature is increased from 30 to 150°C.¹⁵

There is no general correlation between thermal stability and radiation resistance. For instance, irradiated polytetrafluoroethylene (Teflon^R) readily undergoes main-chain scission while polysiloxanes are efficiently crosslinked, although both polymers are heat resistant.⁹ At elevated temperatures, radiation may accelerate the usual thermal degradation reactions because thermal initiation characterized by a high activation energy (about 20 to 80 kcal/g-mole¹⁶) is replaced by radiation initiation, which has a much lower activation energy.⁵ The threshold temperature for thermal degradation can be decreased significantly if the material is irradiated before (or during) heating.

¹⁵ Jellinek 1983. H. H. G. Jellinek, ed., Degradation and Stabilization of Polymers, Vol. 1, Elsevier, New York, 1983.

¹⁶ Madorsky 1964. S. L. Madorsky, Thermal Degradation of Organic Polymers, Interscience Publishers, John Wiley & Sons, New York, 1964.

3.1.2.3.1.3 Pressure

Pressure up to 50 psig may slightly lower G values as a result of back reactions. Experiments conducted in a vacuum measure more of the gas generated than do experiments conducted at ambient pressure, in which some of the gases can remain dissolved in the material being irradiated.

The decrease in segmental motions in polybutadiene with increasing pressure led to a corresponding decrease in G values for chain scission in polybutadiene¹⁷ and an increase in G values for crosslinking.

3.1.2.3.1.4 Atmosphere in Which Irradiation Occurs

Measured total gas G values depend on the atmosphere in which the irradiation occurs, especially whether or not any oxygen is present. In most polymers, oxygen retards or completely eliminates formation of a cross-linked network. Even polymers that otherwise would crosslink will degrade in the presence of oxygen.⁵ Radiation-induced oxidation initially consumes dissolved oxygen that has diffused into the material from the surrounding oxygen-containing atmosphere.⁵ The efficiency of radiolytic oxidation of polymers under otherwise equal conditions depends on the dose rate and on other factors determining the rate at which oxygen can permeate the sample (e.g., oxygen pressure, sample thickness, oxygen solubility and ability to penetrate through the material, irradiation temperature, and polymer phase state).⁵

Organic solvents can change the net effect of radiolysis by permeating the material and reacting chemically. Reactions of trapped radicals may occur with chemically active molecules (such as oxygen or solvents) that have diffused into the sample after irradiation ceases.⁵ These effects are most pronounced in materials that have been irradiated in the absence of oxygen. Intense degradation of polymers that have been pre-irradiated in the absence of oxygen has been observed when the polymers are exposed to oxygen.⁵

Most G values are measured in a vacuum, in air, or in pure oxygen. In the vacuum experiments, a larger amount of evolved gas may be measured because gas molecules will be pulled out of the materials rather than remain dissolved in the materials. A few experiments have been conducted in atmospheres different from air or pure oxygen, such as oxygen plus carbon tetrachloride, chloroform vapor, or nitrous oxide; or air saturated with water vapor. (The results of these experiments are discussed in later chapters.)

Various thermal, chemical, and radiolytic oxidation processes occurring in the CH-TRU waste materials, the packaging materials, and the waste containers themselves will react with the oxygen initially present inside the innermost waste bags. Eventually, these processes could deplete the oxygen inside the transport package cavity.

The gases that could be present inside the transport package include the following: (1) air; (2) nitrogen, argon, or helium used to inert the cavity; (3) nitrogen plus hydrogen and carbon

¹⁷ Sasuga 1975. T. Sasuga and M. Takehisa, "Effect of High Pressure on Radiation-Induced Cross-Linking of Synthetic Rubbers," *J. Macromol. Sci.-Phys. B11*, pp. 389-401, 1975.

dioxide, with trace amounts of carbon monoxide, oxygen, and methane; (4) any of the above plus vapor from absorbed water or other liquids. These liquids may include various oils and solvents. For example, some of the solvents that could be present in the wastes include: 1,1,1-trichloroethane, carbon tetrachloride, 1,1,2-trichloro-1,2,2 trifluoroethane (Freon), methylene chloride, methanol, xylene, and butanol.

3.1.2.3.1.5 Total Absorbed Dose

As irradiation of a material proceeds, the end products of radiolysis (called primary products) may increase to such a concentration in the material that they are irradiated or react with some of the free radicals or other species to form secondary products. It follows that the G value (slope of the yield of a product versus dose curve) may decrease as the absorbed dose increases (assuming that the products are more stable under irradiation than the parent material), and the concentration of the product may ultimately reach a steady-state limit.⁴ Many of the common plastics contain saturated carbon-carbon bonds. Radiolysis of these materials results in release of hydrogen and an increase in unsaturation. Unsaturated hydrocarbon liquids have much lower $G(H_2)$ values than do related saturated hydrocarbon liquids. Therefore, the degraded material in the plastics should be more stable than the parent material with respect to gas formation, leading to lower $G(H_2)$ values with absorbed dose. Eventually, all of the available hydrogen will have been released from the material. The decrease in G values with absorbed dose has also been called a "matrix-depletion" effect. To avoid this complication, G values are often expressed as initial G values or as the G values extrapolated to zero absorbed dose.

On the other hand, radiolysis of plastics where additives are used to achieve stability, such as PVC, could result in higher G values with increasing absorbed dose as the additives are consumed.

Absorbed dose effects can disappear at higher temperatures. For example, for irradiation of crystalline polyethylene at 25°C, the value of $G(H_2)$ decreased from about 3.7 to 3.2 as the absorbed dose increased from near zero to 15 Mrad (0.15 MGy).¹⁸ For the same sample, irradiated at 120°C, virtually no change in $G(H_2)$ with increasing radiation dose was reported.

Several reports discuss absorbed dose effects for alpha radiolysis. For Cm-244 irradiation of paper tissue, Bibler observed a decrease in $G(\text{gas})$ from an initial value of 1.9 to about 0.8 after 17 days.¹⁹ Zerwekh's data show decreases in $G(\text{gas})$ values by about 50% in 250 days of irradiation from Pu-238.¹³

For alpha irradiation, the absorbed dose for waste materials is applicable only to the mass of the waste reached by the alpha particles. The range of alpha particles in low density materials for $4 < E < 8$ MeV is given by (see Section 3.1.2.3.2.1):

¹⁸ Mandelkern 1972. L. Mandelkern, "Radiation Chemistry of Linear Polyethylene," in The Radiation Chemistry of Macromolecules, Vol. I, Academic Press, New York, 1972, ed. M. Dole.

¹⁹ Bibler 1976. N. E. Bibler, "Radiolytic Gas Production During Long-Term Storage of Nuclear Wastes," E. I. DuPont de Nemours and Company, Savannah River Laboratory, DP-MS-76-51, American Chemical Society Meeting (preprint), October 27-29, 1976.

$$\text{Range(cm)} = [1.24 \times E(\text{MeV}) - 2.62] \times [1.2\text{E-}3 \text{ g/cm}^3 / (\text{density of material})].$$

The density of plastics and paper is approximately 1 g/cm³. The range of a 5.14 MeV alpha particle (Pu-239 alpha) in plastics or paper would be 4.6E-3 cm, while the range of 5.59 MeV alpha particle (Pu-238 alpha) would be 5.2E-3 cm.

The alpha particle track is cylindrical, with 90% of the ions present within a diameter of 1E-2 microns. The remaining 10% are recoil electrons with sufficient energy to produce their own ionization(s). Such ions are present out to about 0.2 microns from the center of the track.²⁰

The volume of material most affected by an alpha particle can, therefore, be approximated by a cylinder of diameter 0.01E⁻⁴ cm and length equal to the range of the alpha particle. For 5.59-MeV alpha particles, the estimated volume of irradiated material is 4.1E-15 cm³. For 5.14-MeV alpha particles, the estimated volume of irradiated material is 3.6E-15 cm³. The corresponding dose absorbed by that material from one alpha particle is given by:

$$\text{Dose (rad)} = \frac{\text{Decay energy (eV)} \times 1 \text{ rad} / [6.24\text{E}13 \text{ eV/g}]}{\text{Volume (cm}^3) \times \text{density (g/cm}^3)}$$

Therefore, the dose absorbed by material irradiated by a Pu-238 or Pu-239 alpha particle is 22-23 Mrad. With time, the particle tracks will begin to overlap, and the dose absorbed by the material will increase. For a given particle size of PuO₂, for example, absorbed dose effects should be observed much more quickly during Pu-238 irradiation, which produces a factor of about 200 times the disintegrations per second of Pu-239 irradiation.

Several conclusions may be reached from this discussion:

- (1) The gas-generation rates from materials irradiated to absorbed doses much less than 22 Mrad are expected to be greater than expected for alpha radiolysis of these materials in CH-TRU wastes.
- (2) A particle of Pu-238 oxide will have an activity over 200 times the activity of the same size Pu-239 oxide particle. Absorbed dose effects should occur much sooner with Pu-238 contamination than with Pu-239 contamination.
- (3) G values measured using Pu-238 contamination should be extrapolated to initial G values before the results are applied to Pu-239 contamination to minimize the difference in absorbed dose effects.

²⁰ NAS 1976. National Academy of Sciences, "Health Effects of Alpha-Emitting Particles in the Respiratory Tract," EPA 520/4-76-013, October 1976.

3.1.2.3.1.6 Dose Rate

Some radicals are fairly stable and may build up to quite high concentrations. Under these conditions they may react with other radicals, rather than with the material being irradiated. If this occurs, the G values may exhibit a nonlinear dependence on the dose rate. For example, a radiation-initiated chain reaction can result in a G value for products that is inversely proportional to the square root of the dose rate.⁴ In a number of experiments, however, the G values for molecular gas products for specific materials were independent of dose rate for the ranges studied [e.g., Bibler 1976¹⁹, Chapiro 1962¹⁰ (p. 415)].

Some apparent dose rate effects are caused by an increase in the material's temperature. Since the major portion of the absorbed radiation energy is converted to heat, at high dose rates the rate of heat release to the environment can be insufficient, resulting in an increase in temperature. Many chemical reactions have activation energies in the range of 20-50 kcal/mole. Consequently, it is feasible that at high absorbed dose rates (i.e., at high localized material temperatures), reaction pathways different from those occurring at low dose rates may dominate.⁹

Gillen and co-workers have documented evidence of physical and chemical dose-rate effects in gamma radiolysis of polymers in oxygen-containing environments as part of their efforts to perform accelerated aging simulations. Much of this work is summarized in Bonzon (1986)²¹.

Physical dose-rate effects appear to be a common occurrence for gamma radiation aging of polymeric materials. Evidence for dose-rate effects was observed for polyolefins and ethylene-propylene rubber, while no noticeable dose-rate effects were noted for a chloroprene rubber, silicone, and two chlorosulfonated polyethylene materials. The dose-rate effects ranged from insignificant to very large, depending on such factors as polymer type, aging conditions, sample geometry, and the degradation parameter being monitored. (Change in tensile elongation was commonly used in these studies to detect radiation damage.) More mechanical degradation was produced for a given total dose as the dose rate was lowered. Diffusion-limited oxidation processes were shown to be the cause of such effects. When the oxidation processes in a material use up dissolved oxygen faster than it can be replenished from the atmosphere surrounding the material (through diffusion), a heavily oxidized layer of material is formed near the sample surfaces, and oxygen depletion occurs in the sample interior. As the dose rate is reduced, oxidation of the sample increases due to the longer times available for the diffusion processes.

Oxidation-controlled dose-rate effects are less likely to occur for alpha irradiation of polymers from surface contamination. In order for the reactions to be dose-rate independent, oxygen must diffuse only to a depth equal to the range of the alpha particles. Physical dose-rate effects are minimized in gamma irradiation experiments by using thin films.²¹

²¹ Bonzon 1986. L. L. Bonzon, et al., "Status Report on Equipment Qualification Issues -- Research and Resolution," Sandia National Laboratories, NUREG/CR-4301, SAND85-1309, November 1986.

Other chemical dose-rate effects were observed in the interactions between radiation and thermal degradation. Deterioration in polyethylene and polyvinyl chloride cable materials was found in the containment building of the Savannah River nuclear reactor.²² The degradation in material properties was much higher than expected for the maximum dose [2 Mrad (0.02 MGy)] experienced by the cable materials at the relatively low operating temperature of 43°C. Experiments performed to model this behavior showed that the most severe mechanical degradation was found when irradiation occurred at elevated temperature. The observed degradation was much greater than the sum of the damage caused by separate exposure to radiation and to the elevated temperature. This effect was also attributed to an oxidation mechanism, in which peroxides initially formed by the radiation are then thermally decomposed.

Chemical dose-rate effects caused by synergistic behavior of radiation and elevated temperature would also occur for alpha irradiation when oxygen is present. The magnitude of these effects could be reduced by removing any remaining oxygen before the irradiated materials are heated.

3.1.2.3.1.7 Specific Material Composition

Many of the radiolysis experiments reported in the radiation chemistry literature were performed to examine the chemical reactions occurring in the pure material. However, commercial plastics differ from the pure polymers because they contain large fractions of various additives, such as stabilizers and plasticizers. These materials can significantly influence the amount and species of gases generated by thermal degradation and radiolysis. See Attachment A of this appendix and Section 3.1.4 for more detailed discussions.

3.1.2.3.1.8 Extreme Upper Bound Estimate for Gas Generation G Values in Most Organic Liquids and Polymers

For most materials, bond dissociation energies can be used to estimate an extreme upper bound to the number of gas molecules produced by radiolysis per unit energy absorbed. Dissociation energies of chemical bonds in common polymers range from about 65 kcal/g-mol (C-Cl) to 108 kcal/g-mol (C-F), with carbon-carbon bonds in the middle of the range (75-85 kcal/g-mol)³. The carbon-hydrogen bond dissociation energy is about 90-100 kcal/g-mole (3.9-4.4 eV/molecule).

Hydrogen is the major gaseous product from radiolysis of most organic liquids and polymers that contain hydrogen. In the simplest case, a hydrogen molecule conceptually could be formed by breaking two C-H bonds and recombining the two hydrogen atoms. If all the radiation energy went into breaking bonds, then the energy needed to form one hydrogen molecule is given by twice the bond dissociation energy, or $2 \times (3.9-4.4 \text{ eV})/\text{molecule}$. This required energy results in an extreme upper bound G value estimated to be about 12 molecules generated per 100 eV of energy absorbed. This is an extreme upper bound because it ignores the H atoms that recombine with the parent molecule and the energy that is dissipated as heat.

²² Gillen 1982. K. T. Gillen, R. L. Clough, and L. H. Jones, "Investigation of Cable Deterioration in the Containment Building of the Savannah River Nuclear Reactor," NUREG CR-2877, SAND81-2613, August 1982.

Most measured G values lie between 0.1 and 10.⁴ Higher G values usually indicate a chain reaction has occurred. For example, the radiolysis products may chemically degrade the parent material, as occurs from HCl generated in pure PVC.

3.1.2.3.2 Factors Affecting the Fraction of Energy Absorbed by a Material

Factors affecting the fraction of energy absorbed by a material include the range of effectiveness of the radiation in the material, distribution of radioactive contaminants, and (in the case of alpha radiolysis) particle size of the radioactive contaminant (such as PuO₂ particles).

3.1.2.3.2.1 Range of Effectiveness of the Radiation

The range of alpha particles in gases, liquids, and solids must be considered both when comparing alpha with gamma radiolysis experiments on specific materials, and when evaluating the gas generation rates expected from actual waste drums. For example, the range of alpha particles in air at 0°C and 760 mm Hg pressure is approximated by Cember (1978)⁸:

$$\text{Range(cm)} = [1.24 \times E(\text{MeV})] - 2.62, \text{ for } 4 < E < 8 \text{ MeV.}$$

For 5.5 MeV alpha particles, the range in air would be 4.2 cm. The presence of water vapor or other vapors would decrease that distance. The range of alpha particles in biological tissue, or other materials of low density, is given by Cember (1978)⁸:

$$\begin{aligned} \text{Range} &= \text{Range}(\text{air}) \times (\text{density of air})/(\text{density of material}) \\ &= 4 \text{ cm} \times (1.2\text{E-}3 \text{ g/cm}^3)/(\text{density of material}). \end{aligned}$$

Plastics and cellulose (or liquid water) have densities of about 1 g/cm³. Therefore the range of alpha particles in typical combustible wastes or absorbed aqueous solutions is estimated to be about 5E-3 cm [(5E-3 cm x 1E4 microns/cm = 50 microns; 5E-3 cm/(2.54 cm/in) x 1E3 mils/in = 2 mils)].

Several conclusions that can be reached from the above calculations are:

- (1) For low-density materials less than about 2 mils thick, both alpha particles and gamma rays can penetrate completely through the material.
- (2) Materials more than about 4 cm away from all alpha-emitting radionuclides should not experience any alpha radiolysis.
- (3) Radiolysis of gases or vapors within 4 cm of alpha-emitting radionuclides will occur unless the alpha particles are first absorbed by other materials.

3.1.2.3.2.2 Distribution of Radioactive Contaminants

The distribution of radioactive contaminants can affect the rate of gas generation. This is especially important when the materials being irradiated are heterogeneous. For example, consider a drum containing mixed combustible and dry metal waste, where the thick metal pieces

are individually wrapped with plastic, and the activity all results from alpha decay. Several possible distributions of the alpha activity include the following:

- (1) All the activity is located in the interior of the metal pieces.
- (2) All of the activity is located on the exterior of the metal pieces, in contact with both the plastic wrapping and the metal pieces.
- (3) All of the activity is uniformly distributed in the mixed combustible waste.

The rate of gas production will be different for each of the three cases. In Case 1, no radiolytic gas will be generated. In Case 2, gas could be generated at a rate up to one-half the rate characteristic of plastic (no radiolytic gas is generated by metal). In Case 3, gas will be generated at a rate equal to the weighted average G value for the mixed combustibles. An upper-bound estimate of the quantity of radiolytic gas generated from a mixture of materials can be calculated by assuming that all of the emitted alpha energy is absorbed by the material having the highest G value.

If a plutonium dioxide particle is located on a surface, up to half the alpha particles may interact with gases or vapors above the contaminated surface, unless another surface is in contact with the first. The quantity of gas generated may be greater than calculated based only on the surface-contaminated material if a significant fraction of the atmosphere above the surface consists of organic vapors.

3.1.2.3.2.3 Particle Size of the Contaminant

The plutonium contaminants in CH-TRU wastes are usually in particle form as PuO₂ or hydroxides but may also be in the form of plutonium nitrate from solution in nitric acid. If the plutonium is in particle form, some of the alpha particles will interact with plutonium or oxygen atoms (in the process known as self-absorption), rather than with the waste material. Attachment B of this document presents a calculation of the fraction of alpha decay energy escaping from a particle of PuO₂ as a function of the PuO₂ particle radius.

The gas generation rate reported from particulate contamination could then be less than the rate predicted using maximum G values and all of the activity measured in the waste using segmented gamma scan, passive/active neutron interrogation, or other assay methods. For example, the G(H₂) value for Pu-238 dissolved in nitric acid was observed to be about 2.5 times the G(H₂) value for 2-micron particles of the oxide.²³ (These particles had probably agglomerated to larger particles.)

²³ Bibler 1979. N. E. Bibler, "Gas Production from Alpha Radiolysis of Concrete Containing TRU Incinerator Ash, Progress Report 2, August 1, 1978 - November 30, 1978," E. I. DuPont de Nemours and Company, Savannah River Laboratory, DPST-78-150-2, April 1979.

3.1.2.3.3 Use of G Values Measured by Non-Alpha Irradiation

Alpha radiolysis predominates in the CH-TRU wastes. However, many radiolysis experiments have been performed using gamma (or other) radiation. Some differences are found in the gases produced in alpha radiolysis versus gamma radiolysis, but the results in most cases are very similar, as shown in Sections 3.1.3, 3.1.4, and 3.1.5. The quantities and compositions of the evolved gases should be comparable when:

- (1) The total absorbed dose for the gamma radiolysis experiment is similar to the total absorbed dose for the alpha radiolysis experiment.
- (2) The dose rate for the gamma radiolysis experiment is similar to the dose rate for the alpha radiolysis experiment.
- (3) For materials that are surface contaminated in an alpha radiolysis experiment, the gamma radiolysis experiment is performed on powders or thin films, to minimize diffusion effects in bulk materials.

3.1.3 Radiolysis of Liquids, Vapors, and Gases

G values for liquids are applicable to the following three waste forms: liquids absorbed onto various waste materials, liquids incorporated into a matrix such as concrete, and liquids used as plasticizers in plastics and rubbers. Radiolysis of vapors near contaminated surfaces may occur. The organic liquids are grouped into families based on their functional groups.⁷ The functional group is the atom or group of atoms that defines the structure of a particular family of organic compounds, and, at the same time, determines their properties. For example, the functional group in alcohols is the -OH group, while in alkenes the functional group is the carbon-carbon double bond. A large part of organic chemistry is the chemistry of the various functional groups. A particular set of properties can be associated with a particular group wherever it is found. When a molecule contains a number of different functional groups, the properties of the molecule are expected to be roughly a composite of the properties of the various functional groups. (The properties of a particular group may be modified by the presence of another group, however.) Functional groups in macromolecules also determine their chemical reactions.

The major products of radiolysis are also influenced by molecular structure.⁶ Chemical bonds are not broken randomly even though the excitation energy may exceed the bond dissociation energy. For solid materials for which the G values are unknown, structurally related organic liquids can provide estimates of maximum G values.

The radiolysis data are organized by families of liquids, which are based on functional groups (see Attachment A of this document for more details). Where data are available, G values at different LETs are shown.

Liquids that have G values for flammable gas greater than 4.1 are: saturated hydrocarbons, alcohols, ethers, ketones, and organic acids. Liquids that have G values for flammable gases less than 4.1 include unsaturated hydrocarbons, aromatic hydrocarbons, water, esters, halogenated hydrocarbons, aromatic halides, and commercial lubricant oils. G values for flammable gases for

organic nitrogen compounds are low for those having aromatic characteristics or C-N triple bonds.

3.1.3.1 Radiolysis of Saturated Hydrocarbons

Saturated hydrocarbons contain only hydrogen and carbon atoms and single carbon-carbon bonds. They include most of the common petroleum fuels. An example of a saturated hydrocarbon is hexane, with the following structure:

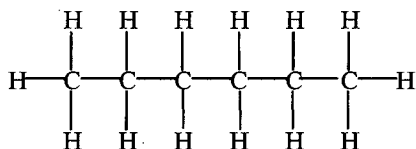


Table 3.1-2 presents G values for saturated hydrocarbons for irradiation at room temperature in vacuum. G(gas) is the G value for all gas produced.

From Table 3.1-2, the bounding G(H₂) value is 5.6 for saturated hydrocarbons in the liquid phase at room temperature. In addition to hydrogen, other flammable gases may be generated. Newton²⁴ has observed some general characteristics of gas generation from saturated hydrocarbons. Normal saturated hydrocarbons yield principally hydrogen, with methane being produced only from the end groups. Therefore, the ratio of hydrogen to methane increases with increasing molecular weight. With branched-chain hydrocarbons (such as isobutane or neopentane), relatively more methane is produced, and the yield of methane increases with the number of methyl groups on the hydrocarbon chain.

Hall⁶ reports an activation energy of about 3 kcal/mole for the G(H₂) value for the liquid phase of neopentane and n-hexane. (See Section 3.1.3.4.1.1 for the use of activation energies in calculating the temperature dependence of G values.)

Table 3.1-2 — G Values for Saturated Hydrocarbons

Material	G(H ₂)	G(CH ₄)	G(gas) ^a	Comments	Reference
<u>Vapor phase</u>					
propane	8.2	0.4		alpha; vacuum	(1)
butane	9.0	1.2		alpha; vacuum	(1)
pentane	7.3	0.8		alpha; vacuum	(1)
hexane	5.6	0.8		alpha; vacuum	(1)
isobutane	7.4	2.7		alpha; vacuum	(1)
neopentane	2.0	2.0		alpha; vacuum	(1)

²⁴ Newton 1963. A. S. Newton, "Chemical Effects of Ionizing Radiation," in Radiation Effects on Organic Materials, Academic Press, New York, 1963, eds. R. O. Bolt and J. G. Carroll.

Table 3.1-2 — G Values for Saturated Hydrocarbons (Concluded)

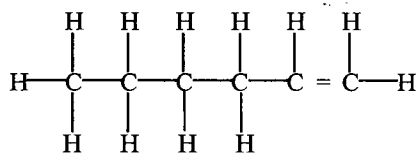
Material	G(H ₂)	G(CH ₄)	G(gas) ^a	Comments	Reference
<u>Liquid phase</u>					
pentane	4.2	0.4		electron; vacuum	(1)
	4.2	0.2	5.4	electron; vacuum	(2)
hexane	5.0	0.2	5.2	electron; vacuum	(1)
	5.0	0.1	7.2	electron; vacuum	(2)
cyclohexane	5.6	0.1	5.7	electron; vacuum	(1)
	5.3	0	5.3	alpha; vacuum	(1)
	7.7	--		fission fragments; vacuum	(3)
heptane	4.7	0.1		electron; vacuum	(1)
octane	4.8	0.1		electron; vacuum	(1)
	4.6	0.1		gamma; air	(4)
	4.2	--		alpha; air	(4)
nonane	5.0	0.1		electron; vacuum	(1)
decane	5.2	0.1		electron; vacuum	(1)
dodecane	4.9	0.1		electron; vacuum	(1)
hexadecane	4.8	0		electron; vacuum	(1)
2-methylpentane	4.0	0.5		electron; vacuum	(1)
2,2-dimethyl-butane	2.0	1.2		electron; vacuum	(1)
neopentane	1.6	3.7	5.6	gamma; vacuum	(2)

Refs.: (1) Spinks 1976³, p. 365; (2) Hall 1963⁶, p. 71; (3) Gaumann 1968²⁵; (4) Bibler 1977²⁶.

Note: ^aG(gas) includes miscellaneous gaseous hydrocarbons C₂-C₄.

3.1.3.2 Radiolysis of Unsaturated Hydrocarbons

Unsaturated hydrocarbons are hydrocarbons that have at least one double or triple carbon-carbon bond. Examples include acetylene, ethylene, 1-hexene, and cyclohexene. The compound 1-hexene has the following structure.



G(H₂) values for unsaturated hydrocarbons are generally much smaller than for saturated hydrocarbons, even when the only structural difference occurs in a small area of a long molecule (e.g., hexane compared to 1-hexene). Table 3.1-3 gives G values for three unsaturated hydrocarbons.

²⁵ Gauman, 1968.

²⁶ Bibler 1977. N. E. Bibler and E. G. Orebaugh, "Radiolytic Gas Production from Tritiated Waste Forms, Gamma and Alpha Radiolysis Studies," E. I. DuPont de Nemours and Company, Savannah River Laboratory, DP-1459, July 1977.

Radiolysis products of liquid cyclohexene and their G values are listed in Table 3.1-4 for both gamma and alpha (1.5 MeV) radiation.³

Table 3.1-3 — G Values for Three Unsaturated Hydrocarbons

Material	G(H ₂)	G(CH ₄)	G(gas) ^a	Comments	Reference
ethylene ^b	1.2	0.1	2.8	electron; vacuum	(1)
cyclohexene	1.3	0	1.3	gamma; vacuum	(2)
	3.0	0	3.0	alpha; vacuum	(2)
1-hexene	0.8	0	0.8	electron; vacuum	(1)

Refs.: (1) Hall 1963⁶, p.78; (2) Spinks 1976³, p. 384.

Notes: ^aG(gas) includes C₂H₂.

^bGas phase.

Table 3.1-4 — Radiolysis Products and G Values for Liquid Cyclohexene

Product	G (Product)	
	⁶⁰ Co γ-Ray	1.5 MeV α
H ₂	1.3	3.0
cyclohexane	1.0	0.3
2,2'-bicyclohexenyl (II)	1.8-1.9	0.4
3-cyclohexylcyclohexene (III)	0.5-0.6	0.5
bicyclohexyl (IV)	0.2	0.1
polymer, unidentified dimer (as C ₆ units)	8.9-9.8	6.1

Ref.: Spinks 1976³, Table 8.6.

3.1.3.3 Radiolysis of Aromatic Hydrocarbons

An aromatic hydrocarbon has a closed ring structure and resonance-stabilized unsaturation. The stability of aromatic compounds is attributed to the presence in the aromatic ring system of electrons in pi orbitals, which can dissipate energy throughout the ring system. This reduces the probability that excited or ionized aromatic molecules will dissociate. Alternative modes of energy dissipation are favored that do not result in dissociation of the molecule.³ Examples include benzene, xylene, and discrete-ring polyphenyls. All of the aromatic hydrocarbons have very low G values for hydrogen and total gas, as shown in Table 3.1-5.

Aromatic hydrocarbons are good protective agents for a large number of chemicals because they have many low-lying excited states, have low ionization potentials, and are themselves radiation resistant.²⁴ The transfer of energy from higher excited states or charge exchange with the ion of the primary compound results in dissipation of energy in the aromatic hydrocarbon. For example, cyclohexane is protected from radiolytic decomposition by small amounts of added benzene. Internal protective agents can be built into molecules by adding aromatic groups.

Table 3.1-5 — G Values for Several Aromatic Hydrocarbons

Material	G(H ₂)	G(CH ₄)	G(gas)	Comments	Reference
benzene	0.6	0	0.8	alpha; vacuum	(1)
	~0	~0	~0	gamma; vacuum	(1)
	~0	~0	~0	electron; vacuum	(3)
toluene	0.6	0	0.6	alpha; vacuum	(1)
	0.1	~0	0.1	gamma; vacuum	(1)
	0.1	~0	0.1	electron; vacuum	(2)
p-xylene	0.2	0	0.2	gamma; vacuum	(1)
ethyl benzene	0.2	~0	0.2	electron; vacuum	(2), (3)
	0.2	~0	0.2	gamma; vacuum	(1)
	0.2	~0	0.2	reactor; vacuum	(2)
isopropyl benzene	0.2	0.1	0.3	gamma; vacuum	(1)
	0.2	0.1	0.3	electron; vacuum	(2), (3)
	0.3	0.1	0.4	alpha; vacuum	(3)
	0.2	0.1	0.3	reactor; vacuum	(2)
tert-butyl benzene	0.1	0.1	0.2	electron; vacuum	(2), (3)
	0.2	~0	0.2	reactor; vacuum	(2)
mesitylene	0.2	~0	0.2	electron; vacuum	(3)
biphenyl	a	a	~0	electron; vacuum	(2)
	a	a	0.1	reactor; vacuum	(2)
p-terphenyl	~0	~0	~0	electron; vacuum	(2)
	~0	~0	~0	reactor; vacuum	(2)

Refs.: (1) Spinks 1976³, p. 388; (2) Hall 1963⁶, p. 91; (3) Rad. Effects 1963²⁷, p. 63.

Notes: ^anot listed;
~0 denotes a value <0.1.

3.1.3.4 Radiolysis of Water

Table 3.1-6 presents G values for radiolysis of water. G(H₂) strongly depends on LET, increasing by a factor of 3-4 from gamma radiolysis to alpha radiolysis. (Note that LET for alpha particles decreases for increasing alpha particle energy that is greater than 1.5 MeV.)

²⁷ Rad. Effects 1963. "Radiation Effects Handbook," S-146, Institute of Electrical and Electronics Engineers, Inc., June 1963.

The maximum $G(\text{H}_2)$ value for water is 1.6 for alpha radiation. The maximum $G(\text{O}_2)$ value for water would be 0.8. Addition of nitrates to water lowers the production of hydrogen, but can increase the production of oxygen.

Bibler²⁸ measured gas evolution from aerated nitric acid or sodium nitrate-0.4-M H_2SO_4 irradiated by Cm-244 and Pu(IV)-239 alpha particles. The nitrate ions scavenged the precursors of hydrogen and reduced $G(\text{H}_2)$ as observed in gamma radiolysis experiments. Above 1-M NO_3^- concentration, oxygen and nitrite ions were produced as a result of direct energy absorption by nitrate ions.

Table 3.1-6 — G Values for Water^{a,b}

Radiation Type	pH	$G(\text{H}_2)$	Reference
<u>Vapor phase</u> gamma, e	not given	0.5	(1)
<u>Liquid phase</u> gamma, e	0.5	0.4	(1),(2)
	3 to 13	0.45	(1),(2)
6.4 MeV He ⁺⁺	not stated	1.1 ^d	(2)
²⁴⁴ Cm alpha (5.8 MeV)	not stated	1.3	(3)
5.3 MeV alpha (Po) ^c	0.5	1.6	(1)
²⁵² Cf alpha, beta, and fission fragments	0.4M- H_2SO_4	1.7	(4)

Refs.: (1) Spinks 1976³, p. 258; (2) Burns 1981²⁹; (3) Bibler 1974²⁷; (4) Bibler 1975³⁰.

Notes: ^a"e" means accelerated electrons.

^b $G(\text{O}_2)$ values not reported; maximum $G(\text{O}_2)$ would be 1/2 $G(\text{H}_2)$.

^cPo = polonium.

^d $G(\text{H}_2)$ value from curve fit to data from seven authors at a wide range of LET values.

The $G(\text{H}_2)$ value in alpha radiolysis experiments was found to decrease sharply from about 1.3 for zero concentration of NO_3^- , to 0.7 at 1-M NO_3^- , to about 0.25 at 2.5-M NO_3^- . The decrease

²⁸ Bibler 1974. N. E. Bibler, "Curium-244 Radiolysis of Nitric Acid. Oxygen Production from Direct Radiolysis of Nitrate Ions," *J. Phys. Chem.* **78**, pp. 211-215, 1974.

²⁹ Burns 1981. W. G. Burns and H. E. Sims, "Effect of Radiation Type in Water Radiolysis," *J. Chem. Soc., Faraday Trans. I* **77**, pp. 2803-2813, 1981.

³⁰ Bibler 1975. N. E. Bibler, "Radiolysis of 0.4 M Sulfuric Acid Solutions with Fission Fragments from Dissolved Californium-252. Estimated Yields of Radical and Molecular Products that Escape Reactions in Fission Fragment Tracks," *J. Phys. Chem.* **79**, pp. 1991-1995, 1975.

in $G(\text{H}_2)$ was more pronounced for Co-60 gamma irradiation than for alpha irradiation. This effect has been attributed by Bibler and others to nitrate ions being more efficient hydrogen scavengers for gamma irradiation than for alpha irradiation. The $G(\text{O}_2)$ variation with NO_3^- concentration was approximately linear, from about $G(\text{O}_2)=0.25$ at zero concentration NO_3^- to $G(\text{O}_2)=0.75$ at 5.6-M NO_3^- . Agitation of the samples was necessary to release all of the generated O_2 , much of which otherwise stayed in solution.

Bibler²⁹ reports measurements of gas produced from irradiation of 0.4-M sulfuric acid by Cf-252, which is a transuranic isotope that decays by alpha emission as well as spontaneous fission. The total absorbed dose from Cf-252 is due to alpha particles, fission fragments, and beta particles from decay of the fission fragments. The net $G(\text{H}_2)$ value reported from all contributions was 1.7. The fission fragment contribution (LET of 400 eV/A) was calculated to have $G(\text{H}_2)=2.1$.

$G(\text{H}_2)$ values and equilibrium concentrations of H_2 for irradiated water are controlled by a back reaction of H_2 with the OH^- radical to form water.^{31,25} This back reaction is much more efficient for gamma radiation than for alpha radiation, resulting in a $G(\text{H}_2)$ value for gamma radiolysis 3-4 times lower than that for alpha radiolysis. The gas pressure above the water also was found to reach an equilibrium value at a much lower pressure for gamma radiolysis than for alpha radiolysis.

Another scavenger species that could compete with H_2 for OH^- is Cl^- , present in salt brines. The results of an experimental program to measure gas generation from radiolysis of salt brines are reported by Gray (Gray 1984³⁰). The brine was prepared by dissolving Permian Basin salt, consisting primarily of NaCl with a small amount of calcium sulfate, in deionized water. The irradiations were conducted in pressure vessels. The alpha radiolysis tests were terminated as the pressure approached the capacity of the pressure transducers. Gas compositions for both gamma and alpha radiolysis were roughly two parts H_2 to one part O_2 in most cases. The gamma radiolysis experiments reached an equilibrium pressure of about 100 atm, while the alpha radiolysis experiments were extrapolated to reach an equilibrium pressure of about 275 atm.

Alpha radiolysis experiments conducted by Bibler (Bibler 1981³²) on the free water in concrete demonstrated that below 100°C, the H_2 production rate is independent of temperature and radiation dose rate.

³¹ Gray 1984. W. J. Gray and S. A. Simonson, "Gamma and Alpha Radiolysis of Salt Brines," PNL-SA-12746, 1984 Fall Meeting of the Materials Research Society in Boston, Mass., November 1984.

³² Bibler 1981. N. E. Bibler, "Gas Production from Alpha Radiolysis of Concrete Containing TRU Incinerator Ash, Progress Report 4, September 1, 1979 - August 31, 1980," E. I. DuPont de Nemours and Company, Savannah River Laboratory, DPST-80-150-2, March 1981.

3.1.3.5 Radiolysis of Alcohols

Alcohols are compounds of the general formula ROH, where R is any alkyl or substituted alkyl group.⁷ The group may be open-chain or cyclic; it may contain a double bond, a halogen atom, or an aromatic ring. All alcohols contain the hydroxyl (-OH) group, which determines the properties characteristic of this family. Compounds in which the hydroxyl group is attached directly to an aromatic ring are called phenols, and differ markedly from the alcohols. A glycol is a dihydroxy alcohol, containing two hydroxyl groups. For example, ethylene glycol has the structure

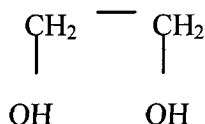


Table 3.1-7 presents G values for many alcohols.

3.1.3.6 Radiolysis of Ethers

Ethers are compounds of the general formula R-O-R, Ar-O-R, or Ar-O-Ar.⁷

Table 3.1-8 presents G values for many ethers. The maximum reported value of G(H₂) is 3.6. Almost all of the other radiolysis gases or vapors are also flammable. Branching in the alkyl group decreases hydrogen evolution but increases hydrocarbon yields.⁶

3.1.3.7 Radiolysis of Aldehydes and Ketones

Aldehydes are compounds of the general formula RCHO; ketones are compounds of the general formula RR'CO.⁷ The groups R and R' may be aliphatic or aromatic. Both aldehydes and ketones contain the carbonyl group, C=O, and are often referred to collectively as carbonyl compounds. It is the carbonyl group that largely determines the chemistry of aldehydes and ketones. For example, the structure of acetone is

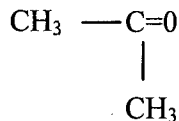


Table 3.1-9 presents G values for propionaldehyde. Table 3.1-10 illustrates the effect of LET on the gaseous products of acetone. Table 3.1-11 presents G values for several ketones, including acetone. The maximum total G value for flammable gas production from gamma or alpha radiolysis of these aldehydes or ketones is 3.1.

The series consisting of formaldehyde, acetaldehyde, and acetone was irradiated in the gas phase with electrons.⁶ Hydrogen, CO, and CO₂ were the principal products from formaldehyde. Replacing one or both hydrogen atoms of the formaldehyde molecule with CH₃ groups (giving acetaldehyde or acetone) resulted in lower radiolytic production of CO₂ and H₂, but gave substantial yields of alkanes and alkenes. This result was considered by those authors to be as expected on the basis of a group-to-product correlation.

Table 3.1-7 — G Values for Alcohols

Material	G(H ₂)	G(CO)	G(CH ₄)	G(gas) ^{a,b}	Comments	Reference
<u>Vapor phase</u>						
ethanol	10.8	1.2	0.9	12.9	electron; vacuum	(1)
methanol	10.8	1.0	0.3	12.1	gamma; vacuum	(1)
<u>Liquid phase</u>						
ethanol	5.0	0.1	0.6	5.7	gamma; vacuum	(1)
	3.5	0.1	0.4	4.5	alpha; vacuum	(2)
	4.1	0.1	0.4	4.6	alpha; vacuum	(3)
methanol	5.4	0.1	0.7	6.2	gamma; vacuum	(1)
	3.5	0.2	0.4	4.5	alpha; vacuum	(2)
	4.0	0.2	0.2	4.4	gamma; vacuum	(3)
methanol	major product is formaldehyde				gamma; oxygen	(1)
1-propanol	4.4	--	--	4.4 ^c	gamma; vacuum	(1)
	2.8	0.1	0.1	3.0	alpha; vacuum	(3)
2-propanol	3.7	--	1.5	5.2 ^c	gamma; vacuum	(1)
n-propanol	2.8	--	0.1	3.9	alpha; vacuum	(2)
1-butanol	4.6	--	--	4.6 ^c	gamma; vacuum	(1)
	3.6	0.1	0.1	4.3	alpha; vacuum	(3)
t-butanol	1.0	--	3.6	4.6 ^c	gamma; vacuum	(1)
n-butanol	3.6	--	0.1	4.3	alpha; vacuum	(2)
1-octanol	3.5	0.1	~0	3.7	alpha; vacuum	(3)
1-decanol	3.5	~0	~0	3.6	alpha; vacuum	(3)

Refs.: (1) Spinks 1976³, pp. 410, 417, 420; (2) Rad Effects, 1963²⁶, pp. 59-61; (3) Hall 1963⁶, p. 92.

Notes: ^aWater vapor is generated but is not included.

^bOther highly volatile products, such as formaldehyde, acetylene, ethylene, ethane, acetaldehyde, ethyl ether, and others, are also generated. G(gas) values greater than the sum of G(H₂), G(CO), and G(CH₄) have included these vapors.

^cOnly major products were listed.

Table 3.1-8 — G Values for Ethers in the Liquid Phase

Material	G(H ₂)	G(CO)	G(CH ₄)	G(gas) ^a	Comments	Reference
ethyl ether	3.4	--	0.4	3.8	gamma; vacuum	(1)
	3.6	0.1	0.2	3.9	alpha; vacuum	(2)
ethyl n-butyl ether	3.3	0.1	0.1	3.5	alpha; vacuum	(2)
dibutyl ether	2.9	--	0.1	3.0	gamma; vacuum	(1)
n-butyl ether	2.7	0.1	0.1	2.9	alpha; vacuum	(2)
ethyl tertbutyl ether	2.0	0.1	0.8	2.9	alpha; vacuum	(2)
isopropyl ether	2.2	~0	1.5	8.4	gamma; vacuum	(3)
	2.4	0.1	0.9	5.8	alpha; vacuum	(3)
di-isopropyl ether	2.4	--	1.7	4.1	gamma; vacuum	(1)
dioxan	2.1	0.3	--	2.4	gamma; vacuum	(1)
tetrahydrofuran	2.6	--	--	2.6	gamma; vacuum	(1)

Refs.: (1) Spinks 1976³, pp. 421-423; (2) Hall 1963⁶, p. 98; (3) Newton 1963²⁴, p. 55.

Note: ^aOther gases or highly volatile products, such as formaldehyde, acetylene, ethylene, ethane, acetaldehyde, alcohols, and others, are also generated. G(gas) values greater than the sum of G(H₂), G(CO), and G(CH₄) have included these other gases or vapors.

Table 3.1-9 — G Values for Propionaldehyde

Material	G(H ₂)	G(CO)	G(CH ₄)	G(gas) ^a	Comments
propionaldehyde	1.2	1.6	0.1	4.4	electron; vacuum

Refs.: Hall 1963⁶, p. 102.

Note: ^aG(gas) includes C₂-C₄ hydrocarbons.

Table 3.1-10 — Effect of LET on the Gaseous Products of Acetone

Radiation -dE/dx(eV/nm)	⁶⁰ Co-γ 0.2	6.9-MeV He-ions 131	67-MeV C-ions 390	65.7-MeV N-ions 553
G(H ₂)	0.96	1.47	2.36	2.71
G(CO)	0.56	0.80	1.05	1.22
G(CH ₄)	1.76	0.97	0.99	0.96
G(C ₂ H ₄)	0.04	0.12	0.21	0.24
G(C ₂ H ₆)	0.30	0.50	0.56	0.64
G(gas)	3.62	3.86	5.17	5.77

Ref.: Spinks 1976³, Table 8.19.

Table 3.1-11 — G Values for Three Ketones

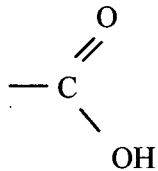
Material	G(H ₂)	G(CO)	G(CH ₄)	G(gas) ^a	Comments	Reference
acetone	1.0	0.6	1.8	3.6	gamma; vacuum	(1)
	1.5	0.8	1.0	3.9	alpha; vacuum	(1)
	0.9	0.8	2.6	4.8	gamma; vacuum	(2)
methyl ethyl ketone	1.2	0.8	0.9	6.8	gamma; vacuum	(2)
diethyl ketone	1.2	1.5	0.1	7.7	gamma; vacuum	(2)

Refs.: (1) Spinks 1976³, p. 427; (2) Hall 1963⁶, p. 102.

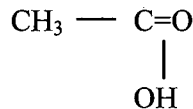
Note: ^aG(gas) includes C₂-C₄ hydrocarbons.

3.1.3.8 Radiolysis of Carboxylic Acids

Carboxylic acids contain the carboxyl group



attached to either an alkyl group (RCOOH) or an aryl group (ArCOOH).⁷ For example, acetic acid, CH₃COOH, has the structure



Whether the group is aliphatic or aromatic, saturated or unsaturated, substituted or unsubstituted, the properties of the carboxyl group are essentially the same.

Table 3.1-12 gives G values for two carboxylic acids that are liquids at room temperature. G values for some carboxylic acids that are solids at room temperature are given in Section 3.1.5.

Table 3.1-12 — G Values for Carboxylic Acids (Liquids at Room Temperature)

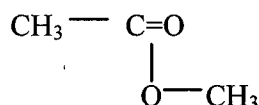
Material	G(H ₂)	G(CO)	G(CO ₂)	G(CH ₄)	G(gas)	Comments	Reference
acetic acid	0.5	0.2	5.4	3.9	10.5	gamma; vacuum	(1)
	0.5	0.4	4.0	1.4	7.2	alpha; vacuum	(1)
propionic acid	0.8	0.3	3.9	0.5	5.5	alpha; vacuum	(2)

Refs.: (1) Spinks 1976³, pp. 428-429; (2) Hall 1963⁶, p. 108.

Note: ^aG(gas) may include C₂; water vapor is also generated but is not included.

3.1.3.9 Radiolysis of Esters

Esters are functional derivatives of carboxylic acids in which the -OH of the carboxyl group has been replaced by -OR'.⁷ Phosphate esters are discussed separately. For example, the structure of methyl acetate is



The emulsifier for Envirostone^R, a gypsum-based material used to solidify organic and low pH aqueous sludges and liquid waste, has been identified as a polyethyl glycol ester. Many plasticizers added to polymers to form commercial plastics are esters, such as dioctyl phthalate. Table 3.1-13 gives G values for many esters. Note that benzyl acetate, which includes a benzene ring in its structure, has a much lower G(H₂) value than the other esters.

Table 3.1-13 — G Values for Esters

Material	G(H ₂)	G(CO)	G(CO ₂)	G(CH ₄)	G(gas) ^a	Comments	Reference
methyl acetate	0.8	1.6	1.0	2.0	5.7	gamma; vacuum	(1)
	0.9	1.6	0.8	2.1	5.6	gamma; vacuum	(2)
	0.6	1.2	0.4	0.8	3.4	electron; vacuum	(2)
ethyl acetate	0.9	1.1	--	1.6	3.6	gamma; vacuum	(2)
isopropyl acetate	0.9	1.2	0.8	0.9	5.6	alpha; vacuum	(2)
	0.5	0.8	0.6	1.0	3.6	electron; vacuum	(2)
n-propyl acetate	0.8	1.1	0.6	0.4	4.0	electron; vacuum	(2)
benzyl acetate	0.1	0.2	1.6	0.8	2.7	electron; vacuum; aromatic character	(2)

Table 3.1-13 — G Values for Esters (Concluded)

Material	G(H ₂)	G(CO)	G(CO ₂)	G(CH ₄)	G(gas) ^a	Comments	Reference
di (2-ethyl) hexyl sebacate	1.0	0.3	0.2	~0	1.8	electron; vacuum	(3)
	1.0	0.3	0.2	~0	1.5	gamma; vacuum	(4)
di (2-ethyl) hexyl adipate	0.9	0.5	0.2	~0	1.7	gamma; vacuum	(4)
pentaerythritol ester	0.8	0.8	0.3	~0 ^b	1.9	gamma; vacuum	(4)

Refs.: (1) Spinks 1976³, p. 430; (2) Hall 1963⁶, p. 104; (3) Rad. Effects 1963²⁶, p. 62; (4) Arakawa 1983a.³³

Note: ^aG(gas) may include C₂ hydrocarbons or vapors from volatile liquids, such as aldehydes, alcohols, or ethers.

^bThe value of 0.3 in the reference appears to be in error (0.03 vs. 0.3).

3.1.3.10 Radiolysis of Phosphate Esters

Phosphate esters have one of the following structures⁷:

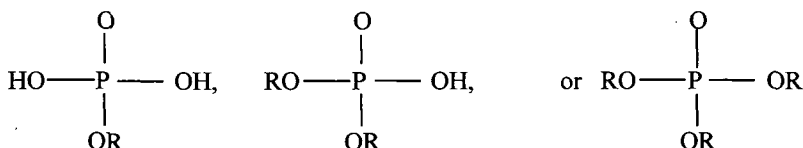


Table 3.1-14 gives G values for phosphate esters. Tricresyl phosphate contains three benzene rings and has a much lower G(H₂) value than either trioctyl or tributyl phosphate.

Table 3.1-14 — G Values for Phosphate Esters

Material	G(H ₂)	G(CO)	G(CO ₂)	G(CH ₄)	G(gas) ^a	Comments	Reference
tricresyl phosphate	0.05	~0	~0	~0	0.06	gamma; vacuum; aromatic character	(1)
tributyl phosphate	2.0	--	--	0.3	2.3	gamma	(2)
trioctyl phosphate	2.3	~0	~0	0.1	2.6	gamma; vacuum	(1)

Refs.: (1) Arakawa 1983a³²; (2) Holland 1978³⁴.

Note: ^aG(gas) may include C₂ hydrocarbons

³³ Arakawa 1983a. K. Arakawa, et al., "Radiation-Induced Gas Evolution from Commercial Lubricant Base Oil," Nuclear Technology 61, pp. 533-539, 1983.

³⁴ Holland 1978. J. P. Holland, et al., "The Radiolysis of Dodecane-Tributylphosphate Solutions," Nuclear Instruments and Methods 153, pp. 589-593, 1978.

Tri-n-butyl phosphate (TBP), an organic ester of phosphoric acid, is used as an extractant in the reprocessing of nuclear fuel. Radiolysis experiments have been conducted to determine the decomposition of TBP in different phases of the extraction system. The Purex process uses solution of TBP in dodecane.³⁵

Ladrielle³⁴ conducted both gamma and alpha radiolysis experiments in solutions of TBP in dodecane at room temperature. The average alpha particle energy from the cyclotron beam interacting with the solution was estimated to be 10.5 MeV. Pure TBP and dodecane were also irradiated. Radiolysis of pure TBP resulted in the formation of mono and dibutylphosphate, butanol, and saturated hydrocarbons (C₅ to C₈). Radiolysis of pure dodecane yielded hydrocarbons (C₅ to C₁₁). Lower molecular weight hydrocarbons (C₄ and below) were neglected in this study.

Holland³³ performed gamma radiolysis experiments on TBP, dodecane, and mixtures of TBP and dodecane. All samples were treated with dry clean helium for a period of four to eight hours. The number of moles of gas volatile at 161 K was determined by PVT analysis. A sample of the gas extracted was analyzed at 40 C by gas chromatography. Values of G(H₂)=6.7 and G(CH₄)=0.05 were determined for dodecane. Corresponding G values for pure TBP were G(H₂)=2.0 and G(CH₄)=0.3. Mixtures of TBP and dodecane were also irradiated, with dodecane electron fractions of 40%, 70%, 80%, 90%, and 95%. Plots of G(H₂) versus TBP electron fraction were nonlinear. The yield of hydrogen was less than would be predicted by the mixture law (the yield of acid was greater).

Aromatic hydrocarbons, such as benzene, toluene, and cyclohexene protect TBP, while saturated hydrocarbons such as hexane, cyclohexane, and dodecane sensitize TBP to radiolytic degradation.³⁶ Carbon tetrachloride also sensitizes TBP radiolysis. Barney found that chlorinated aromatic hydrocarbons also provided more protection to TBP for alpha radiolysis than did the chlorinated unsaturated hydrocarbons. The rate of chloride ion formation in 20% TBP mixtures with various chlorinated hydrocarbon diluents was also measured. The relative rates were in the ratio 1/0.7/0.5 for carbon tetrachloride/trichloroethylene/ tetrachloroethylene. No detectable chloride ion formation was found for 1,2,4-trichlorobenzene or o-dichlorobenzene.

3.1.3.11 Radiolysis of Halogenated Hydrocarbons

Halogenated hydrocarbons are hydrocarbons in which at least one and possibly all of the hydrogen atoms have been replaced by halogen atoms (the major functional group for these materials). Radiolysis of halogenated hydrocarbons can be strongly affected by the presence of oxygen or moisture, and chain reactions can occur involving HCl for chlorinated hydrocarbons.

³⁵ Ladrielle 1983. Ladrielle, et al., "Alpha and Gamma Induced Radiolysis of Tributyl-Phosphate," Radiochem. Radioanal. Letters 59, pp. 355-364, 1983.

³⁶ Barney 1977. G. S. Barney and D. G. Bouse, "Alpha Radiolysis of Tributyl Phosphate - Effect of Diluents," Atlantic Richfield Hanford Company, ARH-ST-153, April 1977.

3.1.3.11.1 Radiolysis of Carbon Tetrachloride

Radiolysis of carbon tetrachloride, CCl_4 , represents a simple example of radiolysis of an organic halogen compound because the radicals produced have limited possible reactions. Only two products are found: chlorine and hexachloroethane (not a gas). The observed G values for both products are 0.65 to 0.75 for gamma radiation.³ When carbon tetrachloride is irradiated in the presence of oxygen, phosgene gas and chlorine are formed, each with a G value for gamma radiation of 4.3.³

Kazanjian³⁷ measured gas generation from carbon tetrachloride contaminated with plutonium dioxide and mixed with calcium silicate to form a paste. The initial atmosphere was air. The only gaseous product found was carbon dioxide, with a G value of 0.6. After the oxygen was completely depleted in about 40 days, the gas production rate became essentially nil. Kazanjian remarked that finding only carbon dioxide was puzzling because previous studies had shown that chlorine and phosgene were the only gaseous products. He hypothesized that chlorine was not detected because of its high reactivity. Phosgene can react with water to form HCl and CO_2 .³⁸ Another possibility is that the calcium silicate, while radiolytically inert, could sorb radiolysis products, such as chlorine. Table 3.1-15 gives G values for carbon tetrachloride.

Table 3.1-15 — G Values for Carbon Tetrachloride

Radiation Type	G(Products)	Comments	Reference
gamma	G(gas)=0.7-0.8 G(Cl_2)=0.7-0.8	vacuum	(1),(2)
gamma	G(gas)=8.6	oxygen	(1)
alpha	G(gas)=0.6 G(CO_2)=0.6	air; CCl_4 mixed with calcium silicate to form a paste	(3)

Refs.: (1) Spinks 1976³, pp. 401-403; (2) Rad. Effects 1963²⁶, p. 62; (3) Kazanjian 1976³⁶.

3.1.3.11.2 Radiolysis of Aromatic Halides

The aromatic halides chlorobenzene, bromobenzene, and iodobenzene consist of a benzene ring with one hydrogen atom replaced by a chlorine, bromine, or iodine atom, respectively.

Table 3.1-16 lists G values for several aromatic halides. Very low $G(\text{H}_2)$ values are found, as for the aromatic hydrocarbons.

³⁷ Kazanjian 1976. A. R. Kazanjian, "Radiolytic Gas Generation in Plutonium Contaminated Waste Materials," Rockwell International, Rocky Flats Plant, RFP-2469, October 1976.

³⁸ Kazanjian 1969. A. R. Kazanjian and A. K. Brown, "Radiation Chemistry of Materials Used in Plutonium Processing," The Dow Chemical Company, Rocky Flats Division, RFP-1376, December 1969.

Table 3.1-16 — G Values for Aromatic Halides

Material	G(Products)	G(gas) ^a
chlorobenzene	G(H ₂)~0; G(HCl)=1.4; G(Cl ₂)~0	1.4
bromobenzene	G(H ₂)~0; G(HBr)=2.3; G(Br ₂)=0.2	2.5
iodobenzene	G(H ₂)~0; G(HI)~0; G(I ₂)=2.0	2.0

Ref.: Spinks 1976³, p. 407.

Note: ^aGamma irradiation in a vacuum.

3.1.3.11.3 Radiolysis of Miscellaneous Halogenated Hydrocarbons

Some of the halogenated hydrocarbons that may be present in CH-TRU wastes are chloroform, methylene chloride, 1,1,1-trichloroethane, and 1,1,2-trichloro-1,2,2-trifluoroethane (Freon-113).

The amounts and species of gases generated from gamma radiolysis of liquid chloroform are dependent on temperature and dose rate and, in particular, on traces of oxygen and moisture that induce chain reactions. Aqueous solutions of chloroform do not decompose by a chain reaction.³ Measured values of G(HCl) from about 5 up to 11 have been reported at 22-25°C (Ottolenghi 1961³⁹, Chen 1960⁴⁰) for pure chloroform.

In the presence of oxygen, chloroform takes part in a radiation-initiated chain reaction. Nearly 100 chloroform molecules are decomposed per 100 eV of energy absorbed⁴¹. Most of the radiolysis products are hydrolyzed by water to produce hydrochloric acid.

Kazanjian³⁶ measured gas generation from the alpha radiolysis of Chlorothene-VG solvent, which is a trade name for 1,1,1-trichloroethane. The samples were mixed with calcium silicate to form a paste. The total pressure decreased for the first 30 days because of oxygen depletion; then it increased because of evolved gases. The main products measured were hydrogen, carbon dioxide, and dichloroethylene. Kazanjian remarked that formation of dichloroethylene inferred the production of hydrogen chloride, and that the hydrogen chloride probably was not detected because of its high reactivity. Calculations using Kazanjian's data show average G values for

³⁹ Ottolenghi 1961. M. Ottolenghi and G. Stein, "The Radiation Chemistry of Chloroform," Radiation Research 14, pp. 281-290, 1961.

⁴⁰ Chen 1960. T. H. Chen, et al., "Radiolysis of Chloroform and Carbon Tetrachloride," J. Phys. Chem. 64, pp. 1023-1025, 1960.

⁴¹ Schulte 1953. J. W. Schulte, et al., "Chemical Effects Produced in Chloroform by Gamma-Rays," J. Am. Chem. Soc. 75, pp. 2222-2227, 1953.

CO₂ and H₂ of 0.3 and 0.2, respectively; and G(gas)=0.7. The G values did not decrease with increasing dose.

Getoff⁴² performed gamma irradiation of oxygenated waste water containing 1,1,1-trichloroethane and found G(Cl)=0.4.

Kazanjian^{37,43} performed gamma radiolysis experiments on Baker reagent-grade trichloroethylene. Trichloroethylene is a highly sensitive compound, and very little energy input is necessary to initiate decomposition. In the absence of air, there were only two major products: hydrochloric acid and chloroacetylene, each with a G value of 0.25. A chain reaction was observed to occur when trichloroethylene was irradiated in the presence of oxygen. Extremely high yields were obtained, but the products were difficult to analyze because of their high reactivity. The major products were determined to be dichloroacetyl chloride, phosgene, and trichloroethylene oxide. There was no HCl or Cl₂ measured. Rapid reaction of the products with water to form HCl made it possible to analyze for total acidity. The total acid yield was measured by shaking the irradiated solvent with water and titrating the mixture with standardized NaOH solution. The G(H⁺) obtained was 4600 at room temperature⁴² and increased with increasing temperature with an activation energy value of 2.2 kcal/mole.

Kazanjian³⁷ also measured the products from gamma irradiation of Alk-Tri^R, a commercial brand of trichloroethylene, which contains diisopropylamine for light stabilization. G(H⁺) was found to be 1600. Acid yields for this material would be expected to increase to the yields obtained for the reagent grade chemical as the additives were depleted through continued irradiation.

Perchloroethylene is expected to have a radiation chemistry similar to that of trichloroethylene and to produce an extremely high yield of acidic products in the presence of oxygen³⁷.

Alfassi and co-workers have performed gamma radiolysis experiments on two Freons, CFCl₃ and CF₂Cl₂, in the liquid phase.^{44,45} A variety of C-F-Cl compounds were found with maximum measured G value for products of 2.6 in the presence of oxygen. All of the products were gases or highly volatile liquids.

Table 3.1-17 gives G values for miscellaneous organic halogen compounds.

⁴² Getoff 1985. N. Getoff and W. Lutz, "Radiation Induced Decomposition of Hydrocarbons in Water Resources," Radiat. Phys. Chem. 25, pp. 21-26, 1985.

⁴³ Kazanjian 1970. A. R. Kazanjian and D. R. Horrell, "The Radiation-Induced Oxidation of Trichloroethylene," J. Phys. Chem. 75, pp. 613-616, 1971.

⁴⁴ Alfassi 1982. Z. B. Alfassi, "The Radiation Chemistry of CFCl₃ in the Liquid Phase," Radiochem. Radioanal. Letters 56, pp. 333-342, 1982.

⁴⁵ Alfassi 1983. Z. B. Alfassi and H. Heusinger, "The Radiation Chemistry of CF₂Cl₂ in the Liquid Phase," Radiat. Phys. Chem. 22, pp. 995-1000, 1983.

3.1.3.12 Radiolysis of Organic Nitrogen Compounds

Organic nitrogen compounds are basically hydrocarbons where a functional group has been replaced by an NO_2 , NH_2 , or other group containing one or more nitrogen atoms. Amides (such as propionamide) are functional derivatives of carboxylic acids in which the $-\text{OH}$ of the carboxyl group has been replaced by $-\text{NH}_2$ ⁷. Amines have the general formula RNH_2 , R_2NH , or R_3N , where R is any alkyl or aryl group. In many of their reactions, the final products depend on the number of hydrogen atoms attached to the nitrogen atom. Two examples of amines are methylamine (CH_3NH_2) and aniline, which has the NH_2 group attached to a benzene ring. Some of the heterocyclic compounds containing nitrogen (such as pyrrole, pyrazole, pyridine, and pyrimidine) have aromatic properties, while others, including 3-pyrroline and pyrrolidene, do not.

G values for radiolysis of organic nitrogen compounds that have aromatic characteristics are low, as were the G values for radiolysis of aromatic hydrocarbons. Table 3.1-18 lists the G values for the products generated by the gamma radiolysis of many liquid organic nitrogen compounds. Ammonia is one of the products formed for a few of the compounds.

Table 3.1-17 — G Values for Miscellaneous Organic Halogen Compounds

Material	G(Products)	Comments	Reference
chloroform ^a	$G(\text{HCl})=5.3$	gamma; vacuum	(1)
methylene chloride	$G(\text{HCl})=4.9$	gamma; vacuum	(2)
1,1,1-trichloroethane	$G(\text{gas})=0.7$; $G(\text{H}_2)=0.2$; $G(\text{CO}_2)=0.3$; $G(\text{dichloroethylene})=0.2$	alpha; with or without O_2 present	(3) ^b
	$G(\text{Cl}^-)=0.4$	gamma; O_2 present in aqueous solution	(4)
trichloroethylene	$G(\text{H}^+)=4600^a$	gamma; oxygen present	(5)
	$G(\text{HCl})=0.25$	gamma; vacuum	(5),(6)
Freons	$G(\text{gas})=2.6(\text{max})$; $G(\text{C-F-Cl compounds})=1.6$; $G(\text{CO}_2)=0-1.1$	gamma; with or without O_2 present	(7),(8)

Refs.: (1) Spinks 1976³, p. 403; (2) Rad. Effects 1963²⁶, p. 62; (3) Kazanjian 1976³⁶; (4) Getoff 1985⁴¹; (5) Kazanjian 1970⁴²; (6) Kazanjian 1969³⁷; (7) Alfassi 1982⁴³; (8) Alfassi 1983⁴⁴.

Notes: ^a $G(\text{H}^+)$ is large for irradiation in oxygen. A chain reaction occurs in the liquid.

^bAverage G values calculated using author's data.

Table 3.1-18 — G Values for Liquid Organic Nitrogen Compounds^a

Material	G(Products)	Comments
nitromethane	G(HCHO)=2.0	
nitrobenzene	G(N ₂)=0.16	
acetonitrile	G(H ₂)=0.67; G(CH ₄)=0.65; G(HCN)=0.2	C N bond
methylamine	G(H ₂)=5.4; G(CH ₄)=0.18	
aniline	G(H ₂)=0.12; G(NH ₃)=0.25; G(C ₆ H ₆)=0.04	contains benzene ring
propionamide	G(H ₂)=0.14; G(CO)=2.6; G(CH ₄)=0.93	
pyrrole	G(H ₂)=0.20	aromatic N-C bonds
3-pyrroline	G(H ₂)=2.34	
pyrrolidine	G(H ₂)=6.35	
pyrazole	G(H ₂)=0.04; G(N ₂)=0.12	aromatic N-C bonds
tetrazole	G(H ₂)=trace; G(N ₂)=0.96	aromatic N-C bonds
pyridine	G(H ₂)=0.025	aromatic N-C bonds
pyrimidine	G(H ₂)=0.030	aromatic N-C bonds

Ref.: Spinks 1976³, Table 8.22.

Note: ^aGamma irradiation in vacuum. Other liquid products are also formed.

A value of G(gas)=10.1 was reported for gamma irradiation at room temperature of mono-n-butylamine (Mirchi 1981⁴⁶). Major gas constituents were hydrogen [G(H₂)=5.6] and ammonia [G(NH₃)=4.0]. For dibutylamine and tri-n-butylamine, measurements of G(H₂) values at room temperature were 3.6 and 2.7, respectively. In all three cases, the total G value for hydrocarbon gases was 0.5.

Diethylenetriaminepentaacetic acid (DTPA) is a polyamino-carboxylic acid used as an eluting agent for the purification of Cm-244 by cation exchange chromatography. DTPA has been irradiated in aqueous solution by alpha and gamma radiation sources (Bibler 1972⁴⁷). In some experiments, the solutions were degassed before irradiation, and the amounts of radiolytically produced gases that were noncondensable at -196°C and at -78°C were determined. The products were identified by mass spectrometry. Gamma radiolysis of solutions of DTPA in 4-M HNO₃ or 0.4-M H₂SO₄ produced CO₂ and H₂, with measured G values of 6.5 and 4.2, respectively. Gases produced in the alpha radiolysis experiments were not reported. However, measured G values for the destruction of DTPA were much lower for the alpha radiolysis experiments than for the gamma radiolysis experiments, indicating that gas production for alpha radiolysis should also be much lower than for gamma radiolysis.

⁴⁶ Mirchi 1981. R. Mirchi, et al., "Selected Problems of Radiation Stability of Some Solvents and Amines Used in the Reprocessing of Nuclear Fuel," *Nukleonika* 26, pp. 827-848, 1981.

⁴⁷ Bibler 1972. N. E. Bibler, "Gamma and Alpha Radiolysis of Aqueous Solutions of Diethylenetriaminepentaacetic Acid," *J. Inorg. Nucl. Chem.* 34, pp. 1417-1425, 1972.

3.1.3.13 Radiolysis of Commercial Lubricants

Commercial lubricants consist of paraffinic, naphthenic, and aromatic hydrocarbons. The aromatics have much lower G values than the paraffins but are largely removed from the oils by refining because of their poor viscosity-temperature properties (Carroll 1963⁴⁸).

G values have been measured for many different commercial lubricants using gamma irradiation at room temperature at a dose rate of 1 Mrad/h and absorbed doses ranging from 100 to 3000 Mrad (Arakawa 1983a³²). Graphs of the amount of evolved gas versus dose were nearly linear even at high absorbed dose, indicating nearly constant G values.

G values for Texaco Regal A motor oil, used in machining operations at the RFETS, were measured by Kazanjian using Co-60 gamma irradiation (Kazanjian 1969³⁷) and alpha irradiation from Pu-239 (Kazanjian 1976³⁶). In the gamma irradiation experiment, samples of the oil were irradiated under vacuum or sealed under 500 torr air. Values of $G(H_2)$ at 8.4 Mrad absorbed dose were 2.3 for the vacuum experiment and 1.8 for the experiment in air. The author did not consider this difference significant. At 8.4 Mrad absorbed dose, $G(-O_2)=1.6$, decreased from a value of 3.0 at 1.4 Mrad.

In the alpha radiolysis experiment, the Texaco oil was contaminated with plutonium dioxide and mixed with calcium silicate to form a paste. About 15% of the alpha energy could have been absorbed by the calcium silicate, which was considered to be radiation stable. In the first experiment the materials were contained in an initial air atmosphere in a valved stainless steel vessel. The oxygen concentration decreased from 21% to 5% over the course of the 100-day experiment. For the second experiment the vessel was evacuated and backfilled with helium. Calculations using Kazanjian's data show that as the absorbed dose increased, the G values for H_2 and total gas increased from about 1.6 to 2.8-2.9 for the first experiment. During the second experiment in vacuum, the G values decreased from about 2.3 to 1.9-2.1. The cause for these changes in G values is unknown. Maximum values for these experiments are listed in Table 3.1-18.

Zerwekh (Zerwekh 1979¹³) measured gas generated from the alpha radiolysis of vacuum pump oil (DuoSeal) absorbed on vermiculite. Two experimental cylinders were prepared. One cylinder contained 62 mg of Pu-238 in the oxide form dispersed in 35 g of oil, which was then absorbed on 17.5 g of vermiculite. The other cylinder contained the same amounts of oil and vermiculite but only half as much PuO_2 . The gases in the cylinders were sampled each time the pressure reached 15-17 psig, and then the pressure was reduced to 1 psig. The O_2 concentration was less than 0.1% at the first sampling. The gas generated was predominantly hydrogen, with a small amount of methane. Concentrations of CO and CO_2 did not exceed 0.7% (each) at any time during the experiment. The maximum $G(gas)$ value observed was about 1.7. The initial $G(gas)$ value observed for the sample contaminated with 32 mg of PuO_2 was about 10% higher than for the sample contaminated with 62 mg of PuO_2 .

⁴⁸ Carroll 1963. J. G. Carroll and R. O. Bolt, "Lubricants," in Radiation Effects on Organic Materials, Academic Press, New York, 1963, eds. R. O. Bolt and J. G. Carroll.

G values for Cm-244 alpha and Co-60 gamma radiolysis of DuoSeal vacuum pump oil absorbed on vermiculite were measured by Bibler (Bibler 1977²⁵) at various dose rates, absorbed doses, and mass fraction of oil. (Vermiculite is a hydrated magnesium-aluminum-iron silicate, and produced no H₂ when irradiated.) Usually, 2.5 ml of the oil was absorbed onto each gram of vermiculite. At low gamma dose rates (1.5-4.8E5 rad/hr), a G(H₂) of 2.0 was calculated based on energy absorbed only by the organic material. The composition of the evolved gas was about 96% H₂, 3% CO₂, and 1% CH₄. Experiments conducted at a dose rate of 1.4E7 rad/hr (gamma) showed that G(H₂) was directly proportional to the amount of organic material present, indicating that the energy absorbed by the vermiculite was not transferred to the organic material.

The corresponding alpha radiolysis experiment using vacuum pump oil absorbed on vermiculite contaminated with 7.2 mg Cm-244 (dose rate 1.4E6 rads/hr) resulted in a G(H₂) value of 2.7. No decrease in G values with increasing absorbed dose was observed for the alpha radiolysis experiment.

Rykon lubricating grease was irradiated under vacuum and in air using a Co-60 gamma source (Kazanjian 1969³⁷). The gas yield was low and consisted mostly of hydrogen, with an approximate value of G(H₂)=1.

Table 3.1-19 gives G values for many commercial lubricants. The maximum G values for commercial lubricants are G(gas)=2.9 and G(H₂) = 2.8.

3.1.3.14 Radiolysis of Gases

Radiolysis of the nitrogen/oxygen mixture found in air produces a small amount of ozone, as well as oxides of nitrogen (Spinks 1976³). Back reactions lead to an equilibrium concentration of these gases of a few ppm for ozone to a few percent for NO₂ and N₂O. The NO yields are much smaller (Kazanjian 1969³⁷). When moisture is present, the main product is nitric acid, which is formed until the water vapor is exhausted (Spinks 1976³, Kazanjian 1969³⁷). G values are around 1 for nitric acid formation but vary with water concentration (Kazanjian 1969³⁷).

Gaseous carbon dioxide is almost unaffected by ionizing radiation (Spinks 1976³), possibly due to a back reaction between CO and ozone to form CO₂ plus O₂.

3.1.4 Radiolysis of Polymers

Radiation effects in organic solids are generally similar to those for the same compound in the liquid state when allowance is made for the restricted mobility of the active species in the solid. Polymers, including materials such as polyethylene, PVC, and cellulose, are common organic solids found in CH-TRU wastes. Attachment A of this document describes the families of polymers and their use in commercial plastics. Other solids, such as solidified organic liquids, aqueous sludges, and bitumen, are discussed in Section 3.1.5. Some of the polymers discussed in this chapter occur in the liquid state at room temperature.

Table 3.1-19 — G Values for Many Commercial Lubricants

Material/ Radiation Type	G(Products)	Comments	Reference
<u>Mineral oils</u>			
gamma	G(gas)=2.8; G(H ₂)=2.7; G(CH ₄)=0.05	vacuum; highest G values for four paraffin oils	(1)
<u>Naphthenic neutral oil</u>			
gamma	G(gas)=0.9; G(H ₂)=0.9	vacuum	(1)
<u>Poly-alpha-olefin oil</u>			
gamma	G(gas)=2.4; G(H ₂)=2.3	vacuum	(1)
<u>Ester lubricants</u>			
gamma	G(gas)=2.6; G(H ₂)=2.3; G(CH ₄)=0.1; G(CO)=0	vacuum; highest G values for 5 oils ^a	(1)
<u>Aromatic lubricants</u>			
gamma	G(gas)=0.6; G(H ₂)=0.5	vacuum; highest G values for 7 aromatic oils	(1)
<u>Silicones</u>			
gamma	G(gas)=2.3; G(H ₂)=0.6 G(CH ₄)=1.4; G(C ₂ H ₆)=0.3	vacuum; highest G values for 2 silicones	(1)
<u>Texaco Regal-A machining oil</u>			
alpha (²³⁹ Pu) ^b	G(gas)=2.9; G(H ₂)=2.8; G(HC) ^c =0.1	in air, before or after oxygen depletion; maximum values; mixed with calcium silicate to form a paste	(2) ^b
gamma	G(H ₂)=2.3	vacuum; 8.4 Mrad	(3)
gamma	G(H ₂)=1.8	500 torr O ₂ ; 8.4 Mrad	(3)
gamma	G(H ₂)=2.1	500 torr O ₂ ; 1.4 Mrad	(3)
<u>DuoSeal vacuum oil</u>			
alpha (²³⁸ Pu)	G(gas)=1.7; G(H ₂)~1.6	in air after oxygen depleted; sorbed on vermiculite	(4)
alpha (²⁴⁴ Cm)	G(gas)=2.8; G(H ₂)=2.7; G(CO ₂)=0.1	in air	(5)
gamma	G(gas)=2.1; G(H ₂)=2.0; G(CO ₂)=0.1	in air; extrapolated to zero dose	(5)
<u>Rycon grease</u>			
gamma	G(H ₂)=1	vacuum or air	(3)

Refs.: (1) Arakawa 1983a³²; (2) Kazanjian 1976³⁶; (3) Kazanjian 1969³⁷; (4) Zerwekh 1979¹³; (5) Bibler 1977²⁵.

Note: ^aIncludes oils based on di-2-ethylhexyl sebacate (DOS), di-2-ethylhexyl adipate (DOA), pentaerythritol ester, tricresyl phosphate (TCP), and trioctyl phosphate (TOP).

^bCalculated using author's data. Assumes all decay energy was absorbed by the oil (85% by weight).

^cHC = hydrocarbons.

The controlling factor in the behavior of polymers under irradiation, as under most other environmental influences, is the chemical structure (Sisman 1963⁴⁹). Additives to improve physical or aging properties affect changes produced by radiation.

For example, polystyrene demonstrates the stabilizing effect of a regularly recurring phenyl group on the main chain (Sisman 1963⁴⁸). The protective effect appears to depend on closeness to the phenyl group (not more than six carbon atoms away). A part of the stability of polystyrene must be assigned to the low mobility of the molecular segments in the solid.

Radiolysis of polymers generally results in two types of reactions: (a) chain scission and (b) crosslinking. Chain scission (degradation) is the term used for breaking of main-chain bonds in polymer molecules, which results in the formation of species of lower molecular weight. When scission of the polymer is predominant, structural strength and plasticity are rapidly lost. The polymer may actually crumble to a powder. Crosslinking results in network structures that are insoluble and infusible because of increased molecular weight and size. Generally, competition occurs between the two reaction mechanisms.

In the absence of oxygen, polymers can be divided into classes according to their tendency to degrade or crosslink. Tables 3.1-20 through 3.1-22 list common polymers in order of their decreasing resistance when irradiated to net molecular-weight change for polymers that

Table 3.1-20 — Radiation Resistance of Common Polymers that Predominantly Crosslink^a

Polymer	Characteristics
poly(vinyl carbazole)	aromatic, N in main chain
polystyrene	aromatic
aniline-formaldehyde	aromatic, N in main chain
Nylon ^R	N in main chain (amide)
polymethyl acrylate	ester
polyacrylonitrile	C-N triple bond
styrene-butadiene rubber	aromatic, unsaturated
polybutadiene	unsaturated
polyisoprene	unsaturated
nitrile-butadiene rubber	C-N triple bond, unsaturated
polyethylene oxide	ether
polyvinyl acetate	ester
polyvinyl methyl ether	
polyethylene	saturated
silicone	

Ref.: Sisman 1963⁴⁸

Note: ^aListed in order of decreasing resistance to net molecular-weight change.

⁴⁹ Sisman 1963. O. Sisman, et al., "Polymers," in Radiation Effects on Organic Materials, Academic Press, New York, 1963, eds. R. O. Bolt and J. G. Carroll.

Table 3.1-21 — Radiation Resistance of Common Polymers that are Borderline Between Predominant Crosslinking and Scission^a

Polymer	Characteristics
polysulfide rubber	S in main chain
polyethylene terephthalate	aromatic, ester
polyvinyl chloride	halogen
polyvinylidene chloride	halogen
polypropylene	saturated

Ref.: Sisman 1963⁴⁸.

Note: ^aListed in order of decreasing resistance to net molecular-weight change.

Table 3.1-22 — Radiation Resistance of Common Polymers that Scission Predominantly^a

Polymer	Characteristics
phenol-formaldehyde	aromatic
polymethyl methacrylate	ester
polyvinyl alcohol	alcohol
polytetrafluoroethylene	halogen
polyisobutylene	saturated
cellulose	alcohol/ether

Ref.: Sisman 1963⁴⁸.

Note: ^aListed in order of decreasing resistance to net molecular-weight change.

predominantly crosslink, are borderline between crosslinking and scission, or that predominantly undergo scission, respectively. Oxygen enhances the degradation of most polymers (polymethyl methacrylate is one exception).

Ether-type oxygen linkages occur in the main chain in polyethylene oxide. Cellulose is made up of glucose residues joined through acetal linkages (ether links formed between hydroxyl and carbonyl groups). Cellulose and cellulose esters and ethers undergo scission, probably resulting from a break in the acetal link rather than rupture of the glucose ring (Sisman 1963⁴⁸).

Commercial plastics and papers contain additives that modify the properties of the base polymer in the material. In general, the additives improve the radiation stability of the commercial materials and reduce G values for flammable gases.

Additives and nonpolymer components can be divided into two categories: active and inert materials. The active additives can be subdivided into two classes: the energy-sink materials and the chemical reactants. The aromatic ring acts as an energy sink incorporated intramolecularly in the polymer. Antioxidants are usually complex aromatic amines or phenols, which should have low G values as a result of their aromatic characteristics (Sisman 1963⁴⁸).

Scission of polymethyl methacrylate has been reduced by the addition of aromatic compounds dissolved in the polymer (Bopp 1963⁵⁰). Protection was shown to be concentration dependent. For several of the additives, no dose dependence was found, indicating that the additives were not being radiolytically degraded, but in other cases, a dose dependence was observed. Antioxidants and aromatic stabilizers and plasticizers are frequently used to enhance durability of mechanical properties. Polyethylene and hydrocarbon rubbers normally require a small quantity of antioxidant for stability during hot processing.

From the observed G values for flammable gas [G(flam gas)], the expected relationships between the G(flam gas) values for structurally related polymers are shown in Table 3.1-23.

Table 3.1-23 — Expected Relative G(flam gas) Values for Polymers from G(flam gas) Values in Structurally Related Liquids

High

Hydrocarbon polymers containing only saturated C-C bonds

Polymers containing alcohol functional groups

Polymers containing ether functional groups

Medium

Hydrocarbon polymers containing unsaturated C-C bonds

Polymers containing ester functional groups

Low

Polymers with aromatic characteristics

Notes: High: liquid G(flam gas)=5-7; Medium: liquid G(flam gas)=2-3; Low: liquid G(flam gas)<1.

Radiolysis experiments on polymers that are discussed in this chapter are organized into the following groups, that follow the approximate order of high to low G values for flammable gas expected for synthetic polymers containing only carbon, hydrogen, nitrogen, and oxygen:

- (1) Hydrocarbon polymers containing only saturated C-C bonds (polyethylene, polypropylene, ethylene-propylene rubber, and polyisobutylene)
- (2) Polymers containing alcohol functional groups (polyvinyl alcohol and polyethylene glycol)
- (3) Polymers containing ether functional groups (cellulose, urea formaldehyde, polyoxymethylene, polypropylene oxide, and polyvinyl formal)
- (4) Hydrocarbon polymers containing unsaturated C-C bonds (polybutadiene and polyisoprene)
- (5) Polymers containing ester functional groups (polymethyl methacrylate and polyvinyl acetate)

⁵⁰ Bopp 1963. C. D. Bopp, et al., "Plastics," in Radiation Effects on Organic Materials, Academic Press, New York, 1963, eds. R. O. Bolt and J. G. Carroll.

- (6) Polymers with aromatic characteristics (polystyrene, polysulfone, polycarbonate, and polyethylene terephthalate and other polyesters)

Additional groupings include halogen-containing polymers and miscellaneous:

- (7) Polymers containing halogens (polyvinyl chloride, polychloroprene, chlorosulfonated polyethylene, polytetrafluoroethylene, polychlorotrifluoroethylene, chlorinated polyether, rubber hydrochloride, and polyvinylidene chloride).
- (8) Miscellaneous polymers (polyamides, ion-exchange resins, and others).

The maximum G values are summarized in Table 3.1-24.

3.1.4.1 Radiolysis of Hydrocarbon Polymers Containing Only Saturated C-C Bonds

Polymers included in this section are polyethylene, polypropylene, ethylene-propylene rubber, and polyisobutylene. The polymers in this group produce hydrogen as the principal radiolysis gas. Small amounts of other hydrocarbons are formed. The maximum $G(H_2)$ value is 4.0 for polyethylene; the maximum $G(\text{flam gas})$ value is 4.1 for polyethylene.

3.1.4.1.1 Polyethylene

Polyethylene has the repeat unit:



Polyethylene materials are generally divided into two classes: low-density polyethylene (LDPE) and high-density polyethylene (HDPE). Polyethylene bags and a 90-mil HDPE rigid drum liner are commonly used polyethylene products that are found in CH-TRU wastes. Unirradiated polyethylene softens in the range of 70 to 90°C, and melts to a viscous liquid at about 115 to 125°C (Spinks 1976³). Some of the G values and gas species produced by radiolysis of polyethylene depend on whether or not oxygen is present.

3.1.4.1.1.1 Radiolysis of Polyethylene in the Absence of Oxygen

When irradiated, polyethylene crosslinks in the absence of oxygen and evolves a considerable amount of gas (80-95% hydrogen along with other simple aliphatic hydrocarbons). The amount of volatile hydrocarbons produced by radiolysis of polyethylene increases while the hydrogen yield decreases, as the degree of chain branching increases. The evolution of hydrogen and hydrocarbon gases is accompanied both by an increase in unsaturation in the polymer chain and by an increase in crosslinking density (Chapiro 1962¹⁰).

Table 3.1-24 — Summary of Maximum G Values for Polymers at Room Temperature^a

Group ^b	Polymer	G(H ₂)	G(flam gas)	G(net gas) ^c
S-HC	polyethylene	4.0	4.1	4.1
	polypropylene	3.3	3.4	3.4
	ethylene-propylene	d	d	d
	polyisobutylene	1.6	2.4	2.4
Al	polyvinyl alcohol	3.1	3.1	3.1
	polyethylene glycol	3.5	3.5	3.5
Eth	cellulose	3.2	3.2	10.2
	cellulose nitrate	e	e	6.0 ^f
	urea formaldehyde	2.4	2.8	2.8
	polyoxymethylene	2.1	5.6	14.1
	polypropylene oxide	1.1	e	e ^f
	polyvinyl formal	e	e	5.6 ^f
U-HC	polybutadiene	0.5	0.5	0.5
	polyisoprene	0.7	0.9	0.9
Est	polymethyl methacrylate	0.4	2.0	4.1
	polyvinyl acetate	0.9	1.4	1.4
Ar	polystyrene	0.2	0.2	0.2
	polysulfone	0.1	0.1	0.1
	polycarbonate	<0.1	<0.1	0.8
	polyesters	0.3	0.3	<0.8
	polyphenyl methacrylate	<0.1	<0.1	1.3
Hal	polyvinyl chloride	0.7	0.7	2.6
	polychloroprene	0.1	0.1	0.7
	chlorosulfonated			
	polyethylene	0.3	0.3	0.6
	polychlorotrifluoroethylene	0	0	1.1
	polytetrafluoroethylene	0	0	<0.3
	chlorinated polyether	0.7	0.8	0.8
	rubber hydrochloride	0	0	<2.1
	polyvinylidene chloride	0	0	<2.1
M	polyamides	1.1	1.2	1.5
	ion-exchange resins	1.7	1.7	2.1

- Notes: ^aValues listed are those most appropriate for CH-TRU waste, i.e., above 10 Mrad absorbed dose or for commercial rather than for pure materials
- ^bS-HC = saturated hydrocarbon, Al = alcohol functional group, Eth = ether functional group, U-HC = unsaturated hydrocarbon, Est = ester functional group, Ar = aromatic character, Hal = halogen functional group, and M = miscellaneous
- ^cG(net gas) is the net G value, and includes depletion of oxygen when applicable
- ^dValues are intermediate between those for polyethylene and those for polypropylene
- ^eNot reported
- ^fCalculated on the basis of G(gas) = factor x G(gas) for polyethylene; factor=1.5 for cellulose nitrate, factor=1.4 for polyvinyl formal, and G(gas)=4.1 for polyethylene

Experimental measurements of G values from radiolysis of polyethylene in a vacuum, using reactor, gamma, accelerated electron, and x-ray radiation, are shown in Table 3.1-25 from Chapiro 1962¹⁰. Chapiro also plotted the data in an Arrhenius plot and found a temperature dependence with an activation energy of about 0.8 kcal/mole. From these data, Chapiro concluded that the G value for hydrogen at room temperature is about 4.1 and about 3.2 near the glass-transition temperature of -120°C. G values for volatile hydrocarbon formation were found to be usually less than 0.1. More recent experiments, discussed later in this section, have measured lower G(H₂) values, and a maximum G(H₂) value is established at G(H₂)=4.0.

One set of gamma irradiation experiments examined the effect of molecular weight on the G(H₂) value for crystalline samples of polyethylene in the absence of oxygen (Mandelkern 1972¹⁸). A maximum value of G(H₂)=4 was found for the higher molecular weights studied (2.5-4.5 x 10⁴); a G(H₂) value as low as 2.8 was found for the lowest molecular weight studied (2 x 10³).

Zerwekh (Zerwekh 1979¹³) contaminated pieces of LDPE bags (0.05 mm thick) with Pu-238 dissolved in 2-M HNO₃. In other experiments, pieces of the HDPE drum liner material (2.3 mm thick, 100% cross-linked) were contaminated with Pu-238 as chloride solution. The materials were allowed to dry, then placed into stainless steel cylinders. Gases were sampled and the pressure reduced to 1 psig when the pressure in a cylinder reached 15-17 psig. Almost all of the oxygen had been depleted by the time of first sampling. Gas compositions were determined using a mass spectrometer. The majority of the gas produced from LDPE in these alpha radiolysis experiments was hydrogen. The maximum G(gas) value measured for LDPE was 1.7.

The HDPE experiment, containing 62 mg of Pu-238, never pressurized to 15 psig (even after 1,300 days). At day 674, a gas sample was taken, and consisted of 5% H₂, 17% CO₂, and 77% N₂, with very small amounts of CH₄, O₂, and CO.

Kosiewicz (Kosiewicz 1981¹²) performed alpha radiolysis experiments on samples of commercial LDPE. The composition of the generated gas was 98% H₂, 1% CH₄, and 1% CO plus CO₂. Kosiewicz has reviewed his experimental data, and has corrected the originally published G values. The measured value of G(gas) was 2.0-2.4. Typically, 50 g of the material was cut into small squares onto which the TRU contaminant (Pu-238 or Pu-239 oxide powder) was distributed. A second piece of the test material was placed over the first to contain the plutonium. The initial atmosphere inside the experimental cylinders was air at local atmospheric pressure at Los Alamos of 77 kPa (11.2 psia). The gases in the cylinders were sampled and the pressures relieved when the pressure had increased to 100 kPa over ambient pressure. The rate of gas generation was calculated from the rate of pressure change. (This method results in an underestimate of the G values for generated gases while oxygen is present inside the experimental cylinder.)

Mitsui (Mitsui 1979⁵¹) measured gas generation from films made from Hizex 1200P polyethylene powder containing no antioxidant that were gamma irradiated in a vacuum. Values of G(H₂) obtained at different temperatures were 3.0 at 30°C, 3.2 at 50°C, 3.4 at 70°C, and 3.6 at

⁵¹ Mitsui 1979. H. Mitsui and Y. Shimizu, "Kinetic Study of the Gamma Radiolysis of Polyethylene," *J. Polym. Sci., Polymer Chem. Ed.* 17, pp. 2805-2813, 1979.

100°C. From these data the authors calculated an activation energy of 0.6 kcal/g-mole for formation of H₂.

Table 3.1-25 — Summary of G Values for Hydrogen and Methane for Radiolysis of Polyethylene in a Vacuum

Material ^a	Type of Radiation and Irradiation Temperature ^b	G(H ₂)	G(CH ₄)
LDPE	reactor (70°C)	4.0	0.08
LDPE	800 keV electrons	5.0	0.9
LDPE	reactor	5.0 ^c	--
LDPE	Co ⁶⁰ gamma	3.75	--
LDPE and HDPE	2 MeV electrons (-196°C to +80°C)	3.1	--
PE	Co ⁶⁰ gamma	4.0	--
PE	reactor (80°C)	7.0	--
HDPE	800 keV electrons		
Marlex-50 ^R	(-170 to 34°C)	3.75	0.07
Marlex-50 ^R	136°C	5.5	0.13
Marlex-50 ^R	240°C	5.8	0.17
LDPE	50 kV x-rays, 13°C	2.5	0.15
LDPE	50 kV x-rays, 80°C	3.0	0.36
HDPE	50 kV x-rays, 10°C	2.8	0.03
HDPE	50 kV x-rays, 80°C	3.0	0.09

Ref.: Chapiro 1962¹⁰, Table IX.I.

Note: ^aLDPE = low density polyethylene; HDPE = high density polyethylene. "High pressure" = "low density"; "low pressure" = "high density"; (Wiley 1986⁵²).

^bLiquid above about 130°C.

^cG(gas).

Kang (Kang 1966⁵³) measured G(H₂) values for polyethylene (Marlex-6002^R film) as a function of temperature and dose. The room temperature G(H₂) value varied from 3.7 (extrapolated to zero dose) to 3.3 (at an absorbed dose of 13 Mrad or more). A large increase in G value from 3.7 to 5.6 was observed when polyethylene was heated from room temperature to the liquid state at 140°C. The G(H₂) values extrapolated to zero dose for the temperatures studied were: 3.68 at room temperature, 3.73 at 60°C, 3.81 at 80°C, 4.05 at 100°C, and 4.11 at 120°C. (The values at 60 and 120°C yield an activation energy of 0.4 kcal/g-mole.)

⁵² Wiley 1986. The Wiley Encyclopedia of Packaging Technology. John Wiley & Sons, New York, 1986, ed. M. Bakker.

⁵³ Kang 1966. H. Y. Kang, et al., "The Radiation Chemistry of Polyethylene. IX. Temperature Coefficient of Cross-Linking and Other Effects," J. Am. Chem. Soc. **89**, pp. 1980-1986, 1966.

Krasnansky (Krasnansky 1961⁵⁴) performed gamma radiolysis experiments (6 Mrad absorbed dose) in vacuum on various commercial packaging materials. The measured value of G(gas) was reported to be between 1.6 and 3.2 for samples of both low- and high-density polyethylene. Both LDPE and HDPE generated 90-91% H₂ and 3% CO₂. The major difference in the observed gas composition was that the HDPE sample produced 6.5% CO and 0.5% propane, while the LDPE sample produced 2.5% propane, 2% ethane, and 1.5% ethene. The authors stated that the relatively high proportion of CO and CO₂ could have been a result of oxidation of the polyethylene prior to the irradiation.

Bowmer (Bowmer 1977⁵⁵) measured G values from two types of LDPE and one type of HDPE at 30 and 150°C using gamma irradiation in a vacuum of small (5-35 mg) or large (0.5-2.5 g) samples. For the small samples, the following G values were obtained at 30°C: HDPE, G(H₂)=2.9, G(HC)=0.01; LDPE-1, G(H₂)=3.5, G(HC)=0.09; LDPE-2, G(H₂)=3.1, G(HC)=0.1. Values for G(H₂) increased by about 11% for LDPE and 53% for HDPE when the irradiation temperature was changed from 30°C to 150°C.

G(H₂) values about 25% lower were observed for the large samples, even when they were heated at 150-200°C for 60-90 minutes to allow volatiles to escape from the materials (Bowmer 1977⁵⁴). This effect was attributed to reactions of double bonds and trapped polymer radicals with hydrogen atoms and molecules for the large samples, for which the hydrogen pressure was an order of magnitude higher than in the small samples.

G values for various gases generated from the irradiation of polyethylene when oxygen is absent or has been depleted are listed in Table 3.1-26 for experiments not reported by Chapiro (Chapiro 1962¹⁰). The highest value of G(H₂) in these experiments at room temperature was 4.0. The data listed in the table for Kosiewicz (Kosiewicz 1981¹²) are values that incorporate a correction for a calculational error in the original data, supplied by that author.

3.1.4.1.1.2 Radiolysis of Polyethylene in the Presence of Oxygen

In an early gamma radiolysis experiment, the change in the total gas pressure was measured for irradiation of high-density polyethylene in pure oxygen. The G value for oxygen consumption [G(-O₂)] was found to be at least twice the sum of the G values for oxygen-containing gas molecules. The rest of the oxygen was assumed to be converted to peroxides and hydroxyl groups in the polyethylene (Dole 1973a⁵⁶).

Relative amounts of gaseous products were measured for gamma irradiation of commercial samples of LDPE and HDPE in air and in vacuum up to 5.6 Mrad absorbed dose.⁵⁷ For both

⁵⁴ Krasnansky 1961. V. J. Krasnansky, et al., "Effect of Gamma Radiation on Chemical Structure of Plastics," SPE (Society of Plastics Eng.) Trans. 1, pp. 133-138, 1961.

⁵⁵ Bowmer 1977. T. N. Bowmer and J. H. O'Donnell, "Nature of the Side Chain Branches in Low Density Polyethylene: Volatile Products from Gamma Radiolysis," Polymer 18, pp. 1032-1040, 1977.

⁵⁶ Dole 1973a. M. Dole, "Oxidation of Irradiated Polymers," in The Radiation Chemistry of Macromolecules, Vol. II, Academic Press, New York, 1973, ed. M. Dole.

⁵⁷ Bersch 1959. C. F. Bersch, et al., "Effect of Radiation on Plastic Films," Modern Packaging 32, pp. 117-168, 1959.

low- and high-density polyethylene, greater amounts of products per gram of material were obtained for irradiation in air than in vacuum (a ratio of 2.0 for LDPE and 1.4 for HDPE). The corresponding ratios of hydrogen production in air versus in vacuum were 1.8 for LDPE and 1.2 for HDPE. The LDPE produced 1.6 times the gaseous products of the HDPE in air, and 1.2 times the products of HDPE in vacuum. The second most abundant product for irradiation in air was carbon dioxide. All of the oxygen in the sample tubes was consumed for both types of polyethylene films. The experiments were repeated for an absorbed dose of 0.93 Mrad. Radiolysis of the LDPE exposed to air generated only carbon dioxide, while the $G(H_2)$ value for HDPE was higher than at 5.6 Mrad. These results contradict trends observed in most other radiolysis experiments on polyethylene and lower the credibility of Bersch's data on polyethylene.

Arakawa⁵⁸ performed gamma radiolysis of low- and high-density polyethylene in the presence of oxygen to examine the effect of antirad additives. For the pure polymers, hydrogen and carbon dioxide were the primary gases evolved. For LDPE, values of $G(H_2)=3.3$ and $G(CO_2)=1.3$ were obtained; for HDPE, values of $G(H_2)=3.2$ and $G(CO_2)=4.1$ were measured. The addition of propyl-fluoranthene, an antirad additive, reduced the $G(H_2)$ values by 15-30%. Radiolysis of an ethylene-propylene copolymer showed that the $G(H_2)$ value was independent of the amount of oxygen present.

Table 3.1-26 — G Values for Polyethylene (Oxygen Depleted or Absent)

Radiation Type	G(Products)	Comments	Reference
gamma	$G(H_2)=6.2$ (max)	no oxygen, 130°C	(1)
gamma	$G(H_2)=2.8-4.0^a$	no oxygen, room temp	(1)
alpha (²³⁸ Pu)	$G(\text{gas})=1.7$ (90-98% H ₂)	oxygen depleted from initial air atmosphere; room temp	(2)
alpha (²³⁸ Pu)	$G(\text{gas})=2.0-2.4$ (98% H ₂ , 1% CH ₄ , 1% CO ₂ + CO)	oxygen depleted from initial air atmosphere; 20°C; corrected data	(3)
gamma	$G(H_2)=3.0$	vacuum; 30°C	(4)
gamma	$G(H_2)=3.2$	vacuum; 50°C	(4)
gamma	$G(H_2)=3.4$	vacuum; 70°C	(4)

⁵⁸ Arakawa 1983b. K. Arakawa, et al., "Radiation-Induced Oxidation of Polymers. Effect of Antioxidant and Antirad Agent on Oxygen Consumption and Gas Evolution," *J. Polym. Sci.: Polym. Chem. Ed.* **21**, 1983 (preprint).

Table 3.1-26 — G Values for Polyethylene (Oxygen Depleted or Absent) (Concluded)

Radiation Type	G(Products)	Comments	Reference
gamma	G(H ₂)=3.6	vacuum; 100°C	(4)
gamma	G(H ₂)=3.7	vacuum; 25°C to 60°C	(5)
gamma	G(H ₂)=3.8	vacuum; 80°C	(5)
gamma	G(H ₂)=4.05	vacuum; 100°C	(5)
gamma	G(H ₂)=4.11	vacuum; 120°C	(5)
gamma	1.6 G(gas) 3.2 (92% H ₂ , 2-8% CO+CO ₂ , 0-6% HC) ^b	vacuum; room temp	(6)
gamma	G(H ₂)=2.9;G(HC)=0.01 ^b	HDPE; vacuum; 30°C	(7)
gamma	G(H ₂)=4.5;G(HC)=0.03 ^b	HDPE; vacuum; 150°C	(7)
gamma	G(H ₂)=3.5;G(HC)=0.09 ^b	LDPE; vacuum; 30°C	(7)
gamma	G(H ₂)=3.9;G(HC)=0.18 ^b	LDPE; vacuum; 150°C	(7)
gamma	G(H ₂)=3.1;G(HC)=0.11 ^b	LDPE; vacuum; 30°C	(7)
gamma	G(H ₂)=3.5;G(HC)=0.36 ^b	LDPE; vacuum; 150°C	(7)

Refs.: (1) Mandelkern 1972¹⁸; (2) Zerwekh 1979¹³; (3) Kosiewicz 1981¹² (data corrected by that author); (4) Mitsui 1979⁵⁰; (5) Kang 1966⁵²; (6) Krasnansky 1961⁵³; (7) Bowmer 1977⁵⁴.

Notes: ^aValues were 3.9, 3.4, 3.6, 4.0, 3.9, 3.2, 3.4, and 2.8, depending on the molecular weight and degree of crystallinity.

^bHC = hydrocarbons.

Fourteen samples of polyethylene sheet used for bags (presumably LDPE) were gamma irradiated in the presence of oxygen (Kazanjian 1969³⁸). Hydrogen was the only significant product, and a value of $G(\text{H}_2)=2.2$ was obtained. Oxygen consumption occurred; a value of $G(-\text{O}_2)=8.1$ was measured.

Kazanjian (Kazanjian 1976³⁶) obtained radiolysis data during the time period when oxygen was being depleted for alpha radiolysis of LDPE bags contaminated with Pu-238 oxide powder (9.0 mg of Pu-238 to 3.6 g of material). The experiment was conducted for a total of 267 days, starting with an air atmosphere. The $G(\text{gas})$ and $G(\text{H}_2)$ values calculated from these data show sharp decreases with time from $G(\text{gas})=1.7$ to $G(\text{gas})=0.7$ and $G(\text{H}_2)=1.3$ to $G(\text{H}_2)=0.7$ after 36 days of exposure. This decrease in G values could have been caused by (1) a very strong dependence of the G values on absorbed dose, (2) much higher G values in the presence of oxygen, or (3) experimental error. The oxygen initially present had been completely depleted by day 21 ($5.8\text{E}22$ eV absorbed energy). The $G(-\text{O}_2)$ value was about 3. Only small quantities of CO or CO₂ were detected, with maximum G values of 0.1 and 0.3, respectively.

Polyethylene and polyethylene oxide were gamma irradiated in oxygen in the presence of carbon tetrachloride (Jellinek 1983¹⁵). In both cases, chloroform was evolved. The $G(\text{scission})$ values increased for polyethylene from about 10 in oxygen to about 32 in oxygen mixed with carbon tetrachloride.

G values for various gases evolved from the irradiation of polyethylene when oxygen is present are listed in Table 3.1-27. The maximum measured value of $G(\text{H}_2)$ at room temperature when oxygen was present was 3.5, with the exception of Bersch's (Bersch 1959⁵⁶) anomalous measurement of $G(\text{H}_2)=5.4$.

3.1.4.1.1.3 Hydrogen G Value for Polyethylene

Even at elevated temperature, almost all of the reported $G(\text{H}_2)$ values for polyethylene are less than 4.0. All of the $G(\text{H}_2)>4$ values that were found in the technical literature are for experiments conducted prior to 1962. The credibility of the experiments is questionable, as noted in the discussion, or the data were obtained using reactor radiation, where calculation of the absorbed dose is questionable. The available $G(\text{H}_2)$ data from alpha radiolysis experiments are in the 1.6-2.4 range. It is concluded that $G(\text{H}_2)=4.0$ and $G(\text{flam gas})=4.1$ for polyethylene provide upper bound $G(\text{H}_2)$ and $G(\text{flam gas})$ values for commercial polyethylene materials.

Table 3.1-27 — G Values for Polyethylene (Oxygen Present)

Radiation Type	G(Products)	Comments	Reference
gamma	G(-O ₂)=10.0, G(H ₂ O)=2.5, G(CO)=1.0, G(CO ₂)=0.6	30°C; only measured gases containing oxygen	(1)
gamma	G(H ₂)=2.2; G(-O ₂)=8.1	LDPE bags; room temp	(2)
gamma	G(gas)=5.3; G(H ₂)=3.5; G(-O ₂)=14.0; G(CO ₂)=1.3; G(CO)=0.6; G(CH ₄)=0.1	LDPE; room temp; pure material; 20 Mrad	(3)
gamma	G(gas)=3.9; G(H ₂)=2.8 G(-O ₂)=7.4; G(CO ₂)=0.9; G(CO)=0.2	LDPE; room temp; contained antirad additive; 20 Mrad	(3)
gamma	G(gas)=8.6; G(H ₂)=3.2 G(-O ₂)=29; G(CO ₂)=4.1; G(CO)=1.3	HDPE; room temp; pure material; 20 Mrad	(3)
gamma	G(gas)=5.6; G(H ₂)=2.2; G(-O ₂)=12.1; G(CO ₂)=2.8; G(CO)=0.6	HDPE; room temp; contained antirad additive; 20 Mrad	(3)
gamma	G(gas)=6.4; G(H ₂)=5.4; G(CO ₂)=0.6; G(CO)=0.1 ^a	LDPE; room temp; commercial material; 5.6 Mrad	(4)
gamma	G(gas)=3.9; G(H ₂)=3.1; G(CO ₂)=0.6 ^b	HDPE; room temp; commercial material; 5.6 Mrad	(4)
gamma	G(gas)=2.7; G(H ₂)=0; G(CO ₂)=2.7	LDPE; room temp; commercial material; 0.93 Mrad	(4)
gamma	G(gas)=8.5; G(H ₂)=4.0; G(CO ₂)=3.4; G(CO)=1.1	HDPE; room temp; commercial material; 0.93 Mrad	(4)
alpha (Pu-238)	G(gas)=1.7; G(H ₂)=1.3; G(-O ₂)=3; G(CO ₂)=0.3; G(HC)=0.1 ^b	LDPE bags; room temp; water vapor also detected.	(5)

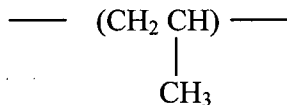
Refs.: (1) Dole 1973a⁵⁵, (2) Kazanjian 1969³⁷, (3) Arakawa 1983b⁵⁷; (4) Bersch 1959⁵⁶; (5) Kazanjian 1976³⁶.

Notes: ^aWater vapor, oxygenated hydrocarbons and unsaturated hydrocarbons also were detected.

^bCalculated from author's data; HC = hydrocarbons; maximum G values are given.

3.1.4.1.2 Polypropylene

Polypropylene has the repeat unit:



Polypropylene is termed isotactic if the methyl groups are on the same side of the chain, and atactic if the arrangement is random. The isotactic polymer is the more common commercially (Bopp 1963⁴⁹).

Polypropylene may be manufactured into fibers (Herculon^R is one example) or into molded shapes. Ful-Flo^R filters used at the RFETS for filtering liquid wastes are made of polypropylene.

The maximum G values for hydrogen and total flammable gas are G(H₂)=3.3 and G(flammable gas)=3.4.

3.1.4.1.2.1 Radiolysis of Polypropylene in the Absence of Oxygen

Hydrogen is the major gas produced from the gamma irradiation of polypropylene in a vacuum at room temperature, as shown in Table 3.1-28. Traces of methane and carbon monoxide are also found (Schnabel 1963⁵⁹).

Polypropylene and other polymers have been gamma irradiated in the presence of carbon tetrachloride or chloroform in order to modify the polymer (Ramanan 1981⁶⁰). When polypropylene fibers were immersed in carbon tetrachloride, generated HCl gas was collected by cooling the irradiated ampoules to 77 K and then breaking them under distilled water. The HCl released was estimated by following the change in pH. High yields of HCl were measured (Ramanan 1981⁶⁰).

3.1.4.1.2.2 Radiolysis of Polypropylene in the Presence of Oxygen

Hegazy (Hegazy 1981a⁶¹) measured a G value for oxygen consumption of about 4 for oxidative radiolysis of isotactic polypropylene (PP) film at ambient temperature and 150 torr initial oxygen pressure (which approximates the oxygen partial pressure in ambient air). The sum of the G values for production of oxygen containing gases (CO₂ and CO) was less than 0.3, suggesting that most of the consumed oxygen had combined with polymer chains.

Table 3.1-29 lists G values for radiolysis of polypropylene in the presence of oxygen.

⁵⁹ Schnabel 1963. W. Schnabel and M. Dole, "Radiation Chemistry of Isotactic and Atactic Polypropylene. I. Gas Evolution and Gel Studies," *J. Phys. Chem.* 67, pp. 295-299, 1963.

⁶⁰ Ramanan 1981. G. Ramanan, et al., "Gamma Irradiation of Polypropylene Fibers in the Presence of Carbon Tetrachloride," *J. Appl. Polym. Sci.* 26, pp. 1439-1451, 1981.

⁶¹ Hegazy 1981a. E. A. Hegazy, et al., "Radiation-Induced Oxidative Degradation of Isotactic Polypropylene," *J. Appl. Polym. Sci.* 26, pp. 1361-1372, 1981.

Table 3.1-28 — G Values for Polypropylene (Oxygen Absent)

Radiation Type	G(Products)	Comments	Reference
gamma	G(gas)=2.4-2.9 G(H ₂)=2.3-2.8, G(CH ₄)=0.1	vacuum; room temp; atactic and isotactic PP	(1)
gamma	G(gas)=3.0; G(H ₂)=2.9; G(CH ₄)=0.1	vacuum; 10 Mrad; room temp; isotactic PP film	(2)
gamma	G(gas)=3.5; G(H ₂)=3.3; G(CH ₄)=0.1	vacuum; 10 Mrad; room temp; isotactic PP powder	(2)
gamma	G(gas) 3.2; (95% H ₂ , 1% CO ₂ , 1% CO, 3% CH ₄)	vacuum; room temp; film	(3)
gamma	G(gas)=3.8; G(H ₂)=3.2; G(CH ₄)=0.1 ^a	vacuum; 0.1 MGy (10 Mrad); room temp; stabi- lized isotactic PP film	(4)
gamma	G(gas)=3.0; G(H ₂)=2.8; G(CH ₄)=0.1 ^a	vacuum; 0.2 MGy (20 Mrad); room temp; stabi- lized isotactic PP film	(4)

Refs.: (1) Geymer 1973⁶²; (2) Hegazy 1981a⁶¹; (3) Krasnansky 1961⁵³; (4) Hegazy 1986⁶³.

Note: ^a Author's G values for gas constituents do not add up to his G(gas) value.

⁶² Geymer 1973. D. O. Geymer, "Radiation Chemistry of Substituted Vinyl Polymers. Polypropylene," in The Radiation Chemistry of Macromolecules, Vol. II, Academic Press, New York, 1973, ed. M. Dole.

⁶³ Hegazy 1986. E. A. Hegazy, et al., "Radiation Effect on Stabilized Polypropylene," Radiat. Phys. Chem. 27, pp. 139-144, 1986.

Table 3.1-29 — G Values for Polypropylene (Oxygen Present)

Radiation Type	G(Products)	Comments	Reference
gamma	G(gas)=3.0; G(H ₂)=2.5; G(CH ₄)=0.1; G(CO)=0.1; G(CO ₂)=0.2, G(-O ₂)=4.2	150 torr O ₂ initial pressure; 20 Mrad; room temp; isotactic PP film	(1)
gamma	G(gas)=2.9; G(H ₂)=2.6; G(CH ₄)=0.1; G(CO)=0.1 G(CO ₂)=0.2; G(-O ₂)=5.0 ^a	150 torr O ₂ initial pressure; 0.2 MGy (20 Mrad); stabilized isotactic PP film	(2)

Refs.: (1) Hegazy 1981a⁶¹; (2) Hegazy 1986⁶³.

Note: ^aAuthor's G values for gas constituents do not add up to his G(gas) value.

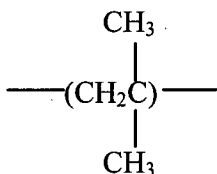
G(scission) values increased for polypropylene from about 5 in oxygen to about 33 in oxygen mixed with carbon tetrachloride vapor (Jellinek 1983¹⁵); chloroform was evolved.

3.1.4.1.3 Ethylene-Propylene Rubber

G values for ethylene-propylene rubbers (EPR, EPDM) are close to G values for polyethylene and polypropylene (Arakawa 1983b⁵⁷, Arakawa 1987⁶⁴, Decker 1973⁶⁵).

3.1.4.1.4 Polyisobutylene

The repeat unit for polyisobutylene is:



Bohm (Bohm 1982⁶⁶) summarized several radiolysis experiments conducted on polyisobutylene. The composition of the gas evolved from polyisobutylene during gamma radiolysis experiments conducted in vacuum was approximately 95% hydrogen and methane, with the remainder composed of isobutylene and other fragments. Values of G(H₂)=1.3-1.6 and G(CH₄)=0.5-0.8 have been reported for gamma radiolysis experiments. A G(gas) value of only 0.9 was measured for mixed reactor radiation. Gas production in polyisobutylene is attributed to the fracture of side chains.

⁶⁴ Arakawa 1987. K. Arakawa, "Oxygen Consumption and Gas Evolution by Radiation-Induced Oxidation in Ethylene-Propylene-Diene Terpolymers," *J. Polym. Sci.: Part A: Polym. Chem.* **25**, pp. 1713-1716, 1987.

⁶⁵ Decker 1973. C. Decker, et al., "Aging and Degradation of Polyolefins. III. Polyethylene and Ethylene-Propylene Copolymers," *J. Polym. Sci.: Polym. Chem. Ed.* **11**, pp. 2879-2898, 1973.

⁶⁶ Bohm 1982. G. Bohm, "Radiation Chemistry," *Rubber Chem. Tech.* **55**, pp. 575-666, 1982.

3.1.4.2 Radiolysis of Polymers Containing Alcohol Functional Groups

Polymers containing alcohol functional groups include polyvinyl alcohol and polyethylene glycol.

Gas generation from polyvinyl alcohol that was gamma irradiated in a vacuum at 12°C, -78°C, and -196°C was measured by Okada (Okada 1967⁶⁷). Over 99% of the gas evolved was hydrogen. G(gas) values were measured to be 3.1 at 12°C, 2.0 at -78°C, and 1.5 at -196°C (maximum activation energy = 0.6 kcal/g-mole). [The corresponding G(gas) value at 25°C would be unchanged from the value at 12°C because of the low activation energy for gas generation.]

Polyethylene glycol (commercial name, Carbowax), having a molecular weight of 6,000, was irradiated using Co-60 gamma rays in a vacuum at room temperature (Nitta 1959⁶⁸). The maximum G(gas) value measured was 3.5. The gas consisted primarily of hydrogen with some methane, acetylene, and carbon monoxide. Experiments conducted on a 4,000-molecular-weight Carbowax at various temperatures showed only a minor change in the G(gas) value from -196°C to 70°C (2.4 to 2.1) (Nitta 1961b⁶⁹).

3.1.4.3 Radiolysis of Polymers Containing Ether Functional Groups

Polymers containing ether functional groups include cellulose, urea formaldehyde, polyoxymethylene, polypropylene oxide, and polyvinyl formal. The polymers in this group generate gases that contain oxygen, even when irradiated in a vacuum. Another polymer in this group is polyethylene oxide. G values for cellulose and urea formaldehyde have been shown to be strongly dependent on the absorbed dose, at least for gamma radiolysis. For absorbed doses greater than 10 Mrad, the maximum value of G(H₂) is 3.2 for cellulose. One of the polymers in this family (polyoxymethylene) generates other flammable gases that cause the G(flam gas) value to exceed 4.1, and another (polyvinyl formal) has a measured G(gas) that is 1.4 times the G(gas) value for polyethylene. For this reason, polyoxymethylene and polyvinyl formal are permitted in CH-TRU wastes only in trace amounts.

3.1.4.3.1 Cellulose

Cellulose is a linear macromolecule consisting of monomeric units with the empirical formula C₆H₁₀O₅. Cellulosic materials commonly present in the CH-TRU wastes include paper, cloth, wood, and Benelex^R, which is composed of wood fiber plus phenolic resin. Other commercial materials that contain cellulose include cellophane, cellulose acetate (used to manufacture Rayon^R, molded items, paints, coatings), and ethyl cellulose (used to manufacture paints, molded items).

⁶⁷ Okada, 1967. T. Okada, "Radiolysis of Poly (Vinyl Alcohol)," in Annual Report of the Japanese Assn. for Radiation Research on Polymers, Vol. 8, pp. 33-43, 1967.

⁶⁸ Nitta 1959. I. Nitta, et al., "Irradiation Effects of Co-60 Radiation on Polyethylene Glycol," in Annual Report of the Japanese Assn. for Radiation Research on Polymers, Vol 1., pp. 320-328, 1959.

⁶⁹ Nitta 1961b. I. Nitta, et al., "Effect of Radiation on Polyethylene Glycol," in Annual Report of the Japanese Assn. for Radiation Research on Polymers, Vol. 3, AEC-tr-6372, pp. 445-453, 1961.

Natural cotton cellulose, having lattice type I, is about 70-80% crystalline and 20-30% amorphous. The other commercially important form of cellulose has lattice Type II, which is commonly referred to as mercerized cotton, and usually consists of regenerated cellulosic materials, paper, and wood products. Cellulose lattice type II is less ordered than cellulose lattice type I and is usually about 60% crystalline.⁷⁰ Differences between these types of cellulose may cause differences in the amount and composition of radiolysis gases.

Authors differ as to whether the presence of oxygen affects the radiation chemistry of cellulose. The results of experiments conducted both in the absence and presence of oxygen are summarized at the end of this section.

Sulfite cellulose, dried to a constant weight at 378 K, was irradiated using Co-60 in sealed, evacuated ampules of known volume, as well as in a medium of air and argon (Ershov 1986⁷¹). The experimental data for each of the media were not reported. The authors stated that the irradiation medium did not appreciably affect the rate at which the products were generated. The dose rate was 20 kGy/h (2 Mrad/h). The volume of gas generated was determined according to the pressure in the ampules. For total absorbed doses from 100-300 kGy (10-30 Mrad) and room temperature, a value of $G(\text{gas})=10.2$ (31% H₂, 59% CO₂, 9% CO, and 1% CH₄) was observed. At liquid nitrogen temperature of 77 K, a value of $G(\text{gas})=6.0$ (48% H₂ and 52% CO₂) was observed.

Concentrations of radiolytically generated carboxyl, carbonyl, and aldehyde groups were measured using thin-layer chromatography for samples of powdered native cellulose that were gamma irradiated in air and in a vacuum (Dziedziela 1984⁷²). No gases were measured. Some of the samples were outgassed for four days before irradiation. In all cases, yields of functional groups increased linearly with absorbed dose, indicating constant G values. For each functional group, the samples irradiated in a vacuum display two straight-line portions, with the low-dose part of the graph coincident with the straight line found for irradiation in oxygen. The authors attribute this effect to traces of oxygen from air still left in the samples, in spite of outgassing, and conclude that formation of functional groups occurs according to the same mechanism as in air up to the exhaustion of oxygen absorbed on the surface of the cellulose. For each functional group, the slope of the second line is much lower, indicating a lower G value in the absence of oxygen. The ratio of the G value in air to the G value in a vacuum for each of the functional groups was equal to 3:1.

⁷⁰ Arthur 1970. J. C. Arthur, Jr., "Graft Polymerization onto Polysaccharides," in Advances in Macromolecular Chemistry 2, Academic Press, London, 1970, ed. by W. M. Pasika, pp. 1-87.

⁷¹ Ershov 1986. B. G. Ershov, et al., "Mechanism of the Radiation Chemical Conversions of Cellulose," translated from Khimiya Vysokikh Energii 20, pp. 142-147, 1986.

⁷² Dziedziela 1984. W. M. Dziedziela and D. Kotynska, "Functional Groups in Gamma-Irradiated Cellulose," Radiat. Phys. Chem. 23, pp. 723-725, 1984.

Cotton cellulose was irradiated under oxygen or nitrogen atmosphere with Co-60 in the dose range 0-130 kGy (0-13 Mrad) (Bludovsky 1984⁷³). The yields of the nongas radiolytic products were measured. The samples were analyzed immediately after irradiation to eliminate any effects of reactions occurring after the irradiation. No differences were observed in the qualitative composition of the products between those produced in nitrogen versus those produced in oxygen atmosphere. In all cases the presence of oxygen increased the yields of radiolytic products. The ratios of the yields varied from nearly 1 up to 1.7. The ratio of the chain scission G value in oxygen to the chain scission G value in nitrogen was 1.3.

Arthur (Arthur 1970⁷⁰) reports the G values for gamma irradiation of cotton cellulose I at absorbed doses of 14E20-42E20 eV/g (22-67 Mrad) in vacuum, oxygen, air, and nitrogen atmospheres. The three measurements in a nitrogen atmosphere at different doses show a total absorbed dose effect, with the G(gas) value reduced from 4.5 at 22E20 eV/g (35 Mrad) to 4.0 at 38E20 eV/g (61 Mrad). All of the difference in G values comes from changes in the G(CO) value with absorbed dose. [The ratio of the G values for carbon-containing gases generated in air or oxygen to the values for gases generated in nitrogen at low dose is about 1.4, which agrees with the data of Bludovsky (Bludovsky 1984⁷³). However, significant differences were seen in the gas composition.]

In one experiment (Dalton 1963⁷⁴), samples of purified American cotton weighing 0.1-2 g were outgassed at 60°C, and electron irradiation was conducted in a vacuum at ambient temperature. The evolved gas consisted almost entirely of hydrogen. A G value near 2 was obtained at (relatively) high doses (75-400 Mrad), while the G value near 6 was obtained at 0.1 Mrad. A G value of about 3 was obtained at 5 Mrad. As discussed in Section 2.3.1.5, the dose experienced by plastics or paper irradiated by Pu-238 or Pu-239 alpha particles is at least 22-23 Mrad. Therefore, the G value of 6 measured for 0.1 Mrad absorbed dose is not applicable to CH-TRU wastes.

Purified American cotton samples were also irradiated in a vacuum without outgassing, and a gas mixture of 82% H₂, 5% CO, and 13% CO₂ was obtained. A value for G(gas) was not reported for that experiment (Dalton 1963⁷⁴). The difference in the gas composition was attributed to oxidation processes involving residual oxygen dissolved in the material.

Kazanjian (Kazanjian 1976³⁶) measured gas consumption and generation from Pu-238 alpha irradiation of both wet and dry Kimwipes^R (paper tissues). The Kimwipes^R were cut up, and the plutonium oxide powder was added to the material in increments and the mixture shaken or stirred in a container. The wet Kimwipes^R contained 11.9 g of water to 4.8 g of paper tissues. The initial atmosphere was air.

⁷³ Bludovsky 1984. R. Bludovsky, et al., "The Influence of Oxygen on the Radiolytical Products of Cellulose," *J. Radioanal. Nucl. Chem. Letters* 87, pp. 69-80, 1984.

⁷⁴ Dalton 1963. F. L. Dalton, et al., "Gas Yields from Electron-Irradiated Cotton Cellulose," *Nature* 200, pp. 862-864, 1963.

G values were calculated using Kazanjian's data for both dry and wet Kimwipes^R. In both cases, the G values decreased as the dose increased. G(gas) decreased from about 1.1 initially to about 0.5 at 6.0E23 eV for dry Kimwipes^R, and from about 0.6 initially to about 0.3 at 4.5E23 eV absorbed dose for wet Kimwipes^R. All of the G values were significantly lower for wet Kimwipes^R compared to the values for dry Kimwipes^R. This is attributed to some of the alpha decay energy being absorbed by water rather than by the cellulose.

The composition of the evolved gas from wet Kimwipes^R was richer in hydrogen than for dry Kimwipes^R (73% vs. 55%) with smaller concentrations of hydrocarbons. The graphs of moles of evolved gas versus time remained approximately linear until oxygen was depleted, then began to decrease in slope. This could be caused by an absorbed dose effect or lower G values in the absence of oxygen.

Zerwekh (Zerwekh 1979¹³) performed alpha radiolysis experiments on two different mixtures of cellulosic materials, one dry mixture and one wet mixture. The dry mixture consisted of paper wipes, paper tissues, embossed paper towel with polyethylene backing, cheesecloth, and cotton laboratory smock material. The final composition of the evolved gas from the dry mixture contained about 60% H₂, 25% CO₂, plus a small amount of CH₄ [estimated from Figure 10 of Zerwekh (Zerwekh 1979¹³)]. The initial composition of the evolved gas contained higher concentrations of CO₂, up to a maximum of about 50%. The wet mixture consisted of damp cheesecloth contaminated with Pu-238 as chloride solution. The final composition of the evolved gas contained about 55% H₂ and 35% CO₂ [estimated from Figure 13 of Zerwekh (Zerwekh 1979¹³)]. The initial composition of the evolved gas contained about 85% H₂ and 5% CO₂. The high initial concentration of H₂ may indicate that radiolysis of the water dominated early in the experiment, but radiolysis of the cheesecloth dominated near the end of the experiment (1,000 days). G(gas) values for dry cellulosic materials fell to about half of their initial values after about 750 days (1.2E25 eV absorbed energy).

In one of Zerwekh's experiments, gas generation from two identical cylinders was compared, where one cylinder was sampled and the pressure relieved at 15 psig, and the other one sampled and the pressure relieved only when the pressure reached 100 psig. From a plot in Zerwekh 1979¹³, the rate of gas pressure buildup in the low-pressure cylinder was about twice the rate of gas pressure buildup in the high-pressure cylinder. The evolved gases had the same composition, but water was also found in the high-pressure cylinder.

Bibler (Bibler 1976¹⁹) conducted alpha radiolysis experiments using Cm-244 solution (5-M nitric acid), which was absorbed by paper tissue that was dried and folded to surround the Cm-244 deposit. The evolved gas collected at constant pressure consisted of 49% H₂, 36% CO₂, and 15% CO. The value of G(gas) decreased to G(gas)=0.6 at 2.5E23 eV absorbed dose. A value of G(gas)=1.9 was measured during the first five hours of one experiment, with the first measurement taken at about 4E19 eV absorbed dose. Three different concentrations of Cm-244, up to a factor of 4 difference, were used in the experiments, and all observations appeared to fit the same curve of G(gas) versus absorbed dose.

Kosiewicz (Kosiewicz 1981¹², corrected) measured G(gas) values of about 1.9 at very low absorbed dose and about 1.5 from paper at a total absorbed dose of about 5E23 eV. The G(gas)

value decreased to half its initial value after an absorbed dose of about $2.5E24$ eV. The radiolytic gas composition was about 61% H_2 , 26% CO_2 , and 13% CO and nearly independent of total absorbed dose. Oxygen was initially present, but was rapidly depleted. Water vapor was not measured. Typically, 50 g of the material was cut into 1.5- to 3.0-cm squares onto which the finely divided plutonium dioxide (either Pu-239 or Pu-238) was distributed. A second piece of the test material was placed over the first to sandwich the plutonium particles. The sample vessel was a stainless steel cylinder instrumented with a pressure gauge or transducer. The gases in the cylinders were sampled and the pressures relieved when the pressure had increased to 100 kPa over the ambient pressure.

One set of experiments on paper was conducted in an argon atmosphere to measure the initial $G(\text{gas})$ value (at low dose) (Kosiewicz 1981¹², corrected). Data points started at absorbed dose as low as about $0.5E23$ eV, for 0.016 Ci of Pu-238 per g of waste. A $G(\text{gas})$ value of 1.4 was estimated. A similar experiment with air as the initial atmosphere reached a maximum $G(\text{gas})=1.4$ at about $4E23$ eV. The first measured value of $G(\text{gas})$ was about 30% lower than the maximum value, probably because oxygen depletion was occurring.

Zerwekh (Zerwekh 1979¹³) measured the rate of gas evolution from mixed cellulosic materials at -13°C , 20°C , and 55°C to be 2.59 kPa/day, 3.45 kPa/day, and 4.93 kPa/day, respectively. The composition of the evolved gas was generally independent of temperature (although the experiment at 55°C also generated a gaseous component of molecular weight about 60). After corrections for thermal expansion of the gas, the activation energy calculated from these data by this author ranges from 0.8 kcal/mole (-13°C , 20°C) to 1.3 kcal/g-mole (20°C , 55°C).

Kosiewicz (Kosiewicz 1981¹²) also performed experiments to measure the temperature dependence of radiolysis of cellulosic materials, represented by paper. High dose rates ($640E5$ nCi/g) were used so that radiolysis would produce the majority of the gas and other potential modes of gas generation, such as thermal degradation, could be neglected. The rate of gas evolution was measured for experiments conducted at both 20 and 70°C . The higher temperature experiment initially had a rate of gas evolution that was 70% greater than for the lower temperature experiment. The difference in the rate of gas evolution was observed to decrease with increasing dose. At $180E23$ eV absorbed dose, the difference had decreased to about 30%. (The activation energy for a 70% or 30% increase would be 2.1 kcal/g-mole or 1.0 kcal/g-mole, respectively.) The composition of the evolved gases was not significantly different for the two experiments.

Table 3.1-30 presents a summary of G values for several cellulosic materials when oxygen is absent or has been depleted. Table 3.1-31 presents the results of irradiation experiments conducted when oxygen is present.

Table 3.1-30 — G Values for Cellulosic Materials (Oxygen Absent or Depleted)

Material/Radiation Type	G(Products)	Comments	Reference
<u>Sulfite cellulose</u> gamma	G(gas)=10.2; G(H ₂)=3.2 (31% H ₂ , 59% CO ₂ , 9% CO, 1% CH ₄)	vacuum, air, or oxygen; room temp; 10-30 Mrad	(1)
<u>Cotton cellulose I</u> gamma	G(gas)=3.7; G(H ₂)=1.3 (35% H ₂ , 22% CO, 43% CO ₂)	vacuum; room temp; 33E20 eV/g (53 Mrad)	(2)
gamma	G(gas)=4.5; G(H ₂)=1.0 (22% H ₂ , 56% CO, 22% CO ₂)	nitrogen; room temp; 22E20 eV/g (35 Mrad)	(2)
gamma	G(gas)=4.1; G(H ₂)=1.0 (24% H ₂ , 51% CO, 24% CO ₂)	nitrogen; room temp; 32E20 eV/g (51 Mrad)	(2)
gamma	G(gas)=4.0; G(H ₂)=1.0 (25% H ₂ , 50% CO, 25% CO ₂)	nitrogen; room temp; 38E20 eV/g (61 Mrad)	(2)
<u>American cotton</u> electrons	G(gas) 6; G(H ₂) 6	vacuum + outgassing; room temp; 0.1 Mrad	(3)
electrons	G(gas)~3; G(H ₂)~3	vacuum + outgassing; room temp; 5 Mrad	(3)
electrons	G(gas)~2.5; G(H ₂)~2.5 (98% H ₂ , 1% CO, 0.4% CO ₂)	vacuum + outgassing; room temp; 25 Mrad	(3)
electrons	G(gas)=2.0	vacuum + outgassing; room temp; 75-100 Mrad	(3)
electrons	G(gas) not reported (82% H ₂ , 5% CO, 13% CO ₂)	vacuum w/o outgassing; room temp; 48 Mrad	(3)
<u>Mixed cellulose (dry)</u> alpha (Pu-238)	G(gas)~0.5; G(H ₂)~0.3 (60% H ₂ , 25% CO ₂ , 15% misc) ^a	oxygen depleted from initial air atmosphere; room temp; after 1,000 days of exposure	(4)
<u>Cheesecloth (wet)</u> alpha (Pu-238)	G(gas)~1.3; G(H ₂)~0.7 (55% H ₂ , 35% CO ₂ , 10% misc) ^a	oxygen depleted from initial air atmosphere; room temp; after 1,000 days of exposure	(4)
<u>Paper</u> alpha (Pu-238, -239)	G(gas) 1.5; G(H ₂) 0.9 (61% H ₂ , 26% CO ₂ , 13% CO)	oxygen depleted from initial air atmosphere; room temp; 3E23eV for 50 g material; corrected data	(5)
<u>Paper</u> alpha (Pu-238, -239),	G(gas)=1.44	argon; room temp; corrected data	(5)

Refs.: (1) Ershov 1986⁷¹; (2) Arthur 1970⁷⁰; (3) Dalton 1963⁷⁴; (4) Zerwekh 1979¹³; (5) Kosiewicz 1981¹²,
corrected.

Note: ^aEstimated from author's data.

Table 3.1-31 — G Values for Cellulosic Materials (Oxygen Present)

Radiation Type	G(Products)	Comments	Reference
<u>Cotton cellulose I</u>			
gamma	G(gas)=6.2; G(H ₂)=1.2 (19% H ₂ , 27% CO, 55% CO ₂)	oxygen; 42E20 eV/g (67 Mrad); room temp	(1)
gamma	G(gas)=5.5; G(H ₂)=0.7 (13% H ₂ , 60% CO, 27% CO ₂)	air; 14E20 eV/g (22 Mrad); room temp	(1)
<u>Mixed cellulotics (dry)</u>			
alpha (Pu-238)	G(gas)~1.6; G(H ₂)~0.6 (40% H ₂ , 40% CO ₂ ; (20% misc) ^b	air; room temp first measurement that was taken	(2)
<u>Cheesecloth (wet)</u>			
alpha (Pu-238)	G(gas)~1.6; G(H ₂)~1.4 (85% H ₂ , 5% CO ₂ , 10% misc) ^b	air; room temp; first measurement that was taken	(2)
<u>Kimwipes^R (dry)</u>			
alpha (Pu-238)	G(gas)=1.1; G(H ₂)=0.6 (55% H ₂ , 9% CO, 32% CO ₂ , 3% HC) ^a	air; room temp	(3)
<u>Kimwipes^R (wet)</u>			
alpha (Pu-238)	G(gas)=0.6; G(H ₂)=0.4 (73% H ₂ , 5% CO, 22% CO ₂) ^a		(3)
<u>Paper tissue</u>			
alpha (Cm-244)	G(gas) 1.9; G(H ₂) 0.9 (49% H ₂ , 36% CO ₂ , 15% CO)	air; room temp	(4)

Refs.: (1) Arthur 1970⁷⁰; (2) Zerwekh 1979¹³; (3) Kazanjian 1976³⁶; (4) Bibler 1976¹⁹.

Note: ^aCalculated from author's data.

^bEstimated from author's data.

3.1.4.3.2 Urea-Formaldehyde

Urea-formaldehyde has been examined as a possible solidification medium for power reactor wastes (Colombo 1977⁷⁵). Gamma radiolysis experiments in vacuum were conducted on a urea-

⁷⁵ Colombo 1977. P. Colombo and R. M. Neilson, Jr., "Properties of Radioactive Wastes and Waste Containers, Quarterly Progress Report July-September 1976," Brookhaven National Laboratory Associated Universities, Inc., BNL-NUREG-50617, 1977.

formaldehyde formulation using Borden Casco-Resin 2^R that was catalyzed with a 25 wt% solution of sodium bisulfate in water. Measured values of G(gas) and G(H₂) were strongly dose-dependent: at 0.1 Mrad, G(gas)=21 and G(H₂)=4.8; at 1 Mrad, G(gas)=8.6 and G(H₂)=6.5; at 10 Mrad, G(gas)=2.8 and G(H₂)=2.4, and at 100 Mrad, G(gas)=2.0 and G(H₂)=1.3

3.1.4.3.3 Polyoxymethylene

Krasnansky (Krasnansky 1961⁵³) measured gas evolution from plastic films exposed to gamma radiation to determine their order of radiation stability. Polyacetyl (polyoxymethane) had a value of G(gas) 8.1 for an absorbed dose of 6 Mrad. For that polymer, the gas consisted of 69% CO₂, 8% H₂, 2% methanol, 15% methane, and 6% dimethyl ether. (The minimum G value for all flammable gases would be about 5.6.)

Dole (Dole 1973d⁷⁶) reported analysis (by gas chromatography) of the gas evolved from electron irradiation of polyoxymethylene at 30°C and 0.1 torr pressure. In addition to hydrogen [G(H₂)=1.7], formaldehyde [G(HCHO)=4], methane [G(CH₄)=0.1], carbon monoxide [G(CO)=0.1] and various oxygen-containing gases were detected. Gases excluded were oxygen, carbon dioxide, C₂ hydrocarbons, methanol, dimethyl ether, and butyl alcohol.

Sobashima (Sobashima 1959⁷⁷) measured G values for gas generation from polyoxymethylene (Delrin 500X from DuPont) exposed to gamma irradiation in vacuum at room temperature. The G(gas) value measured was 14.1 at low doses. The gas composition was the following: 15% H₂, 67% CO₂, 1% CO, 10% CH₄, 1% methyl formate, 2% methyl ether, and 3% other. The maximum G value for flammable gases or vapors would be 4.4. The G(gas) values measured at different irradiation temperatures were G(gas)=6.1 at -196°C, G(gas)=9.4 at 20°C, and G(gas)=22.7 at 50°C (Nitta 1961a⁷⁸).

3.1.4.3.4 Polypropylene Oxide

Polypropylene oxide is more susceptible to degradation under irradiation than polypropylene, and yields less hydrogen (Geymer 1973⁶²). For irradiation in vacuum, measured G values for H₂, CH₄, and CO were 1.0, 0.1, and 0.3 for atactic polypropylene oxide, and 1.1, 0.1, and 0.4 for isotactic polypropylene oxide, respectively. G values for other oxygen-containing gases were not discussed. Measured G(OH) values were 1.8 for atactic polypropylene oxide and 1.7 for isotactic polypropylene oxide, compared to a value of 4.5 for polyoxymethylene.

3.1.4.3.5 Polyvinyl Formal

Polyvinyl formal was one of the many commercial plastics irradiated by Bopp and Sisman using the Oak Ridge National Laboratory (ORNL) Graphite Reactor (see Section 3.1.4.8.4 for more

⁷⁶ Dole 1973d. M. Dole, "Polyoxymethylene," in The Radiation Chemistry of Macromolecules, Vol. II, Academic Press, New York, 1973, ed. M. Dole.

⁷⁷ Sobashima 1959. S. Sobashima, et al., "Irradiation Effects on Polyoxymethylene," in Annual Report of the Japanese Assn. for Radiation Research on Polymers, Vol. 1, AEC-tr-6231, pp. 329-338, 1959.

⁷⁸ Nitta 1961a. I. Nitta, et al., "Effect of Radiation on Polyoxymethylene," in Annual Report of the Japanese Assn. for Radiation Research on Polymers, Vol. 3, AEC-tr-6372, pp. 437-443, 1961.

details). The value of G(gas) measured for polyvinyl formal was 1.4 times the value of G(gas) measured for polyethylene.

3.1.4.4 Radiolysis of Hydrocarbon Polymers Containing Unsaturated C-C Bonds

Polybutadiene and polyisoprene (Latex^R) contain unsaturated C-C bonds. The G values for polybutadiene (and copolymers) and polyisoprene (Latex^R) are given in Table 3.1-32.

Table 3.1-32 — G Values for Polybutadiene (and Copolymers) and Polyisoprene

Material/Radiation Type	G(Products)	Comments	Reference
<u>Polybutadiene and copolymers</u> gamma, electrons, and reactor	G(gas) 0.5; G(H ₂ +CH ₄) 0.5	vacuum or air; room temp	(1)
<u>Latex^R gloves</u> alpha (Pu-238)	G(gas)=0.4;G(H ₂)=0.4	oxygen depleted; room temp	(2)
<u>Isoprene^R gloves</u> alpha (Pu-238)	G(gas)<0.9;G(H ₂)<0.7 ^a	oxygen depleted; room temp	(3)

Refs.: (1) Bohm 1973⁷⁹; (2) Kazanjian 1976³⁶; (3) Zerwekh 1979¹³.

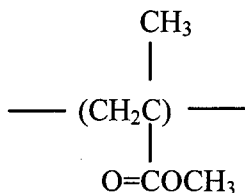
Note: ^aEstimated from author's data.

3.1.4.5 Radiolysis of Polymers Containing Ester Functional Groups

Polymers containing ester functional groups include polymethyl methacrylate (PMMA) and polyvinyl acetate. The maximum measured value of G(flam gas) for these two polymers is 2.0.

3.1.4.5.1 Polymethyl Methacrylate (PMMA)

Polymethyl methacrylate has the repeat unit:



Two common materials made of PMMA are Plexiglas^R and Lucite^R.

⁷⁹ Bohm 1973. G. G. A. Bohm, "Radiation Chemistry of Elastomers," in The Radiation Chemistry of Macromolecules, Vol. II, Academic Press, New York, 1973, ed. M. Dole.

Because PMMA has a high glass-transition temperature (about 106°C), free radicals created within the material at lower temperatures are trapped and can persist days after irradiation. Gases generated from the free radicals are also trapped, and the larger molecular components can be released only by heating the sample (near the glass transition temperature) (Dole 1973c⁸⁰). Even in the absence of oxygen, chain scission dominates. The melting temperature decreases as the absorbed dose increases, from about 140°C at zero dose to about 110°C at 100 Mrad absorbed dose (Jellinek 1978¹¹).

G values for PMMA measured using nonalpha irradiation (probably in a vacuum) differ among authors. The main volatile products formed are H₂, CO₂, CO, CH₄, propane, and methyl methacrylate monomer. The individual G values vary depending on temperature and the type of ionizing radiation; and $G(\text{gas}) < 2$ (Chapiro 1962¹⁰, Bolt 1963¹⁴).

Busfield (Busfield 1982⁸¹) summarized measurements of volatile products from PMMA that was gamma irradiated in vacuum at 30°C. The highest G value for volatile products was 4.1, which included gases and highly volatile liquids including methyl alcohol, dimethyl ether, methyl formate, dimethoxymethane, and methyl acetate. The highest G value for all flammable gases or vapors was 2.2.

Kazanjian (Kazanjian 1976³⁶) measured gas generated from alpha radiolysis of 12.8 g of shredded Plexiglas^R contaminated with 1 g of Pu-239 oxide powder, initially in an air atmosphere. After 100 days of exposure, about half of the remaining gas was replaced with helium, and the experiment continued for an additional 347 days. Calculations were made of G values as functions of absorbed dose using Kazanjian's data. $G(\text{gas})$ values appeared to be gradually decreasing with time from about 2 initially to 1.0 at 450 days (5.0E23 eV absorbed dose) with no apparent differences between the two phases of the experiment. The value of $G(\text{H}_2)$ fell from 0.4 initially to less than 0.2 in the same time period. The initial G value for oxygen consumption was $G(-\text{O}_2) \sim 3.8$. The oxygen was considerably reduced after 19 days but was not completely exhausted.

G values for PMMA are summarized in Table 3.1-33.

⁸⁰ Dole 1973c. M. Dole, "Radiation Chemistry of Substituted Vinyl Polymers. Polymers that Primarily Degrade on Irradiation," in The Radiation Chemistry of Macromolecules, Vol. II, Academic Press, New York, 1973, ed. M. Dole.

⁸¹ Busfield 1982. W. K. Busfield, et al., "Radiation Degradation of Poly (Styrene-co-Methylmethacrylate). 2. Protective Effects of Styrene on Volatile Products, Chain Scission and Flexural Strength," *Polymer* 23, pp. 431-434, 1982.

Table 3.1-33 — G Values for PMMA

Radiation Type	G(Products)	Comments	Reference
alpha (Pu-238)	very low	oxygen depleted; room temp; Lucite ^R	(1)
alpha (Pu-239)	G(gas)=2.0 (23% H ₂ , 42% CO, 23% CO ₂ , 11% CH ₄ , 2% HC) ^a	oxygen depleted; room temp; Plexiglas ^R	(2)
gamma	G(gas)=4.1; G(H ₂)=0.3; G(CO)=1.3 G(CH ₄)=0.6; G(CO ₂)=0.8; G(vapors)=1.1 ^c	vacuum; 30°C; PMMA; worst case of three experiments	(3)
various	G(gas) < 2	vacuum; room temp; PMMA	(4), (5)

Refs.: (1) Zerwekh 1979¹³; (2) Kazanjian 1976³⁶; (3) Busfield 1982⁸¹; (4) Chapiro 1962¹⁰, (5) Bolt 1963¹⁴.

Note: ^aCalculated from author's data; HC = hydrocarbons.

^cVapors include methyl alcohol, dimethyl ether, methyl formate, methyl acetate, and dimethoxymethane.

3.1.4.5.2 Polyvinyl Acetate

Measurements of G values for gas generation from polyvinyl acetate at 20 Mrad absorbed dose from gamma irradiation in a vacuum are reported by Graessley (Graessley 1973⁸²). The value of G(gas) obtained was 1.4. The evolved gas consisted of 64% H₂, 34% CH₄, and 2% CO₂ + CO. Small amounts of acetic acid also were evolved but were not detected in the mass spectrometer analysis.

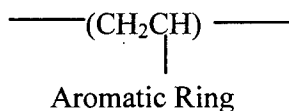
3.1.4.6 Radiolysis of Polymers with Aromatic Characteristics

Polymers having aromatic characteristics include polystyrene, polysulfone, polycarbonate, polyethylene terephthalate and polyesters, and others. These polymers are characteristically low [G(gas) is usually less than 0.8]. Other polymers in this group, for which scant radiolysis data are available, include polyurethane, analine-formaldehyde, styrene-butadiene rubber, phenol-formaldehyde, phenolic resin, epoxy resin, and polyimides.

⁸² Graessley 1973. W. W. Graessley, "Polyvinyl Acetate," in The Radiation Chemistry of Macromolecules, Vol. II, Academic Press, New York, 1973, ed. M. Dole.

3.1.4.6.1 Polystyrene

The repeat unit for polystyrene is:



One common material composed of polystyrene is Styrofoam^R. Polystyrene contains aromatic rings and exhibits the low G values and relatively strong LET effects characteristic of aromatic compounds [$G(\text{H}_2)$ is 0.2 or less] (Parkinson 1973⁸³). Production of very small amounts of methane and benzene by radiolysis has also been observed. Bersch (Bersch 1959⁵⁶) measured $G(\text{H}_2)=0.1$ and $G(\text{gas})=0.3$ for gamma radiolysis of polystyrene in air and $G(\text{gas})<0.1$ in a vacuum. Busfield (Busfield 1982⁸¹) reported an even lower value of $G(\text{H}_2)=0.03$.

The values of $G(\text{scission})$ increased for polystyrene from about 10 in oxygen to about 45 in oxygen mixed with carbon tetrachloride (Jellinek 1983¹⁵).

3.1.4.6.2 Polysulfone

G values for polysulfone have been reported for gamma and electron irradiation of several different materials (Giori 1984⁸⁴). The value of $G(\text{gas})$ ranged from 0.01 to 0.1. Hydrogen, methane, carbon monoxide, and carbon dioxide composed most of the gas generated.

3.1.4.6.3 Polycarbonate

Krasnansky (Krasnansky 1961⁵³) measured gas evolution from commercial polycarbonate powder exposed to gamma radiation in vacuum. The value of $G(\text{gas})$ calculated from his data was less than 0.8. Most of the gas was carbon dioxide or carbon monoxide. The value of $G(\text{H}_2)$ was less than 0.012.

Samples of polycarbonates were irradiated in vacuum at room temperature using a Co-60 source.⁸⁵ The measured value of $G(\text{gas})$ was 0.9, 97% of which was carbon monoxide or carbon dioxide.

3.1.4.6.4 Polyethylene Terephthalate and Other Polyesters

Commercial polyesters include Dacron^R and Mylar^R. Polyethylene terephthalate (PET) is the polymer on which these materials are based. Oxygen atoms appear in the backbone of the molecule as well as in side branches. One or more aromatic rings occur in the backbone or side

⁸³ Parkinson 1973. W. W. Parkinson and R. M. Keyser, "Radiation Chemistry of Substituted Vinyl Polymers. Polystyrene and Related Polymers," in The Radiation Chemistry of Macromolecules, Vol. II, Academic Press, New York, 1973, ed. M. Dole.

⁸⁴ Giori 1984. C. Giori and T. Yamauchi, "Effects of Ultraviolet and Electron Radiations on Graphite-Reinforced Polysulfone and Epoxy Resins," J. Appl. Polym. Sci. 29, pp. 237-249, 1984.

⁸⁵ Amamiya 1959. A. Amamiya and S. Sekigawa, "Irradiation Effects on Polycarbonates," in Annual Report of the Japanese Assn. for Radiation Research on Polymers, Vol 1., pp. 469-476, 1959.

branches; consequently, low G values are expected. Table 3.1-34 lists G values for several polyesters. The hydrogen chloride reported by Krasnansky (Krasnansky 1961⁵³) that was evolved from polyester III was believed to have resulted from the breakdown of the coating on that material.

3.1.4.6.5 Other Polymers Containing Aromatic Rings

Polyphenyl methacrylate produced G values for gamma irradiation in vacuum that were determined to vary from 1.3 for a high molecular weight polymer to 0.7 for a low molecular weight polymer (Raghunath 1983⁸⁶). The majority of the gas in each case was CO. The value of G(H₂) was less than 0.1. Scission of the ester group appeared to be the most important degradation process.

Table 3.1-34 — G Values for Polyesters

Material/Radiation Type	G(Products)	Comments	Reference
<u>PET</u>			
gamma, electrons	G(gas)=0.1-0.3; G(H ₂)=0.01-0.02 (CO+CO ₂ =83-90%)		(1)
gamma	G(gas)=0.3; G(H ₂)<0.1	air; room temp; 5.6 Mrad	(2)
gamma	G(gas)<0.1	vacuum; room temp; 5.6 Mrad	(2)
<u>Polyester I</u>			
gamma	G(gas) 0.2; G(H ₂)<0.1 (34% H ₂ , 56% CO ₂ , 6% HC, 4% other ^{a,b})	vacuum; room temp; 6 Mrad	(3)
<u>Polyester II</u>			
gamma	G(gas) 0.8; G(H ₂)<0.1 (18% H ₂ , 82% CO ₂) ^b	vacuum; room temp; 6 Mrad	(3)
<u>Polyester III</u>			
gamma	G(gas) 0.2; G(H ₂)=0.3 (60% H ₂ , 24% CO ₂ , 16% CH ₄ +HCl)	vacuum; room temp; 6 Mrad	(3)

Refs.: (1) Turner 1973⁸⁷; (2) Bersch 1959⁵⁶; (3) Krasnansky 1961⁵³.

Notes: ^aOther = methyl chloride.

^bCalculated from author's data.

⁸⁶ Raghunath 1983. S. Raghunath, et al., "Effect of Co-60 Gamma-Rays on Polyphenyl Methacrylate Obtained by Gamma-ray Irradiation," *Radiat. Phys. Chem.* 22, pp. 1023-1027, 1983.

⁸⁷ Turner 1973. D. T. Turner, "Radiation Chemistry of Some Miscellaneous Polymers. Polyethylene Terephthalate," *The Radiation Chemistry of Macromolecules*, Vol. II, Academic Press, New York, 1973, ed. M. Dole.

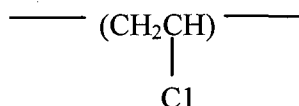
3.1.4.7 Radiolysis of Polymers Containing Halogens

Polymers containing halogen atoms include polymers that also contain hydrogen (e.g., polyvinyl chloride, polychloroprene, chlorosulfonated polyethylene, and polyvinylidene chloride) and polymers that contain no hydrogen (i.e., polytetrafluoroethylene and polychlorotrifluoroethylene).

For the polymers containing both halogen and hydrogen atoms, the G values for production of possible gas species, such as HCl, H₂, etc., are strongly dependent on the plasticizers and stabilizers added to the base polymers. Where G values for commercial materials have been measured, these are used for the maximum G values applicable to CH-TRU wastes, rather than G values for the pure polymers. Maximum values are G(H₂)=0.7-0.8 and G(gas)=3.2.

3.1.4.7.1 Polyvinyl Chloride (PVC)

The repeat unit for polyvinyl chloride (PVC) is:



PVC is found in many of the CH-TRU wastes as a packaging material, such as the 10-mil PVC box liner or 10-mil PVC O-ring bag. Various forms of PVC also appear in combustible wastes. PVC and its copolymers are used in electrical components, in Tygon^R tubing, and in Pylox^R gloves.

The conventional technique for commercial PVC heat stabilization is the addition of a stabilizer or a combination of stabilizers to the polymer. Most PVC heat stabilizers are organometallic salts containing calcium, zinc, barium, cadmium, or lead. Most traditional stabilizers function as hydrogen chloride acceptors, which reduce the catalytic effect of evolved HCl gas (Kelen 1983⁸⁸).

Brittle polymers such as PVC are usually plasticized to produce flexible films and containers. Tricresyl phosphate, the original plasticizer for commercial PVC, has been replaced by phthalic acid esters, such as dioctyl phthalate (DOP). Plasticizers may be external plasticizers, such as the phthalates, or internal plasticizers that form copolymers with vinyl chloride, such as vinyl acetate, ethylene, or methyl acrylate. Citric acid esters, epoxidized oils, and dioctyl adipate are substituted for DOP for food packaging materials. Low molecular weight polyesters are also used as nonvolatile plasticizers (Wiley 1986⁵⁰).

A typical Ca/Zn-stabilized PVC compound for food packaging films consists of 100 parts PVC, 30-70 parts plasticizer, 2-3 parts Ca/Zn stabilizer, 1-2 parts epoxidized soybean oil, and 0.1-0.2 part stearic acid. Electrical insulation and jacketing for wires and cables are generally made from PVC formulations that are stabilized by lead (Kelen 1983⁸⁸).

⁸⁸ Kelen 1983. T. Kelen, Polymer Degradation, Van Nostrand Reinhold Company, New York, 1983.

The strong effect of the plasticizers and stabilizers on the radiolysis of PVC is demonstrated by the differences in the composition of the radiolysis gas, which varies from 85% H₂, to 83% HCl, to 70% CO₂ depending on the specific formulation and whether oxygen is present.

3.1.4.7.1.1 Radiolysis of PVC in the Absence of Oxygen

Values of G(HCl) up to 13 at room temperature, increasing to 23 at 70°C, have been reported for electron irradiation in a vacuum of unstabilized Geon 101^R PVC powder (Miller 1959⁸⁹). The evolved gas was collected in a stainless-steel irradiation cell. The PVC powder was outgassed for several hours while the temperature was raised, then the sample was irradiated to doses of 5-20 Mrad. Following irradiation, the cell was allowed to stand for one hour at room temperature, allowing diffusion of the HCl out of the PVC particles to a constant pressure reading. Cooling of the evolved gas into a liquid nitrogen trap showed that at least 95% was condensable and that little or no hydrogen (noncondensable) was formed. The author assumed all of the condensable product was HCl, which is a reasonable assumption for pure PVC that had been thoroughly outgassed before irradiation. For irradiation at 70°C, the irradiation cell was immediately quenched in liquid nitrogen to cool the sample to room temperature in less than 5 minutes, to avoid collecting gas resulting from purely thermal degradation. G values were also measured at low temperatures, down to -145°C. Very little change in the G value occurred between 0 and -145°C. The minimum value of G(HCl) measured was 5.6.

Lawton (Lawton 1961⁹⁰) performed similar experiments involving electron irradiation of Geon 101^R PVC powder and measured values of G(H₂)=0.4 and G(HCl)=0.5 for irradiation at -196°C. He reported a chain dehydrochlorination process that occurred at temperatures as low as -70°C and concluded that Miller's value (Miller 1959⁸⁹) of G(HCl)=5.6 at -196°C was not the true radiation yield.

The gas yield from irradiation of samples of commercial PVC depends strongly on the materials added to the PVC resin, and even on the solvent used to dissolve the resin. Szymanski (Szymanski 1976⁹¹) reports a value of G(HCl)=8-9 for films prepared by dissolving PVC resin in tetrahydrofuran (THF) and a value of G(HCl)=4-5 for films prepared using cyclohexanone as the solvent. The HCl yield was measured by determining the chloride concentration. Films containing various concentrations of three different stabilizers were prepared using THF, and irradiated with Co-60 gamma radiation at room temperature to a dose of about 3 Mrad. (It is unclear whether oxygen was present during the irradiation.) Addition of 2-3% p-terphenyl or Tinuvin P^R decreased the value of G(HCl) to 5. Addition of 1% Epidian 5^R (an epoxy resin) decreased the value of G(HCl) to about 0.3.

⁸⁹ Miller 1959. A. A. Miller, "Radiation Chemistry of Polyvinyl Chloride," *J. Phys. Chem.* **63**, pp. 1755-1759, 1959.

⁹⁰ Lawton 1961. E. J. Lawton and J. S. Balwit, "Electron Paramagnetic Resonance Study of Irradiated Polyvinyl Chloride," *J. Phys. Chem.* **65**, pp. 815-822, 1961.

⁹¹ Szymanski 1976. W. Szymanski, et al., "Increase of Poly (Vinyl Chloride) Stability Towards Ionizing Radiation. II. Effects of Epidian Addition in PVC Films. III. Effects of the Addition of Ethylene Glycol Bis-beta-Aminocrotonate in PVC Foils," *Nukleonika* **21**, pp. 277-283, 1976.

Additional experiments were performed using PVC films formulated with 18% DOP (plasticizer) and 1-5% metallic soaps as stabilizers. Values of $G(\text{HCl})$ ranged from 1.7 to nearly 0, with most in the range of 0.3-0.7 (Szymanski 1976⁹¹). For three of the films, no HCl was detected. The average value of $G(\text{HCl})$ for 19 formulations of plasticized, stabilized PVC was $G(\text{HCl})_{\text{avg}}=0.54$. A value of $G(\text{HCl})$ for 18% DOP plasticizer but no stabilizer was $G(\text{HCl})=3.1$.

Gamma radiolysis of pure PVC powder and plasticized PVC film was studied with and without oxygen present to determine the effects of additives and oxygen on the gases generated (Hegazy 1981b⁹²). (His experiments conducted with oxygen present are discussed in Section 3.1.4.7.1.2.) Oxygen consumption and gas evolution were measured by gas chromatography and mass spectrometry. The PVC film contained PVC, DOP, epoxy oil, and Ca-Zn stearate compounds in the ratio of 100/50/5/2. The dose rate was 1 Mrad/hr, and the experiments were conducted at room temperature. In the absence of oxygen, the amount of hydrogen produced as a function of absorbed dose remained linear (constant G value) up to about 80 Mrad absorbed dose. CO_2 and CH_4 production began to decrease at about 30 Mrad absorbed dose.

For pure PVC powder irradiated to 10 Mrad absorbed dose in a vacuum, G values obtained were $G(\text{gas})=8.4$, $G(\text{H}_2)=0.2$, and $G(\text{HCl})=8.2$. At 60 Mrad absorbed dose, the values were $G(\text{gas})=5.2$, $G(\text{H}_2)=0.2$, and $G(\text{HCl})=4.9$. The plasticized/stabilized PVC film displayed much lower G values than the pure PVC powder and produced different ratios of gases depending on the absorbed dose. For PVC film irradiated in a vacuum to 10 Mrad absorbed dose, the following G values were obtained: $G(\text{gas})=0.3$, $G(\text{H}_2)=0.1$, and $G(\text{HCl})=0.03$. At 21 Mrad absorbed dose, the values were $G(\text{gas})=0.3$, $G(\text{H}_2)=0.2$, and $G(\text{HCl})=0.03$; while at 60 Mrad absorbed dose, the values were $G(\text{gas})=1.7$, $G(\text{H}_2)=0.2$, and $G(\text{HCl})=1.4$. The increases in $G(\text{gas})$ and $G(\text{HCl})$ with absorbed dose were attributed to degradation of the stabilizers and DOP above 20 Mrad absorbed dose (Hegazy 1981b⁹²), probably through reaction with radiolysis products.

Rigid PVC films containing stabilizers and anti-oxidants in the range of 0.2-0.5 wt% were gamma irradiated in a vacuum and at various oxygen pressures (Zahran 1985⁹³). For a rigid PVC film in a vacuum irradiated to 10 Mrad absorbed dose, G values obtained were $G(\text{gas})=2.9$, $G(\text{H}_2)=0.2$, and $G(\text{HCl})=2.7$; while in a vacuum at 20 Mrad absorbed dose, the values were $G(\text{gas})=2.6$, $G(\text{H}_2)=0.2$, and $G(\text{HCl})=2.4$ (Zahran 1985⁹³). Oxygen consumption and gas evolution were analyzed using gas chromatography.

Arakawa⁹⁴ measured gas evolution and oxygen consumption of PVC gamma irradiated at room temperature in a vacuum and in an oxygen environment and used gas chromatography to determine the gas composition. Three samples containing various plasticizers and stabilizers

⁹² Hegazy 1981b. E. A. Hegazy, et al., "Radiation-Induced Oxidative Degradation of Poly (vinyl Chloride)," J. Appl. Polymer Sci. 26, pp. 2947-2957, 1981.

⁹³ Zahran 1985. A. H. Zahran et al., "Radiation Effects on Poly (vinyl chloride) -- I. Gas Evolution and Physical Properties of Rigid PVC Films," Radiat. Phys. Chem. 26, pp. 25-32, 1985.

⁹⁴ Arakawa 1986. K. Arakawa, et al., "Radiation-Induced Gas Evolution in Chlorine-Containing Polymer. Poly (vinyl chloride), Chloroprene Rubber, and Chlorosulfonated-Polyethylene," Radiat. Phys. Chem. 27, pp. 157-163, 1986.

were tested. One sample (model formulated PVC) contained PVC, DOP, tribasic lead sulfate, stearic acid, and clay #33 in the proportions 100/50/5/1/10. The other two samples were of unknown composition but were considered to be representative of insulating materials used for electric cables. All three samples had G(gas) values of 1.4 or less at 20 Mrad absorbed dose. The gas generated from each of the two unknown samples contained 50% or more CO₂. CO₂ generation has also been noted in the thermal degradation of PVC stabilized using basic lead carbonates (Michell 1986⁹⁵).

From these experiments it appears that the plasticizers added to flexible PVC films, in addition to the stabilizers, have a major effect in reducing the G(HCl) value.

Modified PVC, containing 6.5-15.7 mole % N,N-dimethyl dithiocarbamate or 8.3-17.5 mole% N,N-diethyl dithiocarbamate, was irradiated with gamma rays from Co-60 at room temperature under vacuum (Nakagawa 1976⁹⁶). The evolved gases were measured and analyzed with a mass spectrometer. G values were much lower [G(gas)=0.1-0.3] than those measured for pure PVC, and little (if any) HCl was detected. Major peaks in the mass spectra of the gaseous products were measured at mass 28 (CO₂), mass 32, and mass 60. No peaks were reported at mass 2 (H₂) or mass 16 (CH₄).

Kazanjian (Kazanjian 1969³⁷) measured radiolysis products from nine samples of PVC bag material used at the RFETS irradiated using a Co-60 gamma source. The measured hydrogen G value was G(H₂)=0.11. The tubes containing the irradiated PVC were opened under water, shaken, and titrated with 0.04-N NaOH to determine the yield of water soluble acid. The acid yield, most of which was HCl, gave G(HCl)=0.21.

Kazanjian (Kazanjian 1976³⁶) measured radiolytic gas generation from PVC O-ring bags attached to glove box ports at the RFETS. The bags were cut into pieces and contaminated with PuO₂ powder. Two samples were prepared, one contaminated with 1 g of Pu-239 oxide, the other contaminated with 13.5 mg of Pu-238 oxide. The initial atmosphere was air in each experiment. In both cases, the primary gas produced was hydrogen. Measurements were continued in the Pu-239 experiment after the vessel was partially evacuated to estimate the void volume. No HCl was detected using a mass spectrometer (possibly due to reactions with the stainless steel test vessel or the inlet of the instrument).

G values for hydrogen were calculated from Kazanjian's data for both the Pu-239 and Pu-238 experiments. Taken as a whole, the data are consistent with a value of G(H₂) of about 0.6. At doses above 3E23 eV (about 100 days of exposure), the Pu-238 G(H₂) value appeared to be decreasing slightly.

⁹⁵ Michell 1986. E. W. J. Michell, "True Stabilization: A Mechanism for the Behavior of Lead Compounds and Other Primary Stabilizers Against PVC Thermal Dehydrochlorination," *J. Vinyl Technology* 8, pp. 55-65, 1986.

⁹⁶ Nakagawa 1976. T. Nakagawa and Y. Fujiwara, "Radiation Protection of Poly (vinyl chloride) by N,N-Dialkyl Dithiocarbamate Substitution," *J. Appl. Polym. Sci.* 20, pp. 753-763, 1976.

Kosiewicz (Kosiewicz 1979⁹⁷, Kosiewicz 1981¹²) measured gas generated by alpha radiolysis of PVC Pylox^R gloves. The contaminant, in the form of finely divided powders of PuO₂ (either Pu-239 or Pu-238), was distributed onto squares of the material 2.5-3 cm on a side. A second piece of the test material was placed over the first to sandwich the plutonium. Gases in the cylinders were sampled and the pressures relieved when the pressure had increased to 100 kPa over the ambient pressure of about 77 kPa. The gas composition observed was 85% hydrogen with small amounts of methane, carbon dioxide, and carbon monoxide. No HCl was detected, but it may have been absorbed by the steel cylinder walls or inlet of the measuring instrument. The (Kosiewicz 1981¹², corrected) values of G(gas) were about 0.8 at 20°C for a dose rate of 5E22 eV/day and about 6.3 at 70°C for a dose rate of 3E20 eV/day. The G(gas) value appeared to be increasing with time (Kosiewicz 1979⁹⁷), perhaps indicating depletion of stabilizers or plasticizers was occurring.

Zerwekh (Zerwekh 1979¹³) performed similar experiments using PVC and vinyl Bakelite^R 0.3-mm thick bag materials used to package wastes removed from glove boxes. The materials were cut into pieces approximately 5 x 5 cm and contaminated with Pu-238 dissolved in 2-M HNO₃. The solution was placed on the materials with a medicine dropper in as uniform a pattern as possible. The solution was allowed to evaporate, and then the test materials were loaded into all-glass systems used to reduce absorption of any HCl generated. Orsat-type gas burets were used to collect the gases produced. The maximum radionuclide contamination level was 62 mg of heat-source grade Pu on 52.5 g of waste (specific activity of about 14 Ci/g). Vinyl Bakelite^R produced 100 cm³ of gas in 69 days. The gas contained 4% H₂, 2% CO, 0.9% CO₂, and 0.2% CH₄. No Cl or HCl was detected in the gas using a mass spectrometer, but wet chemical analysis found 0.06% Cl. The PVC bagout material produced only 10 cm³ of gas in 335 days, containing 0.6% H₂, 0.1% CO, 1.0% CO₂, and 0.1% CH₄. The balance of each sample was oxygen-depleted air. [The final O₂ concentrations were not reported, so the G(H₂) and G(gas) values cannot be calculated from Zerwekh's data.]

G values for pure PVC irradiated in a vacuum are listed in Table 3.1-35. HCl is the primary gas produced. Table 3.1-36 lists G values for plasticized or stabilized PVC irradiated in a vacuum or after oxygen depletion.

In most instances, G(H₂) 0.3 at room temperature. The highest value of G(H₂) reported was 0.7 for alpha irradiation. A bounding value at room temperature, therefore, appears to be G(H₂)_{max} = 0.7.

⁹⁷ Kosiewicz 1979. S. T. Kosiewicz, et al., "Studies of Transuranic Waste Storage Under Conditions Expected in the Waste Isolation Pilot Plant (WIPP), Interim Summary Report October 1, 1977--June 15, 1979," Los Alamos National Laboratory, LA-7931-PR.

Table 3.1-35 — G Values for Pure PVC (in Vacuum)

Radiation Type	G(Products)	Comments	Reference
electrons	G(gas)=G(HCl)=13	30°C	(1)
electrons	G(gas)=G(HCl)=23	70°C	(1)
gamma	G(HCl)=4-9	room temp; 3 Mrad; only HCl detectable by measurement technique	(2)
gamma	G(gas)=8.4; G(H ₂)=0.2; G(HCl)=8.2	room temp; 10 Mrad	(3)
gamma	G(gas)=8.8; G(H ₂)=0.3; G(HCl)=8.0	room temp; 20 Mrad	(4)

Refs.: (1) Miller 1959⁸⁹; (2) Szymanski 1976⁹¹; (3) Hegazy 1981b⁹²; (4) Arakawa 1986⁹⁴.

Table 3.1-36 — G Values for Plasticized and/or Stabilized PVC (Oxygen Absent or Depleted)

Material/Radiation Type	G(Products)	Comments	Reference
<u>Films w/stabilizers</u>			
gamma	G(HCl)=0.3-5	vacuum; room temp; 3 Mrad; only HCl detectable by measurement technique	(1)
gamma	G(gas)=2.9; G(H ₂)=0.2; G(HCl)=2.7	vacuum; room temp; 10 Mrad	(2)
<u>Films w/stabilizers and plasticizers</u>			
gamma	G(HCl)=0-1.7 (most 0.3-0.7); G(HCl) _{avg} =0.54	vacuum; room temp; 3 Mrad; only HCl detectable by measurement technique	(1)
gamma	G(gas)=0.3; G(H ₂)=0.1; G(HCl)=0.03 ^a ; G(CO)=0.1; G(CO ₂)=0.1	vacuum; room temp; 10-20 Mrad	(3)
gamma	G(gas)=1.4; G(H ₂)=0.1; G(HCl)=1.2 (8% H ₂ , 83% HCl, 5% CO, 3% CO ₂ , 1.2% HC) ^b	vacuum; room temp; 10 Mrad; three different materials	(4)
	G(gas)=0.7; G(H ₂)=0.2; G(HCl)=0.1 (26% H ₂ , 14% HCl, 8% CO, 50% CO ₂ , 1.4% HC) ^b		
	G(gas)=1.1; G(H ₂)=0.2; G(HCl)=0.1 (15% H ₂ , 8% HCl, 9% CO, 66% CO ₂ , 2% HC) ^b		
alpha (Pu-238, -239)	G(gas)=0.7; G(H ₂)=0.6 (83% H ₂ , 12% CO + CO ₂ , 5% HC) ^b	oxygen depleted; room temp; O-ring bags	(5)
alpha (Pu-238)	G(gas)=0.8; G(H ₂)=0.7 (85% H ₂ , 2% CH ₄ , 6% CO ₂ , 7% CO) ^c	oxygen depleted; 20°C; Pylox ^R gloves; corrected data	(6)
alpha (Pu-238)	G(gas)=6.3; G(H ₂)=5.3 (85% H ₂ , 2% CH ₄ , 6% CO ₂ , 7% CO) ^c	oxygen depleted; 70°C; Pylox ^R gloves; corrected data	(6)

Refs.: (1) Szymanski 1976⁹¹; (2) Zahran 1985⁹³; (3) Hegazy 1981b⁹²; (4) Arakawa 1986⁹⁴; (5) Kazanjian 1976³⁶; (6) Kosiewicz 1981¹² (corrected).

Notes: ^aAt an absorbed dose of 60 Mrad, G(HCl)=1.4.

^bHC = hydrocarbons; calculated using author's data.

^cAn increase from G(H₂)=0.7 to G(H₂)=5.3 between 20°C and 70°C corresponds to an activation energy of 8.1 kcal/mole; see Section 3.1.2.3.1.2.

3.1.4.7.1.2 Radiolysis of PVC in the Presence of Oxygen

Zeppenfeld (Zeppenfeld 1967⁹⁸) irradiated PVC (apparently pure PVC) with Co- gamma rays in the presence of oxygen. The HCl formed was absorbed in water and then titrated. The HCl yield as a function of radiation dose was a straight line through the origin, with a G(HCl) value of 46 at about 95°C (estimated from the author's data). Experiments conducted at several different temperatures between about 84 and 119°C yielded an activation energy of 5 kcal/g-mole. The corresponding value of G(HCl) at 25°C would be 9.4.

Pure PVC powder and PVC film containing PVC, DOP, epoxy oil, and Ca-Zn stearate compounds in the ratio of 100/50/5/2 were irradiated at various oxygen pressures (Hegazy 1981b⁹²). The dose rate was 1 Mrad/h, and the experiments were conducted at room temperature. At an absorbed dose of 20 Mrad with an initial oxygen pressure of 150 torr (the oxygen partial pressure in ambient air), plasticized PVC again produced much less gas than pure PVC. For pure PVC powder, G values measured were G(gas)=10, G(H₂)=0.1, G(HCl)=8.0, and G(-O₂)=11.3. For PVC film, G values measured were G(gas)=2.4, G(H₂)=0.2, G(HCl)=1.7, and G(-O₂)=6. Corresponding results at an oxygen pressure of 500 torr are: for pure PVC powder, G values measured were G(gas)=20.3, G(H₂)=0.1, G(HCl)=15, and G(-O₂)=29; for PVC film, G values measured were G(gas)=5.9, G(H₂)=0.2, G(HCl)=5.0, and G(-O₂)=11 (Hegazy 1981b⁹²).

Rigid PVC films containing stabilizers and anti-oxidants in the range of 0.2-0.5 wt% were gamma irradiated in a vacuum and also at various oxygen pressures (Zahran 1985⁹³). At an absorbed dose of 20 Mrad with an initial oxygen pressure of 150 torr, G values for rigid PVC film were G(gas)=6.1, G(H₂)=0.1, G(HCl)=5.9, and G(-O₂)=2.9.

Gas evolution and oxygen consumption were measured for three samples of PVC containing various plasticizers and stabilizers that were gamma irradiated at room temperature with oxygen present (the O₂ concentration was not stated) (Arakawa 1986⁹⁴). The formulations of these samples are discussed in Section 3.1.6.6.1. Pure PVC powder was also studied. G(gas) for the pure PVC powder was much higher (21.6) than G(gas) for any of the plasticized/stabilized samples (1.4-5.0). Radiolysis of the model-formulation PVC produced primarily HCl, while the two commercial samples of unknown composition produced primarily CO₂ (as was the case for irradiation in vacuum). Values of G(H₂), however, were consistently between 0.2 and 0.3 for all four PVC samples studied.

Examination of the efficiency in forming a gel fraction in gamma radiolysis of plasticized PVC samples in air led Krylova (Krylova 1979⁹⁹) to conclude that the plasticizers were functioning as anti-rad additives. The plasticizers, containing esters with long hydrocarbon chains, appeared to break down more readily than the PVC base polymer. Energy transfer from the PVC molecules to the plasticizer molecules seemed to be occurring.

⁹⁸ Zeppenfeld 1967. G. Zeppenfeld and L. Wuckel, "On the Mechanism of the Radiation Oxidation of Poly (Vinyl Chloride)," in Proceedings of the Second Tihany Symposium, Akademiai Kiado, Budapest, 1967.

⁹⁹ Krylova 1979. S. V. Krylova, et al., "Effect of Plasticizers on the Behavior of Polyvinyl Chloride in γ -Irradiation," Polym. Sci. 21, pp. 749-757, 1979.

Table 3.1-37 lists G values for PVC irradiated in the presence of oxygen. The highest value of $G(\text{H}_2)$ observed for PVC irradiated at room temperature, with or without oxygen present, is $G(\text{H}_2)=0.7$.

3.1.4.7.2 Polychloroprene

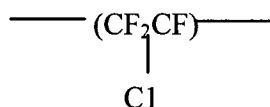
Neoprene rubber is composed of polychloroprene. G values for polychloroprene are listed in Table 3.1-38.

3.1.4.7.3 Chlorosulfonated Polyethylene

Hypalon^R gloves are composed of chlorosulfonated polyethylene. Lead oxide is often incorporated into the glove material to provide gamma shielding. Table 3.1-39 provides G values for chlorosulfonated polyethylene (Hypalon®).

3.1.4.7.4 Polytetrafluoroethylene (PTFE) and Polychlorotrifluoroethylene

Both polytetrafluoroethylene and polychlorotrifluoroethylene contain no hydrogen in their base polymers. Polychlorotrifluoroethylene has the repeat unit:



Bersch (Bersch 1959⁵⁶) measured gas evolution in air and in a vacuum from gamma radiolysis of two brands of Kel-F^R, which has polychlorotrifluoroethylene as the base polymer. The maximum value of $G(\text{gas})$ calculated from Bersch's data was 1.1 in air versus 0.1 in vacuum. Almost all of the radiolysis gas produced in air consisted of CO_2 .

Polytetrafluoroethylene (PTFE) has the repeat unit:



Teflon^R is a trade name for PTFE. Teflon^R is similar in structure to polyethylene; however, all of the hydrogen atoms are replaced by fluorine atoms. Differences in the energy relationships between possible chemical reactions lead to the generation of hydrogen gas from polyethylene but no fluorine gas from Teflon^R (Dole 1973b¹⁰⁰).

¹⁰⁰ Dole 1973b. M. Dole, "Radiation Chemistry of Some Miscellaneous Polymers. Fluoropolymers," in The Radiation Chemistry of Macromolecules, Vol. II, Academic Press, New York, 1973, ed. M. Dole.

Table 3.1-37 — G Values for PVC (Oxygen Present)^a

Material/ Radiation Type	G(Products)	Comments	Reference
<u>Pure PVC</u>			
gamma	G(gas)=10.3; G(H ₂)=0.1; G(HCl)=8.0; G(CO)=1.0; G(CO ₂)=1.2; G(-O ₂)=11.3	150 torr O ₂ ; 20 Mrad; room temp	(1)
gamma	G(gas)=21.6 ^a ; G(H ₂)=0.2 (1% H ₂ , 85% HCl, 4% CO, 10% CO ₂) ^b G(-O ₂)=37.7 ^b	O ₂ pressure not reported ^c ; room temp	(2)
<u>Films w/stabilizers</u>			
gamma	G(gas)=6.1; G(H ₂)=0.1; G(HCl)=5.9; G(-O ₂)=2.9	150 torr O ₂ ; room temp	(3)
<u>Films w/stabilizers and plasticizers</u>			
gamma	G(gas)=2.4; G(H ₂)=0.2; G(HCl)=1.7; G(CO)=0.2; G(CO ₂)=0.2; G(-O ₂)=6	150 torr O ₂ ; 20 Mrad; room temp	(1)
gamma	G(gas)=5.0 ^a ; G(H ₂)=0.3 G(HCl)=2.6 (5% H ₂ , 52% HCl, 6% CO, 37% CO ₂) ^b G(-O ₂)=8.1 ^b	O ₂ pressure not reported; 10 Mrad; room temp	(2)
gamma	G(gas)=1.4 ^a ; G(H ₂)=0.2; G(HCl)=0.2; (15% H ₂ , 15% HCl, 17% CO, 51% CO ₂ , 1% HC) ^b G(-O ₂)=6.9 ^b		(2)
gamma	G(gas)=1.9 ^a ; G(H ₂)=0.2; G(HCl)=0.2; (10% H ₂ , 10% HCl, 9% CO, 70% CO ₂ , 1% HC) ^b G(-O ₂)=6.6 ^b		(2)
gamma	G(H ₂)=0.11; G(HCl)=0.21	G(HCl) determined from G(acid)	(4)

Refs.: (1) Hegazy 1981b⁹²; (2) Arakawa 1986⁹⁴; (3) Zahran 1985⁹³; (4) Kazanjian 1969³⁷.

Note: ^aSee also Kazanjian 1976³⁶.

^bCalculated using author's data.

^cProbably ambient pressure (~760 torr).

Table 3.1-38 — G Values for Polychloroprene

Material/ Radiation Type	G(Products)	Comments	Reference
<u>Pure polychloroprene</u>			
gamma	G(gas)=3.5; G(H ₂)=0.2 (5% H ₂ , 93% HCl, 1% CO ₂) ^a	vacuum; room temp	(1)
gamma	G(gas)=7.7; G(H ₂)=0.3 (4% H ₂ , 39% HCl, 14% CO, 43% CO ₂) ^a	oxygen; room temp	(1)
<u>Commercial Neoprene^R</u>			
alpha (Pu-238)	G(gas)=0.03; G(H ₂)=0.03 (95% H ₂ , 3% CO ₂ , 1% CO, 1% CH ₄)	oxygen depleted; room temp; corrected data	(2)
alpha (Pu-238)	G(gas)<0.1; G(H ₂)<0.1 ^b	oxygen depleted; room temp	(3)
gamma	G(gas)=0.2; G(H ₂)=0.1 (35% H ₂ , 16% HCl, 3% CO, 43% CO ₂ , 3% SO ₂) ^a	vacuum; room temp; model compound	(1)
gamma	G(gas)=0.3; G(H ₂)=0.1 (29% H ₂ , 17% HCl, 1% CO, 50% CO ₂ , 3% SO ₂) ^a	vacuum; room temp; special compound	(1)
gamma	G(gas)=0.6; G(H ₂)<0.1 (6% H ₂ , 7% HCl, 8% CO, 79% CO ₂) ^a	oxygen; room temp; model compound	(1)
gamma	G(gas)=0.7; G(H ₂)=0.1 (17% H ₂ , 9% HCl, 9% CO, 58% CO ₂ , 1% CH ₄ , 6% SO ₂) ^a	oxygen; room temp; special compound	(1)

Refs.: (1) Arakawa 1986⁹⁴; (2) Kosiewicz 1981,¹² corrected (3) Zerwekh 1979¹³.

Notes: ^aCalculated from author's data.

^bEstimated from author's data.

Table 3.1-39 — G Values for Hypalon^R

Material/Radiation Type	G(Products)	Comments	Reference
<u>Pure Hypalon^R</u>			
gamma	G(gas)=5.0; G(H ₂)=0.6 (12% H ₂ , 42% HCl, 9% CO ₂ , 37% SO ₂)	vacuum; room temp	(1)
gamma	G(gas)=7.8; G(H ₂)=0.5 (6% H ₂ , 62% HCl, 2% CO, 20% CO ₂ , 10% SO ₂)	oxygen; room temp	(1)
<u>Commercial Hypalon^R</u>			
alpha (Pu-238)	G(gas)=0.15; G(H ₂)=0.15 (96% H ₂ , 1% CH ₄ , 2% CO ₂ , 1% CO)	oxygen depleted from initial air atmosphere; room temp; temp; corrected data	(2)
alpha (Pu-238)	G(gas)<0.1; G(H ₂)<0.1 ^a	oxygen depleted from initial air atmosphere; room temp; dry box gloves	(3)
alpha (Pu-239)	G(gas)=0.4; G(H ₂)=0.2; (56% H ₂ , 42% CO ₂ , 2% HC) ^b	oxygen present; room temp; Neoprene-Hypalon glove box gloves	(4)
gamma	G(gas)=0.3; G(H ₂)=0.3 (90% H ₂ , 8% CO ₂ , 2% CO)	vacuum; room temp; model compound	(1)
gamma	G(gas)=0.4; G(H ₂)=0.3 (66% H ₂ , 33% CO ₂ , 1% CO)	vacuum; room temp; special compound	(1)
gamma	G(gas)=0.5; G(H ₂)=0.3 (59% H ₂ , 31% CO ₂ , 10% CO)	oxygen; room temp; model compound	(1)
gamma	G(gas)=0.6; G(H ₂)=0.3 (52% H ₂ , 44% CO ₂ , 4% CO)	oxygen; room temp; special compound	(1)

Refs.: (1) Arakawa 1986⁹⁴; (2) Kosiewicz 1981,¹² corrected; (3) Zerwekh 1979¹³; (4) Kazanjian 1976³⁶.

Note: ^aEstimated from author's data.

^bCalculated from author's data.

Teflon^R is one of the most stable polymers with respect to heat, solvents, and most corrosive chemicals. In contrast, this polymer is extremely sensitive to radiation and incurs marked damage to its mechanical properties after relatively low radiation doses.

3.1.4.7.4.1 Radiolysis of PTFE in the Absence of Oxygen

While authors disagree about the details of PTFE radiolysis in the absence of oxygen, they agree that the total gas generation rate is relatively low. Pure PTFE contains no hydrogen, so

radiolysis of commercial Teflon^R should yield little or no hydrogen-containing gases. Table 3.1-40 gives G values for PTFE in the absence of oxygen.

Table 3.1-40 — G Values for PTFE (Oxygen Depleted or Absent)

Radiation Type	G(Products)	Comments	Reference
gamma	G(gas)=0.3 for condensable gases	vacuum; room temp	(1)
reactor	(primarily CF ₄ ; no G value given)		(2)
reactor	G(gas)=0.02-0.05 (CO ₂ + CO)		(2)
alpha (Pu-238)	G(gas)=0.06 (0% H ₂ , 0.2% CH ₄ , 16.8% CO ₂ , 83% CO)	oxygen depleted from initial air atmosphere; room temp; Teflon ^R , corrected data	(3)

Refs.: (1) Dole 1973b¹⁰⁰; (2) Chapiro 1962¹⁰, (3) Kosiewicz 1981, ¹² corrected.

3.1.4.7.4.2 Radiolysis of PTFE in the Presence of Oxygen

Irradiation of PTFE in the presence of oxygen increases the rate of degradation. Gamma irradiation of powdered PTFE resulted in a G value for oxygen consumption of G(-O₂)=5. A G value of 3.5 for condensable gases was measured; a large percentage of the gas was carbonyl fluoride. The G value for condensable gases (0.33) for irradiation in a vacuum was much smaller (Dole 1973b¹⁰⁰).

G(scission) values for PTFE increased from about 7 in oxygen to about 26 in oxygen mixed with carbon tetrachloride vapor (Jellinek 1983¹⁵). The evolved gas was CCl₃F.

Table 3.1-41 gives G values for PTFE in the presence of oxygen.

Table 3.1-41 — G Values for PTFE (Oxygen Present)

Radiation Type	G(Products)	Comments
gamma	G(-O ₂)=5, G(gas)=3.5 for condensable gases	oxygen present; mostly CF ₂ O produced

Ref.: Dole 1973b¹⁰⁰.

3.1.4.7.5 Other Polymers Containing Halogens

Krasnansky (Krasnansky 1961⁵³) measured gas evolution from commercial chlorinated polyether film exposed to gamma radiation in vacuum. The value of $G(\text{gas})$ calculated from his data was less than 0.8, with hydrogen composing 86% of the gas and butene 1.4%.

Bersch (Bersch 1959⁵⁶) measured gas evolution in air and in a vacuum from gamma radiolysis of rubber hydrochloride (Pliofilm^R) and two brands of polyvinylidene chloride. For these polymers, measured G values were much smaller than those for polyethylene [$G(\text{gas})_{\text{max}}=2.1$ for polyvinylidene chloride in vacuum], and the evolved gas for the polymers when irradiated in air consisted mostly of CO_2 .

3.1.4.8 Radiolysis of Miscellaneous Polymers

Radiolysis experiments have been conducted for a variety of additional polymers and commercial plastics.

3.1.4.8.1 Polyamides

Polyamides include materials, such as Nylon^R, which contain H-N bonds as well as H-C and C=O bonds. Nomex^R, used in filters, is an aromatic polyamide (EPRI 1981¹⁰¹). G values for polyamides are summarized in Table 3.1-42. Polyacrylonitrile contains C=N bonds and should also have low G values (see Section 3.1.3.12 for a discussion of structurally-related liquids).

3.1.4.8.2 Ion-Exchange Resins

The vast majority of ion-exchange resins used are synthetic organic resins (Pillay 1986¹⁰²). G values vary, depending on the resin and the ionic form. Pillay (Pillay 1986¹⁰²) reports G values for many different ion-exchange resins. The bounding values are $G(\text{gas})$ 2.1, and $G(\text{H}_2)$ 1.7 for Zeocarb-215^R resin (wet) (Mohorcic 1968¹⁰³). Most $G(\text{gas})$ and $G(\text{H}_2)$ values are much lower. Kazanjian (Kazanjian 1976³⁶) obtained a value of $G(\text{gas})=0.1$ for Dowex-1^R resin.

3.1.4.8.3 Other Miscellaneous Polymers

Some specialty materials have been developed to be highly sensitive to radiation. These include the poly(olefin sulfone)s, which have very high G values for production of SO_2 , hydrogen, and olefins. For example, a value of $G(\text{gas})$ of 71 is reported for polyhexene-1-sulfone (Jellinek 1978¹¹). These materials are not used in common commercial plastics.

¹⁰¹ EPRI 1981. Georgia Institute of Technology, "Radiation Effects on Organic Materials in Nuclear Plants," Electric Power Research Institute, EPRI NP-2129, November 1981.

¹⁰² Pillay 1986. K. K. S. Pillay, "The Effects of Ionizing Radiations on Synthetic Organic Ion Exchangers," J. Radioanaly. Nuc. Chem., Articles 97/1, pp. 135-210, 1986.

¹⁰³ Mohorcic 1968. G. Mohorcic and V. Kramer, "Gasses Evolved by Co-60 Radiation Degradation of Strongly Acidic Ion Exchange Resins," J. Polym. Sci.: Part C, pp. 4185-4195, 1968.

Table 3.1-42 — G Values for Polyamides

Material/ Radiation Type	G(Products)	Comments	Reference
<u>Polymid MXD-6^R</u> gamma	G(gas)=0.1 ^a ;G(H ₂)<0.1 ^a (75% H ₂ , 25% CO ₂)	vacuum; room temp; 36 Mrad	(1)
<u>Nylon 66^R</u> gamma	G(gas)=0.5 ^a ;G(H ₂)=0.4 ^a (82.5% H ₂ , 16% CO, 1.5% CO ₂)	vacuum; room temp; 36 Mrad	(1)
<u>Nylon 6-6^R</u> gamma	G(gas) not reported; G(H ₂)=0.4	vacuum; room temp	(2)
<u>Nylon II^R</u> gamma	G(gas)=1.5 ^a ;G(H ₂)=1.1 ^a (75% H ₂ , 22.5% CO; 0.5% CO ₂ ; 2% CH ₄)	vacuum; room temp; 36 Mrad	(1)
<u>Aromatic polyamide</u> not reported	G(gas) not reported; G(H ₂)=0.01		(3)

Refs.: (1) Krasnansky 1961⁵³; (2) Dole 1983¹⁰⁴; (3) Zimmerman 1973¹⁰⁵.

Note: ^aCalculated from author's data.

The radiation stability of various commercial plastics was studied in the 1950s by members of the ORNL by irradiating the materials in the ORNL Graphite Reactor (Bopp 1953¹⁰⁶, Bopp 1955¹⁰⁷, Bopp 1963⁴⁹). The radiation exposure was converted to absorbed dose using the chemical composition of the material. The data as reported in Bopp (Bopp 1963⁴⁹) were arbitrarily scaled up to match a higher G value for polyethylene, indicating some uncertainty in the absolute values. Because of inherent dosimetry problems in these early studies, these data are used only in a qualitative sense to establish the gas generation potential of the materials with

¹⁰⁴ Dole 1983. M. Dole, "Effects of Radiation Environments on Plastics," in The Effects of Hostile Environments on Coatings and Plastics, American Chemical Society, Washington, D. C., 1983, ed. D. P. Garner, pp. 17-24.

¹⁰⁵ Zimmerman 1973. J. Zimmerman, "Radiation Chemistry of Some Miscellaneous Polymers. Polyamides," The Radiation Chemistry of Macromolecules, Vol. II, Academic Press, New York, 1973, ed

¹⁰⁶ Bopp 1953. C. D. Bopp and O. Sisman, "Radiation Stability of Plastics and Elastomers," Oak Ridge National Laboratory, ORNL-1373, July 1953.

¹⁰⁷ Bopp 1955. C. D. Bopp and O. Sisman, "Radiation Stability of Plastics and Elastomers," *Nucleonics* 13, pp. 28-33, 1955.

respect to polyethylene (one of the materials irradiated). G values obtained from these experiments relative to polyethylene are listed in Table 3.1-43.

Table 3.1-43 — G(gas) Values for Miscellaneous Commercial Plastics (Relative to Polyethylene)

Material	G(gas) Value Relative to Polyethylene ^a
cellulose nitrate	1.5
polyvinyl formal	1.4
polyethylene	1.0
allyl diglycol carbonate	0.6
ethyl cellulose	0.5
methyl methacrylate	0.5
cellulose propionate	0.5
cellulose acetate butyrate	0.4
Nylon ^R	0.4
phenolics (no filler, or cellulosic or mineral filler)	<0.3
urea formaldehyde (cellulosic filler)	0.3
Silastic ^R	0.3
cellulose acetate	0.3
butyl rubber	0.3
natural rubber-butyl rubber mixtures	<0.3
melamine formaldehyde (cellulosic filler)	0.2
Selectron 5038 ^R polyester	0.2
natural rubber with fillers	<0.2
natural rubber	0.1
Thiokol ST ^R	0.09
Neoprene ^R	<0.06
casein plastic	0.05
Mylar ^R film	0.05
Plaskon ^R alkyd	0.03
triallyl cyanurate	0.02
aniline formaldehyde	0.01
furane resin (asbestos & carbon filler)	<0.01
polystyrene	<0.01
styrene-butadiene copolymer	<0.01

Ref.: Bopp 1953¹⁰⁶

Note: ^aCalculated from author's data.

Only two materials, polyvinyl formal and cellulose nitrate, had higher G(gas) values than polyethylene in the ORNL reactor irradiation experiments. The composition of the evolved gas was not reported. The major use of polyvinyl formal is in heat-resistant nonconductive electrical wire enamels and other coatings (Deanin 1972¹⁰⁸). Because of its thermal instability, cellulose nitrate does not have wide application in commonly used materials in general commerce, except

¹⁰⁸ Deanin 1972. R. D. Deanin, Polymer Structure, Properties and Applications, Changers Books, Boston, 1972.

in photographic film and lacquers (cellulose nitrate commonly is the film remaining after the volatile constituents have evaporated) (Deanin 1972¹⁰⁸). As a result, polyvinyl formal and cellulose nitrate will be present in the CH-TRU wastes only in trace amounts.

3.1.5 Radiolysis of Non-Polymer Solids

Other common solid materials in the CH-TRU wastes are solidified liquid wastes, solid organic acids, asphalt, and miscellaneous inorganic materials.

3.1.5.1 Radiolysis of Solidified Liquid Wastes

Solidified liquid wastes include sludges, concretes, and gel-like or monolithic structures that bind liquid wastes so that free liquids are minimized.

3.1.5.1.1 Aqueous Sludges

One common sludge is produced at the RFETS by the neutralization of nitric acid solutions in the plutonium recovery process. The sludge consists of hydroxides of calcium, sodium, potassium, silicon, magnesium, aluminum, iron, and other metals at lower concentrations (Kazanjian 1981¹⁰⁹). The water and nitrate content of the sludge can vary.

Kazanjian (Kazanjian 1981¹⁰⁹) conducted experiments on this sludge to determine the radiolytic gas yields as a function of water and nitrate content. The nitrate concentration in the material was determined to be 10.2 wt%, and the water content was 52 wt%. The water content was varied either by drying or adding water to the as-received sludge. Mass spectrometric analysis of the gases evolved under drying conditions showed that the weight loss was essentially all due to water evaporation. In order to examine the effect of the nitrates on gas yields, nitrate salts were removed by washing the sludge with water. All of the experiments were conducted at lowered pressure to permit more accurate analysis of the evolved gases using mass spectrometry.

The experiments were conducted using gamma radiation. The dose rate was 4.45E5 rad/h, except for the 75% water sample, which was irradiated at 3.8E5 rad/h.

The results show that decreasing the water content of the sludge decreases the rate of gas generation. Small amounts of CO and NO_x were also observed. Removing nitrates from the sludge changed the amount and composition of the evolved gas. Oxygen generation was virtually eliminated. Hydrogen evolution in these samples, which contained about 65% water, was up to three times greater than hydrogen evolution obtained from sludge containing nitrate. The measured value of G(H₂) varied from 0.23 to 0.43. [The largest G(H₂) value observed (0.43) is very close to the value of 0.45 for G(H₂) measured for gamma irradiation of liquid water at high pH (see Section 3.1.3.4).] A maximum value of G(O₂) of 0.9 was found in the nitrate sludges from the radiolysis of nitrates. These findings are in agreement with other experiments on the radiolysis of nitric acid and solid inorganic nitrates.

¹⁰⁹ Kazanjian 1981. A. R. Kazanjian and M. E. Killion, Results of experiments on radiolytic gas generation from sludge, Rockwell International, Rocky Flats Plant, personal communication.

Sludge from waste water processing at Mound Laboratory, composed primarily of carbon, iron, and calcium compounds, is immobilized in Portland cement (Lewis 1983¹¹⁰). A sample of the sludge was contaminated with heat-source plutonium dioxide, consisting of particles averaging 20 microns in size, and mixed with cement. The sludge/cement contained 20 wt% water. The G(gas) value measured was 0.21 (for generated gases only), consisting almost entirely of hydrogen; the G(-O₂) value was 0.13. A small amount of nitrogen was also generated.

Gas generation from cemented caustic waste resulting from immobilization at Mound Laboratory of 1-N NaOH contaminated scrubber solution in Portland cement is reported in Lewis (Lewis 1983¹¹⁰). The caustic waste was contaminated with heat-source plutonium in the form of PuO₂ particles averaging 20 microns in size. The caustic/cement waste form contained 22 wt% water. The measured G(gas) value was 0.26, consisting of about equal amounts of oxygen and hydrogen [G(O₂)=0.11 and G(H₂)=0.13]. A small amount of nitrogen was also generated.

3.1.5.1.2 Concretes

The cement-based and other hydraulic binders used for immobilization of wastes require water in their curing reactions. Generally, some excess water remains in the materials in a closed-pore system (Dole 1986¹¹¹). Radiolysis of this unbound water contributes most of the gas generation from within these solidified radioactive wastes.

High-level radioactive sludges at the SRS were simulated using Fe₂O₃, MnO₂, or equimolar mixtures of the two compounds, which were solidified in high-alumina cement (Bibler 1976¹⁹, Bibler 1978¹¹²). For all tests, the simulated wastes were 40 wt% of the dry cement-waste mixtures. Irradiation of this material with Co-60 gamma rays generated a gas consisting predominantly of hydrogen. The hydrogen pressure reached a steady-state value; higher pressures corresponded to higher dose rates. The equilibrium pressure also depended on the specific material being irradiated, with equilibrium pressures in descending order for Fe₂O₃-cement, neat cement, and MnO₂-cement. In all three cases, oxygen was partially consumed to form hydrogen peroxide, as verified by chemical analysis of the irradiated concrete.

In alpha radiolysis experiments conducted on the same concretes, oxygen was a product as well as hydrogen, composing 20 to 50% of the evolved gas. Up to 200 psi, no steady-state pressure was reached. The average value of G(H₂) was 0.21 (Bibler 1978¹¹²).

¹¹⁰ Lewis 1983. E. L. Lewis, "TRU Waste Certification: Experimental Data and Results," Monsanto Research Corporation, Mound Laboratory, MLM-3096, September 1983.

¹¹¹ Dole 1986. L. R. Dole and H. A. Friedman, "Radiolytic Gas Generation from Cement-Based Waste Hosts for DOE Low-Level Radioactive Wastes," preprint of a presentation at the Symposium on the Effects of Radiation on Materials, Seattle, Washington, June 1986.

¹¹² Bibler 1978. N. E. Bibler, "Radiolytic Gas Production from Concrete Containing Savannah River Plant Waste," E. I DuPont de Nemours and Company, Savannah River Laboratory, DP-1464, January 1978.

The effect of adding NO_3^- or NO_2^- ions was also examined (Bibler 1978¹¹²). In low-dose-rate (0.09 Mrad/hr) gamma radiolysis tests, added NO_3^- or NO_2^- did not lead to additional pressurization. O_2 was still consumed, and H_2 was still produced. At the high dose rate (28 Mrad/hr), O_2 was a product, indicating that a different radiolytic process dominates at this dose rate. Also, a steady-state pressure was not reached.

Gas generation from a concrete consisting of a mixture of Portland cement and gypsum-perlite plaster mixed with water in the ratio of approximately 1.7:1 was measured by Bibler (Bibler 1977²⁵). The value of $G(\text{gas})$ measured in the gamma radiolysis experiment was 0.03. Hydrogen was the only gas produced. As the hydrogen pressure increased, back reactions occurred to reduce the rate of hydrogen formation, resulting in a steady-state pressure that depended on the dose rate. Oxygen in the air was partially consumed, and nitrogen was unaffected. For the alpha radiolysis tests, Cm-244 was dissolved in the water used to make the concrete, ensuring that the Cm-244 was in direct contact with the elements in the concrete. In four tests with varying amounts of Cm-244, $G(\text{H}_2)$ was constant and equal to 0.6, a value 20 times greater than measured in the gamma radiolysis experiment. As with gamma radiolysis, oxygen was partially consumed and nitrogen was unaffected. However, a steady-state pressure was not attained even at about 200 psi of hydrogen.

Bibler (Bibler 1980¹¹³) conducted a series of alpha radiolysis experiments to study radiolysis of CH-TRU wastes immobilized in concrete, especially incinerator ash. Drying the concrete at 200°C reduced the water content from 35 to 7.4% (80% reduction) but greatly reduced the $G(\text{H}_2)$ value from 0.38 to 0.0002. The water remaining was thought to be involved in hydration reactions and not as easily degraded as the free water remaining in the concrete after curing.

The similarity in the radiolysis results for concrete and water led Bibler (Bibler 1977²⁵) to conclude that the metal oxides of the concrete do not significantly alter the radiation chemistry of the water, even when the water is incorporated in the concrete. In gamma radiolysis tests, O_2 in the air sealed in the container was partially consumed, while N_2 was unaffected. A steady-state H_2 pressure up to 45 psig was attained. Higher equilibrium pressures were seen for the higher dose rates in the experiment. The values of $G(\text{H}_2)$ were measured to be 0.03 for all dose rates.

In the alpha radiolysis experiments on concrete, a value of $G(\text{H}_2)=0.6$ was measured, independent of the amount of Cm-244. This $G(\text{H}_2)$ value was a factor of 20 times higher than the $G(\text{H}_2)$ value measured for gamma radiolysis. As with gamma radiolysis, oxygen was partially consumed while N_2 was unaffected. In contrast to gamma radiolysis, a steady-state pressure was not attained even to about 200 psig H_2 .

Tests were also performed (Bibler 1979²³) to determine if self-absorption of alpha energy would occur when plutonium dioxide particles were added to concrete. The amount of energy absorbed by a particle depends on the size of the particle and its density. The value of $G(\text{H}_2)$ was decreased by about a factor of 2 for concrete containing PuO_2 particles having an average size of

¹¹³ Bibler 1980. N. E. Bibler, "Radiolytic Gas Generation in Concrete Made with Incinerator Ash Containing Transuranium Nuclides," in Scientific Basis for Nuclear Waste Management, Vol. 2, pp. 585-592, 1980.

2 microns and a density about 80% of the maximum density, compared to concrete containing plutonium dissolved in nitric acid. (The particles may have agglomerated to form larger particles.) The calculated range of the Pu-238 alpha particles (in PuO₂ of the maximum theoretical density of 11.4 g/cm³) is 11 microns (Bibler 1979²³).

Bibler (Bibler 1979²³, Bibler 1980¹¹⁴) reported gas generation experiments on three types of concrete containing simulated TRU incinerator ash: high-alumina cement, Portland Type I cement, and Portland-pozzolanic cement. Simulated incinerator ash containing primarily CaO and TiO₂ was mixed with dry cement (30 wt% ash, 70 wt% cement). Pu-238 solution was added, and the resulting paste was transferred to a mold and cured to allow 30-40% of the free water to evaporate. G(H₂) values ranged from 0.3 to 0.6. G(H₂) values were unaffected by either dose rate or the pH of the water used to make the concrete. G(H₂) could be decreased by reducing the water content of the concrete and by adding an organic acid (EDTA) to the concrete.

Bibler (Bibler 1979²³, Bibler 1980¹¹⁴) conducted further experiments on high-alumina and Portland Type I cements. He determined that addition of NO₃⁻ or NO₂⁻ ions to the water used to make the concrete lowered the alpha radiolysis G(H₂) values by a factor of 20 for 6-M NO₃⁻ or a factor of 2.4 for 3-M NO₂⁻. Oxygen was also produced from the concrete containing 6-M NO₃⁻, while oxygen was consumed in the concrete containing 3-M NO₂⁻.

Radiolysis experiments conducted at 70 and 100°C indicated that G(H₂) for concretes does not increase with temperature below 100°C (Bibler 1979²³, Bibler 1980¹¹⁴). In fact, decreases in the hydrogen generation rate were noted, caused by evolution of free water from the concretes.

Bibler (Bibler 1979²³) also compared G(H₂) values measured for dissolved TRU contaminants versus contaminants present as small particles. When Pu-238 was added as PuO₂, G(H₂) for high-alumina concrete was 0.21 compared to 0.55 determined using dissolved Pu-238. G(H₂) for Portland Type I cement was 0.28 compared to 0.65. The PuO₂ particles used had an initial average size of 2 microns initially but could have agglomerated to larger particles.

Radiolysis of simulated radioactive waste immobilized in cement-based grouts was examined by Dole (Dole 1986¹¹¹). All specimens were cured for 28 days before the radiolysis gases were collected. Some dewatered specimens were dried at elevated temperature for seven days in order to establish the role of the porewater in the production of radiolysis gases. Cm-244 was used as the contaminant in the alpha radiolysis experiments. Two waste streams were simulated: current acid waste and double-shell slurry (DSS) waste. Both waste streams were acidic and contained metal sulfates and nitrates. The cement used was low alumina cement. The authors stated that the gas tightness of their containers was unreliable, and seals were broken as the pressure increased. G(gas) values for the current acid waste samples were estimated that ranged from 0.32 to 0.43 for alpha radiolysis. When samples were dried at elevated temperature following cure, no evolved gas was detected. The DSS samples had much lower G(gas) values of 0.04-0.15 for alpha radiolysis and 0.02 for gamma radiolysis. Gas compositions remaining in the vessels at the end of the tests indicated generation of hydrogen in all of the tests; production of oxygen was reported in all six of the alpha radiolysis experiments using current acid waste. Only

the DSS waste was examined by both alpha and gamma radiolysis, and conflicting data were obtained for the two alpha radiolysis experiments.

Very low G values have been reported from irradiation of water present as the hydrate in crystals (Zagorski 1983¹¹⁴). Water in the hydrates appears to exhibit the property of an energy sink. This has been attributed to the presence of a hydrated electron that can absorb energy by changing its state. For example, KOH · 0.5 H₂O was irradiated up to 1 MGy absorbed dose without generation of any observable H₂, O₂, or H₂O₂. The authors stated that this concept is also applicable to hydrates of organic materials.

3.1.5.1.3 Adsorbed or Absorbed Liquids

Radiolysis of adsorbed or absorbed liquids indicates that the sorbing medium can either be inert to radiation or can transfer energy to the sorbed liquid. Unless experimental data demonstrate that the binding medium is radiolytically inert (e.g., vermiculite), all of the radiation energy should be assumed to interact with the sorbed liquid.

Bibler (Bibler 1977²⁵) reported gamma and alpha radiolysis experiments on octane or a commercial vacuum pump oil sorbed onto vermiculite. Hydrogen was evolved, and oxygen was consumed. G(H₂) was found to vary linearly with the mass fraction of organic material. This suggested that the vermiculite absorbed some of the emitted energy, and it acted as an inert diluent (no energy transfer occurred between the vermiculite and the organic liquid). The extrapolated G(H₂) values for 100% liquid were 3 for octane and 1.6 for oil at high dose rate. At lower dose rates, the G(H₂) values reported were 4.5 for octane and 2.0 for oil. Radiolysis gases were produced in the nominal ratio of H₂/CO₂/CH₄ = 1.0/0.03/0.01.

Kinetic studies of water radiolysis in the presence of oxide systems have shown that the exposure of an oxide plus adsorbed water system to gamma radiation can result in energy transfer from the oxide to the water molecules (Garibov 1983¹¹⁵). Oxides studied included SiO₂, SiO₂-Al, SiO₂-Ca, Er₂O₃, La₂O₃, and Al₂O₃. Values of G(H₂) measured indicate that the energy transferred from the oxide to the adsorbed water molecules can easily be 3-5 times the energy that is originally absorbed by the water. Very little gas generation was observed from irradiation of silica gel that had been evacuated to remove adsorbed water (Krylova 1967). Lower values of G(H₂) were observed when the silica gel was purified. This effect was attributed to recombination of hydrogen precursors by the organic impurities on the surface of the silica gel.

Garibov (Garibov 1983¹¹⁶) also examined the effect of temperature on charge transfer in silica gel. Increasing the temperature at which the sample was irradiated decreased the value of G(H₂) measured. This was attributed to a greater desorption rate of water molecules from the oxide surface, which inhibited effective energy transfer to adsorbed molecules, and to thermal annealing of radiation defects in the oxide phase.

¹¹⁴ Zagorski 1983. Z. P. Zagorski, "Applied Aspects of Radiation Chemistry of Hydrates," in Proceedings of the Fifth Tihany Symposium on Radiation Chemistry, Akademiai Kiado, Budapest, 1983, pp. 331-336.

¹¹⁵ Garibov 1983. A. A. Garibov, "Water Radiolysis in the Presence of Oxides," in Proceedings of the Fifth Tihany Symposium on Radiation Chemistry, Akademiai Kiado, Budapest, 1983, pp. 377-384.

Vereshchinskii (Vereschinskii 1964¹¹⁶) summarized radiolysis experiments conducted on pentane adsorbed on zeolites or silica gel. The observed values of $G(H_2)$ were examined as a function of the electron fraction of pentane when the system pentane-solid was irradiated. The total dose absorbed by the system was used in calculating the $G(H_2)$ value. The results depended to a great extent on the identity of the solids studied. In most cases, more hydrogen was generated than would be expected without energy transfer from the adsorbent to the pentane. The charge transfer appeared to affect only one mono-layer of the adsorbed liquid. In contrast, radiolysis of water adsorbed on zeolites indicated that there is no energy transfer in that system (Krylova 1967).

3.1.5.2 Radiolysis of Solid Organic Acids

$G(H_2)$ values for some organic acids that are solid at room temperature have been reported in the range from 1.2 to 2.3 (Bolt 1963¹⁴). $G(\text{gas})$ values for the same materials range from 1.8 to 4.1. The maximum G value for flammable gas was 2.6. A value of $G(\text{CO}_2)$ up to 14 has been reported for one of the organic acids (isobutyric acid) (Spinks 1976³).

3.1.5.3 Radiolysis of Asphalt

A value of $G(\text{gas})$ for bitumen (asphalt) for low absorbed dose was estimated to be 1.3, with hydrogen being the primary gas evolved (Kosiewicz 1980¹¹⁷, corrected). No dependence was seen on temperature from 20 to 70°C. Gamma radiolysis experiments reported by Burnay (Burnay 1987¹¹⁸) measured lower G values.

3.1.5.4 Radiolysis of Soil

Gas evolution from plutonium-contaminated soil was reported by Pajunen (Pajunen 1977¹¹⁹). The soil was removed from the Z-9 Trench, which had been used as a liquid waste disposal site for the Plutonium Finishing Plant at the Hanford site. The waste solutions were acidic and consisted of aluminum, magnesium, calcium, and other metal nitrate salt wastes; degraded solvents (15% tributyl phosphate or dibutylbutyl phosphate in CCl_4); and other organics, such as solvent washings, fabrication oil, and other waste materials from hood and equipment flushes (Ludowise 1978¹²⁰). The top 30 cm of soil in the trench was mined. The soil moisture content ranged between 0.2 and 25.5 wt%, averaging approximately 5 wt%. Organic content averaged 7.1 wt % with a range of 0.2 to 46.4 wt %. The highest value of $G(\text{gas})$ calculated from Pajunen's data was 1.6, for a soil having a combined organic and moisture content of about 15

¹¹⁶ Vereshchinskii 1964. I. V. Vereshchinskii and A. K. Pikaev, Introduction to Radiation Chemistry, Israel Program for Scientific Translations, Ltd., Jerusalem, 1964.

¹¹⁷ Kosiewicz 1980. S. T. Kosiewicz, "Gas Generation from the Alpha Radiolysis of Bitumen," Nuclear and Chemical Waste Management 1, pp. 139-141, 1980.

¹¹⁸ Burnay 1987. S. G. Burnay, "Comparative Evaluation of and Radiation Effects in a Bitumenisate," Nuclear and Chemical Waste Management 7, pp. 107-127, 1987.

¹¹⁹ Pajunen 1977. A. O. Pajunen, "Radiolytic Evolution of Gases from Z-9 Soils," Rockwell Hanford Operations, RHO-CD-13, July 1977.

¹²⁰ Ludowise 1978. J. D. Ludowise, "Report on Plutonium Mining Activities at 216-Z-9 Enclosed Trench," Rockwell International, Rockwell Hanford Operations, RHO-ST-21, September 1978.

wt%. The typical composition of the gas generated by the soils was 50% N₂, 14% O₂, 23% H₂, and 13% CO₂.

Soil samples from Mound Laboratory property were contaminated with heat-source plutonium in the form of PuO₂ particles averaging 20 microns in size (Lewis 1983¹¹⁰). Gas generation was measured from a soil sample that contained about 5 wt% water. The G(gas) value was 0.22, with G(H₂)=0.15 and G(CO₂)=0.07. Oxygen was consumed, with G(-O₂)=0.10.

3.1.5.5 Radiolysis of Dry, Solid Inorganic Materials

Dry, solid inorganic materials do not generate hydrogen gas but may produce other gases (frequently oxygen).

Some common inorganic chemicals used in processing aqueous wastes include ferric sulfate, calcium chloride, and magnesium sulfate. One treatment process produces a precipitate of the hydrated oxides of iron, magnesium, aluminum, silicon, etc. (Kazanjian 1981¹⁰⁹). Various nitrates and carbonates can also be present (Clements 1985a¹²¹, Clements 1985b¹²²).

The yield of nitrite ions is more frequently measured in gamma radiolysis of solid nitrates than is the oxygen yield. For stoichiometric decomposition, a value of G(O₂) should be one-half of the G(NO₂⁻) value. A value of G(O₂)<1.3 has been determined (Johnson 1970¹²³). G values measured for gamma radiolysis of barium, potassium, and sodium chlorates had G(Cl⁻)<0.8 and G(O₂)<4.0.

For alkali and alkaline earth perchlorates, values of G(Cl⁻)<1.1 and G(O₂)<5.3 were measured. Careful tests were conducted to detect the presence of ozone and free chlorine, but neither of those gases was observed (Johnson 1970¹²⁴).

3.1.6 Comparison of Laboratory G Values With Effective G Values Measured for Drums of CH-TRU Wastes

Actual CH-TRU wastes consist of general laboratory waste (glass, crucibles), combustible materials (paper, plastic), organic shielding materials (Benelex^R, Plexiglas^R), metals, sludges or concreted wastes, and various other materials. The materials are contaminated with TRU radionuclides in solution (such as dilute nitric acid) or in particle form (such as PuO₂).

Typically, several different contaminated materials are present in a given waste container. The G value calculated for actual CH-TRU wastes is an effective G value. All of the radioactivity present in the waste container is assumed to be absorbed by the waste materials, when actually some self-absorption of the alpha decay energy occurs inside particulate contamination.

¹²¹ Clements 1985a. T. L. Clements, Jr. and D. E. Kudera, "TRU Waste Sampling Program: Volume I--Waste Characterization," EG&G Idaho, Inc., EGG-WM-6503, September 1985.

¹²² Clements 1985b. T. L. Clements, Jr. and D. E. Kudera, "TRU Waste Sampling Program: Volume II--Gas Generation Studies," EG&G Idaho, Inc., EGG-WM-6503, September 1985.

¹²³ Johnson 1970. E. R. Johnson, The Radiation-Induced Decomposition of Inorganic Molecular Ions, Gordon and Breach Science Publishers, New York, 1970.

Effective G values have been measured for drums of actual CH-TRU wastes. On the whole, the effective hydrogen G values are much lower than maximum hydrogen G values for the waste forms based on the material in the waste form with the highest G value. For drums of combustible wastes, the maximum $G(H_2)$ value determined in controlled experiments was 2.1 versus a possible value of 4.0 based on laboratory experiments. For drums of sludge, the maximum $G(H_2)$ value measured was 0.3 versus a possible value of 1.6 based on laboratory experiments.

Sources of information for gas generated from actual CH-TRU wastes include examinations of drums retrieved from storage at the Idaho National Engineering and Environmental Laboratory (INEEL) (Clements 1985a¹²²) and at LANL (Warren 1985¹²⁴, Clements 1985a¹²²), and experiments measuring gas composition and pressure for newly generated drums of wastes at the RFETS (Clements 1985b¹²³, Kazanjian 1985¹²⁵), at LANL (Clements 1985b¹²³, Zerwekh 1986¹²⁶) and at the SRS (Ryan 1982¹²⁷).

3.1.6.1 Retrieved Drums of CH-TRU Wastes

G values for radiolytic gas production from unvented retrieved drums can only provide lower limits, because of uncertainties in the rates at which gases can permeate through the drum gaskets or diffuse through gaps between the gaskets and sealing surfaces. [Tests conducted at INEEL indicate that drums will vent when pressurized above 20 psig (Clements 1985a¹²²).] Only gas in the drum headspace was sampled, and the concentrations of generated gases could have been higher inside the waste bags.

A total of 209 waste containers (199 drums) of wastes that originated at the RFETS were retrieved from storage at INEEL (Clements 1985a¹²²). A sample of the headspace gas in each drum was taken and analyzed. Internal pressure and void volume for gas accumulation were measured, and the containers were opened and the wastes examined. All but seven of the waste drums had been sealed with nonporous styrene-butadiene gaskets.

A lower limit for the hydrogen G value was calculated (by this author) for each of the drums using reported alpha activity, void space, pressure, time since drum closure, and hydrogen concentration in the headspace. Almost all of the drums had minimum $G(H_2)$ values less than 1.0. Those that had minimum $G(H_2)$ values greater than 1.0 and activity greater than 0.1 Ci (the specific activity of Pu-239 is 0.07 Ci/g) are listed in Table 3.1-44.

¹²⁴ Warren 1985. J. L. Warren and A. Zerwekh, "TRU Waste-Sampling Program," Los Alamos National Laboratory, LA-10479-MS, August 1985.

¹²⁵ Kazanjian 1985. A. R. Kazanjian, et al., "Gas Generation Results and Venting Study for Transuranic Waste Drums," Rockwell International, Rocky Flats Plant, RFP-3739, 1985.

¹²⁶ Zerwekh 1986. A. Zerwekh and J. L. Warren, "Gas Generation and Migration Studies Involving Recently Generated Pu-238-Contaminated Waste for the TRU Waste Sampling Program," Los Alamos National Laboratory, LA-10732-MS, July 1986.

¹²⁷ Ryan 1982. J. P. Ryan, "Radiogenic Gas Accumulation in TRU Waste Storage Drums," E. I. du Pont de Nemours & Co., Savannah River Laboratory, DP-1604, January 1982.

One possible source of a high apparent G value is that the time period for gas generation may have been underestimated. The storage times are based on the dates the drums were sealed, while wastes may have been placed into the drum weeks or months prior to the closure date. Four of the drums had calculated effective G values of 6.0 or higher. These include one drum of combustibles and three drums of cemented sludges and solutions containing organic complexing chemical wastes.

Solidified liquid organic wastes, including cemented sludges and solutions and organic sludges, will not be transported until more information is available on their potential for hydrogen (or other flammable) gas generation.

Combustible waste Drum No. 76-02898 had a calculated $G(H_2)$ value of 6.0, which is above the bounding laboratory value of 4 (at room temperature). The most probable explanation for the high calculated $G(H_2)$ value is that the drum contained a significant amount of Am-241. Drum No 76-02898 was lead-lined, a procedure necessary when Am-241 is present in higher concentration than in usual weapons-grade plutonium. This was the only one of the combustible waste containers that was lead lined. The original assay listed 32 g Pu and no Am. A second assay, conducted on a NaI system using a 100-second count (not long enough to measure americium) listed 29 g Pu and no Am. Reassay records showed a measurement of 29 ± 16.3 g Pu.

Drums of CH-TRU wastes were also retrieved at LANL, but those drums had been closed with a gas-permeable sponge-rubber gasket. All of the LANL drums were at ambient pressure, demonstrating that flow or diffusion of gases through the porous gasket had occurred.

3.1.6.2 Newly Generated Waste Experiments

Experiments on newly generated wastes have been conducted at RFETS, LANL, and SRS.

3.1.6.2.1 Rocky Flats Environmental Technology Site Experiments

The gas generated inside each of 16 drums of newly generated wastes contaminated with weapons-grade plutonium was measured over a 13-week period as the second phase of a two-phase experiment (Clements 1985¹²³, Kazanjian 1985¹²⁴). Wastes were assayed as individual packages or by radiochemical analysis to determine total alpha activity. In Phase I, the drums were vented for three months using one of three potential venting devices (a filter, a semi-permeable gasket, or a Hanford vent clip). Drum pressure and gas concentrations in the drum headspaces were measured. At the conclusion of Phase I, the drums were purged with air, and a gas sample was taken to obtain the initial gas composition for the second phase of the study. In all cases the plug in the lid of the rigid liner was left out, so that the rigid liner was not a primary barrier for gas escape.

Table 3.1-44 — Data for RFETS Retrieved Waste Drums with $G(H_2)_{min} > 1.0^{a,b}$

ID No.	Waste Form	Activity (Ci)	Time (days)	Gauge Pressure (mmHg)	Void Vol. (l)	Gas Composition						Minimum G Values			
						H ₂	O ₂	N ₂	Ar	CO ₂	HC	G(H ₂)	G(CO ₂)	G(HC)	G(gas)
22-01194	Combustibles	0.30	276	2.0	181	0.4	18.8	79.2	0.9	0.2	0.3	1.0	0.6	0.7	2.3
02-39371	combustibles ^c	1.78	245	28.5	182	2.1	0.1	96.5	1.1	0.0	0	1.1	0	0	1.1
02-39465	combustibles	0.74	227	-19.0	179	0.9	17.2	79.4	0.9	1.1	0.3	1.1	1.3	0.3	2.7
02-39195	combustibles	0.15	307	-36.0	168	0.3	12.5	83.3	0.9	2.1	0.3	1.4	8.4	1.2	10.9
744-3829	cmt s&s	0.16	263	13.5	77	0.8	1.7	95.0	1.1	0.8	0.1	1.7	0.2	0.3	2.1
76-01642	spc slud	0.74	880	-43.0	151	7.5	5.6	85.2	1.0	0.0	0.6	1.9	0	0.2	2.1
76-02898	combustibles	2.15	326	87.5	171	18.2	0.0	64.6	0.8	15.2	0.8	6.0	5.0	0.2	11.3
744-3841	cmt s&s	0.15	256	5.4	76	2.7	2.8	91.8	1.1	0.0	0.3	6.3	0	0.6	6.9
744-3837	cmt s&s	0.17	256	5.5	38	6.2	0.2	90.7	1.1	0.0	0	6.4	0	0	6.4
744-2389	cmt s&s	0.20	4439	154.0	162	32.4	0.1	64.2	0.8	0.0	2.3	8.6	0	0.6	9.2

Notes: ^a cmt s&s = cemented sludges and solutions consisting of organic complexing chemical wastes; spc slud = an uncemented sludge packaged in polyethylene bottles inside a drum; HC = hydrocarbons.

^b Ambient pressure at RFETS is about 613 mmHg; ambient pressure at INEEL is about 640 mmHg.

^c Contained Ful-Flo^R (polypropylene) filters coated with grease.

The drum lids were sealed to the drums using Permatex Form-a-Gasket^R. The drums were pressure tested and considered to be sealed if they held a pressure of 155 torr above atmospheric pressure for 3 hours with a pressure loss of no more than 5 torr. Two of the drums developed leaks of 41 torr and 28 torr. These values were not considered in determining the gas generation rates. The drum pressure and gas composition of samples taken from the drum headspace were recorded weekly. Gas compositions were determined by mass spectrometry.

While no gas samples were taken from inside the waste bags, the gas generation rates calculated from the drum headspace samples should give the gas generation rates inside the waste bags. In these experiments, hydrogen generated inside the inner waste bags had permeated through the layers of plastic in the drum into the drum headspace, and the hydrogen concentration increased linearly with time. When this occurs, the hydrogen concentrations in the inner waste bags, drum liner bags, and drum headspaces are all increasing at the same rate.

The G values for hydrogen, carbon dioxide, hydrocarbons, and total gas were calculated for each of the drums in the cited reports. Plots of hydrogen gas production versus time that are shown in the reports appear linear, indicating that absorbed dose effects were minimal. The G values so obtained are listed in Table 3.1-45. Figure 3.1-1 shows Ar, CO₂, H₂, hydrocarbons, and isopropanol partial pressures as functions of time for a drum containing leaded rubber gloves (Figure #16 in Table 3.1-45). (The isopropanol is attributed to the Permatex Form-a-Gasket^R material.)

The high values of G(H₂) for the organic setup waste form (solidified organics) are much greater than the G(H₂) values of less than 3 that have been measured for oils. The radionuclide content of the drums was confirmed by reassaying samples of the sludge. The authors (Clements 1985b¹²³, Kazanjian 1985¹²⁶) suggested that corrosion of the mild steel drum could be responsible for the high rate of hydrogen production. Corrosion can produce hydrogen gas in an anaerobic, wet atmosphere, which were the conditions inside each of the two drums after the first week of the experiment.

The relatively large amounts of CO₂ generated in several of the drums could have been caused by microbial action or chemical reactions. Measured G(H₂) values for combustibles (maximum of 2.1) are all well within the maximum G value of 4 at room temperature established in Section 3.1.4. Measured G(H₂) values for inorganic sludges (maximum of 0.3) are much lower than the maximum G(H₂) value of 1.6 for water.

Table 3.1-45 — Effective G Values for RFETS Newly-Generated Waste Drums

Fig #	Waste Form Description	Effective G values			
		H ₂	CO ₂	HC	Total
1	inorganic sludge	0.30	0.01	--	0.31
2	inorganic sludge	0.28	0.01	--	0.29
3	inorganic sludge	0.19	0.01	--	0.92 ^a
4	inorganic sludge	0.16	0.01	0.02	0.19
5	organic setup	15.1	0	--	15.1
6	organic setup	22.5	0	--	22.5
7	dry combustibles	2.1	1.6	--	3.7
8	dry combustibles	1.4	1.3	0.9	3.6
9	dry combustibles	0.79	0.47	--	1.26
10	dry combustibles	0.39	5.1	--	5.49
11	wet combustibles	0.74	0.17	--	0.91
12	wet combustibles	0.52	0.28	0.25	1.05
13	plastic & rubber	1.1	2.2	--	3.3
14	plastic & rubber	0.65	0.77	--	1.42
15	leaded rubber	0.32	6.4	--	6.72
16	leaded rubber	0.95	0.49	0.07	1.51

Notes: ^aIncludes G(O₂)=0.72. All other G(O₂)s were negative.

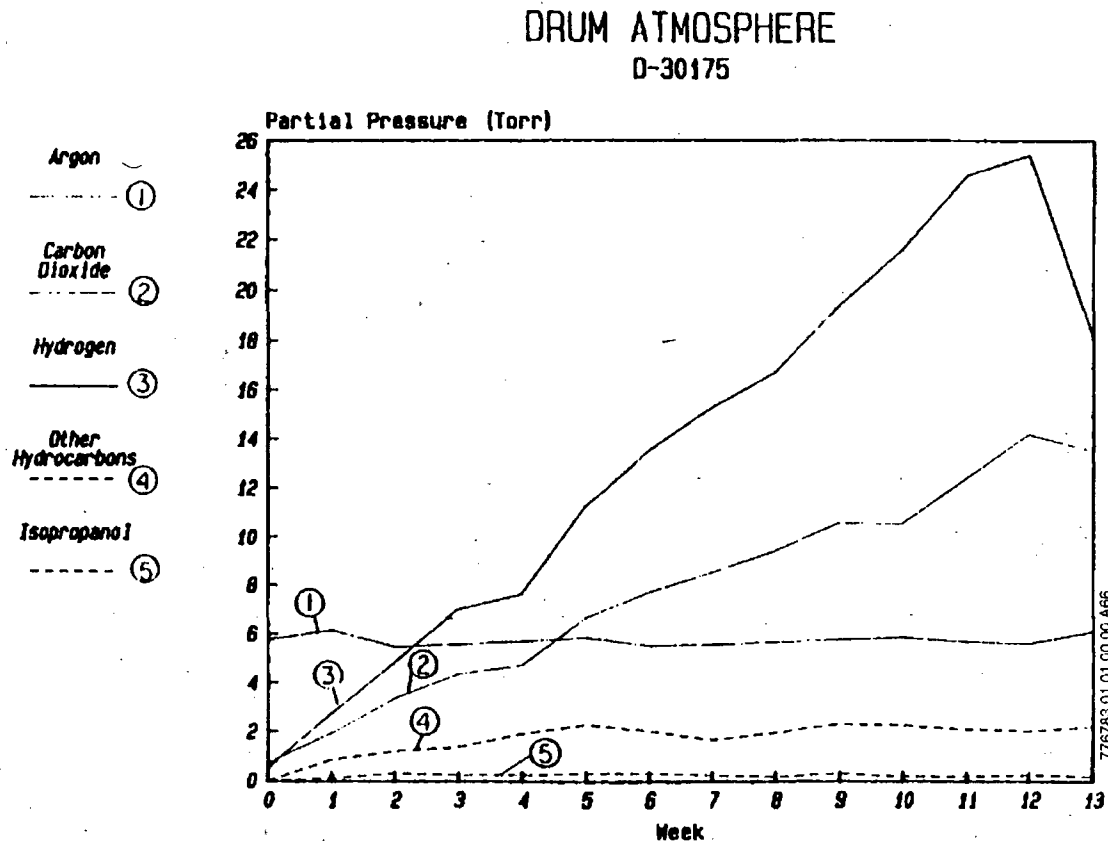


Figure 3.1-1 — Partial Pressures of Various Gases in a Drum of Newly-Generated Waste from RFP (Leaded Rubber Gloves)

3.1.6.2.2 Los Alamos National Laboratory Experiments

In the LANL experiments, six high-activity newly generated Pu-238 waste drums were examined to determine gas generation rates and the ability of filters to limit the hydrogen concentration in the drum. Two additional drums of wastes provided information on the permeation of hydrogen through the 90-mil high-density polyethylene rigid liner. The experiments were separated into the same two phases as the RFETS experiments.

All of the drums selected contained combustible materials. Each waste package within the drum was individually assayed using segmented gamma scan techniques, and the assay results for the individual packages were added to obtain the total activity. The wastes had been generated from three to eight months before the gas generation phase of the experiments began.

Gas generation data for five of the six drums of waste for which void volumes could be measured are listed in Table 3.1-46. An ambient atmospheric pressure at Los Alamos of 579 mm Hg was assumed for all cases. (Actual ambient pressures were obtained for sampling dates, but using those pressures did not reduce the scatter of the measurements.)

No observable decrease in G values appeared to occur in these experiments until after about 100 days into the experiment (for wastes that had been generated three to eight months before the experiments began). In another 200 days, the G values had dropped to about one-half of their initial values. A plot of gas yields versus time for drum BFB-116 is shown in Figure 3.1-2. The composition of the generated gas was 46% CO₂, 41% H₂, 12% CO, and 1% CH₄, comparable to the gas composition measured in laboratory radiolysis experiments on Hypalon^R or Neoprene^R.

3.1.6.2.3 Savannah River Site Experiments

SRS initiated a series of experiments in 1976 to acquire data on drum pressures and gas compositions under actual storage conditions at SRS (Ryan 1982¹²⁸). Four drums were filled with highly contaminated material consisting of typical SRS waste. Data were collected on a monthly basis for over four years. The waste materials were contained in plastic bags that were placed within a 90-mil-thick high-density polyethylene liner. The liner was sealed with an adhesive. The drum lids were locked on over a neoprene-butadiene O-ring gasket (specified to be nonporous), with a galvanized ring bolt. While sealing compound was used to hold the gasket in place on the drum lid, no adhesive was applied to the lower surface of the gasket. Valves and airtight bulkhead fittings were connected to each drum wall before the drums were filled with waste. A detailed inventory and radioactive material assay were conducted of each bag of waste materials. The test drums were placed in concrete culverts. The culverts, 7-ft high by 7-ft dia. cylindrical containers with 6-in. thick walls, were designed to contain 14 drums of waste in two tiers of seven. The culvert lids were grouted in place and sealed with epoxy.

About 100 days after the experimental drums had been filled with waste and sealed, the drums were placed into the culvert. Two thermocouple wires were included in the instrumentation, one attached to the drum that contained the greatest amount of radioactivity (Drum No. 122), the other suspended in the culvert to read the air temperature. Ryan (Ryan 1982¹²⁸) reported most of the temperature data only for outside air. Where data were available, the drum surface

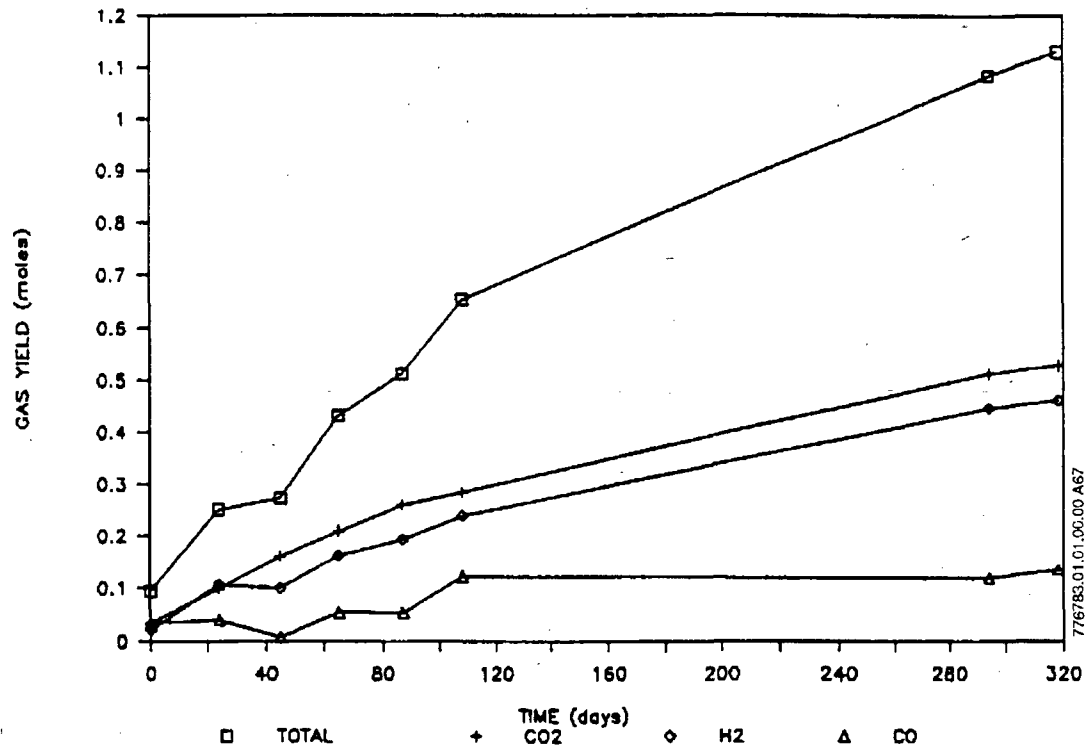
Table 3.1-46 — Effective G Values for LANL Newly-Generated Waste Drums^a

Drum No.	Waste Form Description	Pkg.	Dates		²³⁸ Pu		Void Vol. ^c		Effective G Values		
			Start	End	g	Ci	I	H2	Initial Total	H2	Final Total
BFB-112	plastic, leaded gloves	7/28/83	4/10/84	2/22/85	1.2	16.8	198.1	0.3	0.6 ^b	0.1	0.3
BFB-114	plastic, rags	9/23/83	12/29/83	3/30/84	15.6	218.4	201.1	0.4	0.7	0.1	0.6
BFB-116	leaded gloves	10/27/83	4/10/84	2/22/85	2.28	31.9	210.3	0.2	0.5 ^b	0.1	0.2
BFB-118	rags, plastics, metals, metal oxides	10/27/83	4/10/84	1/29/85	4.92	68.9	201.3	0.4	0.8 ^b	0.2	0.4
BFB-120	leaded gloves	1/03/84	8/10/84	3/06/85	1.6	22.4	215.6	0.2	0.4	0.1	0.3

Notes: ^aCalculated using authors' data; Drum BFB-113 has been omitted because of the scarcity of data in the sealed condition.

^bInitial G values apply to the first 100 days of the 300-day experiment.

^cVoid volume for drum BFB-114 is the volume inside the rigid liner; other void volumes include the void between the rigid liner and the drum.



776783.01.01.00.00.A67

Figure 3.1-2 — Gas Yields vs. Time LANL Drum BFB-116 (Leaded Rubber Gloves)

temperature typically was no more than 5°C different from the outside air temperature, although one measurement showed a difference of 12°C.

The first gas samples were drawn 101 days after the drums were sealed. Subsequent samples were taken about every 30 days. The composition of ambient air was determined as part of the standardization of each gas analysis and was, on the average, 79% N₂, 21% O₂, and 0.1% CO₂. [The 1% Ar that is present in ambient air was not reported.]

Ryan (Ryan 1982¹²⁸) plotted drum gas concentrations versus time and drum gauge pressures versus time. The gas composition of the culvert atmosphere was also measured. The largest hydrogen concentration measured in a culvert air sample was about 0.7 mole %. No appreciable hydrogen concentration was measured inside the culvert until day 993. Ryan stated that a significant quantity of gas was escaping from the drums at all times. This conclusion appears to be based on the maximum G values calculated from the largest (or close to largest) increases in the amounts of gas present, and then extrapolating the pressures from those G values. Ryan concluded that G(gas) appeared to be at least equal to 1.0 and more likely about 2.0.

Ryan's data (concentrations for each gas species, air temperature, gauge pressure, drum void volume, activity, and sampling date) were entered onto a LOTUS spreadsheet that calculates moles of gas and G values as functions of time. Drums 119 and 121 appear to have leaked, while drums 120 and 122 could have been well sealed, at least for most of the four-year period. Plots of gauge pressure and total moles of gas present are shown in Figures 3.1-3 and 3.1-4 for drum 122. The cyclical behavior of the gauge pressure versus time plot corresponds to annual temperature variations.

Figure 3.1-5 shows a plot of G(H₂) versus time, with the points chosen by Ryan checked. The plot illustrates the variability in the experimental data. The greatest slope of the curve (ignoring wide swings in the data) occurs at the beginning of the experiment, with $G(H_2)_{\max}=0.2$. Similar evaluations performed for the other three drums show that the G values appear to be much less than 1, in agreement with laboratory data for the radiolysis of rubber.

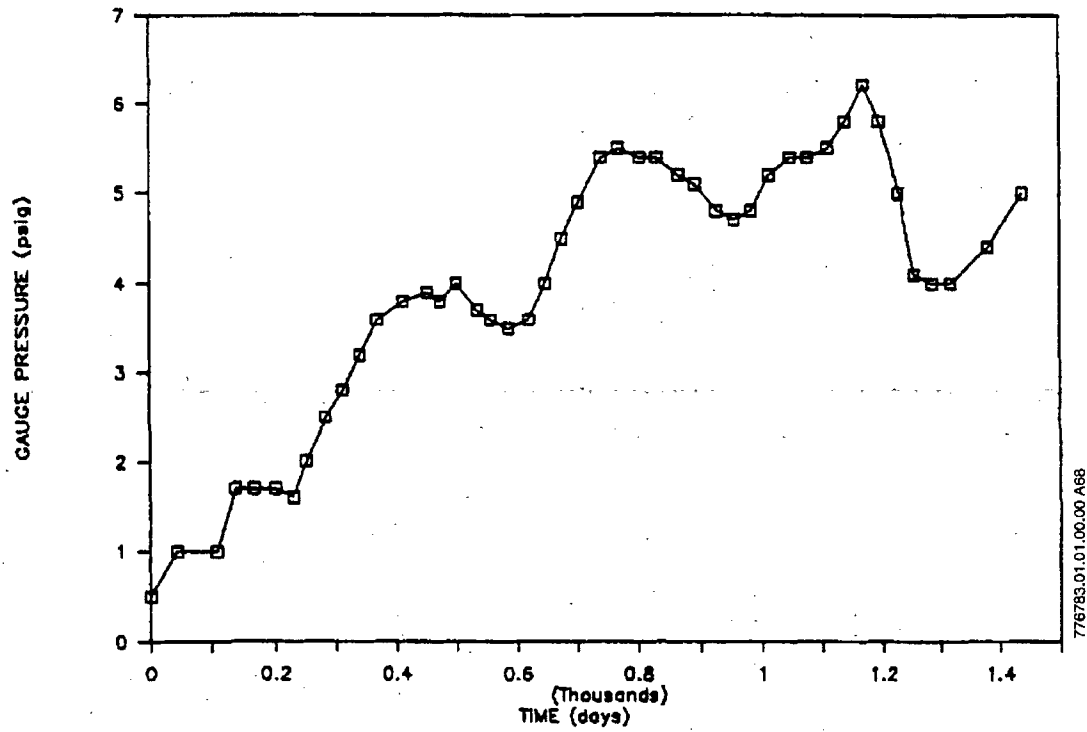
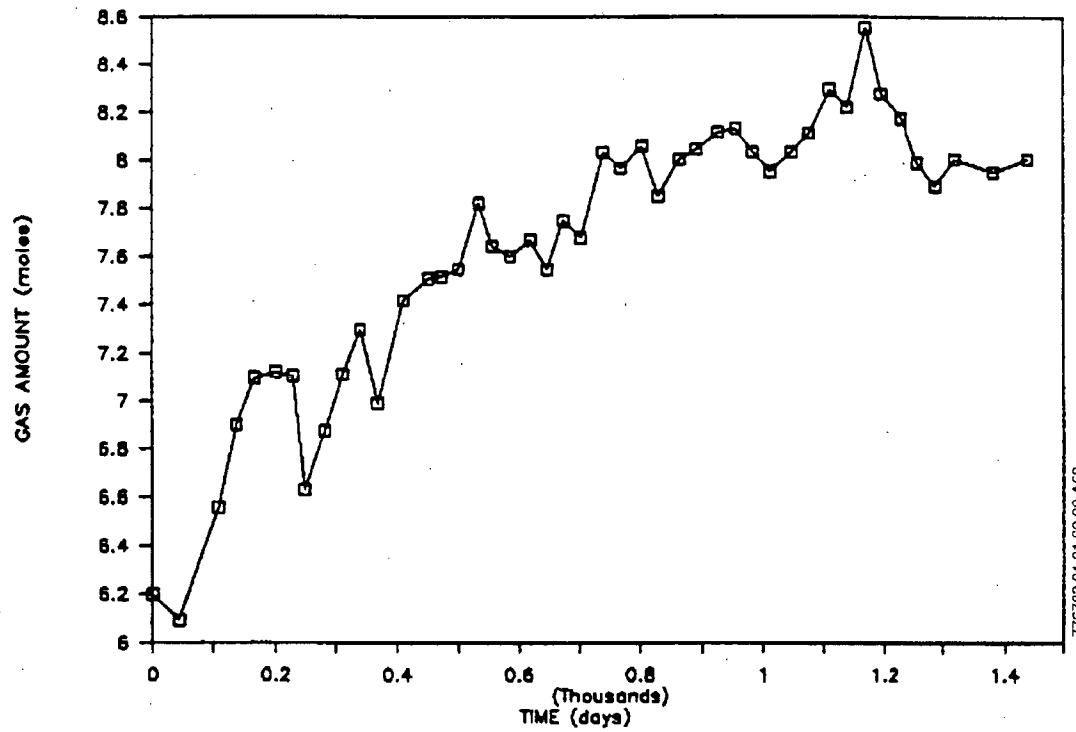


Figure 3.1-3 — Gauge Pressure in Drum 122 vs. Time



776783.01.01.00.00 A69

Figure 3.1-4 — Moles of Gas Present in Drum 122 vs. Time

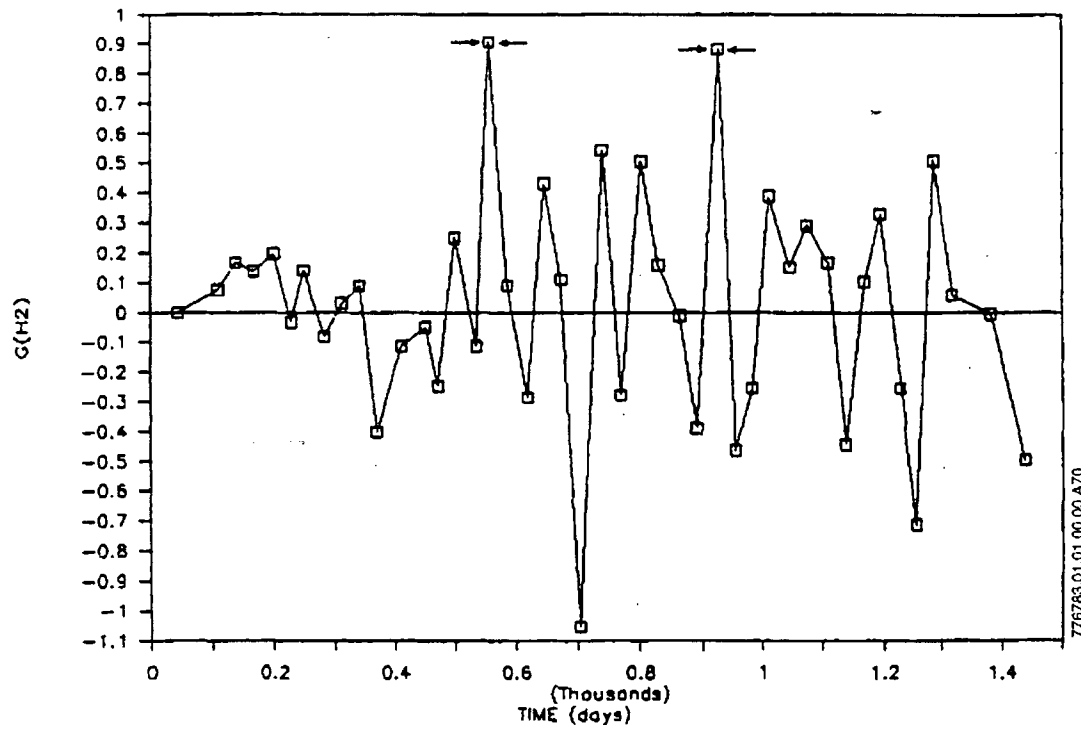


Figure 3.1-5 — $G(H_2)$ vs. Time for Drum 122

Attachment A

Chemical Properties and Commercial Uses of Organic Materials

Executive Summary

Almost all of the materials that are potential generators of gas from radiolysis are organic materials (water and inorganic materials containing water being the primary exceptions). These organic materials are hydrocarbons or their derivatives containing oxygen, nitrogen, halogens, or other atoms. Naturally occurring organic materials that are present in the CH-TRU wastes, such as cellulose, also may generate radiolytic gas.

Basic families of organic liquids are described in Section A1.1. Polymers and their use in commercial materials are discussed in Section A1.2. Section A1.3 illustrates structural features of many commercial polymers.

A1.1 Families of Organic Liquids

Common names for families of organic liquids are: the hydrocarbons [alkanes (paraffins), alkenes (olefins), alkynes, cyclic hydrocarbons, and aromatic hydrocarbons]; the oxygenated organic compounds [ethers, esters, alcohols, aldehydes, ketones, and organic acids]; and the organic derivatives of ammonia (called amines). Compounds having the same formula but different structures and properties are called isomers (Pierce 1970¹). (Higher-molecular-weight members of these families may be solids at room temperature rather than liquids.)

Hydrocarbons, as the name implies, contain only hydrogen and carbon atoms. Except for methane (CH₄), the carbon atoms form chains that consist of two or more atoms. The main chain may also contain side branches of atoms.

The alkanes are saturated hydrocarbons in which only carbon-carbon single bonds occur. All of the alkane names end in "-ane," such as methane, ethane, propane, and butane. In the petroleum industry, a high-temperature process called cracking of the saturated hydrocarbons causes the molecules to separate into fragments that then recombine at random to form other hydrocarbons and hydrogen gas. The alkanes are used as fuels to generate energy by oxidation (combustion). The addition of halogens forms such compounds as carbon tetrachloride, chloroform, trichloroethylene, hydrogen chloride, and other halogenated compounds.

The alkenes (olefins) are unsaturated hydrocarbons that contain double carbon-carbon bonds. All of the names of the alkenes end in "-ene," such as ethene, propene, and butene. Many of the olefins polymerize, forming macromolecules having gram molecular masses on the order of 10⁴ to 10⁶.

In the alkynes, the double bond of the alkenes is replaced by a triple carbon-carbon bond. Acetylene is one of the common alkynes.

¹ Pierce 1970. J. B. Pierce, The Chemistry of Matter, Houghton Mifflin Company, Boston, 1970.

Cyclic hydrocarbons may be alkanes (such as cyclohexane), alkenes, or alkynes. All of the cyclic alkanes have saturated carbon-carbon bonds.

Aromatic hydrocarbons contain a benzene ring and include benzene, toluene, naphthalene, and xylene. Aromatic compounds may be formed by joining benzene rings together through the elimination of hydrogen, for example, biphenyl (two benzene rings). Naphthalene is an example of a condensed-ring structure and is used in the manufacture of alkyd resins. A hydrogen atom on a benzene ring can be replaced by other chemical species through halogenation, sulfonation, or nitration. Toluene is formed by replacing one of the hydrogen atoms in benzene by a methyl (CH_3) group. Xylene is formed by replacing two of the hydrogens by methyl groups. The location of the substituted groups determines the isomer (ortho, meta, para). Phenol is formed by adding a hydroxyl group (OH) to the benzene molecule and is used in the formation of Bakelite[®] plastics and glues.

Organic compounds may also contain oxygen. The oxygen atoms may be bonded between carbon atoms to form ethers or esters. Oxygen atoms may bond to single carbon atoms to form alcohols (ROH), ketones (RCOR'), aldehydes (RCOH), or carboxylic acids (RCOOH).

Individual alcohols are named by adding the suffix "-ol" to the name of the corresponding alkane, such as "methanol." Several different isomers of alcohols are possible as the number of carbons in the chain increases, such as in propanol and butanol. More than one hydroxyl (OH) group may be present in the molecule, such as for ethylene glycol and glycerol.

Aldehydes are formed by oxidation of alcohols which have an hydroxyl group on a terminal carbon atom. The simplest aldehyde is formaldehyde. It reacts with phenol and urea to form phenol-formaldehyde and urea-formaldehyde resins.

Ketones are formed by oxidation of a secondary alcohol. The simplest ketone is acetone.

The organic (carboxylic) acids contain the group $-\text{COOH}$ attached to either an alkyl or an aryl group. Examples of these acids are formic acid, acetic acid, oleic acid, and oxalic acid. Long-chain organic acids are called fatty acids.

The reaction of a carboxylic acid with an alcohol produces an ester (RCOOR') plus water. Common names for esters end in "-ate." When there are no double or triple bonds between the carbon atoms, the materials are solids; otherwise, they are liquids at room temperature. Esters of low molecular mass are used as solvents, artificial flavors, and components in perfumes. Waxes contain esters formed by the reaction of long-chain acids and alcohols. Fatty-acid esters of glycerol are found in vegetable oils and animal fats. The less volatile esters (such as dioctyl phthalate) are commonly used as plasticizers. The reaction of fats with boiling sodium hydroxide solution forms soaps.

Amines are organic derivatives of ammonia. Amines are used in the production of polyamides, such as Nylon[®]. Proteins are also polyamides.

A1.2 Polymers

Polymers are natural or synthetic materials that are composed of very large molecules containing repeating structural units called monomers. The structural features of many commercial polymers are shown in Section A1.3.

Knowledge of the repeat unit can aid in interpreting or predicting the gases generated by radiolysis (or thermal degradation). Additives also can affect the gas generation potential of commercial materials made from polymers. Polymers composed of more than one kind of repeat unit are termed copolymers.

Various additives are combined with the base polymer or polymers in compounding to produce the final commercial composition and properties of a plastic. Liquid plasticizers are added to polymers such as polyvinyl chloride (PVC) or cellulose esters to increase their flexibility. These compounds are chosen for their relatively low volatility but may be lost from a material that is heated or aged for long periods of time. Plasticizers in PVC commonly compose about 30-40% of the total material. Most of the plasticizers are less solvent- and chemical-resistant than the polymer to which they are added. Many plasticizers may be extracted by oils or dry-cleaning solvents. Most of the plasticizers are combustible, and lower the flame resistance and softening points of the total composition (Deanin 1972²).

Stabilizers are added to the polymer to increase resistance to heat, ultraviolet light, or other forms of degradation. Most plastics contain antioxidants, which may be consumed eventually by chemical reactions with oxygen. Polymers that crosslink are often rendered quite sensitive to oxidative degradation by radiation. The use of effective antioxidants can significantly improve their radiation resistance. Materials added to obtain other desirable properties could result in a final product which is less radiation resistant than the base polymer. However, this does not appear to happen often. Inorganic fillers are usually effective in increasing radiation resistance by dilution of the base polymer (EPRI 1981³).

Organic phosphates and halogenated compounds are frequently added to polymers to increase their flame resistance. At the same time, these additives may decrease thermal and other types of stability, particularly if they contain organic halogen compounds (Deanin 1972²).

The CH-TRU wastes consist of commercial materials, containing plasticizers and stabilizers that can affect radiolytic gas production (both the composition and amount of gas). For this reason, maximum G values measured for commercial materials provide more realistic upper bounds for radiolytic gas generation than do the G values measured for pure polymers.

² Deanin 1972. R. D. Deanin, Polymer Structure, Properties and Applications, Changers Books, Boston, 1972.

³ EPRI 1981. Georgia Institute of Technology, "Radiation Effects on Organic Materials in Nuclear Plants," Electric Power Research Institute, EPRI NP-2129, November 1981.

Chain lengths on the order of a hundred thousand monomer units are not uncommon in polymers (Sisman 1963⁴). Branched or network structures may be present. Most linear commercial polymers have a small amount of branching caused by impurities in the starting material or side reactions during the polymerization process. Polymers may be amorphous, crystalline, or contain regions of each. The linear polymers are used in a wide variety of molded and extruded objects. The solubility of linear polymers in solvents permits their use as paints, coatings, and films. Other applications include fibers, fabrics, tires, hoses, and gaskets.

Polymers are useful as electrical and thermal insulators. The rigidity and hardness of cross-linked polymers have been utilized in molded objects, which can be produced economically by thermally initiating cross-linking reactions within the mold. Polymers having network structures are generally insoluble. They have a strong tendency to retain their shape through rubber-like elasticity in materials with a low density of cross links or through high rigidity and hardness in heavily cross-linked materials (Sisman 1963⁴).

Table A1.2-1 lists the families of plastics (Dean 1987⁵). Cross-references of commercial names with the base polymers are available in Desk-Top Data Bank (1977⁶, 1979⁷, 1980⁸).

A1.2.1 Acetals

Acetal homopolymers are prepared from formaldehyde and consist of high-molecular-weight linear polymers of formaldehyde. They are among a group of high-performance engineering thermoplastics that resemble Nylon[®] in appearance (but not in properties). Trade names include Delrin[®] and Celcon[®]. Prolonged exposure to elevated temperatures results in the liberation of increasing amounts of formaldehyde. Acetals have relatively low radiation stability (Harper 1975⁹). Major applications for polyoxymethylene (an acetal) are in business machines, automotive gears and bearings, plumbing fittings, such as tub assemblies, and in consumer articles, such as aerosol containers (Deanin 1972²).

⁴ Sisman 1963. O. Sisman, et al., "Polymers," in Radiation Effects on Organic Materials, Academic Press, New York, 1963, eds. R. O. Bolt and J. G. Carroll.

⁵ Dean 1987. J. A. Dean, Handbook of Organic Chemistry, McGraw-Hill Book Company, New York, 1987.

⁶ Desk-Top Data Bank 1977. Desk-Top Data Bank, Elastomeric Materials, The International Plastics Selector, Inc., San Diego, 1977.

⁷ Desk-Top Data Bank 1979. Desk-Top Data Bank, Films, Sheets, and Laminates, The International Plastics Selector, Inc., San Diego, 1979.

⁸ Desk-Top Data Bank 1980. Desk-Top Data Bank, Commercial Names and Sources for Plastics and Additives, The International Plastics Selector, Inc., San Diego, 1980.

⁹ Harper 1975. C. A. Harper, Handbook of Plastics and Elastomers, McGraw-Hill Book Company, New York, 1975.

Table A1.2-1 — Families of Plastics

Acetals

Acrylics

Polymethyl methacrylate (PMMA)

Polyacrylonitrile (PAN)

Alkyds

Alloys

Acrylic-polyvinyl chloride alloy

Acrylonitrile-butadiene-styrene-polyvinyl chloride alloy (ABS-PVC)

Acrylonitrile-butadiene-styrene-polycarbonate (ABS-PC)

Allyls

Allyl-diglycol-carbonate polymer

Diallyl phthalate (DAP) polymer

Cellulosics

Cellulose acetate resin

Cellulose-acetate-propionate resin

Cellulose-acetate-butyrate resin

Cellulose nitrate resin

Ethyl cellulose resin

Rayon[®]

Chlorinated polyether

Epoxy

Fluorocarbons

Polytetrafluoroethylene (PTFE)

Polychlorotrifluoroethylene

Perfluoroalkoxy (PFA) resin

Fluorinated ethylene-propylene (FEP) resin

Polyvinylidene fluoride

Ethylene-chlorotrifluoroethylene copolymer

Ethylene-tetrafluoroethylene copolymer

Polyvinyl fluoride

Melamine-formaldehyde

Melamine phenolic

Nitrile resins

Phenolics

Polyamides

Nylon[®]s

Aromatic Nylon[®]s

Polyamide-imide

Polyaryl ether

Polycarbonate

Polyesters

Polyethylene terephthalate (PET)

Unsaturated polyesters

Table A1.2-1 — Families of Plastics (Concluded)

Polyimide

Polymethyl pentene

Polyolefins

Low-density polyethylene (LDPE)

High-density polyethylene (HDPE)

Ultrahigh-molecular-weight polyethylene

Polypropylene

Polybutylene

Polyallomers

Polyphenylene oxide

Polyphenylene sulfide

Polyurethanes

Silicones

Styrenics

Polystyrene

Acrylonitrile-butadiene-styrene (ABS) copolymer

Styrene-acrylonitrile (SAN) copolymer

Styrene-butadiene copolymer

Sulfones

Polysulfone

Polyether sulfone

Polyphenyl sulfone

Thermoplastic elastomers

Urea-formaldehyde

Vinyls

Polyvinyl chloride (PVC)

Polyvinyl acetate (PVAC)

Polyvinylidene chloride

Polyvinyl butyrate

Polyvinyl formal

Polyvinyl alcohol

Ref: Dean 1987⁵.**A1.2.2 Acrylics**

Polyacrylates are derivatives of acrylic acid. They are frequently used as coatings or paints. Polyethyl acrylate is used as a component of synthetic rubbers in which resistance to oils and high temperatures is important (Bopp 1963¹⁰). Polymethyl methacrylate (PMMA), a related compound, has common trade names of Plexiglas[®] and Lucite[®]. Acrylics are also made into fibers and fabrics, such as Orlon[®], Acrilan[®], and Creslan[®] (Rutherford 1963¹¹).

¹⁰ Bopp 1963. C—D. Bopp, et al., "Plastics," in Radiation Effects on Organic Materials, Academic Press, New York, 1963, eds. R. O. Bolt and J. G. Carroll.

¹¹ Rutherford 1963. H. A. Rutherford, "Textiles," in Radiation Effects on Organic Materials, Academic Press, New York, 1963, eds. R. O. Bolt and J. G. Carroll.

Polyacrylonitrile (PAN) is a member of the acrylic family that includes nitrogen atoms in its structure. Its major use is in the production of wool-like fibers used in sweaters, blankets, and carpeting (Deanin 1972²).

A1.2.3 Alkyds

Alkyds are thermosetting plastics that are widely used for molded electrical parts. They have high degrees of cross-linking (Deanin 1972²) and are chemically similar to polyester resins (Harper 1975⁹).

A1.2.4 Alloys

Polymer alloys are physical mixtures of structurally different homopolymers or copolymers. The mixture is held together by secondary intermolecular forces such as dipole interaction, hydrogen bonding, or van der Waals' forces. The physical properties of these alloys are averages based on composition (Dean 1987⁵). Polymer alloys include acrylic-polyvinyl chloride, acrylonitrile-butadiene-styrene-polyvinyl chloride (ABS-PVC), and acrylonitrile-butadiene-styrene-polycarbonate (ABS-PC). ABS alloyed or blended with polycarbonate results in a thermoplastic that is easier to process, has high heat and impact resistance, and is cheaper than polycarbonate alone.

A1.2.5 Allyls

Allyl polymers are linear thermoplastic structures. Molding compounds with mineral, glass, or synthetic fiber filling are used for electrical components. Allyl polymers include allyl-diglycol-carbonate and diallyl phthalate (DAP). Their benzene rings, a high degree of cross-linking, and the usual glass fiber reinforcement provide high rigidity and strength. Primary applications are in molded structural electrical insulation. Diallyl phthalate resin is also used for surfacing laminates in furniture and paneling (Deanin 1972²).

A1.2.6 Cellulosics

Cellulosics are a class of polymers that are prepared by various treatments of purified cotton or special grades of wood cellulose. Trade names include Tenite[®], Ethocel[®], and Forticel[®]. Cellulosics are among the toughest of thermoplastics, are generally economical, and are good insulating materials (Harper 1975⁹). The most prominent industrial cellulosics are cellulose acetate, cellulose acetate butyrate, cellulose propionate, and ethyl cellulose.

Cellulose butyrate, propionate, and acetate are tough and rigid, and useful for applications where clarity, outdoor weatherability, and aging characteristics are needed. The materials are fast-molding plastics and can be manufactured to have hard, glossy surfaces (Bopp 1963¹⁰). Major applications of these cellulose esters include blister packaging, pencils, lighting fixtures, tool handles, and tubing (Deanin 1972²). Ethyl cellulose is compatible with many other resins and with most plasticizers. These properties, along with its compatibility with cellulose nitrate, are responsible for its use in paints and as a coating for fabrics (Bopp 1963¹⁰).

Incompletely nitrated cellulose nitrate is used in molded objects, and as a constituent of lacquers and photographic film. Because of its flammability and tendency to decompose at high temperatures, cellulose nitrate is not used as a compression or injection molding material (Bopp 1963¹⁰). The nitrogen content for cellulose nitrate plastics is usually about 11%, for lacquers and cement base it is 12%, and for explosives it is 13% (Dean 1987⁵).

Cotton and cellulose acetate (Rayon[®]) are two cellulose derivatives that are made into fibers. Cellulose derivatives (cotton and wood) are blended in making paper. Cellophane is also based on cellulose (Deanin 1972²). Cellulose triacetate is used primarily in motion picture film and magnetic recording tape (Deanin 1972²). Cellulose ethers have applications where low temperature impact strength is needed, such as in instrument cases, electrical appliance parts, and tool handles. Different processing produces a polymer that is completely soluble in water and is used primarily as a thickening agent in foods, shampoo, latex paints, paper, and adhesives (Deanin 1972²).

A1.2.7 Epoxy

Epoxy and unsaturated polyesters are cross-linking resins that can be cured by chemical agents with little or no application of heat or pressure. They are frequently used in paints and finishes (Bopp 1963¹⁰).

A1.2.8 Fluorocarbons

Fluorocarbons include polytetrafluoroethylene (PTFE), polychloro-trifluoroethylene, perfluoroalkoxy (PFA) resin, fluorinated ethylene-propylene (FEP) resin, polyvinylidene fluoride, ethylene-chlorotrifluoroethylene copolymer, ethylene-tetrafluoroethylene copolymer, and polyvinyl fluoride.

These polymers have good abrasion and solvent resistance and electrical properties. Polyvinyl fluoride is used only as a film (Dean 1987⁵).

Polytetrafluoroethylene is the base polymer for Teflon[®]. Polychloro-trifluoroethylene resins may be processed by melting and can be molded as extruded. Kel-F[®] is one of the trade names (Harper 1975⁹). PFA resins are used as electrical insulations in flat cables and circuitry and in laminates used in electrical and mechanical applications. Fluorinated ethylene/propylene copolymer has applications in capacitors, cables, flexible belting, textile finishing, and printing (Deanin 1972²).

A1.2.9 Nitrile Resins

The principal monomer of nitrile resins is acrylonitrile (see Section B.2.1).

A1.2.10 Polyamides

Polyamides are called nylons, which include hard materials used in mechanical parts as well as soft materials used for fibers and textiles. Aromatic nylons (also called aramids) are high temperature nylons such as Nomex[®]. Nomex[®] is used in sheet, fiber, and paper form for insulation (Harper 1975⁹) and in filters.

A1.2.11 Polyaryl Ether

Polyaryl ether is one of the relatively new thermoplastics that can be used for engineering applications in the automotive, appliance, and electrical industries. One trade name is Arylon[®] (Harper 1975⁹).

A1.2.12 Polycarbonate

Polycarbonates have high performance characteristics in engineering designs, which require very high impact strength. As with most plastics containing aromatic groups, polycarbonates have high radiation stability (Harper 1975⁹).

A1.2.13 Polyesters

Polyesters are used in the production of film and fibers. Glass reinforced polyesters are used in automotive, electrical/electronic, and other industrial applications replacing other plastics or metals. The basic polymer is polyethylene terephthalate (PET). Brand names include Mylar[®] (sheet) and Dacron[®] (fiber). Unsaturated polyesters are discussed under "Epoxies".

A1.2.14 Polyimides

Polyimides can be used at the highest temperatures among the commercially available plastics, and they are the strongest and most rigid (Harper 1975⁹). These materials can be used in various forms, including moldings, laminates, films, coatings, and adhesives.

A1.2.15 Polymethyl Pentene

Polymethyl pentene is another thermoplastic based on the ethylene structure. Applications for this material have been developed in the fields of lighting and in the automotive, appliance, and electrical industries (Harper 1975⁹).

A1.2.16 Polyolefins

The family of polyolefins includes various polyethylenes (low-density polyethylene, high-density polyethylene, ultrahigh-molecular-weight polyethylene), polypropylenes, polyethylene oxide, polypropylene oxide, and polybutylene.

Polypropylenes are chemically similar to polyethylenes (Harper 1975⁹). The material is termed isotactic if the methyl groups are on the same side of the chain and atactic if the arrangement is random. The isotactic polymer is more frequently used commercially (Sisman 1963⁴). The polymer is used to make molded items or fibers (Herculon is one example).

Commercial polyethylene oxide is waxy and fibrous. Because of its water solubility, it is used as a plasticizer and as an additive in non-polymeric materials rather than as a base polymer (Bopp 1963¹⁰).

Treatment of polyethylene with chlorine and sulfur dioxide decreases the crystallinity of the polyethylene and results in a rubbery material. Applications include wire and cable insulation,

liquid roof coatings, gaskets, floor tile, and shoe soles (Deanin 1972²). One trade name is Hypalon[®], which is used in fabricating glovebox gloves.

Polybutylene low-molecular-weight polymers are viscous liquids used in compounding adhesives, caulks, and sealants. High-molecular weight polymers are used in elastomers and sealants, such as butyl rubber (Deanin 1972²).

Polyallomers are polyolefin-type thermoplastic polymers produced from two or more different monomers, such as propylene and ethylene. In general, the properties of polyallomers are similar to those of polyethylenes and polypropylenes (Harper 1975⁹).

A1.2.17 Polyphenyl Polymers

Polyphenylene oxide is formulated by the oxidative coupling of phenolic monomers. This material is used for engineering applications. One trade name is Noryl[®]. Polyphenylene sulfide is a crystalline polymer, and is used for coatings and molded materials. One trade name is Ryton[®].

A1.2.18 Polyurethanes

The most common usage of polyurethane is in foams, which may be flexible or rigid (Deanin 1972²). These foams have applications as insulation, structural reinforcement, packaging, and gaskets (Harper 1975⁹).

A1.2.19 Silicones

Silicones are also called polysiloxanes. They are characterized by their three-dimensional branched-chain structure. Various organic groups (such as methyl, phenyl, vinyl) introduced within the polysiloxane chain impart certain characteristics and properties. Applications include waterproofing, paper coatings, elastomers, sealants, medical equipment, and transformers (Deanin 1972²).

A1.2.20 Styrenics

Polystyrene can be regarded as a substituted polyethylene with phenyl groups on alternate carbon atoms (Sisman 1963⁴). Polystyrene is highly rigid at room temperature, but the rigidity may be decreased and the impact strength increased by the addition of plasticizers. It can be used in moldings or in small electrical components, as well as in containers and other packaging items (Sisman 1963⁴). Common trade names are Lustrex[®] and Styron[®].

Styrene-acrylonitrile (SAN) copolymers are random, amorphous copolymers whose properties vary with molecular weight and copolymer composition. SAN resins are rigid, hard, transparent thermoplastics (Dean 1987⁵). Acrylonitrile-butadiene-styrene (ABS) copolymer is a thermoplastic resin. Trade names include Marbon Cicolac[®], Bason[®], and Lustran[®]. ABS plastics have hardness and rigidity without brittleness, at moderate costs (Harper 1975⁹). Styrene-butadiene copolymers are used in gaskets.

A1.2.21 Sulfones

Polysulfones are rigid, strong thermoplastics, and can be molded, extruded, or thermoformed into a wide variety of shapes. The chemical structure is highly resonating (contains benzene rings), resulting in high stability (Harper 1975⁹). Copolymers with olefins, however, have low radiation stability (Jellinek 1978¹²).

A1.2.22 Thermosetting Plastics

Thermosetting plastics are insoluble and infusible because of their three-dimensional structure. They are used chiefly as molding powders and as binders for laminates. Examples are phenol-formaldehyde, urea-formaldehyde, and melamine-formaldehyde. Common uses are in molded household items. Laminated sheets and tubes are widely used in electrical components or molded components of industrial equipment (Bopp 1963¹⁰).

A1.2.23 Vinyls

Vinyl polymers are structurally based on the ethylene chain (Harper 1975⁹).

Polyvinyl chloride (PVC) is a material with a wide range of rigidity or flexibility. PVC can be plasticized with a wide variety of materials to produce soft, yielding plastics. Without plasticizers, PVC is a strong, rigid material that can be machined, heat-formed, or welded by solvents or heat. Typical uses include wire and cable insulation and foam applications. PVC can also be made into film and sheet (Harper 1975⁹). Other uses are as a fabric coating, for upholstery and similar household articles, and for hoses and tubular items (Bopp 1963¹⁰).

Polyvinyl acetate (PVAC) is used in latex paints because of its quick-drying and self-priming properties, and resistance to weathering. It is also used in hot-melt and solution adhesives (Dean 1987⁵). Copolymers of polyvinylidene chloride and PVC are used to make Saran (Bopp 1963¹⁰).

Polyvinyl alcohol is made by the hydrolysis of polyvinyl acetate. It is soluble in water and resistant to most organic solvents. It is used in solvent-resistant hoses, diaphragms, and gaskets, and in coatings, textile sizing, and as an adhesive (Bopp 1963¹⁰).

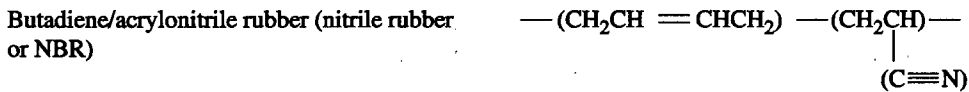
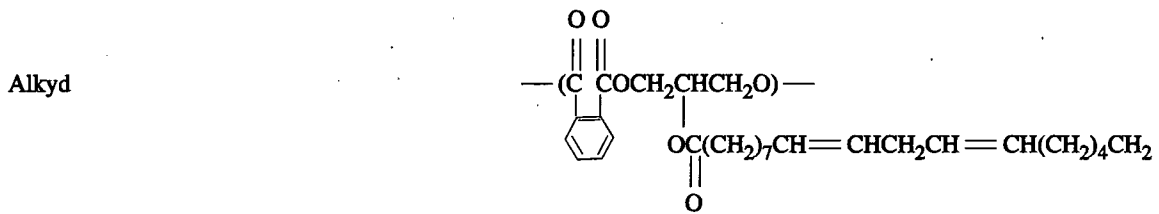
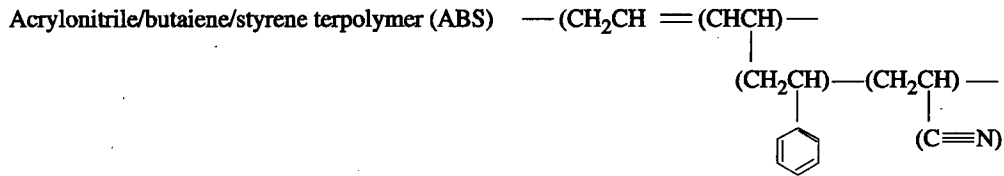
Polyvinyl acetals, consisting of polyvinyl butyral, polyvinyl formal, and polyvinyl acetal, are the most abundantly used plastics related to polyvinyl alcohol. Polyvinyl formal is used in coating electrical wire. Polyvinyl acetal is tough and easy to mold, and is used for bottle caps, combs, and as a binder in heavily filled molded items. Polyvinyl butyral is a very important item of commerce as the interlayer in safety glass (Bopp 1963¹⁰).

A1.3 Structural Features of Commercial Polymers

The structural features of many commercial polymers are shown in Table A1.3-1.

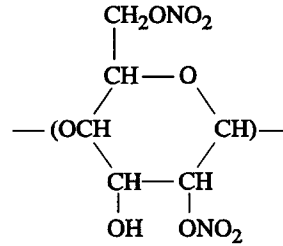
¹² Jellinek 1978. H. H. G. Jellinek, Aspects of Degradation and Stabilization of Polymers, Elsevier Scientific Publishing Company, New York, 1978.

Table A1.3-1 — Structural Features of Commercial Polymers

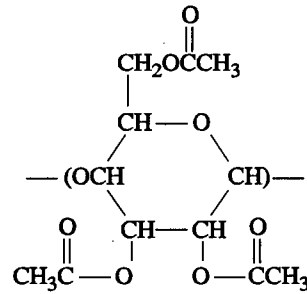


**Table A1.3-1 — Structural Features of Commercial Polymers
(Continued)**

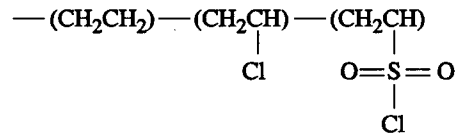
Cellulose Nitrate



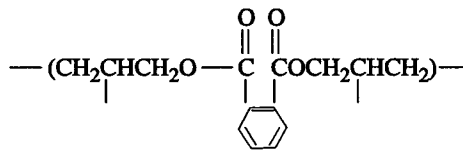
Cellulose Triacetate



Chlorosulfonated Polyethylene



Diallyl Phthalate



Epoxy Resin

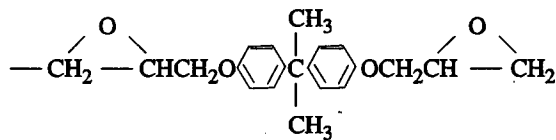
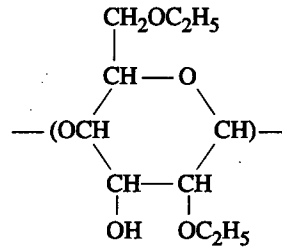
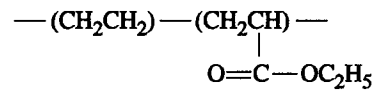


**Table A1.3-1 — Structural Features of Commercial Polymers
(Continued)**

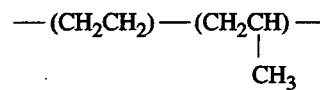
Ethyl Cellulose



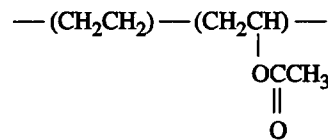
Ethylene/Ethyl Acrylate Copolymer



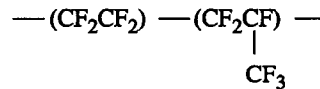
Ethylene/Propylene Copolymer



Ethylene/Vinyl Acetate Copolymer



Fluorinated Ethylene/Propylene Copolymer



Melamine-Formaldehyde

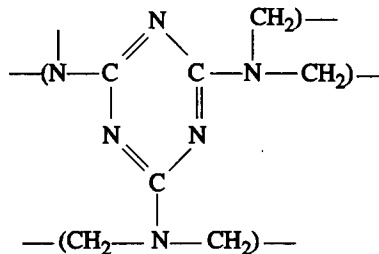
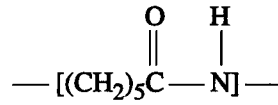
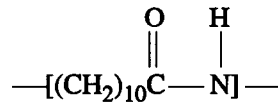


**Table A1.3-1 — Structural Features of Commercial Polymers
(Continued)**

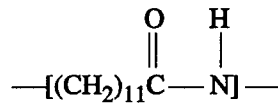
Nylon 6



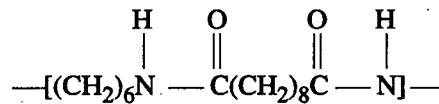
Nylon 11



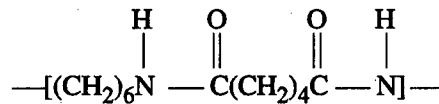
Nylon 12



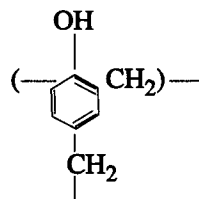
Nylon 610



Nylon 66



Phenol-formaldehyde



Phenoxy Resin

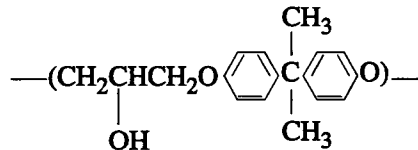
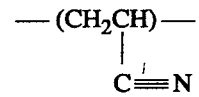
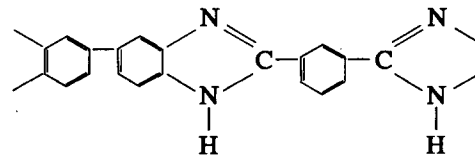


**Table A1.3-1 — Structural Features of Commercial Polymers
(Continued)**

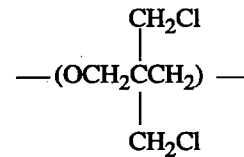
Polyacrylonitrile



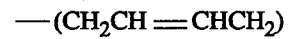
Polybenzimidazole



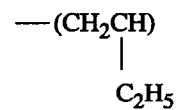
Poly-3,3-bis (chloromethyl) oxetane (Penton)



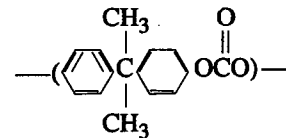
Polybutadiene



Poly-1-Butene



Polycarbonate



Polychloroprene (neoprene)

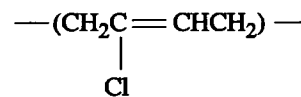
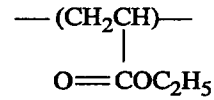
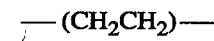


**Table A1.3-1 — Structural Features of Commercial Polymers
(Continued)**

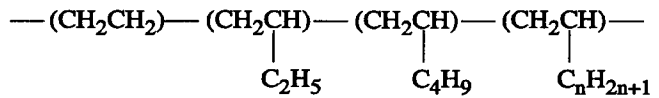
Polyethyl Acrylate



High-Density Polyethylene



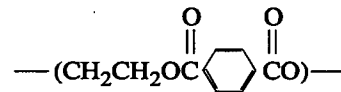
Low-Density Polyethylene



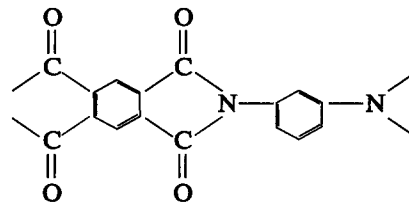
Polyethelene Oxide



Poly(ethelene terephalate)



Polyimide



Polyisobutylene

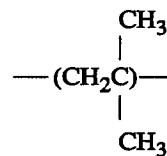
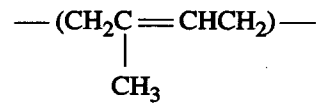
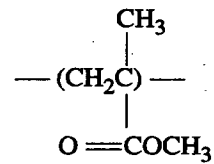


**Table A1.3-1 — Structural Features of Commercial Polymers
(Continued)**

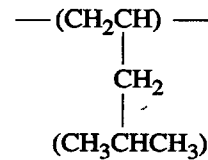
Polyisoprene (Natural Rubber)



Polymethyl Metacrylate



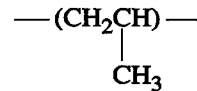
Poly (4-methylpentene-1)



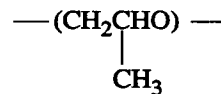
Polyoxymethylene (Acetal)



Polypropylene



Polypropylene-Oxide



Poly-p-xylylene

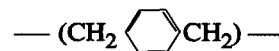
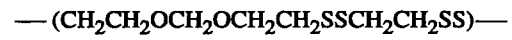
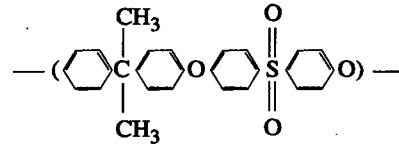


**Table A1.3-1 — Structural Features of Commercial Polymers
(Continued)**

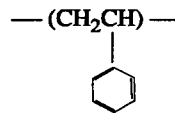
Polysulfide Elastomer



Polysulfone



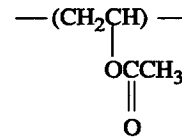
Polystyrene



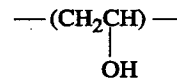
Polytetrafluoroethylene



Polyvinyl Acetate



Polyvinyl Alcohol



Polyvinyl Butyral

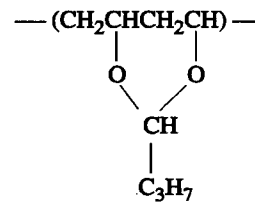
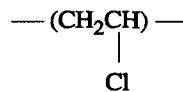
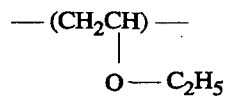


**Table A1.3-1 — Structural Features of Commercial Polymers
(Continued)**

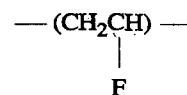
Polyvinyl Chloride



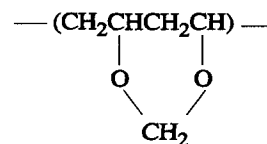
Polyvinyl Ethyl Ether



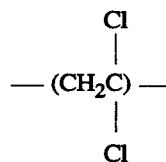
Polyvinyl Fluoride



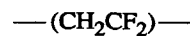
Polyvinyl Formal



Polyvinylidene Chloride



Polyvinylidene Fluoride



Polyvinyl Pyrrolidone

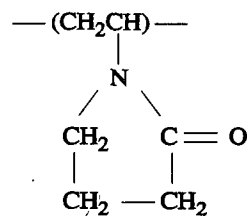
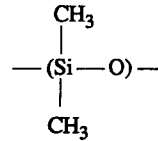
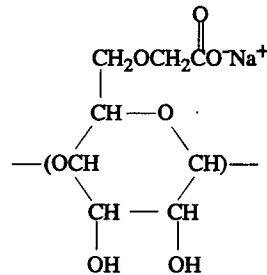


**Table A1.3-1 — Structural Features of Commercial Polymers
(Concluded)**

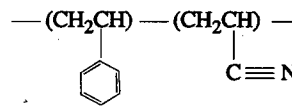
Silicone



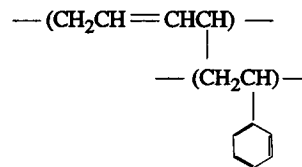
Sodium Carboxymethyl Cellulose (CMC)



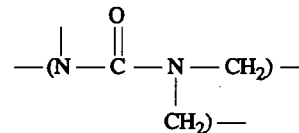
Styrene/Acrylonitrile Copolymer



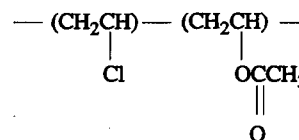
Impact Styrene



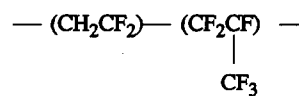
Urea-Formaldehyde



Vinyl Chloride Vinyl Acetate Copolymer



Vinylidene Fluoride/Hexafluoroporylene Copolymer



Attachment B

Absorption of Alpha Decay Energy Inside Particles of PuO₂

Executive Summary

This attachment derives the fraction of alpha decay energy escaping from a spherical particle of PuO₂ of radius r . The rate of energy deposition is calculated from an estimated Bragg curve for PuO₂.

B1.1 Introduction

Let

s = stopping distance of alpha particles in PuO₂,

a = radius of spherical particles of PuO₂.

E_0 = energy generated per unit volume.

The solution is separated into three cases: for Case I, the diameter of the particle is less than the stopping distance ($2a < s$), for Case II, the stopping distance is between the radius and the diameter of the particle ($a \leq s \leq 2a$), and for Case III, the radius of the particle is greater than the stopping distance ($s < a$).

The rate of alpha particle energy deposition inside the PuO₂ particle is calculated based on the estimated Bragg curve shown in Figure B1-1. This curve was generated by the program TRIM-88 "The Transport of Ions in Matter," copyrighted by J. P. Biersack and J. F. Ziegler (discussed in Ziegler 1985¹).

The highest atomic number nucleus included in the program is U(92), so UO₂ with the density of PuO₂ (11.4 g/cm³) was used to simulate PuO₂. Figure B1-2 shows the alpha particle energy in MeV versus distance traveled from its origin for alpha particles having initial energies of 5.15 MeV (Pu-239) and 5.49 MeV (Pu-238). [The total distance along the particle's path is somewhat greater, due to straggling that occurs at low energies when collisions of the alpha particle with nuclei become more important than interactions of the alpha particle with electrons.]

B2.1 Case I, $2a < s$

The geometry of Case I is shown in Figure B2-1. The fraction of energy reaching point Q from point P along r' is

$$E_F = f(E_0, r') \quad (\text{B2-1})$$

¹ Ziegler 1985. J. F. Ziegler, J. P. Biersack, and U. Littmark, The Stopping and Range of Ions in Solids, Vol. I, Pergamon Press, New York, N.Y., 1985.

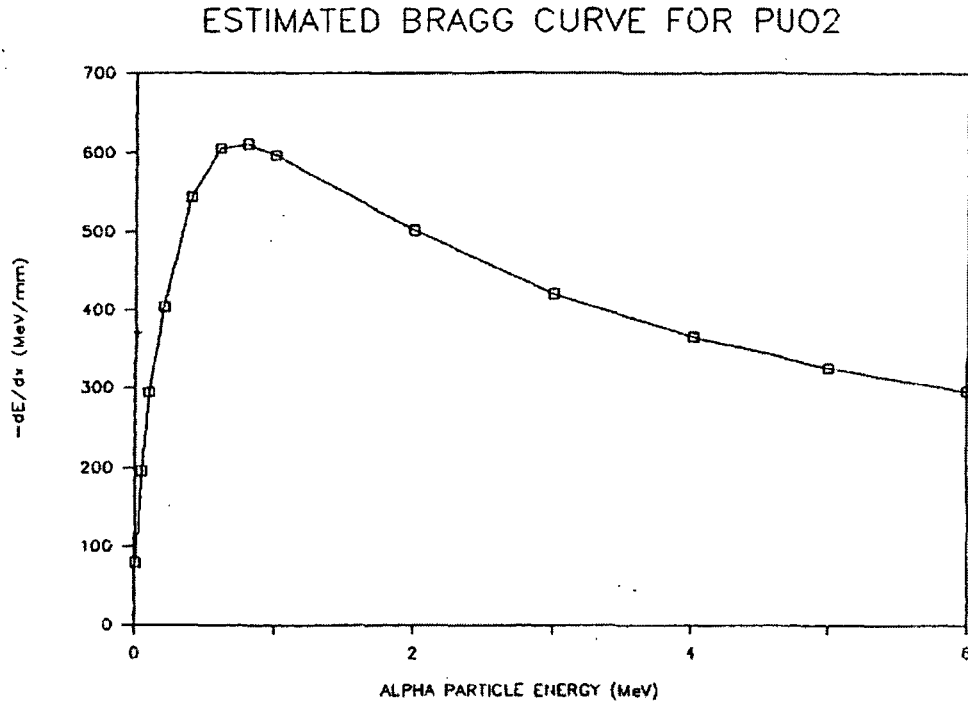


Figure B1-1
Estimated Bragg Curve for PuO₂

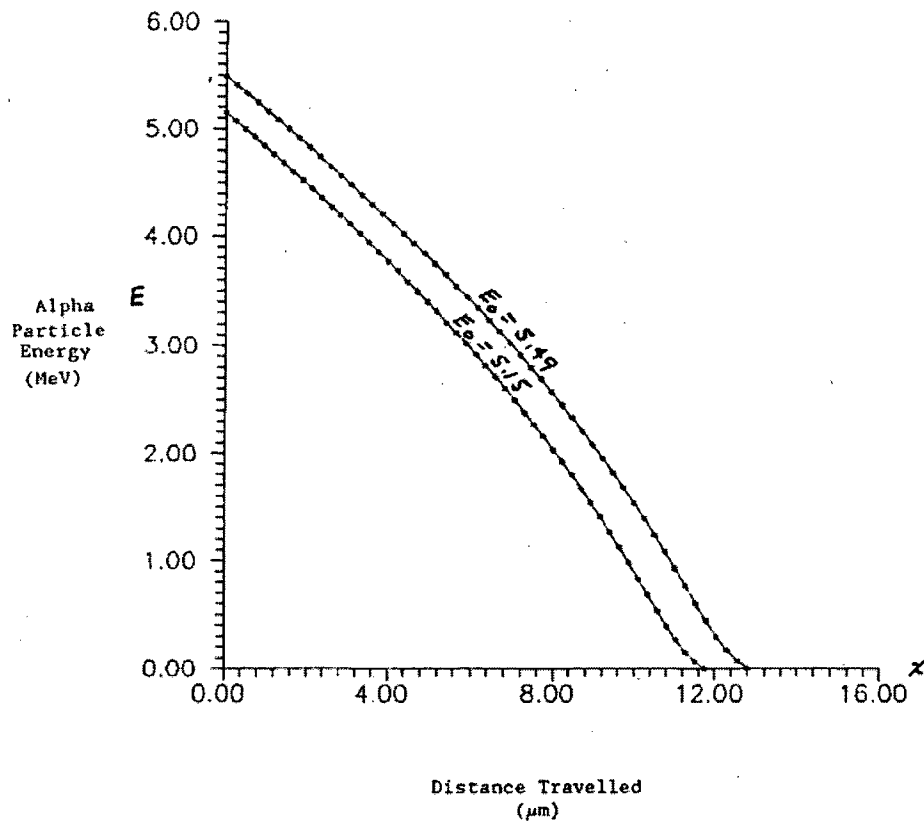


Figure B1-2
Alpha Particle Energy vs. Distance Traveled from Point of Origin

Where:

$$r'^2 = a^2 + r^2 - 2 ar \cos \omega \quad (\text{B2-2})$$

since $r' < a$ for this case, and $f(E_0, r')$ is shown graphically in Figure B1-2 for two values of E_0 .

The fraction of the area of a sphere centered at P, subtended by $d\phi$ and revolved about the x axis is

$$A = \frac{r' d\phi 2\pi r' \sin \phi}{4\pi r'^2} \quad (\text{B2-3})$$

The total energy reaching the boundary, a, from point P is

$$\rho(r) = 1/2 \int_0^\pi f(E_0, r') \sin \phi d\phi \quad (\text{B2-4})$$

The total energy from all points, P, in the sphere is

$$E = \int_0^a 4\pi r^2 \rho(r) dr = 2\pi \int_0^a r^2 \int_0^\pi f(E_0, r') \sin \phi d\phi dr \quad (\text{B2-5})$$

The fraction of energy generated in the sphere and escaping from the surface is

$$\frac{E}{E_r} = \frac{2\pi}{4/3 \pi a^3 E_0} \int_0^a r^2 \int_0^\pi f(E_0, r') \sin \phi d\phi dr \quad (\text{B2-6})$$

where r' is defined in Eq. (B2-2).

The law of signs allows $\cos \omega$ to be expressed in terms of ϕ where

$$\frac{r'}{\sin \omega} = \frac{a}{\sin(\pi - \phi)} = \frac{a}{\sin \phi}, \quad (\text{B2-7})$$

$$r' = \frac{a \sin \omega}{\sin \phi} = \sqrt{a^2 + r^2 - 2 ra \cos \omega}, \quad (\text{B2-8})$$

$$\frac{a^2 \sin^2 \omega}{\sin^2 \phi} = a^2 + r^2 - 2 ra \cos \omega, \quad (\text{B2-9})$$

$$\frac{a^2}{\sin^2 \phi} (1 - \cos^2 \omega) = a^2 + r^2 - 2ra \cos \omega, \quad (\text{B2-10})$$

$$\frac{a^2}{\sin^2 \phi} \cos^2 \omega - 2ra \cos \omega + a^2 + r^2 - \frac{a^2}{\sin^2 \phi} = 0, \quad (\text{B2-11})$$

$$\frac{a^2}{\sin^2 \phi} \cos^2 \omega - 2ra \cos \omega + r^2 - \frac{a^2 \cos^2 \phi}{\sin^2 \phi} = 0, \quad (\text{B2-12})$$

$$\cos \omega = \frac{2ra \pm \sqrt{4r^2 a^2 - \frac{4a^2}{\sin^2 \phi} \left[r^2 - a^2 \frac{\cos^2 \phi}{\sin^2 \phi} \right]}}{\frac{2a^2}{\sin^2 \phi}} \quad (\text{B2-13})$$

$$= \left[r \pm \sqrt{-\frac{r^2 \cos^2 \phi}{\sin^2 \phi} + \frac{a^2 \cos^2 \phi}{\sin^4 \phi}} \right] \frac{\sin^2 \phi}{a} \quad (\text{B2-14})$$

$$= \frac{r}{a} \sin^2 \phi \pm \frac{|\cos \phi| |\sin \phi|}{a} \sqrt{\frac{a^2}{\sin^2 \phi} - r^2}, \quad (\text{B2-15})$$

$$= \frac{r}{a} \sin^2 \phi + \frac{\cos \phi}{a} \sqrt{a^2 - r^2 \sin^2 \phi}. \quad (\text{B2-16})$$

The positive solution is chosen since when $\phi = 0$, $\omega = 0$ and when $\phi = \pi$, $\omega = \pi$, and when $r = 0$, $\omega = \phi$.

Therefore,

$$\cos \omega = \frac{r}{a} \sin^2 \phi + \cos \phi \sqrt{1 - \left(\frac{r}{a}\right)^2 \sin^2 \phi}. \quad (\text{B2-17})$$

B2.2 Case II, $a \leq s \leq 2a$

Case II is divided into two subcases. Figure B2-2 shows the geometry for Case IIa where $r \leq s-a$. The geometry for Case IIb is shown in Figure B2-3 where $r > s-a$.

For Case IIa, tangency occurs when $r = s-a$. The total energy reaching the boundary, a , is

$$\rho(r) = \int_0^\pi f(E_o, r') \frac{r' d\phi \ 2\pi r' \sin \phi}{4\pi r'^2} \quad (\text{B2-18})$$

since $r' < s$.

For Case IIb intersection occurs for $r' = s$. From Figure B2-3,

$$a^2 = r^2 + s^2 - 2rs \cos(\pi - \phi(r, s)), \quad (\text{B2-19})$$

$$= r^2 + s^2 + 2rs \cos \phi(r, s), \quad (\text{B2-20})$$

$$\phi(r, s) = \cos^{-1} \frac{a^2 - r^2 - s^2}{2rs} \quad (\text{B2-21})$$

The total energy reaching the boundary, a, is

$$\rho(r) = \int_0^{\phi(r,s)} f(E_o, r') \sin \phi \ d\phi \ dr \quad (\text{B2-22})$$

Where r' is given in Eq. (B2-2) and $\cos \omega$ is defined in Eq. (B2-17).

The fraction of energy generated in the sphere and escaping from the surface is

$$\begin{aligned} \frac{E}{E_T} = \frac{1.5}{a^3 E_o} & \left[\int_0^{s-a} r^2 \int_0^{\phi(r,s)} f(E_o, r') \sin \phi \ d\phi \ dr \right. \\ & \left. + \int_{s-a}^a r^2 \int_0^{\phi(r,s)} f(E_o - r') \sin \phi \ d\phi \ dr \right] \end{aligned} \quad (\text{B2-23})$$

or

$$\frac{E}{E_T} = \frac{3}{2a^3 E_o} \int_0^a r^2 \int_0^{\phi(r,s)} f(E_o, r') \sin \phi \ d\phi \ dr \quad (\text{B2-24})$$

where

$$\phi(r, s) = \pi \quad \text{if } r \leq s - a \quad (\text{B2-25})$$

$$= \cos^{-1} \left[\frac{a^2 - r^2 - s^2}{2rs} \right] \quad \text{if } r > s - a \quad (\text{B2-26})$$

B2.3 Case III, $s < a$

In this case, the energy reaching the boundary a from point P is confined to a shell of thickness s as shown in Figure B2-4. The total energy is given by

$$\rho(r) = \int_0^{\phi(r,s)} f(E_0, r') \frac{r' d\phi 2\pi r' \sin \phi}{4\pi r'^2} \quad (\text{B2-27})$$

where Equation (B2-26) defines $\phi(r, s)$.

The fraction of energy generated in the sphere and escaping from the surface is

$$\frac{E}{E_T} = \frac{2\pi E_0}{4/3 \pi a^3 E_0} \int_{a-s}^a r^2 \int_0^{\phi(r,s)} f(E_0, r') \sin \phi d\phi dr. \quad (\text{B2-28})$$

B2.4 Numerical Solution

The fractional energy equations, E/E_T , were evaluated for particles with radii, a , between 0 and 100 microns and initial energies of 5.15 and 5.49 MeV. Adaptive 8-point Legendre-Gauss integration was performed with GAUS8 (see VanDevender 1984² and Cowell 1984³). An integration error tolerance of 10^{-4} was used. Figures B2-5 and B2-6 display fractional energy for $0 \geq a \geq 100$ and $0 \leq a \leq 20$, respectively, for $E_0 = 5.15$ MeV. Table B2-1 lists the fraction of energy escaping from particles of various radii.

² VanDevender 1984. W. H. VanDevender, "Slatec Mathematical Subprogram Library Version 2.0," Sandia National Laboratories, SAND84-0281, April 1984.

³ Cowell 1984. W. R. Cowell, Sources and Development of Mathematical Software. Prentice Hall, New York, N.Y., 1984.

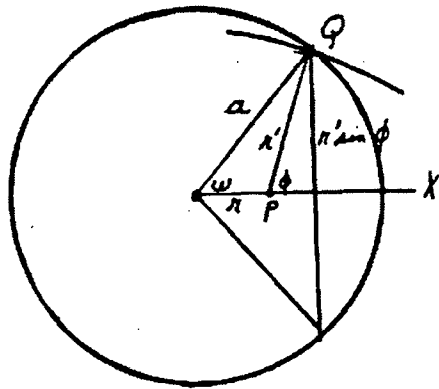


Fig. B2-1 Case I $2a < s$

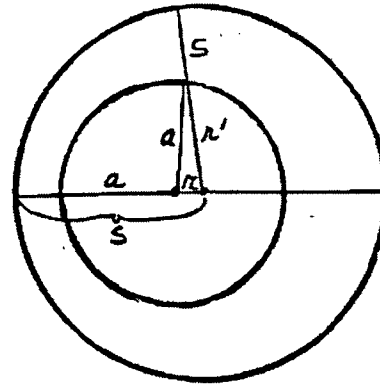


Fig. B2-2 Case IIa $r \leq s-a$

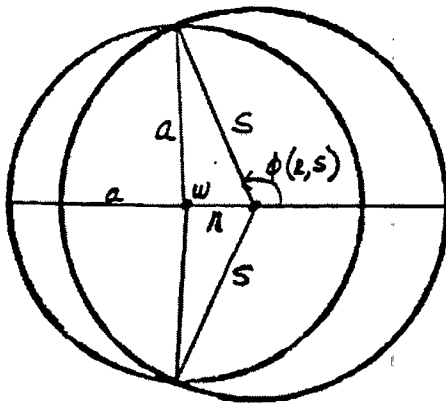


Fig. B2-3 Case IIb $r > s-a$

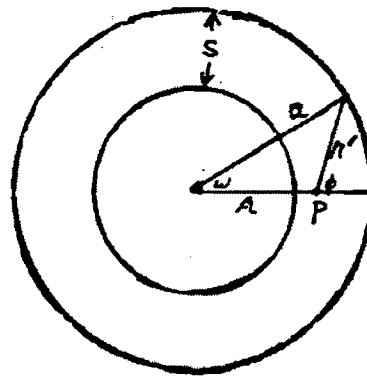


Fig. B2-4 Case III $s < a$

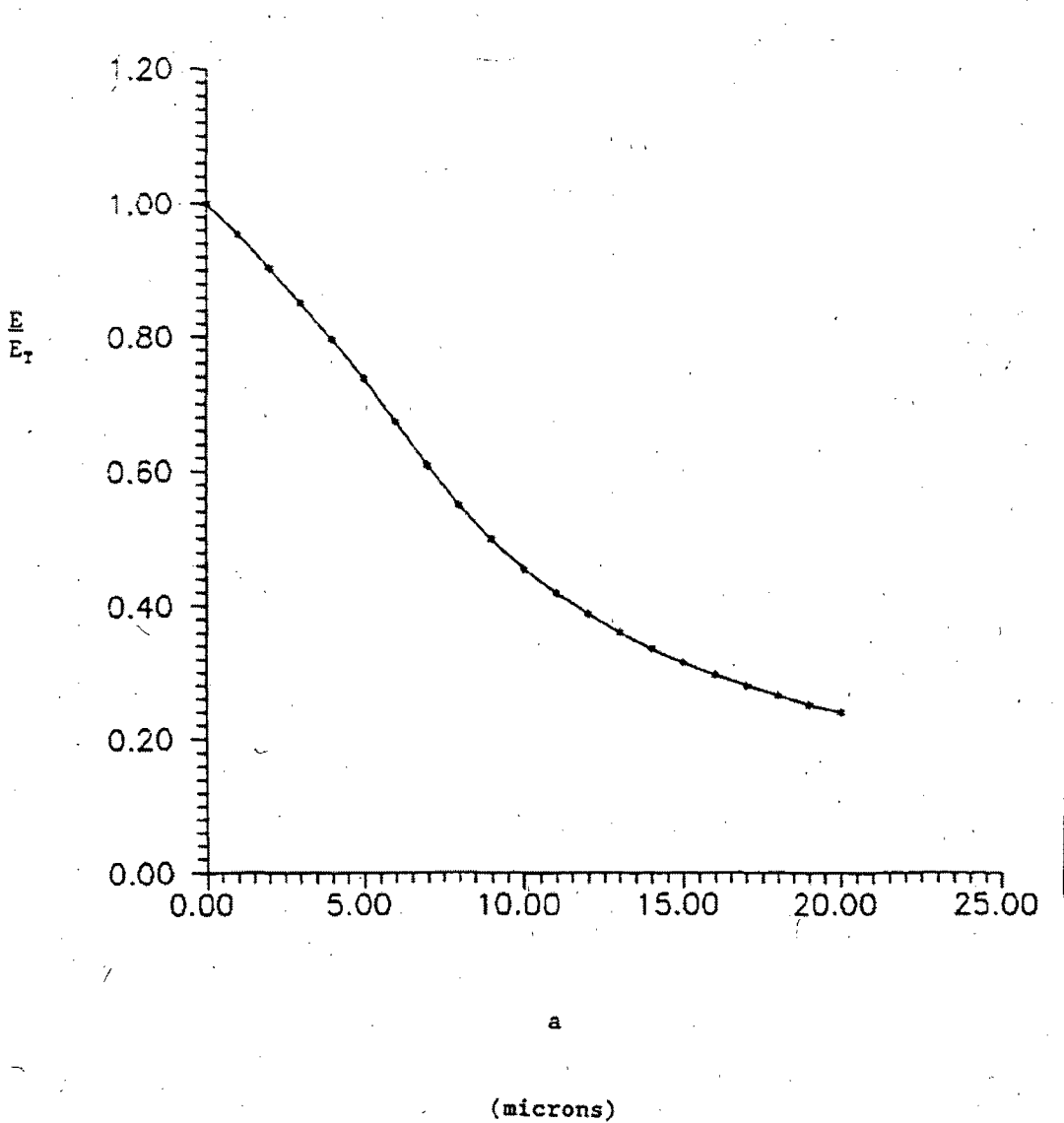


Figure B2-5
PuO₂ Fractional Energy vs. Radius for E₀ = 5.15 MeV

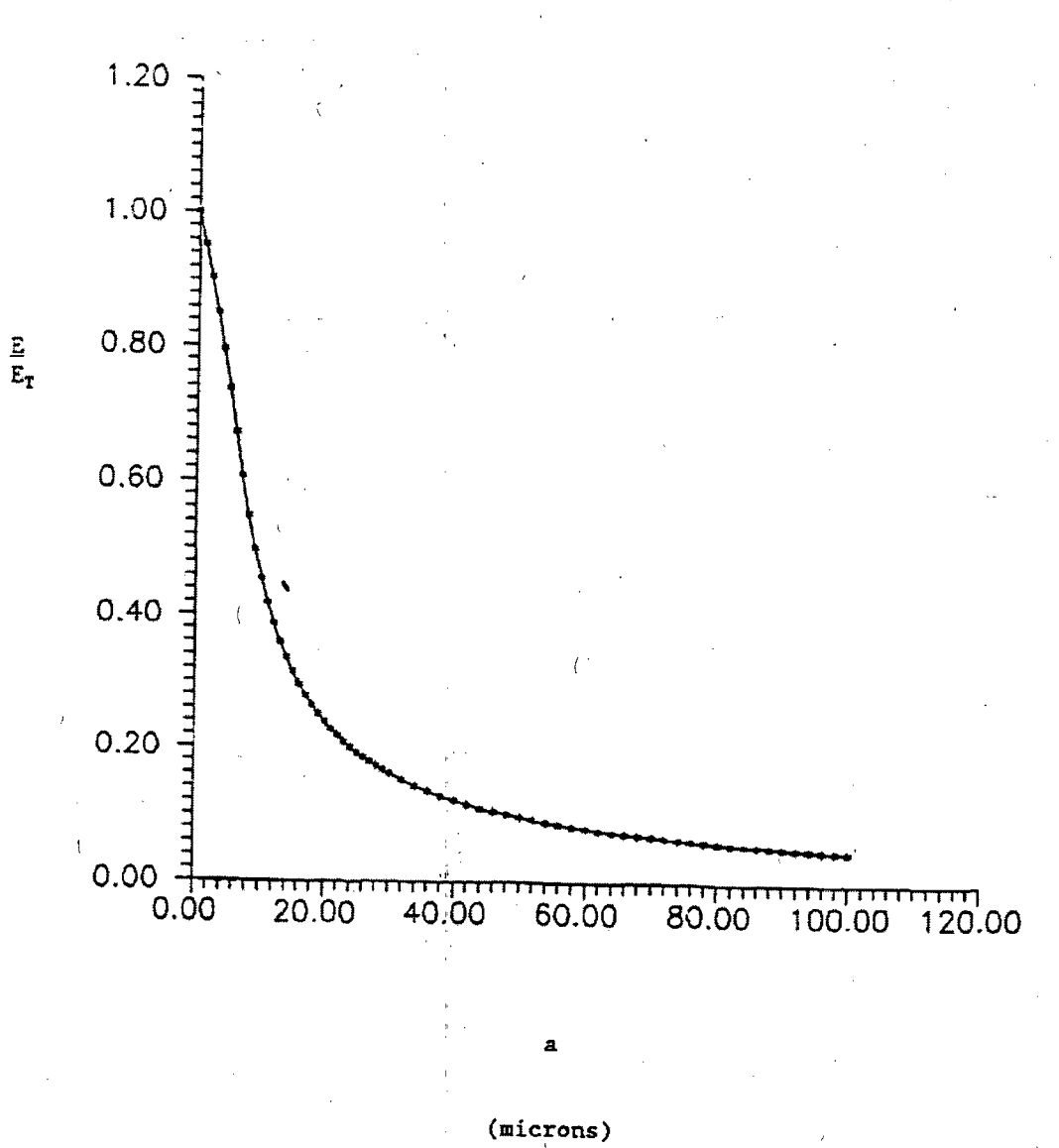


Figure B2-6
PuO₂ Fractional Energy vs. Radius E₀ = 5.15 MeV

Table B2-1 — Fraction of Alpha Particle Energy Escaping from PuO₂ Particles as a Function of Particle Radius and Initial Energy

Particle Radius (μm)	Fraction of Energy Escaping	
	$E_0 = 5.15 \text{ MeV}$	$E_0 = 5.49 \text{ MeV}$
9.5	0.476	0.515
7.0	0.607	0.647
4.5	0.766	0.790
3.5	0.823	0.840
2.5	0.877	0.888
1.5	0.927	0.934
0.75	0.964	0.967
0.28	0.987	0.988

This page intentionally left blank.

APPENDIX 3.2

EFFECTIVE G VALUES FOR CH-TRU WASTE MATERIAL TYPES

This page intentionally left blank.

3.2 Effective G Values for CH-TRU Waste Material Types

3.2.1 Summary

This appendix determines the effective G values for payload shipping categories of contact-handled transuranic (CH-TRU) waste materials, based on the radiolytic G values for waste materials that are discussed in detail in Appendix 3.1 of the CH-TRU Payload Appendices. The effective G values take into account self-absorption of alpha decay energy inside particulate contamination, the fraction of energy absorbed by nongas-generating materials, and the dose absorbed by the target matrix material.

Increasing dose (defined as the product of the decay heat and elapsed time from waste generation to date of compliance evaluation and expressed in units of watt*year) decreases the flammable gas generation rate of hydrogenous materials (such as plastics and combustibles) due to depletion of hydrogen in the target material in the vicinity of alpha-emitting sources. This effect has been demonstrated for a variety of materials present in TRU waste by a number of researchers.¹ Extensive radiolytic testing of polyethylene (PE), polyvinyl chloride (PVC), and cellulose has established a steady-state, dose-dependent G value for each material when a container has attained a dose level of 0.012 watt*year.¹ The applicability of dose-dependent G values for CH-TRU waste types is further described in Appendix 3.3 of the CH-TRU Payload Appendices.

CH-TRU waste materials in payloads for the transportation packaging are described according to the following waste types (I, II, III, or IV) or can be divided into waste material types (I.1, I.2, I.3, II.1, II.2, II.3, III.1, III.2, III.3, and IV.1):

- I. Solidified aqueous or homogeneous inorganic solids (that contain water)
 - I.1 Absorbed, adsorbed, or solidified inorganic liquids (nuclides may be in solution and energy transfer may occur between the liquid and the inorganic binder).
 - I.2 Soils, solidified particulates, or sludges formed from precipitates.
 - I.3 Concreted inorganic particulate waste having a maximum of 30 weight percent unbound water.
- II. Solid inorganic materials
 - II.1 Solid inorganic materials packaged in organic materials.
 - II.2 Solid inorganic materials packaged in metal cans.

¹ Idaho National Engineering and Environmental Laboratory, 1999, "TRUPACT-II Matrix Depletion Program Final Report," INEL/EXT-98-00987, Rev. 1, Idaho National Engineering and Environmental Laboratory, Idaho Falls, Idaho.

- II.3 Homogeneous solid inorganic materials with unbound absorbed ambient moisture (≤ 6 percent by weight) in metal cans.
- III. Solid organic materials
 - III.1 Solid organic materials (including some absorbed liquids and cemented organics).
 - III.2 Homogeneous mixed organic (10 percent by weight) and inorganic (90 percent by weight) materials packaged in metal cans.
 - III.3 Homogeneous mixed organic (10 percent by weight) and inorganic (90 percent by weight) materials packaged in organic materials.
- IV. Solidified organic materials. Waste Type IV (Waste Material Type IV.1) is in the test category since a bounding G value has not been established and is not addressed in this appendix.

Effective G values are determined for use in calculating concentrations of potentially flammable gases, quantities of HCl that could be generated, and for net gas generated (equal to the total amount of gas generated minus the amount of oxygen consumed, if applicable). Factors are also provided that allow G values at room temperature to be corrected for a higher or lower waste temperature. Table 3.2-1 summarizes the effective G values at an assumed room temperature of 70°F.

3.2.2 Introduction

As described in Appendix 3.1 of the CH-TRU Payload Appendices, an effective G value, G_{eff} , is defined by:

$$G_{\text{eff}} = \sum_M (F_M \times G_M)$$

F_M = fraction of energy absorbed by material M
 G_M = maximum G value for a material M

where the sum is over all materials present inside a waste container.

The G value itself is determined primarily by the chemical properties of the material and its temperature. The value of F is determined primarily by the size of the particles containing the radionuclides, the distribution of radioactivity on the various materials present inside the waste container, and the stopping distance of alpha particles in air, in the waste materials, or in the waste packaging materials.

Table 3.2-1 — Effective G Values for Waste Material Types at Room Temperature

Waste Material Type	Effective G Values		
	Flammable Gas	HCl	Net Gas ^a
I.1	1.6	~0	2.4
I.2	1.3	~0	2.0
I.3	0.4	~0	0.6
II.1 (watt*year ≤0.012)	1.7	0.3	1.7
II.1 (watt*year >0.012)	0.32	0.3	1.7
II.2	0	0	0
II.3	0.08	0	0.12
III.1 (watt*year ≤0.012)	3.4	0.5	8.4
III.1 (watt*year >0.012)	1.09	0.5	8.4
III.2 (watt*year ≤0.012)	0.34	0.05	0.84
III.2 (watt*year >0.012)	0.11	0.05	0.84
III.3 (watt*year ≤0.012)	1.85	0.29	2.35
III.3 (watt*year >0.012)	0.4	0.29	2.35

a Net gas is equal to the total amount of gas generated minus the amount of oxygen consumed.

Waste materials have been placed into three general waste types: solidified aqueous or homogeneous inorganic solids (containing bound and unbound water), solid inorganic materials, and solid organic materials. For the purpose of determining bounding G values, a distinction is made between the use of organic (e.g., plastic bags) and inorganic (e.g., metal cans) packaging materials for Waste Types II and III. All three waste types can be packaged using organic packaging materials (e.g., plastic bags or cardboard cartons); solid inorganic materials and homogeneous mixed organic and inorganic materials can also be packaged in metal cans, resulting in different G values. The G values for the organic packaging provide the maximum G values applicable for solid inorganic materials (except for waste in metal cans). PE, PVC, and cellulose (e.g., paper, cardboard, and wood) are the most common solid organic materials present in the CH-TRU wastes. Radiolytic G values for generation of flammable gases, HCl, and net gas for these materials provide upper bounds for the G values for solid organic waste materials that are present in greater than trace quantities. For pressure calculations, a G value for net gas has been determined that includes the effect of oxygen consumption, if oxygen was present in the experiment.

3.2.3 G Values for Waste Materials

For flammable gas generation or total pressure, the maximum G values for materials are used. For generation of HCl, an average G(HCl) value is used. This average G(HCl) value has been calculated from literature G values for PVC formulations that are most common in general commerce. The G(HCl) values used in determining the average G(HCl) value are included in those discussed in Appendix 3.1 of the CH-TRU Payload Appendices and are shown in Table 3.2-2. An average G(HCl) was used in the calculations because of wide variations in

formulation of PVC film materials and the very low values observed for actual bagging materials used at the waste generator sites (Table 3.2-2).

Table 3.2-2 — G(HCl) Values Measured for Common PVC Formulations at Room Temperature

PVC Formulation	Rad. Type/Dose	Oxygenated Atmosphere	G(HCl)	Contribution to G(HCl) _{avg}
19 types, 18% DOP plasticizer, 1-5% metallic soaps as stabilizers	gamma/ 3 Mrad	no	0-1.7 0.54 (avg)	10.26
1 type, 2 dose extremes, 50 phr DOP plasticizer, 5 phr epoxy oil, 2% Ca-Zn stabilizer	gamma/ 20-60 Mrad	no	0.03-1.4 0.72 (avg)	1.44
50 phr DOP plasticizer, 5 phr tribasic lead sulfate, 1 phr stearic acid, 10 phr clay #33	gamma/ 10 Mrad	no	1.2	1.2
50 phr DOP plasticizer, 5 phr epoxy oil, 2% Ca-Zn stabilizer	gamma/ 20 Mrad	yes	1.7	1.7
50 phr DOP plasticizer, 5 phr tribasic lead sulfate, 1 phr stearic acid, 10 phr clay #33	gamma/ 10 Mrad	yes	2.6	2.6
O-ring bags used at RFETS	gamma	yes	0.2	0.2
O-ring bags used at RFETS	alpha	yes	none detected	0
Bag materials used at Los Alamos National Laboratory	alpha	yes	none detected	0
$G(HCl)_{avg} = 17.4/27 =$				0.64

Notes: avg = Average
DOP = Dioctyl phthalate
HCl = Hydrochloric acid
Mrad = Millirad
phr = Parts per hundred resin
PVC = Polyvinyl chloride
RFETS = Rocky Flats Environmental Technology Site

The use of an average value of 0.64 for G(HCl) is considered bounding for the following reasons.

- Gas sampling programs (discussed in Appendices 5.3 and 6.2 of the CH-TRU Payload Appendices) at the Idaho National Engineering and Environmental Laboratory (INEEL) and Rocky Flats Environmental Technology Site (RFETS) did not detect HCl gas in the headspace of any of the 249 drums of CH-TRU waste that were sampled. In addition to drum headspace sampling, twenty-two drums of waste were sampled for gases, within successive layers of confinement up to and including the innermost layer of the waste. In all cases, HCl was never detected in any layer of confinement.
- Experimentally derived G(HCl) values for waste materials frequently found in CH-TRU wastes are listed in Table 6.2-1 of Appendix 6.2 of the CH-TRU Payload Appendices. All the values for G(HCl) are very low for both alpha and gamma radiolysis experiments. These data indicate that the potential for HCl production from radiolysis of commonly used PVC materials in CH-TRU waste is minimal and less than the average G(HCl) value of 0.64 from the literature results.

The temperature dependence of G values is approximated by the Arrhenius equation (see Appendix 3.1 of the CH-TRU Payload Appendices):

$$G(T_2) = G(T_1) \exp\left[\frac{E_a}{R} \left(\frac{T_2 - T_1}{T_2 \times T_1}\right)\right]$$

where, E_a is the activation energy in cal/g-mole for a gas species, R is the ideal gas constant (1.99 cal/g-mole-K), and T is the absolute temperature. The value of the activation energy can change when a material melts or otherwise significantly changes its physical properties (such as becoming brittle).

Table 3.2-3 summarizes G values from Appendix 3.1 of the CH-TRU Payload Appendices that provide maximum G values for the waste types and an average G(HCl) value for PVC calculated in Table 3.2-2. The activation energy for calculating G values at temperatures other than room temperature is also given. No temperature dependence has been observed for radiolysis of water (in the liquid state or solidified in concrete) from room temperature to 100°C.

For all waste types, PVC is the bounding material for G(HCl). Water is the bounding material for G(net gas) and G(flammable) in Waste Type I and Waste Material Type II.3. G(net gas) is equal to G(total) minus any measured consumption of oxygen. For Waste Material Type II.1, PE is the bounding material for G(flammable gas) and G(net gas). PE is the bounding material for G(flammable gas), and cellulose is the bounding material for G(net gas) for Waste Type III containers that have not met the 0.012 watt*year dose criteria. Cellulosics are the bounding material for G(flammable gas) for Waste Type III containers that have satisfied the 0.012 watt*year dose criteria. For applicable waste material types satisfying the watt*year criteria and using

Table 3.2-3 — Summary of Maximum G Values for Bounding Materials in Waste Types at Room Temperature

Waste Material	G Value ^a			Activation Energy ^b
	Flammable Gas	HCl	Net Gas	
Water	1.6	0	2.4	0
Polyethylene	4.1 ^c 0.64 ^d	0	4.1	0.8
Polyvinyl chloride Maximum	0.7 ^c 0.54 ^d	2.6	2.6	3.0 (HCl) 8.1 (H ₂)
Average	N/A	0.64	N/A	3.0 (HCl)
Cellulose	3.2 ^c 1.09 ^d	0	10.2	2.1

a G values are in units of molecules per 100 eV of energy at 70°F.

b Activation energies are in units of kcal/g-mole.

c Watt*year criteria not satisfied.

d Watt*year criteria satisfied.

dose-dependent G values, only the dose-dependent flammable gas G value is calculated, as HCl and net gas G values are conservatively assumed to be the same as for the corresponding waste material type that has not satisfied the watt*year criteria.

3.2.4 Fraction of Alpha Decay Energy Absorbed in Particles

Most CH-TRU wastes consist of materials that have been contaminated with particles of radioactive material, usually in the oxide form. The solid inorganic materials (e.g., glass and metal) and the solid organic materials (e.g., paper and plastic) meet this description. The solidified aqueous sludges and most other homogeneous solids consist of precipitated solids and radioactivity in particulate form. The major exceptions are liquids containing dissolved radioactivity that may be present as bound liquid within the solid mass, as opposed to water of hydration.

The equation for effective G value can be rewritten as:

$$G_{\text{eff}} = \sum_M (F_P \times F_M) \times G_M$$

$$= \sum_M (F_M \times G_M) \times F_P$$

where, F_P = fraction of energy emerging from the particles
 F_M = fraction of energy absorbed by material M
 G_M = maximum G value for material M.

Attachment B of Appendix 3.1 of the CH-TRU Payload Appendices describes a mathematical calculation of the fraction of alpha decay energy that escapes from a spherical particle containing uniformly distributed TRU nuclides. Attachment A of this appendix shows that a maximum of 82 percent of the alpha decay energy escapes from particles of PuO₂ when the particle size distribution is taken into account.

For waste containing contamination in solution (i.e., solidified wastes), a maximum of 100 percent of the alpha decay energy may emerge from the particles. For waste forms using dose-dependent G values, a value of 1.0 is used for the fraction of energy emerging from the particles, because the experimentally determined dose-dependent G values provided in Table 3.2-3 already account for particle size distribution and were conducted with materials representative of TRU waste.

3.2.5 Effective G Values for Waste Types

3.2.5.1 Waste Type I – Solidified Aqueous or Homogeneous Inorganic Solids

This waste type includes soil and concreted or sludge wastes that do not contain more than trace amounts (<1 weight percent) of organic materials (with the exception of organic packaging materials). The materials are well mixed.

For this waste type, the radioactive materials are dispersed throughout the solidified or solid mass, and the fraction of the alpha decay energy absorbed by the plastic bags or high-density polyethylene rigid (HDPE) liner is negligible. The range of alpha particles (t) in water is only about 5E-3 cm. Only a shell at most equal to the surface area of the waste volume and 5E-3 cm thick, will emit alpha particles that can reach the plastic. For a cylindrical waste volume having radius r and height h, the fraction of alpha particles that can reach the plastic packaging materials is given by:

$$P = \frac{t \times 2\pi r(r+h)}{\pi r^2 h} = \frac{2t(r+h)}{rh}$$

For waste with an approximate volume of one gallon (with a radius of three inches and height of eight inches), $P = 1.8E-3$. This provides an upper bound for the fraction of alpha particles that can interact with the plastic packaging materials for Waste Type I.

Water is the only material present in solidified aqueous or homogeneous inorganic solids in other than trace quantities that could generate potentially flammable gases. The maximum values for water provide the maximum values for solidified inorganic waste containing water.

3.2.5.1.1 Waste Material Type I.1

For Waste Material Type I.1, any inorganic absorbents or solidification agents can be used. Because energy transfer can occur between some inorganic materials and water, the fraction of available energy absorbed by the water is assumed to be 1.0. The activity may be present as particles or in solution encapsulated by the solidification materials.

The effective G value for Waste Material Type I.1 is given by:

$$G_{\text{eff},1.1} = \sum_M (F_M \times G_M) \times F_P$$

$$= [1.8\text{E-}3 \times G(\text{plastic}) + 1.0 \times G(\text{water})] \times 1.0$$

Therefore, the effective G values for potentially flammable gas, HCl, and net gas are given respectively by:

$$G(\text{flam gas}) = [1.8\text{E-}3 \times 4.1 + 1.0 \times 1.6] \times 1.0 = 1.6$$

$$G(\text{HCl}) = [1.8\text{E-}3 \times 0.64] \times 1.0 = \sim 0$$

$$G(\text{net gas}) = [1.8\text{E-}3 \times 4.1 + 1.0 \times 2.4] \times 1.0 = 2.4.$$

3.2.5.1.2 Waste Material Type I.2

For Waste Material Type I.2 (solidified particulates, soil or sludges) data presented in Appendix 3.1 of the CH-TRU Payload Appendices demonstrate that energy transfer can occur between many of the materials and the water. For Waste Material Type I.2, therefore, all of the energy available is assumed to be absorbed by the water. The sludges are formed by precipitating the radionuclides from solution, so the radionuclides should be present in the form of particles.

The effective G value for Waste Material Type I.2 is given by:

$$G_{\text{eff},1.2} = \sum_M (F_M \times G_M) \times F_P$$

$$= [1.8\text{E-}3 \times G(\text{plastic}) + 1.0 \times G(\text{water})] \times 0.82$$

Therefore the effective G values for flammable gas, HCl, and net gas are given respectively by:

$$G(\text{flam gas}) = [1.8\text{E-}3 \times 4.1 + 1.0 \times 1.6] \times 0.82 = 1.3$$

$$G(\text{HCl}) = [1.8\text{E-}3 \times 0.64] \times 0.82 = \sim 0$$

$$G(\text{net gas}) = [1.8\text{E-}3 \times 4.1 + 1.0 \times 2.4] \times 0.82 = 2.0.$$

3.2.5.1.3 Waste Material Type I.3

For Waste Material Type I.3 (concreted inorganic particulate waste), data presented in Appendix 3.1 of the CH-TRU Payload Appendices demonstrate that energy transfer does not occur between the cement and the bound or unbound water, and the G value for the bound water (water of hydration) is close to zero. The unbound water content of the cured concrete is limited to 30 weight percent. For Waste Material Type I.3, therefore, only 30 percent of the energy available is absorbed by the water.

The effective G value for Waste Material Type I.3 is given by:

$$G_{\text{eff,I.3}} = \sum_M (F_M \times G_M) \times F_p$$

$$= [1.8\text{E-}3 \times G(\text{plastic}) + 0.30 \times G(\text{water})] \times 0.82$$

Therefore the effective G values for flammable gas, HCl, and net gas are given respectively by:

$$G(\text{flam gas}) = [1.8\text{E-}3 \times 4.1 + 0.30 \times 1.6] \times 0.82 = 0.4$$

$$G(\text{HCl}) = [1.8\text{E-}3 \times 0.64] \times 0.82 = 0$$

$$G(\text{net gas}) = [1.8\text{E-}3 \times 4.1 + 0.30 \times 2.4] \times 0.82 = 0.6.$$

Water within concreted wastes is actually found in two forms. Part of the water is chemically bound during the hydration of the cement phases. The remaining water is unbound or loosely bound and is part of the excess water added to make the freshly mixed cement paste workable. In an average cemented sludge (e.g., RFETS, RF 114A), the amount of water added to the cement/sludge mixture at the time of mixing, plus the water contained in the sludge totals approximately 37 percent by weight of the mixture. The water content of the sludge is conservatively assumed to be 50 percent by volume. After only 50 percent hydration, attained within 6 to 7 days of mixing,² 5.7 percent water by weight of the mixture is bound within the cement phases. This leaves approximately 31 percent unbound water by weight. Some of this water is lost due to evaporation during mixing and curing. Bibler reports that concrete (simulating Savannah River Plant cemented sludge) cured at ambient conditions for two to five days had lost 30 to 40 weight percent of the free water to evaporation.³ This results in a free water content of 19 to 22 percent by weight.

Calculation of the total porosity of the concrete after 50 percent hydration at the water/cement ratio prescribed by RFETS (0.775) yielded 45 volume percent. If the concrete were 100 percent saturated at the porosity, the maximum unbound (free water) moisture content would be only 32 weight percent. Again, evaporation is expected to remove 30 to 40 percent of the free water during the curing leaving 19 to 22 weight percent free water. Even assuming a high relative humidity during the curing process, 30 percent represents an estimated upper bound for this free water moisture content.

The experiment referred to in Section 3.1.5.1.2 of Appendix 3.1 of the CH-TRU Payload Appendices appears to use initial moisture content of the cement/sludge mixture, before

² Mindess, S., and J. F. Young, 1981, Concrete, Prentice-Hall, Inc., Englewood Cliffs, NJ.

³ Bibler, N. E., 1979, "Gas Production From Alpha Radiolysis of Concrete Containing TRU Incinerator Ash, Progress Report 2, August 1 - November 30, 1978," E.I. Du Pont De Nemours and Co., Savannah River Laboratory, Aiken, South Carolina.

hydration occurs.⁴ The initial moisture content of the mix was 35 weight percent. After drying at 200°C, it was reported that 7.4 percent moisture content by weight remained. This refers to the water bound by hydration of the cement minerals after approximately 36 days curing time plus water contained in the cement gel pores. Cement gel porosity refers to the pore space within the structure of the hydrated cement phases. The pores measure less than 10 nanometers and water contained in these pores is nonevaporable and can be considered bound within the cement.² The gel porosity is small and makes up only ~15 percent of the total porosity. The unbound (free water) content of the sample reported to contain 35 percent water is approximately (35 - 7.4 percent) or 27.6 percent by weight.

Examples of acceptable materials for Waste Material Types I.1, I.2 and I.3 that can be present in quantities greater than or equal to one weight percent are listed in Section 4.0 of the CH-TRAMPAC. Any other inorganic material is also acceptable in Waste Type I.

3.2.5.2 Waste Type II – Solid Inorganic Materials

This waste type includes surface-contaminated inorganic materials, such as glass, metal, ceramics, and fiberglass. The waste materials must be dry (Note: Waste Material Type II.3 may have less than or equal to 6 weight percent unbound absorbed ambient moisture) and free of oil, grease, or other organics except for trace quantities (less than 1 weight percent). The wastes may be packaged first inside plastic bags (II.1) or metal cans (II.2 and II.3), then in drums, which are lined with plastic bags (polyethylene or PVC) and/or the rigid high-density polyethylene liner, or placed directly into payload containers.

Due to the short range of an alpha particle and surface irregularities, the surface-contaminated inorganic wastes will, on the average, absorb half of the alpha decay energy escaping from particulate contamination. (The other half of the alpha decay energy could be absorbed by air, the packaging materials, or other inorganic waste materials.) The assumption is made that the remaining half of the alpha decay energy is absorbed by the packaging materials. The inorganic materials are considered to generate no net gas.

Examples of acceptable materials for Waste Type II are listed in Section 4.0 of the CH-TRAMPAC. Any other dry, solid, inorganic material is acceptable for Waste Type II.

3.2.5.2.1 Waste Material Type II.1—Dose Criteria Not Satisfied (Watt*Year ≤0.012)

The effective G value for Waste Material Type II.1 is given by:

$$G_{\text{eff,II.1}} = \sum_M (F_M \times G_M) \times F_P$$

$$= [0.5 \times G(\text{plastic}) + 0.5 \times G(\text{inorganics})] \times 0.82$$

⁴ Bibler, N. E., 1980, "Radiolytic Gas Generation in Concrete Made with Incinerator Ash Containing TRU Nuclides," Scientific Basis for Nuclear Waste Management, Vol. 2, Plenum Publishing, Corp., New York, NY.

Therefore the effective G values for flammable gas, HCl, and net gas are given respectively by:

$$G(\text{flam gas}) = [0.5 \times 4.1 + 0.5 \times 0] \times 0.82 = 1.7$$

$$G(\text{HCl}) = [0.5 \times 0.64 + 0.5 \times 0] \times 0.82 = 0.3$$

$$G(\text{net gas}) = [0.5 \times 4.1] \times 0.82 = 1.7$$

3.2.5.2.2 Waste Material Type II.1—Dose Criteria Satisfied (Watt*Year >0.012)

The effective G value for Waste Material Type II.1 is given by:

$$\begin{aligned} G_{\text{eff,II.1}} &= \sum_M (F_M \times G_M) \times F_P \\ &= [0.5 \times G(\text{plastic}) + 0.5 \times G(\text{inorganics})] \times F_P \end{aligned}$$

Therefore the effective G value for flammable gas is:

$$G(\text{flam gas}) = [0.5 \times 0.64 + 0.5 \times 0] \times 1.0 = 0.32$$

3.2.5.2.3 Waste Material Type II.2

The effective G value for Waste Material Type II.2 is equal to zero, since the inorganic materials and metal containers generate no gas from radiolysis.

3.2.5.2.4 Waste Material Type II.3

Waste Material Type II.3 is a homogeneous solid inorganic waste with ≤ 6 percent (by weight) unbound absorbed ambient moisture packaged in metal containers. The effective G value for Waste Material Type II.3 with 6 percent water and 94 percent inorganic material and packaging is given by:

$$\begin{aligned} G_{\text{eff,II.3}} &= \sum_M (F_M \times G_M) \times F_P \\ &= [0.06 \times G(\text{water}) + 0.94 \times G(\text{inorganic})] \times 0.82 \end{aligned}$$

Therefore, the effective G values for flammable gas, HCl, and net gas are given respectively by:

$$G(\text{flam gas}) = [0.06 \times 1.6 + 0.94 \times 0] \times 0.82 = 0.08$$

$$G(\text{HCl}) = [0.06 \times 0 + 0.94 \times 0] \times 0.82 = 0$$

$$G(\text{net gas}) = [0.06 \times 2.4 + 0.94 \times 0] \times 0.82 = 0.12$$

Acceptable materials for Waste Material Type II.3 wastes are listed in the CH-TRAMPAC.

3.2.5.3 Waste Type III – Solid Organic Materials

This waste type includes surface-contaminated solid organic materials, such as plastics, paper, cloth, Plexiglas®, and Benelex®. The materials may contain absorbed water, commercial greases, oils or organic liquids having sufficiently low G values. Cemented organic process solids are included in this category.

3.2.5.3.1 Waste Material Type III.1—Dose Criteria Not Satisfied (Watt*Year ≤0.012)

The surface-contaminated organic wastes or their organic packaging are assumed to absorb 100 percent of the available alpha decay energy. Any gas generated by inorganic materials (which are also permitted in this category) would be oxygen, which will be used in the oxidation of the plastic packaging materials. Therefore, any inorganic materials present are considered to generate no net gas.

The effective G value for Waste Material Type III.1 is given by:

$$\begin{aligned} G_{\text{eff,III.1}} &= \sum_M (F_M \times G_M) \times F_p \\ &= [1.0 \times G(\text{solid organic})] \times 0.82 \end{aligned}$$

Therefore the effective G values for flammable gas, HCl, and net gas are given respectively by:

$$G(\text{flam gas}) = [1.0 \times 4.1] \times 0.82 = 3.4$$

$$G(\text{HCl}) = [1.0 \times 0.64] \times 0.82 = 0.5$$

$$G(\text{net gas}) = [1.0 \times 10.2] \times 0.82 = 8.4$$

Acceptable materials for Waste Material Type III.1 wastes are listed in Section 4.0 of the CH-TRAMPAC.

Materials for which the G value at room temperature for flammable gas could be greater than 4.1 are limited to trace quantities (<1 weight percent) based on current data. These materials are cellulose nitrate, polyvinyl formal, polyoxymethylene, and poly(olefin sulfone)s, as determined in Appendix 3.1 of the CH-TRU Payload Appendices. Other polymers containing ether functional groups may also have high G (flammable gas) values.

3.2.5.3.2 Waste Material Type III.1—Dose Criteria Satisfied (Watt*Year >0.012)

The surface-contaminated organic wastes or their organic packaging are assumed to absorb 100 percent of the available alpha decay energy. Any gas generated by inorganic materials (which are also permitted in this category) would be oxygen, which will be used in the oxidation of the plastic packaging materials. Therefore, any inorganic materials present are considered to generate no net gas.

The effective G value for Waste Material Type III.1 is given by:

$$G_{\text{eff,III.1}} = \sum_M (F_M \times G_M) \times F_P$$

$$= [1.0 \times G(\text{solid organic})] \times F_P.$$

Therefore the effective G value for flammable gas is:

$$G(\text{flam gas}) = [1.0 \times 1.09] \times 1.0 = 1.09.$$

Acceptable materials for Waste Material Type III.1 wastes are listed in Section 4.0 of the CH-TRAMPAC.

Materials for which the G value at room temperature for flammable gas could be greater than for cellulose are limited to trace quantities (<1 weight percent) based on current data. These materials are cellulose nitrate, polyvinyl formal, polyoxymethylene, and poly(olefin sulfone)s, as determined in Appendix 3.1 of the CH-TRU Payload Appendices. Other polymers containing ether functional groups may also have high G (flammable gas) values.

3.2.5.3.3 Waste Material Type III.2—Dose Criteria Not Satisfied (Watt*Year ≤ 0.012)

Waste Material Type III.2 is a homogeneous mixture made up of ≤ 10 percent (by weight) solid organic material and ≥ 90 percent (by weight) solid inorganic material packaged in metal containers. The effective G value for Waste Material Type III.2 is calculated proportionally from Waste Material Types III.1 (10 percent) and II.2 (90 percent). The effective G value is given by:

$$G_{\text{eff,III.2}} = \sum_M (F_M \times G_M) \times F_P$$

$$= [0.1 \times G(\text{solid organic}) + 0.9 \times G(\text{solid inorganic})] \times 0.82$$

Therefore, the effective G values for flammable gas, HCl, and net gas are given respectively by:

$$G(\text{flam gas}) = [0.1 \times 4.1 + 0.9 \times 0] \times 0.82 = 0.34$$

$$G(\text{HCl}) = [0.1 \times 0.64 + 0.9 \times 0] \times 0.82 = 0.05$$

$$G(\text{net gas}) = [0.1 \times 10.2 + 0.9 \times 0] \times 0.82 = 0.84$$

Acceptable materials for Waste Material Type III.2 wastes are listed in Section 4.0 of the CH-TRAMPAC.

3.2.5.3.4 Waste Material Type III.2—Dose Criteria Satisfied (Watt*Year > 0.012)

Waste Material Type III.2 is a homogeneous mixture made up of ≤ 10 percent (by weight) solid organic material and ≥ 90 percent (by weight) solid inorganic material packaged in metal containers. The effective G value for Waste Material Type III.2 is calculated proportionally from Waste Material Types III.1 (10 percent) and II.2 (90 percent). The effective G value is given by:

$$G_{\text{eff,III.2}} = \sum_M (F_M \times G_M) \times F_P$$

$$= [0.1 \times G(\text{solid organic}) + 0.9 \times G(\text{solid inorganic})] \times F_P.$$

Therefore, the effective G value for flammable gas is:

$$G(\text{flam gas}) = [0.1 \times 1.09 + 0.9 \times 0] \times 1.0 = 0.11$$

Acceptable materials for Waste Material Type III.2 wastes are listed in Section 4.0 of the CH-TRAMPAC.

3.2.5.3.5 Waste Material Type III.3—Dose Criteria Not Satisfied (Watt*Year ≤ 0.012)

Waste Material Type III.3 is a homogeneous mixture made up of ≤ 10 percent (by weight) solid organic material and ≥ 90 percent (by weight) solid inorganic material packaged in plastic. The effective G value for Waste Material Type III.3 is calculated proportionally from Waste Material Types III.1 (10 percent) and II.1 (90 percent). The effective G value is given by:

$$G_{\text{eff,III.3}} = \sum_M (F_M \times G_M) \times F_P$$

$$= \{0.1 \times G(\text{solid organic}) + 0.9 \times [0.5 \times G(\text{plastic}) + 0.5 \times G(\text{inorganics})]\} \times 0.82$$

Therefore, the effective G values for flammable gas, HCl, and net gas are given respectively by:

$$G(\text{flam gas}) = \{0.1 \times 4.1 + 0.9 \times [0.5 \times 4.1 + 0.5 \times 0]\} \times 0.82 = 1.85$$

$$G(\text{HCl}) = \{0.1 \times 0.64 + 0.9 \times [0.5 \times 0.64 + 0.5 \times 0]\} \times 0.82 = 0.29$$

$$G(\text{net gas}) = \{0.1 \times 10.2 + 0.9 \times [0.5 \times 4.1 + 0.5 \times 0]\} \times 0.82 = 2.35$$

Acceptable materials for Waste Material Type III.3 wastes are listed in Section 4.0 of the CH-TRAMPAC.

3.2.5.3.6 Waste Material Type III.3—Dose Criteria Satisfied (Watt*Year > 0.012)

Waste Material Type III.3 is a homogeneous mixture made up of ≤ 10 percent (by weight) solid organic material and ≥ 90 percent (by weight) solid inorganic material packaged in plastic. The effective G value for Waste Material Type III.3 is calculated proportionally from Waste Material Types III.1 (10 percent) and II.1 (90 percent). The effective G value is given by:

$$G_{\text{eff,III.3}} = \sum_M (F_M \times G_M) \times F_P$$

$$= \{0.1 \times G(\text{solid organic}) + 0.9 \times [0.5 \times G(\text{plastic}) + 0.5 \times G(\text{inorganics})]\} \times F_P.$$

Therefore, the effective G value for flammable gas is:

$$G(\text{flam gas}) = \{0.1 \times 1.09 + 0.9 \times [0.5 \times 0.64 + 0.5 \times 0]\} \times 1.0 = 0.40$$

Acceptable materials for Waste Material Type III.3 wastes are listed in Section 4.0 of the CH-TRAMPAC.

Attachment A

Mass-Weighted Fraction of Energy Escaping from PuO₂ Particles

A.1 Introduction

This attachment demonstrates that a maximum of 82 percent of the alpha decay energy escapes from particles of PuO₂ when the particle size distribution is taken into account.

A.2 Mass-Weighted Fraction of Energy Escaping from PuO₂ Particles

Attachment B of Appendix 3.1 of the CH-TRU Payload Appendices describes a mathematical calculation of the fraction of alpha decay energy that escapes from a spherical particle containing uniformly distributed TRU nuclides.

As the PuO₂ particle radius exceeds the stopping distance of the alpha particles, some of the alpha particles are completely absorbed within the PuO₂ particle. Only the outer shell of the PuO₂ particle (11-12 μm thick) contains radionuclides whose alpha particles can escape from the PuO₂ particle.

Many different particle-size distributions for PuO₂ have been reported in the literature. Mishima⁵ in his examination of transport methods for PuO₂ powder for fuel considered thirteen different distributions. The PuO₂ used for fuel fabrication is required to be finely divided powder or coprecipitate so that it can be intimately blended with UO₂ to form a mixed oxide fuel. It is unlikely that the PuO₂ found in surface-contaminated waste would be as fine a powder as is used in fuel fabrication. HEPA filters in glovebox exhaust systems will trap the smaller particles, which more easily become airborne. Size distributions for aerosols are applicable only to HEPA filters (which typically have inorganic filtration media). Small particles can also agglomerate, creating larger particles.

The particle size distribution used in this document was chosen by Schwendiman⁶ as most appropriate for evaluating leakage from a transportation container for PuO₂ powder. The distribution corresponds to 1000°C calcined plutonium oxalate with a 15-minute dispersion prior to measurement. This particle size distribution is listed in Table A-1. The particle size distributions in most wastes are expected to have larger mean particle sizes.

These data were converted to mass fraction of particles having diameters between two values, and the mass fraction was assigned to a diameter corresponding to the range midpoint. The fraction of the alpha decay energy escaping from each size particle was calculated using Table B2-1 of Appendix 3.1 of the CH-TRU Payload Appendices, Attachment B. The results

⁵ Mishima, J., and C. G. Lindsey, "Investigation into the Feasibility of Alternative Plutonium Shipping Forms," Pacific Northwest Laboratory, Battelle Memorial Institute, NUREG/CR-3007, PNL-4507, 1983.

⁶ Schwendiman, L. C., "Supporting Information for the Estimation of Plutonium Oxide Leak Rates through Very Small Apertures," Battelle, Pacific Northwest Laboratories, BNWL-2198, NRC-12, 1977.

and the mass-weighted total energy escaping from the PuO₂ particles are tabulated in Tables A-2 and A-3.

The conclusion drawn is that at most 82 percent of the alpha decay energy from particulate contamination is available to interact with waste materials.

Table A-1 — PuO₂ Particle Size Distribution

Particle Diameter and Smaller (μm)	Cumulative Percent by Weight
20	100
18	99
10	81
8	56
6	39
4	20
2	4
1	1
0.5	0.15
0.1	0.1

Source: Schwendiman, L. C., "Supporting Information for the Estimation of Plutonium Oxide-Leak Rates through Very Small Apertures," Battelle, Pacific Northwest Laboratories, BNWL-2198, NRC-12, 1977.

Table A-2 — Mass-Weighted Total Energy Escaping from PuO₂ Particles for Pu-239

Midpoint Particle Radius (μm)	Fraction of Alpha Energy Escaping	Mass Fraction in Distribution	Mass-Weighted Fraction of Energy Escaping
9.5	0.48	0.01	0.005
7.0	0.61	0.18	0.110
4.5	0.77	0.25	0.193
3.5	0.82	0.17	0.139
2.5	0.88	0.19	0.167
1.5	0.93	0.16	0.149
0.75	0.96	0.03	0.029
0.28	0.99	0.01	0.010
TOTAL			0.802

Note: Particles have the size distribution given in Table A-1.

Table A-3 — Mass-Weighted Total Energy Escaping from PuO₂ Particles for Pu-238

Midpoint Particle Radius (μm)	Fraction of Alpha Energy Escaping	Mass Fraction in Distribution	Mass-Weighted Fraction of Energy Escaping
9.5	0.52	0.01	0.005
7.0	0.65	0.18	0.117
4.5	0.79	0.25	0.198
3.5	0.84	0.17	0.143
2.5	0.89	0.19	0.169
1.5	0.93	0.16	0.149
0.75	0.97	0.03	0.029
0.28	0.99	0.01	0.010
TOTAL			0.820

Note: Particles have the size distribution given in Table A-1.

APPENDIX 3.3

USE OF DOSE-DEPENDENT G VALUES FOR CH-TRU WASTES

This page intentionally left blank.

3.3 Use of Dose-Dependent G Values for CH-TRU Wastes

3.3.1 Background

This appendix describes controlled studies and experiments that quantify the reduction in the rate of hydrogen gas generation (G value) over time based on the total dose received by the target matrix. Over time and with constant exposure to radiation, hydrogen is removed from the hydrogenous waste or packaging material (the matrix), thus decreasing the number of hydrogen bonds available for further radiolytic breakdown (the matrix is depleted). Therefore, when the alpha-generating source is dispersed in the target matrix, it will affect only that portion of the target material that is present in a small spherical volume surrounding the source particle. As the amount of available hydrogen is reduced over time, the effective G value decreases with increasing dose to a limit that is defined as the "dose-dependent G value." This phenomenon of matrix depletion has been studied and observed in previous studies (see Appendix 3.1 of the CH-TRU Payload Appendices). A formal study was recently undertaken to quantify dose-dependent G values under strictly controlled conditions and evaluate their applicability to contact-handled transuranic (CH-TRU) wastes.¹ This appendix summarizes the results of this study and derives dose-dependent G values for CH-TRU waste materials, as applicable.

3.3.2 Overview of the Matrix Depletion Program

The Matrix Depletion Program (MDP), established as a joint venture by the U.S. Department of Energy (DOE) National TRU Waste Program and the DOE Mixed Waste Focus Area, is comprised of the following elements:

1. Laboratory experiments for the assessment of effective G values as a function of dose for matrices expected in CH-TRU wastes (polyethylene, polyvinyl chloride, cellulose, etc.), as well as an assessment of the impact of other variables (isotope, temperature, etc.) on the dose-dependent G values.
2. Measurements of effective G values and hydrogen concentrations in real waste and comparisons with dose-dependent G values.
3. Analysis to calculate effective G values from fundamental nuclear and molecular mechanisms.

A total of 60 one-liter test cylinders containing the simulated CH-TRU waste materials were used, with two replicates for each test. Solid waste matrices (plastics and cellulose) were prepared by sprinkling the radioactive isotope powders over the matrix, folding the matrix over the contaminated surfaces, securing them, and placing them in test cylinders. Solidified waste matrices (cement) were mixed with a solution of dissolved plutonium oxide, water, and sodium

¹ Idaho National Engineering and Environmental Laboratory, "TRUPACT-II Matrix Depletion Program Final Report," *INEL/EXT-98-00987*, Rev. 1, prepared for the U.S. Department of Energy, Idaho Operations Office, Idaho Falls, Idaho (1999).

hydroxide to adjust the pH. The test cylinders were connected to measurement devices that facilitated sampling of generated gases and quantifying the gas generation over time. The entire test apparatus was controlled by a personal computer through LABVIEW software.

All activities of the MDP were performed under a documented quality assurance (QA) program that specified the performance-based QA/quality control requirements for all aspects of the program.² The experiments under the MDP were designed using an U.S. Environmental Protection Agency established procedure to formulate data quality objectives. QA objectives for the MDP were defined in terms of precision, accuracy, representativeness, completeness, and comparability. All data were validated and verified pursuant to the performance objectives of the program. The MDP was run for a duration of approximately three years.

3.3.3 Results and Conclusions from the MDP

Results from the MDP are described in detail in the MDP final report¹ and are summarized in Table 3.3-1 in terms of the dose-dependent G values for each matrix tested.

Table 3.3-1 — Experimental Dose-Dependent G Values

Matrix	Current Waste Material Type G Value	Number of Observations	Mean	Standard Deviation	95% Upper Tolerance Limit
Cement	1.3	202	0.25	0.18	0.58
Dry Cellulose	3.4	302	0.27	0.18	0.59
Polyethylene	3.4	186	0.23	0.22	0.64
Polyvinyl Chloride	3.4	99	0.14	0.19	0.50
Wet Cellulose	3.4	276	0.44	0.36	1.09

Source: Idaho National Engineering and Environmental Laboratory, "TRUPACT-II Matrix Depletion Program Final Report," *INEL/EXT-98-00987*, Rev. 1, prepared for the U.S. Department of Energy, Idaho Operations Office, Idaho Falls, Idaho (1999).

For all matrices, these dose-dependent G values were achieved within a maximum dose of 0.006 watt*year (product of watts times years). For example, for a waste container with a watt loading of 0.1 watt, the dose-dependent G value shown in Table 3.3-1 would be reached after 0.06 years or 22 days. The lower the watt loading, the longer it would take for the watt*year criteria to be satisfied and the dose-dependent G value to be applicable.

² Connolly, M.J., G.R. Hayes, T.J. Krause, and J.S. Burt, "TRUPACT-II Matrix Depletion Quality Assurance Program Plan," *INEL95/0361*, Rev. 1, Idaho National Engineering and Environmental Laboratory, Idaho Falls, Idaho (1997).

The following conclusions can be drawn from the results of the MDP:

- Increasing dose (product of the decay heat loading and elapsed time) decreases the effective G value for hydrogen due to depletion of the matrix in the vicinity of the alpha-emitting radioactive source particle. The lower G value, called the “dose-dependent G value,” is applicable after a dose of 0.006 watt*years.
- As with initial G values, the dose-dependent G values are a function of the waste matrix.
- Dose-dependent G values for wet cellulosics were higher than those for dry cellulosics because of the presence of water.
- The dose-dependent G values were independent of temperature based on testing performed at room temperature and at 140°F.
- Experiments performed with different particle sizes show that while initial G values could be higher for smaller particle sizes, the dose-dependent G values for all particle sizes tested are bounded by the values shown in Table 3.3-1.
- Previous experiments that included agitation of cylinders similar to those used in the MDP indicated that agitation did not affect dose-dependent G values.¹
- Isotopic composition did not have a significant impact on the dose-dependent G values based on experiments performed with two different isotopes of Pu (Pu-238 and Pu-239).

Data from actual CH-TRU waste containers at the Rocky Flats Environmental Technology Site and the Idaho National Engineering and Environmental Laboratory show that even when compared to the mean dose-dependent G values from the matrix depletion experiments, G values from real waste containers are lower. Theoretical analysis, using nuclear and molecular level mechanisms, also shows that hydrogen generation from radiolysis and matrix depletion is consistent with the experimental results from the MDP.

3.3.4 Effects of Agitation on Dose-Dependent G Values

The effects of agitation on dose-dependent G values have been evaluated by previous studies at both the laboratory-scale and drum-scale levels, and agitation has been found to have no impact on dose-dependent gas generation rates. Agitation could occur under transportation conditions but, as shown below, does not cause redistribution of the radionuclides to a nondepleted portion of the waste matrix and therefore does not cause an increase in the dose-dependent G values as shown in this section.

The earliest study of the effects of agitation on gas generation rates was performed by Zerwekh at the Los Alamos National Laboratory (LANL) in the late 1970s.³ Zerwekh prepared an experimental array of 300-cm³ stainless steel pressure cylinders, each loaded with 52.5 grams of a single or a combination of TRU waste matrix materials. Materials tested included cellulosics, polyethylene (PE) (low-density) bags, PE (high-density) drum liner material, and other typical TRU waste material. Net gas G values as a function of elapsed time were derived for each of the test cylinders and showed the characteristic decrease in G value with dose. Thorough mechanical shaking of two of the cylinders on two different occasions did not affect the rate of gas generation.³

In a second study, researchers at LANL retrieved six drums of ²³⁸Pu contaminated waste from storage to study gas generation.⁴ The wastes were contained in 30-gallon drums and consisted of either mixed cellulosic wastes or mixed combustible wastes. The drums ranged in age from four to ten years. Two of the drums containing mixed combustible wastes were tumbled end over end in a drum tumbler for four hours.⁴ The researchers also reported G values for three drums of newly generated waste that were previously characterized. All six retrieved drums had measured G values that were lower than those measured for newly generated drums. The researchers concluded that the retrieved drums' effective hydrogen G values corroborate the matrix depletion observed for the laboratory-scale experiments in Zerwekh (1979)³. Also, because of the vigorous nature of the agitation experienced by two of the four-year-old drums, the researchers concluded that radionuclide redistribution does not occur under transportation conditions.³

More recently, experiments on alpha radiolysis were conducted at LANL by Smith et al.⁵ to determine radionuclide loading limits for safe on-site storage of containers at LANL. Simulated TRU waste matrices in the form of cellulose (cheesecloth and computer paper) and PE (bottle and bag material forms) were contaminated with pre-weighed amounts of ²³⁸PuO₂ powder. The first PE experiment (referred to as PE test cylinder 1) used a PE bottle to allow any potential later redistribution of the radionuclide particles to fresh matrix surfaces. The radionuclide powder was poured into the bottle, which was sealed and gently rolled to allow contamination of the sides of the bottle. The bottle was returned to an upright position and the lid was punctured with an approximately 0.5-inch diameter hole to allow free movement of generated gas from the bottle to the test canister. It was noted that the ²³⁸PuO₂ powder adhered to the walls of the bottle and very little, if any, collected at the bottom. The remaining five test sample matrices were prepared by uniformly sprinkling the powder across a letter-sized sheet of the waste matrix, folding the sheet in toward the center from each end, and finally rolling each sheet into a cylindrical shape of about 2 by 4 inches. The six test matrices were placed inside six cylindrical, 2.06 liter stainless steel sealed canisters. Gas samples were extracted periodically and analyzed by mass spectrometry.

³ Zerwekh, A., "Gas Generation from Radiolytic Attack of TRU-Contaminated Hydrogenous Waste," LA-7674-MS, Los Alamos National Laboratory, Los Alamos, New Mexico (1979).

⁴ Zerwekh, A., J. Warren, and S. Kosiewicz, "The Effect of Vibration on Alpha Radiolysis of Transuranic (TRU) Waste," Proceedings of Symposium on Waste Management, Tucson, Arizona (1993).

⁵ Smith, M.C., E.L. Callis, J.H. Capps, E.M. Foltyn, R.S. Marshall, and J. Espinoza, "Alpha Radiolytic Gas Generation: Determination of Effective G-values," Benchmark Environmental Corporation, Albuquerque, New Mexico (1997).

The first test canister for each waste material was subjected to vigorous dropping, rolling several times, and shaking on day 188 to simulate drum handling and transportation that could result in redistribution of the $^{238}\text{PuO}_2$ to fresh nondepleted portions of the waste matrix. Any agitation effects were expected to be most pronounced for the test canister containing the PE bottle in PE test cylinder 1, because some aggregation of the powder at the bottom of the bottle was expected. However, no change in the effective hydrogen G value was observed for either the cellulose or PE test canisters.

In summary, three separate studies have investigated the ability of agitation to redistribute radionuclide particles to nondepleted surfaces of TRU waste matrices. All three studies conclusively showed that the dose-dependent G values are not impacted by agitation during transportation. Application of dose-dependent effective G values is discussed in Section 3.3.5.

3.3.5 Application of Dose-Dependent G Values to CH-TRU Wastes

Dose-dependent G values are applicable to CH-TRU waste materials of Waste Types II and III. Waste Type I, Solidified Inorganic Solids, will be governed by the initial G values under all conditions because the solidified, aqueous nature of these waste forms, in theory, precludes observation of matrix depletion (as the matrix near the Pu is depleted, water can move to replace the depleted matrix). Similarly, if CH-TRU waste materials of Waste Types II and III contain absorbed, adsorbed, or solidified aqueous materials, matrix depleted G values cannot be used. The presence of absorbed, adsorbed, or solidified aqueous materials precludes the observation of matrix depletion and requires the use of initial G values for Waste Types II and III that include such materials although the watt*year criteria (watt*year >0.012) may be met.

In addition, waste in shielded containers is conservatively assigned an initial G value (no credit for matrix depletion) due to the potentially higher contribution of gamma energy to the container decay heat compared to other CH-TRU waste forms. Although a large portion of the decay heat in these containers is from alpha and beta radiation and will result in matrix depletion, no credit is taken for this in the shielded container.

The watt*year criteria used to apply dose-dependent G values is twice the highest value recorded in the experiments. The dose-dependent G values chosen for CH-TRU waste materials of Waste Types II and III are the 95% upper tolerance limit values shown in Table 3.3-1. The application of dose-dependent G values to the waste types is as follows:

- Waste Type II: Dose-dependent G value (H_2) for containers meeting a watt*year criteria of 0.012 is governed by assuming polyethylene as the packaging material, with a G value (H_2) of 0.64.
- Waste Type III: Dose-dependent G value (H_2) for containers meeting a watt*year criteria of 0.012 is governed by wet cellulosic materials in the waste, with a G value (H_2) of 1.09.

Dose-dependent G values are not applicable to Waste Type I or to waste packaged in shielded containers.

As can be seen from Table 3.3-1, the above dose-dependent G values represent conservative values that are more than two times the mean value from the experiments.

APPENDIX 3.4

SHIPPING PERIOD – GENERAL CASE

This page intentionally left blank.

3.4 Shipping Period — General Case

3.4.1 Introduction

The purpose of this appendix is to develop, on a conservative basis, the time for the shipping period from closure until venting that should be considered for the analysis of gas generation in TRUPACT-II and HalfPACT.

3.4.2 Background

A large number of shipments of contact handled transuranic (CH-TRU) waste to the Waste Isolation Pilot Plant (WIPP) from U.S. Department of Energy (DOE) facilities have been planned. These shipments will be made by a fleet of trucks, each capable of transporting up to three packages, or by rail. The analysis in this appendix is presented for the case of shipments by truck. Shipments by rail shall meet the 60-day total maximum shipping period requirement for truck shipments. A 20-day shipping period is applicable to shipments to destinations (WIPP or other receiving site) within a radius of approximately 1,000 miles, as presented in Appendix 3.5 of the CH-TRU Payload Appendices. Using administrative controls, a 10-day shipping period is applicable for shipments to WIPP or other receiving site as presented in Appendix 3.6 of the CH-TRU Payload Appendices. For Content Code LA 154, a shipping period of 5 days to WIPP is justified, as presented in Appendix 6.12 of the CH-TRU Payload Appendices.

The packages are loaded on specially designed trailers and travel over the routes shown in Figure 3.4-1. The waste transportation activity will span a 25-year period. Because of the large number of trips and because of the agreements for notification to the states through which these shipments will pass on their way to WIPP or other receiving site, a state-of-the-art satellite tracking system will be employed to monitor the progress and position of each shipment. This monitoring capability will be available to authorities in the affected states as well as the transportation management people at the WIPP site and other receiving sites.

3.4.3 Approach

The approach to be taken in establishing the shipping period will be to develop a normal or expected shipment time based on the planned loading, transport, and unloading times. Then a maximum shipment time will be based on adding to the normal shipment time delays caused by a number of factors. This maximum shipment time will assume that each of these delays occurs. The probability of each of these delays occurring is small. The joint probability of all of these delays occurring would be extremely small. Thus the development of a maximum shipment time based on the sum of extended delays for each of the factors is considered to have a large margin of error. In the event that a particular shipment is experiencing delays (for one reason or another) resulting in an abnormal shipment time, close monitoring of the delay by WIPP will ensure minimum delays in the schedule.

Security Related Information

Figure Withheld Under 10 CFR 2.390

Figure 3.4-1—TRU Waste Generator/Storage Site and Potential Shipment Corridor States

3.4.3.1 Normal or Expected Shipment Time

The normal transport time is the sum of the times associated with loading the packages, the normal transit time, and the unloading of the packages. The loading time to be considered as important is the time interval from closing (sealing) the inner containment vessel (ICV) until the truck leaves the waste shipper's facility. The transit time is that time interval beginning with departure from the shipper's facility and ending with the arrival at the WIPP site or other receiving site. The unloading time is that time interval beginning with the arrival at the receiving site and ending with the venting of the ICV. This total time defines the expected shipment time.

3.4.3.2 Off-Normal or Maximum Shipment Time

The maximum shipment time includes those delays that could extend the shipment time. These delays are:

- Delays in loading or releasing the truck at the shipper's facility.

- Delays in transit caused by adverse weather conditions leading to road closures, or road closures due to accidents involving other vehicles.
- Accidents involving the shipment vehicle. These delays would include the time required for notification of appropriate authorities (including the DOE Emergency Response Team), and the time to take corrective action. This corrective action may involve transfer of the packages to a back-up truck, which would require the services of heavy equipment.
- Delays in transit caused by mechanical problems with the truck. This factor would include such things as tire problems, broken belts and hoses, and any other such minor problems.
- Delays caused by one or both of the drivers becoming ill.
- Delays in unloading the packages at the WIPP site or other receiving site. These could potentially be caused by factors such as truck arrival at the start of a long holiday weekend or equipment problems at the receiving site.

3.4.4 Discussion

3.4.4.1 Normal or Expected Shipment Time

As stated previously, the normal or expected shipment time is that time interval beginning with the sealing of the ICV at the shipper's facility and ending with the venting of the ICV at the WIPP site or other receiving site.

3.4.4.1.1 Package Loading

The package is designed so that it can be loaded within one hour. The loading operation is facilitated by design features and contents handling methods aimed at a quick turnaround during either loading or unloading. For example, the closure lids on both the inner containment vessel and outer confinement vessel are fastened with a breech-lock type of mechanism. The contents are handled in vertical sets as a payload assembly, and only one lift is required. All steps in the loading process (from attaching the lifting fixture to the crane until the lift fixture lift links are disconnected from the outer closure following loading) can be accomplished in two hours or less. Thus the time associated with loading the three packages for a single shipment is expected to be less than eight hours. However, to be conservative, one day (24 hours) is allotted for this activity.

3.4.4.1.2 Transit Time

Specific routes have been selected for transport of waste between the DOE facilities and from each of the DOE facilities to the WIPP site. The distances for the primary DOE facilities to the WIPP site are given in Table 3.4-1.

These shipments will all be made by trucks having two drivers. Regulations governing maximum driving and on-duty times are given in 49 CFR 395, "Hours of Service of Drivers."¹

These regulations permit a driver to drive not more than ten (10) hours following eight (8) consecutive hours off duty or, be in the on-duty status not more than fifteen (15) hours. If the fifteen hours on-duty status is reached, a driver must be out of the vehicle in an off-duty status for eight hours. Drivers using sleeper berth equipment may cumulate the eight (8) hours off duty (for the ten hour on-duty status) resting in the sleeper in two separate periods (each period must be at least two hours) totaling eight (8) hours. Drivers cannot be on duty more than seventy (70) hours in eight consecutive days. By using the two drivers and a rotational on-duty/off-duty system of approximately five (5) hours, the vehicle can be maintained operational for twenty-four (24) hours per day for seven days.

Table 3.4-1 — Normal Transit Times

To WIPP From	Distance (Miles)	Transit Time in Hours (Miles per Hour)				Transit Time in Days (Miles per Hour)			
		40	45	50	55	40	45	50	55
ANL	1404	35.1	31.2	28.1	25.5	1.5	1.3	1.2	1.1
Hanford	1847	46.2	41.0	36.9	33.6	1.9	1.7	1.5	1.4
INL	1484	37.1	33.0	29.7	27.0	1.5	1.4	1.2	1.1
Knolls-NFS	1573	39.3	35.0	31.5	28.6	1.6	1.5	1.3	1.2
LANL*	352	8.8	7.8	7.0	6.4	0.4	0.3	0.3	0.3
LLNL	1345	33.6	29.9	26.9	24.5	1.4	1.2	1.1	1.0
NTS*	1017	25.4	22.6	20.3	18.5	1.1	0.9	0.8	0.8
ORNL	1493	37.3	33.2	29.9	27.1	1.6	1.4	1.2	1.1
RFETS*	666	16.7	14.8	13.3	12.1	0.7	0.6	0.6	0.5
SNL	326	8.2	7.2	6.5	5.9	0.3	0.3	0.3	0.2
SRS	1447	36.2	32.2	28.9	26.3	1.5	1.3	1.2	1.1
WVDP	2391	59.8	53.1	47.8	43.5	2.4	2.2	2.0	1.8

*See Appendix 3.5 of the CH-TRU Payload Appendices for the justification of a shorter shipping period determination for these sites, which are within an approximately 1,000 mile radius of WIPP.

Experience at the Idaho National Laboratory has shown that shipments of this type can achieve an average speed of 45 mph. This average speed includes stops for vehicle inspections every two hours, fueling, meals, driver relief and state vehicle inspections.

¹ Title 49, Code of Federal Regulations, Section 395 (49 CFR 395), "Hours of Service of Drivers."

The normal transit time ranges from 0.3 day for shipments from Los Alamos National Laboratory or Sandia National Laboratory to 2.2 days for shipments from the West Valley Demonstration Project as shown in Table 3.4-1. For the purpose of conservatism, 3 days is assumed for a maximum normal transit time.

3.4.4.1.3 Unloading

Normal unloading will be accomplished in less than a day. Once the truck has undergone the health physics survey and security checks, the tractor is disconnected, and a trailer jockey is connected to the trailer. The trailer and packages are cleaned, and the trailer is moved to the unloading area. The packages are removed from the trailer and placed into the unloading area. The outer and inner lids are removed after the containment vessels have been vented through a facility gas-handling system, and other procedural steps are then taken. The normal unloading of a trailer with three packages will be accomplished in less than one day. The unloading time is, thus, conservatively assigned a value of one day.

3.4.4.1.4 Total Normal or Expected Shipment Time

The total normal or expected shipment time is three to five days depending on the origin of the waste. Normal loading time is one day, transit time is one to three days and unloading time is one day.

3.4.4.2 Off-Normal or Maximum Shipping Time

3.4.4.2.1 Loading Delays

There are a number of factors that could extend the time interval between the sealing of the ICV and the truck getting under way:

- Loading could begin on a day preceding a holiday weekend.
- Difficulty testing the ICV or Outer Confinement Vessel (OCV) seals.
- Handling equipment failure.

In the most severe sequence, one package of the load would already have been filled and sealed. Loading could begin on a day preceding a long (holiday) weekend. If, for example, loading began on a Friday preceding a three-day weekend, loading would not be completed until the following Tuesday. This would result in a four-day loading period.

The inner or outer seal may fail the leak test, which would generally call for some maintenance. The worst case would probably be a failure in the leak test equipment that could take up to two days to correct.

The crane or the lifting fixture with center of gravity load compensation could also fail, forcing a delay in any further package loading until corrected. This could also take two days.

It would be very unlikely for more than two of these scenarios to happen simultaneously, so a total of six days is deemed to be a reasonable maximum time to account for delays associated with loading. If there were conditions that could cause long, totally unanticipated delays, the packages can be vented at the shipper's facility.

3.4.4.2.2 Transit Time Delays

There are several factors that could extend the maximum normal transit time of three days. Adverse weather conditions could lead to delays and road closures. A telephone survey of each of the states in the waste shipment corridor states was conducted to ascertain a reasonable time to assume for weather delays. Table 3.4-2 provides the results of this survey. One can conclude from this survey that weather conditions may close a major highway for two to five days. Long-term interruptions in normal traffic caused by bridge outages etc., would result in rerouting traffic to alternate routes. Accidents involving other vehicles could also cause delays and road closures of up to a day. It is concluded that a total transit delay of five (5) days is reasonable to assume for weather delays or road closures.

Accidents involving the shipment vehicle itself could cause lengthy delays. These delays would include the accident response time for notifying appropriate authorities (including Radiological Assistance Teams, if required) and the time to take corrective action or to mitigate the accident. One day is conservatively assumed for the response to the accident. (In addition to normal accident responses, monitoring of the satellite tracking system would also facilitate an early response to accidents). Corrective action may involve retrieving the packages from a damaged trailer (including the possibility that the truck could be over an embankment), and transferring them to a back-up truck. Special equipment such as cranes may be required to carry out these operations. An accident mitigation time of five days will be assumed. This time includes the time for delivery of a back-up truck, and the time to move in special heavy equipment and rig special lifting fixtures to retrieve and transfer the packages to the back-up vehicle.

Table 3.4-2 — Survey of Weather Related Delays on Interstate Highways of the TRU Waste Shipment Corridor Sites

State/City	Office Contacted	Date Contacted	Type of Weather Related Delays	Highway
1. Alabama/Montgomery	State DOT	2/4/88	24 hrs. max.	All
2. Arizona/Phoenix	Dept. of Public Safety	2/4/88	8 hrs. maximum for any type of emergency.	All
3. Arkansas/Little Rock	State DOT Construction of Maintenance	2/17/88	1/2 day maximum.	All
4. California/Sacramento	State DOT Highway Dept.	2/18/88	2 days due to snow every 2 to 3 years. Few minutes to 2 to 3 weeks due to flood. 2 weeks due to earthquake. Detours provided.	I-5 I-15 Route 14
5. Colorado/Denver	State DOT	2/5/88	12 hrs. maximum.	
6. Georgia/Atlanta	State DOT Maintenance	2/2/88	No information available.	
7. Idaho/Boise	State DOT	2/4/88	3 to 4 hrs. due to blizzard.	
8. Illinois/Springfield	State DOT	2/7/88	10 days because a bridge pier slipped. (Trucks were off the road for 14 days). Detours provided.	Northbound I-90, I-94
9. Indiana/Indianapolis	Dept. of Highway Operations	2/5/88	2 days due to snowstorm or blizzard/wind.	I-65
10. Kentucky/Frankfort	State DOT Highway Maintenance	2/5/88	8 hrs. maximum.	
11. Louisiana/Baton Rouge	State DOT Office of Highway Traffic and Planning	2/3/88	No information available.	
12. Mississippi/Jackson	State DOT Highway Dept.	2/17/88	None.	
13. Missouri/Jefferson City	Highway Patrol	2/4/88	1/2 to 1 day due to flooding. 1 to 1-1/2 days with detours provided.	I-70
14. Nevada/Carson City	State DOT Maintenance Div.	2/4/88	4 to 8 hrs. due to snow.	I-80
15. New Mexico/Santa Fe	State DOT	2/9/88	Closed periodically due to snow and/or wind but for a very short period of time.	Interstate
16. Ohio/Columbus	State DOT	2/5/88	8 hrs. maximum.	All
17. Oklahoma/Oklahoma City	State DOT	2/5/88	1 month due to a bridge was washed out on Cimmaron River.	I-35
18. Oregon/Salem	State DOT	2/4/88	8 hrs. maximum. Generally, usage of highway stopped for trucks/oversized vehicles for up to 8 hours for icy conditions	Interstate
19. South Carolina/Columbia	State DOT State Dept. of Health and Control	2/3/88	No information but generally 8 hrs. maximum.	

Table 3.4-2 — Survey of Weather Related Delays on Interstate Highways of the TRU Waste Shipment Corridor Sites (Continued)

State/City	Office Contacted	Date Contacted	Type of Weather Related Delays	Highway
20. Tennessee/Nashville	State DOT	2/3/88	96 hours due to rain. 72 Hours due to rain/high water level.	State Route 54 N in Haywood County State Route 188
21. Texas/Austin	State DOT	2/16/88	2 to 3 hours due to flooding. 8 hours maximum due to snow.	I-20
22. Utah/Salt Lake City	State DOT Traffic Engr.	2/4/88	4 to 5 hours due to blizzard.	I-15
23. Washington/Olympia	State DOT	2/4/88	2 days due to avalanche.	I-90
24. Wyoming/Cheyenne	State DOT Motor Vehicle Safety	2/4/88	4 to 5 days predominantly due to weather.	I-80

Delays in transit could be caused by routine mechanical problems with the truck. These problems could include tire failures, broken belts and hoses, electrical failures and similar minor problems; or more significant problems necessitating bringing a back-up truck into service. It is conservatively assumed that appropriate responses to mechanical failures of the truck can be made in four days.

Lastly, one or both of the drivers could become ill during the trip, necessitating the possibility that one driver must do all the driving or relief drivers would have to be sent to wherever the truck is parked. If one driver has to do all the driving, the transit time would be doubled (i.e., add three days). If relief drivers are required, a two-day delay will occur to allow for travel time of the replacement driver(s).

3.4.4.2.3 Unloading Delays

Delays in unloading the packages at the WIPP site or other receiving site could be caused by a number of factors: A truck could arrive at the receiving site late on a Friday preceding a three day weekend, and the normal processing and unloading would not be completed until the following Tuesday, causing a delay in unloading of approximately 4-1/2 to 5 days. There could be equipment problems that could cause delays in unloading the packages. Venting and handling equipment could break down. A total unloading time of four days will be assumed if unloading begins just before a regular weekend or five days for a holiday weekend. This is a reasonable maximum time to account for delays associated with unloading because the packages can be vented at the receiving site (using workers overtime) if a totally unanticipated chain of delays were to occur.

3.4.4.2.4 Total Off-Normal or Maximum Shipment Time

The total off-normal or maximum shipment time is summarized in Table 3.4-3. A maximum shipment time of 31 days is projected assuming the worst-case scenario of all off-normal occurrences happening in the same shipment.

Table 3.4-3 — Shipment Time Summary

Activity	Time (Days)
Normal Shipment Time	
Loading	1
Transit Time	1-3
Unloading	1
Maximum Normal Shipment Time	3-5
Off-Normal or Maximum Shipment Time ^a	
Loading	6
Transit Time	
• Normal (maximum)	3
• Weather delays and road closures	5
• Accident response	1
• Accident Mitigation	5
• Truck maintenance problems	4
• Driver illness	2
Unloading	5
Maximum Off-Normal Shipment Time	31

^aAdding all the times for relatively low-probability, independent delays provides a conservative value for the maximum off-normal transit time.

3.4.5 Summary and Conclusions

The total normal or expected shipment time from the DOE facilities to the WIPP site or other receiving site will be three to five days with the longest time associated with the trip from the West Valley Demonstration Project to WIPP. The maximum or off-normal shipment time that has been postulated to occur as a consequence of a series of accidents or other off-normal events and delays is 31 days. This maximum shipment time is six times the maximum normal expected shipment time. This justifies using a 31-day period for the basis of determining potential buildup of flammable concentrations in the package under the specified normal conditions with the absence of venting or operational controls during transport. However, to add an additional margin of safety, the shipping period is nearly double the total off-normal shipment time or 60 days, which is more than an order of magnitude longer than the maximum normal shipment time.

This page intentionally left blank.

APPENDIX 3.5

SHIPPING PERIOD – CLOSE-PROXIMITY SHIPMENTS

This page intentionally left blank.

3.5 Shipping Period—Close-Proximity Shipments

3.5.1 Introduction

This appendix presents the shipping period determination for close-proximity shipments (i.e., within a radius of approximately 1,000 miles). The three U.S. Department of Energy (DOE) facilities nearest to the Waste Isolation Pilot Plant (WIPP) (i.e., Los Alamos National Laboratory [LANL], Rocky Flats Environmental Technology Site [RFETS], and Nevada Test Site [NTS]) are within a radius of approximately 1,000 miles of WIPP. For close-proximity shipments, the TRUPACT-II or HalfPACT is loaded at the site, transported within a radius of approximately 1,000 miles, and vented within a maximum of 20 days from the closure (or sealing) of the inner containment vessel (ICV). The basis for the 20-day shipping period is defined in this appendix.

3.5.2 Approach

The shipping period is defined to begin with closure (or sealing) of the ICV during loading at the shipping facility and end with venting of the ICV during unloading at the receiving facility. Conservative time estimates for the following activities were used in determining the shipping period for close-proximity shipments:

- Loading time
- Transport time
- Unloading time.

3.5.2.1 Loading Time

The loading time begins with the sealing of the ICV and ends with the departure of the shipment of the package from the site. All steps in the normal, or expected, loading process for a single package (from attaching the lifting fixture to the crane until the lift fixture lift links are disconnected from the outer closure following loading) can be accomplished in two hours or less. Thus, the time associated with loading the three packages for a single truck shipment is expected to be less than eight hours. However, the maximum expected loading time is conservatively estimated as 24 hours (1 day).

The potential factors that could delay the expected loading time are as follows:

- Initiating loading on a day preceding a holiday weekend
- Difficulty associated with testing the ICV or outer confinement vessel (OCV) seals
- Failure associated with payload handling equipment.

Loading could be delayed if initiated on a day preceding a holiday weekend or other scheduled facility closure period. This could result in a maximum loading time of 4 days. Potential delays associated with leak testing or payload handling equipment failures are typically reduced to a matter of hours by the backup or replacement equipment typically available at each shipping

facility. However, even with available standby equipment, any equipment failure is likely to result in a lost day due to the time required to identify the problem, attempt corrective measures, and then access the backup or replacement equipment. As a result, a 1-day delay is deemed adequate for either seal testing or payload handling equipment failures. Although unlikely, if loading is assumed to be initiated on a day preceding a holiday weekend and either a seal testing or payload handling equipment failure is assumed to occur simultaneously, 5 days could be required to load three payloads. It should be noted that if excessive loading delays beyond 5 days were to occur due to unanticipated events, the packages could be vented at the shipping facility.

3.5.2.2 Transport Time

The transport time begins with the departure of the shipment from the site and ends with the arrival of the shipment at the receiving site. The transport time is dependent upon the distance between the shipping and receiving sites. For close-proximity shipments, the distance will be within a radius of approximately 1,000 miles. The normal, or expected, travel time for a distance of 1,000 miles is 25 hours based on an average speed of 40 miles per hour (mph). This average speed takes into account stops for vehicle inspections every two hours, fueling, meals, driver relief, and state vehicle inspections.

The potential factors that could delay the expected transport time are as follows:

- Adverse weather
- Vehicle accidents
- Mechanical problems with the truck
- Driver illness.

Adverse weather could result in transport time delays due to road closures, slower driving speeds, or unforeseen stops. Based on actual delays experienced to date by TRUPACT-II shipments, the average delay time attributed to weather is 23 hours (~1 day). Procedures at sites ensure that shipments are not initiated at times when adverse weather exists or is forecasted. Using operational experience, a 60-hour (2.5-day) delay is deemed adequate for any delay caused by adverse weather conditions.

Vehicle accidents have the potential for the longest transport time delays due to the time required to respond and perform required corrective actions. Based on the training programs provided to local emergency response personnel along the transport routes, accident response time would be minimal (less than one hour). However, additional time may be required for notification and response of other appropriate authorities such as Radiological Assistance Teams (if required). Deployment of other appropriate authorities from either the receiving or shipping facility, whichever is closer, would take no more than 0.5 day to reach an accident scene. The accident mitigation time for close-proximity shipments is considered to be prompt due to the relatively short distance that would be required to provide equipment to perform corrective measures. A backup truck and trailer, as well as special equipment (such as a crane and special lifting fixtures) could be required to return the shipment to the road. Either the shipping or receiving facility, whichever is closer, could provide accident mitigation equipment and personnel.

Therefore, up to 3 days is considered appropriate for completing accident corrective action. This time includes deployment of a backup truck and trailer, retrieving and transferring the packages to the backup vehicle, and performing any necessary surveys and/or inspections to confirm the shipment is prepared for transport.

Truck maintenance associated with common mechanical problems could result in transport time delays. The majority of routine mechanical problems (flat tires, belt or hose failures, etc.) can be rectified in a matter of hours. A worst-case mechanical problem would result in the need for a replacement truck, which is included in the time estimated for vehicle accident mitigation as described above.

The last remaining potential scenario for delaying the transport time is driver illness. The relatively short distances between close-proximity sites would enable prompt replacement of the ill driver(s). No more than 0.5 day would be required to provide a replacement driver if deployed from either the shipping or receiving facility, whichever is closer.

As a result, a 6.5-day transport time accounts for any unexpected impact to the expected transport time.

3.5.3 Unloading Time

The unloading time begins with the arrival of the shipment at the receiving site and ends with the venting of the ICV. The normal, or expected, unloading of a trailer with three packages will be accomplished in less than 0.5 day. However, the maximum expected unloading time is conservatively estimated at 24 hours (1 day).

The potential factors that could delay the expected unloading time are as follows:

- Shipment arrival preceding a holiday weekend
- Failure associated with venting or handling equipment.

Unloading could be delayed if the shipment arrives on a day preceding a holiday weekend or other scheduled facility closure period. This could result in a maximum unloading time of 4 days. Potential delays associated with venting or handling equipment failures are typically reduced to a matter of hours by the backup or replacement equipment typically available at each receiving facility. However, even with available standby equipment, any equipment failure is likely to result in a lost day due to the time required to identify the problem, attempt corrective measures, and deploy the backup or replacement equipment. As a result, a 1-day delay is deemed accurate for either venting or payload handling equipment failures. Although unlikely, if unloading is assumed to be initiated on a day preceding a holiday weekend and either a venting or payload handling equipment failure is assumed to occur simultaneously, 5 days could be required to unload three payloads. It should be noted that the packages could be vented, even if not completely unloaded, at the receiving facility within 5 days.

3.5.4 Summary and Conclusions

Based on an expected loading time of 24 hours, an estimated expected transport time of approximately 25 hours, and an expected unloading time of 24 hours, the maximum expected shipping period is approximately 3 days. The maximum shipment time that has been used in this analysis is based on conservative time estimates for loading (5 days), transport (6.5 days), and unloading (5 days). The additional contingency of a 3.5-day margin of safety results in a maximum shipping period of 20 days. Table 3.5-1 provides a summary of the activities comprising the shipping period.

Table 3.5-1 – Shipping Period Analysis Summary

Activity	Normal Expected Time (days)	Maximum Time Used in Analysis (days)
Loading Time	<1	5
Transport Time	~1	6.5
Unloading Time	<1	5
Margin of Safety	–	3.5
Shipment Time	3	20

This analysis justifies using a 20-day period as the basis for determining potential buildup of flammable concentrations in the package under the specified off-normal conditions with the absence of venting or operational controls during transport.

With twice the expected shipping period being just 6 days, the use of a 20-day shipping period is conservative. Data available for more than 1,800 shipments to the WIPP in more than 5 years show 20 days to be an extremely conservative estimate of shipping period. Sample shipping time data based on 1,467 shipments to WIPP from the three sites within a radius of approximately 1,000 miles are shown in Table 3.5-2. As shown, all shipments were made within a period of two days.

Table 3.5-2 — Sample Shipping Time Data

To WIPP From	Total Number of Shipments as of 04-20-04	Average Shipping Time (hours)*	% of Time Shipments are Completed within Average Time	Shipping Time Delays	
				Duration of Maximum Delay	Explanation
LANL	71	9	98%	1 day	Delay occurred at LANL as the result of generator site issues prior to shipment departure
NTS	7	30	100%	N/A	N/A
RFETS	1,389	18	99%	2 days	Weather delay; delay occurred at RFETS prior to shipment departure and en route following departure

*Average shipping times are estimated based on average speeds of 50 miles per hour and include time associated with safety inspections, fuel and food stops, and driver breaks.

N/A = Not applicable.

The 20-day shipping period justified herein may be used for any shipment to a destination within a radius of approximately 1,000 miles. For shipments to WIPP from within a radius of approximately 1,000 miles (i.e., from LANL, RFETS, and NTS), the 20-day shipping period may be used.

This page intentionally left blank.

APPENDIX 3.6

SHIPPING PERIOD – CONTROLLED SHIPMENTS

This page intentionally left blank.

3.6 Shipping Period — Controlled Shipments

3.6.1 Introduction

This appendix presents the shipping period determination for shipments designated as controlled shipments. For these shipments, the TRUPACT-II or HalfPACT is loaded at the site, transported from the site to the Waste Isolation Pilot Plant (WIPP) or other receiving site, and vented within a maximum of 10 days from the closure (or sealing) of the inner containment vessel (ICV). The basis for the 10-day shipping period is defined in this appendix. The use of a 10-day controlled shipment is an option available to sites that elect to impose administrative controls to ensure compliance with the conditions described herein.

3.6.2 Approach

The shipping period is defined to begin with closure (or sealing) of the ICV during loading at the shipping facility and end with venting of the ICV during unloading. Conservative time estimates for the following activities were used in determining the shipping period for controlled shipments:

- Loading time
- Transport time
- Unloading time.

3.6.2.1 Loading Time

The loading time begins with the sealing of the ICV and ends with the departure of the shipment of the package from the site. Activities to be completed during the loading time include leak testing and handling of the loaded package(s). As directed by site procedures for controlled shipments, these activities must be completed within 24 hours. If these activities are delayed beyond 24 hours, the package(s) must be vented and the closure process repeated in accordance with the administrative controls described in Section 6.2.3 of the Contact-Handled Transuranic Waste Authorized Methods for Payload Control (CH-TRAMPAC).

3.6.2.2 Transport Time

The transport time begins with the departure of the shipment from the site and ends with the arrival of the shipment at the receiving site. The transport time is dependent upon the distance between the two sites and capabilities for efficient response to potential transport time delays. As shown in Table 3.6-1, at an average speed of 40 miles per hour (mph) the longest travel time from a site to WIPP is 59.8 hours [corresponding to the 2,391 mile distance from the West Valley Demonstration Project (WVDP) to WIPP]. Controlled shipments shall be made only when the shipping distance between the two sites is bound by that shown for the WVDP to WIPP in Table 3.6-1. This average speed takes into account stops for vehicle inspections every two hours, fueling, meals, driver relief, and state vehicle inspections. Controlled shipments between sites are not allowed if the proposed travel distance exceeds 2,391 miles.

Table 3.6-1 — Normal Transit Times

To WIPP From	Distance (Miles)	Transit Time in Hours (Miles per Hour)				Transit Time in Days (Miles per Hour)			
		40	45	50	55	40	45	50	55
ANL	1404	35.1	31.2	28.1	25.5	1.5	1.3	1.2	1.1
Hanford	1847	46.2	41.0	36.9	33.6	1.9	1.7	1.5	1.4
INL	1484	37.1	33.0	29.7	27.0	1.5	1.4	1.2	1.1
Knolls-NFS	1573	39.3	35.0	31.5	28.6	1.6	1.5	1.3	1.2
LANL	352	8.8	7.8	7.0	6.4	0.4	0.3	0.3	0.3
LLNL	1345	33.6	29.9	26.9	24.5	1.4	1.2	1.1	1.0
NTS	1017	25.4	22.6	20.3	18.5	1.1	0.9	0.8	0.8
ORNL	1493	37.3	33.2	29.9	27.1	1.6	1.4	1.2	1.1
SNL	326	8.2	7.2	6.5	5.9	0.3	0.3	0.3	0.2
SRS	1447	36.2	32.2	28.9	26.3	1.5	1.3	1.2	1.1
WVDP	2391	59.8	53.1	47.8	43.5	2.4	2.2	2.0	1.8

The potential factors that could delay the normal transport time are as follows:

- Adverse weather
- Vehicle accidents
- Mechanical problems with the truck
- Driver illness.

Administrative controls in place at the shipping site prohibit the initiation of a controlled shipment at times when adverse weather exists or is forecasted. Any transport time delays associated with adverse weather are expected to be minimal and are, therefore, adequately covered by the margin of safety included in this analysis (see Section 3.6.4).

Prompt emergency response, truck maintenance, and driver or equipment replacement during the transport of controlled shipments is ensured by the application of additional resources.

Administrative controls applied to all CH-TRU waste shipments regardless of destination require the designation of a shipment as a “controlled shipment” prior to initiation of the shipment from the site. This designation provides a trigger that requires additional resources to be available in order to provide accelerated response to avoid any significant delay during the transport time. This controlled shipment protocol is in addition to the routine use of the TRANSCOM system at WIPP, which provides continuous tracking of the shipment during transport regardless of its destination (i.e., to WIPP or other receiving site).

Vehicle accidents have the potential for the longest transport time delays due to the time required to respond and perform required corrective actions. Based on the training programs provided to local emergency response personnel along the transport routes, accident response time would be minimal (less than one hour). However, additional time may be required for notification and response of other appropriate authorities such as Radiological Assistance Teams (if required). Deployment of other appropriate authorities from WIPP, the shipping facility, or other intermediate site, whichever is closer, would take no more than 1 day to reach an accident scene. Prompt mitigation of any accident is ensured by the application of WIPP protocol for controlled

shipments. Due to the additional resources available during controlled shipments, up to 2 days is considered appropriate for completing accident corrective actions. This time includes deployment of a backup truck and trailer, retrieving and transferring the package(s) to the backup vehicle, and performing any necessary surveys and/or inspections to confirm the shipment is prepared for continued transport.

Truck maintenance associated with common mechanical problems could result in transport time delays. The majority of routine mechanical problems (flat tires, belt or hose failures, etc.) can be rectified in a matter of hours. A worst-case mechanical problem would result in the need for a replacement truck, which is included in the time estimated for vehicle accident mitigation as described above.

The last remaining potential scenario for delaying the transport time is driver illness. The additional resources available for controlled shipments ensure prompt replacement of an ill driver. The time required to replace a driver is conservatively estimated as 1 day.

As a result of WIPP protocols applied to shipments designated as controlled shipments, a 4-day transport time accounts for any unexpected impact to the expected transport time.

3.6.3 Unloading Time

The unloading time begins with the arrival of the shipment at the receiving site and ends with the venting of the ICV. Normal unloading will be accomplished in less than one day (24 hours). Section 6.2.3 of the CH-TRAMPAC outlines administrative controls imposed to ensure venting of the ICV within 9 days of shipment departure from the shipping site.

3.6.4 Summary and Conclusions

Based on a loading time of 24 hours, an estimated transport time of less than 60 hours, and an unloading time of 24 hours, the normal expected shipping period for controlled shipments is 4 to 5 days. Using a conservatively estimated maximum transport time of 5 days, the maximum expected shipping period for controlled shipments is 7 days. The additional contingency of a 3-day margin of safety results in a maximum shipping period of 10 days. Table 3.6-2 provides a summary of the activities comprising the shipping period.

Table 3.6-2 – Shipping Period Analysis Summary

Activity	Normal Expected Time (days)	Maximum Time Used in Analysis (days)
Loading Time	<1	1
Transport Time	<2.5	5
Unloading Time	<1	1
Margin of Safety	–	3
Shipment Time	4-5	10

This analysis justifies using a 10-day period as the basis for determining compliance with gas generation requirements under rigorous operational controls during loading, transport, and unloading as specified in this appendix.

Sample shipping time data based on over 5,000 shipments of CH-TRU waste to WIPP are shown in Table 3.6-3. As shown, all shipments have been made in well under 10 days even without the use of administrative controls specified in this appendix. Therefore, the controlled shipments completed under the conditions specified in this appendix will readily comply with the 10-day shipping period.

Only shipments designated as controlled shipments and, therefore, subject to the protocol described in this appendix and the administrative controls specified in Section 6.2.3 of the CH-TRAMPAC for loading and unloading are eligible for evaluation using the 10-day shipping period.

Table 3.6-3 — Sample Shipping Time Data

To WIPP From	Total Number of Shipments as of 06-13-06	Average Shipping Time (hours)①	% of Time Shipments are Completed within Average Time	Shipping Time Delays	
				Duration of Maximum Delay	Explanation
ANL-E	13	38	100%	N/A	N/A
ANL-W	1	34	100%	N/A	N/A
Hanford	282	45	82%	5 days	Repairs at generator site on loading equipment
INL	1,721	36	80%	5 days	Weather delay; delay occurred en route; shipment was returned to INL and delayed prior to second departure
LANL	207	9	94%	1 day	Delay occurred at LANL as the result of generator site issues prior to shipment departure
LLNL	18	33	99%	1 hour	Delay in route
NTS	48	30	99%	9 hours	Delay in departure
RFETS	2,045	18	96%	2 days	Weather delay; delay occurred at RFETS prior to shipment departure and en route following departure
SRS	675	32	86%	3.7 days	Weather delay; delay occurred at SRS prior to shipment departure

① Average shipping times are estimated based on average speeds of 50 miles per hour and include time associated with safety inspections, fuel and food stops, and driver breaks.

N/A = Not applicable.

APPENDIX 3.7

**ASPIRATION OF UNVENTED PAYLOAD CONTAINERS
OF CH-TRU WASTE**

This page intentionally left blank.

3.7 Aspiration of Unvented Payload Containers of CH-TRU Waste

3.7.1 Introduction

Payload containers of contact-handled transuranic (CH-TRU) waste at U.S. Department of Energy (DOE) sites that have been stored in an unvented condition (without a filter or equivalent venting mechanism and/or without a punctured/vented liner) have the potential to accumulate hydrogen gas during storage. Prior to transport in a TRUPACT-II or a HalfPACT package, each container shall be vented for a sufficient period of time to aspirate. This is required to reduce the concentration of hydrogen present at the time of venting to steady state concentrations (generation rate equals release rate) within each of the layers of confinement in a payload container. Once steady state concentrations are achieved, there will be no change in the concentration of hydrogen in each of the volumes of confinement. "Venting" refers to the puncturing of the drum lid and rigid liner lid (if present) and the installation of one or more filter vent(s) or equivalent venting mechanism(s) in the drum lid of a payload container. The period of time for which a payload container needs to be vented before qualifying for transport in a package is defined as the "aspiration time." This appendix derives the aspiration times needed for unvented payload containers of waste for each payload shipping category.

Section 3.7.2 presents three options available to the sites to meet the aspiration requirements. Section 3.7.3 describes the methods used to derive the aspiration times including the computational procedure. A discussion of tables that must be used to determine the aspiration times for each payload shipping category is presented in Section 3.7.4. Specific procedures to be followed by the sites to implement any of the three options are presented in Section 3.7.5. All sites with unvented payload containers of waste shall follow one or more of these procedures as part of the waste qualification process.

3.7.2 Options to Determine Aspiration Times

Sites with unvented payload containers of waste have the following options to determine the aspiration time for a payload container. All of the options use bounding values for the hydrogen generation rates. For payload containers with waste types in packaging configurations that do not generate any flammable gas, aspiration is not required (i.e., Waste Material Type II.2). It is assumed that during the storage period and subsequent aspiration, hydrogen is being generated in the payload container at this bounding rate. These generation rates are the maximum allowable for each of the shipping categories. These rates are not a function of the G values, but depend on the packaging configurations within the payload containers. Since all the parameters used in the calculations are the same for containers with the same packaging configuration within a waste type (i.e., I, II, III, and IV), the aspiration times for the waste material types of a waste type (e.g., I.1, I.2, and I.3) are the same. In the aspiration tables for common shipping categories presented in Section 5.3 of the Contact-Handled Transuranic Waste Authorized Methods for Payload Control (CH-TRAMPAC), no distinction has therefore been made (or is necessary) between waste material types.

3.7.2.1 Option 1 - Aspiration Time Based on Date of Drum Closure

The aspiration time using Option 1 is calculated based on the amount of time that a payload container has been closed without venting. This option uses the bounding hydrogen generation rate for the payload shipping category (Appendices 2.3 and 6.7 of the CH-TRU Payload Appendices), and assumes that all of the hydrogen generated within the storage period will accumulate in the layers of confinement of the payload container. This approach will give a conservative estimate of the aspiration time, since the actual hydrogen generation rate will be less than the bounding value, and may decrease during storage due to matrix depletion. In addition, some of the hydrogen generated during storage may not be retained in the payload container. Many payload containers have gaskets that are manufactured to allow selected diffusion of hydrogen.

This analysis has been extended up to a possible accumulation of 40% hydrogen in the headspace of the payload container. As will be discussed in subsequent sections, this concentration is about an order of magnitude higher than the average concentration of hydrogen measured in sampling programs of CH-TRU waste drums at the DOE sites. If the DOE sites choose to implement this option, the age (period of time that the container has been closed) of the payload container will determine the aspiration time as shown in Section 5.3 of the CH-TRAMPAC.

3.7.2.2 Option 2 - Headspace Gas Sampling At The Time Of Venting

The second option is divided into two sub-options:

- Option 2A — Sampling of Container Headspace
- Option 2B — Sampling of Rigid Liner Headspace.

3.7.2.2.1 Option 2A — Container Headspace Gas Sampling at the Time of Venting

This option requires the sampling of payload containers for the container headspace concentration of hydrogen prior to puncturing the rigid drum liner. (Container headspace is the region between the payload container and the outermost layer of confinement, usually the rigid liner). This option allows credit for actual hydrogen generation rates inside the payload container during storage. In addition, this option allows credit for any diffusion of hydrogen through the gasket that can occur during storage. The aspiration time is determined based on the concentration of hydrogen in the container headspace. Bounding values for hydrogen generation are used to simulate the aspiration after venting. The required aspiration time for common shipping categories as a function of the headspace hydrogen concentration is presented in Section 5.3 of the CH-TRAMPAC. If the sites decide to implement this option, the payload container must be sampled for the container headspace concentration of hydrogen at the time of venting.

3.7.2.2.2 Option 2B — Rigid Drum Liner Headspace Gas Sampling at the Time of Venting

This option requires the sampling of payload containers for the rigid drum liner headspace concentration of hydrogen at the time of puncturing the rigid drum liner. (Rigid drum liner headspace is the region between the rigid drum liner and the next layer of confinement, usually a bag.) Bounding values for hydrogen are used to simulate the aspiration after venting. The required aspiration time for common shipping categories as a function of the rigid liner headspace hydrogen concentration is presented in Section 5.3 of the CH-TRAMPAC. If the sites decide to implement this option, the payload container must be sampled for the rigid drum liner headspace concentration of hydrogen at the time of venting.

3.7.2.3 Option 3 - Headspace Gas Sampling During Aspiration

The third option involves the sampling of payload containers for the container headspace concentration of hydrogen at least two weeks after venting. This accounts for actual hydrogen generation and release rates inside the container up to the time of sampling. Bounding values for hydrogen generation and release are then used to simulate the aspiration from the time of sampling. The required aspiration time for common shipping categories as a function of the headspace hydrogen concentration is presented in Section 5.3 of the CH-TRAMPAC. This option is similar to Option 2A except for the time of sampling the payload container. If the sites decide to implement this option, the payload container must be sampled for the headspace concentration of hydrogen at least two weeks after venting.

3.7.3 Derivation of Aspiration Times

3.7.3.1 Quantification of Aspiration Time Parameters

The purpose of this sub-section is to quantify the parameters which determine the aspiration times for each of the payload shipping categories. For common parameters, the values used are identical to those used in the calculation of decay heat limits (Appendices 2.3 and 6.7 of the CH-TRU Payload Appendices). These parameters include pressure, temperature, allowed hydrogen generation rates, and hydrogen release rates. The values of the release rates for the various confinement layers are summarized in Table 3.7-1. The release rates in the second column, expressed in units of liters/day/mole fraction, were computed using the ideal gas law.

Void Volumes for Waste Types: The total void volume for each waste type was determined by averaging the void volumes that were measured as part of the TRU Waste Sampling Program.¹ Containers that met the WAC restrictions and had a measured void volume were included in the calculations of average void volume. The aspiration model developed in this appendix is directly applicable to these waste containers.

¹ Clements, T.L., Jr., and D.E. Kudera, September 1985, "TRU Waste Sampling Program: Volume I, Waste Characterization," Report EGG-WM-6503," Idaho National Engineering Laboratory, Idaho Falls, Idaho.

Table 3.7-1 — Hydrogen Release Rates for Confinement Layers Used in Calculations

Confinement Layer	Release Rate (moles/sec/mole fraction)	Release Rate (liters/day/mole fraction)
Small Inner Bag ^a	5.58E-7 (Waste Type II, III)	1.163
	4.17E-7 (Waste Type I)	0.869
Large Drum Liner Bag	4.67E-6	9.734
Rigid Drum Liner (<u>intact without a puncture</u> ; this value was used in the accumulation step of the computa- tional procedure)	1.83E-8	0.038 ^b
Rigid Drum Liner (<u>punctured</u> ; used in the aspiration step of the computa- tional procedure)	5.09E-5	106.097
Carbon Composite Filter ^a	1.90E-6 (Waste Type II, III)	3.960
	1.37E-6 (Waste Type I)	2.856

^a See Appendix 6.9 of the CH-TRU Payload Appendices for explanations of minimum release rates. The difference in release rates is due to the temperature at which the decay heat limit is calculated.

^b All values in the Table except for the release rates of an intact rigid liner without a puncture are from Appendix 6.7 of the CH-TRU Payload Appendices. The release rates for an intact rigid liner without a puncture are calculated from Kudera (Kudera, D.E., B.W. Brown, M.G. Bullock, K.S. Monti, and R.D. Sanders, Sr., September 1986, "Evaluation of the Aspiration Rate of Hydrogen from a Waste Drum," Informal Report EEG-WSM-7228, Idaho National Engineering Laboratory, Idaho Falls, Idaho).

A portion of the total void volume (28 liters) was assigned to the annular space (volume between drum and rigid liner) void volume². This is based on actual measurement of the drum and liner dimensions. The remaining void volume was distributed proportionately to other layers of confinement based on the input values supplied to the PERM model, also developed as part of a study to determine aspiration rates at INEL.² The total void volume and the distribution of this volume among the different layers of confinement are summarized below.

Waste Type I. Solidified aqueous or homogeneous inorganic solids

Annular void	= 28.0 liters
Rigid liner void	= 26.7 liters
Multiple bag void	= 34.0 liters
<hr/>	
Total void volume	= 88.7 liters

Waste Type II. Solid inorganic materials

Annular void	= 28.0 liters
Rigid liner void	= 13.9 liters
Multiple bag void	= 125.1 liters
<hr/>	
Total void volume	= 167.0 liters

Waste Type III. Solid organic materials (including some absorbed liquids and cemented solid organics)

Annular void	= 28.0 liters
Rigid liner void	= 20.4 liters
Multiple bag void	= 107.0 liters
<hr/>	
Total void volume	= 155.4 liters

In order to provide a conservative estimate for allocating the available void volume between the individual layers of confinement for multiple layers of bags, an effective release rate through all of the layers of bags in a drum was computed by summing the individual bag release rates in parallel, i.e.,

$$\frac{1}{Q_{\text{eff}}} = \Sigma \frac{1}{q_i}$$

where

² Kudara, D.E., B.W. Brown, M.G. Bullock, K.S. Monti, and R.D. Sanders, Sr., September 1986, "Evaluation of the Aspiration Rate of Hydrogen from a Waste Drum," Informal Report EEG-WSM-7228, Idaho National Engineering Laboratory, Idaho Falls, Idaho.

- Q_{eff} = effective release rate through all layers of bags, (moles/sec/mole fraction)
- q_i = release rate through layer (bag) "i," (moles/sec/mole fraction).

A sensitivity study was made to assess the change in aspiration time due to changes in the effective release rate from layers of bags. This assessment varied the distribution of the available void among the number of assumed bag confinement layers. The results indicate that the conservative approach is to assume the available void is in the innermost bag layer of confinement with outer layers (bags) having minimal void volumes. By adding all available void volume to the innermost layer, the summed release rate provides the longest aspiration time. A numerical example of this sensitivity study is provided in Table 3.7-2. Therefore, only the following three void volumes are used in the computations:

- a summed void volume inside the bags
- the void volume between the outermost bag and the rigid drum liner, and
- the annular void volume between the rigid drum liner and the drum.

Hydrogen Gas Generation Rates: The hydrogen gas generation rates used in estimating the aspiration times are as follows:

- For analytical categories, the maximum values for each payload shipping category are used
- For test categories, the measured values are used.

3.7.3.2 Mathematical Framework

The aspiration times for each option were calculated using the analytical solutions of the differential equations which describe the unsteady-state mass balances on hydrogen within each confinement volume of a payload container. As discussed in subsection 3.7.3.1, a maximum of three void volumes are used in the computations.

Two systems of differential equations have been solved for the following cases:

- a payload container with two void volumes and no bags
- a payload container with three void volumes.

Table 3.7-2 — Aspiration Times With Different Bag Void Volume DistributionsASSUMPTIONS

1. All parameters except for the void volume distribution are the same in all cases. These were picked only for the purpose of a numerical example.
2. The total void volume for the bags is the same in all cases, and equal to 104.2 liters.

CASE 1: Summing of bag void volumes (Approach used in model).

Bag Void Volume = 104.2 liters

Aspiration Time = 435 days

CASE 2: Two bags with void volumes

Bag 1 Void Volume = 100 liters

Bag 2 Void Volume = 4.2 liters

Aspiration Time = 429 days

CASE 3: Two bags with void volumes (Equal distribution between bags)

Bag 1 Void Volume = 52.1 liters

Bag 2 Void Volume = 52.1 liters

Aspiration Time = 370 days

CASE 4: Three bags with void volumes

Bag 1 Void Volume = 34.73 liters

Bag 2 Void Volume = 34.73 liters

Bag 3 Void Volume = 34.73 liters

Aspiration Time = 351 days

The assumptions that have been made in deriving the governing equations are:

- Hydrogen is an ideal gas and the ideal gas law applies
- The pressure and temperature are assumed to be one atmosphere and 21°C respectively. The assumption of isobaric conditions provides the longest aspiration times, since, with pressurization, the partial pressure of hydrogen would be greater implying faster aspiration than under isobaric conditions.
- Hydrogen is assumed to be nonreactive with any materials in the payload container.
- Hydrogen gas generation rates are not reduced by depletion of the waste matrix and thus remain constant.
- During aspiration simulations, the concentration of hydrogen outside the payload container is assumed to be zero.

The following list defines the variables that are used in equations for a payload container with two void volumes and no bags.

Nomenclature List: Payload Container With Two Voids and No Bags

<u>Symbol</u>	<u>Definition</u>
$X_1(t)$	mole fraction hydrogen within the drum liner void at time, t.
$X_2(t)$	mole fraction hydrogen within the headspace at time, t.
X_{10}	mole fraction hydrogen within the drum liner void at the time of venting.
X_{20}	mole fraction hydrogen within headspace of a drum at the time of venting.
R_1	The effective release rate of hydrogen from the rigid liner divided by the rigid liner void volume.
R_2	The effective release rate of hydrogen from the rigid liner divided by the headspace void volume.
R_3	The effective release rate of hydrogen from the container divided by the headspace void volume.
t	Time.
CG	The hydrogen gas generation rate per innermost confinement layer.

R	The gas law constant.
T	Absolute temperature.
P	Absolute pressure.
V ₁	Void volume within innermost confinement layer.

For brevity in the equations a parameter G will be defined as:

$$G = CG \times R \times T / (P \times V_1)$$

Differential Equations for a Payload Container With Two Void Volumes and No Bags

$$dX_1/dt = G - R_1(X_1 - X_2) \quad (1A)$$

$$dX_2/dt = R_2(X_1 - X_2) - R_3X_2 \quad (1B)$$

Solutions to Equations 1A and 1B For a Payload Container With Two Void Volumes and No Bags:

$$\begin{aligned}
 X_1(t) = & (R_2 + R_3)G / (P_1P_2) \\
 & - \{X_{10}P_1^2 - [(R_2+R_3)X_{10} + R_1X_{20} + G]P_1 + (R_2+R_3)G\} / \{P_1(P_2 - P_1)\} \exp(-P_1t) \\
 & - \{X_{10}P_2^2 - [(R_2+R_3)X_{10} + R_1X_{20} + G]P_2 + (R_2+R_3)G\} / \{P_2(P_1 - P_2)\} \exp(-P_2t)
 \end{aligned} \quad (2A)$$

$$\begin{aligned}
 X_2(t) = & GR_2 / (P_1P_2) \\
 & - \{X_{20}P_1^2 - [R_2X_{10} + R_1X_{20}]P_1 + R_2G\} / \{P_1(P_2 - P_1)\} \exp(-P_1t) \\
 & - \{X_{20}P_2^2 - [R_2X_{10} + R_1X_{20}]P_2 + R_2G\} / \{P_2(P_1 - P_2)\} \exp(-P_2t)
 \end{aligned} \quad (2B)$$

where,

$$A_1 = R_1 + R_2 + R_3 \quad (2C)$$

$$P_1 = (A_1 + \text{SQRT}(A_1^2 - 4R_1R_3)) / 2 \quad (2D)$$

$$P_2 = R_1R_3 / P_1 \quad (2E)$$

Nomenclature List: Payload Container With Three Voids

<u>Symbol</u>	<u>Definition</u>
$X_1(t)$	mole fraction hydrogen within innermost void at time, t.
$X_2(t)$	mole fraction hydrogen within the rigid liner void at time, t.
$X_3(t)$	mole fraction hydrogen within the headspace at time, t.
X_{10}	mole fraction hydrogen within innermost void at the time of venting.
X_{20}	mole fraction hydrogen within the rigid liner void at the time of venting.
X_{30}	mole fraction hydrogen within the headspace at the time of venting.
R_1	The effective release rate of hydrogen from all bags divided by the innermost void volume.
R_2	The effective release rate of hydrogen from all bags divided by the rigid liner void volume.
R_3	The effective release rate of hydrogen from the rigid liner divided by the liner void volume.
R_4	The effective release rate of hydrogen from the rigid liner divided by the headspace void volume.
R_5	The effective release rate of hydrogen from the container divided by the headspace void volume.

The other variables have been defined previously in the list for two void volumes.

Differential Equations for a Payload Container With Three Void Volumes

$$dX_1/dt = G - R_1(X_1 - X_2) \quad (3A)$$

$$dX_2/dt = R_2(X_1 - X_2) - R_3(X_2 - X_3) \quad (3B)$$

$$dX_3/dt = R_4(X_2 - X_3) - R_5X_3 \quad (3C)$$

Solutions to Equation 3A, 3B, and 3C for a Payload Container With Three Void Volumes

$$X_1(t) = \{X_{10}P_1^3 - Z_{11}P_1^2 + Z_{12}P_1 - Z_{13}\} / \{P_1(P_2 - P_1)(P_3 - P_1)\} \exp(-P_1t) \\ + \{X_{10}P_2^3 - Z_{11}P_2^2 + Z_{12}P_2 - Z_{13}\} / \{P_2(P_1 - P_2)(P_3 - P_2)\} \exp(-P_2t)$$

$$\begin{aligned}
& + \{X_{10}P_3^3 - Z_{11}P_3^2 + Z_{12}P_3 - Z_{13}\} / \{P_3(P_1 - P_3)(P_2 - P_3)\} \exp(-P_3t) \\
& + Z_{13} / (P_1P_2P_3)
\end{aligned} \tag{4A}$$

$$\begin{aligned}
X_2(t) = & \{X_{20}P_1^3 - Z_{21}P_1^2 + Z_{22}P_1 - Z_{23}\} / \{P_1(P_2 - P_1)(P_3 - P_1)\} \exp(-P_1t) \\
& + \{X_{20}P_2^3 - Z_{21}P_2^2 + Z_{22}P_2 - Z_{23}\} / \{P_2(P_1 - P_2)(P_3 - P_2)\} \exp(-P_2t) \\
& + \{X_{20}P_3^3 - Z_{21}P_3^2 + Z_{22}P_3 - Z_{23}\} / \{P_3(P_1 - P_3)(P_2 - P_3)\} \exp(-P_3t) \\
& + Z_{23} / (P_1P_2P_3)
\end{aligned} \tag{4B}$$

$$\begin{aligned}
X_3(t) = & \{X_{30}P_1^3 - Z_{31}P_1^2 + Z_{32}P_1 - Z_{33}\} / \{P_1(P_2 - P_1)(P_3 - P_1)\} \exp(-P_1t) \\
& + \{X_{30}P_2^3 - Z_{31}P_2^2 + Z_{32}P_2 - Z_{33}\} / \{P_2(P_1 - P_2)(P_3 - P_2)\} \exp(-P_2t) \\
& + \{X_{30}P_3^3 - Z_{31}P_3^2 + Z_{32}P_3 - Z_{33}\} / \{P_3(P_1 - P_3)(P_2 - P_3)\} \exp(-P_3t) \\
& + Z_{33} / (P_1P_2P_3)
\end{aligned} \tag{4C}$$

where,

$$Z_{11} = (R_2 + R_3 + R_4 + R_5)X_{10} + R_1X_{20} + G \tag{4D}$$

$$Z_{12} = (R_2 + R_3 + R_4 + R_5)G + (R_2R_4 + R_2R_5 + R_3R_5)X_{10} + R_1(R_4 + R_5)X_{20} + R_1R_3X_{30} \tag{4E}$$

$$Z_{13} = (R_2R_4 + R_2R_5 + R_3R_5)G \tag{4F}$$

$$Z_{21} = R_2X_{10} + (R_1 + R_4 + R_5)X_{20} + R_3X_{30} \tag{4G}$$

$$Z_{22} = R_2(R_4 + R_5)X_{10} + R_1(R_4 + R_5)X_{20} + R_1R_3X_{30} + R_2G \tag{4H}$$

$$Z_{23} = R_2(R_4 + R_5)G \tag{4I}$$

$$Z_{31} = R_4X_{20} + (R_1 + R_2 + R_3)X_{30} \tag{4J}$$

$$Z_{32} = R_2R_4X_{10} + R_1R_4X_{20} + R_1R_3X_{30} \tag{4K}$$

$$Z_{33} = R_2R_4G \tag{4L}$$

$$A_1 = R_1 + R_2 + R_3 + R_4 + R_5 \tag{4M}$$

$$A_2 = R_1(R_3 + R_4 + R_5) + R_2(R_4 + R_5) + R_3R_5 \tag{4N}$$

$$A_3 = R_1 R_3 R_5 \quad (4O)$$

$$P_1 = [(A_1 - A_3/C) + \text{SQRT}\{(A_1 - A_3/C)^2 - 4C\}]/2 \quad (4P)$$

$$P_2 = C/P_1 \quad (4Q)$$

$$P_3 = A_3/(\quad (4R)$$

and C is a positive root of the cubic equation

$$C^3 - A_2 C^2 + A_1 A_3 C - A_3^2 = 0 \quad (4S)$$

3.7.3.3 Computational Procedure

A consistent set of steps were followed in computing the aspiration time for each of the payload shipping categories for each of the three options. The steps for each option will be detailed in this subsection. An example of how aspiration times are specified for each of the three options is included in Attachment A of this appendix for shipping category 10 0040 0190 (or alphanumeric shipping category I.3A2).

Option 1 - Aspiration Time Based On Date of Drum Closure

1. Assuming a payload container has been closed for a time period (t_s) compute the concentration of hydrogen within each of the voids via Equations 2A, and 2B for a container with two void volumes and using Equations 4A, 4B, and 4C for a container with three void volumes.
2. Recalculate R_i 's to account for the puncturing of the rigid liner at the time of venting.
3. Calculate the concentration, X_s , which is 1.05 times the steady-state value in the headspace. The steady state head space concentration is obtained from Equations 2B and 4C by letting time approach infinity. Hence, from Equation 2B for the case of a container with two voids the concentration (X_s) in the headspace is:

$$X_s = 1.05GR_2/(P_1P_2).$$

From Equation 4C for a container with three voids the concentration (X_s) in the headspace is:

$$X_s = 1.05Z_{33}/(P_1P_2P_3)$$

5. Calculate the maximum concentration in the headspace (X_p) after venting. This is done by taking the derivative of Equations 2B and 4C with respect to time, setting the

derivative equal to zero and solving for time. At this time, (t_p) the concentration is thus a maximum.

6. Calculate the maximum headspace concentration X_p corresponding to the time t_p using Equations 2B and 4C.
7. If the maximum concentration X_p is less than X_s then there is no need to aspirate and thus the aspiration time (t_a) is zero. Otherwise, the aspiration time (t_a) is calculated using Equations 2B and 4C. The bisection method³ is used to numerically solve for t_a in the nonlinear Equations 2B and 4C.

Option 2A - Container Headspace Gas Sampling At The Time Of Venting

1. Assuming that the concentration of hydrogen in the container headspace at the time of venting is $X_2(t_s)$ for a container with two void volumes or $X_3(t_s)$ for a container with three void volumes, solve Equations 2B or 4C respectively for the storage time, $t=t_s$, which corresponds to these headspace concentrations.
2. Compute the concentrations in the other void volumes, $X_1(t_s)$ and in $X_2(t_s)$ for three void volumes using Equations 2A or 4A and 4B at this storage time t_s . The concentrations $X_1(t_s)$, $X_2(t_s)$ and $X_3(t_s)$ are then assigned as the initial conditions X_{10} , X_{20} and X_{30} respectively in the aspiration Equations 2A and 2B and 4A, 4B and 4C.
3. Recalculate the R_i 's to account for the puncturing of the rigid liner at the time of venting.
4. Calculate the concentration, (X_s), which is 1.05 times the steady-state value in the headspace. The steady state headspace concentration is obtained from Equations 2B and 4C by letting time approach infinity. Hence, from Equation 2B, for the case of a container with two voids the concentration (X_s) in the headspace is:

$$X_s = 1.05GR_2/(P_1P_2).$$

From Equation 4C for a container with three voids the concentration (X_s) in the headspace is:

$$X_s = 1.05Z_{33}/(P_1P_2P_3)$$

5. Calculate the maximum concentration in the headspace (X_p) after venting. This is done by taking the derivative of Equations 2B and 4C with respect to time, setting the derivative equal to zero and solving for time. At this time, (t_p) the concentration is thus a maximum.

³ Reklaitis, G.V., A. Ravindran, and K.M. Ragsdell, 1983, "Engineering Optimization: Methods and Applications," John Wiley and Sons, New York, New York.

6. Calculate the maximum headspace concentration X_p corresponding to the time t_p using Equations 2B and 4C.
7. If the maximum concentration X_p is less than X_s then there is no need to aspirate and thus the aspiration time (t_a) is zero. Otherwise, the aspiration time (t_a) is calculated using Equations 2B and 4C. The bisection method³ is used to numerically solve for t_a in the nonlinear Equations 2B and 4C.

Option 2B - Rigid Drum Liner Headspace Gas Sampling At The Time Of Venting

1. Assuming that the concentration of hydrogen in the rigid liner headspace at the time of venting is $X_1(t_s)$ for a container with two void volumes or $X_2(t_s)$ for a container with three void volumes, solve Equations 2A or 4B respectively for the storage time, $t=t_s$, which corresponds to these headspace concentrations.
2. Compute the concentrations in the other void volumes, $X_1(t_s)$ using Equations 2B for the case of two void volumes or $X_1(t_s)$ and $X_3(t_s)$ using Equations 4A and 4C for the case of three void volumes at this storage time t_s . The concentrations $X_1(t_s)$, $X_2(t_s)$ and $X_3(t_s)$ are then assigned as the initial conditions X_{10} , X_{20} and X_{30} respectively in the aspiration Equations 2A and 2B and 4A, 4B and 4C.
3. Recalculate the R_i 's to account for the puncturing of the rigid liner at the time of venting.
4. Calculate the concentration, (X_s), which is 1.05 times the steady-state value in the headspace. The steady state headspace concentration is obtained from Equations 2B and 4C by letting time approach infinity. Hence, from Equation 2B, for the case of a container with two voids the concentration (X_s) in the headspace is:

$$X_s = 1.05GR_2/(P_1P_2).$$

From Equation 4C for a container with three voids the concentration (X_s) in the headspace is:

$$X_s = 1.05Z_{33}/(P_1P_2P_3)$$

5. Calculate the maximum concentration in the headspace (X_p) after venting. This is done by taking the derivative of Equations 2B and 4C with respect to time, setting the derivative equal to zero and solving for time. At this time, (t_p) the concentration is thus a maximum.
6. Calculate the maximum headspace concentration X_p corresponding to the time t_p using Equations 2B and 4C.
7. If the maximum concentration X_p is less than X_s then there is no need to aspirate and thus the aspiration time (t_a) is zero. Otherwise, the aspiration time (t_a) is calculated using

Equations 2B and 4C. The bisection method³ is used to numerically solve for t_a in the nonlinear Equations 2B and 4C.

Option 3 - Headspace Gas Sampling During Aspiration

1. Assume that the concentration of hydrogen in the headspace during aspiration is $X_2(t_p)$ for a container with two void volumes or $X_3(t_p)$ for a container with three void volumes. In order to determine the longest aspiration time, this concentration will be equivalent to the maximum concentration in the headspace after venting.
2. The concentrations X_{10} , X_{20} , and X_{30} at the time of venting are not known and must be evaluated in order to calculate the aspiration time. The steps involved in this evaluation are:
 - 2A. For an assumed storage time t_s prior to venting compute the concentrations in all void volumes, $X_1(t_s)$, $X_2(t_s)$ and $X_3(t_s)$, using Equations 2A, and 2B or 4A, 4B, and 4C.
 - 2B. Assign concentrations $X_1(t_s)$, $X_2(t_s)$ and $X_3(t_s)$ as the initial conditions X_{10} , X_{20} and X_{30} respectively, in the container, at the time of venting.
 - 2C. Recalculate the R_i 's to account for the puncturing of the drum liner at the time of venting.
 - 2D. Calculate the maximum concentration in the headspace (X_m) after venting. This is done by taking the derivative of Equation 2B or 4C with respect to time, setting the derivative equal to zero and solving for this time, (t_m) and evaluating X_m using Equation 2B or 4C. At this time (t_m) the concentration is thus a maximum.
 - 2E. Compare the concentration X_m with $X_2(t_p)$ or with $X_3(t_p)$ and modify the storage time t_s accordingly using the bisection method³.
 - 2F. Repeat steps 2A through 2E until the storage time, t_s is evaluated to an accuracy of at least 1/100 of a day.
3. Calculate the concentration (X_s) which is 1.05 times the steady-state value in the headspace. The steady state headspace concentration is obtained from Equations 2B and 4C by letting time approach infinity. Hence, from Equation 2B, for the case of a container with two voids the concentration (X_s) in the headspace is:

$$X_s = 1.05GR_2/(P_1P_2).$$

From Equation 4C for a container with three voids the concentration (X_s) in the headspace is:

$$X_s = 1.05Z_{33}/(P_1P_2P_3)$$

4. The aspiration time, (t_a) is calculated using Equations 2B and 4C. The bisection method³ is used to numerically solve for t_a in the nonlinear Equations 2B and 4C.

The aspiration times for Options 1 and 2 have been calculated up to a maximum concentration of 40 mole percent hydrogen in the container headspace, even though a majority of the stored waste containers are expected to have concentrations well below this value. The highest observed hydrogen concentration in a waste drum that could qualify for transport in a package is 32.4 mole percent.¹ Data collected as part of the TRU Waste Sampling Program¹ shows that the average hydrogen concentration in the headspace of the containers was 1.5 mole percent, with a standard deviation of 2.8 mole percent. These numbers include payload containers in Waste Types I, II, and III. Hence, a 40 mole percent hydrogen concentration in the container headspace should provide a bounding case for all of the stored waste, even if the waste had been stored for lengthy periods of time.

3.7.4 Aspiration Times for Shipping Categories

Example aspiration times under each of the options for common shipping categories are presented in Section 5.3 of the CH-TRAMPAC. The tables are categorized as per the waste type (I, II and III). The aspiration times using Option 1 are a function of the storage time for the payload containers. The aspiration times using Options 2A and 2B are a function of the headspace hydrogen concentration at the time of venting. The aspiration times using Option 3 are a function of the headspace hydrogen concentration, taken at least two weeks after the payload container had been vented.

3.7.5 Drum Aspiration Procedure

The procedures that will be followed in determining the aspiration time for a payload container are specified in this section. Three acceptable methods are available to the sites for establishing the required duration of aspiration. The first requires that the date of closure of the drum be known. The second involves sampling the headspace hydrogen concentration at the time of drum liner puncturing and installation of a filter vent. The third is based on sampling the headspace at least two weeks after the initiation of the payload container aspiration. A step-by-step procedure for the three options is presented in Section 5.3 of the CH-TRAMPAC.

Attachment A

This attachment provides a specific example for each of the three options in determining the aspiration times for the shipping category 10 0040 0190 (or I.3A2). As described in earlier sections of the Appendix, the mathematical basis for the three options is the same. The independent variable (with the aspiration time being the dependent variable) in the three options is different - the age of the waste in Option 1, the headspace hydrogen concentration at the time of venting in Option 2, and the headspace hydrogen concentration at the time of sampling (at least two weeks after venting) in Option 3.

Figure 3.7-1 is a plot of the hydrogen concentration in the different confinement layers in a payload container as a function of time. The container is a drum with two bag layers and a rigid drum liner. As mentioned in Section 3.7.3.1, the void volume in the layers of bags is combined into one single void volume; hence only three concentration profiles (labeled the inner bag, drum liner, and headspace) are shown in Figure 3.7-1. The figure is plotted from the program by calculating the hydrogen concentrations in the void volumes at different time steps.

From time $t=0$ to time $t=t_1$ in Figure 3.7-1, the container is closed and hydrogen accumulates in the different layers as shown. The container is vented at time t_1 , with the drum liner punctured and the drum fitted with a filter vent or equivalent venting mechanism. The sharp increase in the headspace hydrogen concentration at this point is due to equilibration of the gases between the drum headspace and the void volume in the liner. The drum starts to aspirate at time t_1 , and approaches the steady state concentration in all layers at time t_3 . The drum can be part of a payload after time t_3 and will comply with the 5% limit on the hydrogen concentration at the end of the 60-day shipping period.

The method of arriving at the aspiration times under each of the three options is described below for the case of this payload container.

Aspiration Time from Option 1: Under Option 1, the aspiration time is determined from the storage time of the waste, indicated as time t_1 on Figure 3.7-1.

The aspiration time required is $(t_3 - t_1)$. The aspiration times for different storage periods are derived similarly. These are the values reported for common shipping categories in Section 5.3 the CH-TRAMPAC. In the table, storage time of the waste (age) is read from the first column, rounded up to the next highest month.

Aspiration Time from Option 2: Under Option 2, the aspiration time is determined from the container (Option 2A) or rigid liner (Option 2B) headspace hydrogen concentration at the time of venting. In this example, the measured hydrogen concentration for a drum stored for t_1 days is approximately 3% in the container headspace (Option 2A) or approximately 20% in the rigid liner headspace (Option 2B). The aspiration time for this headspace concentration is again $(t_3 - t_1)$. The aspiration times for different headspace concentrations can be derived similarly. These are the values reported for common shipping categories in Section 5.3 of the CH-TRAMPAC.

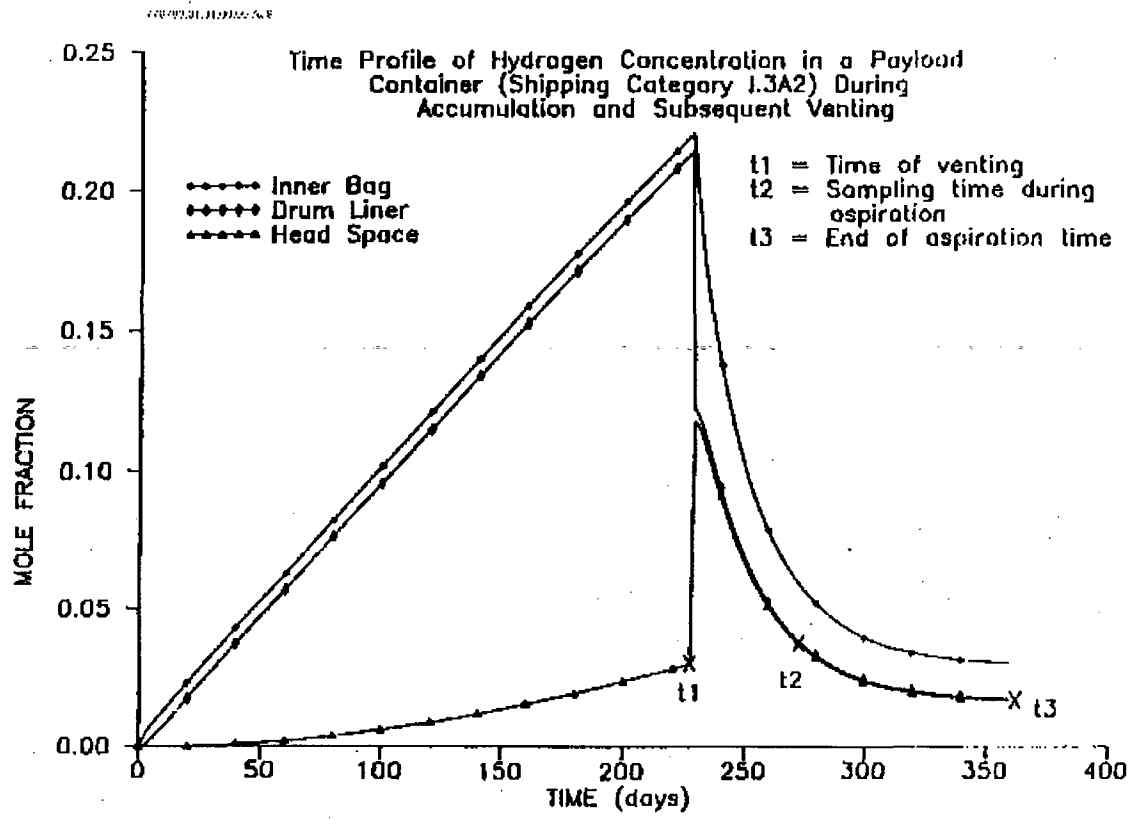


Figure 3.7-1—Time Profile of Hydrogen Concentration in a Payload Container (Shipping Category 1.3A2) During Accumulation and Subsequent Venting

Aspiration Time from Option 3: From Option 3, the aspiration time is determined from the headspace hydrogen concentration, measured at least two weeks from the time of venting. For this example (Figure 3.7-1), the measured headspace hydrogen concentration is 3.8% after aspiring for a time of $(t_2 - t_1)$. The additional aspiration time required is $(t_3 - t_2)$. The aspiration times for different samples of the headspace concentration can be derived similarly. These are the numbers reported for common shipping categories in Section 5.3 of the CH-TRAMPAC.

In summary, three options have been presented for the DOE sites to determine the required aspiration time for a given unvented payload container. The procedures to be followed by the sites in determining these aspiration times are completely mechanical as outlined in Section 5.3 of the CH-TRAMPAC. The aspiration times determined using Options 1, 2, and 3 are summarized in tables contained in Section 5.3 of the CH-TRAMPAC for common shipping categories.

This page intentionally left blank.

APPENDIX 3.8

SPECIFICATION FOR CLOSURE OF INNER CONFINEMENT LAYERS

This page intentionally left blank.

3.8 Specification for Closure of Inner Confinement Layers

For the payload of CH-TRU waste, a confinement layer is defined as follows:

A confinement layer is any boundary around a volume greater than four liters that restricts, but does not prohibit, the release of hydrogen gas across the boundary.

Examples of confinement layers are plastic bags (smaller inner bags or larger container liner bags) with the allowable closure methods described below and metal containers fitted with filter vents. Note: Punctured plastic bags, liner bags open at the end, pieces of plastic sheeting wrapped around the waste for handling, and metal containers with lid closures that allow free hydrogen release are not considered as confinement layers. Bags (in a fully expanded condition), containers, or other closed inner packagings that are less than four liters in size are not considered as layers of confinement. Per CH-TRAMPAC Section 2.8, sealed containers greater than four liters in size are not allowed.

Drum liner bags shall be made of materials belonging to the class of polyethylene (PE) or polyvinyl chloride (PVC) with a nominal thickness between 5 - 15 mils and having a surface area of at least 1.6 m². (This area is equal to that of a rigid drum liner – therefore, any bag larger in size than the drum liner will meet this specification.) SWB liner bags shall be made of materials belonging to the class of PE or PVC, unless another material is shown to be equivalent by testing or analysis.

The only allowable methods of closure for plastic bags (greater than four liters in size in a fully expanded condition) used for waste confinement are the following:

- Twist and tape closure
- Fold and tape closure
- Heat-seal closure or twist and tape closure with a minimum of one filter vent
- Unvented heat-seal closure for a bag with a minimum surface area of approximately 390 square inches. For example, a tube of plastic that is heat-sealed on both ends, with nominal dimensions of 14 inches by 14 inches when flattened, would have a surface area of $14 \times 14 \times 2 = 392$ square inches. Larger bags are allowed, as the surface area for gas release is greater.

When the method of closure is twist and tape, the waste bag that is ready to be closed should be twisted at the end and then taped tightly. The twisted portion of the bag that is taped should generally have a length of six inches; however, procedures for twist and tape may be site specific. Site-specific health and safety procedures shall govern the precautions to be taken by the operators. Supplemental sealing devices such as clamps or heat sealing shall not be used unless the hydrogen release has been quantified and is greater than or equal to that of the twist and tape bag closure (see Appendices 6.7 and 6.13 of the CH-TRU Payload Appendices). Quantification of hydrogen release can either be by testing or analysis.

The fold and tape procedure is applicable but not restricted to bags used in the SWB for which twisting the top end is not practical.

Vented heat-sealed bags may be used to address site health and safety issues in specific configurations when the other closure methods may be difficult (see Section 2.5 of the CH-TRAMPAC). Appendix 3.11 of the CH-TRU Payload Appendices defines the authorized use of heat-sealed filtered bags. Unvented heat-sealed bags may be used provided they meet the requirements of this appendix.

Plastic bags that are closed by the twist and tape or fold and tape methods may also be vented for site-specific purposes.

Any other type of confinement layer (other than the types of plastic bags or metal or other rigid containers described) used at the sites shall be shown, by testing or analysis, to be equivalent to one of the allowable confinement layers for purposes of minimum hydrogen release. "Equivalency" shall be established by demonstration of a hydrogen release rate greater than or equal to the approved confinement layers.

APPENDIX 3.9

**DETERMINATION OF STEADY-STATE VOC CONCENTRATIONS
FROM DACs**

This page intentionally left blank.

3.9 Determination of Steady-State VOC Concentrations from DACs

3.9.1 Introduction

If a concentration of flammable volatile organic compounds (VOCs) in the payload container headspace of less than or equal to 500 parts per million (ppm) cannot be established based on waste generation procedures or records of process knowledge, headspace gas sampling for flammable VOCs is required. Prior to performing headspace sampling, drum age criteria (DACs) need to be met for headspace samples to be valid. DACs are estimates of time required for VOCs in a payload container to reach 90 percent of the equilibrium steady-state concentration within the different layers of confinement. Alternately, the headspace sample taken before the DAC has been met can be used to determine the 90 percent steady-state concentration in a waste container. The 90 percent steady-state concentration can then be correlated to the VOC concentration in the innermost layer of confinement by the use of prediction factors (PFs), which are multipliers to be applied to the headspace concentration. The methodology used for determining the steady-state (90%) VOC concentration from DACs (or measurement) and PFs is based on Liekhus et al., October 2000.¹ Three options are available:

- Option 1 **No DACs Required.** If the concentration of flammable VOCs in a payload container can be shown to be less than or equal to 500 ppm from the waste generation procedures or records of process knowledge, then no DACs or PFs are required. Option 1 is discussed in Section 3.9.2.1.
- Option 2 **Assignment of DACs for Common Packaging Configurations.** DACs for common representative packaging configurations used for contact-handled transuranic (CH-TRU) waste at the sites are presented in look-up tables. Under Option 2, there are three container venting and sampling scenarios. Option 2 and the associated scenarios and look-up tables are discussed in detail in Section 3.9.2.2.
- Option 3 **Calculation of Steady-State VOC Concentrations for Specific Packaging Configurations.** For specific packaging configurations not covered by Option 2, the steady-state VOC concentration can be determined based on sampling (measurement) using the methodology described in Liekhus et al., October 2000.¹ Option 3 is described in Section 3.9.2.3.

A list of flammable VOCs identified by the sites in CH-TRU waste is provided as Table 3.9-1. If additional flammable VOCs (i.e., not listed in Table 3.9-1) are identified in concentrations greater than 500 ppm, Section 5.2.5.3.2 of the Contact-Handled Transuranic Waste Authorized Methods for Payload Control (CH-TRAMPAC) specifies a formalized process for including these VOCs in the analysis for compliance with the flammable (gas/VOC) limits.

¹ Liekhus, K.J., S.M. Djordjevic, M. Devarakonda, M.J. Connolly, October 2000, "Determination of Drum Age Criteria and Prediction Factors Based on Packaging Configurations," INEEL/EXT-2000-01207, Idaho National Engineering and Environmental Laboratory, Idaho Falls, Idaho.

Table 3.9-1 — List of Flammable Volatile Organic Compounds Identified by Sites in CH-TRU Wastes^a

Acetone
Benzene
1-Butanol
Chlorobenzene
Cyclohexane
1,1-Dichloroethane
1,2-Dichloroethane
1,1-Dichloroethene
cis-1,2-Dichloroethene
Ethyl benzene
Ethyl ether
Methanol
Methyl ethyl ketone
Methyl isobutyl ketone
Toluene
1,2,4-Trimethylbenzene
1,3,5-Trimethylbenzene
Xylenes

^aIf additional flammable VOCs are identified in concentrations greater than 500 ppm total, the methodology documented in Section 5.2.5.3.2 of the CH-TRAMPAC shall be used.

3.9.2 Options For Determining DACs

The three options for determining DACs are discussed in the following sections. Figure 3.9-1 presents a flow chart for determining the appropriate option.

3.9.2.1 Option 1: No Drum Age Criteria Required

If the concentration of flammable VOCs in a payload container can be shown to be less than or equal to 500 ppm from the waste generation procedures or records of process knowledge, then no DACs or PFs are applicable.

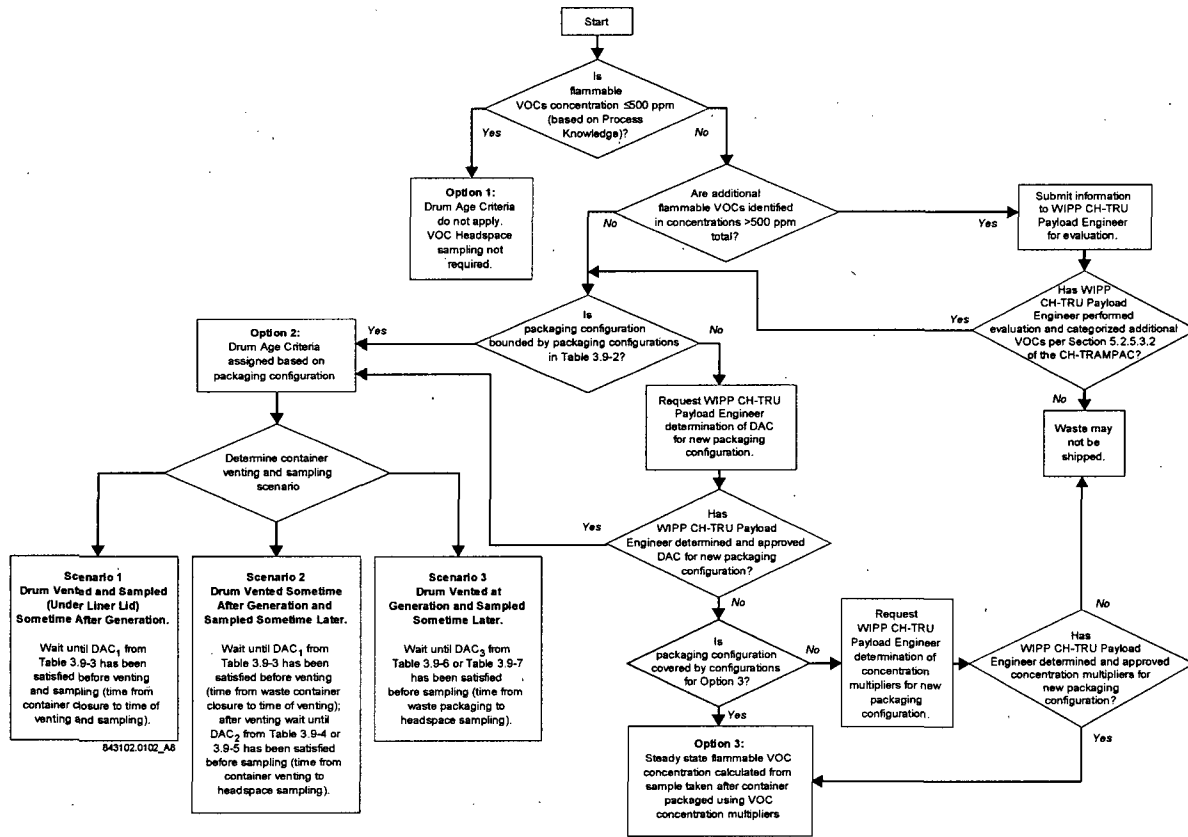


Figure 3.9-1 — Determination of DAC Option

If the concentration of flammable VOCs cannot be determined from the waste generation procedures or the records of process knowledge, headspace sampling must be performed and Option 2 or Option 3 below must be used.

3.9.2.2 Option 2: Drum Age Criteria for Common Packaging Configurations

The derivation of the DACs for Option 2 is based on specific packaging configurations and waste types commonly used at the TRU waste sites. The selection of representative packaging configurations for the DAC analysis under Option 2 was based on the following criteria:

- A review of the CH-TRU Waste Content Codes (CH-TRUCON) document² showing that currently, the majority of content code packaging configurations can be summarized into a set of common configurations. These configurations are divided into two groups: (1) packaging configurations included in either Waste Type I or Waste Type IV (solidified waste) content codes, and (2) packaging configurations included in either Waste Type II or Waste Type III (solid waste) content codes.
- A projection of future waste packaging configurations expected at U.S. Department of Energy (DOE) sites based on experience to date.
- A preliminary sensitivity analysis performed to determine which factors most influence the DACs.

The sensitivity analysis shows that four factors need to be considered when calculating the DACs. These factors include:

- Presence of a rigid drum liner
- Size of the hole in the drum liner lid
- Payload container filter diffusivity
- Number of plastic bags.

Other characteristics of packaging configurations were determined to have little or no impact on the DACs (e.g., filters on the plastic bags). For this reason, only the above-mentioned factors are considered in calculating DACs for the common waste packaging configurations.¹

A computer program was used to calculate the DAC values for some of these common packaging configurations. The computer program is based on a VOC transport model that estimates the transient VOC gas-phase concentration throughout a waste container. The model consists of a series of material balance equations describing the transient VOC transport with

² U.S. Department of Energy (DOE), "CH-TRU Waste Content Codes (CH-TRUCON)," current revision, DOE/WIPP 01-3194, U.S. Department of Energy, Carlsbad Field Office, Carlsbad, New Mexico.

respect to a given layer of confinement. The governing equations for the model are presented in Liekhus et al., October 2000¹, and Connolly et al., June 1998³.

Considering only the number of layers of confinement, the common packaging configurations currently described in the CH-TRUCON document² can be bound by the packaging configurations presented in Table 3.9-2.

Table 3.9-2 — Common CH-TRU Waste Packaging Configurations

Packaging Configuration	Waste Types II and III	Waste Types I and IV
Packaging Configuration 1 (55-gallon drums)	No inner bags, no liner bags	
Packaging Configuration 2 (55-gallon drums)	Up to 4 bag layers, up to 1 of which is a liner bag	Any configuration with 1 liner bag
Packaging Configuration 3 (55-gallon drums)	Up to 6 bag layers, up to 2 of which are liner bags	Any configuration with 2 liner bags
Packaging Configuration 4 (pipe components)	Up to 2 inner bags and 1 filtered metal can inside a pipe component (headspace sample taken inside the pipe component)	
Packaging Configuration 5 (SWBs or TDOPs)	SWB or TDOP with up to 1 bag layer (inner or liner)	
Packaging Configuration 6 (SWBs or TDOPs)	SWB or TDOP with up to 6 bag layers, up to 1 of which is a liner bag	
Packaging Configuration 7 (85- and 100-gallon drums)	85-gallon or 100-gallon drum with filtered inner lid (no inner or liner bags and no rigid liners)	

For example, a packaging configuration consisting of a single plastic bag in a 55-gallon drum for Waste Type II or III could be conservatively placed into Configuration 2 (i.e., the DAC for a packaging configuration consisting of 1 inner bag would be less than or equal to that for 3 inner bags and 1 liner bag). Similarly, a configuration of 2 inner bags and 2 liner bags in a 55-gallon drum for these waste types would be assigned to Configuration 3. In addition, filtered bag layers are also conservatively assigned to the configurations in Table 3.9-2. For example, a configuration of Waste Type II with 3 filtered inner bags and 1 filtered liner bag in a 55-gallon drum is bounded by Packaging Configuration 2. For Waste Types I and IV in 55-gallon drums, one or two liner bags are the configurations most commonly used. The DAC analysis conservatively assumes for solidified wastes that only the top of the liner bag is available for VOC transport. The presence of inner bags makes the entire liner bag area available and hence the DACs are bound by the configurations in Table 3.9-2.¹

Any site requiring the transportation of TRU waste in the TRUPACT-II or HalfPACT that cannot be covered under a packaging configuration included in Table 5.2-3 must request the

³ Connolly, M.J., S.M. Djordjevic, K.J. Liekhus, C.A. Loehr, L.R. Spangler, June 1998, "Position for Determining Gas Phase Volatile Organic Compound Concentrations in Transuranic Waste Containers," INEEL-95/0109, Rev. 2, Idaho National Engineering and Environmental Laboratory, Idaho Falls, Idaho.

determination of an appropriate DAC by submitting a request in writing to the WIPP CH-TRU Payload Engineer.

The WIPP CH-TRU Payload Engineer shall assign a conservative DAC for a packaging configuration not covered under Table 5.2-3 using the governing equations and methodology.^{1,3} Compliance with all other transportation requirements of the CH-TRAMPAC document shall also be demonstrated. The WIPP CH-TRU Payload Engineer does not have the authority to change the transportation requirements for the TRUPACT-II or the HalfPACT as specified in the CH-TRAMPAC document without approval from the NRC. Section 1.5 of the CH-TRAMPAC describes the process for WIPP CH-TRU Payload Engineer approval of packaging configurations as part of the TRUCON code approval process.

DACs are defined for three unique venting and sampling scenarios (Figure 3.9-1). These drum venting and sampling scenarios are defined by the time elapsed after container closure and venting, as follows:

- t_1 = time (days) elapsed after container closure until venting
 t_2 = time (days) elapsed after venting.

Scenario 1: The drum liner headspace (under liner lid) can be sampled at the time of venting if t_1 is greater than DAC_1 . The drum age criterion DAC_1 is defined as the time for a representative VOC to reach a concentration of at least 90% of its equilibrium concentration before drum venting. Table 3.9-3 presents the DAC_1 values.

Table 3.9-3 — DAC_1 Values (in Days)

Waste Type	DAC_1 (days)
Waste Types I and IV	127
Waste Types II and III	53

Scenario 2: For drums generated in an unvented condition and subsequently vented, the drum headspace can be sampled in a vented drum if t_1 is greater than DAC_1 and t_2 is greater than DAC_2 .

The drum age criterion DAC_2 is defined as the time for a representative VOC to reach a headspace concentration of at least 90% of its steady-state concentration after venting a waste drum that was unvented for at least DAC_1 . DAC_2 values are calculated for the two categories of waste types under Scenario 1 with four different opening sizes in the punctured drum liner lid and three different drum filter diffusivities.

In other words, under this scenario, if the drum has remained in an unvented condition for a period of at least 53 days for Waste Types II and III and 127 days for Waste Types I and IV, equilibration of VOCs is complete inside the drum. When the drum is subsequently vented, a time period for the appropriate DAC_2 listed in Table 3.9-4 or 3.9-5 is needed before sampling to ensure reequilibration between the liner and the drum headspace.

Table 3.9-4 — Packaging-Specific DAC₂ Values (in Days) for Solidified Waste (Waste Types I and IV)

Drum Filter Minimum Hydrogen Diffusivity (m/s/mf)	Liner Lid Opening			
	0.3-inch Diameter Hole	0.375-inch Diameter Hole	0.75-inch Diameter Hole	1-inch Diameter Hole
1.9×10^{-6}	36	30	23	22
3.7×10^{-6}	30	25	19	18
3.7×10^{-5}	13	11	11	11

m/s/mf = mole per second per mole fraction.

Table 3.9-5 — Packaging-Specific DAC₂ Values (in Days) for Solid Waste (Waste Types II and III)

Drum Filter Minimum Hydrogen Diffusivity (m/s/mf)	Liner Lid Opening			
	0.3-inch Diameter Hole	0.375-inch Diameter Hole	0.75-inch Diameter Hole	1-inch Diameter Hole
1.9×10^{-6}	29	22	13	12
3.7×10^{-6}	25	20	12	11
3.7×10^{-5}	7	6	6	4

m/s/mf = mole per second per mole fraction.

Scenario 3: If t_1 is less than DAC₁ when the container is vented, the container headspace can be sampled when t_2 is greater than DAC₃. Also, for newly generated payload containers that were vented at the time of generation, the container headspace can be sampled after DAC₃ has been exceeded.

The drum age criterion DAC₃ is defined as the time for a representative VOC to reach a headspace concentration of at least 90% of its steady-state concentration. DAC₃ values are calculated for the two categories of waste types each with different packaging configurations, different opening sizes in the drum liner lid as well as the case of no rigid liner inside the drum, and different filter diffusivities. The appropriate DAC₃ values are listed in Tables 3.9-6 and 3.9-7.

Table 3.9-6 — Packaging-Specific DAC₃ Values (in Days) for Solidified Waste (Waste Types I and IV)

Packaging Configuration 1						
Drum Filter Minimum Hydrogen Diffusivity (m/s/mf)	Liner Lid Opening				No Lid	No Liner
	0.3-inch Diameter Hole	0.375-inch Diameter Hole	0.75-inch Diameter Hole	1-inch Diameter Hole		
1.9×10^{-6}	131	95	37	24	4	4
3.7×10^{-6}	111	85	36	24	4	4
3.7×10^{-5}	28	28	23	19	4	4

Packaging Configuration 2						
Drum Filter Minimum Hydrogen Diffusivity (m/s/mf)	Liner Lid Opening				No Lid	No Liner
	0.3-inch Diameter Hole	0.375-inch Diameter Hole	0.75-inch Diameter Hole	1-inch Diameter Hole		
1.9×10^{-6}	213	175	108	92	56	18
3.7×10^{-6}	188	161	105	90	56	17
3.7×10^{-5}	80	80	75	71	49	10

Packaging Configuration 3						
Drum Filter Minimum Hydrogen Diffusivity (m/s/mf)	Liner Lid Opening				No Lid	No Liner
	0.3-inch Diameter Hole	0.375-inch Diameter Hole	0.75-inch Diameter Hole	1-inch Diameter Hole		
1.9×10^{-6}	283	243	171	154	107	34
3.7×10^{-6}	253	225	166	151	106	31
3.7×10^{-5}	121	121	115	110	84	13

Packaging Configuration 4	
Pipe Component Filter Minimum Hydrogen Diffusivity (m/s/mf)	Headspace Sample Taken Inside Pipe Component
1.9×10^{-6}	152

Table 3.9-6 — Packaging-Specific DAC₃ Values (in Days) for Solidified Waste (Waste Types I and IV) (Continued)

Packaging Configuration 5	
Minimum Total Filter Diffusivity (m/s/mf)	Headspace Sample Taken Inside Direct Load SWB/TDOP
7.4 x 10 ⁻⁶ (SWB)	15
3.33 x 10 ⁻⁵ (TDOP)	15

Packaging Configuration 6	
Minimum Total Filter Diffusivity (m/s/mf)	Headspace Sample Taken Inside Direct Load SWB/TDOP
7.4 x 10 ⁻⁶ (SWB)	56
3.33 x 10 ⁻⁵ (TDOP)	56

Packaging Configuration 7^a			
Drum Filter Minimum Hydrogen Diffusivity (m/s/mf)	Inner Lid Filter Vent Minimum Hydrogen Diffusivity (m/s/mf)		
	7.4 x 10⁻⁶	1.85 x 10⁻⁵	9.25 x 10⁻⁵
3.7 x 10 ⁻⁶	13	7	2
7.4 x 10 ⁻⁶	10	6	2
1.85 x 10 ⁻⁵	6	4	2

^aHeadspace sample taken between inner and outer drum lids. If headspace sample is taken inside the filtered inner drum lid prior to placement of the outer drum lid, then a DAC₃ value of 2 days may be used. m/s/mf = mole per second per mole fraction.

Table 3.9-7 — Packaging-Specific DAC₃ Values (in Days) for Solid Waste (Waste Types II and III)

Packaging Configuration 1						
Drum Filter Minimum Hydrogen Diffusivity (m/s/mf)	Liner Lid Opening				No Lid	No Liner
	0.3-inch Diameter Hole	0.375-inch Diameter Hole	0.75-inch Diameter Hole	1-inch Diameter Hole		
1.9×10^{-6}	131	95	37	24	4	4
3.7×10^{-6}	111	85	36	24	4	4
3.7×10^{-5}	28	28	23	19	4	4

Packaging Configuration 2						
Drum Filter Minimum Hydrogen Diffusivity (m/s/mf)	Liner Lid Opening				No Lid	No Liner
	0.3-inch Diameter Hole	0.375-inch Diameter Hole	0.75-inch Diameter Hole	1-inch Diameter Hole		
1.9×10^{-6}	175	138	75	60	30	11
3.7×10^{-6}	152	126	73	59	30	11
3.7×10^{-5}	58	57	52	47	28	8

Packaging Configuration 3						
Drum Filter Minimum Hydrogen Diffusivity (m/s/mf)	Liner Lid Opening				No Lid	No Liner
	0.3-inch Diameter Hole	0.375-inch Diameter Hole	0.75-inch Diameter Hole	1-inch Diameter Hole		
1.9×10^{-6}	199	161	96	80	46	16
3.7×10^{-6}	175	148 ^a	93	79	46	16
3.7×10^{-5}	72	72	67	62	42	10

Packaging Configuration 4	
Pipe Component Filter Minimum Hydrogen Diffusivity (m/s/mf)	Headspace Sample Taken Inside Pipe Component
1.9×10^{-6}	152

Table 3.9-7 — Packaging-Specific DAC₃ Values (in Days) for Solid Waste (Waste Types II and III) (Continued)

Packaging Configuration 5	
Minimum Total Filter Diffusivity (m/s/mf)	Headspace Sample Taken Inside Direct Load SWB/TDOP
7.4 x 10 ⁻⁶ (SWB)	15
3.33 x 10 ⁻⁵ (TDOP)	15

Packaging Configuration 6	
Minimum Total Filter Diffusivity (m/s/mf)	Headspace Sample Taken Inside Direct Load SWB/TDOP
7.4 x 10 ⁻⁶ (SWB)	56
3.33 x 10 ⁻⁵ (TDOP)	56

Packaging Configuration 7 ^b			
Drum Filter Minimum Hydrogen Diffusivity (m/s/mf)	Inner Lid Filter Vent Minimum Hydrogen Diffusivity (m/s/mf)		
	7.4 x 10 ⁻⁶	1.85 x 10 ⁻⁵	9.25 x 10 ⁻⁵
3.7 x 10 ⁻⁶	13	7	2
7.4 x 10 ⁻⁶	10	6	2
1.85 x 10 ⁻⁵	6	4	2

^aDAC of 142 days is applicable provided that the packaging configuration does not exceed 3 inner bags and 2 liner bags. This DAC value for this bounding packaging configuration has been previously used to address headspace sampling issues at the sites for disposal purposes.

^bHeadspace sample taken between inner and outer drum lids. If headspace sample is taken inside the filtered inner drum lid prior to placement of the outer drum lid, then a DAC₃ value of 2 days may be used.

m/s/mf = mole per second per mole fraction.

Because direct load TDOPs require a greater minimum hydrogen diffusivity value than SWBs, the SWB packaging configurations (Packaging Configurations 5 and 6) bound the direct load TDOP packaging configurations. Packaging Configuration 6 also includes bin overpack configurations with the headspace sample taken inside the bin.

Packaging Configuration 7 describes 85- and 100-gallon drums with a vented inner lid and no additional inner layers of confinement and no rigid liners. Sampling is performed between the inner and outer lids or inside the inner lid. The DAC values for an 85- or 100-gallon drum with no additional inner layers of confinement and no rigid liners are listed in Tables 3.9-6 and 3.9-7. If a 100-gallon drum contains a compacted 55-gallon drum containing a rigid drum liner, the 55-gallon drum must meet the appropriate 55-gallon drum DAC (DAC₃), listed in Tables 3.9-6 or 3.9-7, to ensure that VOC solubility associated with the presence of the 55-gallon rigid drum liner does not impact the DAC for the 100-gallon drum.

3.9.2.3 Option 3: Calculation of Steady-State VOC Concentrations for Specific Packaging Configurations

The steady-state VOC concentration for specific packaging configurations can be conservatively calculated by sampling the container headspace after container packaging and by the use of VOC concentration multipliers.¹ A VOC concentration multiplier is defined as the ratio of 90 percent of the steady-state VOC concentration in the sampling headspace divided by the VOC headspace concentration at a given time. The VOC concentration multipliers are determined by solving the governing transport equations.¹

Therefore, Option 3 consists of sampling the container headspace at a point in time and multiplying by the appropriate VOC concentration multiplier. Option 3 is applicable to waste packaging configurations containing metal cans and pipe overpacks, which may require long time periods to achieve steady state. Three example packaging configurations of vented metal containers inside a vented drum are utilized in Option 3 as shown in Tables 3.9-8 through 3.9-11. These cases bound other packaging configurations with an equal or lesser number of bag layers (including filtered bags) in a similar fashion as described in Option 2. Cases where filtered cans are placed inside filtered cans are described by the bounding configuration containing a filtered can and filtered pipe component. VOC concentration multipliers for specific configurations with different filter characteristics are provided in Tables 3.9-8 through 3.9-11. Similar to the process described in Section 3.9.2.2, for configurations not covered by Tables 3.9-8 through 3.9-11, the site may request that the WIPP CH-TRU Payload Engineer direct the determination of appropriate concentration multipliers using the packaging configuration information and the governing equations and methodology¹.

Table 3.9-8 – VOC Concentration Multipliers(Filtered Inner Containers and Drum Filter Minimum Hydrogen Diffusion Characteristic = 1.9×10^{-6} mole/sec/mole fraction)

Volatile Organic Compound	Days	Waste Drum Packaging Configuration											
		2IB-PC-DL-DF*				3IB-FC-2LB-DL-DF*				2IB-FC-PC-DL-DF*			
		75	150	300	600	75	150	300	600	75	150	300	600
Carbon Tetrachloride		5.5	2.9	1.7	1.1	7.8	3.9	2.2	1.4	14.9	5.4	2.4	1.4
Cyclohexane		6.6	2.6	1.4	1.0	11.6	4.2	1.9	1.2	10.5	3.8	1.8	1.1
Methanol		2.8	1.8	1.2	1.0	4.0	2.4	1.5	1.1	5.3	2.6	1.5	1.1
Methylene chloride (Dichloromethane)		3.2	1.8	1.2	1.0	4.5	2.5	1.5	1.1	7.5	3.1	1.6	1.1
Toluene		22.7	11.5	6.0	3.2	32.6	15.5	7.7	4.0	64.9	22.9	9.5	4.5
1,1,1-Trichloroethane		4.3	2.3	1.4	1.0	6.2	3.2	1.8	1.2	11.2	4.2	2.0	1.2
Trichloroethene		11.2	5.7	3.1	1.8	15.4	7.6	4.0	2.2	31.2	11.1	4.8	2.4
1,1,2-Trichloro-1,2,2-trifluoroethane		4.5	2.1	1.3	1.0	6.7	3.1	1.7	1.1	9.9	3.6	1.7	1.1
p-Xylene		45.1	22.8	11.7	6.1	74.4	33.2	15.7	7.8	136.9	47.6	19.2	8.8
Acetone		3.1	1.8	1.2	1.0	4.5	2.4	1.5	1.1	7.4	2.9	1.5	1.0
1-Butanol		4.8	2.6	1.6	1.1	6.7	3.5	2.0	1.3	12.7	4.8	2.2	1.3
Chloroform		3.5	2.0	1.3	1.0	5.0	2.7	1.6	1.1	8.9	3.5	1.7	1.1
1,1-Dichloroethene		3.3	1.8	1.2	1.0	4.8	2.5	1.5	1.1	7.8	3.0	1.5	1.0
Methyl ethyl ketone		4.1	2.2	1.4	1.0	5.8	3.0	1.8	1.2	10.3	3.9	1.9	1.2
Methyl isobutyl ketone		7.1	3.6	2.0	1.3	10.1	5.0	2.7	1.6	19.6	6.9	3.0	1.6
1,1,2,2-Tetrachloroethane		17.0	8.8	4.6	2.6	23.8	11.6	5.9	3.1	49.4	17.5	7.3	3.6
Tetrachloroethene		9.1	4.7	2.6	1.6	12.5	6.3	3.3	1.9	26.4	9.4	4.0	2.1
Benzene		4.2	2.3	1.4	1.0	5.9	3.1	1.8	1.2	10.7	4.1	2.0	1.2
Bromoform		20.1	10.3	5.4	3.0	28.5	13.7	6.9	3.6	57.2	20.4	8.6	4.1
Chlorobenzene		10.2	5.3	2.9	1.7	14.1	7.0	3.7	2.1	29.7	10.6	4.5	2.3
1,1-Dichloroethane		3.3	1.9	1.2	1.0	4.8	2.6	1.5	1.1	8.3	3.3	1.6	1.1
1,2-Dichloroethane		4.5	2.5	1.5	1.1	6.2	3.3	1.9	1.2	11.7	4.5	2.1	1.3
Cis-1,2-Dichloroethene		3.4	1.9	1.2	1.0	4.8	2.6	1.5	1.1	8.4	3.3	1.7	1.1
Ethyl benzene		10.8	5.4	2.9	1.7	15.1	7.4	3.9	2.2	31.5	11.0	4.6	2.3
Ethyl ether		4.1	2.0	1.2	1.0	6.1	2.9	1.6	1.1	8.4	3.2	1.6	1.1
1,3,5-Trimethylbenzene		18.1	9.0	4.7	2.6	26.1	12.4	6.2	3.3	55.9	19.0	7.6	3.6
1,2,4-Trimethylbenzene		20.6	10.3	5.3	2.9	30.0	14.1	7.0	3.7	64.3	21.8	8.7	4.1
o-Xylene		12.4	6.3	3.4	1.9	17.4	8.5	4.4	2.4	36.9	12.9	5.3	2.6
m-Xylene		10.8	5.5	2.9	1.7	15.2	7.4	3.9	2.2	31.8	11.1	4.6	2.3

*IB = Inner bag; PC = Vented pipe component; FC = Filtered can; LB = Drum liner bag; DL = Drum liner; DF = Drum filter vent.

Table 3.9-9 — VOC Concentration Multipliers

(Filtered Inner Containers Minimum Hydrogen Diffusion Characteristic = 3.7×10^{-6} mole/sec/mole fraction; Drum Filter Minimum Hydrogen Diffusion Characteristic = 1.9×10^{-6} mole/sec/mole fraction)

Volatile Organic Compound	Days	Waste Drum Packaging Configuration											
		2IB-PC-DL-DF*				3IB-FC-2LB-DL-DF*				2IB-FC-PC-DL-DF*			
		75	150	300	600	75	150	300	600	75	150	300	600
Carbon tetrachloride		4.1	2.2	1.4	1.0	6.2	3.2	1.8	1.2	8.5	3.6	1.9	1.2
Cyclohexane		5.0	2.2	1.3	1.0	11.1	4.1	1.9	1.2	7.1	2.9	1.6	1.1
Methanol		2.3	1.5	1.1	1.0	3.5	2.2	1.4	1.0	3.6	2.1	1.3	1.0
Methylene chloride (Dichloromethane)		2.4	1.5	1.1	1.0	3.6	2.0	1.3	1.0	4.6	2.2	1.3	1.0
Toluene		15.8	8.1	4.3	2.4	23.5	11.2	5.7	3.0	35.3	14.4	6.7	3.4
1,1,1-Trichloroethane		3.2	1.8	1.2	1.0	5.1	2.7	1.6	1.1	6.6	2.9	1.6	1.1
Trichloroethene		7.9	4.1	2.3	1.4	11.2	5.6	3.0	1.7	17.2	7.1	3.5	1.9
1,1,2-Trichloro-1,2,2-trifluoroethane		3.5	1.8	1.1	1.0	6.1	2.9	1.6	1.1	6.3	2.7	1.5	1.0
p-Xylene		31.1	15.8	8.2	4.3	52.7	23.5	11.2	5.7	72.8	29.2	13.3	6.5
Acetone		2.4	1.4	1.0	1.0	3.8	2.1	1.3	1.0	4.6	2.1	1.3	1.0
1-Butanol		3.5	2.0	1.3	1.0	5.2	2.8	1.6	1.1	7.3	3.2	1.7	1.1
Chloroform		2.6	1.6	1.1	1.0	3.9	2.2	1.4	1.0	5.3	2.4	1.4	1.0
1,1-Dichloroethene		2.5	1.5	1.0	1.0	4.1	2.2	1.4	1.0	4.8	2.2	1.3	1.0
Methyl ethyl ketone		3.1	1.7	1.2	1.0	4.8	2.5	1.5	1.1	6.1	2.7	1.5	1.1
Methyl isobutyl ketone		5.3	2.7	1.6	1.1	8.3	4.1	2.3	1.4	11.2	4.6	2.3	1.4
1,1,2,2-Tetrachloroethane		11.8	6.1	3.3	1.9	16.5	8.1	4.2	2.3	26.6	11.0	5.2	2.7
Tetrachloroethene		6.4	3.4	2.0	1.3	9.1	4.6	2.5	1.5	14.4	6.0	2.9	1.7
Benzene		3.1	1.8	1.2	1.0	4.6	2.5	1.5	1.1	6.3	2.8	1.6	1.1
Bromoform		13.8	7.2	3.8	2.2	19.6	9.5	4.9	2.6	30.9	12.8	6.0	3.1
Chlorobenzene		7.2	3.8	2.2	1.4	10.3	5.2	2.8	1.7	16.2	6.7	3.3	1.8
1,1-Dichloroethane		2.5	1.5	1.1	1.0	3.9	2.1	1.3	1.0	5.0	2.3	1.3	1.0
1,2-Dichloroethane		3.3	1.9	1.2	1.0	4.7	2.5	1.5	1.1	6.7	3.0	1.7	1.1
Cis-1,2-Dichloroethene		2.5	1.5	1.1	1.0	3.8	2.1	1.3	1.0	5.0	2.3	1.4	1.0
Ethyl benzene		7.7	4.0	2.2	1.4	11.5	5.7	3.0	1.8	17.3	7.0	3.3	1.9
Ethyl ether		3.3	1.7	1.1	1.0	5.6	2.7	1.5	1.1	5.5	2.4	1.4	1.0
1,3,5-Trimethylbenzene		12.8	6.5	3.4	2.0	19.7	9.4	4.8	2.6	30.1	11.8	5.4	2.8
1,2,4-Trimethylbenzene		14.5	7.3	3.9	2.2	22.3	10.6	5.3	2.9	34.3	13.4	6.1	3.1
o-Xylene		8.8	4.6	2.5	1.5	13.0	6.4	3.4	1.9	20.0	8.1	3.8	2.1
m-Xylene		7.7	4.0	2.2	1.4	11.6	5.7	3.0	1.8	17.4	7.0	3.4	1.9

*IB - Inner bag; PC = Vented pipe component; FC = Filtered can; LB = Drum liner bag; DL = Drum liner; DF = Drum filter vent.

Table 3.9-10 — VOC Concentration Multipliers

(Filtered Inner Containers Minimum Hydrogen Diffusion Characteristic = 1.9×10^{-6} mole/sec/mole fraction; Drum Filter Minimum Hydrogen Diffusion Characteristic = 3.7×10^{-6} mole/sec/mole fraction)

Volatile Organic Compound	Days	Waste Drum Packaging Configuration											
		2IB-PC-DL-DF*				3IB-FC-2LB-DL-DF*				2IB-FC-PC-DL-DF*			
		75	150	300	600	75	150	300	600	75	150	300	600
Carbon Tetrachloride		3.9	2.1	1.3	1.0	5.3	2.8	1.6	1.1	9.3	3.5	1.7	1.1
Cyclohexane		4.3	1.9	1.1	1.0	6.9	2.6	1.4	1.0	6.4	2.5	1.3	1.0
Methanol		2.1	1.4	1.1	1.0	2.8	1.8	1.2	1.0	3.5	1.9	1.2	1.0
Methylene chloride (Dichloromethane)		2.3	1.4	1.0	1.0	3.2	1.8	1.2	1.0	4.8	2.1	1.2	1.0
Toluene		15.5	7.9	4.2	2.3	22.3	10.7	5.4	2.9	40.0	14.2	6.0	3.0
1,1,1-Trichloroethane		3.0	1.7	1.1	1.0	4.2	2.3	1.4	1.0	7.1	2.8	1.4	1.0
Trichloroethene		7.7	4.0	2.3	1.4	10.6	5.3	2.8	1.7	19.4	7.0	3.1	1.7
1,1,2-Trichloro-1,2,2-trifluoroethane		3.2	1.6	1.1	1.0	4.3	2.1	1.3	1.0	6.2	2.4	1.3	1.0
p-Xylene		30.7	15.6	8.0	4.3	50.7	22.7	10.9	5.5	84.1	29.4	11.9	5.6
Acetone		2.3	1.4	1.0	1.0	3.1	1.8	1.2	1.0	4.8	2.0	1.2	1.0
1-Butanol		3.4	1.9	1.2	1.0	4.7	2.5	1.5	1.1	8.0	3.1	1.6	1.1
Chloroform		2.5	1.5	1.1	1.0	3.5	2.0	1.3	1.0	5.7	2.4	1.3	1.0
1,1-Dichloroethene		2.3	1.4	1.0	1.0	3.3	1.8	1.2	1.0	5.0	2.1	1.2	1.0
Methyl ethyl ketone		2.9	1.6	1.1	1.0	4.0	2.2	1.4	1.0	6.5	2.6	1.4	1.0
Methyl isobutyl ketone		4.9	2.6	1.5	1.1	6.8	3.4	1.9	1.2	12.2	4.4	2.0	1.2
1,1,2,2-Tetrachloroethane		11.7	6.1	3.3	1.9	16.5	8.1	4.2	2.3	30.6	11.0	4.7	2.4
Tetrachloroethene		6.3	3.4	1.9	1.3	8.6	4.4	2.4	1.5	16.4	6.0	2.7	1.5
Benzene		3.0	1.7	1.2	1.0	4.1	2.2	1.4	1.0	6.8	2.7	1.4	1.0
Bromoform		13.8	7.2	3.8	2.2	19.7	9.6	4.9	2.7	35.4	12.7	5.4	2.7
Chlorobenzene		7.1	3.7	2.1	1.3	9.7	4.9	2.7	1.6	18.4	6.7	3.0	1.6
1,1-Dichloroethane		2.4	1.4	1.0	1.0	3.3	1.9	1.2	1.0	5.4	2.2	1.2	1.0
1,2-Dichloroethane		3.2	1.8	1.2	1.0	4.4	2.4	1.5	1.1	7.4	3.0	1.5	1.0
Cis-1,2-Dichloroethene		2.4	1.5	1.1	1.0	3.4	1.9	1.2	1.0	5.4	2.3	1.3	1.0
Ethyl benzene		7.4	3.8	2.1	1.4	10.3	5.1	2.7	1.6	19.5	6.9	3.0	1.6
Ethyl ether		2.9	1.5	1.0	1.0	3.9	2.0	1.2	1.0	5.3	2.2	1.2	1.0
1,3,5-Trimethylbenzene		12.4	6.2	3.3	1.9	17.7	8.4	4.3	2.4	34.4	11.8	4.8	2.4
1,2,4-Trimethylbenzene		14.1	7.1	3.7	2.1	20.3	9.7	4.9	2.7	39.6	13.6	5.5	2.7
o-Xylene		8.5	4.4	2.4	1.5	11.9	5.9	3.1	1.8	22.8	8.1	3.5	1.8
m-Xylene		7.4	3.8	2.2	1.4	10.3	5.1	2.8	1.6	19.7	7.0	3.0	1.6

*IB = Inner bag; PC = Vented pipe component; FC = Filtered can; LB = Drum liner bag; DL = Drum liner; DF = Drum filter vent.

Table 3.9-11 — VOC Concentration Multipliers(Filtered Inner Containers and Drum Filter Minimum Hydrogen Diffusion Characteristic = 3.7×10^{-6} mole/sec/mole fraction)

Volatile Organic Compound	Days	Waste Drum Packaging Configuration											
		2IB-PC-DL-DF*				3IB-FC-2LB-DL-DF*				2IB-FC-PC-DL-DF*			
		75	150	300	600	75	150	300	600	75	150	300	600
Carbon Tetrachloride		3.1	1.8	1.2	1.0	4.5	2.4	1.5	1.1	5.8	2.6	1.4	1.0
Cyclohexane		3.4	1.6	1.1	1.0	6.7	2.6	1.4	1.0	4.4	2.0	1.2	1.0
Methanol		1.8	1.3	1.0	1.0	2.6	1.7	1.2	1.0	2.6	1.6	1.1	1.0
Methylene chloride (Dichloromethane)		1.9	1.3	1.0	1.0	2.7	1.6	1.1	1.0	3.2	1.7	1.1	1.0
Toluene		12.0	6.2	3.3	1.9	17.6	8.5	4.4	2.4	23.9	9.8	4.7	2.5
1,1,1-Trichloroethane		2.5	1.5	1.0	1.0	3.7	2.0	1.3	1.0	4.6	2.1	1.2	1.0
Trichloroethene		6.0	3.2	1.9	1.2	8.5	4.3	2.4	1.4	11.7	5.0	2.5	1.5
1,1,2-Trichloro-1,2,2-trifluoroethane		2.6	1.4	1.0	1.0	4.1	2.0	1.2	1.0	4.2	1.9	1.2	1.0
p-Xylene		23.6	12.0	6.3	3.4	39.6	17.8	8.6	4.4	49.1	19.8	9.1	4.5
Acetone		1.9	1.2	1.0	1.0	2.8	1.6	1.1	1.0	3.2	1.6	1.1	1.0
1-Butanol		2.8	1.6	1.1	1.0	3.9	2.2	1.4	1.0	5.1	2.3	1.4	1.0
Chloroform		2.1	1.3	1.0	1.0	3.0	1.7	1.2	1.0	3.7	1.8	1.1	1.0
1,1-Dichloroethene		2.0	1.2	1.0	1.0	2.9	1.7	1.1	1.0	3.3	1.6	1.1	1.0
Methyl ethyl ketone		2.4	1.4	1.0	1.0	3.5	1.9	1.3	1.0	4.2	2.0	1.2	1.0
Methyl isobutyl ketone		4.0	2.1	1.3	1.0	5.9	3.0	1.7	1.2	7.6	3.2	1.7	1.1
1,1,2,2-Tetrachloroethane		9.0	4.8	2.6	1.6	12.7	6.3	3.3	1.9	18.1	7.6	3.7	2.0
Tetrachloroethene		4.9	2.7	1.6	1.1	6.9	3.6	2.0	1.3	9.9	4.2	2.1	1.3
Benzene		2.4	1.5	1.1	1.0	3.5	1.9	1.3	1.0	4.4	2.1	1.2	1.0
Bromoform		10.6	5.6	3.0	1.8	15.0	7.3	3.8	2.1	21.1	8.8	4.2	2.3
Chlorobenzene		5.5	3.0	1.8	1.2	7.8	4.0	2.2	1.4	11.0	4.7	2.4	1.4
1,1-Dichloroethane		2.0	1.3	1.0	1.0	2.9	1.7	1.1	1.0	3.5	1.7	1.1	1.0
1,2-Dichloroethane		2.6	1.5	1.1	1.0	3.6	2.0	1.3	1.0	4.7	2.2	1.3	1.0
Cis-1,2-Dichloroethene		2.0	1.3	1.0	1.0	2.9	1.7	1.1	1.0	3.5	1.7	1.1	1.0
Ethyl benzene		5.9	3.1	1.8	1.2	8.5	4.3	2.3	1.4	11.7	4.8	2.4	1.4
Ethyl ether		2.4	1.3	1.0	1.0	3.7	1.9	1.2	1.0	3.7	1.7	1.1	1.0
1,3,5-Trimethylbenzene		9.7	4.9	2.7	1.6	14.5	7.0	3.6	2.0	20.2	8.0	3.8	2.0
1,2,4-Trimethylbenzene		11.0	5.6	3.0	1.8	16.5	7.9	4.0	2.2	23.1	9.2	4.3	2.3
o-Xylene		6.7	3.5	2.0	1.3	9.7	4.8	2.6	1.6	13.6	5.6	2.7	1.6
m-Xylene		5.9	3.1	1.8	1.2	8.5	4.3	2.4	1.4	11.8	4.9	2.4	1.4

*IB = Inner bag; PC = Vented pipe component; FC = Filtered can; LB = Drum liner bag; DL = Drum liner; DF = Drum filter vent.

3.9.3 Methodology for Determining Packaging-Specific PFs

This section describes the methodology used for determining the PFs for a given packaging configuration. This methodology is based on the analysis presented in Liekhus et al., October 2000,¹ and Connolly et al., June 1998.³ The PF is a variable with a unique value for each VOC and packaging configuration that, when multiplied by the measured VOC concentration in the container headspace, determines the concentration of the VOC in the innermost confinement layer. The PFs are applicable in cases where the headspace flammable VOC concentration exceeds 500 ppm.

At steady-state conditions, there is no accumulation of VOCs within any layer of confinement, the concentrations of VOCs are constant within each layer of confinement, and the VOC transport rate across each layer of confinement is equal to a constant rate. The equations describing VOC transport across layers of confinement are presented in Liekhus et al., October 2000.¹

The relationship for the innermost confinement layer VOC concentration as a function of the measured container headspace VOC concentration is:

$$y_{icl} = y_{hs} \left[1 + n_{cf} D_{voc-cf} \left(\sum_{i=1}^{nl} \frac{n_i}{K_i} \right) \right]$$

where

- y_{icl} = innermost confinement layer VOC mole fraction (dimensionless)
- y_{hs} = VOC mole fraction within container headspace void volume (dimensionless)
- n_i = number of type “i” confinement layers in packaging configuration
- n_{cf} = number of container filters in packaging configuration
- K_i = transport characteristic of type “i” confinement layer (molecule [mol] sec⁻¹)
- nl = number of different confinement layer types.
- D_{voc-cf} = VOC-container filter diffusion characteristic (mol sec⁻¹), which is calculated using the following equation:

$$D_{VOC-cf} = \frac{D_{VOC-air}}{D_{H_2-air}} D_{H_2-cf}$$

where

$D_{VOC-air}$ = VOC diffusivity in air (cubic centimeters [cm²] sec⁻¹)

D_{H_2-air} = hydrogen diffusivity in air (cm² sec⁻¹)

D_{H_2-cf} = hydrogen-container filter diffusion characteristic (mol sec⁻¹).

Multiplying both sides of equation 1 by a conversion factor (10⁶ ppm/mole fraction) yields the following equation for the prediction factor:

$$Y_{icl} = Y_{hs} \left[1 + n_{cf} D_{voc-cf} \left(\sum_{i=1}^{nl} \frac{n_i}{K_i} \right) \right]$$

where

Y_{icl} = innermost confinement layer VOC concentration (ppm)

Y_{hs} = measured VOC concentration in container headspace (ppm).

Thus, the prediction factor, PF, is:

$$PF = \left[1 + n_{cf} D_{voc-cf} \left(\sum_{i=1}^{nl} \frac{n_i}{K_i} \right) \right]$$

Using this equation, the PFs for any packaging configuration can be established.

PFs are not applicable if the sample is taken after the appropriate DAC has been met inside the rigid liner of an unvented drum (Scenario 1), since all layers are at the equilibrium concentration.

APPENDIX 3.10

**DETERMINATION OF FLAMMABLE GAS/VOLATILE ORGANIC
COMPOUND CONCENTRATIONS BY MEASUREMENT**

This page intentionally left blank.

3.10 Determination of Flammable Gas/Volatile Organic Compound Concentrations by Measurement

This appendix summarizes the logic and methodology of using headspace flammable gas/volatile organic compound (VOC) measurements for evaluating compliance with flammable gas/VOC concentrations during transport in the TRUPACT-II and HalfPACT packages. As described in Chapter 5.0 of the Contact-Handled Transuranic Waste Authorized Methods for Payload Control (CH-TRAMPAC) document, headspace gas/VOC measurement is one option for the following test category wastes:

- Containers that could potentially exceed 500 parts per million (ppm) flammable VOCs in the innermost confinement layer
- Containers that exceed decay heat limits or analytically determined hydrogen gas generation rate limits.

3.10.1 Calculation of Drum Flammable Gas Generation Methods: AltMeth

This section applies when the concentration of flammable VOCs is less than 500 ppm in the innermost layer of the payload container. The methodology is based on sampling the waste container headspace or inside the rigid drum liner for flammable gases to calculate the actual drum flammable gas generation rate. The use of headspace gas sampling results is an extension of the methodology for deriving aspiration times of contact-handled transuranic (CH-TRU) waste containers as documented in Appendix 3.7 of the CH-TRU Payload Appendices.

Containers are categorized as either (a) sealed and then vented or (b) newly packaged and vented. The conceptual model is described below:

- A payload container with either two or three void volumes is filled with waste within the innermost layer of confinement (multiple bag layers are conservatively classified as a single void with an equivalent resistance). The container is either sealed or vented with one or more filters at the time of waste packaging.
- Flammable gas is generated within the waste.
- Flammable gas accumulates and is transported across layers of confinement.
- After some time, sealed containers are vented and the headspace gas or the headspace inside the rigid drum liner may be sampled for flammable gas.
- At some point during aspiration or venting, the container headspace may be sampled for flammable gases.

3.10.1.1 Mathematical Model

The generation of flammable gas within the innermost confinement layer and subsequent transport across the various confinement layers of an actual container can be simulated by solving the differential equations that describe the unsteady-state mass balances on flammable gas within each confinement layer of the actual container. To account for the various packaging configurations and container conditions, two sets of differential equations must be solved along with the appropriate initial conditions that represent the initial state of a container. The two sets represent (a) a container with two void volumes, and (b) a container with three void volumes.

3.10.1.2 Differential Equations for a Container with Two Void Volumes

Differential Equations (1) and (2) represent the mass balances on flammable gas in a container with two void volumes.

$$\frac{dC_1}{dt} = G - R_1(C_1 - C_2) \quad (1)$$

$$\frac{dC_2}{dt} = R_2(C_1 - C_2) - R_3C_2 \quad (2)$$

where,

C_1 = Mole or volume fraction of flammable gas within the drum liner void volume at time t (dimensionless).

C_2 = Mole or volume fraction flammable gas within the drum headspace at time t (dimensionless).

G = $C_g R T / (P V_1)$.

R_1 = Effective release rate of flammable gas from the container liner divided by the innermost void volume (day^{-1}).

R_2 = Effective release rate of flammable gas from the container liner divided by the headspace void volume. One value based on the release rate from an intact liner is used in the equations for the concentration in a sealed container. A different value is used with the aspiration equations based on the release of flammable gas from the punctured rigid liner hole (day^{-1}).

R_3 = Effective release rate of flammable gas from the container divided by the headspace void volume. One value based on the permeation characteristics of the drum gasket is used to calculate the concentration in a sealed container. A different value is used based on a combination of diffusion characteristic across the drum filter and permeation characteristic across the drum gasket to calculate concentrations in an aspirating container (day^{-1}).

t = Time(s)/day.

R = Universal gas constant (82.057 atm cm³/mol K).

T = Absolute temperature (K).

V₁ = Void volume within the innermost confinement layer (cm³).

C_g = Flammable gas generation rate within the innermost confinement layer (mol/sec).

The following initial conditions represent the initial state of the container. At the time of container generation, there is no flammable gas within the container and the initial concentrations, C₁₀ and C₂₀, are set equal to zero. If the container is sealed at the time of generation and then vented, the concentrations predicted in a sealed container at the time of venting serve as initial conditions for the differential equations that describe the mass balances of the aspirating container.

$$C_1(t=0) = C_{10} \quad (3)$$

$$C_2(t=0) = C_{20} \quad (4)$$

The solution to differential equations (1) and (2) is given by the following set of equations.

$$C_1(t) = (R_2 + R_3) G / (P_1 P_2) \quad (5)$$

$$- \{C_{10} P_1^2 - [(R_2 + R_3) C_{10} + R_1 C_{20} + G] P_1 + (R_2 + R_3) G\} / \{P_1 (P_2 - P_1)\} \exp(-P_1 t)$$

$$- \{C_{10} P_2^2 - [(R_2 + R_3) C_{10} + R_1 C_{20} + G] P_2 + (R_2 + R_3) G\} / \{P_2 (P_1 - P_2)\} \exp(-P_2 t)$$

$$C_2(t) = G R_2 / (P_1 P_2) \quad (6)$$

$$- \{C_{20} P_1^2 - [R_2 C_{10} + R_1 C_{20}] P_1 + R_2 G\} / \{P_1 (P_2 - P_1)\} \exp(-P_1 t)$$

$$- \{C_{20} P_2^2 - [R_2 C_{10} + R_1 C_{20}] P_2 + R_2 G\} / \{P_2 (P_1 - P_2)\} \exp(-P_2 t)$$

where,

$$A_1 = R_1 + R_2 + R_3 \quad (7)$$

$$P_1 = (A_1 + \sqrt{A_1^2 - 4 R_1 R_3}) / 2 \quad (8)$$

$$P_2 = R_1 R_3 / P_1 \quad (9)$$

3.10.1.3 Differential Equations for a Container with Three Void Volumes

Differential Equations (10), (11), and (12) represent the mass balances on flammable gas in a container with three void volumes.

$$\frac{dC_1}{dt} = G - R_1(C_1 - C_2) \quad (10)$$

$$\frac{dC_2}{dt} = R_2(C_1 - C_2) - R_3(C_2 - C_3) \quad (11)$$

$$\frac{dC_3}{dt} = R_4(C_2 - C_3) - R_5C_3 \quad (12)$$

where,

$$G = C_g R T / (P V_1)$$

C_1 = Mole or volume fraction flammable gas within the innermost void volume at time t (dimensionless).

C_2 = Mole or volume fraction flammable within the rigid drum liner at time t (dimensionless).

C_3 = Mole or volume fraction flammable within the drum headspace at time t (dimensionless).

R_1 = Effective release rate coefficient of hydrogen from all bags divided by the innermost void volume (day^{-1}).

R_2 = Effective release rate coefficient of hydrogen from all bags divided by the rigid liner void volume (day^{-1}).

R_3 = Effective release rate coefficient of flammable gas from the rigid liner divided by the liner void volume. (One value based on the release from an intact liner is used in the equations for the concentration profiles in a sealed container. A different value is used with the aspiration equations based on the release of flammable gas from the punctured drum liner.) (day^{-1}).

R_4 = Effective release rate coefficient of flammable gas from the rigid liner divided by the container headspace void volume. (One value based on the permeation characteristics of the drum gasket is used to calculate the concentration in a sealed container. A different value is used based on a combination of diffusion characteristic across the drum filter and permeation characteristic across the drum gasket to calculate concentrations in an aspirating container.) (day^{-1}).

R_5 = Effective release rate coefficient of flammable gas from the container divided by the container headspace void volume. (One value based on the permeation characteristics of the drum gasket is used to calculate the concentration in a sealed container. A different value is used based on a combination of diffusion characteristic across the drum filter and permeation characteristic across the drum gasket to calculate concentrations in an aspirating container.) (day^{-1}).

The following initial conditions represent the initial state of the container. At the time of container generation, there is no flammable gas within the container and the initial concentrations, C_{10} , C_{20} , and C_{30} are set equal to zero. If the container is sealed at the time of generation and then vented, the concentrations predicted in a sealed container at the time of venting serve as initial conditions for the differential equations that describe the mass balances of the aspirating container.

$$C_1(t = 0) = C_{10} \quad (13)$$

$$C_2(t = 0) = C_{20} \quad (14)$$

$$C_3(t = 0) = C_{30} \quad (15)$$

The solution to differential equations (10), (11) and (12) is given by the following set of equations.

$$\begin{aligned} C_1(t) = & \{C_{10}P_1^3 - Z_{11}P_1^2 + Z_{12}P_1 - Z_{13}\} / \{P_1(P_2 - P_1)(P_3 - P_1)\} \exp(-P_1 t) \\ & + \{C_{10}P_2^3 - Z_{11}P_2^2 + Z_{12}P_2 - Z_{13}\} / \{P_2(P_1 - P_2)(P_3 - P_2)\} \exp(-P_2 t) \\ & + \{C_{10}P_3^3 - Z_{11}P_3^2 + Z_{12}P_3 - Z_{13}\} / \{P_3(P_1 - P_3)(P_2 - P_3)\} \exp(-P_3 t) \\ & + Z_{13} / (P_1 P_2 P_3) \end{aligned} \quad (16)$$

$$\begin{aligned} C_2(t) = & \{C_{20}P_1^3 - Z_{21}P_1^2 + Z_{22}P_1 - Z_{23}\} / \{P_1(P_2 - P_1)(P_3 - P_1)\} \exp(-P_1 t) \\ & + \{C_{20}P_2^3 - Z_{21}P_2^2 + Z_{22}P_2 - Z_{23}\} / \{P_2(P_1 - P_2)(P_3 - P_2)\} \exp(-P_2 t) \\ & + \{C_{20}P_3^3 - Z_{21}P_3^2 + Z_{22}P_3 - Z_{23}\} / \{P_3(P_1 - P_3)(P_2 - P_3)\} \exp(-P_3 t) \\ & + Z_{23} / (P_1 P_2 P_3) \end{aligned} \quad (17)$$

$$\begin{aligned} C_3(t) = & \{C_{30}P_1^3 - Z_{31}P_1^2 + Z_{32}P_1 - Z_{33}\} / \{P_1(P_2 - P_1)(P_3 - P_1)\} \exp(-P_1 t) \\ & + \{C_{30}P_2^3 - Z_{31}P_2^2 + Z_{32}P_2 - Z_{33}\} / \{P_2(P_1 - P_2)(P_3 - P_2)\} \exp(-P_2 t) \\ & + \{C_{30}P_3^3 - Z_{31}P_3^2 + Z_{32}P_3 - Z_{33}\} / \{P_3(P_1 - P_3)(P_2 - P_3)\} \exp(-P_3 t) \\ & + Z_{33} / (P_1 P_2 P_3) \end{aligned} \quad (18)$$

where,

$$Z_{11} = (R_2 + R_3 + R_4 + R_5) C_{10} + R_1 C_{20} + G \quad (19)$$

$$Z_{12} = (R_2 + R_3 + R_4 + R_5) G + (R_2 R_4 + R_2 R_5 + R_3 R_5) C_{10} + R_1 (R_4 + R_5) C_{20} + R_1 R_3 C_{30} \quad (20)$$

$$Z_{13} = (R_2 R_4 + R_2 R_5 + R_3 R_5) G \quad (21)$$

$$Z_{21} = R_2 C_{10} + (R_1 + R_4 + R_5) C_{20} + R_3 C_{30} \quad (22)$$

$$Z_{22} = R_2 (R_4 + R_5) C_{10} + R_1 (R_4 + R_5) C_{20} + R_1 R_3 C_{30} + R_2 G \quad (23)$$

$$Z_{23} = R_2 (R_4 + R_5) G \quad (24)$$

$$Z_{31} = R_4 C_{20} + (R_1 + R_2 + R_3) C_{30} \quad (25)$$

$$Z_{32} = R_2 R_4 C_{10} + R_1 R_4 C_{20} + R_1 R_3 C_{30} \quad (26)$$

$$Z_{33} = R_2 R_4 G \quad (27)$$

$$A_1 = R_1 + R_2 + R_3 + R_4 + R_5 \quad (28)$$

$$A_2 = R_1 (R_3 + R_4 + R_5) + R_2 (R_4 + R_5) + R_3 R_5 \quad (29)$$

$$A_3 = R_1 R_3 R_5 \quad (30)$$

$$P_1 = [(A_1 - A_3 / C) + \sqrt{(A_1 - A_3 / C)^2 - 4C}] / 2 \quad (31)$$

$$P_2 = C / P_1 \quad (32)$$

$$P_3 = A_3 / (P_1 P_2) \quad (33)$$

where C is a positive root of the cubic equation

$$C^3 - A_2 C^2 + A_1 A_3 C - A_3^2 = 0 \quad (34)$$

The first step in applying the methodology is to establish the container history (i.e., dates of drum packaging, venting, and sampling). Next, the container headspace flammable gas concentration is obtained. The equations documented earlier are solved iteratively adjusting the flammable gas generation rate until the predicted flammable gas generation rate provides a headspace flammable gas concentration that matches the sampled headspace flammable gas

concentration. A validated software program can be used to apply this methodology to determine compliance with the 5-percent limit on hydrogen concentration by sampling the headspace of a container.

3.10.2 Calculation of Flammable Gas/Voc Concentrations: FAMP

The Flammability Assessment Methodology Program (FAMP) was established to investigate the flammability of gas mixtures found in CH-TRU waste containers. Central to the program was experimental testing and modeling to predict the gas mixture lower explosive limit (MLEL) of gases observed in CH-TRU waste containers. Flammability testing was conducted by the National Institute for Occupational Safety and Health (NIOSH) Pittsburgh Research Laboratory (PRL), as described in Loehr et al., 1997.¹ The MLELs of the gas mixtures in the flammability tests were used to develop and evaluate models for predicting the flammability of CH-TRU waste drum contents that could potentially have flammable gas/VOC mixtures. A summary of the test design, equipment and procedures, and results is provided below.

3.10.2.1 Experimental Design

The experimental design focused on investigating classes of compounds, including nonflammable VOCs, to predict MLELs and to provide data that represent a variety of CH-TRU waste gas mixtures for evaluating MLEL models. Table 3.10-1 lists the compounds (flammable VOCs, nonflammable VOCs, and flammable gases) observed in CH-TRU waste containers and considered in the FAMP. Flammable VOCs were classified according to their chemical structural characteristics and lower explosive limit (LEL) group (Table 3.10-2). The functional groups considered were aromatics, ketones, alcohols, and alkanes/alkenes. The LEL groups were designated by LELs of 0.9% to 1.3%, 1.4% to 2.6%, and 5.6% to 6.7%. In general, there is a correlation between functional and LEL group. LEL groups were chosen as classifications for flammable VOCs by functional and LEL groups.

In addition to LEL groups as classifications for flammable VOCs, flammable gases and nonflammable VOCs were two additional classes of compounds considered in the experimental design. Test mixtures for flammability testing were determined based on the following factors:

- Presence or absence of a flammable VOC from one or more of the three LEL groups
- Presence or absence of hydrogen
- Presence or absence of a nonflammable VOC.

VOCs were selected to represent compound classes based on prevalence in CH-TRU waste and on physical characteristics that facilitated testing.

¹ Loehr, C.A., S.M. Djordjevic, K.J. Liekhus, and M. J. Connolly (1997). Flammability Assessment Methodology Program Phase I: Final Report. INEEL/EXT-97-01073. Idaho National Engineering and Environmental Laboratory, Idaho Falls, Idaho.

Table 3.10-1 — Flammable and Nonflammable Volatile Organic Compounds and Flammable Gases Considered in the Flammability Assessment Methodology Program

Flammable VOCs	Nonflammable VOCs	Flammable Gases
Acetone Benzene 1-Butanol Chlorobenzene Cyclohexane 1,1-Dichloroethane 1,2-Dichloroethane 1,1-Dichloroethene Cis-1,2-Dichloroethene Ethyl benzene Ethyl ether Methanol Methyl ethyl ketone Methyl isobutyl ketone Toluene 1,2,4-Trimethylbenzene 1,3,5-Trimethylbenzene m-Xylene o-Xylene p-Xylene	Bromoform Carbon tetrachloride Chloroform Formaldehyde Methylene chloride 1,1,2,2-Tetrachloroethane Tetrachloroethene 1,1,1-Trichloroethane Trichloroethene 1,1,2-Trichloro-1,2,2-trifluoroethane	Hydrogen Methane

Table 3.10-2 — Classification of Flammable Volatile Organic Compounds

Flammable VOC	Structural Type	Functional Group Number	LEL (vol. %)	LEL Group Number
Acetone	Ketone	2	2.6	2
Benzene	Aromatic	1	1.3	1
1-Butanol	Alcohol	3	1.7	2
Chlorobenzene	Aromatic	1	1.3	1
Cyclohexane	Cycloalkane	-	1.3	1
1,1-Dichloroethane	Alkane	4	5.6	3
1,2-Dichloroethane	Alkane	4	~5	3
1,1-Dichloroethene	Alkene	4	6.5	3
cis-1,2-Dichloroethene	Alkene	4	5.6	3
Ethyl benzene	Aromatic	1	1.0	1
Ethyl ether	Ether	-	1.9	2
Methanol	Alcohol	3	6.7	3
Methyl ethyl ketone	Ketone	2	1.9	2
Methyl isobutyl ketone	Ketone	2	1.4	2
Toluene	Aromatic	1	1.2	1
1,2,4-Trimethylbenzene	Aromatic	1	0.9	1
1,3,5-Trimethylbenzene	Aromatic	1	1.0	1
o-Xylene	Aromatic	1	1.1	1
m-Xylene	Aromatic	1	1.1	1
p-Xylene	Aromatic	1	1.1	1

A full factorial design of the experimental factors plus a quarter replication and minus combinations that resulted in no gas in the mixture resulted in a test matrix of 38 gas mixtures. Replicate runs were included in the test matrix to assess the experimental error. All runs were performed in a random order to help ensure that experimental errors and factor effects were properly estimated and not confounded with experimental procedure trends and other possible experimental effects.

The experimental test mixtures consisted of hydrogen and four VOCs, including 1,2-dichloroethane, to represent chlorinated hydrocarbons and alkanes; methyl ethyl ketone (2-butanone) to represent oxygenated hydrocarbons and ketones; toluene to represent aromatic hydrocarbons; and carbon tetrachloride to represent nonflammable VOCs. These VOCs were chosen to represent the LEL and, thus, the functional groups, because they have sufficient vapor pressures to remain in the gas phase under conditions of standard temperature and pressure. Ethyl ether (an ether) and cyclohexane (a cycloalkane) were not included in the test mixtures because they are not prevalent in CH-TRU waste. The test mixtures contained equimolar amounts of the above constituents as shown in Table 3.10-3.

In planning the experiments, errors were anticipated for measuring the actual concentration of a mixture component injected into the test chamber, the component vapor pressure and associated

temperature, and the actual final mixture pressure. The required overall data quality objective (DQO) was to maintain the error in the experimental MLEL result to less than 5%.

Table 3.10-3 — Experimental Test Mixtures and MLEL Results

Mixture No.	1,2 - Dichloroethane (vol. %)	Methyl ethyl ketone (vol. %)	Toluene (vol. %)	Hydrogen (vol. %)	Carbon tetrachloride (vol. %)	MLEL(%)
1	20	20	20	20	20	3.40±0.10
2	100	0	0	0	0	4.85±0.05
3	50	50	0	0	0	2.65±0.05
4	33	33	33	0	0	1.95±0.03
5	25	25	25	25	0	2.40±0.05
6	33	33	0	33	0	3.40±0.07
7	25	25	0	25	25	5.15±0.05
8	33	33	0	0	33	4.85±0.10
9	25	25	25	0	25	2.80±0.05
10	50	0	50	0	0	2.05±0.03
11	33	0	33	0	33	3.50±0.05
12	33	0	33	33	0	2.65±0.05
13	25	0	25	25	25	3.95±0.05
14	50	0	0	50	0	5.35±0.20
15	33	0	0	33	33	9.7±0.50
16	50	0	0	0	50	Not Determined
17	0	100	0	0	0	1.95±0.03
18	0	50	0	0	50	4.65±0.03
19	0	50	50	0	0	1.45±0.05
20	0	50	0	50	0	3.15±0.07
21	0	25	25	25	25	2.90±0.05
22	0	0	100	0	0	1.20±0.03
23	0	0	50	0	50	2.90±0.05
24	0	0	50	50	0	2.05±0.03
25	0	0	33	33	33	3.65±0.10
26	0	0	0	100	0	5.00±0.40
27	0	0	0	50	50	10.8±0.80
28	0	33	33	0	33	2.45±0.05
29	0	33	33	33	0	2.00±0.05
30	0	33	0	33	33	5.20±0.10
31	0	0	0	0	100	Not Flammable
32	0	0	0	0	0	Not Applicable
33	33	0	33	0	33	3.45±0.10
34	0	33	33	0	33	2.35±0.05
35	33	0	0	33	33	10.1±0.50
36	0	33	0	33	33	5.20±0.07
37	0	0	0	0	0	Not Applicable
38	50	50	0	0	0	2.70±0.05
39	0	0	50	50	0	2.05±0.03
40	25	25	25	25	0	2.40±0.10

3.10.2.2 Flammability Testing Equipment and Procedures

A heavy-walled, stainless steel test chamber with an approximate volume of 19 liters was used for the gas mixture flammability tests. The chamber has been used extensively for dust and gas explosibility measurements. Such chambers are now the standard laboratory chambers for dust explosibility measurements², and are highly useful for gas explosibility measurements as well. They are considerably larger than the 5-liter spherical glass flasks specified in the ASTM vapor flammability test procedure^{2,3}, but are consistent with the ASTM standard. The larger size of the chamber allowed for the potential use of stronger igniters to ensure the absence of ignition limitations when measuring flammability limits, and minimized wall effects on flammability. The question of ignition limitations and wall effects are particularly important in testing halogenated VOCs. The equipment used objective pressure criteria for explosions rather than a purely visual and subjective criteria as in ASTM E681-94³.

The chamber was equipped with viewing ports and various access ports for pressure and temperature sensors, electronic ignition, evacuation, gas admission, and VOC liquid injection. Ignition was attempted using a 41-joule energy spark, and the resulting pressure trace was monitored to determine flammability or nonflammability for each test. By using the test chamber, stronger ignition sources could be used to ensure the absence of ignition limitations when measuring flammability limits, and minimizing wall effects (i.e., heat losses) on flammability.

A computer-controlled data acquisition system was used to display the pressure, rate of pressure rise (dP/dt), and temperature data versus time. The partial pressures of the VOCs, hydrogen, and air were monitored using two Viatran pressure transducers for the explosion pressures and a Baratron pressure transducer for the component pressures. Chamber temperature was monitored by a Chromel-Alumel (type K) thermocouple.

The PRL measured the MLEL in dry air at a total pressure of 1 atm for the VOC mixtures. All testing used known amounts of the appropriate individual components. To ensure complete volatilization of the VOCs, each component was introduced under reduced pressure into the test chamber. Once the appropriate components were introduced into the chamber and pressures were checked to ensure proper component concentrations, the chamber was brought to atmospheric pressure using dry air. Once a uniform mixture was obtained, the test was started by energizing the appropriate ignition source and recording pressure and temperature. Ignition of the mixture was identified by the pressure rise of the test chamber vessel. A positive ignition was required for those test mixtures that contain a flammable gas.

² American Society for Testing and Materials (ASTM) (1997) E1515-96. Standard Test Method for Minimum Explosible Concentration of Combustible Dusts, American Society for Testing and Materials, West Conshohocken, Pennsylvania.

³ American Society for Testing and Materials (ASTM) (1994) E681-94. Standard Test Method for Concentration Limits of Flammability of Chemicals, American Society for Testing and Materials, West Conshohocken, Pennsylvania.

This was accomplished by increasing the component concentrations, while maintaining the required component ratio, until the sample gave a positive ignition. The ignition source selected was of sufficient energy and duration as to avoid ignition limitations as discussed below.

An initial testing phase was completed prior to initiation of testing the 38 gas mixtures in order to verify and establish the following:

- *LEL of the individual components (hydrogen and VOCs).* The LELs determined through the initial testing were compared to values previously determined at the PRL for hydrogen and taken from the literature for the VOCs.
- *Criterion (i.e., pressure rise) for a positive ignition.* Based on the preliminary testing and comparisons to earlier measurements, a pressure rise of 0.5 psi was chosen as the LEL criterion.
- *Equipment performance.*
- *An appropriate ignition source for flammability tests.* Preliminary tests on the LELs of toluene and methyl ethyl ketone had used a stored spark energy of 17 joules. The LELs were found to be in agreement with the reported values from closed flammability tubes. Despite the apparent adequacy of the spark energy used, it was determined to use an even more energetic spark of 41 joules for the test series to help ensure that the more difficult to ignite halogenated VOCs (e.g., 1,2-dichloroethane) and mixtures (those with 1,2-dichloroethane or carbon tetrachloride) would not be ignition limited. Switching to the higher capacitance spark did not reduce the LEL for methyl ethyl ketone. There was, therefore, no indication that the more energetic spark was “overdriving” the chamber mixture, nor was there any expectation that the actual thermal energy deposited in the chamber by the spark (about 1 joule) could possibly do so.

The following measurements were made during an experimental run:

- *Pressure Measurements.* Individual component partial pressure (VOCs, hydrogen, and air) and total chamber pressure were established before each test. The time development of chamber pressure and rate of pressure rise in the chamber were recorded once the appropriate ignition source was energized. The pressure rise criterion, which was determined experimentally, was used to establish ignition of the test gas mixture. In addition to the pressure transducer used to measure component pressures (Baratron), two pressure transducers (Viatran) were used to measure the gas mixture explosion pressure.
- *Temperature measurements.* Test chamber temperature was monitored during each test using a Chromel-Alumel (type K) thermocouple and recorded as a function of time. The thermocouple was able to give qualitative data on flame propagation and temperature, but did not have the response time to allow the monitoring of the actual

peak explosion temperature. Because the thermocouple was cemented in place inside the reaction chamber, it was considered impractical to recalibrate the temperature output on a regular basis. Therefore, the temperature output was treated as a relative rather than an absolute measurement, with more significance given to the measured explosion temperature rise than on the absolute initial starting temperature.

- *Concentration Measurements.* The partial pressure of all gases (VOCs, hydrogen, and air) was used to determine concentrations prior to running a test.

Prior to their use, instruments used in the flammability tests were checked against known standards. Pressure transducers with built in calibrations were checked daily.

3.10.2.3 Experimental Results

The lowest flammable concentration in air of all mixtures specified in the experimental design was determined in the 19-liter laboratory chamber using a strong spark ignition source. Except for 1,2-dichloroethane, the LELs of pure VOCs were within the narrow range of literature values cited by the PRL. The experimental LEL for 1,2-dichloroethane is below the range of values cited in the literature, but may be more accurate because a larger chamber was used in combination with a more energetic spark and it is known that the halogenated species are prone to exhibiting wall effects and ignition limitations. Experimental MLELs generally agreed with calculated values for the mixtures to within 10%.¹

Partial pressures of the VOC and hydrogen components were used to determine test mixture composition and concentration in air for MLEL determinations. Mixture explosion pressure and temperature data were also measured during the experimental tests. Temperature rise measurements and visual observations of the flame propagation were found to correlate well with pressure rise measurements.¹ MLELs for the various test mixtures listed in Table 3.10-3 are based on pressure versus component concentration data plots.

The precision of the MLELs reported in Table 3.10-3 is based on the number of data points in the near vicinity of the LEL value, how close the data points are to the LEL, the effect of using a range of pressure rise criteria (0.5 ± 0.2 psi), and sensitivity of explosion pressures near the LEL. The relative precision values from replicate runs, less than or equal to 5% of the LEL value, is consistent with the DQO identified in the FAMP Test Plan.⁴

The largest uncertainty in the MLEL determinations was due to a gradual increase in explosion pressure with hydrogen concentration and the dominance of hydrogen in some mixtures, particularly the hydrogen and carbon tetrachloride mixture, which combines the lightest, most diffusible molecule, hydrogen, with the heaviest VOC, carbon tetrachloride, selected for the experimental tests. The flammability of equimolar mixtures containing hydrogen is expected to be more influenced by hydrogen because of its diffusivity and reactivity as a fuel. This behavior

⁴ Connolly, M.J., S.M. Djordjevic, L. Evans, and C.A. Loehr (1997). Flammability Assessment Methodology Program Test Plan, Revision 0. INEL 96/0352. Idaho National Engineering and Environmental Laboratory, Idaho Falls, Idaho.

is greatest when other mixture components are much heavier and slower than hydrogen, such as the halogenated components carbon tetrachloride and 1,2-dichloroethane. The other hydrogen-containing mixtures and the pure VOC mixtures (excluding hydrogen and carbon tetrachloride) show a sharp discontinuity at the flammability boundary and, therefore, have more well-defined MLEL and LEL values.¹

3.10.2.4 Model Development, Evaluation, and Selection

The FAMP evaluated seven models for predicting MLELs for gas mixtures, including (a) the original method of Le Chatelier; (b) a modified Le Chatelier method based on accounting for the nonflammable VOC proportion in the mixture; (c) a group contribution factor method, which accounts for the compound stoichiometry; (d) a group contribution factor method that accounts only for flammable VOCs (Flammable Group method); (e) a group contribution method that uses experimental LELs as input; (f) predictions using the American Society for Testing and Materials code, CHETAH; and (g) linear regression of test MLELs on proportions of compounds in the classifications used for flammability testing. In addition, the effects of imposing bias on relatively unbiased models was investigated.

Model predictions for the test mixtures were compared to MLELs determined in flammability testing. Statistics on measures of the degree of consistency of agreement between predicted and test MLELs were generated. An evaluation of the models was also performed using innermost layer concentrations for 532 drums characterized under the CH-TRU waste characterization program at the Idaho National Engineering and Environmental Laboratory and the Rocky Flats Environmental Technology Site.

In applying the models to actual drum data, it was found that some methods resulted in unrealistic MLELs. For instance, all methods except the Flammable Group method resulted in extremely high MLELs predicted for some drums. Based on the results of model evaluations and because of favorable results in the experimental-based evaluations, the Flammable Group model was selected as a conservative approach to determine the MLEL of a mixture of flammable VOCs and flammable gas.

The Flammable Group method is based on an extension of the method presented in the American Institute of Chemical Engineers (AIChE) Procedure B: Method for Estimating Lower Flammability Limit of Pure Compounds in the Data Prediction Manual.³ This method predicts the MLEL of a mixture based on knowledge of the chemical structure of each individual component in the mixture. The MLEL will be calculated by the following equation:

$$MLEL = \frac{100\%}{\sum f_i \times GCF_i} \quad (35)$$

where,

MLEL = mixture lower explosive limit (vol %)

f_i = fraction of flammable gas i in mixture on an air free and nonflammable VOC free basis (i.e., the concentration of flammable compound i divided by the sum of the concentrations of flammable VOCs and flammable gas).

GCF_i = group contribution factor for compound i .

The GCF for a compound is calculated by the following method:

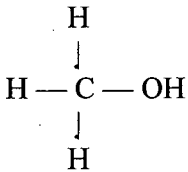
$$GCF_i = \sum n_j * GF_j \quad (36)$$

where,

n_j = number of group type j in compound i

GF_j = group factor for group type j .

Table 3.10-4 contains the FAMP calculated group factor (GF) values for the various groups used to determine the GCF for a compound of interest. As an example, the GCF for methanol (CH_3OH) or structurally as



is calculated as 1 C group + 4 H groups + 1 O group or $(9.10) + (4*2.17) + (-2.68) = 15.1$. The GCF values for various flammable VOCs identified by the sites in CH-TRU waste are listed in Table 3.10-5. GCF values for additional flammable VOCs may be calculated by the WIPP CH-TRU Payload Engineer in the same manner. See Section 5.2.5.3.2 of the CH-TRAMPAC for the process of adding flammable VOCs.

Table 3.10-4 — FAMP Group Factor (GF) Values

Group	Group Factor
C	9.10
H	2.17
H ₂	20.0
O	-2.68
N	1.38
Cl	-4.38
C=C	14.07
F (Number of H atoms > Number of F atoms)	-4.18
F (Number of H atoms < Number of F atoms)	-2.55
I	17.5
S	10.9
P	9.6

Table 3.10-5 — Compound Group Contribution Factors

Compound	Group Contribution Factor (GCF)
Flammable VOCs	
Acetone	37.64
Benzene	82.53
1-Butanol	55.42
Chlorobenzene	75.98
Cyclohexane	80.64
1,1-Dichloroethane	18.12
1,2-Dichloroethane	18.12
1,1-Dichloroethene	9.65
cis-1,2-Dichloroethene	9.65
Ethyl benzene	109.41
Ethyl ether	55.42
Methanol	15.1
Methyl ethyl ketone	51.08
Methyl isobutyl ketone	77.96
Toluene	95.97
1,2,4-Trimethylbenzene	122.85
1,3,5-Trimethylbenzene	122.85
o-Xylene	109.41
m/p-Xylene	109.41
Flammable Gases	
Hydrogen	20
Methane	20

APPENDIX 3.11

**USE OF FILTERED BAGS AS CONFINEMENT LAYERS
FOR CH-TRU WASTES**

This page intentionally left blank.

3.11 Use of Filtered Bags as Confinement Layers for CH-TRU Wastes

3.11.1 Introduction

Contact-handled-transuranic (CH-TRU) waste is typically packaged in closed, unfiltered plastic bags within authorized payload containers. However, filtered bags may also be used as layers of confinement within authorized payload containers for the shipment of specific CH-TRU waste forms in the TRUPACT-II and the HalfPACT. Filtered bags are used primarily for two purposes: (1) increasing allowable decay heat limits and (2) addressing site safety concerns for specific packaging configurations. This appendix describes the test procedures and analyses that validate the use of filtered bags, and provides the technical basis for increased allowable decay heat limits for specific shipping categories using filtered bags.

3.11.2 Description of Filtered Bag

The filtered bag is a plastic bag installed with a minimum of one filter vent. An example of a filtered bag configuration is presented in Figure 3.11-1. Other configurations meeting the requirements of Section 2.5 of the Contact-Handled Transuranic Waste Authorized Methods for Payload Control (CH-TRAMPAC), "Filter Vents," are acceptable. Appendix 3.8 of the CH-TRU Payload Appendices presents the specifications for allowable closure methods for any layers of confinement used in payload containers. Section 2.5 of the CH-TRAMPAC provides the specification for the plastic bag filter vent.

3.11.3 Testing

The flow rate and hydrogen diffusion characteristics of the bag filters were measured in experimental programs, designed similar to those for the filters used for the payload containers.^{1,2} In the first series of tests, conducted in 1990, flow was measured as a function of differential air pressure across the filter vent, and diffusion was measured at zero differential pressure, with 4.78%, by volume, hydrogen in nitrogen.³ Four bag filters were tested under both dry and wet conditions, and the test data were used to calculate filter flow and diffusion coefficients for each. The results indicate that flow increases linearly with pressure at a rate of 5.9 standard liters per minute (slpm)/pounds per square inch gauge (psig). This rate exceeds the minimum filter flow requirement specified by Section 2.5 of the CH-TRAMPAC (i.e., 1 slpm at 1 psig). Table 3.11-1 presents the flow coefficients of each tested filter.

¹ Peterson, S.H., E.E. Smeltzer, and R.D. Straw, March 1990, "Determination of Flow and Hydrogen Diffusion Characteristics of Carbon Composite Filters Used at the Waste Isolation Pilot Plant," Purchase Order No. 75WRS36917IZ, Westinghouse Science and Technology Center, Pittsburgh, Pennsylvania.

² Callis, E.L., J.H. Capps, M.C. Smith, and R.S. Marshall, 1995, "Hydrogen Venting Characteristics of Commercial Carbon-Composite Filters and Applications to TRU Waste," LA-UR-95-1447, Los Alamos National Laboratory, Los Alamos, New Mexico.

³ Callis, E.L., January 23, 1996, "Summary of January 1996 Filter Measurements," Letter Report to IT Corporation, Los Alamos National Laboratory, Los Alamos, New Mexico.

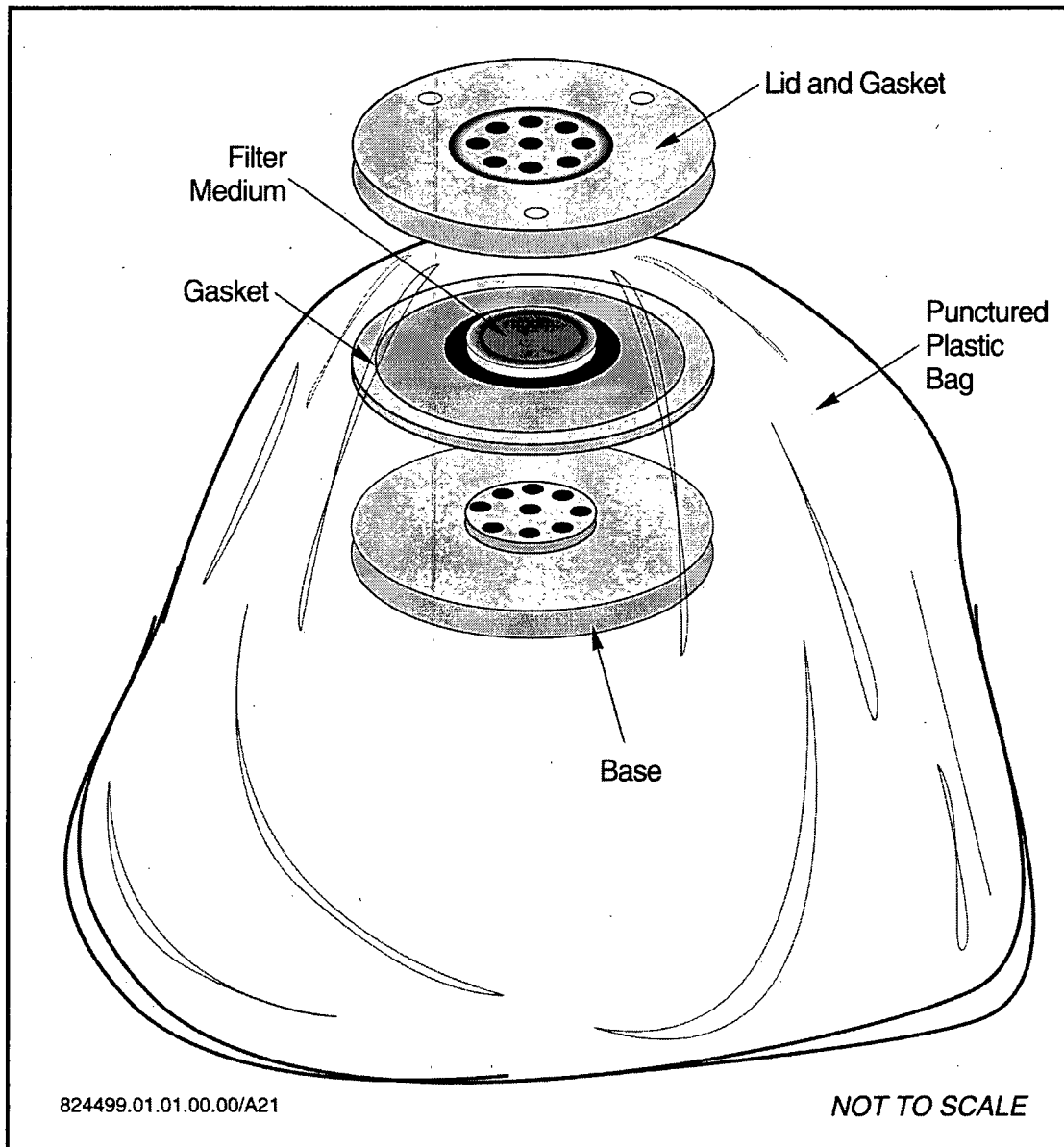


Figure 3.11-1 — Example of One Type of Filtered Bag

Table 3.11-1 — Flow Coefficients of Bag Filters Tested with Compressed Air, 0.2 to 10 psig

Filter Model	Filter Identification	Mean Flow Coefficient (slpm/psig)
NFT-030	WH-05	5.8
	WH-06	6.5
	WH-07	5.9
	WH-08	5.5
	AVERAGE	5.9

Source: Peterson, S.H., E.E. Smeltzer, and R.D. Straw, March 1990, "Determination of Flow and Hydrogen Diffusion Characteristics of Carbon Composite Filters Used at the Waste Isolation Pilot Plant," Purchase Order No. 75WRS36917IZ, Westinghouse Science and Technology Center, Pittsburgh, Pennsylvania.

Diffusion measurements in these tests showed that the hydrogen diffusivity values of the filters ranged from 4.17E-06 to 4.32E-06 mole/second/mole fraction (mol/sec/mol fraction) (Table 3.11-2).

Table 3.11-2 — Diffusion Coefficients of Bag Filters

Filter Model	Filter Identification	Diffusion Coefficient (mol/sec/mol Fraction)
NFT-030	WH-05	4.32E-06
	WH-06	4.26E-06
	WH-07	4.17E-06
	WH-08	4.31E-06
	AVERAGE	4.27E-06

Source: Peterson, S.H., E.E. Smeltzer, and R.D. Straw, March 1990, "Determination of Flow and Hydrogen Diffusion Characteristics of Carbon Composite Filters Used at the Waste Isolation Pilot Plant," Purchase Order No. 75WRS36917IZ, Westinghouse Science and Technology Center, Pittsburgh, Pennsylvania.

Table 3.11-3 presents a comparison of diffusion results for wet and dry filters. At applied pressures less than or equal to 1 psig the wet filters were ineffective.¹ At pressures greater than 1 psig, the water was forced out of the filter and the flow measurements paralleled that of the dry filter. A conservative approach precludes the use of filtered bags to directly package CH-TRU waste where the filters could come in contact with water (i.e., Waste Material Types I.1 [absorbed, adsorbed, or solidified inorganic liquids], I.2 [soils, solidified particulates, or sludges formed from precipitates], or Waste Type IV [solidified organics]). It should be noted that the CH-TRU waste forms do not exist as free liquids and are not likely to affect filter performance. Therefore, the use of a heat-sealed filtered bag as the innermost layer of confinement to package CH-TRU waste is limited to Waste Material Types I.3, II.1, III.1 and III.3 provided that there is no potential for contact of the filters with water. Waste Material Types II.2, II.3, and III.2, which by definition include a metal can as the innermost layer of confinement, may use heat-sealed

filtered bags outside of the innermost metal can. For other waste material types, heat-sealed filtered bags are not allowed as the innermost layer of confinement.

Table 3.11-3 — Comparison of Wet and Dry Diffusion Coefficients of Bag Filters

Filter Model	Filter Identification	Diffusion Coefficient (mol/sec/mol fraction)	
		Dry	Wet
NFT-030	WH-05	4.32E-06	0.040E-06
	WH-06	4.26E-06	0.044E-06
	WH-07	4.17E-06	0.022E-06
	WH-08	4.31E-06	0.041E-06
	AVERAGE	4.27E-06	0.037E-06

Source: Peterson, S.H., E.E. Smeltzer, and R.D. Straw, March 1990, "Determination of Flow and Hydrogen Diffusion Characteristics of Carbon Composite Filters Used at the Waste Isolation Pilot Plant," Purchase Order No. 75WRS36917IZ, Westinghouse Science and Technology Center, Pittsburgh, Pennsylvania.

In the second series of tests, conducted in 1995, 12 bag filters were tested for hydrogen diffusivity, with the results shown in Table 3.11-4.² The hydrogen diffusivity values ranged from 1.075E-05 mol/sec/mol fraction to 1.217E-05 mole/sec/mol fraction, with an average value of 1.127E-05 mol/sec/mol fraction. As may be seen by a comparison of Tables 3.11-2 and 3.11-4, these results are higher (approximately 3.7 times) than the results from the initial testing in 1990. Further investigations and retesting of the initial filters showed that the differences could be attributed to an improved design of the filters, which provided for nine gas release holes (in the 1995 filters) instead of only five (in the 1990 filters).³ The use of bag filters is based only on the newer design. The minimum diffusivity value of 1.075E-05 mol/sec/mol fraction obtained in the 1995 testing will be used in the minimum specifications for the bag filters (Section 2.5 of the CH-TRAMPAC). As specified in Section 2.5 of the CH-TRAMPAC, high-diffusivity bag filters (HDBF) may be used to decrease the resistance to hydrogen diffusivity. The HDBFs allow credit to be taken for filters for which a hydrogen diffusivity value that is equal to or greater than 2 times, 5 times, 25 times, or 100 times the minimum specification for the bag filter has been demonstrated and documented through testing. As with other filter requirements, site-specific procedures ensure compliance with this limit through procurement and administrative controls. The value specified in Section 2.5 of the CH-TRAMPAC is used in determining the hydrogen release rate through the bag filters in the calculation of the decay heat limit for shipping categories using filtered bags (Section 3.11.5).

Table 3.11-4 — Diffusion Coefficients of Bag Filters

Filter Model	Filter Identification	Diffusion Coefficient (mol/sec/mol fraction)
NFT-030	LANL 1	1.105E-05
	LANL 2	1.116E-05
	LANL 4	1.170E-05
	LANL 6	1.130E-05
	LANL 13	1.128E-05
	LANL 14	1.145E-05
	LANL 15	1.217E-05
	LANL 16	1.075E-05
	LANL 25	1.092E-05
	LANL 26	1.125E-05
	LANL 27	1.121E-05
	LANL 28	1.105E-05
	AVERAGE	1.127E-05

Source: Callis, E.L., J.H. Cappis, M.C. Smith, and R.S. Marshall, 1995, "Hydrogen Venting Characteristics of Commercial Carbon-Composite Filters and Applications to TRU Waste," LA-UR-95-1447, Los Alamos National Laboratory, Los Alamos, New Mexico.

3.11.4 Shipping Category

Filtered bags shall be used only in packages as described in Section 3.11.3, Testing. The use of filtered bags in waste packaging configurations must be specified in approved content codes.

In the alpha-numeric shipping category notation scheme used until June 1999, the presence of filtered bags in a shipping category was indicated by using an alpha trailer designation of "f" in conjunction with the notation for the total number of bags. This designation indicated that all plastic bags were filtered bags. For example, the notation II.1A2f indicated CH-TRU Waste Material Type II.1 packaged in one 55-gallon drum with two filtered bags, each containing a minimum of one filter vent. In the numeric shipping category notation initiated in June 1999, the resistance of filtered bags is represented in the last four digits of the shipping category, as detailed in Appendix 2.2 of the CH-TRU Payload Appendices.

Filtered bags may be closed by any method, including heat-sealing. For estimation of gas release rates and decay heat limits, it is conservatively assumed that the bag closure allows no gas release (i.e., the bag is heat-sealed).

3.11.5 Decay Heat Limits

Decay heat limits, expressed as watts per payload container, are established for all shipping categories of authorized payload containers. Limits for the allowable decay heat value for each shipping category are specified in order to control the potential for combustible gas accumulation. The method for calculating decay heat limits for different shipping categories is provided in Appendix 2.3 of the CH-TRU Payload Appendices.

Because filtered bags allow higher rates of gas release, the maximum decay heat limits for specific shipping categories containing filtered bags may be increased. Allowable decay heat limits for shipping categories using filtered bags were calculated using data for hydrogen diffusivity through the bag filters and permeation through the liner bag(s). The calculation of decay heat limits is derived in Appendix 2.3 of the CH-TRU Payload Appendices, and is the same for the shipping categories using filtered bags, with the release rates being based on the testing described in this appendix.

APPENDIX 4.1

DESCRIPTION OF STANDARD PIPE OVERPACK

This page intentionally left blank.

4.1 Description of Standard Pipe Overpack

4.1.1 Introduction

The standard pipe overpack, also referred to as pipe overpack payload container, pipe overpack configuration, or pipe overpack assembly, consists of a pipe component, also referred to as pipe container, positioned by dunnage within a 55-gallon drum with a rigid liner. It is designed to be used for the shipment of specific contact-handled transuranic waste forms in the TRUPACT-II and the HalfPACT. Appendix 1.3.1 of the TRUPACT-II Safety Analysis Report¹ (SAR), Appendix 1.3.1 of the HalfPACT SAR², and Section 2.9.2 of the Contact-Handled Transuranic Waste Authorized Methods for Payload Control³ (CH-TRAMPAC) describe the materials of construction, sizes, and other dimensional specifications for the standard pipe overpack. The purpose of the standard pipe overpack is to provide criticality control, shielding, and containment of fine particulate waste material and to increase the maximum fissile gram equivalent (FGE) loading within the package. This allows for the shipment of up to 7 pipe overpacks in a HalfPACT or up to 14 pipe overpacks in a TRUPACT-II with payload container and packaging FGE limits as presented in Section 4.1.6 of this appendix. This appendix describes the test procedures and analyses that validate the use of the standard pipe overpack, and provides the technical basis for the FGE limits for shipments of pipe overpacks. Appendices 4.2, 4.3, and 4.4 of the CH-TRU Payload Appendices describe the analyses that validate the use of shielded configurations of the pipe overpack and provide the technical basis for the shipment of specific gamma- and neutron-emitting wastes in shielded pipe overpacks in the TRUPACT-II and HalfPACT.

¹ U.S. Department of Energy (DOE), *TRUPACT-II Shipping Package Safety Analysis Report*, USNRC Certificate of Compliance 71-9218, U.S. Department of Energy, Carlsbad Field Office, Carlsbad, New Mexico.

² U.S. Department of Energy (DOE), *HalfPACT Shipping Package Safety Analysis Report*, USNRC Certificate of Compliance 71-9279, U.S. Department of Energy, Carlsbad Field Office, Carlsbad, New Mexico.

³ U.S. Department of Energy (DOE), *Contact-Handled Transuranic Waste Authorized Methods for Payload Control* (CH-TRAMPAC), U.S. Department of Energy, Carlsbad Field Office, Carlsbad, New Mexico.

4.1.2 Description

The standard pipe overpack consists of a pipe component surrounded by fiberboard and plywood dunnage within a standard 55-gallon drum with a rigid polyethylene liner and lid. A schematic of the pipe overpack is shown in Figure 4.1-1.

The pipe component^{4,5} provides three significant control functions with regard to waste materials: (1) criticality control, (2) shielding, and (3) containment of fine particulate waste material. The testing and analyses described in the following sections demonstrate the effectiveness of the pipe overpack design for normal conditions of transport and hypothetical accident conditions.

The pipe component is a stainless steel, cylindrical pipe with a welded or formed bottom cap and a bolted stainless steel lid sealed with a butyl rubber or ethylene propylene O-ring (Figure 4.1-2, Appendix 1.3.1 of the HalfPACT SAR, and Appendix 1.3.1 of the TRUPACT-II SAR). The pipe component is approximately 2 feet long and is available with either a 6-inch (in.) (0.280-in. nominal thickness) or a 12-in. (0.250-in. nominal thickness) diameter. The pipe component must be installed with a filter vent; Section 2.5 of the CH-TRAMPAC provides the specification for the pipe component filter vent. The pipe component is centered in the standard 55-gallon steel drum with dunnage consisting of fiberboard packing and plywood (see Figure 4.1-1).

⁴ 6-inch Pipe Component Test Unit Fabrication Drawings:

Rocky Flats Environmental Technology Site, March 1995. Residue Container Fabrication Drawing, P15630, Rocky Flats Environmental Technology Site.

Rocky Flats Environmental Technology Site, September 1996. 6-inch Residue Container Assembly Drawing, SNMP 1001, Rocky Flats Environmental Technology Site.

⁵ 12-inch Pipe Component Test Unit Fabrication Drawings:

Rocky Flats Environmental Technology Site, October 1994. Residue Container Fabrication Drawing, P15706, Rocky Flats Environmental Technology Site.

Rocky Flats Environmental Technology Site, September 1996. 12-inch Residue Container Assembly Drawing, SNMP 1019, Rocky Flats Environmental Technology Site.

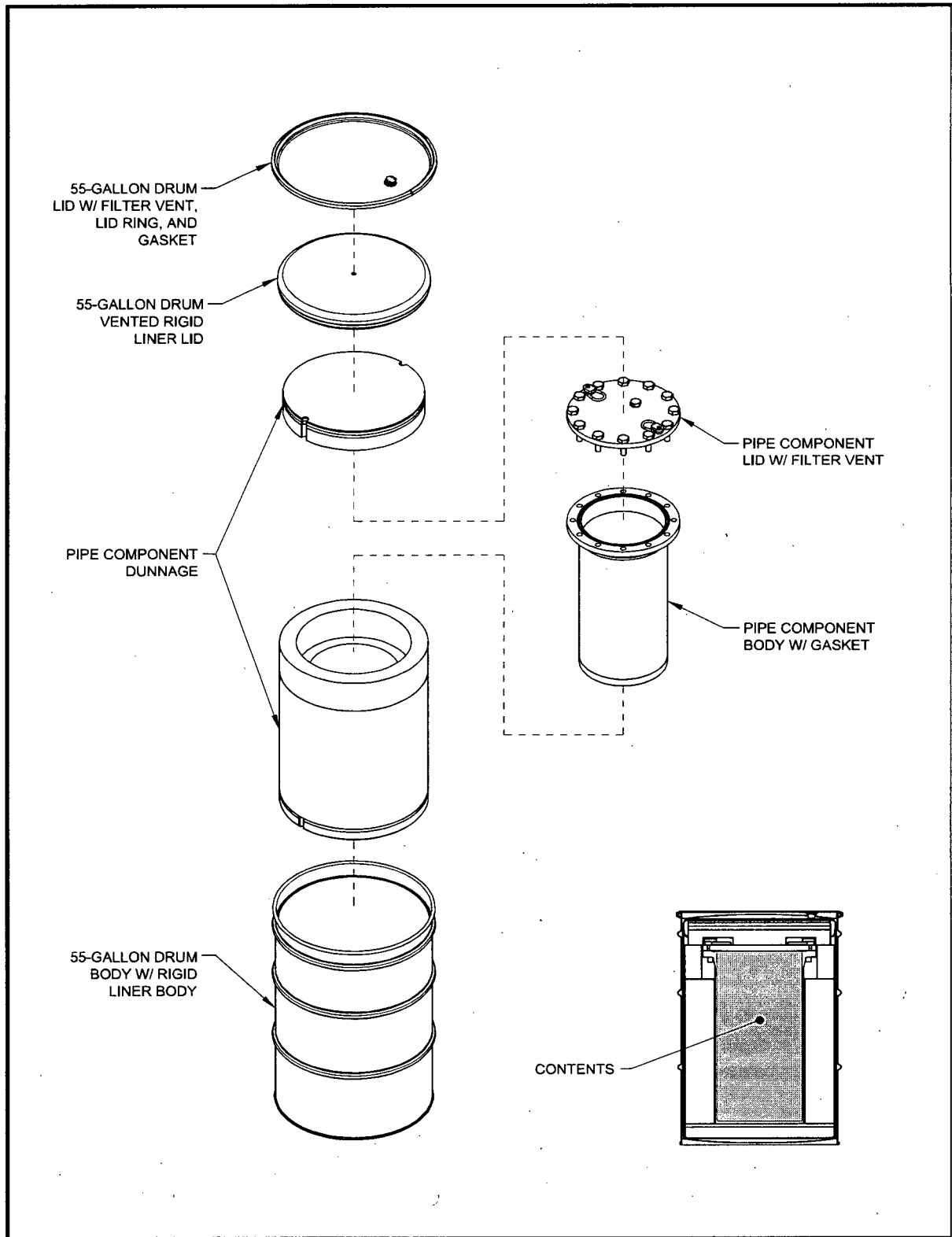
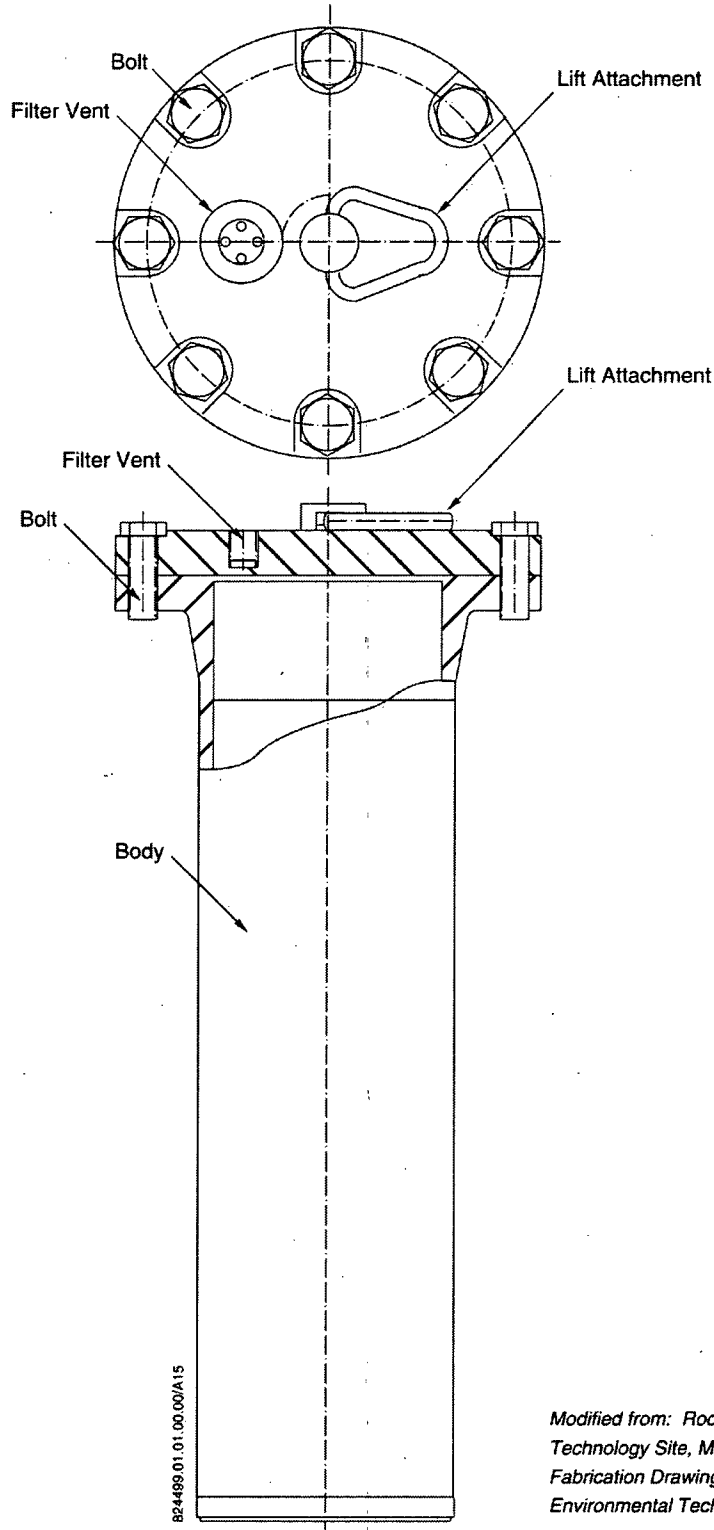


Figure 4.1-1 – Standard Pipe Overpack



*Modified from: Rocky Flats Environmental
Technology Site, May 1994. Residue Container
Fabrication Drawing, P15631, Rocky Flats
Environmental Technology Site.*

Figure 4.1-2 – Pipe Component

4.1.3 Description of Test Program for the Standard Pipe Overpack

A test program was developed and implemented to demonstrate the structural integrity of the pipe overpack under hypothetical accident conditions. Normal conditions of transport are also bounded by the test program. The test program procedures and results are documented in independent reports^{6,7} and are summarized in this section.

Two series of testing, consisting of 30-foot top- and side-impact drops of loaded pipe overpacks, have been performed. The drop tests simulated the interaction effects of other fully loaded pipe overpacks within a TRUPACT-II without subjecting an actual TRUPACT-II packaging to the tests. This resulted in more conservative analyses of the performance of the pipe overpack, since potential damage to the pipe overpacks would be less severe within a TRUPACT-II or HalfPACT.

In the first series of testing, the empty weights of the 6-in. and 12-in. diameter pipe components were approximately 87 pounds and 195 pounds, respectively. Two 6-in. diameter aluminum rods weighing nominally 66 pounds total were placed one on top of the other in each 6-in. nominal diameter pipe component; and six 5.5-in. diameter aluminum rods weighing nominally 167 pounds total were placed in two layers of three in each 12-in. nominal diameter pipe component (Figure 4.1-3a). Nominal loaded weights of the 6-in. and 12-in. diameter pipe components were 153 pounds and 362 pounds, respectively. Six "dummy" pipe components were loaded with steel rods to approximately equal the loaded weights of the test pipe components. The purpose of the "dummy" pipe components was to complete the payload configuration; these components were not tested. The loaded pipe components were overpacked within standard 55-gallon drums. Nominal loaded weights of the pipe overpacks, containing the 6-in. and 12-in. diameter pipe components, were 328 pounds and 504 pounds, respectively.

The second series of testing was similar to the first and was conducted following a revision to the 12-in. diameter pipe component design. The design was revised to remove nonessential weight from the pipe component flange and lid. The revised 12-in. diameter lid design, similar to that of the 6-in. diameter pipe component, is thicker and eliminates the need for a shielding plate to be attached to the lid under the filter opening. This design increases the available payload weight by 60 pounds over the original design. The modifications to the 6-in. diameter pipe component design are negligible. The design drawings included in the SARs for the TRUPACT-II and HalfPACT encompass both the original and the revised pipe component designs.

⁶ Ammerman, D.J., and J.G. Bobbe, October 1995. "Rocky Flats Pipe Component Testing," TTC-1434, Sandia National Laboratories, Albuquerque, New Mexico.

⁷ Ammerman, D.J., J.G. Bobbe, M. Arviso, and D.R. Bronowski, April 1997. "Testing in Support of Transportation of Residues in the Pipe Overpack Container," TTC-1477, Sandia National Laboratories, Albuquerque, New Mexico.

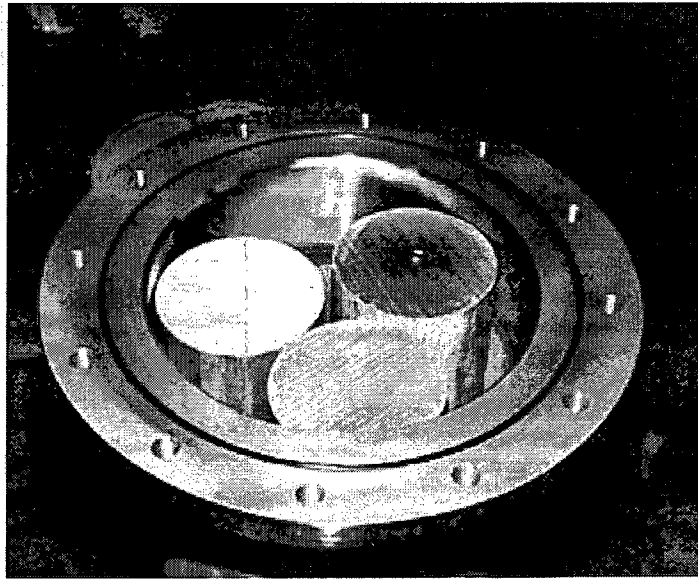


Figure 4.1-3a. Loaded Pipe Component (12-inch diameter)

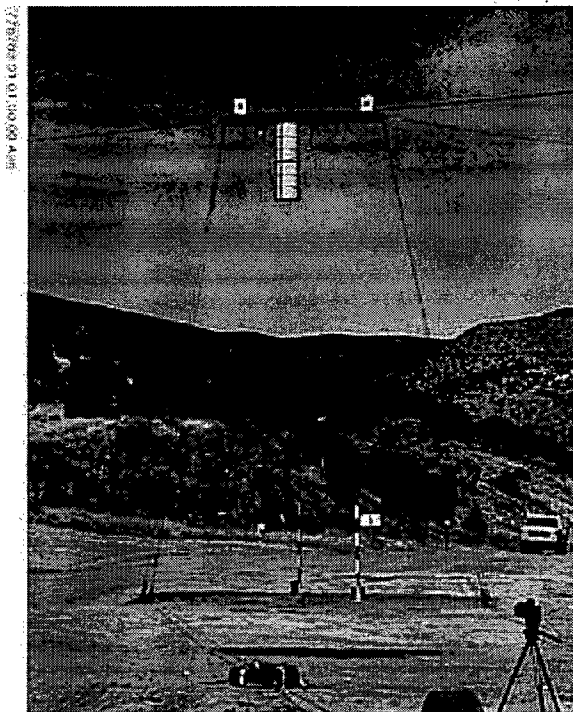


Figure 4.1-3b. Top-Impact Drop Test Set-up

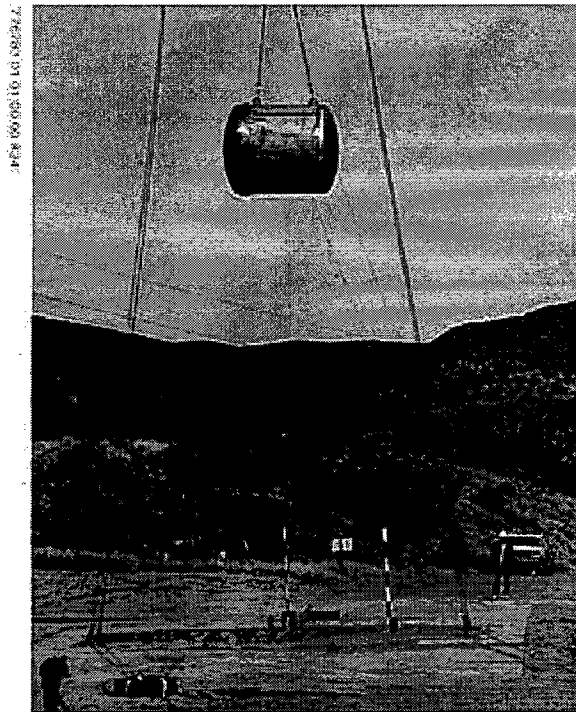


Figure 4.1-3c. Side-Impact Drop Test Set-up

Figure 4.1-3 – Test Program Photographs of the Standard Pipe Overpack (Pre-Test)

For the second series of tests, the nominal loaded weights of the 6-in. diameter pipe component and pipe overpack closely approximated the corresponding weights of the first test series. However, the nominal loaded weight of the revised 12-in. diameter pipe component was 407 pounds, which included contents weighing 225 pounds. The nominal loaded weight of the pipe overpack containing the 12-in. diameter pipe component was 547 pounds. The tests were designed to qualify not only TRUPACT-II payload assemblies of pipe overpacks, containing fourteen 6-in. or fourteen 12-in. diameter pipe components, but also a mixed assembly of pipe overpacks, containing a 7-pack of all 6-in. diameter and a 7-pack of all 12-in. diameter pipe components.

Three top-impact drop tests were performed during both series of tests. In each test, two drums were strapped end-to-end as if positioned for transport within a TRUPACT-II (Figure 4.1-3b). Top-impact drop tests were performed for the following three configurations of pipe overpacks:

- Two 55-gallon drums containing 6-in. diameter pipe components
- Two 55-gallon drums containing 12-in. diameter pipe components
- Two 55-gallon drums; one containing a 12-in. diameter pipe component and one containing a 6-in. diameter pipe component with the 6-in. impacting first.

One side-impact test was performed by dropping an uncertified but functional TRUPACT-II inner containment vessel (ICV) with a payload assembly, including a top layer of seven pipe overpacks containing 6-in. diameter pipe components and a bottom layer of seven pipe overpacks containing 12-in. diameter pipe components (Figure 4.1-3c and Figure 4.1-4). The drop demonstrated a worst case, since potential damage to the pipe overpacks would be less severe within the entire TRUPACT-II packaging, which includes 10 inches of impact-absorbing foam.

A leakage rate test using helium and a mass spectrometer leak detector was performed before and after each drop test to evaluate the containment provided by the pipe component. The pipe components used in the testing were fitted with leak-test ports to allow connection to the leak detector. The leak-test port is not a feature of the pipe component production model. To facilitate the test, the opening in the pipe component filter was sealed with vacuum putty. This allowed the gasket between the filter and the pipe component lid to be leak-tested. After the post-drop leak test, the filters were removed and an evaluation of filter performance was conducted by the filter manufacturer.

4.1.4 Results of Test Program for the Standard Pipe Overpack

The first test series was completed at Sandia National Laboratories/New Mexico in March 1995.³ Testing of the revised pipe component was completed at the same location in December 1996.⁴ There was no loss of containment in any drop test, and all pipe components had a leakage rate of less than 1×10^{-7} cc/sec. The filters showed no damage from the drop tests. Following the leak test, the filters were removed from the pipe components and verified by the filter manufacturer to have maintained undiminished flow and filtering characteristics in accordance with the requirements of Section 2.5 of the CH-TRAMPAC.

This page intentionally left blank.

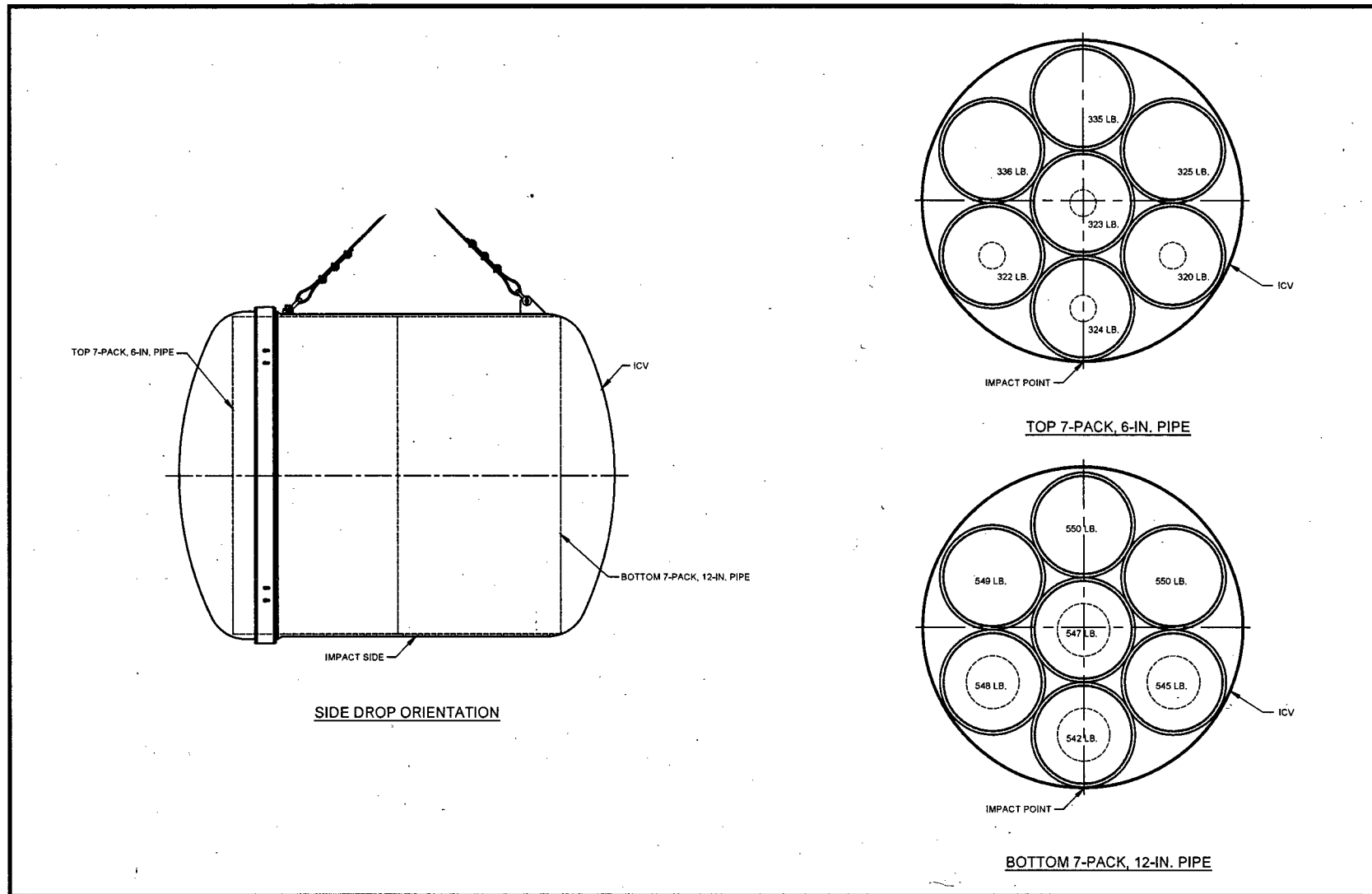


Figure 4.1-4 – Side Drop Configuration and Weights

This page intentionally left blank.

In the first test series, some of the bolts in the lids were observed to be loose upon post-test inspection of the two 6-in. diameter pipe components tested in the top-impact drop test. The cause of this anomaly was traced to the specification for bolt fabrication that allowed protruding die marks on the bearing surface of the bolts. During the top-impact drops, the protruding die marks cut into the surface of the pipe component lid causing a reduction of bolt tension. Although this irregularity did not affect the ability of the pipe components to maintain closure and pass the leak tests, the anomaly was corrected by modifying the specification for the screw-fasteners so that the result is a flat bearing-surface and uniform contact pressure.

The only other pipe overpack deformation observed during this test series was to the shielding plate of the 12-in. diameter pipe component lid. During the top-impact drop tests, the force of the pipe component contents pushed the shielding plate, which is located below the filter, closer to the lid surface. The shielding plate prevents radiation emission through the filter vent and protects the filter media from potential damage if impacted by the component contents. While these functions were not compromised by the movement of the shielding plate, the abnormality was corrected in the production 12-in. diameter pipe components.

The 6-in. diameter pipe component and the revised 12-in. diameter pipe component do not have shielding plates. The lids of these designs are thicker than that of the original 12-in. diameter pipe component design and encase the bottom portion of the filter vent opening. Therefore, the lids of the 6-in. diameter pipe component and the revised 12-in. diameter pipe component provide adequate shielding without the addition of shielding plates.

Additionally, the maximum axial drum crush observed during the end drop test was 3.98 in. and 3.63 in. for the 6-in. and 12-in. pipe overpacks, respectively. The maximum diametrical drum crush observed during the side drop test was 4.31 in. and 2.25 in. for the 6-in. and 12-in. pipe overpacks, respectively.

In summary, the results of the test program for the standard pipe overpack demonstrate that under hypothetical accident conditions, the 6-in. and 12-in. diameter pipe components (both original and revised designs) maintain containment of material and do not incur any damage (see Figure 4.1-5).

4.1.5 Structural Analysis of the Standard Pipe Overpack

The pipe component is constructed of grade 304 stainless steel. Protective fiberboard and plywood packing material is used to center the pipe component within a standard 55-gallon drum to constitute a pipe overpack. In the original testing, the 20 pipe components involved in the drop tests sustained no visible damage or deformation with the exception of the minor items noted in Section 4.1.4, which have been corrected. The 14 pipe components that were leak tested showed no loss in containment capability. The capability of the pipe components to maintain structural integrity during hypothetical accident testing is due to the design and material construction of the closures.

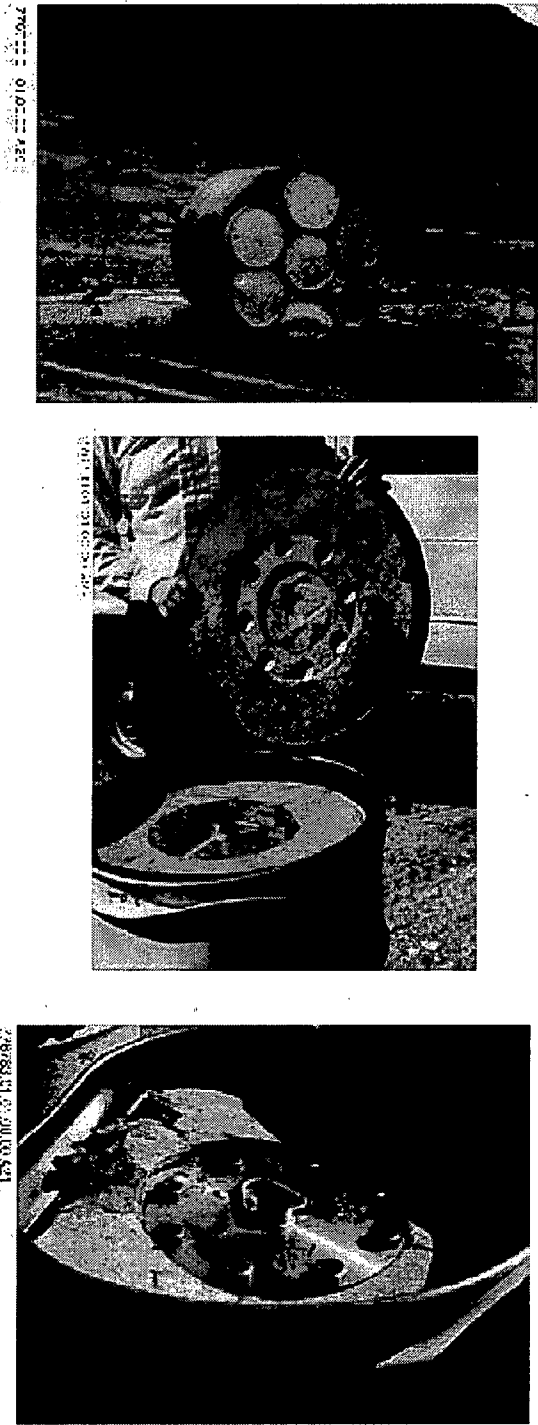


Figure 4.1-5 – Test Program Photographs of the Standard Pipe Overpack (Post-Test)

The observed maximum drum crush values reported in Section 4.1.4 result in idealized minimum right-circular cylinder dimensions for the 6-in. and 12-in. pipe overpacks of 18.19 in. outside diameter by 29.27 in. height and 20.25 in. outside diameter by 29.62 in. height, respectively, utilized in the criticality analysis summarized in Section 4.1.6.

A butyl rubber or ethylene propylene O-ring seals the lid to the pipe component body. Both O-ring materials have a sustained temperature capability of 250 degrees Fahrenheit (°F), which exceeds temperatures realized within the TRUPACT-II ICV during previous testing. Likewise, the neoprene gasket that seals the filter housing to the lid has a 250°F temperature capability. The filter design used in the pipe component functions within specifications at temperatures ranging from well below -40°F to over 280°F. The filters have been shown to survive independent drop tests and impact tests.⁸

4.1.6 Criticality Analysis of the Standard Pipe Overpack

A criticality analysis was performed for two different payload cases, depending on the quantities of special reflector materials in the payload container (see Chapter 6.0 of TRUPACT-II SAR or Chapter 6.0 of HalfPACT SAR for description of special reflector materials), as described below:

- Case E: For Case E, the contents of the pipe overpack payload container contain less than or equal to 1% by weight quantities of special reflector materials. The pipe overpack payload container may contain greater than 1% by weight quantities of special reflector materials provided that one of the following conditions is met:
 - The special reflector materials are chemically or mechanically bound to the fissile material such that no reconfiguration or release of the bond is possible under normal or accident conditions, or
 - The special reflector materials are present in thicknesses and/or packing fractions that render them less effective than a 25% polyethylene/75% water equivalent reflector per the limits in Table 6.2-1 of the TRUPACT-II or HalfPACT SAR.
- Case F: For Case F, the contents of the pipe overpack payload container contain greater than 1% by weight quantities of special reflector materials that do not meet the exceptions listed for Case E.

The criticality analysis demonstrates that a TRUPACT-II shipment of 14 pipe overpacks with contents meeting the requirements of Case E at 200 FGE of ²³⁹Pu each (for a total of 2,800 FGE per TRUPACT-II) or a HalfPACT shipment of 7 pipe overpacks with 200 FGE each (for a total of 1,400 FGE per HalfPACT) ensures compliance with the requirements of Title 10, Code of Federal Regulations (CFR), Sections 71.55 and 71.59 (10 CFR 71.55 and 71.59).⁹ Additionally, shipments of pipe overpacks with contents meeting the requirements of Case F at 140 FGE for each payload container and 980 and 1960 FGE per HalfPACT and TRUPACT-II, respectively,

⁸ Nuclear Filter Technology, Inc., February 1995. "The Effect of Extreme Temperatures, Impacts, and Vibrations on Nuclear Filter Technology, Inc.'s NucFil 013," Nuclear Filter Technology, Inc., Wheat Ridge, Colorado.

⁹ Packaging Technology, Inc., May 2004, "Pipe Overpack Criticality Analysis for the TRUPACT-II Package," ED-076, Packaging Technology, Inc., Tacoma, Washington.

ensure compliance with 10 CFR 71.55 and 71.59. Based on an infinite array of undamaged or damaged packages, the criticality transport index is 0.0.

The key parameters in the pipe overpack analysis for Case E are (1) the maximum fissile loading per pipe component is 200 FGE, (2) no more than 1% by weight quantities of special reflector materials are present or greater than 1% by weight quantities of special reflectors are either bound to the fissile material or meet the limits in Table 6.2-1 of the TRUPACT-II or HalfPACT SAR, (3) the spacing between the components (i.e., effective drum diameter) is reduced by the maximum amount reported in Section 4.1.5, and (4) the package arrays are infinite arrays stacked two high.

The key parameters in the pipe overpack analysis for Case F are (1) the maximum fissile loading per pipe component is 140 FGE, (2) the spacing between the components (i.e., effective drum diameter) is reduced by the maximum amount reported in Section 4.1.5, and (3) the package arrays are infinite arrays stacked two high.

The detailed analysis presented in Packaging Technology, 2004⁶, presents the results of a series of SCALE 4.4 CSAS25 module¹⁰ (KENO-Va version 4) calculations that establish a maximum system reactivity ($k_s + 2\sigma$) of less than 0.933 and the corresponding Upper Subcriticality Limit (USL) of 0.9377. Therefore, the shipment of 200 FGE or 140 FGE per pipe overpack for Cases E and F, respectively, in the TRUPACT-II and HalfPACT is safely subcritical.

4.1.7 Shielding Analysis of the Standard Pipe Overpack

The evaluation of compliance with the radiation dose rate limits for NCT and HAC required by 10 CFR §71.47 is presented in Chapter 5 of the TRUPACT-II and HalfPACT SARs^{1,2} for the standard pipe overpack payload configuration. When the TRUPACT-II and HalfPACT packages are loaded with assemblies of standard pipe overpacks containing gamma and/or neutron source terms that are limited per Section 3.3 of the CH-TRAMPAC³, the package meets the NCT radiation dose rate requirements of 200 mrem/hr at the surface of the package and 10 mrem/hr at 2 meters from the surface of the package under exclusive use. As a result, the packages also comply with the HAC dose rate requirement of 1 rem/hr at 1 meter from the surface of the package.

4.1.8 Authorized Payload Contents for the Standard Pipe Overpack

As demonstrated in Section 4.1.7, *Shielding Analysis of the Standard Pipe Overpack*, when loaded with gamma and/or neutron emitting isotopes with maximum activity limits summarized in the CH-TRAMPAC, the standard pipe overpack payload meets the NCT and HAC dose rate limits. As demonstrated in Section 4.1.6, *Criticality Analysis of the Standard Pipe Overpack*, when loaded with fissile material with maximum mass limits summarized for Cases E and F, the standard pipe overpack payload meets the calculated reactivity limit and is safely subcritical.

¹⁰ SCALE4.4., "Modular Code System for Performing Standardized Computer Analyses for Licensing Evaluation for Workstations and Personal Computers," RSICC code package C00545/MNYCP00, Oak Ridge National Laboratory, September 1998.

4.1.9 Conclusion

The standard pipe overpack consists of a pipe component positioned by dunnage within a 55-gallon drum with a rigid liner and lid. The tests and analyses summarized by this appendix demonstrate the ability of the pipe overpack to provide three significant control functions: (1) criticality control, (2) shielding, and (3) containment of fine particulate waste material during normal conditions of transport and hypothetical accident conditions.

The primary purpose of the pipe overpack is to allow the shipment of up to 7 pipe overpacks in a HalfPACT or up to 14 pipe overpacks in a TRUPACT-II, each with a maximum FGE loading of 200 g for payloads with contents meeting the requirements for Case E and 140 g for payloads with contents meeting the requirements for Case F. The results of the criticality analyses show that a payload of pipe overpacks is subcritical in all cases. As determined by the criticality analyses, the FGE limit is 2,800 g per TRUPACT-II and 1,400 g per HalfPACT for Case E shipments of waste packaged in standard pipe overpacks and 1,960 g per TRUPACT-II and 980 g per HalfPACT for Case F shipments of waste packaged in standard pipe overpacks.

The shielding evaluation shows that, when the standard pipe overpack is in compliance with the maximum activity limits summarized in the CH-TRAMPAC, the dose rate limits for NCT and HAC are met.

This page intentionally left blank.

APPENDIX 4.2

DESCRIPTION OF S100 PIPE OVERPACK

This page intentionally left blank.

4.2 Description of S100 Pipe Overpack

4.2.1 Introduction

The S100 pipe overpack is based closely on the standard pipe overpack described in Appendix 4.1 of the CH-TRU Payload Appendices. It differs from the standard pipe overpack in that most of the cane fiberboard dunnage is replaced with neutron shielding material. In addition, neutron shielding material is placed within the pipe component, above, below, and around the payload. It is intended for the shipment of sealed neutron sources in the TRUPACT-II and the HalfPACT. Appendix 1.3.1 of the TRUPACT-II Safety Analysis Report (SAR), Appendix 1.3.1 of the HalfPACT SAR, and Section 2.9.3 of the Contact-Handled Transuranic Waste Authorized Methods for Payload Control (CH-TRAMPAC) describe the materials of construction, size, and other dimensional specifications for the S100 pipe overpack. Up to 14 S100 pipe overpacks may be shipped in the TRUPACT-II, and up to 7 S100 pipe overpacks may be shipped in the HalfPACT. This appendix describes the structural, criticality, and shielding basis of the S100 pipe overpack.

4.2.2 Description

The S100 pipe overpack consists of a 6-inch (in.) pipe component surrounded by neutron shielding material on the sides and by cane fiberboard and plywood dunnage on the top and bottom, within a 55-gallon drum with a rigid polyethylene liner and lid. A schematic of the S100 pipe overpack is shown in Figure 4.2-1. The 6-in. pipe component used in the S100 pipe overpack is identical to the 6-in. pipe component used in the standard pipe overpack described in Appendix 4.1 of the CH-TRU Payload Appendices. Furthermore, the pipe component is placed within the drum, using the same type of cane fiberboard and plywood dunnage below the lower surface of the pipe component and above the upper surface of the pipe component. The space around the sides of the pipe component is filled with a neutron shielding material. The neutron shield may be in the form of a casting (such as a commercial neutron shielding casting compound), a solid monolith (such as a molded or machined unit of solid plastic), or fabricated component (such as a tightly wound roll of plastic film or other built-up fabrication). The minimum properties of the neutron shielding material are given in Section 4.2.6. The neutron shield extends from the lower edge of the pipe component up to the top surface of the lid of the pipe component, and rests on the lower plywood dunnage. The S100 Pipe Overpack is shown in Figure 4.2-1. To provide shielding for the top and bottom of the pipe component, rigid high-density polyethylene plugs approximately 6 in. in diameter and 6.5 in. long are placed below the payload (in the bottom of the pipe component), and above the payload (below the lid of the pipe component) as shown in Figure 4.2-1. A rigid high-density polyethylene shield sleeve is placed between the two end plugs, as shown in Figure 4.2-1.

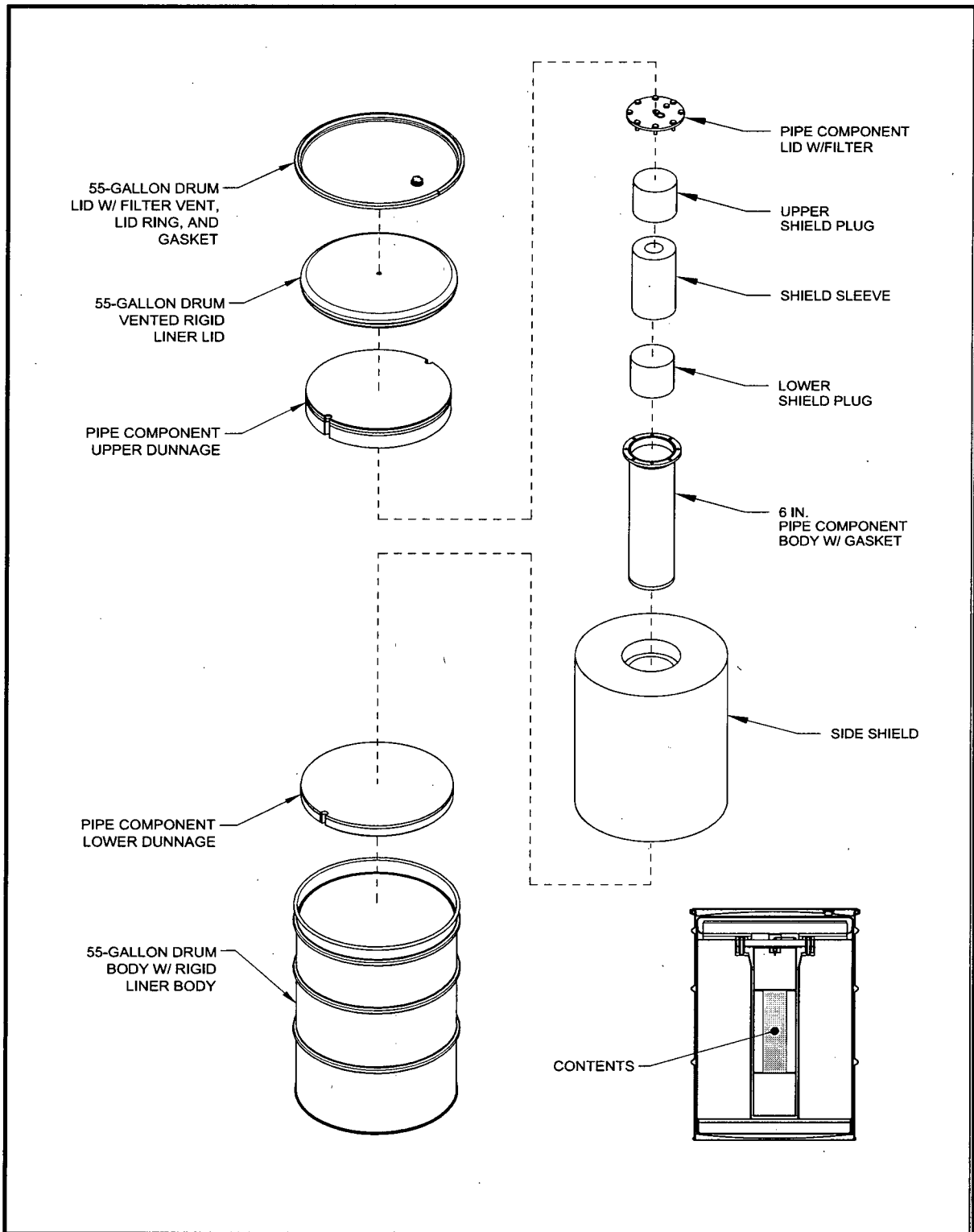


Figure 4.2-1 — S100 Pipe Overpack

The pipe component is a stainless steel, cylindrical pipe of 0.280 in. nominal thickness with a welded or formed bottom cap and a bolted stainless steel lid sealed with a butyl or ethylene-propylene rubber O-ring. The pipe component is approximately 2 feet (ft.) long and has an inner diameter of 6 in. The S100 pipe component is identical to the description of the standard 6-in. pipe component, including the filter vent, found in Appendix 4.1 of the CH-TRU Payload Appendices. The S100 pipe component provides three significant control functions: 1) criticality, 2) shielding, and 3) confinement of the payload. The S100 pipe overpack is designed for the transport of specific sealed neutron source waste forms. The following sections demonstrate the effectiveness of the S100 pipe overpack design for normal conditions of transport (NCT) and hypothetical accident conditions (HAC). All demonstrations are by analysis or by reference to the standard pipe overpack, unless stated otherwise.

4.2.3 Structural Analysis for Normal Conditions of Transport

Under NCT, the S100 pipe overpack remains leaktight and retains the sealed neutron sources within the pipe component. Since the pipe component remains leaktight under HAC as demonstrated in Section 4.2.4, this bounds all NCT, and demonstrations specific to NCT are not necessary.

The maximum damage that could occur to the shielding material in a normal condition free drop is evaluated as follows. As specified in Section 2.9.3 of the CH-TRAMPAC, the maximum weight of the loaded S100 pipe overpack is 550 pounds (lbs). The normal condition free drop height is 3 ft., or 36 in. The maximum damage to the shielding by crush deformation occurs in the side drop orientation. In this orientation, the weight of five of the drums in one layer may be conservatively assumed to be supported by a single drum in the lowest position as shown in Figure 4.2-2. (The two drums on either side of the lowest position each support their own weight.) A determination of crush distance is found by conservatively assuming that 25% of the drop energy of five drums is absorbed by the crush of the neutron absorbing material on one side of the lowest drum, where the percentage of energy absorbed by the neutron absorbing material is derived in Section 4.2.4. The drop energy (E), measured in inch-pounds (in.-lbs), to be absorbed by the neutron shield is:

$$E = 0.25 * (550 \text{ lbs} * 5 * 36 \text{ in.}) = 24,750 \text{ in. - lbs}$$

At the maximum payload temperature of 170°F, the minimum crush strength of the neutron shielding material is $\sigma = 300$ pounds per square inch (psi). Therefore, to absorb this energy, the volume (V), measured in cubic inches (in³), of crushed material is:

$$V = \frac{E \text{ in. - lbs}}{\sigma \text{ psi}} = 82.50 \text{ in}^3$$

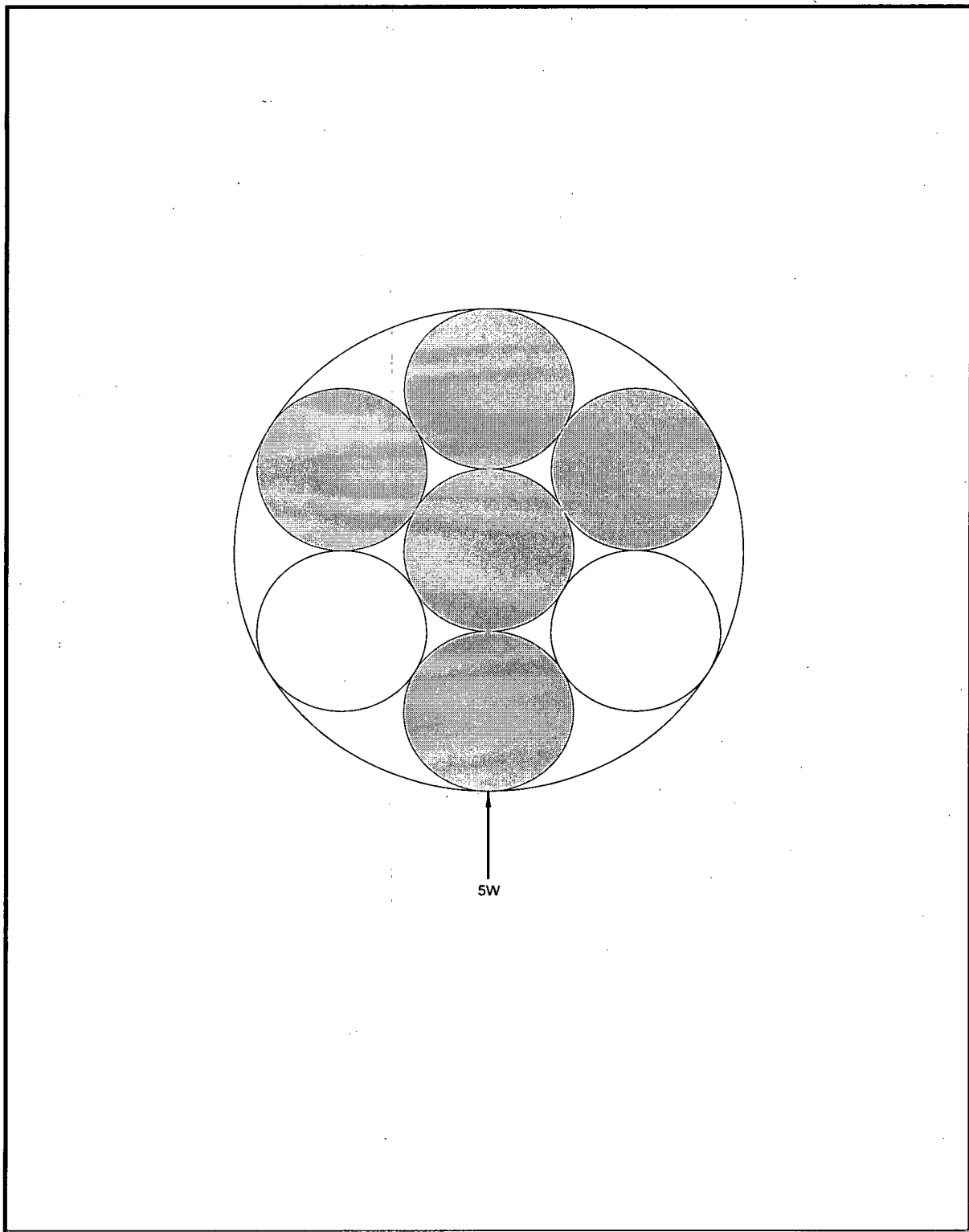


Figure 4.2-2 — NCT Side Drop Drum Loading Diagram

The volume is in the form of a segment of a cylinder having a length equal to the length of the neutron shielding material, or $L = 26.7$ in. The area (A) of the segment is therefore

$$A = \frac{V \text{ in}^3}{L \text{ in.}} = 3.08 \text{ in}^2$$

Based on the area of the circular segment and on the outer diameter of the shield material of 21.5 in., the depth of crush is computed to be 0.63 in. A conservative value of 2 inches is used in the normal condition shielding analysis discussed in Section 4.2.6 of this appendix.

As an alternative to specifying the shielding material crush strength, a test of the full-scale shielding component may be performed. The test shall demonstrate that the shield is capable of absorbing an amount of energy equal to 24,750 in-lbs with 2 in. or less of radial deformation. The energy absorbed may be calculated by integration of the force-deflection curve or other equivalent means. The test must be performed with a material temperature of at least 170°F.

If cast neutron shielding material is used, some moisture may be hydrated by the material upon solidification. At the maximum payload container temperature of 170°F, this moisture could produce a partial pressure of only 6 psi absolute, which would be the case for any moist payload. Therefore, the shielding material does not cause the pressure within the ICV to exceed the bounding maximum value of 61.2 psi absolute given in Section 2.6 of the TRUPACT-II and HalfPACT SARs.

4.2.4 Structural Analysis for Hypothetical Accident Conditions

Under HAC, the S100 pipe overpack remains leaktight and retains the sealed neutron sources within the pipe component. It is shown in Section 4.2.6 that an adequate level of biological shielding for HAC is achieved without any aid from the shielding in the S100 pipe overpack. Since the shielding in the S100 pipe overpack is not required for the HAC shielding analysis, the damage to the shielding material in the accident free drop does not need to be quantified. However, the reduced effective drum diameter, which prescribes the resultant pipe component spacing utilized in the criticality analysis, does need to be quantified.

To demonstrate that the pipe component remains leaktight and retains the sealed neutron sources within the pipe component in a 30 ft. free drop, reference is made to the testing of the Standard Pipe Overpack, as documented in Appendix 4.1 of the CH-TRU Payload Appendices. To account for design differences of the S100 Pipe Overpack, an additional test was performed, as documented below. Normal conditions of transport are bounded by these tests.¹

The testing of the Standard Pipe Overpack, as documented in Appendix 4.1 of the CH-TRU Payload Appendices, consisted of two types of tests: 1) end drop testing, in which a stacked

¹ Packaging Technology, Inc., July 2002, "30' Free Drop Test Report for the S100 Overpack," TR-013, Packaging Technology, Inc., Tacoma, Washington.

arrangement of drums was dropped from a height of 30 ft. in an end drop orientation, i.e., along the axis of the drums, and 2) side drop testing, in which a bare TRUPACT-II ICV filled with test drums was dropped from 30 ft. in a horizontal orientation. Since, in the S100 design, the energy absorbing configuration at each axial end of the pipe component is identical to the Standard Pipe Overpack design, it was not necessary to repeat the end drop testing. In the side drop testing, however, the load path is through the material that is placed around the sides of the pipe component. In the prior Standard Pipe Overpack testing, this material was Celotex dunnage, and in the S100, it is made of neutron shielding material, which could have a different force-deflection behavior than the dunnage. Therefore, to clearly demonstrate that the S100 remains leaktight under hypothetical accident conditions, an additional drop test was performed.

The test consisted of a drop of a single, bare S100 package from a height of 30 ft. in a horizontal orientation onto an essentially unyielding surface. This test was conservative relative to a hypothetical accident drop inside a TRUPACT-II, since it neglected all of the impact absorption ability of the TRUPACT-II, and consequently, the impact was much higher. In addition, it was not necessary to place any weight on top of the S100 to represent the weight of the 'overburden' of drums ordinarily present within the ICV in a side drop orientation. This is because the effect of 'overburden' drums was conservatively included in the Standard Pipe Overpack drop testing using the 12-in. pipe component as follows:

- The 12-in. pipe version of the Standard Pipe Overpack weighed 547 lbs, which is essentially the same weight as the S100 at 550 lbs, and therefore the 'overburden' loading is equivalent;
- The 12-in. pipe component had a smaller nominal wall thickness and larger diameter than the 6-in. pipe component used in the S100, and thus was more liable to deformation under a given load;
- The 12-in. pipe component was surrounded by approximately 4.2 inches of Celotex dunnage, while the 6-in. pipe component in the S100 was surrounded by approximately 7 inches of neutron shielding, thus affording greater protection from the 'overburden' loads.

The test of the S100 focused, therefore, on the deceleration forces imposed on the 6-in. pipe component due to impact. Since the shielding material is generally stronger than the Celotex dunnage used to surround the 6-in. pipe component in the Standard Pipe Overpack, the impact forces on the pipe component in the S100 could be greater in a hypothetical accident free drop. Since the S100 is dropped bare, without any energy absorption materials present except the shield itself, it is very conservative compared to conditions within a complete TRUPACT-II or HalfPACT.

A helium mass spectrometer leakage rate test was performed before and after the drop test to evaluate the containment provided by the pipe component. There was no loss of leaktight containment as a result of the drop test. The leakage rate of the S100 pipe component after the 30 ft. drop was less than 1×10^{-7} cubic centimeters per second, air. In addition, the function of the filter vent in the lid of the pipe component was unimpaired, as verified by the filter manufacturer after the test.

The maximum radial crush of the S100 pipe overpack and the resulting minimum effective drum diameter from a 30 ft. free drop is determined by comparison of the crush strength and energy absorbing properties of the S100 Pipe Overpack's side neutron shield material and the 6-in. Standard Pipe Overpack's Celotex dunnage. The comparison demonstrates that the side neutron shield material will see less deformation than the Celotex material such that the maximum radial crush and resulting minimum effective drum diameter of 4.31 in. and 18.19 in., respectively observed in the 6-in. Standard Pipe Overpack drop testing and used in the S100 Pipe Overpack criticality analysis is conservative. The following analysis determines the percentage of total drop energy absorbed by the Celotex dunnage in the 6-in. Standard Pipe Overpack 30 ft. side drop.

Following the side drop crush logic provided in Section 4.2.3, the total drop energy from a 30 ft. side drop of an array of 6-in. standard pipe overpacks with a maximum weight of 328 lbs each (as specified in Section 2.9.2 of the CH-TRAMPAC) is given as follows:

$$E_{TOT} = (328 \text{ lbs} * 5 * 360 \text{ in.}) = 590,400 \text{ in.} - \text{lbs}$$

The actual energy absorbed by the Celotex dunnage in the lower drum can be determined from the measured radial drum crush value of 4.31 in. Based on the depth of crush and the outer diameter of the Celotex material of 21.5 in, the area (A) of the circular segment is computed to be 51.86 in². The crushed volume is in the form of a segment of a cylinder having a length equal to the length of the Celotex material, or L = 26.7 in. The crushed volume (V) is therefore

$$V = A \text{ in}^2 * L \text{ in.} = 1,384.66 \text{ in}^3$$

Based on the average plateau crush strength of Celotex at 150 °F of 90 psi², the actual energy (E) absorbed by the Celotex dunnage is

$$E_{ACT} = V \text{ in}^3 * \sigma \text{ psi} = 124,619 \text{ in.} - \text{lbs}$$

Therefore, the percentage of total to absorbed energy (f) is given as

$$f = \frac{E_{ACT}}{E_{TOT}} * 100 = 21\%$$

A conservative percentage of 25% is utilized in both the NCT and HAC crush determinations for the neutron shield material in the S100 pipe overpack. Accounting for the increased weight of the loaded S100 pipe overpack over that of the 6-in. standard pipe overpack and taking into

² Walker, M.S., January 1991, "Packaging Materials Properties Data", Y/EN-4120, Martin Marietta Energy Systems, Inc., Oak Ridge, Tennessee.

account the fraction of total energy absorbed, the energy absorbed by the neutron shield material in a 30 ft. drop is given as follows:

$$E = 0.25 * (550 \text{ lbs} * 5 * 360 \text{ in.}) = 247,500 \text{ in. - lbs}$$

Following the calculational methodology employed for the NCT case with the minimum crush strength of the neutron shield material of $\sigma=300$ psi at 170°F, the resulting maximum depth of crush of the neutron shield material is 3.01 in. where $V=825.00 \text{ in}^3$, $A=30.90 \text{ in}^2$, and $L=26.7$ in. Thus, the crush depth of neutron shielding material in the S100 pipe overpack is less than that observed for the 6-in. standard pipe overpack.

As an alternative to specifying the shielding material crush strength, a test of the full-scale shielding component may be performed. The test shall demonstrate that the shield is capable of absorbing an amount of energy equal to 247,500 in-lbs with 4 in. or less of radial deformation. The energy absorbed may be calculated by integration of the force-deflection curve or other equivalent means. The test must be performed with a material temperature of at least 170°F. This energy absorption requirement is in addition to that specified for the NCT requirements (i.e., 24,750 in-lbs with 2 in. or less of radial deformation).

4.2.5 Criticality Analysis

A criticality analysis was performed for two different payload cases, depending on the quantities of special reflector materials in the payload container (see Chapter 6.0 of TRUPACT-II SAR or Chapter 6.0 of HalfPACT SAR for description of special reflector materials), as described below:

- Case E: For Case E, the contents of the pipe overpack payload container contain less than or equal to 1% by weight quantities of special reflector materials. The pipe overpack payload container may contain greater than 1% by weight quantities of special reflector materials provided that one of the following conditions is met:
 - The special reflector materials are chemically or mechanically bound to the fissile material such that no reconfiguration or release of the bond is possible under normal or accident conditions, or
 - The special reflector materials are present in thicknesses and/or packing fractions that render them less effective than a 25% polyethylene/75% water equivalent reflector per the limits in Table 6.2-1 of the TRUPACT-II or HalfPACT SAR.
- Case F: For Case F, the contents of the pipe overpack payload container contain greater than 1% by weight quantities of special reflector materials that do not meet the exceptions listed for Case E.

The criticality analysis demonstrates that a TRUPACT-II shipment of 14 pipe overpacks with contents meeting the requirements of Case E at 200 FGE of ^{239}Pu each (for a total of 2,800 FGE per TRUPACT-II) or a HalfPACT shipment of 7 pipe overpacks with 200 FGE each (for a total of 1,400 FGE per HalfPACT) ensures compliance with the requirements of Title 10, Code of

Federal Regulations (CFR), Sections 71.55 and 71.59 (10 CFR 71.55 and 71.59).³ Additionally, shipments of pipe overpacks with contents meeting the requirements of Case F at 140 FGE for each payload container and 980 and 1960 FGE per HalfPACT and TRUPACT-II, respectively, ensure compliance with 10 CFR 71.55 and 71.59. Based on an infinite array of undamaged or damaged packages, the criticality transport index is 0.0.

The key parameters in the pipe overpack analysis for Case E are (1) the maximum fissile loading per pipe component is 200 FGE, (2) no more than 1% by weight quantities of special reflector materials are present or greater than 1% by weight quantities of special reflectors are either bound to the fissile material or meet the limits in Table 6.2-1 of the TRUPACT-II or HalfPACT SAR, (3) the spacing between the components (i.e., effective drum diameter) is reduced by the maximum amount reported in Section 4.2.4, and (4) the package arrays are infinite arrays stacked two high.

The key parameters in the pipe overpack analysis for Case F are (1) the maximum fissile loading per pipe component is 140 FGE, (2) the spacing between the components (i.e., effective drum diameter) is reduced by the maximum amount reported in Section 4.2.4, and (3) the package arrays are infinite arrays stacked two high.

The detailed analysis presented in Packaging Technology, 2004³, presents the results of a series of SCALE 4.4 CSAS25 module⁴ (KENO-Va version 4) calculations that establish a maximum system reactivity ($k_s + 2\sigma$) of less than 0.933 and the corresponding Upper Subcriticality Limit (USL) of 0.9377. Therefore, the shipment of 200 FGE or 140 FGE per pipe overpack for Cases E and F, respectively, in the TRUPACT-II and HalfPACT is safely subcritical.

4.2.6 Shielding Analysis

The payload of the S100 pipe overpack consists of neutron-emitting, actinide-bearing sealed sources, shown in Table 4.2-1. Source terms used in this analysis are for neutron emission and spectra for alpha-n reactions calculated by the SOURCES Version 4A computer code.⁵ Of the sources shown in the table, the ²³⁸Pu Be was determined to be the governing source for shielding calculations,⁶ since it had the highest calculated unshielded dose rate of all the sources that will be transported in the S100.

³ Packaging Technology, Inc., May 2004, "Pipe Overpack Criticality Analysis for the TRUPACT-II Package," ED-076, Packaging Technology, Inc., Tacoma, Washington.

⁴ SCALE4.4., "Modular Code System for Performing Standardized Computer Analyses for Licensing Evaluation for Workstations and Personal Computers," RSICC code package C00545/MNYCP00, Oak Ridge National Laboratory, September 1998.

⁵ Wilson, W.B., R.T. Perry, W. Charlton, et al., 1999, "SOURCES 4A: A Code for Calculating (alpha, n) Spontaneous Fission, and Delayed Neutron Sources and Spectra," LA-13639-MS, Los Alamos National Laboratory, Los Alamos, New Mexico.

⁶ Gogol, S.L., and J. R. Bland, August 2002, "A Comparison of Dose Rates from (alpha, n) and Spontaneous Fission Neutron Sources," LA-UR-02-5120, Los Alamos National Laboratory, Los Alamos, New Mexico.

Table 4.2-1 S100 Pipe Overpack Payloads

$^{241}\text{Am Be}$	$^{238}\text{Pu O}$	$^{239}\text{Pu Li}$	^{241}Am
$^{238}\text{Pu Be}$	$^{239}\text{Pu O}$	$^{238}\text{Pu B}$	^{238}Pu
$^{239}\text{Pu Be}$	$^{244}\text{Cm O}$	$^{239}\text{Pu F}$	^{239}Pu
$^{241}\text{Am O}$	$^{241}\text{Am Li}$	$^{238}\text{Pu }^{13}\text{C}$	^{244}Cm

The radiation generated by the payload is in the form of neutrons and a relatively small amount of gamma radiation. Some additional gamma radiation is generated by capture of thermal neutrons in the neutron shielding. However, the gamma radiation remains a small fraction of the neutron radiation level.

Neutron shielding is afforded by placement of the pipe component within an annulus of shielding material, having an inner diameter of 7 in. and an outer diameter of 21.5 in. (conservatively neglecting the thickness of the drum poly liner). The side neutron shielding extends along the entire length of the pipe component as shown in Figure 4.2-1. The upper and lower shield plugs (6 in. in diameter and 6.5 in. long) and shield sleeve are made of solid high-density polyethylene and are placed within the pipe component. The side neutron shield may be in the form of a casting (such as a commercial neutron shielding casting compound), a solid monolith (such as a molded or machined unit of solid plastic), or fabricated component (such as a tightly wound roll of plastic film or other built-up fabrication). None of the materials of construction of the S100 pipe overpack, including the neutron shielding material, generate hydrogen gas in excess of 10^{-10} moles hydrogen per second per liter of headspace as a consequence of neutron or gamma irradiation by the payload sources.⁷ A combination of the neutron shielding material and the materials of construction of the S100 pipe overpack provide sufficient shielding for both neutron and gamma radiation.

Any material used for the side neutron shield must meet minimum requirements for neutron attenuation and mechanical strength. Neutron attenuation must be at least as good as the reference material, which has an atomic fraction composition of 0.667 hydrogen and 0.333 carbon. A test shall be performed on any alternate materials used for the side shield assembly. The test sample, neutron source, test setup, and acceptance criteria shall be defined in a test specification. The acceptance criteria shall be that the measured neutron attenuation of the equivalent shielding material shall be equal to or greater than the attenuation predicted for the reference material, using the actual test setup and the shielding analysis code.

The side neutron shielding material will have a minimum mechanical strength at a temperature of 170°F. The strength shall be defined as a minimum unit compressive crush strength of 300 psi. Alternatively, it may be defined as a maximum radial deformation of the full-scale shielding component under compressive load. The component must absorb a minimum of 24,750 in-lb. of

⁷ Bustos, L.D., W.F. Sandoval, R. Villarreal, and L.R. Field, October 2000, "Hydrogen Generation Rate Potential from Neutron and Gamma Ray Interactions with Shielding/Packaging Materials Contained in the S100 Pipe Component Overpack," Los Alamos National Laboratory, Los Alamos, New Mexico.

energy with a maximum deformation of 2 in. and a minimum of 247,500 in.-lb. of energy with a maximum deformation of 4 in., when loaded between the inner dimensions and outer dimensions of the component. Equivalent materials will not generate hydrogen gas in excess of 10^{-10} moles hydrogen per second per liter of headspace gas as a consequence of neutron or gamma irradiation.

Dose rate calculations were performed for a single S100 pipe overpack and for a TRUPACT-II in both the as-loaded and post-NCT free drop configurations.⁸ The results were used to determine the maximum loading of the S100 pipe overpack such that the regulatory dose rate limits will be met in each case for NCT and HAC. In the analysis, the bounding payload of ²³⁸Pu Be was used, as discussed above. Source gamma radiation was negligible and was not included, but capture gamma dose rate contribution was included in the calculated integrated dose rate. Dose rate calculations were made for a single S100 pipe overpack as presented for loading into a TRUPACT-II, for a TRUPACT-II as presented for transport with a payload of 14 identical S100 pipe overpacks each having the maximum payload, and for a TRUPACT-II including a conservative representation of NCT free drop damage with a payload of 14 identical S100 pipe overpacks each having the maximum payload. (The HAC case is discussed below.) Dose rates were calculated at the surface and at defined distances from the containers as shown in Table 4.2-2. As shown in the table, the limiting dose is for the TRUPACT-II package including NCT free drop damage, and is equal to 10 mrem/hr at a distance of 2 meters from the package surface. The corresponding S100 pipe overpack surface dose limit is 179 mrem/hr. This means that, as long as the surface dose rate of any S100 pipe overpack transported in a TRUPACT-II is at or below 179 mrem/hr, then the dose rate external to the TRUPACT-II will not exceed 10 mrem/hr at 2 meters including NCT free drop damage, nor will any of the other, less governing regulatory limits be exceeded. The TRUPACT-II calculations govern the case of the HalfPACT. Each S100 pipe overpack will be surveyed before loading into a TRUPACT-II or HalfPACT to ensure compliance with the limiting surface dose rate of 179 mrem/hr, as given in Section 3.2 of the CH-TRAMPAC.

The damage to the TRUPACT-II and payload under NCT is assumed to occur in the 3 ft. side drop, and is discussed in Section 4.2.3. The drums are modeled as resting on the inside of the TRUPACT-II ICV, which is resting on its side, and the bottom drum is crushed by a bounding distance of 2 in. The 2 in. of crushed shielding is conservatively assumed to be lost.

⁸ Packaging Technology, Inc., August 2002, "Dose Rate Calculations for the S100 Pipe Overpack," ED-071, Packaging Technology, Inc., Tacoma, Washington.

Table 4.2-2 Maximum Dose Rates for S100 Pipe Overpack and TRUPACT-II

	Maximum Dose Rate (mrem/hr)	Limits (mrem/hr)④
S100 Surface	179 ±0.82	200
TRUPACT-II side Surface (undamaged) ①②	58.0 ±0.85	200
TRUPACT-II 2 meters (undamaged)	7.33 ±0.14	10
TRUPACT-II 5 meters (undamaged)③	1.76 ±0.04	2
TRUPACT-II side Surface (damaged)	128 ±1.4	200
TRUPACT-II 2 meters (damaged)	9.85 ±0.15	10

Notes:

1. TRUPACT-II contains 14 identical S100 pipe overpacks, each with a maximum surface dose rate of 179 mrem/hr or less.
2. Side dose rate governs over top or bottom dose rates.
3. The 5 meter distance corresponds to the normally occupied space of the truck cab.
4. Limits established by CH-TRAMPAC (S100 surface) or 10 CFR 71.47(b) (TRUPACT-II).

For HAC, the drums, neutron shielding material, pipe components, and internal dunnage are conservatively removed from consideration in the shielding calculation, and the sum total of all activity in the S100 payload is concentrated as a single point source resting on the inside surface of the TRUPACT-II ICV. In accordance with 10 CFR 71.51(a)(2), the dose point is located 1 meter from the external surface of the package. This is equivalent to a total distance from the source of 1 meter plus the minimum crushed wall thickness of the TRUPACT-II or HalfPACT. For simplicity and conservatism, the calculations assume that there is no material of any kind between the source and the dose point. The crushed wall thickness is found by subtracting the HAC 30-foot free drop side orientation crush damage from the original wall thickness of the package as follows. The outer diameter of the package is 94.38 inches, and the inner diameter of the ICV is 73.63 inches, which gives an undamaged wall thickness of 10.38 inches. The maximum crush damage is found in Table 2.10.3-1 of the TRUPACT-II SAR for Test No. 2, as equal to 3.63 inches. The remaining wall thickness is then equal to $10.38 - 3.63 = 6.75$ inches. In the shielding calculations, a value of 6.5 inches is conservatively used. As already discussed, no material is assumed to fill this space. The resulting maximum allowable activity within the TRUPACT-II is a total of 406 Ci, and the resulting conservative dose rate is 999 mrem/hr at 1 meter from the crushed TRUPACT-II surface, which meets the requirements of 10 CFR 71.51(a)(2). As for NCT, the TRUPACT-II HAC calculations govern the case of the HalfPACT.

4.2.7 Authorized Payload Contents

As demonstrated in Section 4.2.6, when loaded with sealed neutron sources of the types specified in Table 4.2-1 (the authorized contents), the S100 pipe overpack meets all regulatory dose rate limits. The bounding payload is defined in three ways: (1) a maximum dose rate on the surface of the S100 pipe overpack of 179 mrem/hr for any S100 pipe overpack placed into the TRUPACT-II or HalfPACT, (2) a maximum activity of 406 Ci within a single TRUPACT-II or HalfPACT, and (3) a maximum payload of 200 FGE per S100 pipe overpack, or a total of 2,800 FGE per TRUPACT-II or 1,400 FGE per HalfPACT when the contents meet the requirements of Case E, or (4) a maximum payload of 140 FGE per S100 pipe overpack, or a total of 1,960 FGE per TRUPACT-II or 980 FGE per HalfPACT when the contents meet the requirements of Case F. Section 4.2.5 demonstrates that 200 FGE per S100 pipe overpack is safely subcritical for Case E shipments and that 140 FGE per S100 pipe overpack is safely subcritical for Case F shipments.

4.2.8 Conclusion

The S100 pipe overpack design is based on the standard pipe overpack. It consists of a 6-in. pipe component within a 55-gallon drum, including a rigid liner and lid. Dunnage is placed above and below the pipe component, and neutron shielding material is placed on the sides of the component. Within the pipe component are placed rigid high-density polyethylene shield plugs and insert. The analyses summarized in this appendix demonstrate the ability of the S100 pipe overpack to provide three significant control functions under NCT and HAC: (1) criticality, (2) shielding, and (3) confinement of the payload.

The primary purpose of the S100 pipe overpack is to allow the shipment of sealed neutron sources of the types listed in Table 4.2-1. The structural analysis shows that the pipe component remains leaktight and the neutron sources remain confined within the pipe component in conservatively bounded normal and accident free drops. For criticality, it is shown that 200 FGE per S100 pipe overpack for Case E payloads is safely subcritical and 140 FGE per S100 pipe overpack is safely subcritical for Case F payloads. The shielding analysis shows that, with the maximum authorized contents, the dose rate limits for NCT and HAC (including appropriate shielding damage assumptions in each case) are met.

This page intentionally left blank.

APPENDIX 4.3

DESCRIPTION OF S200 PIPE OVERPACK

This page intentionally left blank.

4.3 Description of S200 Pipe Overpack

4.3.1 Introduction

The S200 pipe overpack is based closely on the standard pipe overpack described in Appendix 4.1 of the CH-TRU Payload Appendices. It differs from the standard pipe overpack through the addition of a gamma shield insert located by dunnage inside the pipe component. It is intended for the shipment of transuranic waste forms with high gamma energies in the TRUPACT-II and HalfPACT. Appendix 1.3.1 of the TRUPACT-II Safety Analysis Report (SAR), Appendix 1.3.1 of the HalfPACT SAR, and Section 2.9.4 of the Contact-Handled Transuranic Waste Authorized Methods for Payload Control (CH-TRAMPAC) describe the materials of construction, sizes, and other dimensional specifications for the S200 pipe overpack. Up to 14 S200 pipe overpacks may be shipped in the TRUPACT-II, and up to 7 S200 pipe overpacks may be shipped in the HalfPACT. This appendix describes the structural, criticality, and shielding basis of the S200 pipe overpack.

4.3.2 Description

The S200 pipe overpack consists of a gamma shield insert located by rigid polyurethane foam dunnage inside a standard 12-inch (in.) pipe component which is, in turn, located by cane fiberboard and plywood dunnage within a standard 55-gallon drum with a rigid polyethylene liner and lid. A schematic of the S200 pipe overpack is shown in Figure 4.3-1. The 12-in. pipe component, cane fiberboard and plywood dunnage, and 55-gallon drum with rigid polyethylene liner and lid are identical to the standard pipe overpack described in Appendix 4.1 of the CH-TRU Payload Appendices.

The gamma shield insert is a lead two-component assembly consisting of a cylindrical body with an integral bottom cap and a detachable lid. The shield insert is available in two sizes; the S200-A shield insert has a nominal thickness of 1.000 in. and the S200-B shield insert has a nominal thickness of 0.600 in. The overall dimensions of the S200-A and S200-B shield inserts are nominally 10.125 in. diameter by 10.625 in. long and 9.325 in. diameter by 17.825 in. long, respectively. The rigid polyurethane foam dunnage fills the bottom and annular space between the shield insert and the 12-in. pipe component to position the insert near the lid of the pipe component.

The pipe component provides three significant control functions: (1) criticality control, (2) shielding, and (3) confinement of the waste material. Additionally, the gamma shield insert also provides a shielding control function. The following sections demonstrate the effectiveness of the S200 pipe overpack design for normal conditions of transport (NCT) and hypothetical accident conditions (HAC). All demonstrations are by analysis or by reference to the standard pipe overpack analysis and testing, unless stated otherwise.

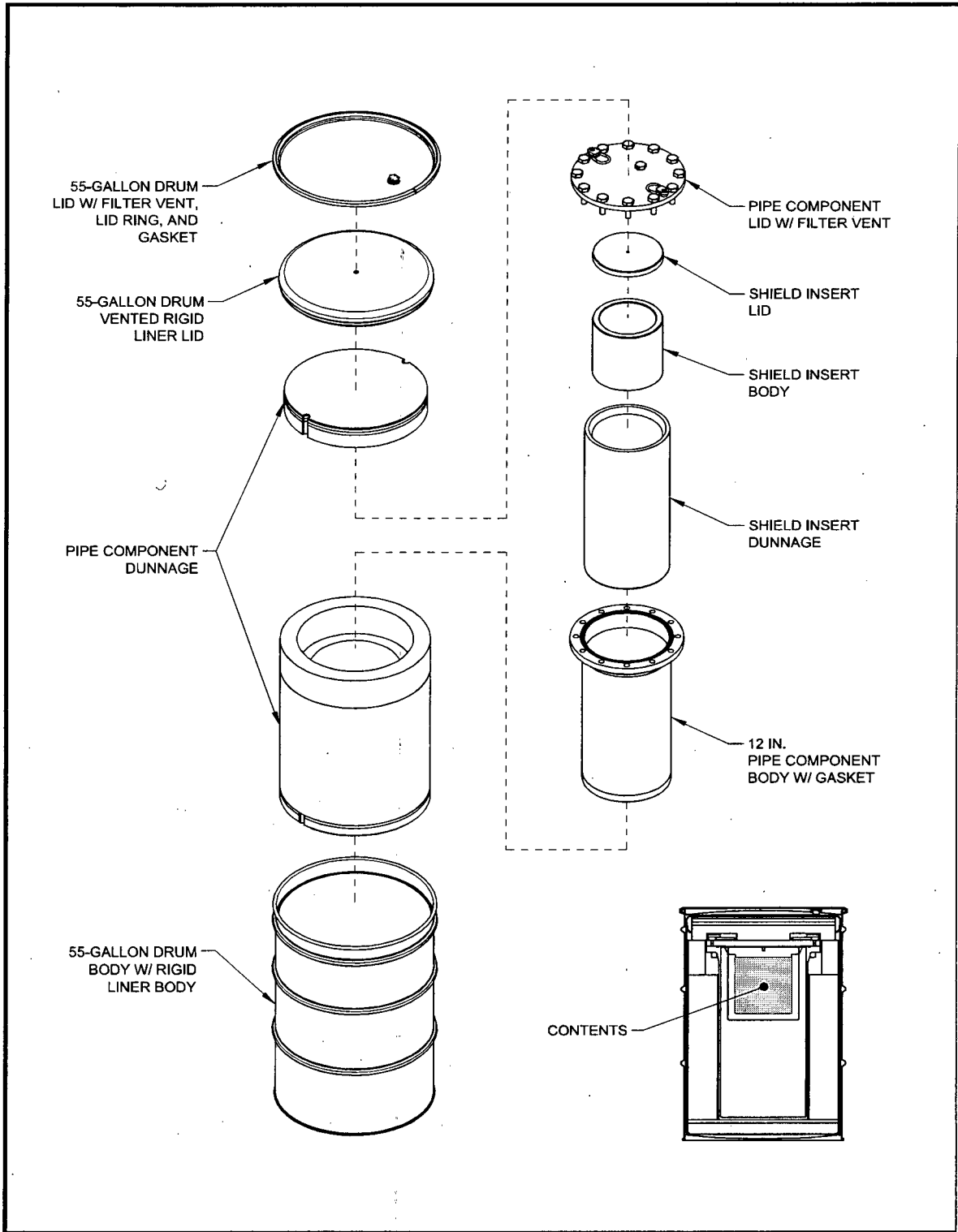


Figure 4.3-1 — S200 Pipe Overpack

4.3.3 Structural Analysis For NCT

The structural effectiveness of the S200 pipe overpack for NCT is demonstrated by showing that the waste contents are confined within the pipe component. The structural effectiveness of the pipe component for NCT is bounded by the structural effectiveness evaluation for HAC given in Section 4.3.4. It is shown in Section 4.3.6 that an adequate level of biological shielding for NCT is afforded by the materials of construction of the TRUPACT-II and HalfPACT, pipe components, and shield inserts themselves, with the 55-gallon drum, fiberboard dunnage, and foam dunnage providing only a distance attenuation contribution. The maximum deflection and resulting radial shift of the pipe overpack array for the NCT side drop, which is limiting for shielding calculations, is bounded by the HAC side drop analysis provided in Section 4.3.4. Additionally, the spacing between pipe components (i.e., effective drum diameter) utilized in the criticality analysis is also bounded by the HAC side drop analysis provided in Section 4.3.4. The following analysis evaluates the maximum damage to the shield insert rigid polyurethane foam dunnage in the end and side drop orientations and thereby shows that the shield lid remains engaged with the shield body and quantifies the maximum shift of the shield insert inside the pipe component.

The shield insert is positioned inside the pipe component by rigid polyurethane foam dunnage with a maximum clearance between the pipe component and shield insert lid of 0.125 in. The shield insert lid has a step feature that has a minimum length of 0.500 in. Therefore, limiting the axial crush of the foam dunnage to less than $(0.500 - 0.125) = 0.375$ in. in any drop orientation ensures that the shield lid remains engaged with the shield body. The maximum crush deformation of the foam in the end drop orientation may be bounded by assuming all of the drop energy of the shield insert and contents is absorbed by the foam beneath the shield insert body. The drop energy (E) to be absorbed for the S200-A and S200-B shield inserts is the product of the weight of the shield insert and contents in pounds (lbs) and the height of the drop (36 in.):

$$E_{S200-A} = (202 \text{ lbs}) (36 \text{ in.}) = 7,272 \text{ in.-lbs}$$

$$E_{S200-B} = (206 \text{ lbs}) (36 \text{ in.}) = 7,416 \text{ in.-lbs}$$

Under NCT, the average temperature of the contents of a drum is bounded by a temperature of 170°F for the case where decay heat is uniformly distributed among all drums, as shown in Table 3.4-1 of the HalfPACT SAR. The minimum parallel-to-rise compressive strength of the rigid polyurethane foam material is $\sigma = 400$ pounds per square inch (psi) at 170°F. Therefore, to absorb this energy, the volume (V) of the crush material in cubic inches (in^3) is:

$$V_{S200-A} = E_{S200-A} / \sigma = (7272 \text{ in.-lbs}) / (400 \text{ psi}) = 18.180 \text{ in}^3$$

$$V_{S200-B} = E_{S200-B} / \sigma = (7416 \text{ in.-lbs}) / (400 \text{ psi}) = 18.540 \text{ in}^3$$

This volume is in the form of a right circular cylinder with a diameter equal to the shield body that generates the following crush area (A) in square inches (in^2):

$$A_{S200-A} = (\pi/4) (D_{S200-A})^2 = (\pi/4) (10.125 \text{ in.})^2 = 80.516 \text{ in}^2$$

$$A_{S200-B} = (\pi/4) (D_{S200-B})^2 = (\pi/4) (9.325 \text{ in.})^2 = 68.295 \text{ in}^2$$

The bounding axial crush of the foam dunnage and resulting maximum separation of shield body and lid (H) is defined as:

$$H_{S200-A} = V_{S200-A} / A_{S200-A} = (18.180 \text{ in}^3) / (80.516 \text{ in}^2) = 0.226 \text{ in.}$$

$$H_{S200-B} = V_{S200-B} / A_{S200-B} = (18.540 \text{ in}^3) / (68.295 \text{ in}^2) = 0.271 \text{ in.}$$

Therefore, the minimum positive engagement between the shield body and lid in a maximum axial foam crush event is 0.104 in.

The maximum radial shift of the shield insert within the pipe component is also bounded through a volumetric crush analysis. The drop energy is the same as that defined above. The minimum perpendicular-to-rise compressive strength of the rigid polyurethane foam material is $\sigma = 300$ psi at 170°F. Therefore, to absorb this energy, the volume of the crush material is:

$$V_{S200-A} = E_{S200-A} / \sigma = (7272 \text{ in.-lbs}) / (300 \text{ psi}) = 24.240 \text{ in}^3$$

$$V_{S200-B} = E_{S200-B} / \sigma = (7416 \text{ in.-lbs}) / (300 \text{ psi}) = 24.720 \text{ in}^3$$

The product of the shield body length (L) and the crescent-shaped area generated by the radial shift defines the crush volume. Therefore, the area of crush material is given by:

$$A_{S200-A} = V_{S200-A} / L_{S200-A} = (24.240 \text{ in}^3) / (9.625 \text{ in.}) = 2.518 \text{ in}^2$$

$$A_{S200-B} = V_{S200-B} / L_{S200-B} = (24.720 \text{ in}^3) / (17.225 \text{ in.}) = 1.435 \text{ in}^2$$

The bounding radial crush of the foam dunnage and resulting maximum radial shift of the shield body and lid (R) is defined as:

$$R_{S200-A} = A_{S200-A} / D_{S200-A} = (2.518 \text{ in}^2) / (10.125 \text{ in.}) = 0.249 \text{ in.}$$

$$R_{S200-B} = A_{S200-B} / D_{S200-B} = (1.435 \text{ in}^2) / (9.325 \text{ in.}) = 0.154 \text{ in.}$$

The side drop crush distances are accounted for in the NCT shielding analysis discussed in Section 4.3.6.

4.3.4 Structural Analysis for HAC

The structural effectiveness of the S200 pipe overpack for HAC is demonstrated by showing that the waste contents remain confined within the pipe component. It is shown in Section 4.3.6 that an adequate level of biological shielding for HAC is afforded by the materials of construction of the TRUPACT-II or HalfPACT and pipe components, themselves, without any aid from the shield inserts inside the pipe components. The 55-gallon drum and fiberboard dunnage provides only a distance attenuation contribution. Since the shield insert in the S200 pipe overpack is not required for the HAC shielding analysis, the damage to the shielding material in the accident free

drop does not need to be quantified. However, the maximum deflection and resulting radial shift of the pipe overpack array will be quantified for the side drop orientation, which is limiting for shielding calculations. The following comparative analysis shows that the contents remain confined within the pipe component under the HAC free drop. Additionally, the analysis shows the maximum deflection of pipe overpacks and the resulting stacked array configuration resulting from the HAC free side drop.

As shown in Table 2.9-7 of Section 2.9.2 of the CH-TRAMPAC, the weight of the 12-in. standard pipe component contents is bounded by a value of 225 lbs. Additionally, as shown in Table 2.9-16 of Section 2.9.4 of the CH-TRAMPAC, the total weight of the S200 pipe overpack shield insert, dunnage, and contents is bounded by a value of 225 lbs. Because the design of the standard and S200 pipe overpacks are structurally identical except for items inside the pipe component and since the weight limit for items inside the pipe component are identical, all structural evaluations of the standard pipe overpack apply to the S200 pipe overpack. Ammerman and Bobbe, 1995,¹ demonstrates the leak tightness of the standard pipe overpack when subjected to HAC testing. Therefore, the waste contents will remain confined within the pipe component under the HAC free drop.

Additionally, Ammerman and Bobbe¹ report a 20.250 in. minimum deformed pipe overpack diameter resulting from a free side drop orientation. Therefore, conservatively using a 20.000 in. 55-gallon drum diameter bounds the radial shift of the pipe component with respect to the S200 pipe overpack at $(22.500 - 20.000)/2 = 1.250$ in.. The resulting stacked array of 14 S200 pipe overpacks resting against the TRUPACT-II inner containment vessel is accounted for in the HAC shielding analysis discussed in Section 4.3.6. The maximum drum crush values reported in Ammerman and Bobbe of 20.25 in. outside diameter by 29.62 in. height are directly utilized in the criticality analysis summarized in Section 4.3.5.

4.3.5 Criticality Analysis

A criticality analysis was performed for two different payload cases, depending on the quantities of special reflector materials in the payload container (see Chapter 6.0 of TRUPACT-II SAR or Chapter 6.0 of HalfPACT SAR for description of special reflector materials), as described below:

- **Case E:** For Case E, the contents of the pipe overpack payload container contain less than or equal to 1% by weight quantities of special reflector materials. The pipe overpack payload container may contain greater than 1% by weight quantities of special reflector materials provided that one of the following conditions is met:
 - The special reflector materials are chemically or mechanically bound to the fissile material such that no reconfiguration or release of the bond is possible under normal or accident conditions, or

¹ Ammerman, D.J., and J.G. Bobbe, October 1995. "Rocky Flats Pipe Component Testing," TTC-1434, Sandia National Laboratories, Albuquerque, New Mexico.

- The special reflector materials are present in thicknesses and/or packing fractions that render them less effective than a 25% polyethylene/75% water equivalent reflector per the limits in Table 6.2-1 of the TRUPACT-II or HalfPACT SAR.
- Case F: For Case F, the contents of the pipe overpack payload container contain greater than 1% by weight quantities of special reflector materials that do not meet the exceptions listed for Case E.

The criticality analysis demonstrates that a TRUPACT-II shipment of 14 pipe overpacks with contents meeting the requirements of Case E at 200 FGE of ^{239}Pu each (for a total of 2,800 FGE per TRUPACT-II) or a HalfPACT shipment of 7 pipe overpacks with 200 FGE each (for a total of 1,400 FGE per HalfPACT) ensures compliance with the requirements of Title 10, Code of Federal Regulations (CFR), Sections 71.55 and 71.59 (10 CFR 71.55 and 71.59).² Additionally, shipments of pipe overpacks with contents meeting the requirements of Case F at 140 FGE for each payload container and 980 and 1960 FGE per HalfPACT and TRUPACT-II, respectively, ensure compliance with 10 CFR 71.55 and 71.59. Based on an infinite array of undamaged or damaged packages, the criticality transport index is 0.0.

The key parameters in the pipe overpack analysis for Case E are (1) the maximum fissile loading per pipe component is 200 FGE, (2) no more than 1% by weight quantities of special reflector materials are present or greater than 1% by weight quantities of special reflectors are either bound to the fissile material or meet the limits in Table 6.2-1 of the TRUPACT-II or HalfPACT SAR, (3) the spacing between the components (i.e., effective drum diameter) is reduced by the maximum amount reported in Section 4.3.4, and (4) the package arrays are infinite arrays stacked two high.

The key parameters in the pipe overpack analysis for Case F are (1) the maximum fissile loading per pipe component is 140 FGE, (2) the spacing between the components (i.e., effective drum diameter) is reduced by the maximum amount reported in Section 4.3.4, and (3) the package arrays are infinite arrays stacked two high.

The detailed analysis presented in Packaging Technology, 2004², presents the results of a series of SCALE 4.4 CSAS25 module³ (KENO-Va version 4) calculations that establish a maximum system reactivity ($k_s + 2\sigma$) of less than 0.933 and the corresponding Upper Subcriticality Limit (USL) of 0.9377. Therefore, the shipment of 200 FGE or 140 FGE per pipe overpack for less than or equal to 1% or greater than 1% by weight quantities of special reflector materials, respectively in the TRUPACT-II and HalfPACT is safely subcritical.

² Packaging Technology, Inc., May 2004, "Pipe Overpack Criticality Analysis for the TRUPACT-II Package," ED-076, Packaging Technology, Inc., Tacoma, Washington.

³ SCALE4.4., "Modular Code System for Performing Standardized Computer Analyses for Licensing Evaluation for Workstations and Personal Computers," RSICC code package C00545/MNYCP00, Oak Ridge National Laboratory, September 1998.

4.3.6 Shielding Analysis

Adequate shielding is provided in the S200 pipe overpack and TRUPACT-II or HalfPACT shipping configuration to ensure that no radioactive payload will exceed the dose rate limits established by 10 CFR 71.47(a) for NCT or 10 CFR 71.51(a)(2) for HAC. Compliance with dose rate limits specified in Section 3.2 of the CH-TRAMPAC for individual S200 pipe overpacks and loaded TRUPACT-IIs or HalfPACTs will be achieved by pre-shipment radiological surveys. Compliance with NCT and HAC radiation dose rate limits will be ensured by limiting radionuclide quantities to satisfy the most-limiting NCT or HAC radiation dose rate limits for worst-case, reconfigured source and post-accident shielding geometries.

A shielding analysis of the S200 pipe overpack and TRUPACT-II shipping configuration was performed to establish the allowable quantities of the radionuclides shown in Table 4.3-1. The analysis utilized a point-source methodology developed by T. Rockwell III for gamma sources and the Nelson methodology for neutron sources.^{4, 5, 6}

Table 4.3-1 — Radionuclide Inventory

³ H	⁸⁵ Kr	¹⁰³ Ru	¹²³ Te	^{144m} Pr	²⁰⁹ Tl	²¹⁴ Po	²²⁷ Ac	²³⁶ U	²⁴⁴ Pu	²⁵⁰ Bk
¹⁴ C	⁸⁶ Rb	¹⁰⁶ Ru	^{123m} Te	¹⁴⁶ Pm	²⁰⁹ Pb	²¹⁵ Po	²²⁸ Ac	²³⁷ U	²⁴¹ Am	²⁴⁹ Cf
²² Na	⁸⁹ Sr	^{103m} Rh	^{125m} Te	¹⁴⁷ Pm	²¹⁰ Pb	²¹⁶ Po	²²⁷ Th	²³⁸ U	²⁴² Am	²⁵⁰ Cf
³² P	⁹⁰ Sr	¹⁰⁶ Rh	¹²⁷ Te	¹⁴⁶ Sm	²¹¹ Pb	²¹⁸ Po	²²⁸ Th	²³⁹ U	^{242m} Am	²⁵¹ Cf
⁵¹ Cr	⁸⁸ Y	¹⁰⁷ Pd	^{127m} Te	¹⁴⁷ Sm	²¹² Pb	²¹¹ At	²²⁹ Th	²⁴⁰ U	²⁴³ Am	²⁵² Cf
⁵⁴ Mn	⁹⁰ Y	^{109m} Ag	¹²⁵ I	¹⁵¹ Sm	²¹⁴ Pb	²¹⁷ At	²³⁰ Th	²³⁷ Np	²⁴⁵ Am	²⁵⁴ Cf
⁵⁵ Fe	^{90m} Y	¹¹⁰ Ag	¹²⁹ I	¹⁵⁰ Eu	²⁰⁷ Bi	²¹⁹ Rn	²³¹ Th	²³⁸ Np	²⁴⁰ Cm	²⁵² Es
⁵⁹ Fe	⁹¹ Y	^{110m} Ag	¹³¹ I	¹⁵² Eu	²¹⁰ Bi	²²⁰ Rn	²³² Th	²³⁹ Np	²⁴² Cm	²⁵³ Es
⁵⁷ Co	⁸⁸ Zr	¹⁰⁹ Cd	¹³⁴ Cs	¹⁵⁴ Eu	²¹¹ Bi	²²² Rn	²³⁴ Th	²⁴⁰ Np	²⁴³ Cm	²⁵⁴ Es
⁵⁸ Co	⁹⁰ Zr	^{113m} Cd	¹³⁵ Cs	¹⁵⁵ Eu	²¹² Bi	²²¹ Fr	²³¹ Pa	^{240m} Np	²⁴⁴ Cm	²⁵⁵ Es
⁶⁰ Co	^{90m} Zr	^{119m} Sn	¹³⁷ Cs	¹⁵² Gd	²¹³ Bi	²²³ Fr	²³³ Pa	²³⁶ Pu	²⁴⁵ Cm	
⁵⁹ Ni	⁹³ Zr	^{121m} Sn	¹³³ Ba	¹⁵³ Gd	²¹⁴ Bi	²²³ Ra	²³⁴ Pa	²³⁸ Pu	²⁴⁶ Cm	
⁶³ Ni	⁹⁵ Zr	¹²³ Sn	¹³⁷ Ba	¹⁶⁸ Tm	²⁰⁹ Po	²²⁴ Ra	^{234m} Pa	²³⁹ Pu	²⁴⁷ Cm	
⁶⁴ Cu	⁹⁵ Nb	¹²⁶ Sn	^{137m} Ba	¹⁸² Ta	²¹⁰ Po	²²⁵ Ra	²³² U	²⁴⁰ Pu	²⁴⁸ Cm	
⁶⁵ Zn	^{95m} Nb	¹²⁵ Sb	¹⁴¹ Ce	¹⁹⁸ Au	²¹¹ Po	²²⁶ Ra	²³³ U	²⁴¹ Pu	²⁵⁰ Cm	
⁷³ As	⁹⁹ Tc	¹²⁶ Sb	¹⁴⁴ Ce	²⁰⁷ Tl	²¹² Po	²²⁸ Ra	²³⁴ U	²⁴² Pu	²⁴⁷ Bk	
⁷⁹ Se	^{99m} Tc	^{126m} Sb	¹⁴⁴ Pr	²⁰⁸ Tl	²¹³ Po	²²⁵ Ac	²³⁵ U	²⁴³ Pu	²⁴⁹ Bk	

⁴ T. Rockwell III, et al., Reactor Shielding Design Manual, TID-7004, First Edition, March 1956, U.S. Atomic Energy Commission, Oak Ridge, Tennessee.

⁵ R.D. Wilson, Neutron Dose Rate Estimates for the 72-B Cask Using the Nelson Methodology, ENG-RCAL-021, Rev. 0, March 1999, Waste Management Federal Services, Inc., Northwest Operations, Richland, Washington.

⁶ IT Corporation, June 2001, "Shielding Analysis of the S200 Pipe Overpack," IT Corporation, Albuquerque, New Mexico.

The primary shielding for the payload in the NCT configuration is the stainless steel and lead provided by the shield insert, pipe component, and TRUPACT-II. HAC configurations utilize the stainless steel in the pipe component and TRUPACT-II. A detailed description of the shield configurations utilized in the shielding analysis is presented in IT Corporation, 2001.⁶

The shielding analysis presented in IT Corporation, 2001,⁶ calculates the maximum allowable radionuclide activity per S200 pipe overpack in the NCT at the surface, NCT at 2 meters, and HAC at 1 meter configurations inside a TRUPACT-II. The minimum of the calculated configuration activities is defined as the limiting activity and presented for both the S200-A and S200-B shield insert configurations in Table 4.3-2. The limiting activity per S200 pipe overpack provided in Table 4.3-2 is also conservative for the HalfPACT configuration because the number of S200 pipe overpacks (and the resulting total activity) is half that of the TRUPACT-II configuration.

Table 4.3-2 — Limiting Activity per S200 Pipe Overpack

Radio-nuclide Name	S200-A Limiting Activity (Ci)	S200-B Limiting Activity (Ci)
³ H	unlimited	unlimited
¹⁴ C	unlimited	unlimited
²² Na	3.722E-02	2.343E-02
³² P	unlimited	unlimited
⁵¹ Cr	1.226E+01	1.226E+01
⁵⁴ Mn	8.440E-02	4.331E-02
⁵⁵ Fe	unlimited	unlimited
⁵⁹ Fe	4.192E-02	2.577E-02
⁵⁷ Co	2.641E+01	2.641E+01
⁵⁸ Co	8.829E-02	4.471E-02
⁶⁰ Co	1.906E-02	1.195E-02
⁵⁹ Ni	unlimited	unlimited
⁶³ Ni	unlimited	unlimited
⁶⁴ Cu	7.156E+00	4.600E+00
⁶⁵ Zn	9.129E-02	5.486E-02
⁷³ As	1.055E+03	1.055E+03
⁷⁹ Se	unlimited	unlimited
⁸⁵ Kr	1.363E+02	3.709E+01
⁸⁶ Rb	5.643E-01	3.353E-01
⁸⁹ Sr	7.224E+02	3.920E+02
⁹⁰ Sr	unlimited	unlimited
⁸⁸ Y	1.709E-02	1.110E-02
⁹⁰ Y	1.328E+06	9.330E+05
^{90m} Y	6.476E-01	2.442E-01
⁹¹ Y	1.572E+01	9.695E+00
⁸⁸ Zr	9.496E-01	7.384E-01
⁹⁰ Zr	unlimited	unlimited
^{90m} Zr	unlimited	unlimited
⁹³ Zr	1.975E+07	1.975E+07
⁹⁵ Zr	1.248E-01	5.705E-02
⁹⁵ Nb	1.100E-01	5.212E-02
^{95m} Nb	8.103E+00	8.103E+00
⁹⁹ Tc	1.693E+07	1.693E+07
^{99m} Tc	1.385E+01	1.385E+01

Radio-nuclide Name	S200-A Limiting Activity (Ci)	S200-B Limiting Activity (Ci)
¹⁰³ Ru	6.524E-01	1.750E-01
¹⁰⁶ Ru	unlimited	unlimited
^{103m} Rh	1.618E+05	1.618E+05
¹⁰⁶ Rh	6.710E-01	2.764E-01
¹⁰⁷ Pd	unlimited	unlimited
^{109m} Ag	2.974E+03	2.974E+03
¹¹⁰ Ag	3.900E+00	1.594E+00
^{110m} Ag	2.521E-02	1.351E-02
¹⁰⁹ Cd	2.974E+03	2.974E+03
^{113m} Cd	7.540E+03	7.540E+03
^{119m} Sn	6.826E+02	6.826E+02
^{121m} Sn	5.948E+03	5.948E+03
¹²³ Sn	7.589E+00	4.521E+00
¹²⁶ Sn	1.726E+02	1.726E+02
¹²⁵ Sb	5.782E-01	1.908E-01
¹²⁶ Sb	4.239E-02	1.826E-02
^{126m} Sb	9.044E-02	3.658E-02
¹²³ Te	unlimited	unlimited
^{123m} Te	7.703E+00	7.703E+00
^{125m} Te	1.542E+03	1.542E+03
¹²⁷ Te	7.613E+01	4.597E+01
^{127m} Te	1.323E+03	5.207E+02
¹²⁵ I	1.647E+03	1.647E+03
¹²⁹ I	1.465E+03	1.465E+03
¹³¹ I	9.832E-01	5.754E-01
¹³⁴ Cs	6.216E-02	2.832E-02
¹³⁵ Cs	unlimited	unlimited
¹³⁷ Cs	2.181E-01	8.747E-02
¹³³ Ba	1.142E+00	1.142E+00
¹³⁷ Ba	unlimited	unlimited
^{137m} Ba	2.060E-01	8.261E-02
¹⁴¹ Ce	2.011E+01	2.011E+01
¹⁴⁴ Ce	1.539E+02	1.539E+02
¹⁴⁴ Pr	1.779E+00	1.126E+00

Table 4.3-2 — Limiting Activity per S200 Pipe Overpack (Continued)

Radio-nuclide Name	S200-A Limiting Activity (Ci)	S200-B Limiting Activity (Ci)
^{144m} Pr	5.304E+01	3.512E+01
¹⁴⁶ Pm	1.958E-01	8.003E-02
¹⁴⁷ Pm	1.175E+06	1.175E+06
¹⁴⁶ Sm	unlimited	unlimited
¹⁴⁷ Sm	unlimited	unlimited
¹⁵¹ Sm	3.504E+05	3.504E+05
¹⁵⁰ Eu	1.001E-01	4.605E-02
¹⁵² Eu	5.488E-02	3.263E-02
¹⁵⁴ Eu	4.915E-02	2.843E-02
¹⁵⁵ Eu	1.743E+02	1.743E+02
¹⁵² Gd	unlimited	unlimited
¹⁵³ Gd	1.898E+02	1.898E+02
¹⁶⁸ Tm	8.380E-02	4.045E-02
¹⁸² Ta	4.298E-02	2.631E-02
¹⁹⁸ Au	9.004E-01	4.886E-01
²⁰⁷ Tl	2.733E+01	1.469E+01
²⁰⁸ Tl	1.497E-02	9.959E-03
²⁰⁹ Tl	2.596E-02	1.678E-02
²⁰⁹ Pb	unlimited	unlimited
²¹⁰ Pb	2.589E+03	2.589E+03
²¹¹ Pb	1.786E+00	8.441E-01
²¹² Pb	4.342E+00	4.342E+00
²¹⁴ Pb	1.681E+00	1.589E+00
²⁰⁷ Bi	4.786E-02	2.598E-02
²¹⁰ Bi	unlimited	unlimited
²¹¹ Bi	8.296E+00	8.296E+00
²¹² Bi	6.418E-01	3.564E-01
²¹³ Bi	2.920E+00	1.052E+00
²¹⁴ Bi	3.569E-02	2.213E-02
²⁰⁹ Po	1.519E+01	8.164E+00
²¹⁰ Po	7.613E+03	3.813E+03
²¹¹ Po	1.055E+01	5.124E+00
²¹² Po	unlimited	unlimited
²¹³ Po	2.147E+03	1.038E+03

Radio-nuclide Name	S200-A Limiting Activity (Ci)	S200-B Limiting Activity (Ci)
²¹⁴ Po	unlimited	unlimited
²¹⁵ Po	2.053E+03	9.111E+02
²¹⁶ Po	4.824E+03	2.419E+03
²¹⁸ Po	unlimited	unlimited
²¹¹ At	6.139E+01	2.565E+01
²¹⁷ At	1.968E+03	8.069E+02
²¹⁹ Rn	7.163E+00	7.163E+00
²²⁰ Rn	3.632E+02	1.115E+02
²²² Rn	8.103E+02	2.176E+02
²²¹ Fr	2.066E+01	2.066E+01
²²³ Fr	1.078E+01	5.211E+00
²²³ Ra	5.380E+00	5.380E+00
²²⁴ Ra	5.031E+01	5.031E+01
²²⁵ Ra	3.668E+02	3.668E+02
²²⁶ Ra	1.065E+02	1.065E+02
²²⁸ Ra	5.749E+03	5.749E+03
²²⁵ Ac	8.245E+01	7.320E+01
²²⁷ Ac	3.927E+04	3.927E+04
²²⁸ Ac	7.672E-02	4.385E-02
²²⁷ Th	4.786E+00	4.786E+00
²²⁸ Th	7.082E+02	7.082E+02
²²⁹ Th	2.522E+01	2.522E+01
²³⁰ Th	1.352E+03	1.336E+03
²³¹ Th	2.833E+02	2.833E+02
²³² Th	2.841E+03	2.809E+03
²³⁴ Th	9.901E+02	9.901E+02
²³¹ Pa	1.330E+01	1.330E+01
²³³ Pa	2.262E+00	2.262E+00
²³⁴ Pa	5.300E-02	2.859E-02
^{234m} Pa	3.751E+00	2.161E+00
²³² U	8.615E+02	8.463E+02
²³³ U	1.179E+03	1.130E+03
²³⁴ U	1.202E+03	1.185E+03
²³⁵ U	5.003E+00	5.003E+00

Table 4.3-2 — Limiting Activity per S200 Pipe Overpack (Continued)

Radio-nuclide Name	S200-A Limiting Activity (Ci)	S200-B Limiting Activity (Ci)	Radio-nuclide Name	S200-A Limiting Activity (Ci)	S200-B Limiting Activity (Ci)
²³⁶ U	1.301E+03	1.286E+03	²⁴⁵ Am	2.809E+01	2.809E+01
²³⁷ U	1.002E+01	1.002E+01	²⁴⁰ Cm	1.241E+02	1.227E+02
²³⁸ U	1.459E+01	1.443E+01	²⁴² Cm	7.823E+01	7.722E+01
²³⁹ U	8.798E+00	4.327E+00	²⁴³ Cm	6.475E+00	6.475E+00
²⁴⁰ U	7.356E+02	7.356E+02	²⁴⁴ Cm	4.356E+00	4.306E+00
²³⁷ Np	1.416E+02	1.416E+02	²⁴⁵ Cm	2.649E+01	2.619E+01
²³⁸ Np	8.656E-02	4.996E-02	²⁴⁶ Cm	1.885E-02	1.864E-02
²³⁹ Np	5.101E+00	5.101E+00	²⁴⁷ Cm	1.175E+00	7.922E-01
²⁴⁰ Np	8.373E-02	4.282E-02	²⁴⁸ Cm	6.126E-05	6.057E-05
^{240m} Np	3.198E-01	1.524E-01	²⁵⁰ Cm	7.043E-06	6.963E-06
²³⁶ Pu	5.764E+02	5.597E+02	²⁴⁷ Bk	5.606E+00	5.606E+00
²³⁸ Pu	6.171E+02	6.087E+02	²⁴⁹ Bk	5.710E+03	5.644E+03
²³⁹ Pu	9.319E+02	8.655E+02	²⁵⁰ Bk	6.133E-02	3.558E-02
²⁴⁰ Pu	1.158E+02	1.145E+02	²⁴⁹ Cf	1.175E+00	1.175E+00
²⁴¹ Pu	3.874E+06	3.874E+06	²⁵⁰ Cf	5.989E-03	5.921E-03
²⁴² Pu	1.334E+00	1.318E+00	²⁵¹ Cf	1.237E+01	1.237E+01
²⁴³ Pu	9.208E+01	9.208E+01	²⁵² Cf	1.548E-04	1.530E-04
²⁴⁴ Pu	5.548E-03	5.485E-03	²⁵⁴ Cf	4.781E-06	4.727E-06
²⁴¹ Am	2.788E+02	2.788E+02	²⁵² Es	4.418E-01	2.180E-01
²⁴² Am	7.973E+05	7.973E+05	²⁵³ Es	4.677E+01	4.453E+01
^{242m} Am	1.095E+02	1.095E+02	²⁵⁴ Es	3.681E+01	3.681E+01
²⁴³ Am	1.409E+02	1.409E+02	^{254m} Es	9.086E-03	8.561E-03

Note: The designation of "unlimited" is made for any radionuclide whose limiting activity is greater than 1×10^8 curies (Ci).

4.3.7 Authorized Payload Contents

As demonstrated in Section 4.3.5, TRUPACT-II shipments of 14 S200 pipe overpacks and HalfPACT shipments of 7 S200 pipe overpacks containing 200 FGE per pipe overpack with contents meeting the requirements of Case E are subcritical in all cases. Therefore, the FGE limit for each S200 pipe overpack with Case E contents is 200 FGE. A maximum TRUPACT-II payload of 14 S200 pipe overpacks and HalfPACT payload of 7 S200 pipe overpacks have allowable FGE limits of 2,800 FGE and 1,400 FGE, respectively for Case E payloads. The FGE limit for Case F payloads is 140, 980, and 1,960 FGE for the S200 pipe overpack, HalfPACT, and TRUPACT-II, respectively.

Section 3.2 of the CH-TRAMPAC requires that each individual S200 pipe overpack and loaded TRUPACT-II or HalfPACT be measured prior to shipment to verify compliance with a dose rate limit of 200 millirem per hour (mrem/hr) at the surface. Additionally, Section 3.2 of the CH-TRAMPAC requires that each loaded TRUPACT-II or HalfPACT be measured prior to shipment to verify compliance with a dose rate limit of 10 mrem/hr at 2 meters. The results of the shielding analyses show that, when the S200 pipe overpack is loaded to the activity limits listed in Table 4.3-2 using a sum of partial fractions for multiple radionuclides, the dose rate limit requirements of 10 CFR 71.47(a) and 10 CFR 71.51(a)(2) are met for a TRUPACT-II loaded with 14 S200 pipe overpacks and a HalfPACT loaded with 7 S200 pipe overpacks.

4.3.8 Conclusion

The S200 pipe overpack design is very closely based on the standard pipe overpack. It consists of a standard 12-in. pipe component within a 55-gallon drum, including a rigid liner and lid. A gamma shield insert is placed inside the pipe component and located by polyurethane foam dunnage. The analyses summarized in this appendix demonstrate the ability of the S200 pipe overpack to provide three significant control functions under NCT and HAC: (1) criticality, (2) shielding, and (3) confinement of the waste contents. The payload of the S200 pipe overpack is transuranic waste with high gamma energies.

The structural analysis shows that the waste contents remain confined within the pipe component in conservatively bounded NCT and HAC free drops. For criticality, it is shown that 200 FGE per S200 pipe overpack is safely subcritical for Case E payloads and 140 FGE per S200 pipe overpack is safely subcritical for Case F payloads. The shielding analysis shows that, with maximum allowable activity specified in Table 4.3-2, the dose limits for NCT and HAC are met.

APPENDIX 4.4

DESCRIPTION OF S300 PIPE OVERPACK

This page intentionally left blank.

4.4 Description of S300 Pipe Overpack

4.4.1 Introduction

The S300 pipe overpack is based closely on the standard pipe overpack described in Appendix 4.1 of the CH-TRU Payload Appendices. It differs from the standard pipe overpack through the addition of neutron shielding within the pipe component. It is intended for the shipment of sealed neutron sources in the TRUPACT-II and HalfPACT. Appendix 1.3.1 of the TRUPACT-II Safety Analysis Report (SAR), Appendix 1.3.1 of the HalfPACT SAR, and Section 2.9.5 of the Contact-Handled Transuranic Waste Authorized Methods for Payload Control (CH-TRAMPAC) describe the materials of construction, sizes, and other dimensional specifications for the S300 pipe overpack. Up to 14 S300 pipe overpacks may be shipped in the TRUPACT-II, and up to 7 S300 pipe overpacks may be shipped in the HalfPACT. This appendix describes the structural, criticality, and shielding basis of the S300 pipe overpack.

4.4.2 Description

The S300 pipe overpack consists of a neutron shield insert placed inside a standard 12-inch (in.) pipe component which is, in turn, located by cane fiberboard and plywood dunnage within a standard 55-gallon drum with a rigid polyethylene liner and lid. A schematic of the S300 pipe overpack is shown in Figure 4.4-1. All of the components of the S300 pipe overpack, except the neutron shield insert, are identical to the 12-in. version of the standard pipe overpack described in Appendix 4.1 of the CH-TRU Payload Appendices.

The neutron shield insert is a two-part assembly consisting of a cylindrical body and stepped lid. With the exception of necessary clearances, the insert fits within and fills the 12-in. pipe component. The insert lid is held in place by the lid of the pipe component. The insert is made from solid, high-density polyethylene (HDPE), and has a nominal wall thickness of 4.13 inches.

The pipe component provides three significant control functions: (1) criticality control, (2) shielding, and (3) confinement of the sealed neutron sources. The following sections demonstrate the effectiveness of the S300 pipe overpack design for normal conditions of transport (NCT) and hypothetical accident conditions (HAC). All demonstrations are by analysis or by reference to the standard pipe overpack analysis and testing, unless stated otherwise.

4.4.3 Structural Analysis for NCT

The structural effectiveness of the S300 pipe overpack for NCT is demonstrated by showing that the source material contents are confined within the pipe component. The structural effectiveness of the pipe component for NCT is bounded by the structural effectiveness evaluation for HAC given in Section 4.4.4. It is shown in Section 4.4.6 that an adequate level of biological shielding for NCT is afforded by the shield insert itself, with all other materials providing mainly a distance attenuation function. The maximum deflection and resulting radial shift of the pipe overpack array for the NCT side drop, which is limiting for shielding calculations, is bounded by the HAC side drop analysis provided in Section 4.4.4. Additionally,

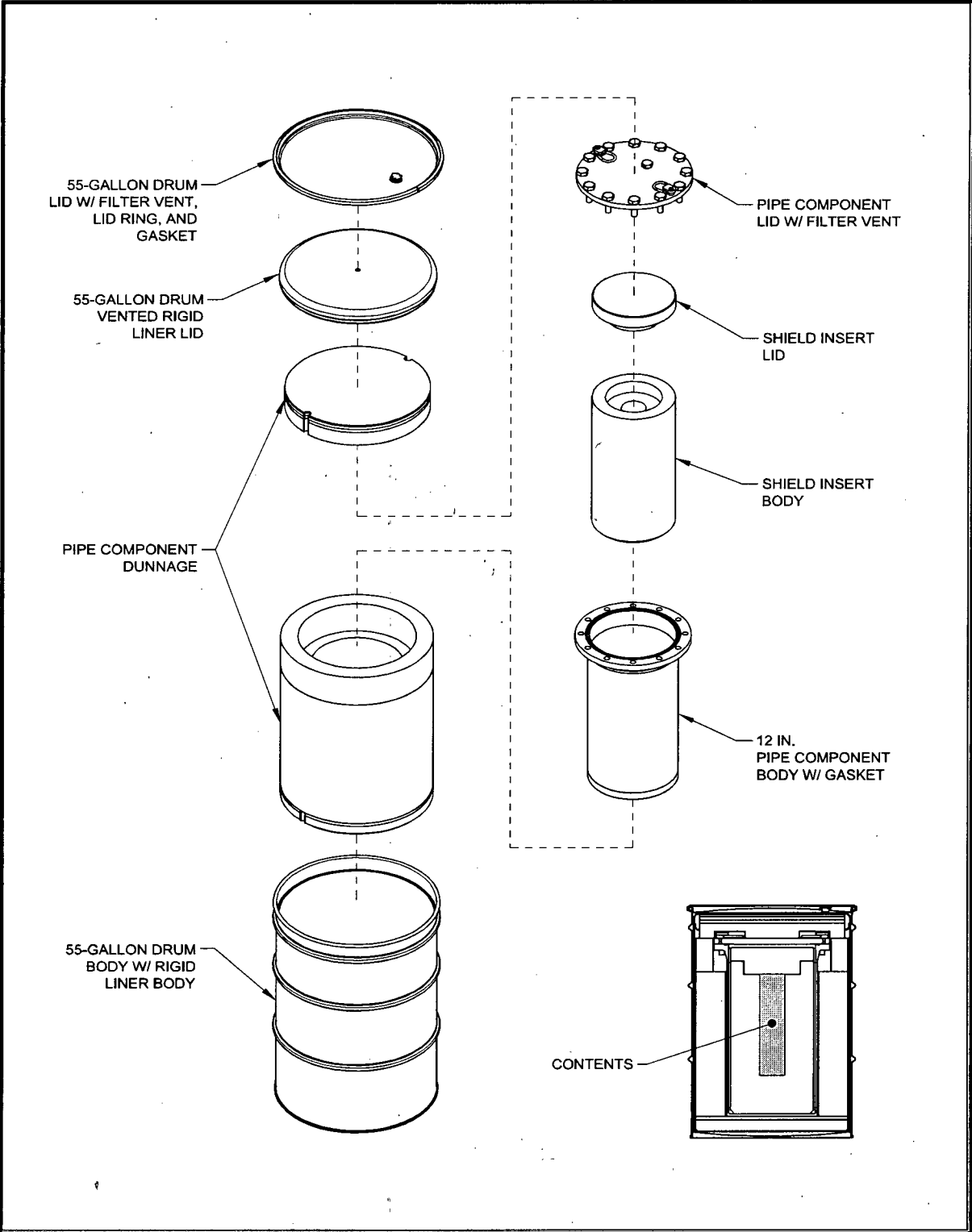


Figure 4.4-1 — S300 Pipe Overpack

the spacing between pipe components (i.e., effective drum diameter) utilized in the criticality analysis is also bounded by the HAC side drop analysis provided in Section 4.4.4.

4.4.4 Structural Analysis for HAC

The structural effectiveness of the S300 pipe overpack for HAC is demonstrated by showing that the source material contents remain confined within the pipe component. It is shown in Section 4.4.6 that an adequate level of biological shielding for HAC is afforded by distance attenuation considering the most conservative post-accident configuration of the TRUPACT-II or HalfPACT and pipe components. Since the shield insert in the S300 pipe overpack is not required for the HAC shielding analysis, the damage to the shielding material in the HAC free drop does not need to be quantified. However, the maximum deflection and resulting radial shift of the pipe overpack array will be quantified for the side drop orientation, which is limiting for shielding calculations. The following comparative analysis shows that the contents remain confined within the pipe component under the HAC free drop. Additionally, the analysis shows the maximum deflection of pipe overpacks and the resulting stacked array configuration resulting from the HAC free drop.

As shown in Table 2.9-7 of Section 2.9.2 of the CH-TRAMPAC, the weight of the 12-in. standard pipe component contents is bounded by a value of 225 lbs. Additionally, as shown in Table 2.9-20 of Section 2.9.5 of the CH-TRAMPAC, the total weight of the S300 pipe overpack shield insert and contents is also bounded by a weight of 225 lbs. Because the design of the standard and S300 pipe overpacks are structurally identical, and because the weight limit for items inside the pipe component are identical, all structural evaluations of the standard pipe overpack apply to the S300 pipe overpack. Ammerman and Bobbe, 1995,¹ demonstrates the leak tightness of the standard pipe overpack when subjected to HAC testing. Therefore, the source materials will remain confined within the pipe component under the HAC free drop.

Additionally, Ammerman and Bobbe¹ report a 20.250 in. minimum deformed pipe overpack diameter resulting from a free side drop orientation. Therefore, conservatively using a 20.000 in. 55-gallon drum diameter bounds the radial shift of the pipe component with respect to the S300 pipe overpack at $(22.500 - 20.000)/2 = 1.250$ in. The resulting stacked array of 14 S300 pipe overpacks resting against the TRUPACT-II inner containment vessel is accounted for in the HAC shielding analysis discussed in Section 4.4.6. The maximum drum crush values reported in Ammerman and Bobbe of 20.25 in. outside diameter by 29.62 in. height are directly utilized in the criticality analysis summarized in Section 4.4.5.

4.4.5 Criticality Analysis

A criticality analysis was performed for two different payload cases, depending on the quantities of special reflector materials in the payload container (see Chapter 6.0 of TRUPACT-II SAR or Chapter 6.0 of HalfPACT SAR for description of special reflector materials), as described below:

¹ Ammerman, D.J., and J.G. Bobbe, October 1995. "Rocky Flats Pipe Component Testing," TTC-1434, Sandia National Laboratories, Albuquerque, New Mexico.

- Case E: For Case E, the contents of the pipe overpack payload container contain less than or equal to 1% by weight quantities of special reflector materials. The pipe overpack payload container may contain greater than 1% by weight quantities of special reflector materials provided that one of the following conditions is met:
 - The special reflector materials are chemically or mechanically bound to the fissile material such that no reconfiguration or release of the bond is possible under normal or accident conditions, or
 - The special reflector materials are present in thicknesses and/or packing fractions that render them less effective than a 25% polyethylene/75% water equivalent reflector per the limits in Table 6.2-1 of the TRUPACT-II or HalfPACT SAR.
- Case F: For Case F, the contents of the pipe overpack payload container contain greater than 1% by weight quantities of special reflector materials that do not meet the exceptions listed for Case E.

The criticality analysis demonstrates that a TRUPACT-II shipment of 14 pipe overpacks with contents meeting the requirements of Case E at 200 FGE of ^{239}Pu each (for a total of 2,800 FGE per TRUPACT-II) or a HalfPACT shipment of 7 pipe overpacks with 200 FGE each (for a total of 1,400 FGE per HalfPACT) ensures compliance with the requirements of Title 10, Code of Federal Regulations (CFR), Sections 71.55 and 71.59 (10 CFR 71.55 and 71.59).² Additionally, shipments of pipe overpacks with contents meeting the requirements of Case F at 140 FGE for each payload container and 980 and 1960 FGE per HalfPACT and TRUPACT-II, respectively, ensure compliance with 10 CFR 71.55 and 71.59. Based on an infinite array of undamaged or damaged packages, the criticality transport index is 0.0.

The key parameters in the pipe overpack analysis for Case E are (1) the maximum fissile loading per pipe component is 200 FGE, (2) no more than 1% by weight quantities of special reflector materials are present or greater than 1% by weight quantities of special reflectors are either bound to the fissile material or meet the limits of Table 6.2-1 of the TRUPACT-II or HalfPACT SAR, (3) the spacing between the components (i.e., effective drum diameter) is reduced by the maximum amount reported in Section 4.4.4, and (4) the package arrays are infinite arrays stacked two high.

The key parameters in the pipe overpack analysis for Case F are (1) the maximum fissile loading per pipe component is 140 FGE, (2) the spacing between the components (i.e., effective drum diameter) is reduced by the maximum amount reported in Section 4.4.4, and (3) the package arrays are infinite arrays stacked two high.

² Packaging Technology, Inc., May 2004, "Pipe Overpack Criticality Analysis for the TRUPACT-II Package," ED-076, Packaging Technology, Inc., Tacoma, Washington.

The detailed analysis presented in Packaging Technology, 2004², presents the results of a series of SCALE 4.4 CSAS25 module³ (KENO-Va version 4) calculations that establish a maximum system reactivity ($k_s + 2\sigma$) of less than 0.933 and the corresponding Upper Subcriticality Limit (USL) of 0.9377. Therefore, the shipment of 200 FGE or 140 FGE per pipe overpack for Cases E and F, respectively, in the TRUPACT-II and HalfPACT is safely subcritical.

4.4.6 Shielding Analysis

The payload of the S300 pipe overpack consists of neutron-emitting, actinide-bearing sealed sources, shown in Table 4.4-1. Source terms used in this analysis are for neutron emission and spectra for alpha-n reactions calculated by the SOURCES Version 4A computer code.⁴ Of the sources shown in the table, the ²³⁸Pu Be was determined to be the governing source for shielding calculations,⁵ since it had the highest calculated unshielded dose rate of all the sources that will be transported in the S300.

Table 4.4-1 S300 Pipe Overpack Payloads

²⁴¹ Am Be	²³⁸ Pu O	²³⁹ Pu Li	²⁴¹ Am
²³⁸ Pu Be	²³⁹ Pu O	²³⁸ Pu B	²³⁸ Pu
²³⁹ Pu Be	²⁴⁴ Cm O	²³⁹ Pu F	²³⁹ Pu
²⁴¹ Am O	²⁴¹ Am Li	²³⁸ Pu ¹³ C	²⁴⁴ Cm

The radiation generated by the payload is in the form of neutrons and a relatively small amount of gamma radiation. Some additional gamma radiation is generated by capture of thermal neutrons in the neutron shielding. However, the gamma radiation remains a small fraction of the neutron radiation level.

Neutron shielding is provided by the shielding insert placed within the 12-in. pipe component. It has a minimum wall thickness of 4.06 in., and minimum end thicknesses of 3.58 in. at the bottom and 3.94 in. in the lid. None of the materials of construction of the S300 pipe overpack, including the neutron shielding material, generate hydrogen gas in excess of 10^{-10} moles hydrogen per second per liter of headspace as a consequence of neutron or gamma irradiation by the payload sources.⁶ A combination of the neutron shielding material and the materials of

³ SCALE4.4., "Modular Code System for Performing Standardized Computer Analyses for Licensing Evaluation for Workstations and Personal Computers," RSICC code package C00545/MNYCP00, Oak Ridge National Laboratory, September 1998.

⁴ Wilson, W.B., R.T. Perry, W. Charlton, et al., 1999, "SOURCES 4A: A Code for Calculating (alpha, n) Spontaneous Fission, and Delayed Neutron Sources and Spectra," LA-13639-MS, Los Alamos National Laboratory, Los Alamos, New Mexico.

⁵ Gogol, S.L., and J.R. Bland, August 2002, "A Comparison of Dose Rates from (alpha, n) and Spontaneous Fission Neutron Sources," LA-UR-02-5120, Los Alamos National Laboratory, Los Alamos, New Mexico.

⁶ Bustos, L.D., W.F. Sandoval, R. Villarreal, and L.R. Field, October 2000, "Hydrogen Generation Rate Potential from Neutron and Gamma Ray Interactions with Shielding/Packaging Materials Contained in the S100 Pipe Component Overpack," Los Alamos National Laboratory, Los Alamos, New Mexico.

construction of the S300 pipe overpack provide sufficient shielding for both neutron and gamma radiation.

Dose rate calculations were performed for a single S300 pipe overpack and for a TRUPACT-II in both the as-loaded and post-NCT free drop configurations.⁷ The results were used to determine the maximum loading of the S300 pipe overpack such that the regulatory dose rate limits will be met in each case for NCT and HAC. In the analysis, the bounding payload of ²³⁸Pu Be was used, as discussed above. Source gamma radiation was negligible and was not included, but capture gamma dose rate contribution was included in the calculated integrated dose rate. Dose rate calculations were made for a single S300 pipe overpack as presented for loading into a TRUPACT-II, for a TRUPACT-II as presented for transport with a payload of 14 identical S300 pipe overpacks each having the maximum payload, and for a TRUPACT-II including a conservative representation of NCT free drop damage with a payload of 14 identical S300 pipe overpacks each having the maximum payload. (The HAC case is discussed below.) Dose rates were calculated at the surface and at defined distances from the containers as shown in Table 4.4-2. As shown in the table, the limiting dose is for the TRUPACT-II package at a distance of 5 meters from the package surface (the truck cab, a normally occupied space), and is equal to 2 millirem per hour (mrem/hr). The corresponding S300 pipe overpack surface dose limit is 155 mrem/hr. This means that, as long as the surface dose rate of any S300 pipe overpack transported in a TRUPACT-II is at or below 155 mrem/hr, then the dose rate external to the TRUPACT-II will not exceed 2 mrem/hr at a distance of 5 meters, nor will any of the other, less governing regulatory limits be exceeded. The TRUPACT-II calculations govern the case of the HalfPACT. Each S300 pipe overpack will be surveyed before loading into a TRUPACT-II or HalfPACT to ensure compliance with the limiting surface dose rate of 155 mrem/hr, as given in Section 3.2 of the CH-TRAMPAC.

⁷ Packaging Technology, Inc., August 2002, "Dose Rate Calculations for the S300 Pipe Overpack," ED-072, Packaging Technology, Inc., Tacoma, Washington.

Table 4.4-2 Maximum Dose Rates for S300 Pipe Overpack and TRUPACT-II

	Maximum Dose Rate (mrem/hr)	Limits (mrem/hr) ^④
S300 Surface	155 ±0.36	200
TRUPACT-II side Surface (undamaged) ^{①②}	64.5 ±0.62	200
TRUPACT-II 2 meters (undamaged)	8.06 ±0.10	10
TRUPACT-II 5 meters (undamaged) ^③	1.97 ±0.03	2
TRUPACT-II side Surface (damaged)	120 ±0.20	200
TRUPACT-II 2 meters (damaged)	9.83 ±0.12	10

Notes:

1. TRUPACT-II contains 14 identical S300 pipe overpacks, each with a maximum surface dose rate of 155 mrem/hr or less.
2. Side dose rate governs over top or bottom dose rates.
3. The 5 meter distance corresponds to the normally occupied space of the truck cab.
4. Limits established by CH-TRAMPAC (S300 surface) or 10 CFR 71.47(b) (TRUPACT-II).

The damage to the TRUPACT-II and payload under NCT is assumed to occur in the 3 ft. side drop, and is discussed in Section 4.4.4. The drums are modeled as resting on the inside of the TRUPACT-II ICV, which is resting on its side. Each drum is conservatively reduced in size to a diameter of 20.0 in., and the array is accordingly compressed and shifted to be in contact with the inside surface of the TRUPACT-II ICV.

For HAC, the drums, neutron shielding material, pipe components, and internal dunnage are conservatively removed from consideration in the shielding calculation, and the sum total of all activity in the S300 payload is concentrated as a single point source resting on the inside surface of the TRUPACT-II ICV. In accordance with 10 CFR 71.51(a)(2), the dose point is located 1 meter from the external surface of the package. This is equivalent to a total distance from the source of 1 meter plus the minimum crushed wall thickness of the TRUPACT-II or HalfPACT. For simplicity and conservatism, the calculations assume that there is no material of any kind between the source and the dose point. The crushed wall thickness is found by subtracting the HAC 30-foot free drop side orientation crush damage from the original wall thickness of the package as follows. The outer diameter of the package is 94.38 inches, and the inner diameter of the ICV is 73.63 inches, which gives an undamaged wall thickness of 10.38 inches. The maximum crush damage is found in Table 2.10.3-1 of the TRUPACT-II SAR for Test No. 2, as equal to 3.63 inches. The remaining wall thickness is then equal to $10.38 - 3.63 = 6.75$ inches. In the shielding calculations, a value of 6.5 inches is conservatively used. As already discussed, no material is assumed to fill this space. The resulting maximum allowable activity within the

TRUPACT-II is a total of 406 Ci, and the resulting conservative dose rate is 999 mrem/hr at 1 meter from the crushed TRUPACT-II surface, which meets the requirements of 10 CFR 71.51(a)(2). As for NCT, the TRUPACT-II HAC calculations govern the case of the HalfPACT.

4.4.7 Authorized Payload Contents

As demonstrated in Section 4.4.6, when loaded with sealed neutron sources of the types specified in Table 4.4-1 (the authorized contents), the S300 pipe overpack meets all regulatory dose rate limits. The bounding payload is defined in three ways: (1) a maximum dose rate on the surface of the S300 pipe overpack of 155 mrem/hr for any S300 pipe overpack placed into the TRUPACT-II or HalfPACT, (2) a maximum activity of 406 Ci within a single TRUPACT-II or HalfPACT, and (3) a maximum payload of 200 FGE per S300 pipe overpack, or a total of 2,800 FGE per TRUPACT-II or 1,400 FGE per HalfPACT when the contents meet the requirements for Case E, or (4) a maximum payload of 140 FGE per S300 pipe overpack, or a total of 1,960 FGE per TRUPACT-II or 980 FGE per HalfPACT when the contents meet the requirements for Case F. Section 4.2.5 demonstrates that 200 FGE per S300 pipe overpack is safely subcritical for Case E contents and that 140 FGE per S300 pipe overpack is safely subcritical for Case E contents.

4.4.8 Conclusion

The S300 pipe overpack design is very closely based on the standard pipe overpack. It consists of a standard 12-in. pipe component within a 55-gallon drum, including a rigid liner and lid. A neutron shield insert is placed inside the pipe component. The analyses summarized in this appendix demonstrate the ability of the S300 pipe overpack to provide three significant control functions under NCT and HAC: (1) criticality, (2) shielding, and (3) confinement of the payload. The payload of the S300 is sealed neutron sources of the types listed in Table 4.4-1. The structural analysis shows that the source material remains confined within the pipe component in conservatively bounded NCT and HAC free drops. For criticality, it is shown that 200 FGE per S300 pipe overpack for Case E payloads is safely subcritical and 140 FGE per S300 pipe overpack is safely subcritical for Case F payloads. The shielding analysis shows that, with the maximum authorized contents, the dose rate limits for NCT and HAC (including appropriate shielding damage assumptions in each case) are met.

APPENDIX 4.5

DESCRIPTION OF SHIELDED CONTAINER

This page intentionally left blank.

4.5 Description of Shielded Container

4.5.1 Introduction

The shielded container is a vented carbon steel and lead cylindrical structure with a removable lid. It is designed to be used for the shipment of specific transuranic waste forms in the HalfPACT package. Drawing 163-008 in Appendix 1.3.1 of the HalfPACT SAR¹ and Section 2.9.10 of the *Contact-Handled Transuranic Waste Authorized Methods for Payload Control* (CH-TRAMPAC)² delineate the materials of construction, sizes, and other dimensional specifications for the shielded container and associated dunnage components.

The shielded container is intended for the shipment of transuranic waste forms with high gamma energies in the HalfPACT. The HalfPACT package can accommodate three (3) shielded containers. As configured for shipment, the shielded container payload assembly remains within the previously established design and certification bases and limits of the HalfPACT package for weight (7,600 pounds) and decay heat (30 watts). Limits on shielded container activity and fissile content are also set consistent with previously implemented and accepted analytic approaches.

This appendix describes the structural, thermal, shielding, and criticality basis of the shielded container payload.

4.5.2 Description

The shielded container, approximately the same size as a standard 55-gallon drum, consists of a twin-shelled, carbon steel cylindrical structure and a lid. Nominally, 1 inch of lead shielding is contained between the 7-gauge inner shell and 11-gauge outer shell. The shells are connected to an upper flange and a 3-inch thick solid steel bottom. The 3-inch thick solid steel lid integrates a silicone rubber gasket, fifteen 1/2-inch, alloy steel closure bolts, two alignment pins to facilitate remote assembly, and a lead-shielded filter port. Three removable lifting eyes are used for handling the shielded container prior to installation within a HalfPACT packaging.

The shielded container is designed to carry one 30-gallon steel payload drum. A partially exploded view of the shielded container, including its 30-gallon payload drum, is provided in Figure 4.5-1. In addition to the 30-gallon payload drum, the shielded container may optionally contain a mesh "bag" to facilitate remote installation of the 30-gallon payload drum into the shielded container. The shielded container must be installed with a filter vent; Section 2.5 of the CH-TRAMPAC provides the minimum specification for the shielded container filter vent.

As illustrated in Figure 4.5-2 and Figure 4.5-3, the shielded container payload system also includes a triangular spaceframe pallet, optional plastic stretch wrap and/or banding around the shielded containers, an optional plastic slipsheet below the three shielded containers, an optional plastic reinforcing plate above the three shielded containers, a radial dunnage assembly surrounding the three shielded containers, and an axial dunnage assembly below and above these components.

¹ U.S. Department of Energy (DOE), *HalfPACT Shipping Package Safety Analysis Report*, USNRC Certificate of Compliance 71-9279, U.S. Department of Energy, Carlsbad Field Office, Carlsbad, New Mexico.

² U.S. Department of Energy (DOE), *Contact-Handled Transuranic Waste Authorized Methods for Payload Control* (CH-TRAMPAC), U.S. Department of Energy, Carlsbad Field Office, Carlsbad, New Mexico.

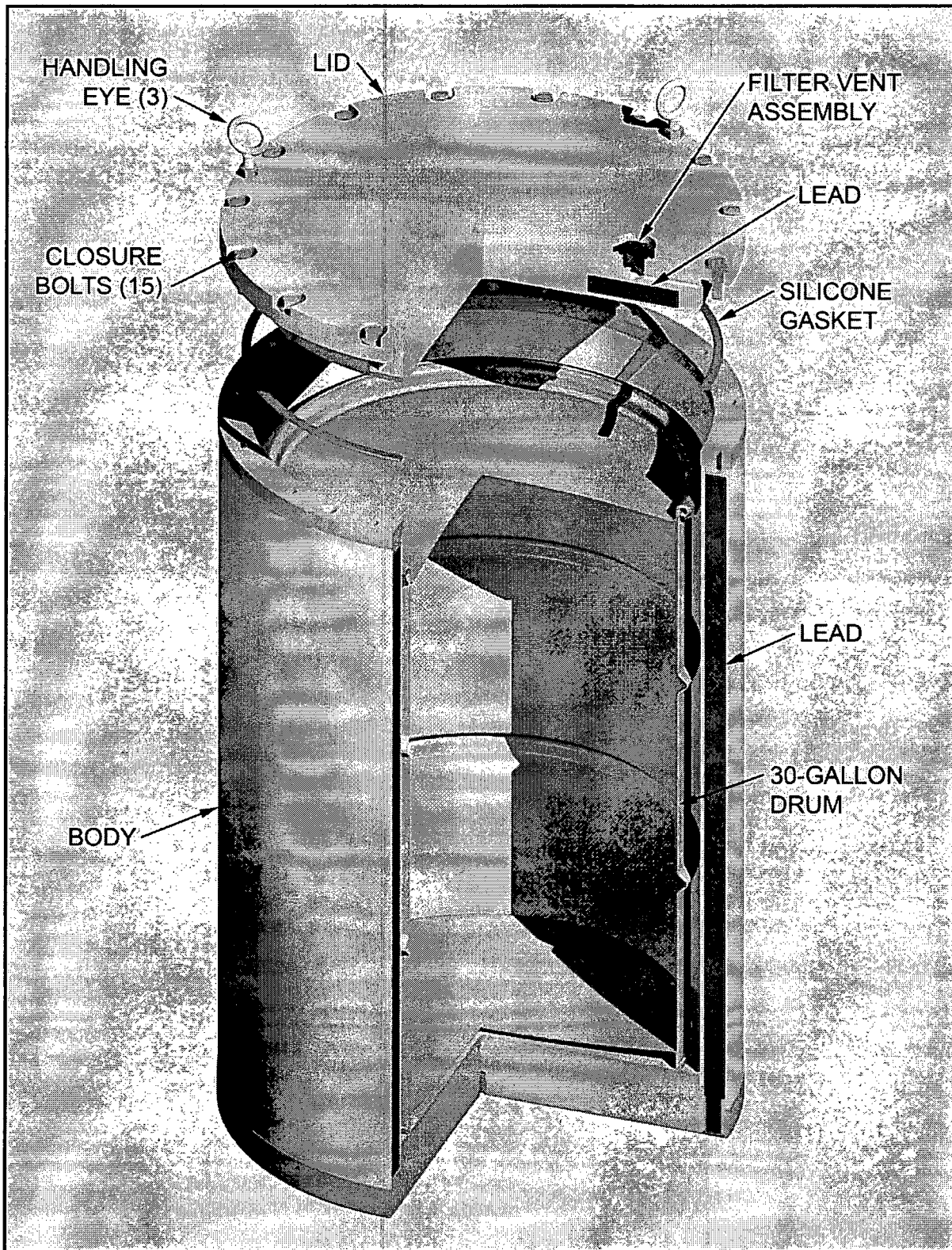


Figure 4.5-1 – Shielded Container Configuration

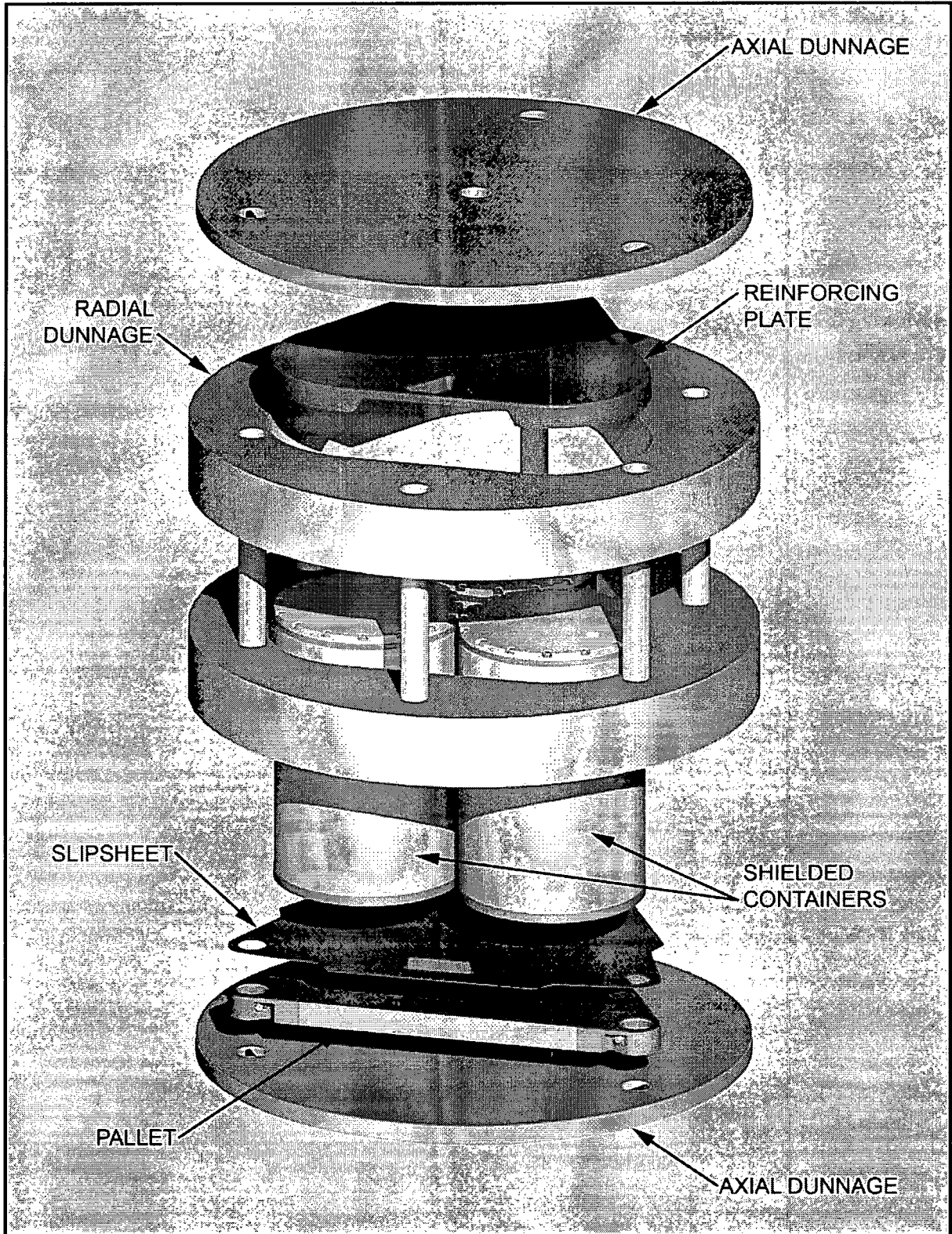


Figure 4.5-2 – Shielded Container Payload Components (Exploded View)

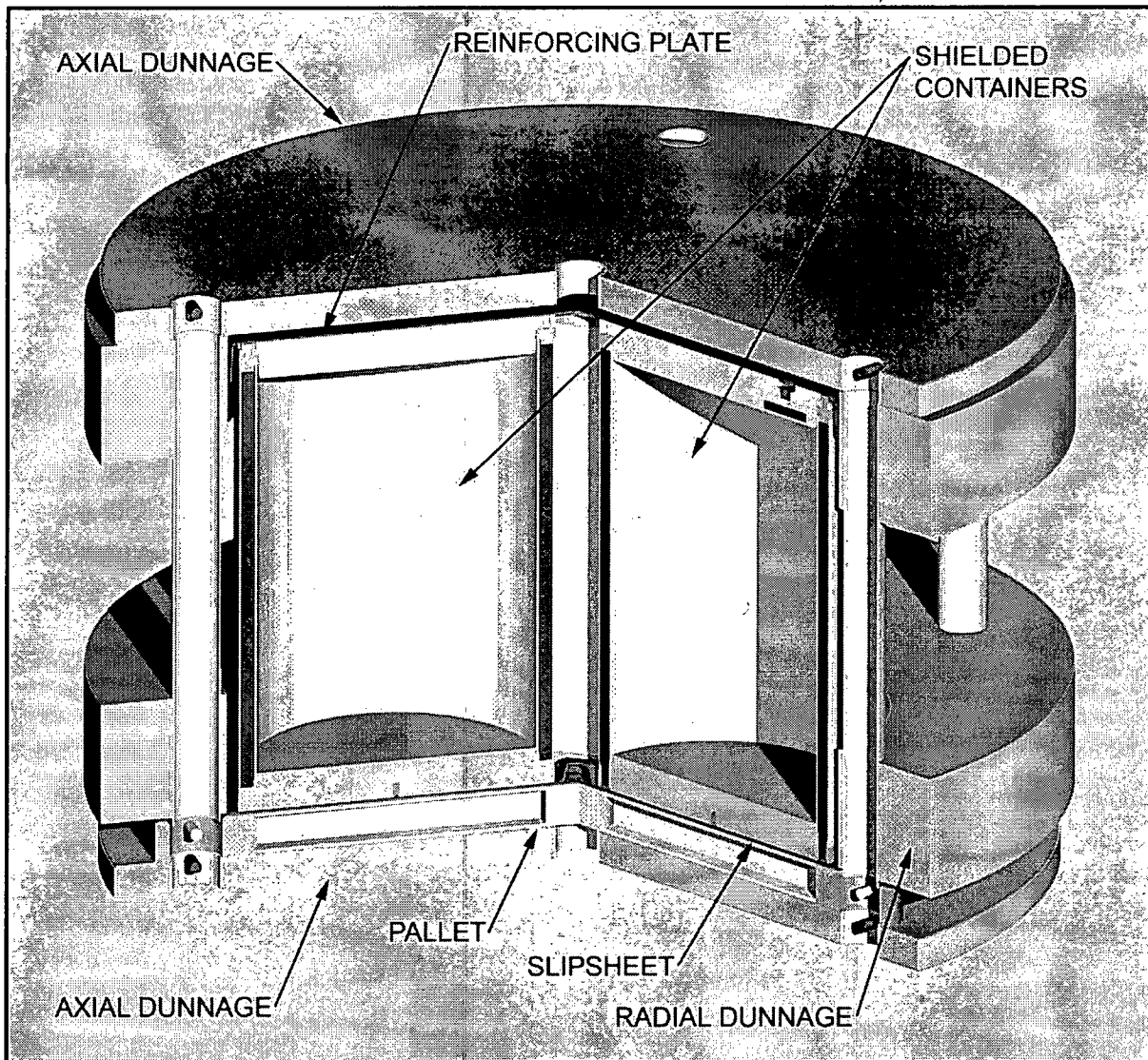


Figure 4.5-3 – Shielded Container Payload Components (Assembled View)

4.5.3 Structural Evaluation

Since the shielded container is vented, it is not subject to pressure loads present within the HalfPACT package's containment boundary.

Based on the following paragraphs, the shielded container payload configuration is, from a HalfPACT packaging perspective, bounded by previous certification testing for the HalfPACT package as currently presented in the HalfPACT SAR.

4.5.3.1 Structural Evaluation for Normal Conditions of Transport

Under normal conditions of transport (NCT), the shielded container maintains both confinement and shielding integrity. Since confinement and shielding integrity has been demonstrated for hypothetical accident conditions (HAC) without loss of fine particulate confinement or degradation

of the shielding material, as discussed in Section 4.5.3.2, *Structural Evaluation for Hypothetical Accident Conditions*, and HAC bounds NCT, demonstrations specific to NCT are not necessary.

4.5.3.2 Structural Evaluation for Hypothetical Accident Conditions

Under HAC, the shielded container confines its contents within its shielded boundary. To demonstrate confinement and shielding integrity of the shielded container, a full-scale test program was conducted.³ Since confinement integrity was maintained, and the shielding material did not reconfigure during HAC testing, NCT is bounded by the HAC test program.

Three shielded containers were assembled on a triangular spaceframe pallet and installed, including axial and radial dunnage assemblies, within a HalfPACT inner containment vessel (ICV). The package was subjected to two 30-foot free drops onto a flat, essentially unyielding, horizontal surface: a vertical end drop and a horizontal side drop. The HalfPACT outer confinement assembly (OCA), with its energy absorbing polyurethane foam, was conservatively omitted from the tests. At the conclusion of the second 30-foot free drop, each shielded container was removed from the ICV, sprayed with water, and visually examined for the presence of fluorescein dye to verify confinement integrity. Each shielded container was subsequently opened and subjected to shielding integrity testing to verify shielding integrity.

To conservatively test to the maximum allowable payload weight of 7,600 pounds within a HalfPACT packaging, each test shielded container utilized a 30-gallon steel drum (approximately 35 pounds empty) filled with approximately 455 pounds of concrete and 70 pounds of sand, for a total loaded weight of 560 pounds.

To address shielded container performance and any potential for adverse effects on the HalfPACT packaging containment and confinement boundaries when transporting shielded containers, it is only necessary to perform 30-foot free drop tests for the flat bottom and side orientations. This is because both the radial dunnage assembly and the axial dunnage assemblies (acting in conjunction with the adjacent aluminum honeycomb end spacers) have been independently designed to absorb 100% of the payload energy associated with a 30-foot drop.

In an end drop orientation, virtually all payload related energy is absorbed by a combination of crushing the aluminum honeycomb end spacer (primary energy absorber) and an axial dunnage assembly (secondary energy absorber). As demonstrated by the bottom end drop testing, the payload pallet structure was minimally deformed and can therefore be assigned no significant energy absorbing role. The radial dunnage assembly also plays no significant energy absorbing role in an end drop and was undamaged.

Conversely, the payload pallet, axial dunnage, and honeycomb end spacer assemblies remain undamaged in a side drop, while the radial dunnage assembly absorbs all the energy associated with the three loaded shielded containers.

Any drop orientation other than end or side would partially crush both the axial and radial energy absorbing dunnage components, but each to a lesser degree than what occurs for the more limiting end and side drop tests. As such, for other drop orientations, loads on both the HalfPACT ICV as well as on the shielded containers themselves are more distributed (i.e., partially shared by both end and side structures) and of lesser magnitude than those experienced in flat end or side drops. Also, from a post-

³ *Regulatory Hypothetical Accident Condition Type B Testing for the HalfPACT Shielded Container Payload*, WP 08-PT.15, Rev. 0, Washington TRU Solutions, December 2007.

HAC shielding point of view, the greatest shift of the shielded containers within the ICV will occur for the end and side drop tests. Finally, the relatively large post-drop residual radial and axial clearances that existed between the shielded containers and the ICV clearly demonstrated that there is no potential for the shielded containers to directly impact, or in any way compromise, the HalfPACT ICV.

Further technical justification for the selected drop orientations, testing at ambient temperature, and testing without internal pressure is provided in Section 5.0 of the test report.³ The position of the three test shielded containers, B01, B02, and B03 is given in Figure 4.5-4.

4.5.3.2.1 End Drop

The end drop was performed using an unprotected HalfPACT ICV that was stiffened at its lower end to conservatively simulate a cold impact deceleration acting on the HalfPACT package of 409g if the OCA were present. Given the circumferentially uniform and permanent deformation that occurred just above the stiffeners at the lower end of the ICV shell in the shielded container end drop test (absent in all prior TRUPACT-II and HalfPACT testing that included an OCA), it is clear that stiffening of the ICV for the shielded container testing conservatively bounded the overall system deceleration that would exist if an OCA was present.

The total deformation to the lower end payload components was approximately 6.2 inches for the ambient temperature testing; the deformation would modestly increase to 6.51 inches for NCT hot conditions. Figure 4.5-5, Figure 4.5-6, Figure 4.5-7, and Figure 4.5-8 illustrate end drop damage to these components. Correspondingly, the maximum estimated acceleration to the shielded containers, including an adjustment for the worst-case cold temperature, was 62.1g. The end drop acceleration was sufficiently low to preclude any amount of lead movement from the end drop test, as demonstrated by subsequent shielding integrity testing and physical sectioning of one of the test shielded containers (see Section 4.5.3.2.3, *Post-Drop Shielding Integrity Testing and Destructive Disassembly*). Potential lead movement at NCT hot conditions is also addressed in Section 5.0 of the test report³ and shown to be insignificant. No damage was visible on the exterior of the shielded containers as a result of the end drop test.

4.5.3.2.2 Side Drop

The side drop was also conservatively performed using an unprotected HalfPACT ICV (i.e., without the energy absorbing HalfPACT OCA). The aluminum honeycomb end spacer, axial dunnage, and pallet assemblies at the ends of the shielded containers remain undamaged in a side drop, but serve to maintain the relative position of the containers within the radial dunnage assembly and ICV. For this reason, the lower honeycomb end spacer and axial dunnage assembly that were damaged in the end drop test were removed and replaced prior to the side drop test with a steel space frame of the correct overall height to re-center the shielded containers within the ICV and radial dunnage assembly.

In the case of a side drop, the radial dunnage assembly must absorb all of the drop-induced kinetic energy of the shielded containers. To maximize damage to the radial dunnage assembly and maximize the load acting on a single shielded container for the side drop test, the shielded containers were oriented to place a single shielded container and the least amount of radial dunnage thickness (9 $\frac{3}{8}$ inches thick) directly in line with the impact point. Figure 4.5-9, Figure 4.5-10, Figure 4.5-11, and Figure 4.5-12 depict the pre-side drop configuration and post-side drop damage.

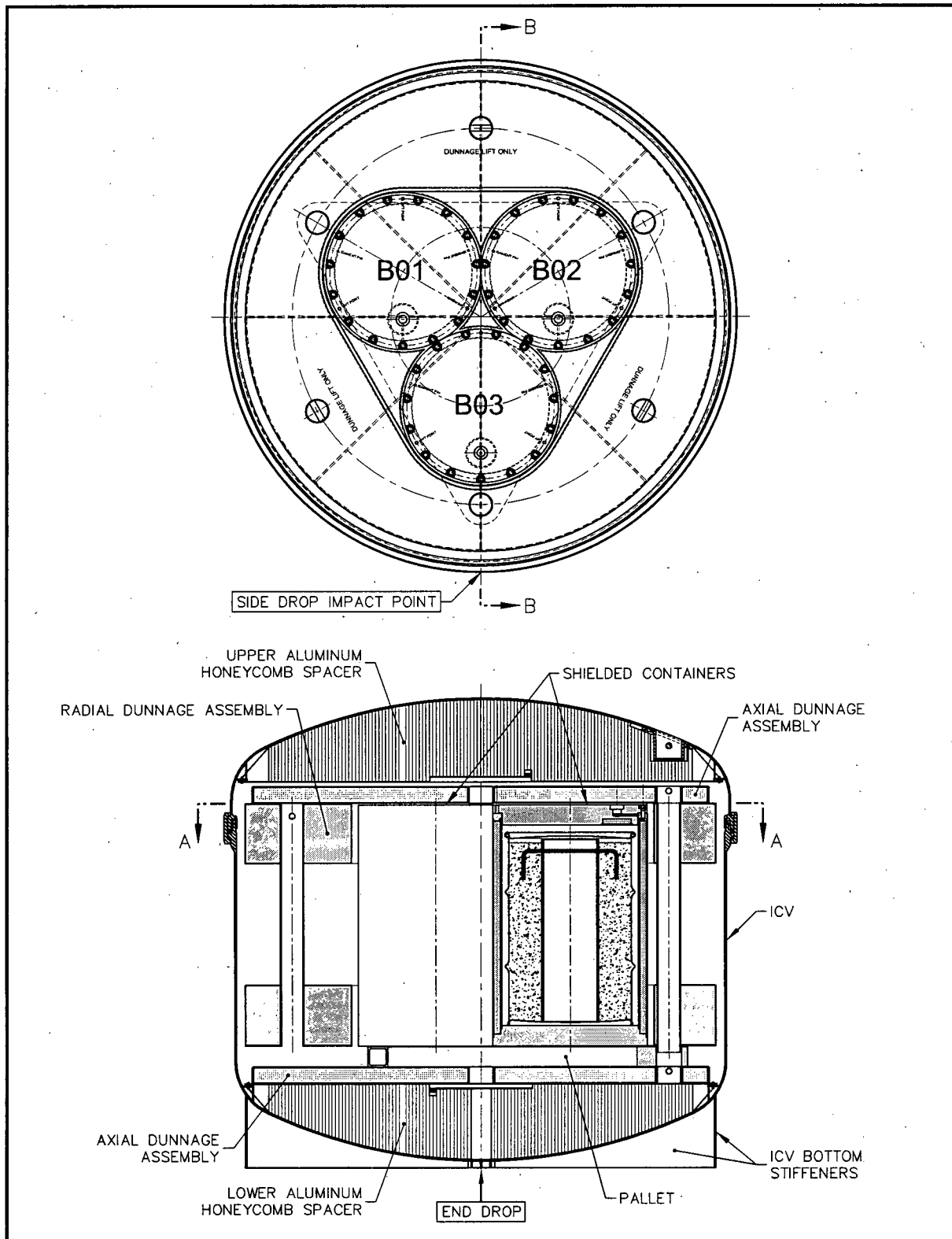


Figure 4.5-4 – Test Configuration and Orientations

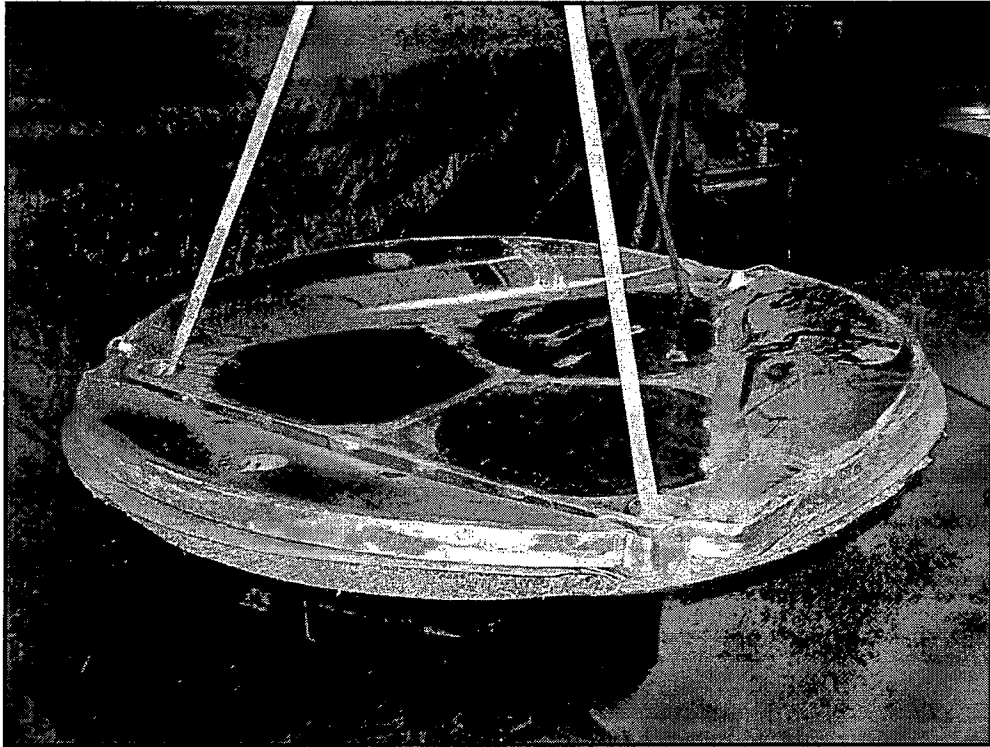


Figure 4.5-5 – End Drop Damage to the Lower Payload Components.

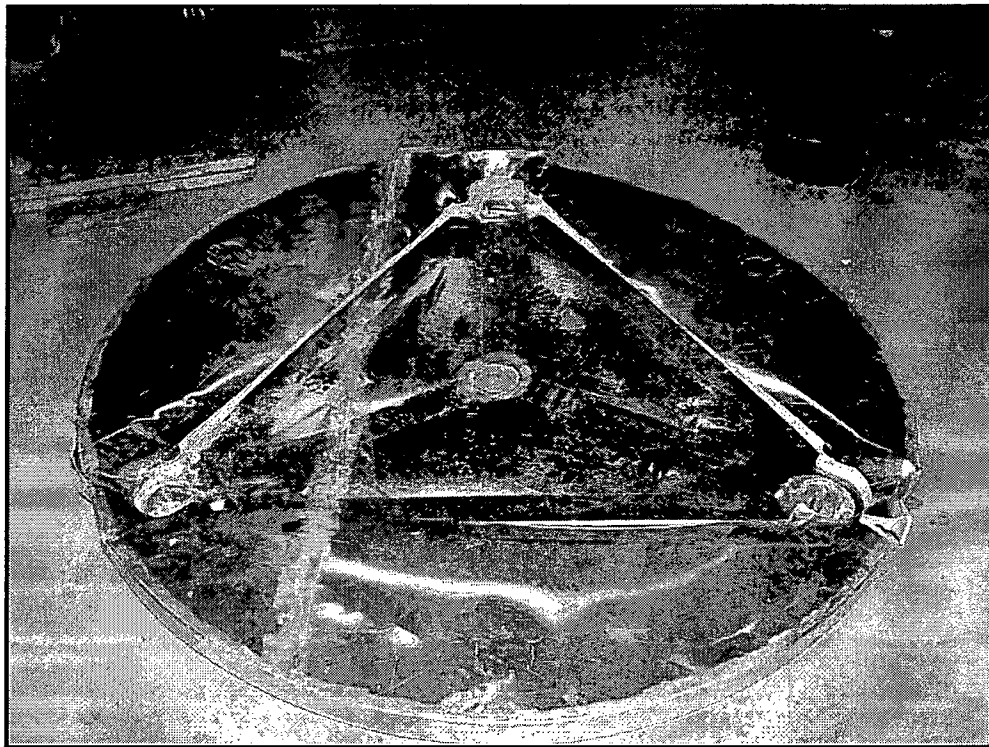


Figure 4.5-6 – End Drop Damage to the Lower Axial Dunnage

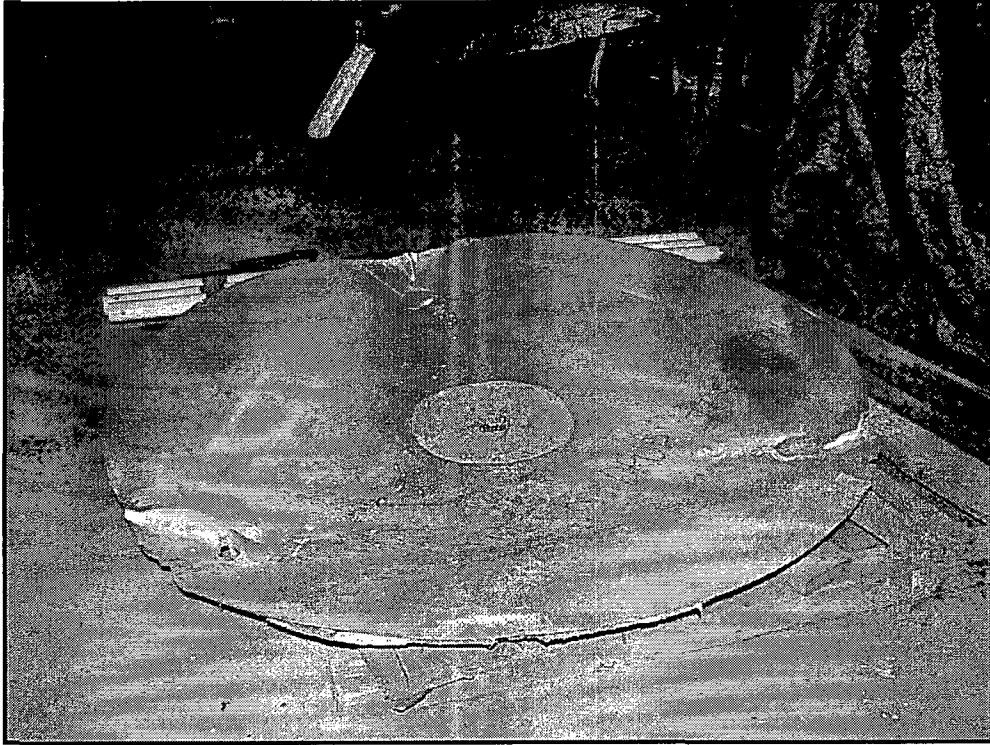


Figure 4.5-7 – End Drop Damage to the Lower Spacer (Top View)

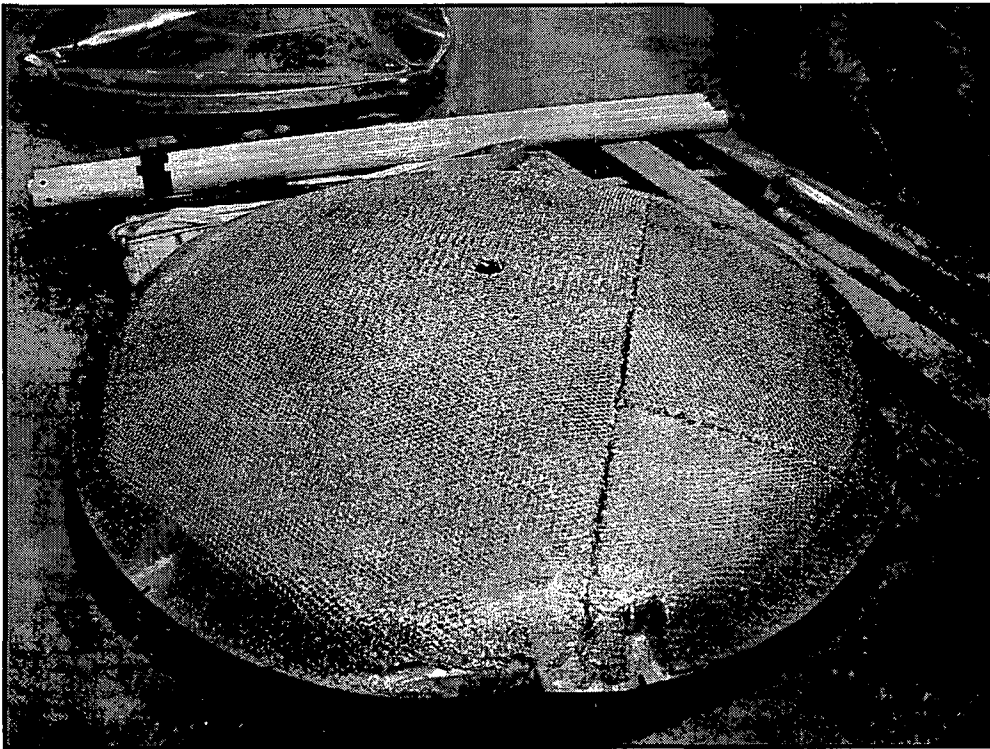


Figure 4.5-8 – End Drop Damage to the Lower Spacer (Bottom View)

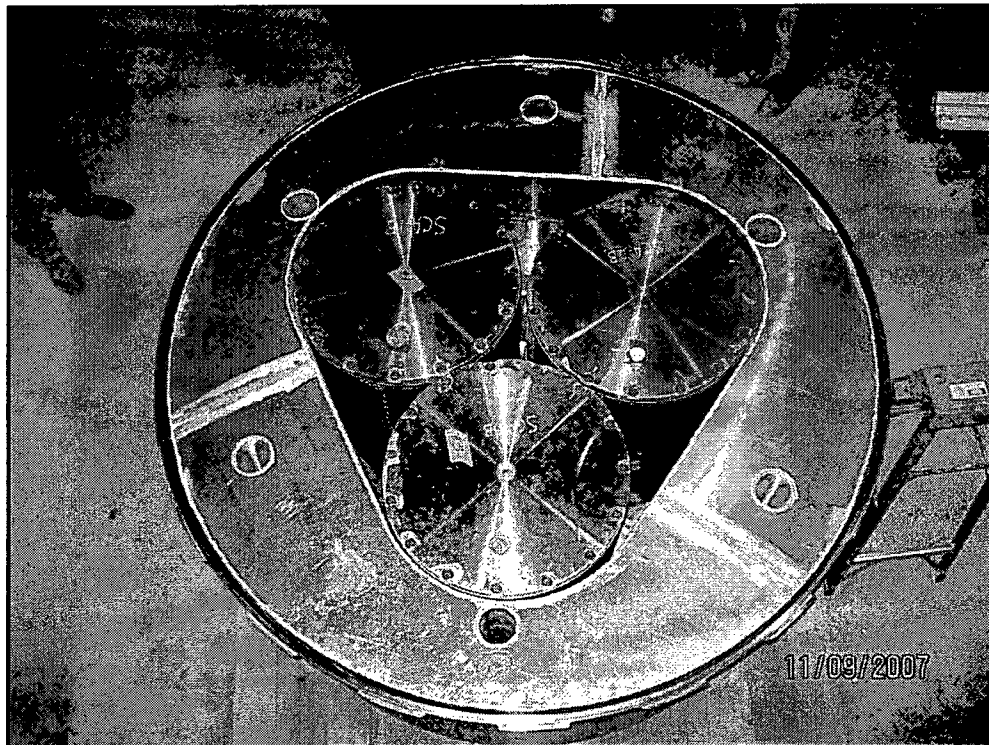


Figure 4.5-9 – Pre-Side Drop Radial Dunnage Configuration

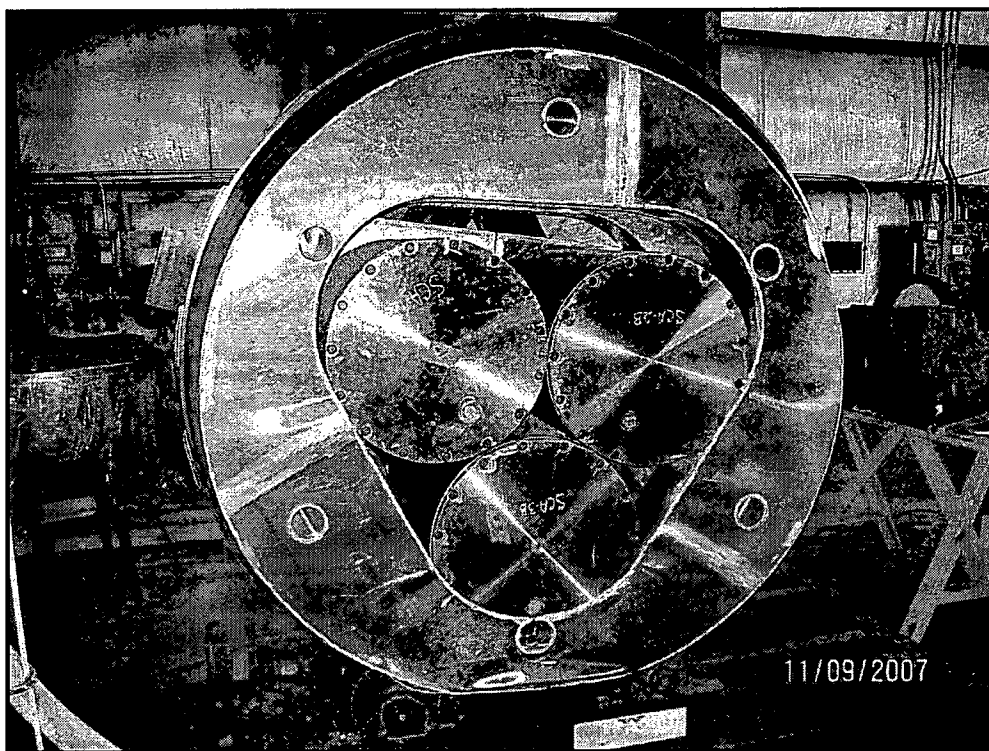


Figure 4.5-10 – Post-Side Drop Radial Dunnage Damage

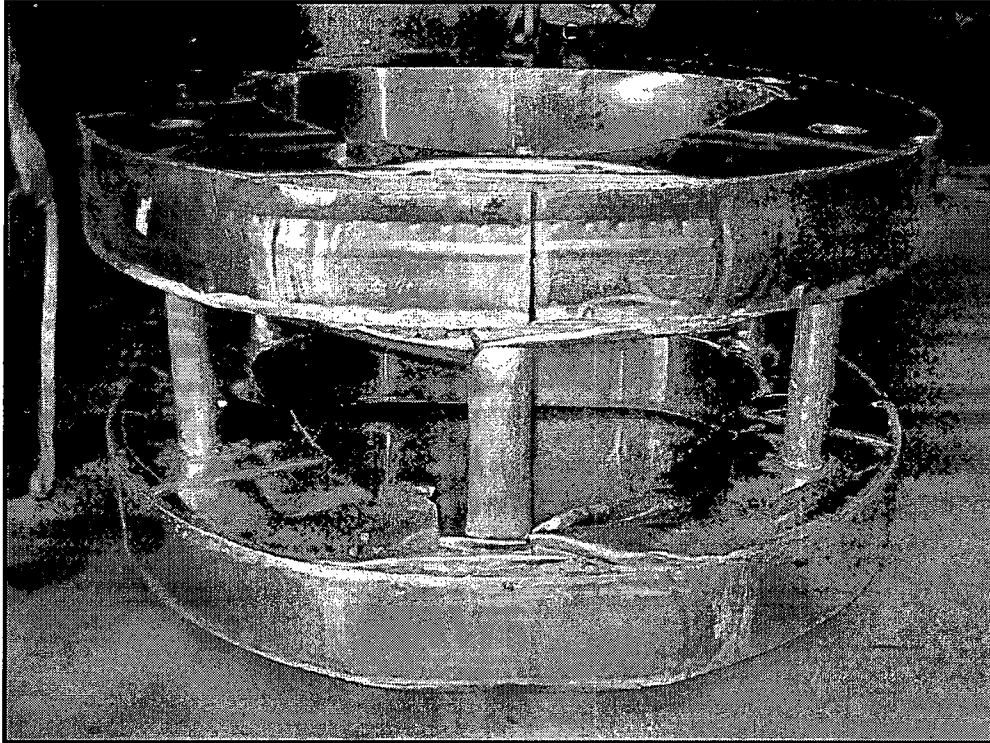


Figure 4.5-11 – Side Drop Damage to the Radial Dunnage (Outside)

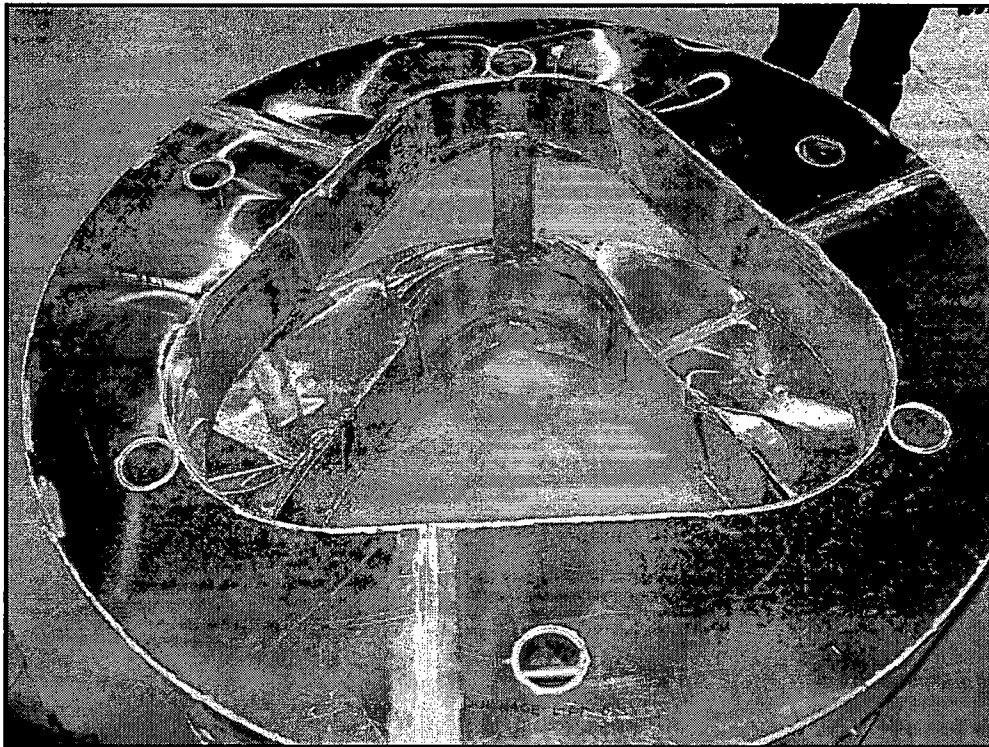


Figure 4.5-12 – Side Drop Damage to the Radial Dunnage (Inside)

The resulting measured deformation of the radial dunnage was 4 $\frac{3}{8}$ inches. Adjusting for the worst-case hot temperature and the minimum allowed radial dunnage room temperature foam crush strength, the estimated maximum deformation becomes 7.07 inches, or 3/4 of the original thickness. Sufficient thickness remains to ensure that all the kinetic energy of the three shielded containers for the side drop event is fully absorbed by the radial dunnage.

Visible damage to the shielded containers was limited to localized flattening of the outer shell-to-flange/base welds that were in contact at shielded container to shielded container interface points during the side drop event.

Section 2.10.3.7.2.2 in the HalfPACT SAR¹ reports a side drop deformation of the OCA of 3 $\frac{3}{4}$ inches. Conservatively assuming no deformation of the radial dunnage occurs, the 3 $\frac{3}{4}$ -inch deformation of the OCA sidewall can be used to establish a bounding lateral acceleration applicable to the shielded containers of 194g. Conservatively treating the shielded container as a simply supported beam, and ignoring any strength from the lead itself, the bending capacity of the shielded container's inner and outer shells is over 400g. Thus, significant design margin exists to prevent yielding of the shells.

4.5.3.2.3 Post-Drop Shielding Integrity Testing and Destructive Disassembly

Pre- and post-drop shielding integrity testing involved the use of a radiation detector and a Co-60 gamma source. A tripod apparatus was mounted to each shielded container's bolting flange and used to control detector/source spacing and location.

A gridded Mylar overlay allowed repeatability; grid spacing was set at 1 $\frac{1}{2}$ inches or less, and the zero circumferential position was arbitrarily set at the outer shell's longitudinal seam weld. Each axial row consisted of 49 sets of readings around the circumference, with 24 total axial rows; 1,176 data points were taken to fully map the lead.

The pre-drop test and post-drop test curves at each axial row tend to track together, with little indication that either localized or global changes to the shielding occurred. With a few exceptions limited to the very ends of the containers, changes in measured dose rates were less than 10%.

In addition to shield integrity testing, two full length cross-sections (wall cut-outs) were taken from test shielded container B03, since it was the container subjected to the most cumulative damage. As can be seen in Figure 4.5-13 and Figure 4.5-14, lead slump did not occur, nor was movement of lead apparent anywhere along the cross-section. Additional detail relative to shielding integrity testing and sectioning of shielded container B03 is provided in Section 6.3 of the test report.³

4.5.3.2.4 Summary of Testing

Key test observations include the following:

1. Post-test visual inspection of the interior and exterior surfaces of the three shielded containers indicated no apparent global or localized deformation or damage to the shielded containers. The solid, concrete-filled rolling hoops in the 30-gallon test payload drums left no visible deformation of the shielded container's inner shell, even through these drums were loaded to exceed the 2,260-pound shielded container gross weight. Visible damage was limited to localized flattening (~2 inches long) of the outer shell-to-flange/base welds in contact at shielded container to shielded container interfaces during the side drop event.

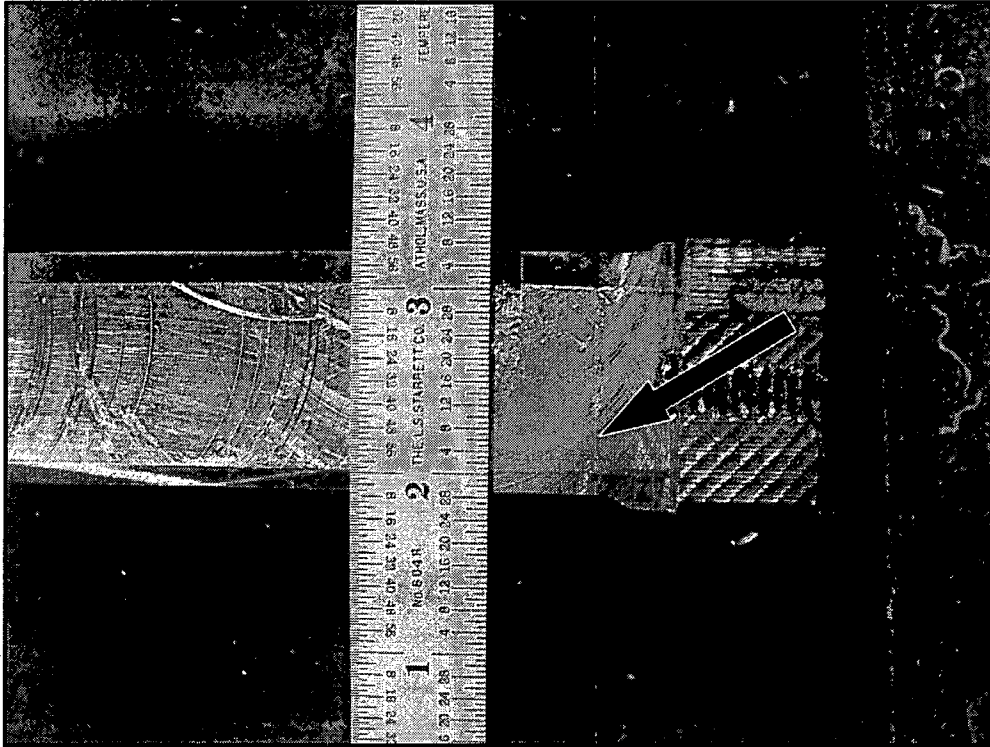


Figure 4.5-13 – Axial Slice in B03 at Lowest Point; Upper End

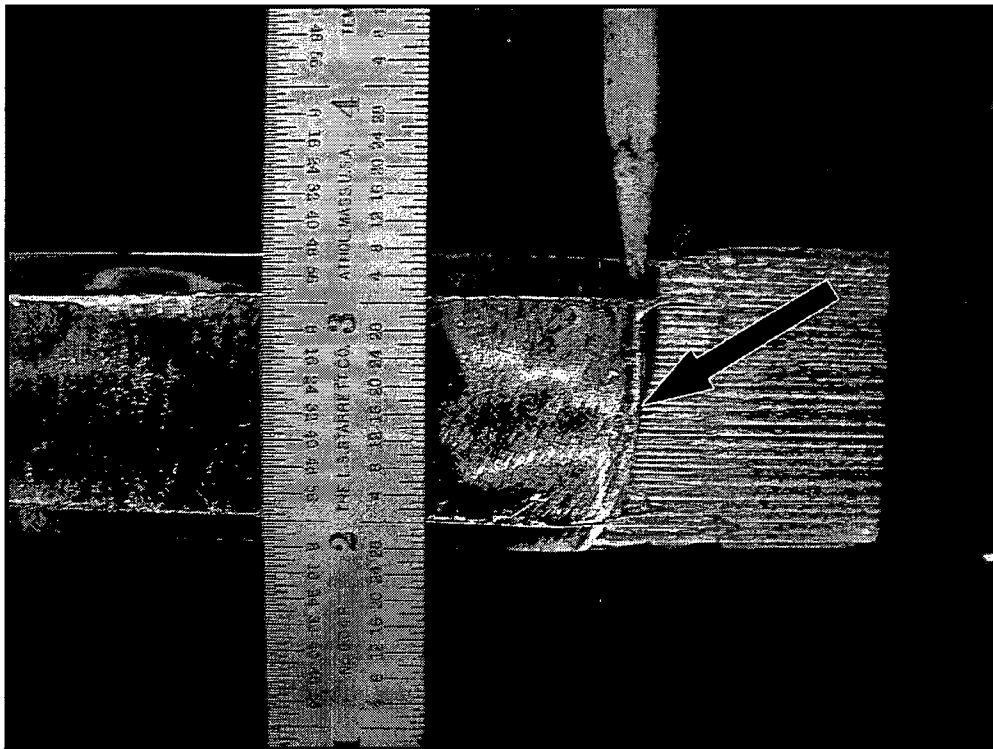


Figure 4.5-14 – Axial Slice in B03 at B02 Interface; Upper End

2. Post-test visual inspection of the HalfPACT ICV shell at its interface with payload dunnage components revealed no localized deformations that could in any way compromise containment integrity.
3. Subsequent to the performance of end and side drop testing, most closure bolts retained full residual torque, and all closure bolts retained some residual torque; 4 bolts on test shielded container B01, no bolts on test shielded container B02, and 1 bolt on test shielded container B03 lost a portion of their torque. In addition, the flour/fluorescein mixture placed within each shielded container was 100% retained throughout the testing. Collectively, these observations readily confirmed confinement integrity of the shielded containers.
4. Pre- and post-test shielding integrity tests coupled with destructive disassemblies of selected shielded container side walls showed no evidence of lead slump or changes of any significance to the shielding capabilities of the design. Post-test visual inspection of the shielded container wall cut-outs revealed some modest global and localized shell deformation, but the magnitudes were very limited, of no structural significance, and not coupled with measurable lead thinning or reduction in shielding.

In summary, the results of the testing program for the shielded containers demonstrate that under HAC the shielded containers maintain both confinement integrity and shielding integrity, and incur little visible damage.

4.5.4 Thermal Evaluation

4.5.4.1 Thermal Evaluation for Normal Conditions of Transport

The thermal analysis⁴ model of the HalfPACT packaging was developed using the computer programs Thermal Desktop⁵ and SINDA/FLUINT⁶. The thermal model of the shielded containers within the HalfPACT packaging is a composite of a newly generated 'solids' model of the shielded containers, the waste contents, and the associated dunnage, pallets, etc. and an existing two-dimensional lumped parameter model of the HalfPACT packaging. Using a feature of the SINDA/FLUINT computer program, these 'submodels' are combined into a single thermal model and solved simultaneously to generate a unified thermal solution. Since the thermal model of the shielded container and its pallet and dunnage assemblies represent a three-dimensional, 180° symmetry model, six segments of the two-dimensional, lumped parameter HalfPACT SAR model, each encompassing a 30° wide segment of the packaging circumference, are combined to form a matching 180° symmetry model of the packaging. Thermal connections between the individual 30° wide, two-dimensional segments are computed based on the model dimensions associated with each model node and the circumferential distance between adjacent segments. The model uses the same material properties for the package's components as used for the HalfPACT SAR analysis.¹

⁴ G. J. Banken, *HalfPACT Shielded Container Thermal Analysis*, P04F.M2.02-03, Rev. 2, AREVA Federal Services LLC, Tacoma, WA, February 2009.

⁵ Thermal Desktop®, Version 4.8, Cullimore & Ring Technologies, Inc., Littleton, CO, 2005.

⁶ SINDA/FLUINT, Systems Improved Numerical Differencing Analyzer and Fluid Integrator, Version 4.8, Cullimore & Ring Technologies, Inc., Littleton, CO, 2005.

The layout of the shielded containers within the HalfPACT packaging requires that a 180° symmetry model be used to allow the simulation of both an even distribution of decay heat loading as well as a case where all the decay heat is concentrated in a single shielded container. This level of analysis requires the modeling of 1½ shielded containers. The modeling uses a combination of surface and solid elements to simulate the container's base, the inner and outer shells, the lead shielding, and the lid. The modeling conservatively assumes a uniform air gap between the lead and the outer shell of the containers due to differential shrinkage between the lead and the carbon steel following lead pour; the gap is assumed to be 0.007 inches at room temperature, and 0 inches at 620 °F.

The 30-gallon drum payload is simulated as a solid with homogenous thermal properties and a volumetric heat generation. The interior dimensions of a generic 30-gallon drum (i.e., 18.25-inch inside diameter and 27.5-inch height) are used to set the volume and surface areas of the payload drum. The payload drum is assumed to be centered in the radial direction and resting on the bottom of the shielded container. However, since the payload drum is assumed to have a rolled rim, no direct contact is assumed between the base of the payload drum and the container. Instead, heat transfer between the payload drum and the container is assumed to be via conduction and radiation across an air gap, with a 1-inch gap at the top, a 1.075-inch gap at the side, and 0.45-inch gap at the bottom.

The pallet and dunnage assemblies are used to provide radial and axial restraint of the containers during transportation and during the regulatory drop events. Heat transfer between the shielded containers and the pallet and dunnage assemblies are modeled as conduction and radiation across the air gaps. The size of the air gaps are determined by the geometry of the design, with the exception that a 0.75-inch air gap is assumed between the surfaces of the shielded containers and the radial dunnage components.

Heat transfer between the shielded containers and the inner surfaces of the HalfPACT ICV are via conduction and radiation. Heat transfer between the shielded containers, the pallet, the axial and radial dunnage assemblies, and the ICV surfaces is simulated as conduction and radiation across the intervening air gaps.

Consistent with Section 3.1.3 of the HalfPACT SAR, maximum steady-state package temperatures with insolation are determined by using a combination of solar heating values. One steady-state analysis is made using the insolation values delineated in 10 CFR §71.71(c)(1), averaged over 24 hours. This action is intended to simulate the slow thermal response that the payload and internal package components have to a varying (i.e., cyclic) solar load. The presence of the HalfPACT's OCA polyurethane foam insulation and the relatively large thermal mass on the inside of the foam isolates (i.e., decouples) the thermal response of the internal components from the "12 hour on / 12 hour off" solar step function cycle applicable to the outside of the package. Thus, the peak temperatures of the components on the inside of the polyurethane foam are determined by applying the insolation values of 10 CFR §71.71(c)(1), averaged over 24 hours, to the exterior of the package. In contrast, the outer sections of the polyurethane foam and the OCA outer shell will respond more quickly to varying external solar loads. Therefore, the maximum steady-state temperatures of the polyurethane foam and OCA outer shell are estimated using another steady-state analysis and the 10 CFR §71.71(c)(1) insolation values averaged over 12 hours applied to the exterior of the package.

The payload within the shielded containers is conservatively assumed to be crumpled paper and to exhibit the thermal conductivity of air and possess zero thermal mass. This conservative representation of the payload bounds the potential temperature rise and temperature limit within a generic payload whose makeup prevents significant heat transfer via radiation and where its thermal conductance is dominated by trapped air spaces.

Table 4.5-1 summarizes the results for the NCT hot condition with insolation applied and 30 watts of decay heat distributed in three shielded containers (10 watts each), contrasted with the similar analysis in the HalfPACT SAR for seven 55-gallon drums. Similarly, Table 4.5-2 summarizes the results for the NCT hot condition with insolation applied and 30 watts of decay heat concentrated in one shielded container, contrasted with the similar analysis in the HalfPACT SAR for seven 55-gallon drums.

Table 4.5-1 – NCT Hot Temperatures with 30 Watts Evenly Distributed

Location	Solar Loading	Temperature (°F) for NCT Hot with Insolation	
		Three Shielded Containers	Seven 55-Gallon Drums (HalfPACT SAR)
Payload Drum Centerline • Shielded Container 1 / Center 55-Gallon Drum • Shielded Container 2 & 3 / Outer 55-Gallon Drums	24-hr avg	222	184
Payload Drum Bulk Average • Shielded Container 1 / Center 55-Gallon Drum • Shielded Container 2 & 3 / Outer 55-Gallon Drums	24-hr avg	179	170
Shielded Container 2 & 3 / Outer 55-Gallon Drums • Shielded Container 2 & 3 / Outer 55-Gallon Drums	24-hr avg	178	168
Shielded Container 1 / Center 55-Gallon Drum • Base • Lid / Seal • Sidewall	24-hr avg	155	156
Shielded Container 1 / Center 55-Gallon Drum • Lid / Seal	24-hr avg	156	156
Shielded Container 1 / Center 55-Gallon Drum • Sidewall	24-hr avg	156	156
Shielded Container 2&3 / Outer 55-Gallon Drums • Base • Lid / Seal • Sidewall	24-hr avg	155	153
Shielded Container 2&3 / Outer 55-Gallon Drums • Lid / Seal	24-hr avg	156	153
Shielded Container 2&3 / Outer 55-Gallon Drums • Sidewall	24-hr avg	156	153
ICV Wall • Maximum • Average • Minimum	24-hr avg	150	153
ICV Wall • Average	24-hr avg	149	149
ICV Wall • Minimum	24-hr avg	148	146
ICV Air • Average	24-hr avg	154	151
Main O-ring Seals • ICV Maximum • OCV Maximum	24-hr avg	148	147
Main O-ring Seals • OCV Maximum	24-hr avg	147	146
OCV Wall • Maximum • Average	24-hr avg	149	150
OCV Wall • Average	24-hr avg	147	147
Polyurethane Foam • Maximum • Bulk Average	12-hr avg	152	155
Polyurethane Foam • Bulk Average	24-hr avg	128	129
OCA Outer Shell • Maximum	12-hr avg	152	155

Table 4.5-2 – NCT Temperatures with 30 Watts Concentrated

Location	Solar Loading	Temperature (°F) for NCT Hot with Insolation	
		All Heat in One Shielded Container	All Heat in Center 55-Gallon Drum (HalfPACT SAR)
Payload Drum Centerline			
• Shielded Container 1 / Center 55-Gallon Drum	24-hr avg	342	340
• Shielded Container 2 & 3 / Outer 55-Gallon Drums	24-hr avg	155	153
Payload Drum Bulk Average			
• Shielded Container 1 / Center 55-Gallon Drum	24-hr avg	224	252
• Shielded Container 2 & 3 / Outer 55-Gallon Drums	24-hr avg	154	153
Shielded Container 1 / Center 55-Gallon Drum			
• Base	24-hr avg	156	163
• Lid / Seal	24-hr avg	158	163
• Sidewall	24-hr avg	158	163
Shielded Container 2&3 / Outer 55-Gallon Drums			
• Base	24-hr avg	155	153
• Lid / Seal	24-hr avg	155	153
• Sidewall	24-hr avg	155	153
ICV Wall			
• Maximum	24-hr avg	150	154
• Average	24-hr avg	149	148
• Minimum	24-hr avg	148	145
ICV Air			
• Average	24-hr avg	154	151
Main O-ring Seals			
• ICV Maximum	24-hr avg	148	145
• OCV Maximum	24-hr avg	147	144
OCV Wall			
• Maximum	24-hr avg	149	150
• Average	24-hr avg	147	146
Polyurethane Foam			
• Maximum	12-hr avg	152	155
• Bulk Average	24-hr avg	128	128
OCA Outer Shell			
• Maximum	12-hr avg	152	155

As can be seen in Table 4.5-1 and Table 4.5-2, temperatures for the shielded container payload configuration are very similar to corresponding temperatures for the 55-gallon drum payload from the HalfPACT SAR, especially for the HalfPACT packaging components. As such, the HalfPACT packaging components maintain the same margin of safety when transporting a shielded container payload compared to transporting a 55-gallon drum payload (or any other currently licensed payload).

4.5.4.2 Thermal Evaluation for Hypothetical Accident Conditions

No safety evaluations for HAC are required for the shielded container payload since the results are bounded by those presented in the HalfPACT SAR. The basis for this conclusion is as follows:

1. The level of heat input into the HalfPACT package during the HAC event is a function of the package's exterior surface area, the thermal mass of the package components, etc., which is essentially unaffected by the makeup of the payload.
2. The temperature response within the payload is a function of its thermal mass and the amount of heat passed to it by the HalfPACT packaging.
3. Since the heat input to the HalfPACT packaging during the HAC event is essentially the same between a package containing a base payload evaluated in the HalfPACT SAR and a package containing a payload of three shielded containers, the thermal HAC response of the HalfPACT package will be bounded by that presented in HalfPACT SAR.
4. Given a similar temperature response for the ICV shell under HAC conditions for either the base payload or the shielded container payload, the thermal response of the shielded container will be inversely proportional to the thermal mass and directly proportional to the surface area of the shielded container payload versus that existing for the base payload. The maximum payload mass (i.e., the packaging contents which includes the payload containers, waste contents, dunnage, pallets, etc) of the shielded container payload is identical to the maximum base payload mass. However, the combined surface area of the shielded container payload is lower than the combined surface area of the base payload drum payload. As such, the rate of heat transfer between the ICV and the shielded containers will be lower under HAC conditions than seen with the base payload due to the lower area for radiation and convection/conduction heat transfer. A lower rate of heat transfer combined with an equal payload mass means the temperature rise experienced by the shielded container payload will be bounded by that experienced by the base payload.

As such, the transient thermal behavior and the rise in the temperatures for the shielded containers within the HalfPACT packaging during the HAC fire event is bounded by that (i.e., $\Delta T = 156^{\circ}\text{F}$ to $290^{\circ}\text{F} = +134^{\circ}\text{F}$) reported for the base payload in Section 3.5.3 of the HalfPACT SAR. Since the melting point for lead is 620°F and the temperature limit for the silicone rubber seal material is 450°F ⁷, a HAC fire event would not reduce the effectiveness of the shielded container.

⁷ ORD 5700, *Parker O-ring Handbook*, 1992, Parker Hannifin Corporation, Cleveland, OH.

4.5.5 Shielding Evaluation

The evaluation of compliance with the radiation dose rate limits for NCT and HAC required by 10 CFR §71.47 is presented in Chapter 5 of the HalfPACT SAR¹ for the shielded container payload configuration. When the HalfPACT package is loaded with an assembly of shielded containers containing gamma and/or neutron source terms that are limited per Section 3.3 of the CH-TRAMPAC², the package meets the NCT radiation dose rate requirements of 200 mrem/hr at the surface of the package and 10 mrem/hr at 2 meters from the surface of the package under exclusive use. As a result, the packages also comply with the HAC dose rate requirement of 1 rem/hr at 1 meter from the surface of the package.

4.5.6 Criticality Evaluation

Shielded containers are designed to transport TRU waste forms with high gamma energies within a HalfPACT package. A criticality evaluation⁸ was performed for two different payload cases: (1) manually compacted waste, and (2) machine compacted waste. A maximum 325 fissile gram equivalent (FGE) of Pu-239 is justified for manually compacted waste, while a lower limit of 245 FGE is justified for machine compacted waste. The methodology and assumptions utilized in the existing HalfPACT SAR are also utilized in the current analysis. The following analyses demonstrate that this configuration complies with the requirements of 10 CFR §71.55 and §71.59. The criticality safety index, per 10 CFR §71.59, is 0.

Two general cases were developed. For Case G⁹ (manually compacted waste), the moderator was modeled as a composition of 25% polyethylene and 75% water (by volume). As polyethylene is a superior moderator than water, this composition results in higher reactivities than would be achieved by water moderation alone. This volume fraction of polyethylene is conservatively higher than the maximum value achievable for manually compacted (i.e., not machine compacted) waste determined by experiment. The reflector is modeled as a mixture of 25% polyethylene, 74% water, and 1% beryllium (by volume). Beryllium is a superior reflector than either water or polyethylene and the inclusion of beryllium is conservative, although at such a small volume fraction, the beryllium has only a small effect on the system reactivity.

For Case H (machine compacted waste), the moderator was modeled as 100% polyethylene. As polyethylene is a superior moderator than water, this composition results in higher reactivities than would be achieved by water moderation alone. The reflector is modeled as a mixture of 99% polyethylene and 1% beryllium (by volume). Beryllium is a superior reflector than polyethylene and the inclusion of beryllium is conservative, although at such a small volume fraction, the beryllium has only a small effect on the system reactivity.

Calculations for the HalfPACT package are performed using the three-dimensional Monte Carlo transport theory code, KENO-V.a v5.0.2, with the CSAS25 utility being used as a driver for the KENO-V.a code; both programs are part of the SCALE-PC v5¹⁰ code system. In this role,

⁸ R. J. Migliore, *HalfPACT Shielded Container Criticality Analysis*, P04F.M2.02-02, Rev. 0, Packaging Technology, Inc., Tacoma, WA, December 2007.

⁹ To avoid confusion, the case designations are selected to be additions to those utilized in the current HalfPACT SAR. Cases G and H are equivalent to Cases A and C, respectively, with modifications specific to the shielded container.

¹⁰ SCALE: *A Modular Code System for Performing Standardized Computer Analyses for Licensing Evaluation*, ORNL/TM-2005/39, Version 5, Vols. I-III, April 2005.

CSAS25 determines nuclide number densities, performs resonance processing, and automatically prepares the necessary input for the KENO-V.a code based on a simplified input description. The 238 energy-group (238GROUPNDF5), cross-section library based on ENDF/B-V cross-section data is used as the nuclear data library for the KENO-V.a code.

The upper subcritical limit (USL) for ensuring that the HalfPACT is acceptably subcritical, as determined in benchmark evaluations, is:

$$\text{USL} = 0.9377$$

The package is considered to be acceptably subcritical if the computed k_{safe} (k_s), which is defined as $k_{\text{effective}}$ (k_{eff}) plus twice the statistical uncertainty (σ), is less than the USL, or:

$$k_s = k_{\text{eff}} + 2\sigma < \text{USL}$$

In all models, the fissile material was assumed to form a single optimally moderated sphere. In actual practice, such a scenario is not credible because each shielded container is limited to 200 FGE. It is extremely unlikely that fissile material could escape from the shielded containers and reconfigure, or travel from one shielded container to another and reconfigure.

Conservative damage assumptions were utilized in both the NCT and HAC analysis. No credit was taken for the torispherical head of the HalfPACT, which would have increased separation distance in the array configuration. All foam and aluminum regions were replaced with reflector at the most reactive density. In the array models, the internal and external reflector densities were varied in order to maximize neutron interaction between packages.

This calculation modeled 1% by weight beryllium to account for the $\leq 1\%$ by weight presence of any special reflector materials. Special reflectors (other than beryllium) that are in $>1\%$ by weight quantities are allowed if they are chemically or mechanically bound to the fissile material. Lead and steel were not considered "special reflectors," although these materials are more reflective than poly/water at large thicknesses. As the shielded containers have thick steel lids and bottoms, and lead side walls clad in steel, the presence of the shielded containers slightly increased the reactivity. Various configurations of fissile sphere and shielded container were utilized. The most reactive configuration (for both single package and array) always occurred when the fissile sphere was in a corner of a shielded container, which maximized reflection.

The maximum reactivity of the single package and infinite array models were nearly identical for most cases. This indicated that neutron communication between packages was rather limited, and the fissile material was largely isolated. Note that differences of approximately 0.002 between the various model results is often simply due to statistical fluctuation. The most reactive HAC single package model, with three shielded containers in a row, the fissile sphere shifted to the upper right corner in the center shielded container, and an H/Pu ratio of 900 ($k_s = 0.9372$), is statistically equivalent to the most reactive HAC array model, with one shielded container modeled at the side and top of the ICV, the fissile sphere located at the side and top of the shielded container, the OCA and external reflector modeled as a void, and an H/Pu ratio of 900 ($k_s = 0.9368$), although the arrangements within the package are quite different. Case G results in higher reactivities than Case H, although Case H has a much lower fissile mass. All results are below the USL of 0.9377.

Case G, the manually compacted waste stream, has a justifiable limit of 325 FGE per HalfPACT, and Case H, the machine compacted waste stream, has a justifiable limit of 245 FGE per HalfPACT. The corresponding results are summarized in Table 4.5-3.

Table 4.5-3 – Summary of Criticality Evaluation Results

Limit	Case G 325 FGE Manually Compacted Waste	Case H 245 FGE Machine Compacted Waste
Normal Conditions of Transport (NCT)		
	k_s	k_s
Single Unit Maximum	0.9354	0.9302
Infinite Array Maximum	0.9355	0.9313
Hypothetical Accident Conditions (HAC)		
	k_s	k_s
Single Unit Maximum	0.9372	0.9298
Infinite Array Maximum	0.9368	0.9340
USL = 0.9377		

4.5.7 Authorized Payload Contents for the Shielded Container

As demonstrated in Section 4.5.5, *Shielding Evaluation*, when loaded with gamma and/or neutron emitting isotopes with maximum activity limits summarized in the CH-TRAMPAC, the shielded container payload meets the NCT and HAC dose rate limits. As demonstrated in Section 4.5.6, *Criticality Evaluation*, when loaded with fissile material with maximum mass limits summarized for Cases G and H in Table 4.5-3, the shielded container payload meets the calculated reactivity limit and is safely subcritical.

4.5.8 Conclusion

The shielded container design consists of a vented carbon steel and lead cylindrical structure with a removable lid, surrounded by axial and radial dunnage, that is to be used for shipment of specific transuranic waste forms in the HalfPACT package.

The analyses summarized in this appendix demonstrate the ability of the shielded container to safely transport limited quantities of gamma and/or neutron emitting isotopes and fissile isotopes. Using geometries consistent with, or conservative with respect to, the structural and thermal analyses, the shielding evaluation showed that the dose rate limits for NCT and HAC (including appropriate shielding damage assumptions in each case) are met with the maximum authorized contents. In addition, the criticality evaluation showed that the reactivity limit is met for manually or machine compacted wastes with specified mass limits.

APPENDIX 4.6

DESCRIPTION OF CRITICALITY CONTROL OVERPACK

This page intentionally left blank.

4.6 Description of Criticality Control Overpack

4.6.1 Introduction

The Criticality Control Overpack (CCO) is an approximately 24-inch diameter, 35-inch tall steel 55-gallon drum with a stainless steel Criticality Control Container (CCC) and plywood Upper and Lower Dunnage assemblies. It is designed to be used for shipment of increased fissile waste contents in the TRUPACT-II and HalfPACT packages. Drawing 163-009 in Appendix 1.3.1 of the TRUPACT-II Safety Analysis Report¹ (SAR) and HalfPACT SAR² and Section 2.9.11 of the *Contact-Handled Transuranic Waste Authorized Methods for Payload Control* (CH-TRAMPAC)³ delineate the materials of construction, sizes, and other dimensional specifications for the CCO.

The TRUPACT-II and HalfPACT packages can accommodate an assembly of fourteen (14) and seven (7) CCOs, respectively. As configured for shipment, the CCO payload assembly remains conservatively within the previously established design and certification bases and limits of the TRUPACT-II and HalfPACT packages for payload weight and decay heat. Limits on CCO activity and fissile content are also set consistent with previously implemented and accepted analytic approaches.

This appendix describes the structural, thermal, shielding, and criticality bases of the CCO payload.

4.6.2 Description

The CCO consists of a steel 55-gallon drum containing a CCC confinement vessel that is centrally positioned within the drum by laminated plywood dunnage. The CCC is constructed of 304/304L stainless steel 6-inch Class 150 standard blind and slip flanges and Schedule 40 pipe (NPS). The lid of the CCC is sealed with an aramid-inorganic/nbr standard ring gasket and retained with eight (8) 3/4-inch heavy hex head stainless steel bolts. The lid and base of the CCC are nominally 1 inch thick and the pipe shell is nominally 0.28 inches thick with an overall assembly height of approximately 29-1/2 inches. The CCO has an approximate tare weight of 230 pounds and a maximum gross weight of 350 pounds. A lifting attachment is optionally integrated into the CCC lid to facilitate handling.

Partially exploded views of the CCO and CCC are provided in Figure 4.6-1 and Figure 4.6-2, respectively. Both the 55-gallon drum and CCC must be fitted with a filter vent; Section 2.5 of the CH-TRAMPAC provides the minimum specification for the CCO filter vents.

¹ U.S. Department of Energy (DOE), *TRUPACT-II Shipping Package Safety Analysis Report*, USNRC Certificate of Compliance 71-9218, U.S. Department of Energy, Carlsbad Field Office, Carlsbad, New Mexico.

² U.S. Department of Energy (DOE), *HalfPACT Shipping Package Safety Analysis Report*, USNRC Certificate of Compliance 71-9279, U.S. Department of Energy, Carlsbad Field Office, Carlsbad, New Mexico.

³ U.S. Department of Energy (DOE), *Contact-Handled Transuranic Waste Authorized Methods for Payload Control* (CH-TRAMPAC), U.S. Department of Energy, Carlsbad Field Office, Carlsbad, New Mexico.

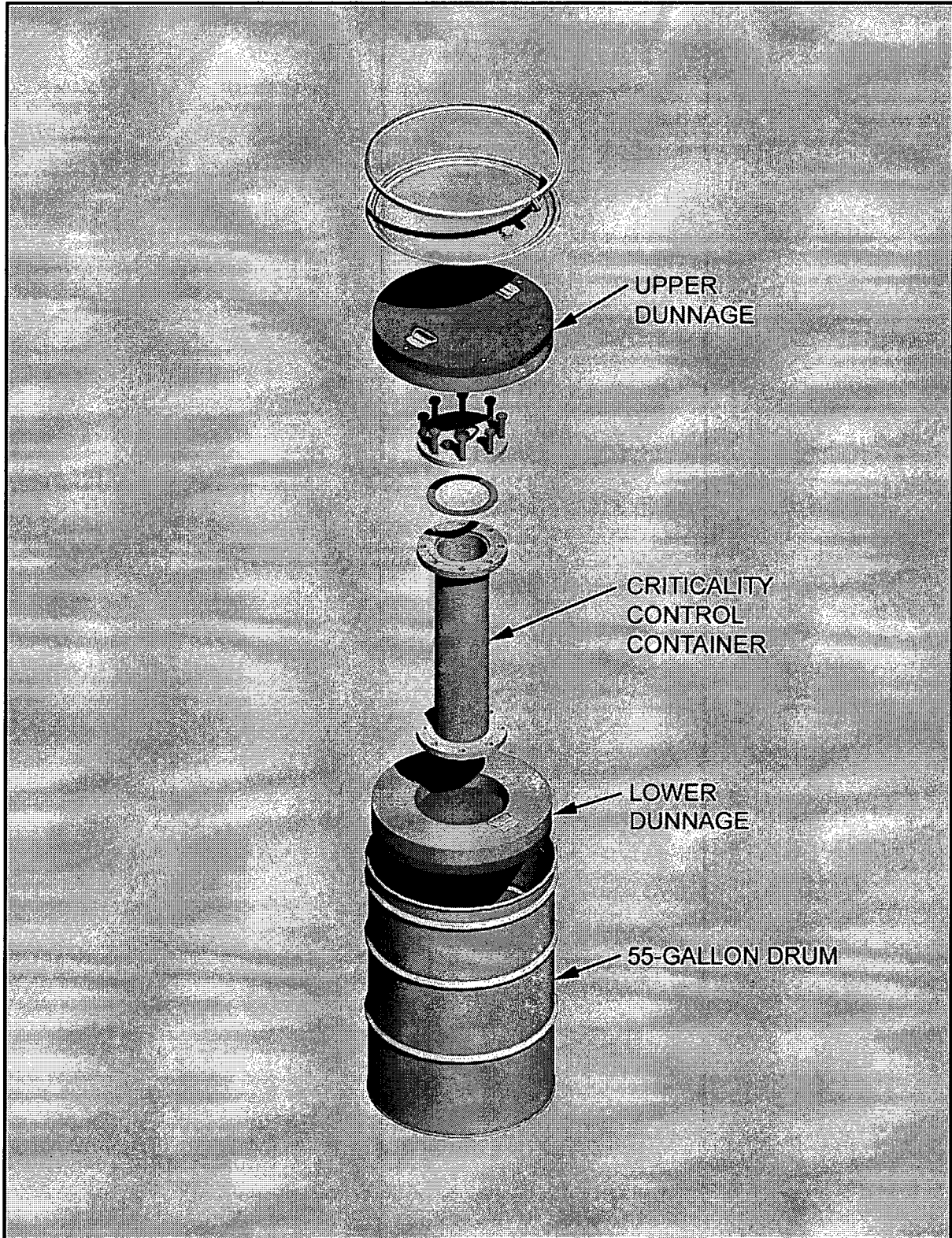


Figure 4.6-1 – Criticality Control Overpack

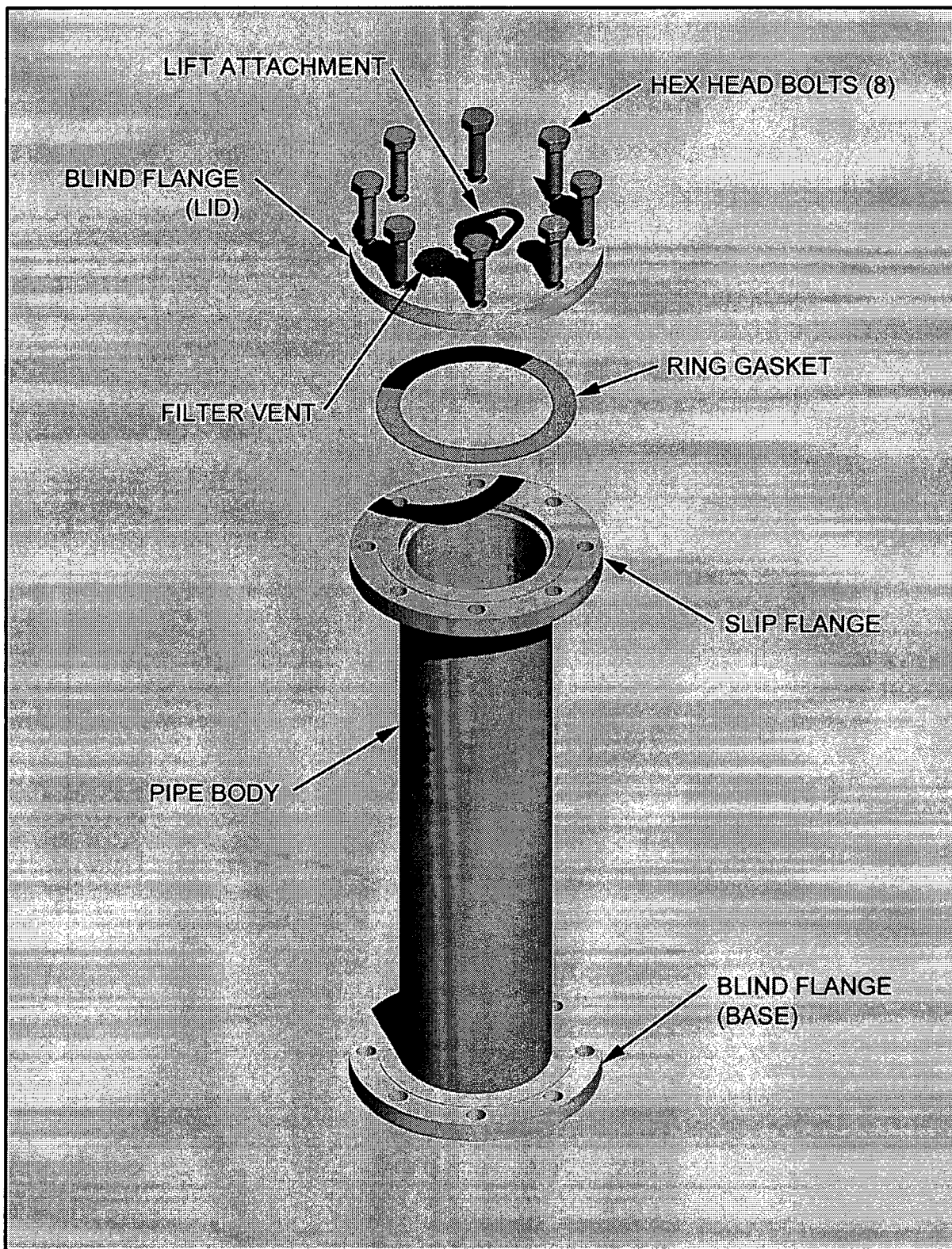


Figure 4.6-2 – Criticality Control Container

4.6.3 Structural Evaluation

The CCO payload configuration is, from a TRUPACT-II and HalfPACT packaging perspective, bounded by previous certification testing for the TRUPACT-II and HalfPACT package as currently presented in the TRUPACT-II and HalfPACT SARs. Therefore, the following structural evaluations are specific to determining the response of the CCOs when subject to transport and accident conditions when transported in the TRUPACT-II and HalfPACT packages.

4.6.3.1 Structural Evaluation for Normal Conditions of Transport

Under normal conditions of transport (NCT), the CCO maintains confinement, shielding integrity, and array spacing for criticality control. Since confinement, shielding integrity, and criticality control has been demonstrated for hypothetical accident conditions (HAC) without loss of fine particulate confinement, as discussed in Section 4.6.3.2, *Structural Evaluation for Hypothetical Accident Conditions*, and HAC bounds NCT, demonstrations specific to NCT are not necessary.

4.6.3.2 Structural Evaluation for Hypothetical Accident Conditions

Under HAC, the CCO retains its contents within the CCC confinement boundary. To demonstrate confinement, shielding integrity, and adequate array spacing for criticality control of the CCO, a full-scale test program was conducted.⁴ Since confinement integrity was maintained, the shielding capability of the container was not reduced, and adequate array spacing was maintained for criticality control during HAC testing, NCT is bounded by the HAC test program.

Two CCO test articles were assembled and attached to side and end drop test fixtures comprised of plate steel to conservatively simulate the overburden forces and boundary conditions associated with a payload assembly of CCOs within the TRUPACT-II packaging Inner Containment Vessel (ICV). The impact-attenuating characteristics of the TRUPACT-II Outer Confinement Assembly (OCA), with its energy-absorbing polyurethane foam, was conservatively neglected from consideration in the tests. Each CCO test article and associated drop test fixture was subjected to a 30-foot free drop onto a flat, essentially unyielding, horizontal surface: one horizontal side drop and one vertical top-down end drop with the CCO at hot (>200 °F) conditions. At the conclusion of the 30-foot free drops, the CCO test articles were dimensionally inspected to determine the radial crush deformation due to the side drop and the axial crush deformation due to the end drop. The CCC test articles were also disassembled from the CCOs, misted with water, and visually examined for the presence of fluorescein dye to verify confinement integrity.

To conservatively test to the maximum allowable CCO gross weight of 350 pounds, each CCO test article was directly loaded with 137 pounds of a 50/50 (by volume) mixture of lead shot and sand topped with a flour/fluorescein indicator mixture, for a total CCO test article weight of 352 pounds.

⁴ Petersen Inc., *Criticality Control Overpack 30-Foot Free Drop Post-Test Summary Report*, Engineering Report 8448-R-001, Rev. 1, Ogden UT, March 2011.

4.6.3.2.1 Technical Basis for the Tests

The following sections supply the technical basis for the chosen free drop test orientations, the use of test fixtures as surrogates for the CCO payload assembly, and the free drop test temperatures and pressures.

4.6.3.2.1.1 Justification for Drop Orientations

To address CCO performance, it is only necessary to perform 30-foot free drop tests for the end and side orientations. Intermediate impact angles simply distribute the interaction forces at lower g-levels between the CCOs and the ICV, whereas the 0° and 90° impact orientations maximize the impact accelerations and localized bearing forces in a manner to maximize the potential for CCC confinement boundary and CCO dunnage crush damage. As such, side and end drop test orientations are bounding for the design.

The requirements of 10 CFR §71.73(c)(1) are satisfied as the drop test orientations are associated with positions for which maximum damage to the CCO is expected.

4.6.3.2.1.2 Justification for Use of Side and End Drop Test Fixtures

Due to the maximum gross weight limit of the CCO being 350 pounds, resulting in a total payload assembly weight that is significantly lower than the 7,265-pound and 7,600-pound payload capacity authorized for the TRUPACT-II and HalfPACT packagings, respectively, the packaging response to a CCO payload is bounded by the current packaging certification tests.

Both the side and end drops are performed on an unprotected (bare) CCO, resulting in higher deformations and acceleration loads to the CCO payload than if inside the impact-attenuating TRUPACT-II or HalfPACT packagings. Therefore, the CCO drop tests are a conservatively bounding determination of the minimum post-drop radial and axial CCO array spacing for the criticality evaluation.

4.6.3.2.1.2.1 Side Drop

As shown in Figure 4.6-3, the CCO side drop test fixture is designed to load the CCO test article with a compressive load equal to four CCOs. The basis for the loading configuration is derived from the configuration depicted in Figure 4.6-5. The total vertical load on the bottom CCO is based on the weight of two CCOs atop the bottom CCO, plus one-half the weight from each of the four side CCOs; the other half of the weight from each of the four side CCOs is assumed to be carried by the ICV. Note that the component of horizontal compressive loading into the bottom CCO caused by the four side CCOs would tend to oppose the vertical compressive load and is, therefore, ignored to maximize overall crush and minimize radial spacing.

4.6.3.2.1.2.2 End Drop

As shown in Figure 4.6-4, the CCO end drop test fixture is designed to load the CCO test article with a compressive axial load equal to one CCO. The end drop test fixture duplicates the two-high drum configuration in the TRUPACT-II package and will result in the maximum overall crush and minimum axial spacing.

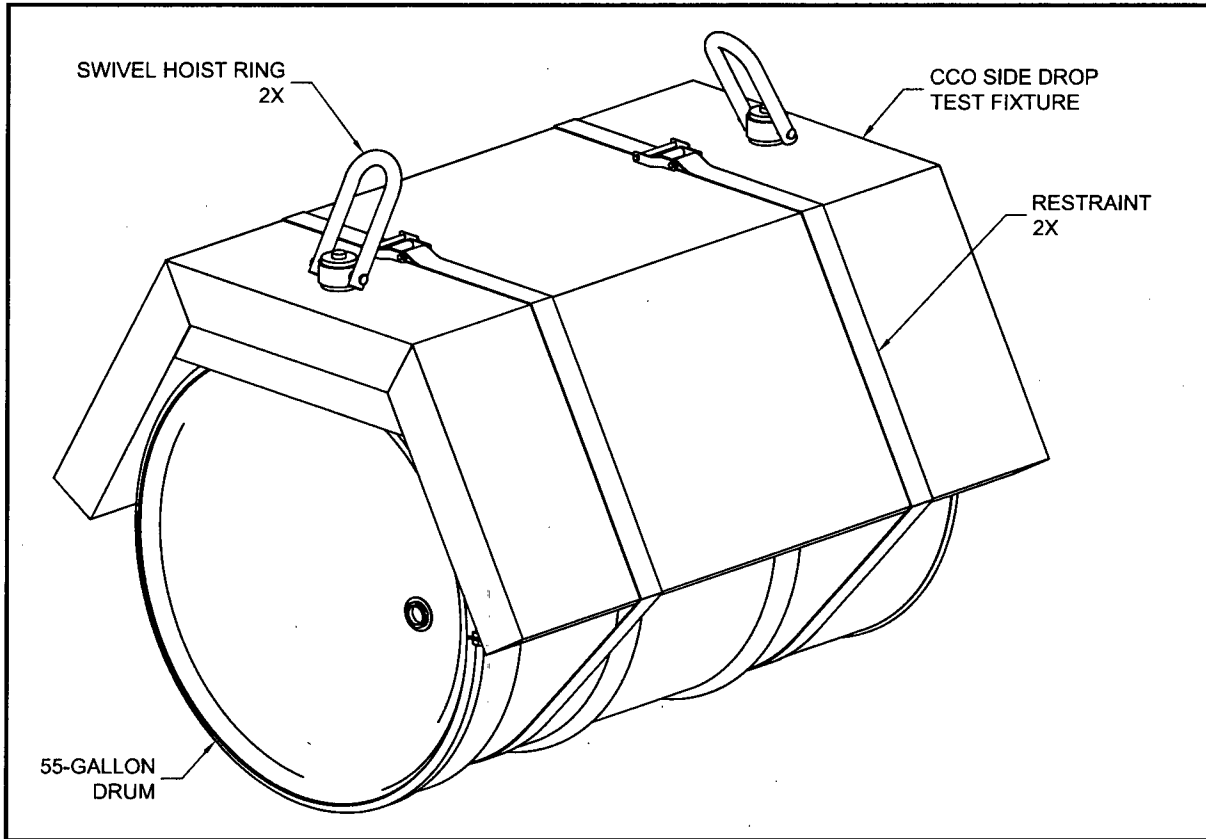


Figure 4.6-3 – Side Drop Test Configuration

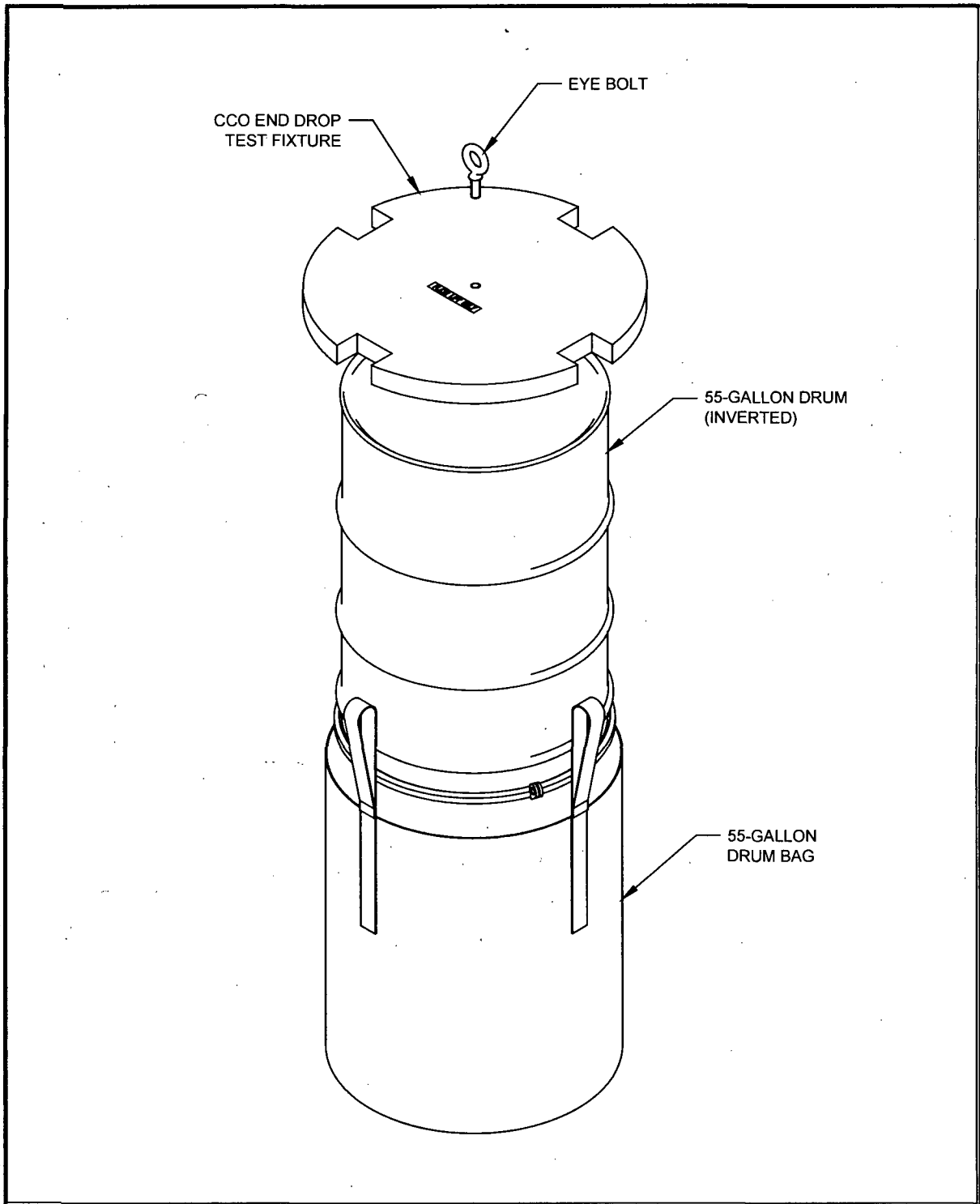


Figure 4.6-4 – End Drop Test Configuration

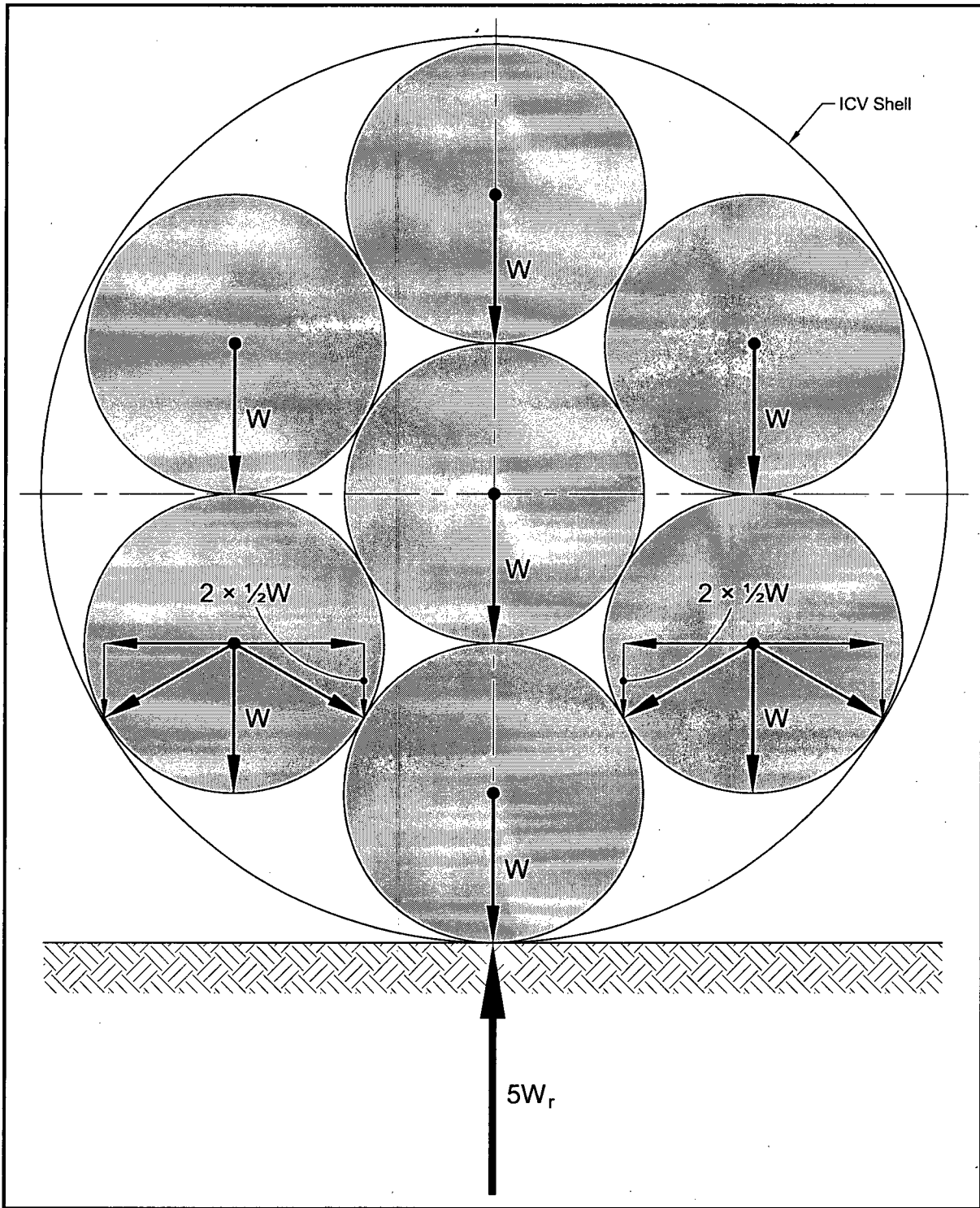


Figure 4.6-5 – Side Loading Free Body Diagram

4.6.3.2.1.3 Justification for Test Temperatures

The CCO side and end drops were performed with the CCO test article conditioned to >200 °F to bound the NCT hot condition. The elevated temperature maximizes the crush deformation of the plywood upper and lower dunnage assemblies, conservatively providing an upper bound on the post-drop CCO payload assembly array spacing for criticality purposes.

4.6.3.2.1.4 Justification for Test Pressure

These CCOs are vented and not subject to differential pressures; hence, internal pressurization of the CCO is not applicable.

4.6.3.2.2 Side Drop Results

The 30-foot hot side drop was performed using a CCO side drop test fixture weighing 1,452 pounds attached to the CCO side drop test article that was dropped in a horizontal orientation to radially impact directly onto the essentially unyielding drop pad surface. The test conservatively simulated the interaction between the lowest CCO and the six upper CCOs in a seven-pack array inside a TRUPACT-II or HalfPACT ICV. The test configuration neglected both the impact-attenuating characteristics of the packaging and the compliance of the upper CCOs in the array to maximize the impact accelerations on the CCC and crush deformation of the dunnage assemblies.

Post-drop inspection of the CCO indicated significant crushing of the 55-gallon drum and internal plywood dunnage assemblies that resulted in a minimum effective diameter of the CCO that measured 16¾ inches at the lid end and 15½ inches at the base end of the container (pre-drop diameter of the 55-gallon drum was Ø24 inches). The upper and lower plywood dunnage assemblies experienced a corresponding radial crush deformation, but the assemblies attenuated the impact and prevented any direct interaction between the CCC and the test fixture/pad. The measured accelerations due to impact were recorded with filtering of the data utilizing a low-pass Butterworth 10-pole filter having a 250 Hz cut-off frequency. A minimum impact acceleration peak, on average from two sensors, of approximately 233 g's was recorded.

Disassembly of the CCO and inspection of the CCC indicated no permanent plastic deformation of any of the confinement boundary components, essentially unaltered preload of the closure bolts (maximum bolt rotation to achieve installation torque value of 3.5°), and no loss of confinement as confirmed via black-light inspection of the assembly with no presence of the fluorescein indicator.

Figure 4.6-6 shows the CCO side drop test article and test fixture assembly prior to the drop test. Figure 4.6-7 shows the assembly during and after the side impact event. Figure 4.6-8 shows the post-test measurement of the effective diameter of the CCO and associated radial crushing of the dunnage assemblies. Figure 4.6-9 shows the CCC after the post-drop test confinement evaluation and bolt residual torque confirmation process, indicating no degradation of the confinement vessel.



Figure 4.6-6 – Side Drop Test Assembly



Figure 4.6-7 – Side Drop Test Assembly During and After Impact



Figure 4.6-8 – Post-Side Drop Inspection of CCO Radial Deformation

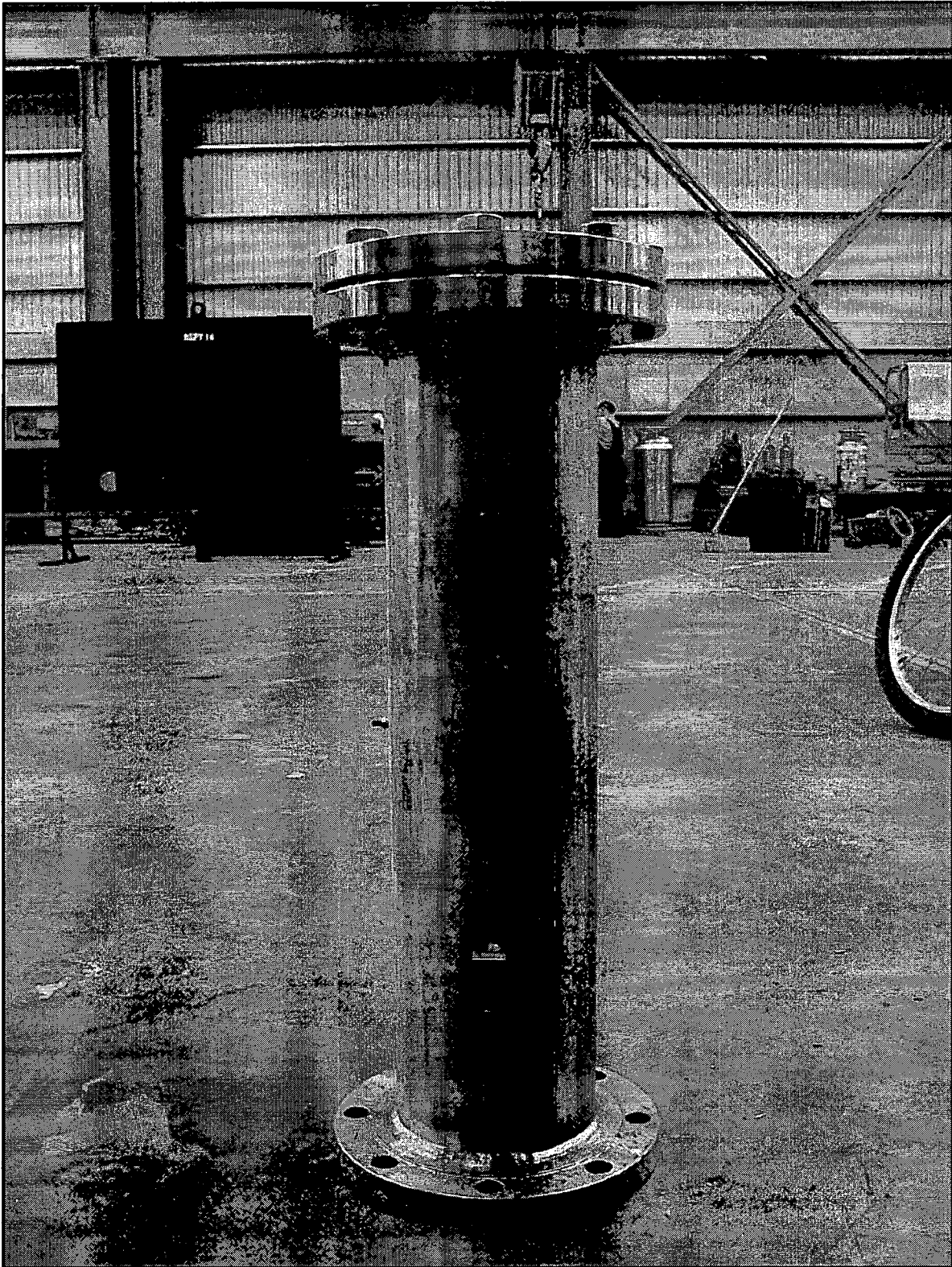


Figure 4.6-9 – Post-Side Drop Evaluation of CCC

4.6.3.2.3 End Drop Results

The 30-foot hot end drop was performed using a CCO end drop test fixture weighing 357 pounds attached to the CCO end drop test article that was dropped in an inverted vertical orientation to axially impact directly onto the essentially unyielding drop pad surface. The test conservatively simulated the interaction between a CCO in a lower seven-pack array and a CCO in an upper seven-pack array inside a TRUPACT-II. The test article was oriented to maximize the loads on the closure interface. The test configuration neglected both the impact-attenuating characteristics of the packaging (e.g., honeycomb payload spacers) and the compliance of the other axially adjacent CCO in the stacked 14-pack arrangement to maximize the impact accelerations on the CCC and crush deformation of the dunnage assemblies.

Post-drop inspection of the CCO indicated measurable crushing of the 55-gallon drum and internal plywood dunnage assemblies that resulted in a minimum effective height of the CCO that measured between 31 $\frac{1}{8}$ inches and 32 inches (pre-drop height of the 55-gallon drum was 35 inches). The upper and lower plywood dunnage assemblies experienced a corresponding axial crush deformation, but the assemblies attenuated the impact and prevented any direct interaction between the CCC and the test fixture/pad. The measured accelerations due to impact were recorded with filtering of the data utilizing a low-pass Butterworth 10-pole filter having a 250 Hz cut-off frequency. A minimum impact acceleration peak, from one reporting sensor, of approximately 411 g's was recorded.

Disassembly of the CCO and inspection of the CCC indicated no permanent plastic deformation of any of the confinement boundary components, essentially unaltered preload of the closure bolts (maximum bolt rotation to achieve installation torque values of 5°), and no loss of confinement as confirmed via black-light inspection of the assembly with no presence of the fluorescein indicator.

Figure 4.6-10 shows the CCO end drop test article and test fixture assembly prior to the drop test. Figure 4.6-11 shows the assembly during and after the end impact event. Figure 4.6-12 shows the post-test measurement of the effective axial height of the CCO and associated axial crushing of the dunnage assemblies. Figure 4.6-13 shows the CCC after the post-drop test confinement evaluation and bolt residual torque confirmation process, indicating no degradation of the confinement vessel.

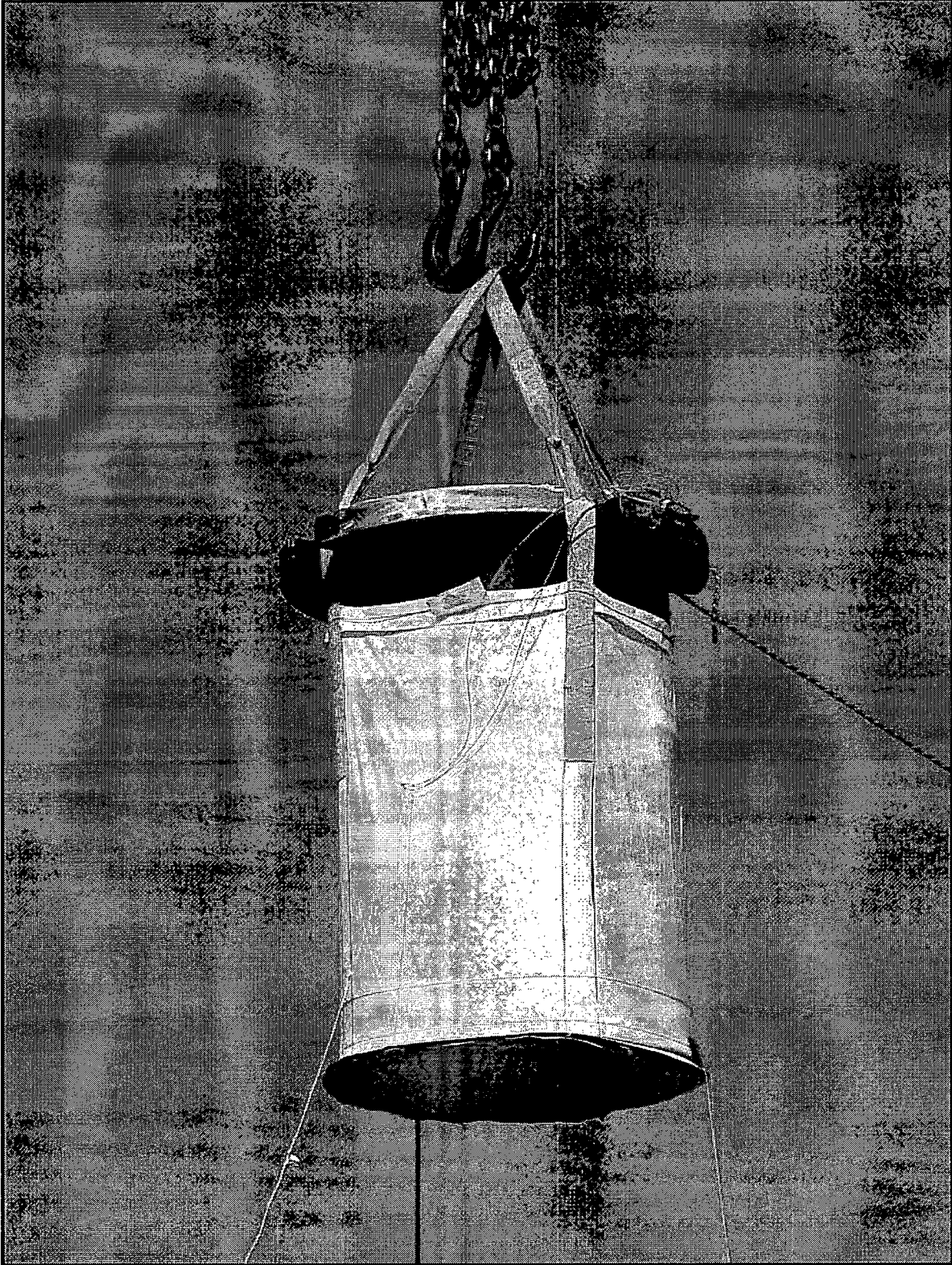


Figure 4.6-10 – End Drop Test Assembly

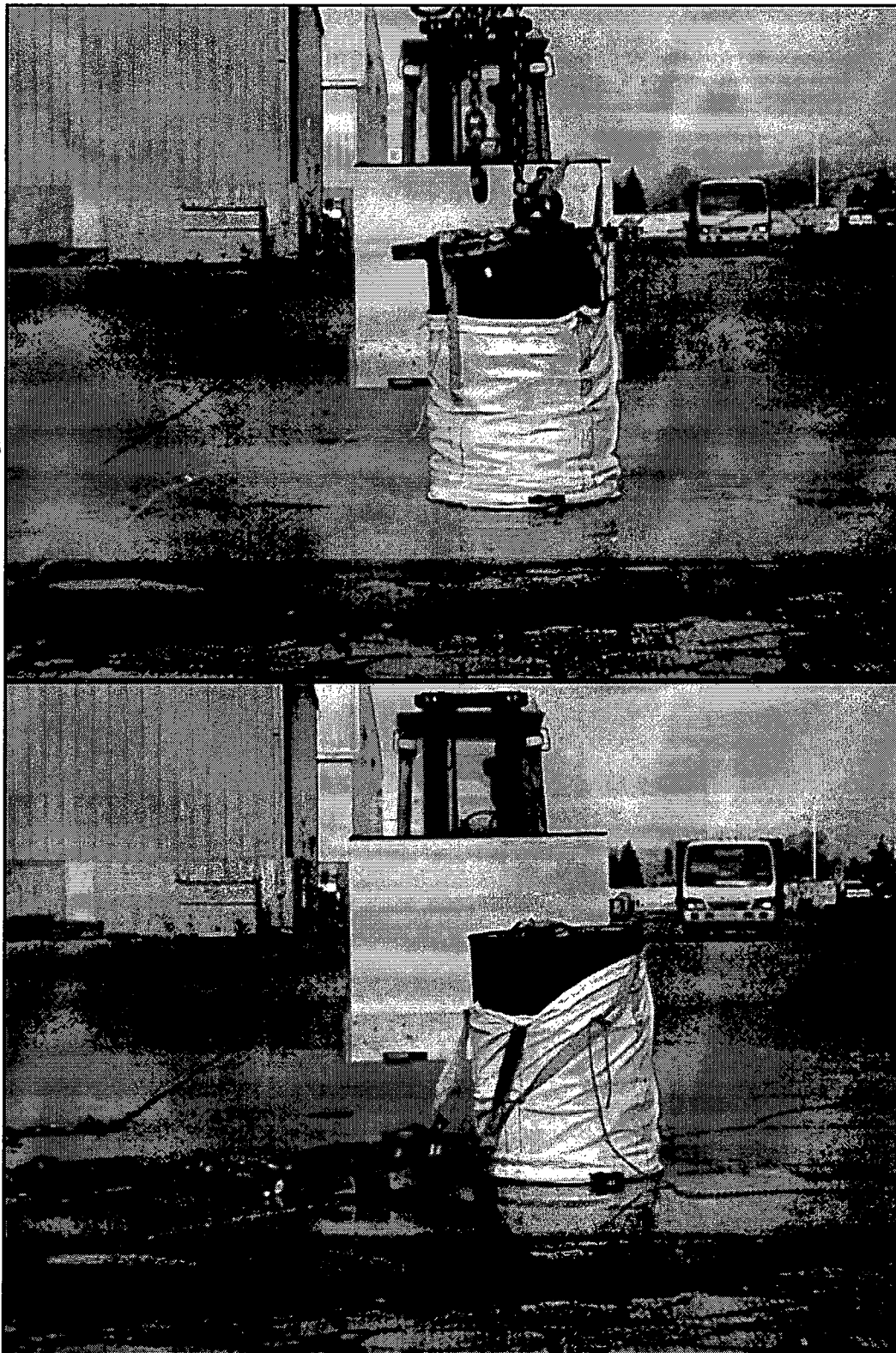


Figure 4.6-11 – End Drop Test Assembly During and After Impact



Figure 4.6-12 – Post-End Drop Inspection of CCO Axial Deformation

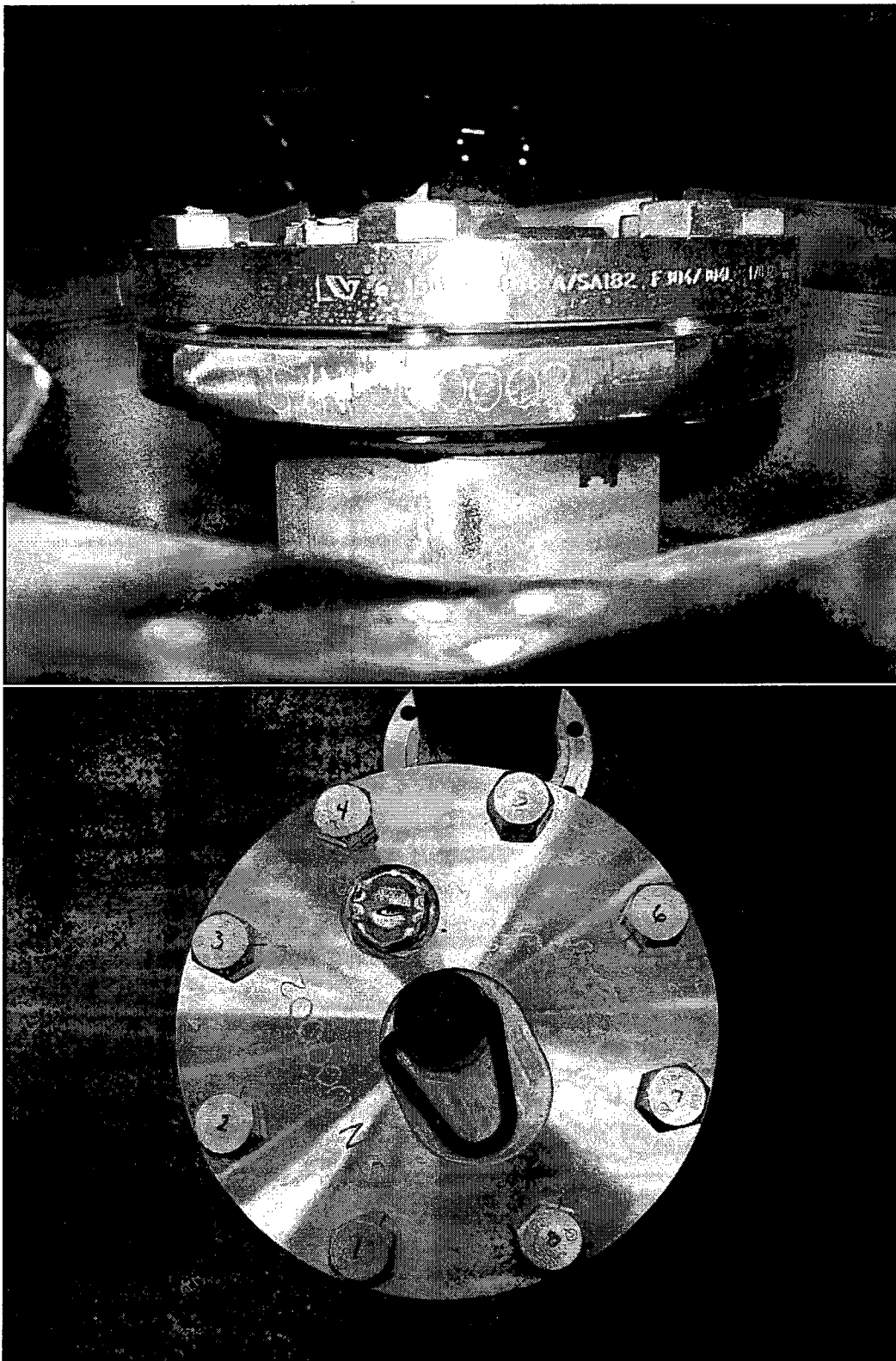


Figure 4.6-13 – Post-End Drop Evaluation of CCC

4.6.3.2.4 Summary of Testing

Key test observations include the following:

1. Post-test visual inspection of the exterior dimensions of the CCO indicated crushing of the upper and lower plywood dunnage assemblies such that the CCC experienced no direct impact with the external impacting surfaces of the test fixture and/or the test pad. The CCC experienced no measurable deformation.
2. The test conditions maximized the crushing of the upper and lower plywood dunnage assemblies by dropping at an elevated temperature using rigid test fixtures to simulate interaction with other CCOs in the payload assembly and by dropping directly onto an essentially unyielding surface rather than onto the impact-attenuating shells and polyurethane foam of the TRUPACT-II and/or HalfPACT ICV/OCA structures.
3. The CCC closure bolts retained essentially full residual torque, where the polar deviation to return the bolts to the initial installation torque was such that 99% of the gasket compression was retained after the drop event. In addition, the flour/fluorescein mixture placed within each CCC was 100% retained throughout the testing. Collectively, these observations readily confirmed confinement integrity of the CCO.

In summary, the results of the testing program for the CCO demonstrate that under HAC the CCO maintains confinement integrity, shielding integrity, and provides defined array spacing for criticality control purposes.

4.6.4 Thermal Evaluation

4.6.4.1 Thermal Evaluation for Normal Conditions of Transport

Thermal analysis models of the TRUPACT-II and HalfPACT packagings with a CCO payload were developed using the computer programs Thermal Desktop⁵ and SINDA/FLUINT⁶. The thermal models are a three-dimensional half-symmetry (180°) finite element and finite difference solid element and surface/planar element and thermal entity representations of the packages. Complete details of the package thermal models, including model dimensions, material properties, boundary conditions, and decay configurations are provided in the calculation package.⁷

Identical modeling approaches were used for the thermal models for the TRUPACT-II and HalfPACT packages with appropriate modifications for the payload cavity height, number of installed payload containers, and decay heat limits and distribution. The CCO geometry is as given in Drawing 163-009 in Appendix 1.3.1 of the TRUPACT-II SAR¹ and HalfPACT SAR². The TRUPACT-II was analyzed when transporting fourteen (14) CCOs, while the HalfPACT was analyzed for transporting seven (7) CCOs. The heat transfer between the various components within the CCOs, between the CCOs and the ICV, and between the ICV/OCA is via radiation and conduction. Convection within the payload cavity is conservatively ignored. Heat transfer between the exterior of the package and the environment is via radiation and natural convection.

The analyses assume that all packaging components are radially centered and all CCO components are radially and axially centered to maximize payload temperatures. Radially shifting the payload to initiate contact between the ICV and adjacent CCO would result in a negligible increase in packaging component and payload temperatures. More significant is the placement of decay heat loads within the packaging payload cavity. Similarly, a fractional shift of CCO components, radially and/or axially, would result in a negligible increase in payload temperatures.

All void spaces within the CCO and packaging cavity are assumed to be filled with air at atmospheric pressure. A paper-based waste stream with the effective conductivity of air is assumed for the payload with a maximum total decay heat loading of 40 watts for the TRUPACT-II package and 30 watts for the HalfPACT package. The distribution of decay heat is varied within the assembly of CCOs to establish the limiting case under the restriction that the maximum decay heat in any single CCO is limited to 20 watts. The decay heat within a CCO is assumed to be equally distributed within the waste volume on a volumetric basis.

The package is mounted in an upright position on its transport trailer or railcar for NCT. This establishes the orientation of the exterior surfaces of the package for determining the free convection heat transfer coefficients and insolation loading. In addition, the bottom of the

⁵ Thermal Desktop®, *A CAD Based System for Thermal Analysis and Design*, Version 5.4, Cullimore & Ring Technologies, Inc., Littleton, CO, 2011.

⁶ SINDA/FLUINT, *General Purpose Thermal/Fluid Network Analyzer*, Version 5.4, Cullimore & Ring Technologies, Inc., Littleton, CO, 2011.

⁷ S. A. Porter, *Criticality Control Overpack Thermal Analysis*, CCO-CAL-0003, Rev. 2, Washington TRU Solutions LLC, Carlsbad, NM, September 2012.

dedicated transport trailer is open, and the bottom of the package is exposed to ambient air instead of resting on the ground or some other semi-adiabatic, conducting surface. Thus, heat transfer from the OCA exterior to the ambient is conducted via free convection and radiation exchange. The insolation values used for heat input to the exterior package surfaces for NCT, as specified in 10 CFR §71.71(c)(1) are as follows: 1) flat base of the package has no applied insolation, 2) all vertical OCA surfaces have an insolation value of 200 gcal/cm² (737.5 Btu/ft²), and 3) the curved OCA torispherical head has an insolation value of 400 gcal/cm² (1,475 Btu/ft²). Consistent with 10 CFR §71.71(b), a 100 °F ambient temperature is used. Insolation is applied in 12-hour “off/on” steps, i.e., a repeating 12-hour “off”, 12-hour “on” cycle for a sufficient period of time (1,200 hours) to allow the hottest location within the package to reach pseudo-steady-state equilibrium.

As summarized below, a set of four primary TRUPACT-II package and four primary HalfPACT package cases were evaluated, both without and with insolation. Additionally included with each set is a zero watt decay heat load as a baseline case for determining the temperature/decay heat relationship for internal pressure calculations.

For the TRUPACT-II package:

- Case 0: 0 watts decay heat in 14 CCOs (0 watts each); baseline case for internal pressure calculations.
- Case 1: 40 watts decay heat evenly distributed in 14 CCOs (2.857 watts each); basic uniform decay heat load case for comparison with existing TRUPACT-II package and payload temperature results.
- Case 2: 40 watts decay heat evenly distributed in the 2 center CCOs (20 watts each); maximum heat load per CCO case with the highest thermal isolation (i.e., centered) that should produce the highest CCO contents temperature.
- Case 3: 40 watts decay heat evenly distributed in 2 axially aligned outer CCOs (20 watts each); highest ICV and OCV seal temperature case, along with Case 4.
- Case 4: 40 watts decay heat evenly distributed in 2 laterally aligned outer CCOs (20 watts each); highest ICV and OCV seal temperature case, along with Case 3.

For the HalfPACT package:

- Case 0: 0 watts decay heat in 7 CCOs; baseline case for internal pressure calculations.
- Case 1: 30 watts decay heat evenly distributed in 7 CCOs (4.286 watts each); basic uniform decay heat load case for comparison with existing HalfPACT package and payload temperature results.
- Case 2: 20 watts decay heat in the center CCO and 10 watts decay heat in one outer CCO; maximum heat load per CCO case with the highest thermal isolation (i.e., centered) that should produce the highest CCO contents temperature, along with Case 3.
- Case 3: 20 watts decay heat in the center CCO and 10 watts decay heat evenly distributed in the 6 outer CCOs; maximum heat load per CCO case with the highest thermal isolation (i.e., centered) that should produce the highest CCO contents temperature, along with Case 2.

- Case 4: 30 watts decay heat evenly distributed in 2 laterally aligned outer CCOs (15 watts each); highest ICV and OCV seal temperature case.

The results of the NCT thermal analyses are provided in Table 4.6-1, Table 4.6-2, Table 4.6-3, and Table 4.6-4. As can be seen in Table 4.6-2 for the TRUPACT-II package with insolation and Table 4.6-4 for the HalfPACT package with insolation, all maximum packaging temperatures and all maximum CCO temperatures are below the respective component maximum allowable temperatures. Additionally, all packaging component temperatures are bounded by the temperatures used in Section 3.4.5, *Maximum Thermal Stresses*, of the TRUPACT-II and HalfPACT SARs to evaluate maximum thermal stresses for NCT. The determination of Maximum Normal Operating Pressure (MNOP) for the CCO payload is presented in Section 3.4.4, *Maximum Internal Pressure*, of the TRUPACT-II and HalfPACT SARs. Thus, the thermal analysis results for the thermal performance of a CCO payload transported within a TRUPACT-II or HalfPACT packaging under NCT conditions demonstrate compliance with the requirements of 10 CFR §71.43(g) and §71.71.

Finally, 10 CFR §71.43(g) stipulates that maximum accessible surface temperatures must be less than 185 °F for a package based on 100 °F ambient conditions without insolation for exclusive use package shipments. As can be seen in Table 4.6-1 for the TRUPACT-II package without insolation and Table 4.6-3 for the HalfPACT package without insolation, all maximum packaging temperatures are below the maximum allowable temperature of 185 °F.

4.6.4.2 Thermal Evaluation for Hypothetical Accident Conditions

The maximum temperatures for the CCO components within the TRUPACT-II and HalfPACT packagings from the HAC fire event may be determined by conservatively combining the experimentally derived differential temperatures measured from HAC fire testing of each package with the worst-case initial pre-fire temperatures from Table 4.6-1 for the TRUPACT-II package and Table 4.6-3 for the HalfPACT package. The worst-case initial pre-fire temperatures are based on the maximum temperature for each component, regardless of the case number. Further conservatism is attained by upwardly adjusting maximum temperatures to account for the difference in the tested payload mass versus the CCO payload mass.

The bounding estimate for the increase in TRUPACT-II and HalfPACT packaging component temperatures due to the lighter CCO payload is determined by taking the heat absorbed by the test payload (i.e., concrete-filled 55-gallon drums) and proportionally redistributing all of that thermal energy to packaging components interior to the OCA outer shell (which is already at the maximum fire temperature of 1,475 °F and incapable of absorbing additional energy). The heat absorbed by the test payload is conservatively calculated by assuming a uniform temperature increase such that the payload bulk average temperature is assumed to be equal to the measured drum shell temperature. The adjusted absorbed heat values are subsequently used to calculate adjusted bulk average temperatures for the packaging components (i.e., OCA foam, OCV structure, ICV structure, honeycomb spacers, payload pallet, and, for the HalfPACT package only, the payload spacer) by using their respective component masses and specific heats. The adjusted packaging component bulk average temperatures are then used to calculate a bounding temperature change (percentage increase) due to a fire event for the package with “no payload” mass.

The “no payload” temperature change percentages are conservatively applied to the packaging components and CCO payload by assuming that the CCO 55-gallon drum adjusted maximum temperature is equal to the adjusted ICV bulk average temperature, with all other packaging component adjusted maximum temperatures equal to the maximum measured fire temperatures increased by the bulk average temperature change percentage for each component. It is conservative to assume that the CCO 55-gallon drum shell is at the bulk average temperature of the ICV structure because, at the point of maximum temperature, heat flow is primarily inward such that the magnitude of temperature increase due to the fire event is progressively less for each component as the heat moves from the OCV to the ICV and into the payload. Additionally, previous fire tests have demonstrated that the maximum surface temperature of the payload container(s) is less than the bulk average temperature of the ICV structure. To account for the pre-fire temperature gradients within the CCO that are due to the insulating effects of the radial gap between the CCC structure and the 55-gallon drum, the maximum temperature differential for each CCO component is assumed to be a function of the maximum temperature differential for the 55 gallon drum and proportional to the pre-fire temperature gradients within the CCO. The detailed calculational process, including example calculations, is provided in Section 5.0, *Thermal Evaluation for Hypothetical Accident Conditions*, in calculation CCO-CAL-0003.⁷

Table 4.6-5 and Table 4.6-6 for the TRUPACT-II and HalfPACT packages, respectively, summarize the predicted HAC temperatures for the major components in each package, none of which exceed defined temperature limits for the materials of construction. Furthermore, the determination of maximum internal pressure under HAC for the TRUPACT-II and HalfPACT packages, presented in Section 3.5.4, *Maximum Internal Pressure*, of the TRUPACT-II and HalfPACT SARs, respectively, is bounding for the CCO payload. Thus, the CCO payload will not impact the safety basis of either the TRUPACT II or HalfPACT packages for HAC, and the requirements of 10 CFR §71.73(c)(3) are satisfied.

Table 4.6-1 – TRUPACT-II Package NCT Steady-State Temperatures (°F) without Insolation

Location	Component(s)	Case 0	Case 1	Case 2	Case 3	Case 4	Limit
Center CCOs	Contents Centerline Maximum	100.0	147.9	285.0	124.9	126.0	N/A
	Contents Centerline Average ^①	100.0	144.7	266.0	124.2	123.6	④
	Contents Bulk Average ^②	100.0	136.6	208.8	124.2	123.6	④
	CCC Structure Maximum	100.0	130.4	162.2	124.9	126.0	2,600
	CCC Gasket Maximum	100.0	128.6	150.6	124.8	125.9	548
	Plywood Dunnage Maximum	100.0	127.6	144.5	126.7	128.2	212
	55-Gallon Drum Maximum	100.0	125.5	131.8	127.0	128.7	2,750
	55-Gallon Drum Average ^②	100.0	124.8	128.5	124.2	123.5	2,750
Outer CCOs (Heated)	Contents Centerline Maximum	—	147.2	—	286.1	286.4	N/A
	Contents Centerline Average ^①	—	143.9	—	266.9	267.7	④
	Contents Bulk Average ^②	—	135.7	—	209.7	210.5	④
	CCC Structure Maximum	—	129.7	—	163.4	163.8	2,600
	CCC Gasket Maximum	—	127.9	—	151.8	151.8	548
	Plywood Dunnage Maximum	—	126.8	—	145.7	145.3	212
	55-Gallon Drum Maximum	—	125.3	—	133.1	132.9	2,750
	55-Gallon Drum Average ^②	—	123.9	—	129.6	130.3	2,750
Outer CCOs (Unheated)	Contents Centerline Maximum	100.0	—	125.0	125.3	124.3	N/A
	Contents Centerline Average ^①	100.0	—	124.2	122.8	121.8	④
	Contents Bulk Average ^②	100.0	—	124.2	122.8	121.8	④
	CCC Structure Maximum	100.0	—	125.0	125.3	124.3	2,600
	CCC Gasket Maximum	100.0	—	124.9	125.2	124.2	548
	Plywood Dunnage Maximum	100.0	—	126.4	127.0	126.3	212
	55-Gallon Drum Maximum	100.0	—	126.7	127.4	130.3	2,750
	55-Gallon Drum Average ^②	100.0	—	124.2	122.7	123.4	2,750
All CCOs	Contents Centerline Average ^①	100.0	144.0	144.5	143.6	142.9	④
	Contents Bulk Average ^②	100.0	135.8	136.3	135.4	134.7	④
	55-Gallon Drum Average ^②	100.0	124.1	124.8	123.9	124.4	2,750
ICV Cavity Air	Bulk Average ^{②③}	100.0	122.9	123.4	122.8	122.9	N/A
ICV Structure	Maximum	100.0	122.4	122.3	126.9	125.0	800
	Bulk Average ^②	100.0	119.5	119.6	119.5	119.2	800
	Minimum	100.0	115.6	115.7	115.3	116.4	800
ICV O-ring Seal	Maximum	100.0	118.2	118.2	121.4	123.2	-40 to 225
OCV Structure	Maximum	100.0	121.2	121.1	125.1	122.7	800
	Bulk Average ^②	100.0	117.4	117.4	117.4	117.2	800
OCV O-ring Seal	Maximum	100.0	114.8	114.8	117.1	118.4	-40 to 225
Polyurethane Foam	Maximum	100.0	121.2	121.1	125.1	122.7	300
	Bulk Average ^②	100.0	108.9	108.9	108.9	108.7	300
OCA Outer Shell	Maximum	100.0	102.7	102.7	103.1	103.2	185

Notes:

- ① Temperature based on an arithmetical average.
- ② Temperature based on an area-weighted average.
- ③ Temperature based on a volume-weighted average.
- ④ Contents temperature limit based on Appendix 6.6 of the *CH-TRU Payload Appendices*.

Table 4.6-2 – TRUPACT-II Package NCT Steady-State Temperatures (°F) with Insolation

Location	Component(s)	Case 0	Case 1	Case 2	Case 3	Case 4	Limit
Center CCOs	Contents Centerline Maximum	118.0	164.1	299.4	141.5	142.9	N/A
	Contents Centerline Average ^①	117.7	161.2	280.8	141.0	140.3	④
	Contents Bulk Average ^②	117.7	153.0	223.6	141.0	140.3	④
	CCC Structure Maximum	118.0	146.6	176.6	141.5	142.9	2,600
	CCC Gasket Maximum	118.0	144.9	165.6	141.4	142.8	548
	Plywood Dunnage Maximum	118.0	144.0	159.9	143.2	144.9	212
	55-Gallon Drum Maximum	118.0	142.2	148.0	143.5	145.4	2,750
	55-Gallon Drum Average ^②	117.7	141.5	145.0	140.9	140.2	2,750
Outer CCOs (Heated)	Contents Centerline Maximum	—	163.5	—	300.5	301.1	N/A
	Contents Centerline Average ^①	—	160.4	—	281.7	282.6	④
	Contents Bulk Average ^②	—	152.2	—	224.5	225.4	④
	CCC Structure Maximum	—	146.0	—	177.8	178.4	2,600
	CCC Gasket Maximum	—	144.3	—	166.7	167.1	548
	Plywood Dunnage Maximum	—	143.3	—	161.1	161.0	212
	55-Gallon Drum Maximum	—	141.8	—	149.2	149.4	2,750
	55-Gallon Drum Average ^②	—	140.7	—	146.0	146.8	2,750
Outer CCOs (Unheated)	Contents Centerline Maximum	118.0	—	141.4	141.9	141.3	N/A
	Contents Centerline Average ^①	117.7	—	141.0	139.6	138.6	④
	Contents Bulk Average ^②	117.7	—	141.0	139.6	138.6	④
	CCC Structure Maximum	118.0	—	141.5	141.9	141.3	2,600
	CCC Gasket Maximum	118.0	—	141.5	141.8	141.2	548
	Plywood Dunnage Maximum	118.0	—	142.9	143.5	143.1	212
	55-Gallon Drum Maximum	118.0	—	143.1	143.8	143.5	2,750
	55-Gallon Drum Average ^②	117.7	—	140.9	139.6	140.2	2,750
All CCOs	Contents Centerline Average ^①	117.7	160.5	161.0	160.1	159.4	④
	Contents Bulk Average ^②	117.7	152.3	152.8	151.9	151.3	④
	55-Gallon Drum Average ^②	117.7	140.8	141.5	140.7	141.1	2,750
ICV Cavity Air	Bulk Average ^{①②}	117.7	139.7	140.2	139.6	139.7	N/A
ICV Structure	Maximum	119.4	139.0	138.9	143.4	142.0	800
	Bulk Average ^①	117.9	136.7	136.8	136.7	136.3	800
	Minimum	116.5	134.4	134.5	133.6	134.2	800
ICV O-ring Seal	Maximum	118.4	135.9	135.8	138.9	140.7	-40 to 225
OCV Structure	Maximum	120.1	137.9	137.8	141.7	139.7	800
	Bulk Average ^①	118.4	135.1	135.2	135.1	134.9	800
OCV O-ring Seal	Maximum	120.1	133.9	133.9	136.1	137.3	-40 to 225
Polyurethane Foam	Maximum	150.6	150.8	150.8	150.8	150.8	300
	Bulk Average ^①	122.5	130.9	130.9	130.9	130.7	300
OCA Outer Shell	Maximum	150.6	150.8	150.8	150.8	150.8	800

Notes:

- ① Temperature based on an arithmetical average.
- ② Temperature based on an area-weighted average.
- ③ Temperature based on a volume-weighted average.
- ④ Contents temperature limit based on Appendix 6.6 of the *CH-TRU Payload Appendices*.

Table 4.6-3 – HalfPACT Package NCT Steady-State Temperatures (°F) without Insolation

Location	Component(s)	Case 0	Case 1	Case 2	Case 3	Case 4	Limit
Center CCO	Contents Centerline Maximum	100.0	157.4	282.8	282.8	122.8	N/A
	Contents Centerline Average ^①	100.0	153.3	264.1	264.1	122.6	④
	Contents Bulk Average ^②	100.0	141.0	206.9	206.9	122.6	④
	CCC Structure Maximum	100.0	131.1	160.1	160.0	122.8	2,600
	CCC Gasket Maximum	100.0	128.2	147.9	147.9	122.5	548
	Plywood Dunnage Maximum	100.0	126.5	141.2	141.2	124.2	212
	55-Gallon Drum Maximum	100.0	123.8	128.1	127.2	124.8	2,750
	55-Gallon Drum Average ^②	100.0	123.3	126.3	126.3	122.5	2,750
Outer CCO(s) (Heated)	Contents Centerline Maximum	—	156.4	203.7	135.7	243.9	N/A
	Contents Centerline Average ^①	—	152.3	194.2	134.1	229.8	④
	Contents Bulk Average ^②	—	140.0	165.6	129.4	186.9	④
	CCC Structure Maximum	—	130.1	142.4	125.6	151.9	2,600
	CCC Gasket Maximum	—	127.2	135.9	124.3	142.4	548
	Plywood Dunnage Maximum	—	125.7	132.5	124.0	137.4	212
	55-Gallon Drum Maximum	—	123.4	126.8	124.5	128.0	2,750
	55-Gallon Drum Average ^②	—	122.3	124.8	122.4	126.0	2,750
Outer CCOs (Unheated)	Contents Centerline Maximum	100.0	—	122.8	—	121.5	N/A
	Contents Centerline Average ^①	100.0	—	122.0	—	120.4	④
	Contents Bulk Average ^②	100.0	—	122.0	—	120.4	④
	CCC Structure Maximum	100.0	—	122.8	—	121.5	2,600
	CCC Gasket Maximum	100.0	—	122.6	—	121.3	548
	Plywood Dunnage Maximum	100.0	—	124.1	—	122.9	212
	55-Gallon Drum Maximum	100.0	—	124.6	—	123.3	2,750
	55-Gallon Drum Average ^②	100.0	—	121.9	—	120.4	2,750
All CCOs	Contents Centerline Average ^①	100.0	152.4	152.6	152.7	151.9	④
	Contents Bulk Average ^②	100.0	140.1	140.4	140.4	139.7	④
	55-Gallon Drum Average ^②	100.0	122.4	122.9	123.0	122.3	2,750
ICV Cavity Air	Bulk Average ^{②③}	100.0	121.1	121.4	121.5	121.0	N/A
ICV Structure	Maximum	100.0	119.6	121.0	119.9	122.3	800
	Bulk Average ^②	100.0	117.6	117.7	117.7	117.6	800
	Minimum	100.0	114.6	114.6	114.6	114.3	800
ICV O-ring Seal	Maximum	100.0	117.0	118.0	117.0	119.1	-40 to 225
OCV Structure	Maximum	100.0	118.6	119.4	118.8	120.7	800
	Bulk Average ^②	100.0	115.6	115.6	115.6	115.6	800
OCV O-ring Seal	Maximum	100.0	113.9	114.6	113.9	115.6	-40 to 225
Polyurethane Foam	Maximum	100.0	118.6	119.4	118.8	120.7	300
	Bulk Average ^②	100.0	107.9	107.9	107.9	107.9	300
OCA Outer Shell	Maximum	100.0	102.4	102.5	102.4	102.6	185

Notes:

- ① Temperature based on an arithmetical average.
- ② Temperature based on an area-weighted average.
- ③ Temperature based on a volume-weighted average.
- ④ Contents temperature limit based on Appendix 6.6 of the *CH-TRU Payload Appendices*.

Table 4.6-4 – HalfPACT Package NCT Steady-State Temperatures (°F) with Insolation

Location	Component(s)	Case 0	Case 1	Case 2	Case 3	Case 4	Limit
Center CCO	Contents Centerline Maximum	117.6	173.5	297.3	297.3	139.4	N/A
	Contents Centerline Average ^①	117.6	169.4	278.7	278.7	139.2	④
	Contents Bulk Average ^②	117.6	157.1	221.5	221.5	139.2	④
	CCC Structure Maximum	117.6	147.1	174.5	174.5	139.4	2,600
	CCC Gasket Maximum	117.6	144.4	162.9	162.9	139.2	548
	Plywood Dunnage Maximum	117.7	142.8	156.6	156.6	140.7	212
	55-Gallon Drum Maximum	117.7	140.2	144.3	143.5	141.3	2,750
	55-Gallon Drum Average ^②	117.5	139.8	142.6	142.6	139.0	2,750
Outer CCO(s) (Heated)	Contents Centerline Maximum	—	172.5	219.1	152.2	258.8	N/A
	Contents Centerline Average ^①	—	168.5	209.8	150.6	244.9	④
	Contents Bulk Average ^②	—	156.2	181.1	145.8	201.9	④
	CCC Structure Maximum	—	146.3	157.8	142.1	166.8	2,600
	CCC Gasket Maximum	—	143.5	151.6	140.8	157.7	548
	Plywood Dunnage Maximum	—	142.0	148.3	140.4	153.0	212
	55-Gallon Drum Maximum	—	139.9	143.2	141.0	144.3	2,750
	55-Gallon Drum Average ^②	—	138.9	141.2	139.0	142.4	2,750
Outer CCOs (Unheated)	Contents Centerline Maximum	117.7	—	139.4	—	138.2	N/A
	Contents Centerline Average ^①	117.6	—	138.7	—	137.2	④
	Contents Bulk Average ^②	117.6	—	138.6	—	137.1	④
	CCC Structure Maximum	117.6	—	139.4	—	138.2	2,600
	CCC Gasket Maximum	117.6	—	139.2	—	138.0	548
	Plywood Dunnage Maximum	117.7	—	140.5	—	139.4	212
	55-Gallon Drum Maximum	117.7	—	141.1	—	139.9	2,750
	55-Gallon Drum Average ^②	117.5	—	138.5	—	137.1	2,750
All CCOs	Contents Centerline Average ^①	117.6	168.6	168.8	168.9	168.2	④
	Contents Bulk Average ^②	117.6	156.3	156.6	156.6	155.9	④
	55-Gallon Drum Average ^②	117.5	139.0	139.5	139.5	138.9	2,750
ICV Cavity Air	Bulk Average ^{①②}	117.5	137.8	138.1	138.1	137.7	N/A
ICV Structure	Maximum	119.2	136.1	137.6	136.0	139.0	800
	Bulk Average ^①	117.8	134.7	134.8	134.8	134.8	800
	Minimum	116.6	133.2	133.0	133.2	132.4	800
ICV O-ring Seal	Maximum	118.1	134.4	135.4	134.4	136.4	-40 to 225
OCV Structure	Maximum	119.8	134.9	136.0	134.8	137.2	800
	Bulk Average ^①	118.3	133.3	133.3	133.3	133.3	800
OCV O-ring Seal	Maximum	119.8	132.7	133.4	132.6	134.3	-40 to 225
Polyurethane Foam	Maximum	150.6	150.7	150.7	150.7	150.8	300
	Bulk Average ^①	122.4	129.8	129.8	129.8	129.8	300
OCA Outer Shell	Maximum	150.6	150.7	150.7	150.7	150.8	800

Notes:

- ① Temperature based on an arithmetical average.
- ② Temperature based on an area-weighted average.
- ③ Temperature based on a volume-weighted average.
- ④ Contents temperature limit based on Appendix 6.6 of the *CH-TRU Payload Appendices*.

Table 4.6-5 – Predicted TRUPACT-II Package HAC Temperatures (°F) with a CCO Payload

Component/Location	TRUPACT-II SAR			CCO Analysis		Limit
	Pre-Fire CTU-2 ^①	Adjusted Max Fire ^②	Adjusted Max ΔT ^③	Pre-Fire CCO ^④	Post-Fire CCO ^⑤	
Maximum CCC Structure	—	—	51.5	163.8	215.3	2,600
Maximum CCC Gasket	—	—	55.6	151.8	207.4	548
Maximum CCO Plywood Dunnage	—	—	57.9	145.7	203.6	482
Maximum CCO 55-Gallon Drum	127.0	190.4	63.4	133.1	196.5	2,750
Bulk Average ICV Cavity Air	127.0	182.4	55.4	123.4	178.8	N/A
Maximum ICV Structure	127.0	224.2	97.2	126.9	224.1	2,600
Maximum ICV O-ring Seal	127.0	203.8	76.8	123.2	200.0	360
Maximum OCV Structure	127.0	450.4	323.4	125.1	448.5	2,600
Maximum OCV O-ring Seal	127.0	259.6	132.6	118.4	251.0	360

Notes:

- ① TRUPACT-II package pre-fire temperatures are taken from Section 3.5.2.2, *CTU-2 Package Conditions and Environment*, of the TRUPACT-II SAR.
- ② With the exception of the CCO 55-Gallon Drum, the Adjusted Max Fire temperatures for the packaging and payload components are equal to the measured fire temperatures for CTU-2 packaging components increased by the temperature change percentages that are based on the “no payload” model. The Adjusted Max Fire temperature for the CCO 55-Gallon Drum is conservatively assumed to be equal to the adjusted bulk average fire temperature for the ICV Structure.
- ③ The Adjusted Max ΔT temperatures are the difference between the Adjusted Max Fire temperatures and the Pre-Fire CTU-2 temperatures.
- ④ The Maximum Pre-Fire CCO Temperatures are taken from Table 4.6-1 referencing the maximum temperature for each component regardless of the case number.
- ⑤ The Post-Fire CCO temperatures are the sum of the Pre-Fire CCO temperatures and the Adjusted Max ΔT temperatures.

Table 4.6-6 – Predicted HalfPACT Package HAC Temperatures (°F) with a CCO Payload

Component/Location	HalfPACT SAR			CCO Analysis		Limit
	Pre-Fire CTU ^①	Adjusted Max Fire ^②	Adjusted Max ΔT ^③	Pre-Fire CCO ^④	Post-Fire CCO ^⑤	
Maximum CCC Structure	—	—	60.2	160.1	220.3	2,600
Maximum CCC Gasket	—	—	65.1	147.9	213.0	548
Maximum CCO Plywood Dunnage	—	—	68.2	141.2	209.4	482
Maximum CCO 55-Gallon Drum	43.0	118.2	75.2	128.1	203.3	2,750
Bulk Average ICV Cavity Air	43.0	121.6	78.6	121.5	200.1	N/A
Maximum ICV Structure	43.0	121.6	78.6	122.3	200.9	2,600
Maximum ICV O-ring Seal	43.0	121.6	78.6	119.1	197.7	360
Maximum OCV Structure	43.0	226.4	183.4	120.7	304.1	2,600
Maximum OCV O-ring Seal	43.0	226.4	183.4	115.6	299.0	360

Notes:

- ① HalfPACT package pre-fire temperatures are taken from Table 3.5-1 of the HalfPACT SAR.
- ② With the exception of the CCO 55-Gallon Drum, the Adjusted Max Fire temperatures for the packaging and payload components are equal to the measured fire temperatures for CTU packaging components increased by the temperature change percentages that are based on the “no payload” model. The Adjusted Max Fire temperature for the CCO 55-Gallon Drum is conservatively assumed to be equal to the adjusted bulk average fire temperature for the ICV Structure.
- ③ The Adjusted Max ΔT temperatures are the difference between the Adjusted Max Fire temperatures and the Pre-Fire CTU temperatures.
- ④ The Maximum Pre-Fire CCO Temperatures are taken from Table 4.6-3 referencing the maximum temperature for each component regardless of the case number.
- ⑤ The Post-Fire CCO temperatures are the sum of the Pre-Fire CCO temperatures and the Adjusted Max ΔT temperatures.

4.6.5 Shielding Evaluation

The evaluation of compliance with the radiation dose rate limits for NCT and HAC required by 10 CFR §71.47 is presented in Chapter 5 of the TRUPACT-II and HalfPACT SARs^{1,2} for the CCO payload configuration. When the TRUPACT-II and HalfPACT packages are loaded with assemblies of CCOs containing gamma and/or neutron source terms that are limited per Section 3.3 of the CH-TRAMPAC³, the package meets the NCT radiation dose rate requirements of 200 mrem/hr at the surface of the package and 10 mrem/hr at 2 meters from the surface of the package under exclusive use. As a result, the packages also comply with the HAC dose rate requirement of 1 rem/hr at 1 meter from the surface of the package.

4.6.6 Criticality Evaluation

CCOs are designed to transport transuranic (TRU) waste forms with high fissile material concentrations within the TRUPACT-II and HalfPACT packages. A criticality evaluation⁸ was performed for payload contents that are manually compacted (i.e., not machine compacted) and contain less than or equal to 1% by weight quantities of special reflector materials. A maximum 380 fissile gram equivalent (FGE) of Pu-239 per CCO is justified for waste forms meeting these requirements. The methodology and assumptions utilized for other approved payloads in the existing TRUPACT-II and HalfPACT SARs are also utilized in the CCO analysis. The following analysis demonstrates that this configuration complies with the requirements of 10 CFR §71.55 and §71.59. The criticality safety index, per 10 CFR §71.59, is 0.

For Case I⁹ (manually compacted waste with less than or equal to 1% by weight quantities of special reflectors), the moderator and surrounding reflector within each CCC was modeled as a composition of 25% polyethylene, 74% water, and 1% beryllium (by volume). As polyethylene is a superior moderator to water, this composition results in higher reactivities than would be achieved by water moderation alone. This volume fraction of polyethylene is conservatively higher than the maximum value achievable for manually compacted (i.e., not machine compacted) waste determined by experiment. Beryllium is a superior reflector to either water or polyethylene, and the inclusion of beryllium is conservative, although at such a small volume fraction, the beryllium has only a small effect on the system reactivity.

The reactivity of CCOs in a HalfPACT package is bounded by the TRUPACT-II analysis. The HalfPACT and TRUPACT-II are essentially identical packages, although the HalfPACT payload region is approximately half the height of the TRUPACT-II. Therefore, the TRUPACT-II may transport 14 CCOs in two layers of seven, while the HalfPACT may transport only a single layer of seven CCOs. The radial spacing of the two packages is identical. Although the HalfPACT ICV is 30 inches shorter, the vertical spacing between the ICVs (e.g., the annular polyurethane insulation) is the same. Thus, the single layer of seven CCOs in the HalfPACT package will have a lower reactivity than the TRUPACT-II package, which has twice the fissile material. For this reason, calculations are performed only for the TRUPACT-II geometry.

Calculations for the TRUPACT-II package are performed using the three-dimensional Monte Carlo transport theory code, KENO-V.a v4.0, with the CSAS25 utility being used as a driver for the KENO-V.a code; both programs are part of the SCALE-PC v4.4¹⁰ code system. In this role, CSAS25 determines nuclide number densities, performs resonance processing, and automatically prepares the necessary input for the KENO-V.a code based on a simplified input description. The 238 energy-group (238GROUPNDF5) cross-section library based on ENDF/B-V cross-section data is used as the nuclear data library for the KENO-V.a code.

⁸ R. J. Migliore, *Criticality Control Overpack Criticality Analysis for TRUPACT-II and HalfPACT*, 01937.01.M009-01, Rev. 0, AREVA Federal Services LLC, Federal Way, WA, February 2012.

⁹ To avoid confusion, the case designator "I" is selected to be a sequential addition to those utilized in the current TRUPACT-II and/or HalfPACT SARs. Case I is equivalent to Case A with modifications specific to the CCO payload.

¹⁰ *SCALE4.4: Modular Code System for Performing Standardized Computer Analyses for Licensing Evaluation for Workstations and Personal Computers*, RSICC code package C00545/MNYCP00, Oak Ridge National Laboratory, September 1998.

The upper subcritical limit (USL) for ensuring that the TRUPACT-II and HalfPACT is acceptably subcritical, as determined in benchmark evaluations, is:

$$\text{USL} = 0.9377$$

Each package is considered to be acceptably subcritical if the computed k_{safe} (k_s), which is defined as $k_{\text{effective}}$ (k_{eff}) plus twice the statistical uncertainty (σ), is less than the USL, or:

$$k_s = k_{\text{eff}} + 2\sigma < \text{USL}$$

In both the NCT and HAC cases, the TRUPACT-II is modeled with reduced outer dimensions consistent with a damaged package. The torispherical heads are also modeled as flat, which brings fuel in stacked packages into close proximity. The steel 55-gallon drum of the CCO is ignored in all models, which is conservative because the steel would absorb neutrons and lower the reactivity. In the NCT models, the spacing provided by the drums is preserved. In the HAC models, reduced drum dimensions consistent with accident geometry are modeled, which results in a highly compressed array within the package. Fuel is modeled as pure Pu-239 homogeneously mixed with a moderator consisting of 74% water, 25% polyethylene, and 1% beryllium (by volume). This is a more reactive moderator than pure water and bounds the observed polyethylene volume fraction in the waste stream. Special reflectors (other than beryllium) that are in >1% by weight quantities are allowed if they are chemically or mechanically bound to the fissile material. The height of the fissile mixture is varied to optimize the moderation. Also, because the drums are stacked in two layers within the ICV, fuel is conservatively arranged so that the fuel is at the bottom of the top layer and at the top of the bottom layer. In all models, the fissile material within each CCC was assumed to form a single optimally moderated cylinder.

The most reactive case is for the HAC array. The HAC array is modeled with an infinite number of packages in the x and y directions, and two packages in the z direction. Because of the infinite number of packages and internal moderation within the CCCs, the HAC array is most reactive with no reflecting material inside the package. The most reactive case has $k_s = 0.9357$, which is below the USL of 0.9377. Addition of any reflecting or moderating material causes a decrease in reactivity. The NCT array shows the same behavior. For the single package cases, maximum reactivity is achieved with some internal reflector. For the NCT single package, the most reactive condition is with the 74/25/1 water/polyethylene/beryllium mixture inside the CCC and full-density water in all other package regions. The presence of plywood dunnage has little influence on the result. For the HAC single package, the most reactive condition is similar to the NCT single package, except with void between the CCC and drum. The system behavior for the HAC single package differs from the NCT single package as a result of the reduced drum diameter in the HAC models. However, the single package reactivity is significantly less than the array reactivity.

Case I has a justifiable limit of 380 FGE per CCO. As such, when maximally loaded with CCOs, the TRUPACT-II and HalfPACT are limited to 5,320 FGE and 2,660 FGE, respectively. The criticality analysis results are summarized in Table 4.6-7.

Table 4.6-7 – Summary of Criticality Evaluation Results for 380 FGE per CCO

Normal Conditions of Transport (NCT)	
Case "I"	k_s
Single Unit Maximum	0.8033
Infinite Array Maximum	0.9002
Hypothetical Accident Conditions (HAC)	
Case "I"	k_s
Single Unit Maximum	0.8209
Infinite Array Maximum	0.9357
USL = 0.9377	

4.6.7 Authorized Payload Contents for the Criticality Control Overpack

As demonstrated in Section 4.6.5, *Shielding Evaluation*, when loaded with gamma and/or neutron emitting isotopes with maximum activity limits summarized in the CH-TRAMPAC, the CCO payload meets the NCT and HAC dose rate limits. As demonstrated in Section 4.6.6, *Criticality Evaluation*, when loaded with fissile material with maximum mass limits, the CCO payload meets the calculated reactivity limit as summarized for Case I in Table 4.6-7 and is safely subcritical.

4.6.8 Conclusion

The CCO design consists of a vented steel 55-gallon drum containing a CCC positioned within the drum by plywood dunnage that is to be used for shipment of specific TRU waste forms in the TRUPACT-II and HalfPACT packages.

The analyses summarized in this appendix demonstrate the ability of the CCO to safely transport limited quantities of gamma and/or neutron emitting isotopes and fissile isotopes. Using geometries consistent with, or conservative with respect to, the structural and thermal analyses, the shielding evaluation showed that the dose rate limits for NCT and HAC are met with the maximum authorized contents. In addition, the criticality evaluation showed that the reactivity limit is met for manually compacted wastes with specified mass limits.

This page intentionally left blank.

APPENDIX 5.1

REAL-TIME RADIOGRAPHY PROCEDURES

This page intentionally left blank.

5.1 Real-Time Radiography Procedures

5.1.1 Description of Real-Time Radiography

Real-time radiography (RTR) is a nondestructive testing method that allows the RTR operator to ascertain the physical waste form within a payload container without opening it. The examination method utilizes X rays to inspect the payload container and contents and allows the operator to view events in progress (real time) such as wave motion of free liquids. A typical RTR system consists of:

1. An X-ray-producing device
2. An imaging system
3. An enclosure for radiation protection
4. A payload container handling system
5. An operator control station.

The X-ray-producing device has controls that allow the operator to vary the voltage, thereby controlling image quality. The voltage can be varied, typically between 150 and 400 kilovolts (kV), to provide an optimum degree of penetration through the waste. For example, high-density material (e.g., solidified liquid) is usually examined with the X-ray device set on the maximum voltage. This ensures maximum penetration through the payload container. Low-density material (e.g., plastics and cellulose) is usually examined at lower voltage settings to improve contrast and image definition. The imaging system typically utilizes a fluorescent screen and a low light television camera.

Payload containers are placed in the RTR vault. Waste drums are placed on a rotating platform. The platform or the X-ray tube and imaging system move up and down to allow total coverage of the drum. X rays are projected through the payload container and onto a fluorescent screen/image intensifier. The resultant image is transferred by a camera to a remotely located television screen. The operator conducts the examination by viewing the remote television screen. The operator scans the contents of the payload container during the examination. Waste boxes cannot be rotated during RTR inspection but are first inspected from one side and then rotated 180 degrees and inspected from the opposite side. The two-sided inspection is performed to compensate for magnification factors. Large magnification factors can occur depending upon the location of an object within a box. Scanning from two sides, 180 degrees apart, allows a higher degree of accuracy for determining sizes and quantities. The two scans, from opposite sides, also provide a higher degree of confidence for detection of objects that may be hidden when scanning from only one side. The waste payload is inspected for correct physical waste form description, sealed containers, pressurized containers, and free liquid waste forms. The RTR operator documents the findings of the RTR examination of each waste payload by several means listed below:

- The results are recorded on an RTR examination form, and this form is included in the waste payload data package. The examination results may also be entered into a computerized data collection system.

- The examination is recorded on a videotape recorder.
- The RTR operator verbally describes the results of the RTR examination on the audio track of the videotape. The audio voice track on the videotape is an additional positive feature of RTR.

The advantage of viewing the examination in real time is that the X-ray device can be adjusted on the spot to obtain optimum imaging conditions, or the system can be stopped to focus on one object. RTR works extremely well for detecting free liquids due to its ability to view events in progress, such as wave motion. The presence of free liquids is verified by jogging the container or handling system (stopping and starting the container rotation) and then watching for the resulting wave motion. Free liquids in pressurized containers are easily detected, thereby assessing two parameters, liquids and pressurized containers. Items that may otherwise go undetected due to being shielded from the X rays by another object are often found because the operator is watching the inspection in real time while rotating or moving the payload container. Interpretation of results and disposition of the inspected payload containers are also accomplished at the time of inspection rather than waiting for X-ray film to be processed.

Operator training and experience are the most important control factor in ensuring the quality of RTR interpretation and inspection. Operator training, qualification, and certification are performed in accordance with Society for Nondestructive Testing (SNT)-TC-1A.¹ SNT-TC-1A is a nationally recognized guideline and is used by employers to train, qualify, and certify employees to perform specific nondestructive tests.

Recertification of operators is based upon evidence of continued satisfactory performance and is performed at least every two years. Unsatisfactory operator performance is cause for decertification. Retraining is required before an operator is again certified to interpret and disposition payload containers.

A training drum containing a variety of different container sizes and holding various amounts of liquid is periodically examined by each operator, as prescribed in the site waste certification and quality assurance (QA) procedures. The test videotape is then reviewed by supervision to ensure that the operator's interpretations remain consistent and accurate. The test tapes are also used for monitoring the imaging system characteristics and identifying other shapes or matrices.

QA oversight functions are performed by independent individuals who review videotape of examined payload containers. The frequency and number of payload containers included in these reviews is determined in accordance with Military Standard (MIL-STD)-105D, "Sampling Procedures and Tables for Inspection by Attributes".²

¹ SNT-TC-1A, August 1984, "Recommended Practice No. SNT-TC-1A, Personnel Qualification and Certification in Nondestructive Testing."

² MIL-STD-105D, April 29, 1963, "Military Standard, Sampling Procedures and Tables for Inspection by Attributes."

RTR has several inherent limitations. X rays with a high enough energy level to penetrate high-density waste forms or shielded containers present an image with such a large latitude that low-density materials (i.e., liquids) will be indiscernible. Therefore, high-density waste forms or shielded payload containers must have the physical waste form verified by other methods (e.g., visual examination during packaging) or be rejected.

RTR inspection is a semi-quantitative examination that can identify and verify the payload container's physical contents. RTR cannot determine the chemical composition of the waste.

This page intentionally left blank.

APPENDIX 5.2

**DOE ASSAY METHODS USED FOR DETERMINATION OF
FISSILE MATERIAL CONTENT AND DECAY HEAT VALUES
OF CH-TRU WASTES**

This page intentionally left blank.

Table of Contents

5.2	DOE Assay Methods Used for Determination of Fissile Material Content and Decay Heat Values of Contact-Handled Transuranic (CH-TRU) Wastes	5.2-1
5.2.1	Introduction	5.2-1
5.2.2	Assay Overview	5.2-3
5.2.3	Assay Methods Descriptions, Characteristics, and Limitations	5.2-6
5.2.3.1	Calorimetry	5.2-6
5.2.3.2	Passive Gamma Assay	5.2-7
5.2.3.3	Radiochemical Methods.....	5.2-14
5.2.3.4	Passive Neutron Coincidence Counting (PNCC) Assays	5.2-15
5.2.3.5	Passive-Active Neutron (PAN) Assay Systems.....	5.2-19
5.2.4	Fissile Material Content and Decay Heat Value Calculations	5.2-41
5.2.5	New Assay Developments.....	5.2-43
5.2.6	QA and QC Practices	5.2-44

List of Tables

	Page
5.2-1 DOE Contractor CH-TRU Waste Generator and/or Storage Sites	5.2-1
5.2-2 CH-TRU Waste Assay Methods	5.2-1
5.2-3 Summary of CH-TRU Waste Assay Methods Presently Used at DOE CH-TRU Waste Generating and Storage Sites	5.2-2
5.2-4 Typical SGS Assay Precisions for WG Pu in Low-Density Wastes Contained in 208-L Drum	5.2-12
5.2-5 Typical SGS Assay Biases	5.2-13
5.2-6 Summary of Typical PNCC Assay Error Contributions for Low-Density Waste Forms	5.2-17

List of Figures

	Page
5.2-1 Schematic Arrangement for Segmented Gamma-Ray Scanning (SGS) System	5.2-9
5.2-2 Schematic PAN System Layout	5.2-20
5.2-3 Moderator Index Measures for PAN Systems Using the Detector Ratio Method	5.2-25
5.2-4 Use of the Moderator Index to Determine Passive Neutron Coincidence Matrix Correction Factors for a PAN System	5.2-27
5.2-5 PAN System Active Assay Matrix Correction Factors Measured at Hanford, INEEL, and SRS with a Set of 20 Standard Matrix Drums	5.2-28
5.2-6 INEEL PAN Standards Measurements (Pink Drum) Performed Over a Three-Year Period	5.2-31
5.2-7 Comparison Assay Data Sets of 200 LLNL CH-TRU Waste Drums	5.2-35
5.2-8 Comparison of 300 Hanford CH-TRU Waste Drum Assays Performed with the PAN System, Passive Neutron Compared to Active Neutron	5.2-36
5.2-9 Assay Comparisons of a Set of 300 RFETS CH-TRU Waste Drums (Graphite Molds Matrix)	5.2-37
5.2-10 Batch Average Pu Assays of 1300 Sludge Drums Performed at RFETS Compared to PAN Assays of the Same Drums Done at INEEL	5.2-38

This page intentionally left blank.

5.2 DOE Assay Methods Used for Determination of Fissile Material Content and Decay Heat Values of Contact-Handled Transuranic (CH-TRU) Wastes

5.2.1 Introduction

The isotopic composition of the waste may be determined from direct measurements taken on the product material during the processing or post-process certification at each site, analysis of the waste, or from existing records. The isotopic composition of the waste need not be determined by direct analysis or measurement of the waste unless process information is not available. Each U.S. Department of Energy (DOE) contractor CH-TRU waste generating and/or storage site may generate and/or store one or more types of waste forms (e.g., sludge, general laboratory waste, etc.) that must be assayed.

The major contractor sites that generate and/or store CH-TRU waste are listed in Table 5.2-1, and the assay techniques used by DOE contractor sites are listed in Table 5.2-2. The specific assay methods utilized at each site are given in Table 5.2-3.

Table 5.2-1 — DOE Contractor CH-TRU Waste Generator and/or Storage Sites

1.	Argonne National Laboratory - East (ANL-E)
2.	Idaho National Engineering and Environmental Laboratory (INEEL)
3.	Lawrence Livermore National Laboratory (LLNL)
4.	Los Alamos National Laboratory (LANL)
5.	Mound Facility (Mound)
6.	Nevada Test Site (NTS)
7.	Oak Ridge National Laboratory (ORNL)
8.	Richland Hanford (RH)
9.	Rocky Flats Environmental Technology Site (RFETS)
10.	Savannah River Site (SRS)

Table 5.2-2 — CH-TRU Waste Assay Methods

1.	Passive Gamma [HPGe, Ge(Li), NaI: transmission-corrected and noncorrected]
2.	Radiochemical assay: gross alpha and gamma spectrometry
3.	Passive neutron coincidence counting (PNCC)
4.	Passive/active neutron assay (PAN)
5.	Calorimetry

Table 5.2-3 — Summary of CH-TRU Waste Assay Methods Presently Used at DOE CH-TRU Waste Generating and Storage Sites^a

Site	SGS or NaI	PNCC	PAN (drum)	PAN (box)	Radiochemistry	Mobile PAN
ANL-E	X				X	
Hanford	X		X			
INEEL			X	X		
LLNL	X				X	X
LANL	X	X	X		X	X
Mound	X				X	
NTS						X
ORNL	X		X			
RFETS	X	X	X	X	X	
SRS	X	X	X			

^aCalorimetry method is also used to obtain quantitative radionuclide content.

The DOE and its site contractors have been historically, and continue to be, the dominant force in assay technology development and implementation, not only within the United States but internationally as well. Some of the assay technologies (passive gamma, radiochemistry, and passive neutron coincidence counting [PNCC]) are highly developed and have a long history of implementation first to nuclear products (in safeguards and material accounting) and eventually to nuclear scraps and wastes. Other assay technologies, such as passive/active neutron (PAN), are newer developments (circa 1980), and were developed especially for application to bulk TRU wastes assays under sponsorship of the DOE. Additional improvements to the assay technology continue to be made and implemented as indicated in this document.

Where practical, the DOE sites perform multiple independent assays of waste packages as well as real-time radiography (RTR) inspection. These independent assays generally take the form of a passive gamma assay (usually segmented gamma-ray scanning [SGS]) at the waste generator site followed by PAN assay at a central certification facility.

These practices, as well as quality assurance (QA) audits and administrative controls, provide assurances that correct values of fissile material and decay heat are assigned to each waste drum. In the case of special-case drums or of significant differences among independent assay measurements, personnel at each site review all available data, including the RTR information and assay records, to determine the appropriate action. If a reasonable assay value cannot be ascertained, remedial action is taken; either reassay if measurement errors are suspected, or repackaging if the drum is suspected of nonconformance with respect to fissile material content or decay heat.

This document describes the nondestructive and destructive assay methods for CH-TRU waste employed by the DOE sites. The assay methods employed by the DOE are shown to be reliable

and accurate means of determining fissile material, radionuclide, and decay heat content of CH-TRU wastes.

Assay topics addressed for an assay method include:

- (1) An overview of the assay method
- (2) Applicability to CH-TRU wastes
- (3) Calibration standards and implementation
- (4) Operator training requirements and practices
- (5) Assay procedures
- (6) Assay precision, bias, and limit of detection.

More details are presented for the SGS and PAN assay methods, which are the primary methods used within the DOE complex.

All systems or methods, except for PAN, have established American Society for Testing and Materials (ASTM), American National Standards Institute (ANSI), and/or U.S. Nuclear Regulatory Commission (NRC) guidelines or methods that describe proper calibration procedures, proper equipment set-up, etc. PAN is a new technique and does not yet have a guideline or method developed. However, comparisons of PAN data with the more established assay methods (e.g., SGS or radiochemistry) are discussed that demonstrate its reliability and accuracy.

QA and quality control (QC) practices used in assay methods are presented. New nondestructive assay developments such as neutron assay imaging are also discussed.

5.2.2 Assay Overview

This section describes the general features of nondestructive assay (NDA) and destructive assay methods used by the DOE site contractors to determine the TRU content of their bulk CH-TRU waste.

ANSI N15.20-1975¹ defines NDA to be “The observation of spontaneous or stimulated nuclear radiations, interpreted to estimate the content of one or more nuclides of interest in the item assayed, without affecting the physical or chemical form of the material.

active assay. Assay based on the observation of radiation(s) induced by irradiation from and external source.

passive assay. Assay based on the observation of naturally occurring or spontaneous nuclear radiation(s).”

¹ ANSI N15.20-1975, “American National Standard Guide to Calibrating Nondestructive Assay Systems.”

Destructive assay refers to chemical analysis in which a sample aliquot is removed from the item (after assuring homogenization of the batch) to be assayed and prepared for alpha and/or gamma counting.

The NRC in NRC Regulatory Guide 5.11² describes the applicable NDA passive measurements: "Radiations attributable to alpha particle decay, to gamma-ray transitions following alpha and beta particle decay, and to spontaneous fission have served as the basis for practical passive NDA measurements."

Gamma rays, X-rays, and/or neutrons, as well as other subatomic particles, are emitted by the various TRU isotopes as they undergo de-excitation to their respective ground states or more stable energy levels. NDA techniques based on detection of each emitted radiation have been developed and utilized for CH-TRU bulk-waste assay.

The passive gamma, passive neutron coincidence counting, radiochemical, and calorimetric methods are techniques, which are described by the ASTM, ANSI, NRC, and American Society of Mechanical Engineers (ASME) standards, guidelines, and/or regulations. These documents^{1,2,3,4,5,6,7,8,9,10} provide information to the user for proper implementation of these techniques.

Characteristics of any assay measurement include precision, bias, and detection limit. Proper calibration methods must also be employed to reduce or eliminate the bias of the assay results. Definitions of each of the above terms are given below and were obtained from

² USNRC Regulatory Guide 5.11, "Nondestructive Assay of Special Nuclear Material Contained in Scrap and Waste," Revision 1, April 1984.

³ ASTM C 853-82, "Standard Test Methods for Nondestructive Assay of Special Nuclear Materials Contained in Scrap and Waste."

⁴ ANSI N15.35, "Guide to Preparing Calibration Material for Nondestructive Assay Systems that Count Passive Gamma Rays."

⁵ ASTM C 696-80, "Methods for Chemical, Mass Spectrometric, and Spectrochemical Analysis of Nuclear-Grade Uranium Dioxide Powders and Pellets."

⁶ ASTM C 697-86, "Methods for Chemical, Mass Spectrometric, and Spectrochemical Analysis of Nuclear-Grade Plutonium Dioxide Powders and Pellets."

⁷ ASTM C 759-79, Methods for Chemical, Mass Spectrometric, Spectrochemical, Nuclear, and Radiochemical Analysis of Nuclear-Grade Plutonium Nitrate Solutions."

⁸ American National Standard Calibration Techniques for the Calorimetric Assay of Plutonium Bearing Solids Applied to Nuclear Materials Control, ANSI-N15.22, American National Standards Institute, New York, 1987.

⁹ Standard Test Method for Determination of Plutonium Isotopic Composition by Gamma-Ray Spectrometry, ASTM C 1030-84, *ibid*.

¹⁰ Standard Test Method for Nondestructive Assay of Special Nuclear Material in Low Density Scrap and Waste by Segmented Passive Gamma-Ray Scanning, ASTM C 853. This draft standard has been referenced with permission from ASTM Subcommittee C-26.10.

ASTM C 859-87¹¹. Examples for each discussed assay method are found in the appropriate sections.

- (1) Precision: A generic term used to describe the dispersion of a set of measured values (also referred to as “random” or “statistical error”).
- (2) Bias: A persistent positive or negative deviation of the method average from the correct value or accepted reference value (also referred to as “constant” or “systematic error”).
- (3) Detection limit: A stated limiting value that designates the lowest concentration or mass that can be estimated or determined with confidence and that is specific to the analytical procedure used.
- (4) Calibration: The determination of the values of the significant parameters by comparison with values indicated by a reference instrument or by a set of reference standards.

Estimates of precision can be calculated by standard error propagation techniques.¹⁰ Radioactive decay is random and described by Poisson statistics. For Poisson statistics, the variance in measuring N events in a detector is equal to N . (The standard deviation is the square root of the variance.)

The precision of a nondestructive assay measurement is not strongly related to the measurement item's adherence to ideal matrix and nuclide density assumptions. For destructive assay methods (e.g., radiochemical), which require sampling, the precision of repeat measurements of a single item will be strongly influenced by a lack of adherence to ideal nuclide density assumptions. However, for SGS systems, measurement bias depends primarily on the adherence of the measurement item to the assumptions of small particle size and homogeneity. Negative assay bias (reported value less than actual value) will be encountered, for example, when the nuclide is present in lumps that attenuate their own radiation to a greater extent than the surrounding material (self-absorption). Radiochemical methods that dissolve material samples will not be affected by lumps. Matrix and nuclide density have no effect on calorimeter measurements. Techniques used to correct for self-absorption effects are used in PNCC and PAN assay techniques.^{3,12,13} Positive assay bias (reported value greater than actual value) can occur when, for example, system multiplication effects become severe at high-plutonium (Pu) sample

¹¹ ASTM C 859-87, “Standard Terminology Relating to Nuclear Materials.”

¹² J. T. Caldwell, R.D. Hastings, G.C. Herrera, W.E. Kunz, E.R. Shunk, “The Los Alamos Second-Generation System for Passive and Active Neutron Assays of Drum-Size Containers,” Los Alamos Formal Report LA-10774-MS, September 1986.

¹³ J. T. Caldwell, et al., “System Evaluation Including Assay Algorithm, Matrix Corrections, and Operational Performance of the Los Alamos Passive/Active Neutron Assay Systems,” Los Alamos Technical Report N2-87-222WP.

loadings during PNCC measurements. Typical techniques used to control this interference are: (1) equivalent reference standards used for calibration, or (2) use of source addition techniques.¹⁴

Of course, to obtain precise assay measurements, count-rate-dependent losses resulting from phenomena such as pulse pileup and analyzer dead-time characteristics must be monitored and corrected. These corrections are not required for calorimeter measurements. Analyzer dead-time is defined as that period of time, which is unique to the analyzer, in which it is unable to accept input signals for analysis. This correction is accomplished through the use of a combination of electronic modules, and/or radioactive sources, and/or computer algorithms (which have been obtained through the assay of calibration standards).

The uncertainty (w) in a measurement is the composite error, including both the precision and bias of the measurement. The uncertainty in a quantity f that is a function of n independent variables x_i is given by:

$$w = \left[\sum_{i=1}^n w_i^2 \right]^{1/2}$$

where w_j is the uncertainty in the variable x_j .

Assay item preparation is generally limited to good waste/scrap segregation practices that produce relatively homogeneous items that are required for any successful waste/inventory management and assay scheme, regardless of the measurement method used.

5.2.3 Assay Methods Descriptions, Characteristics, and Limitations

This section describes the various assay methods, presents their characteristics (precision, bias, and detection limits), and discusses their limitations and applicability to assay of CH-TRU wastes. Assay methods discussed include calorimetry, passive gamma assay (e.g., SGS), radiochemical methods, PNCC, and PAN assay.

5.2.3.1 Calorimetry

Calorimetry has been used for many years in the nuclear weapons program for product assay of weapons grade (WG) Pu. Many of the NDA Pu standards in use throughout the DOE complex have been characterized by calorimetry. A large number of standard radiochemical and gravimetric assay comparisons have been performed to verify the accuracy of calorimetric assay measurements.

Basically, calorimeters measure the heat flow out of contained small packages. Experimental difficulties grow exponentially with package size, so this method is generally used only with small packages, a few liters in volume at most. The primary heat release in WG Pu materials is from alpha and beta decay, and with a knowledge of isotopic composition, precise Pu mass

¹⁴ R. B. Perry, R. W. Brandenburg, and N. S. Beyer, 1972, "The Effect of Induced Fission on Plutonium Assay with a Neutron Coincidence Well Counter," Transactions of the American Nuclear Society, 15 674.

values are readily obtained from virtually any physical or chemical form of Pu material, without knowledge of precise compound stoichiometry (e.g., Pu-to-oxygen ratio).

The kinetic energy of the emitted alpha or beta particle and the energy of the emitted alpha or beta particle and the recoil nucleus is transformed into heat, together with some fraction of the gamma ray energies and conversion electrons that may be emitted by the excited daughter nucleus in lowering its energy to a more stable nuclear configuration. The electrons and low-energy gamma rays are totally absorbed, while the higher-energy gamma rays that may escape from the calorimeter chamber comprise less than 0.01% of the total decay energy. Thus, most of the energy associated with these transitions of the daughter nucleus to ground state, as well as all of the energy associated with the alpha particle and recoil nucleus, is absorbed within the calorimeter.

The calorimeter method measures the total decay heat produced by an item. The relative isotopic abundances of the Pu and americium (Am) nuclides in the mixture and the values of decay heat per gram for each nuclide are used to calculate the average decay heat per gram of nuclide mixture. The total measured decay heat divided by the average decay heat per gram yields the grams of nuclide mixture.

ANSI N-15.22⁸ describes the calorimetry procedure and equipment used for the assay technique. This standard method is used in DOE facilities for calorimetry calibrations, setup, and as the guide to operational measurements.

5.2.3.2 Passive Gamma Assay

5.2.3.2.1 Segmented Gamma Scanning (SGS)

High Resolution (Hyperpure Germanium [HPGe], Lithium-drifted Germanium GE[Li]), Transmission and Count-Rate Corrected Assays.

Overview

The first NDA measurements of TRU isotopes using passive gamma rays were performed by DOE contractor personnel more than 40 years ago. Passive gamma-ray NDA of TRU isotopes is a highly developed technology, and is also the most widely implemented. The introduction more than 20 years ago of germanium solid state detectors and the subsequent incorporation of these detectors into computer-based detection packages has improved the resolution and reliability of these systems. Commercial manufacturers of these systems include Canberra of Meriden, Connecticut, and Nuclear Data of Schaumburg, Illinois.

The number of individual TRU isotopes or their daughters that can be assayed with SGS is large; uranium (U)-233, Pu-238, Pu-239, neptunium (Np)-237, Am-241, Am-243 being among the more common ones. In each case, one or more characteristic moderate-to-high energy gamma rays are emitted in sufficient intensity to permit estimates of quantities in low-to-moderate density waste packages as large as 208-liter (L) drums. The recommended (ASTM C 853-82)¹¹ experimental arrangement for SGS assays is shown in Figure 5.2-1. This

figure displays the essential elements required for SGS assays of TRU isotopes in any package size.

To minimize assay errors due to axial inhomogeneities, assays are performed in segments along a waste package's vertical axis. The effects of radial inhomogeneities are minimized by rotating the drum during the assay measurement. The detector is shielded in such a manner so as to allow the waste drum to be scanned in segments (typically 10 to 20 segments).

Gamma-ray attenuation is measured for each segment with a transmission source in the indicated geometry of Figure 5.2-1. The energy of this source is selected to match that of the gamma-ray line(s) being measured (e.g., Oak Ridge National Laboratory [ORNL] uses a mixed europium (Eu)-152/Eu-154 oxide source for its large array of gamma-emitting radioisotopes [50 keV to 1600 keV], and selenium-75 is typically used for Pu-239 assays).

State-of-the-art counting electronics allow dynamic counting rate ranges of factors of 10^4 to 10^5 or more, with dead-time corrections measured with a second small, low-energy source positioned near the detector. Waste packages are automatically rotated about their vertical axes and cycled through the required segment heights with standardized, computer-controlled electronic motors and precision mechanical turntable/elevator hardware. SGS hardware-software packages are commercially available from several manufacturers.

Applicability to CH-TRU Wastes

A prime factor that determines applicability of SGS to perform assay measurements of CH-TRU waste packages is gamma-ray transmission through the package. Other factors affecting assay measurements include particle self-absorption and nonhomogeneity of the assayed item ("lumping"). Two conditions must be met to optimize assay results. First, the particles containing the nuclide must be small to minimize self-absorption of emitted gamma radiation. Second, the mixture of material within a package segment must be reasonably uniform in order to apply an attenuation correction factor, computed from a single measurement of item transmission through the segment. Variations in item composition and density within a vertical segment lead to indeterminate errors. Such variations should be minimized through strict scrap and waste segregation procedures.

A combination of analytical error analysis³ and experimental usage over many years has determined that transmission factors greater than or equal to 0.5% are required for accurate SGS assays. The physical density of a waste package that this requirement defines depends greatly on the package size [i.e., the radial distance from the gamma-emitting source(s) to detector] and the energy of the gamma rays used for the analysis. Four-liter packages having densities as high as 2 grams per cubic centimeter (g/cm^3) meet the criterion, whereas 208 L packages are limited to densities of 0.5 g/cm^3 or less. To assure compliance with these limits, all current SGS software packages include an automatic warning indicating when the transmission factor for any sector falls below the prescribed limiting value. The routine practice at some sites is to calculate a contribution from that sector based on the lower-limit transmission (e.g., 0.5%).

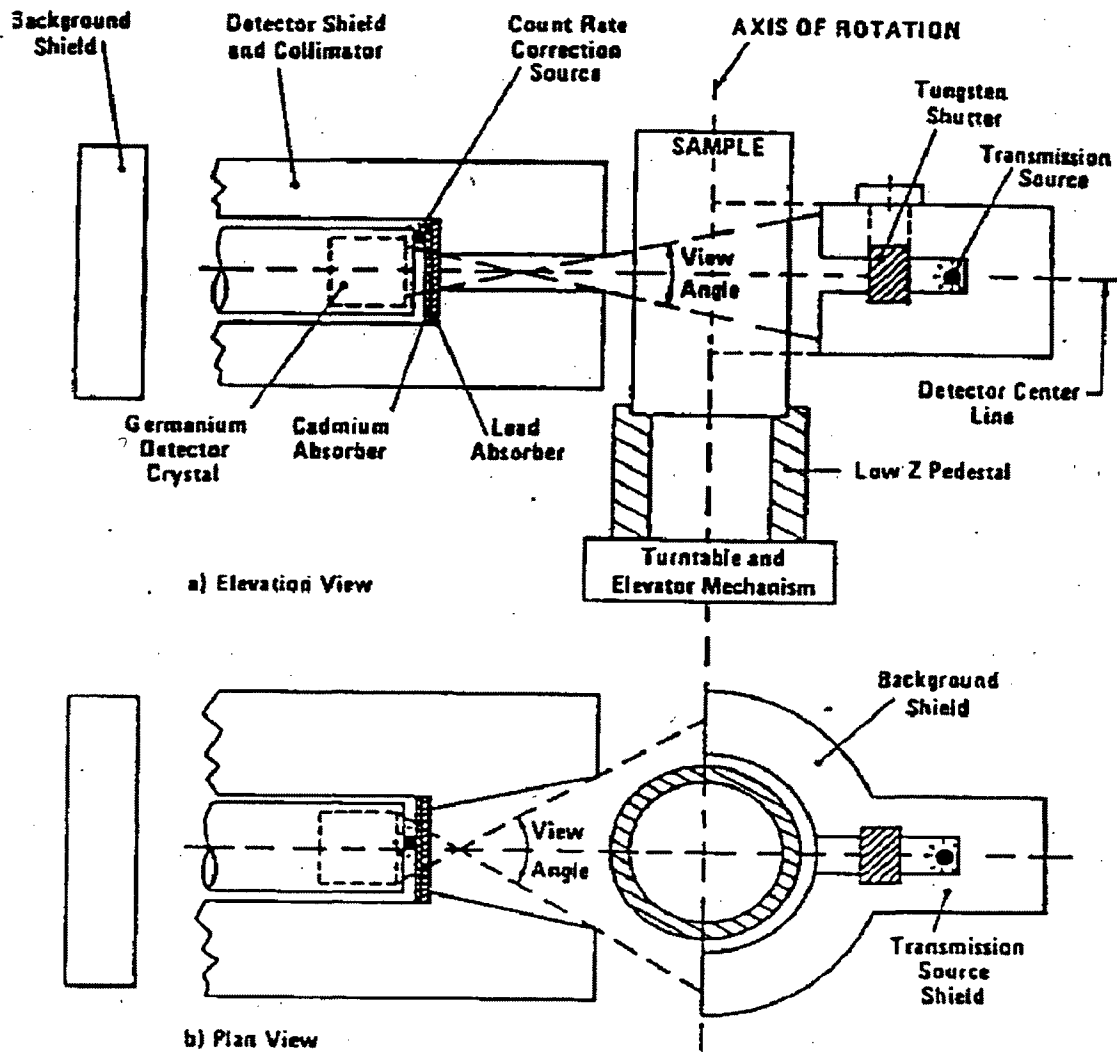


Figure 1
Schematic Arrangement for Segmented Gamma-Ray Scanning (SGS) System

Figure 5.2-1—Schematic Arrangement for Segmented Gamma-Ray Scanning (SGS) System

The reason for maintaining the assay value, rather than disregarding it, is because most SGS transmission failures occur for only one sector out of the 10 to 20 drum sectors assayed. This sector, on the average, contains only a small fraction of the waste drum's total TRU inventory of gamma-emitting isotopes.

On the average, estimating the TRU content for one or two failed segments in this fashion results in only a small overall error for the waste drum. Other sites (e.g., Hanford) flag such drums for management decision on whether the item should be disassembled, examined, and repackaged, or reassayed on a neutron sensing assay instrument, which is less sensitive to density variations. Since the SGS assay value for a transmission failure is truly a lower limit, and as is discussed in detail in Section 5.2.3.4, passive neutron assays generally provide upper limit assay values (especially for WG Pu); the combination of SGS and passive neutron assay methods tends to bracket the actual assay value.

Some matrix forms are inherently unsuitable for SGS analysis. Such forms may contain 'lumps' of nuclide, that is, nuclides contained in small volumes of matrix material having a localized density substantially different from the bulk density of the rest of the container. The dimensions of nuclide particles that constitute a lump vary with the energy of the emitted radiation used for the analytical measurement. The possible magnitude of the problem may be estimated from the following example of attenuating effects. A plutonium metal sphere 0.02 cm in diameter will absorb approximately 4% of the 414 keV, Pu-239 gamma rays produced. Approximately 15% of the 186 keV gamma rays of U-235 will be absorbed in a uranium metal sphere of the same diameter.

As mentioned previously, another condition that will cause measurement problems is presented by containers with several irregular regions, highly variable in density, that prevent the calculation of a valid attenuation correction based on the transmission measurement. In case of such a condition, an analytical method less sensitive to nuclide and matrix densities, such as PNCC, should be employed.

Careful inspection of the transmission and nuclide peak areas for each segment may provide clues when a measurement should be suspect. Sudden, discontinuous changes in the transmission values for adjacent segments or high nuclide count values for isolated segments are examples of signals indicating possible problem items.

Instrument Calibration, Standards Preparation, and Implementation

The recommended DOE facility standard guide used for preparation of SGS standards is ANSI N-15.35.⁴ The recommended DOE facility standard for implementation of these standards is ANSI N-15.20.¹ ANSI N-15.20 calls for the preparation of the calibration material using intimate and stable mixtures of the TRU isotope with matrix material and for preparation of a suitable number of calibration standards to cover the anticipated isotopic concentration region of interest (ROI). In the case of Pu-239, this range is 5 to 200 grams (g) for 208 L drums.

When establishing a calibration curve for the SGS instrument, at least two calibration standards are used for each content code. One standards drum contains a TRU isotopic mass near the low

end of the ROI (e.g., 5g Pu-239) while the other contains a TRU isotopic mass near the high end of the ROI (e.g., 200g Pu-239). Both drums contain waste stream matrix mixtures and densities designed to simulate the waste streams. Some sites use more than the two drums described above to ensure a proper calibration factor. Other sites measurement control programs require standards drums to be measured by the assay instrument multiple times, both before and after each measurement session.

Acceptable ranges for calibration data are specified in the operating procedures (e.g., ORNL accepts a variance of +/- 5%). If assay measurement falls outside the acceptable range, no production assay measurement is performed until the issue has been resolved by a designated NDA expert.

Operator Training Requirements and Practices

Present-day commercial SGS systems, such as the Canberra and Nuclear Data models, are highly-automated, computer-based systems. The instruments are computer-controlled using relatively interactive (“user-friendly”) software. Only trained personnel are allowed to operate the assay equipment. Personnel are qualified according to DOE Order 5480.5.¹⁵

Each site provides a specialized training program for NDA instrument operators. The operators are directed and/or assisted by a designated site NDA expert. Expertise is attained by education and experience.

Assay Procedures

The assay procedures cited in ASTM C 853-82, “Standard Test Methods for Nondestructive Assay of Special Nuclear Materials Contained in Scrap and Waste,”³ are recommended for use at all DOE facilities. These procedures stress usage of proper calibration standards, proper equipment and equipment setup, avoidance of practices (such as misalignment of the waste package) known to result in inaccurate assays, attention to proper record keeping and equipment maintenance, and safe operation of the equipment.

Assay Precision, Bias, and Detection Limit

Assay precision is generally taken to mean measurement repeatability. In the case of typical SGS systems, operated and calibrated according to the recommended procedures, repeatability of results is limited only by statistical counting errors. Counting statistics, in turn, are a strong function of TRU isotopic loading and counting time.

ASTM C 853¹⁰ discusses SGS precision and bias in detail. Some of that discussion follows. The precision of an SGS assay is a function of the precision of the peak areas measured for each segment. The precision of an assay is normally better when the following conditions can be obtained:

¹⁵ DOE Order 5480.5, “Safety of Nuclear Facilities,” September 23, 1986.

- Increased count time
- High transmission source activity
- Low attenuation for gamma radiation in the energy range of interest.

Typical SGS assay precisions for low-density wastes are listed in Table 5.2-4. Certain matrices, such as graphite molds and cemented insulation, whose densities are above the prescribed SGS-applicability limit of 0.5 g/cm^3 for 208 L packages, and drum handling (homogeneity of calibration standards may be jeopardized) can have a deleterious effect on assay precision.³

Table 5.2-4 — Typical SGS Assay Precisions for WG Pu in Low-Density Wastes Contained in 208-L Drum

WG Pu (g)	Precision
1	+/- 100%
10	+/- 10%
30	+/- 3%

(Table 5.2-4 values reflect the assumption that the guidelines given in ASTM C 853-82³ were adhered to in acquiring the data.)

The precision of an assay performed by SGS is not strongly related to the measurement item's adherence to ideal matrix and nuclide density assumptions. However, measurement bias depends primarily on the adherence of the measurement item to the assumptions of small particle size and homogeneity. Negative bias will be encountered when the nuclide is present in lumps that attenuate their own radiation to a greater extent than the surrounding material. Positive bias can result from low transmission items with over-corrected end effects. Items containing high-density areas may be biased either high or low or be unbiased, depending on the relative position of the high density area and the nuclide of interest. In the majority of measurement situations, however, it is expected that when biases exist, measurement results will be lower than true values.

Several SGS and destructive assay comparison studies of several waste forms indicate SGS assay biases of 10% or less, at the 95% confidence level.¹⁶ Assay biases for low-density waste matrices contained in 208-L drum packages are 5% or less. In small package applications (based on numerous Safeguards and Nuclear Materials Accounting applications), SGS assay biases of less than 0.5% have been reported.¹⁶ The basic assay formalism associated with the SGS method, that is, transmission correction and the use of small segments, is conducive to very accurate results if recommended procedures are correctly followed. Heterogeneous matrices and isotopic concentration variations can have a severe and unpredictable effect on assay bias for a given waste drum.

Typical SGS assay biases for two types of wastes are summarized in Table 5.2-5.¹⁶

¹⁶ Fleissner, John G. and Hume, Merril W., "Comparison of Destructive and Nondestructive Assay of Heterogeneous Salt Residues," RFP-3876, March 29, 1986.

Table 5.2-5 — Typical SGS Assay Biases

Waste Type	Biases
Heterogeneous salts	10% ^a
Low-density (e.g., combustibles)	5%

^a Based upon assay of a number of 4-L waste packages prior to placing in a 208-L drum.

(Table 5.2-5 values reflect the assumption that the guidelines given in ASTM C 853-82 were adhered to in acquiring the data.)

SGS assay limit of detection for typical applicable wastes and standard counting times in current routine use in DOE facilities (30 min or less per assay measurement) is about 5g WG Pu. This is based on 30% assay precision. Usually SGS assays are only performed on 208-L drums when screening indicates 10 g or more WG Pu to be present.

SGS Assay Results Comparisons

Calorimetric assay measurements of heterogeneous molten salt residues have provided a total assay value for the Pu and Am, as an NDA comparison (referee) technique for an assessment of SGS assay of RFETS molten salts.¹⁶ Reliable interpretation of the calorimetry measurements depended on an accurate determination of the Am/Pu ratio, since the relative amount of heat produced by the Am in these samples was typically 50% or more.

Gamma-ray spectral isotopic analysis coupled with calorimetry was performed at Mound on nine cans of molten salt, which were subsequently returned to RFETS for dissolution and solution quantification. Results of the Mound measurements show a relative standard deviation range from 0.032% to 0.50% for Pu values and 0.23% to 0.39% for Am values. No biases or statistical differences between pairs or measurements were noted.

5.2.3.2.2 NaI (low-resolution) Assays

Both transmission-corrected and transmission-uncorrected sodium iodide (NaI) assay units are used in DOE facilities. The transmission-uncorrected units are used, for example, at RFETS for low-density wastes containing up to 20 g Pu.

The NaI transmission-corrected assay instruments are special function units, servicing isolated waste streams producing a single type of waste under generally constant conditions. Typically, these NaI units consist of five individual collimated NaI detectors mounted at different heights that view a rotating drum, effecting a five-segment assay. Transmission source geometry is similar to that shown in Figure 5.2-1. The pertinent NDA guidelines outlined in ASTM C 853-82³ are applied to these systems in a fashion similar to that described for SGS units. A two-window pulse height analysis is performed to correct for Am-241 and fission product interferences, and software indicators flag segments containing excessive Am or fission product amounts.

Calibration standards are carefully chosen for the particular waste stream being monitored, and assays are performed in a fashion similar to SGS assays. These units produce, on the average, reliable results as determined by numerous quantitative comparisons with SGS and PAN assays of the same waste drums.¹⁷ Analytical studies of assay biases for these systems indicate +/-10% levels of bias. This has been verified with SGS and PAN comparisons of a large number of drums assayed with these NaI systems.¹⁷ It should also be pointed out that assay standards practices and procedures are adhered to in accordance with ASTM C 853-82 and ANSI N-15.35. Duplicate assays with SGS or PAN (performed at the certification facility) provide additional assurance that proper TRU assay values are being generated with these systems.

5.2.3.3 Radiochemical Methods

The basic application of radiochemical methods in TRU waste assays is in quantifying radioisotopic content of process liquid or sludge waste forms. Before final drying or cementation, a batch of process sludge is contained in a single large tank. The sludge is then mixed for a sufficient period of time to assure a homogenous mixture. This mixture is then sampled at several points while circulating and the samples subjected to routine radiochemical processing and analysis (precipitation and separation followed by alpha and/or gamma spectrometry). The prepared aliquot samples are assayed in a standard alpha spectrometer. In the cases of higher-activity sludges, these samples are assayed using another method (e.g., passive gamma-ray spectroscopy). Assays of samples obtained from individual sludge drums may also be performed.

Using standard analyses, the individual TRU isotopic activities are determined; Pu-239, total Pu (WG Pu), and Am-241. These aliquot sample activities are then used to determine the original batch TRU activity, on an individual isotopic basis. By proper accounting for any volume reduction or increase produced in the drying or cementation process, these batch activities can then be used to determine an individual 208 L drum's specific Pu and Am content, simply by weighing the drum and accounting for the amount of original batch sludge that was deposited in that particular drum. Accurate final drum assays depend upon following the procedure outlined in a careful manner, with maintenance of a homogeneous mixture during both the crucial sampling and drum filling stages.

Standard test methods (e.g., ASTM C 696-80⁵, ASTM C 697-86⁶, and ASTM C 759-79⁷) describe the radiochemical standard aliquot sampling procedures used in the DOE facilities. Assay standards are prepared and used as indicated in the standard test methods. Sampling, weighing of the sample, and handling the sample are done under conditions that assure that the sample is representative of the lot or batch. A lot or batch is defined as any quantity of solution that is uniform in isotopic, chemical, and physical characteristics by virtue of having been mixed in such a manner as to be thoroughly homogeneous. All containers used for a lot or batch are positively identified as containing material from a particular homogeneous solution.

¹⁷ F. J. Schultz and J. T. Caldwell 1988 DOE Model Conference paper.

Assay biases at the final filled-drum stage are difficult to estimate, since they depend primarily on the maintenance of homogeneous mixtures during the sampling, drying/cementing, and final drum-filling stages.

5.2.3.4 Passive Neutron Coincidence Counting (PNCC) Assays

5.2.3.4.1 Overview

PNCC assays include assays conducted on small packages that are summed to give the final reported assay value for a waste container, and the passive portion of the PAN assay system, which is discussed in detail in Section 5.2.3.5.

PNCC method for determination of Pu assay in product materials has been used for Safeguards verification purposes within the DOE complex for more than 20 years. PNCC has also been applied to the assay of TRU-bearing wastes and scraps for many years (ANSI N15-20-1975¹, subsections 20-28). In addition, the NRC Regulatory Guide 5.11² describes NDA techniques acceptable to the NRC for assay of wastes and scraps, which includes PNCC. These standards and regulatory guides are used to ensure proper application by the DOE of PNCC to scrap and waste assay. In fact, DOE laboratories, primarily Los Alamos National Laboratory (LANL), have been largely responsible for the development of PNCC as a reliable assay technique for TRU wastes, as well as for scraps and product.

The prototypical PNCC is comprised of a high-efficiency neutron detector large enough to accommodate the waste package of interest. It operates by detecting the number of time-correlated neutrons being emitted spontaneously by the assay item. In fission events, bursts of 2,3,4,5,... neutrons are emitted simultaneously, and the detection of two or more of these in time coincidence serves to identify the original fission event within the material being measured. Specialized counting electronics (e.g., shift register) have been devised to accomplish and record these measurements. These are discussed in detail in ASTM C 853-82³.

Any TRU isotope that undergoes spontaneous fission at a measurable rate can be quantified by PNCC. Comprising this category are the even isotopes of Pu, curium (Cm), and californium (Cf). Most commonly within the DOE complex, the different grades of Pu [WG, reactor grades (RG) of different isotopic compositions, heat source grade (HSG)] are quantified by coincidence counting of the included mixture of even isotopes of Pu; predominantly Pu-240 for WG and RG, and Pu-238 for HSG. Thus, with knowledge of the Pu isotopes, the observed coincidence rates can be interpreted to yield total Pu mass.

5.2.3.4.2 Applicability to CH-TRU Wastes

The primary requirement for application of PNCC to CH-TRU waste assay is knowledge of the included isotopes, since normally the quantity of interest is the total elemental mass (i.e., total Pu mass) rather than the even isotope masses only. In addition, the wastes should not include mixed-element spontaneous fission emitters. For instance, it is undesirable to have Cm and Cf isotopes present in the same assay item containing Pu isotopes. Most DOE CH-TRU wastes contain Pu even-isotope spontaneous fission emitters. A typical average WG Pu isotope mix

contains 5.8% Pu-240. Pu-240 is responsible for more than 99% of coincidence neutrons detected in typical WG Pu wastes.

5.2.3.4.3 Instrument Calibration, Standards Preparation, and Implementation

Calibration of PNCC instruments, similar to SGS, is obtained by establishing a curve of instrument response versus isotopic mass.^{1,3} A minimum of four calibration points are obtained over the mass range of interest using standards that are representative of the materials being measured. Within each content code, or waste category, the variation due to interference effects within the boundaries defining the limits of that category is measured. Calibration standards are constructed using containers identical to those for the scrap or waste, with contents that are representative of the range of matrix conditions to be encountered. It is not recommended to extrapolate beyond the calibration range established during instrument calibration. Encapsulated Cf-252 sources, such as those used at ORNL for passive PAN calibration, are available to be used for PNCC calibration purposes.

Acceptable ranges for calibration data are specified in the operating procedures. If assay measurement values fall outside the acceptable range, no production assay measurements are performed until the issue has been resolved. Operators contact a designated NDA expert for consultation.

5.2.3.4.4 Operator Training Requirements and Practices

Present-day commercial PNCC systems, such as the JOMAR or National Nuclear models, are highly-automated, computer-based systems. The instruments are computer-controlled using relatively interactive (“user-friendly”) software. Only trained personnel are allowed to operate the assay equipment. Personnel are qualified according to DOE Order 5480.5.¹⁵

Each site provides a specialized training program for NDA instrument operators. The operators are directed and/or assisted by a designated site NDA expert. Expertise is attained by education and experience.

5.2.3.4.5 Assay Procedures

The assay procedures cited in ASTM C 853-82, “Standard Test Methods for Nondestructive Assay of Special Nuclear Materials Contained in Scrap and Waste,”³ are recommended for use at all DOE facilities. These procedures stress usage of proper calibration standards, proper equipment and equipment setup, avoidance of practices (such as misalignment of the waste package) known to result in inaccurate assays, attention to proper record keeping and equipment maintenance, and safe operation of the equipment.

5.2.3.4.6 Assay Precision, Bias, and Limit of Detection

Most PNCC units are used to assay small packages (4-L size), which are then placed into larger waste containers, such as 208-L drums. Assuming proper administrative control of drum filling, this practice greatly reduces the assay errors associated with all PNCC performance effects except counting statistics and isotopics. Additional errors caused by self-multiplication or system dead-time are significant only when strong neutron sources are present.

Sources of assay biases and measurement uncertainties include:

- (a) Counting statistics: A significant source of error at both extremes of count rate. Measurement uncertainty can be significant at very low count rates for all assay conditions. For every high count rates, when the rate is due primarily to a strong (alpha, n) internal source or induced fissions, assay bias is increased.
- (b) Isotopics: For WG Pu waste assay biases produced by systematically incorrect actual Pu isotopics are 3% or less, based on use of historic average WG Pu isotopics. Uncertainties in the measurement of the isotopic composition, generally considered to be unbiased, increase the uncertainty of the assay value.
- (c) Self-multiplication (or induced fissions): Generally a problem when fairly large Pu amounts are present in conjunction with strong (alpha, n) sources within the same drum (measurement value greater than actual value). This phenomenon is a source of potential bias producing uncertainty in the assay value. Multiplication effects should not be significant when TRU gram loadings are low and waste volumes are large.
- (d) System dead-time: A problem when strong neutron sources are present (measurement value is less than actual value). This phenomenon is a source of potential bias with an associated uncertainty.
- (e) Calibration: Typically, assay uncertainties produced by uncertainties in calibration are 3% or less.
- (f) Matrix effects: Matrix effects include neutron poisons (e.g., boron, cadmium) and other neutron emitters [species that spontaneous fission or have strong (alpha, n) reactions] and neutron moderators. See Caldwell et al., 1986¹² for a discussion of moderator error estimation techniques.

Table 5.2-6 provides a summary of typical PNCC assay error contributions for low-density waste forms.

Table 5.2-6 — Summary of Typical PNCC Assay Error Contributions for Low-Density Waste Forms

Error Contribution	WG Pu	Typical Errors
Counting statistics	1 g	+/- 50%
	10 g	+/- 10%
	30 g	+/- 5%
	100 g	+/- 3%
Self-multiplication		+/- 5%
System dead-time		+/- 3%
Isotopics		+/- 3%
Calibration		+/- 3%
Matrix (low-density)		+/- 5-20%

Estimates of PNCC assay uncertainty can be calculated by standard error propagation techniques from the various bias contribution variances. The grams of plutonium calculated by PNCC is a function of net passive coincidence neutron count rate (gross neutron coincidence count rate minus accidental neutron coincidence rate) (SIGP), self-multiplication (MULT), system dead time (SYSDT), isotopics (ISOP), calibration (CALIBP), and moderator index (MI).

For 30 grams of plutonium, the uncertainty in the 30 grams of plutonium is given by (see Section 5.2.2):

$$\begin{aligned} w &= [f(\text{SIGP})^2 + f(\text{MULT})^2 + f(\text{SYSDT})^2 + f(\text{ISOP})^2 + f(\text{CALIBP})^2 + f(\text{MI})^2]^{1/2} \\ &= [(0.05)^2 + (0.05)^2 + (0.03)^2 + (0.03)^2 + (0.03)^2 + (0.20)^2]^{1/2} \\ &= 0.218 \text{ or } 21.8\%. \end{aligned}$$

The passive mass assay value reported by the PNCC assay algorithm would then be:

$$\text{Passive mass (grams)} = 30.00 \text{ +/- } 6.55.$$

Anderson and Lemming, 1982, MLM-3009, Table 5, p. 33,¹⁸ shows overall neutron production rates for several of the more common TRU isotopes and several of the more common matrices that produce significant (alpha, n) reactions. For example, WG Pu, which has an average alpha energy of 5.15 megaelectron-volts (MeV), produces approximately 2 neutrons per second per millicuries-alpha (n/s/mCi-alpha) in an oxide matrix and 215 n/s/mCi-alpha in a fluoride matrix. Pu-238 and Am-241, which have an average alpha particle energy of 5.5 MeV, produce approximately 2.5 n/s/mCi-alpha in an oxide matrix and approximately 310 n/s/mCi-alpha in a fluoride matrix. These values are representative of pure chemicals and alloys. Neutron production rates for waste materials will be less, since the TRU isotopes are more widely dispersed and the alpha particles are less likely to encounter a productive target.

The more usual (alpha, n) reactions that can cause passive assay concerns consist of normal WG Pu in which a sizeable fraction of the Pu is chemically bound to either fluorides or bound in a salt mixture containing aluminum or magnesium. Typically, metal oxide or nitrate forms of TRU isotopes (which produce approximately 0.7 to 2 n/s/mCi-alpha) present no problems for passive neutron assays (both passive PAN and PNCC). In practice, rates ranging to 20 n/s/mCi-alpha do not decrease passive assay precisions drastically as long as the alpha sources present are only those associated with WG or RG Pu. However, waste streams that include additional Am-241 can be difficult to assay passively even if the TRU chemical form is the oxide.

¹⁸ M. E. Anderson and J. F. Lemming, "Selected Measurement Data for Plutonium and Uranium," MLM-3009 (or ISPO-157), November 1982.

5.2.3.5 Passive-Active Neutron (PAN) Assay Systems

5.2.3.5.1 Overview

PAN assay systems consist of two independent assay units—passive and active neutron. The combination of passive and active neutron assays within a common system provides a unique set of information.

The passive assay portion of the PAN method described below is an adaptation of the PNCC method using “self-measurement” matrix corrections. Two complete passive assay detection systems are maintained with separate counting electronics. Two detection systems are used separately or in combination depending upon the neutron count rate. The passive coincidence measurement provides quantitative information on even isotopes present in the waste container, such as Pu-240. The passive singles neutron count rate (difference between total neutron rate and that due to spontaneous fission events) provides semi-quantitative information on alpha particle emitters present in the waste container, such as Am-241. The active assay provides quantitative information on the Pu-239 and other fissile isotope constituents. See Schultz et al., 1984¹⁹ and WIPP-DOE-157, 1989²⁰ for a more complete description of the system.

For WG Pu, the passive coincidence and active assays provide independent total Pu assay values. This fact has been extremely important in verifying the accuracy or determining the bias of the PAN assay measurement technique, as presented in Caldwell, et al., 1986.¹² This formalism has also been verified by extensive comparisons of both passive and active neutron assays with SGS.¹⁰ PAN assays systems have been developed for both drums and boxes (see Section 5.2.5 for discussion of box PAN assay systems). For these relatively large waste containers, effects of the waste material (matrix) on the neutron signals observed cannot be neglected.

5.2.3.5.2 Instrumentation

A basic cross-sectional view of a typical LANL PAN detection system, showing the schematic “interwoven” layout of the two distinct types of neutron detection packages (bare He-3 and cadmium (Cd)-shielded He-3 detector tubes), is shown in Figure 5.2-2.

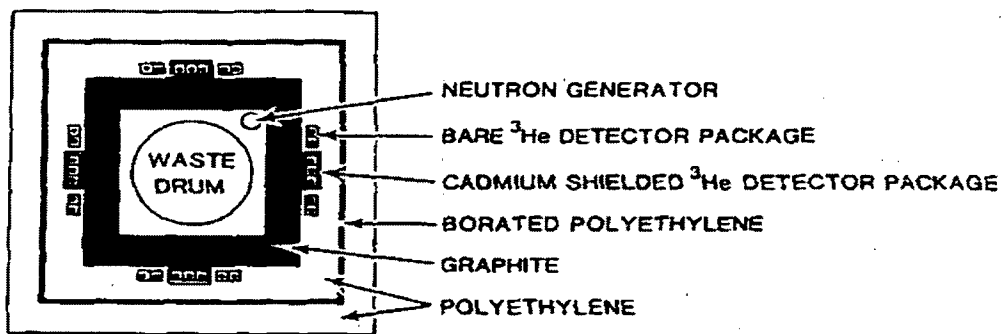
Passive Assay Portion

The passive portion of the PAN assay system utilizes the two types of detection packages to:

- (a) determine a MI used to determine a correction to the assay calculation to account for the matrix characteristics, and

¹⁹ F. J. Schultz, et al., Oak Ridge National Laboratory; J. T. Caldwell et al., Los Alamos National Laboratory, “First-Year Evaluation of a Nondestructive Assay System for the Examination of ORNL TRU Waste,” ORNL-6007, April 1984.

²⁰ “Data Package Format for Certified Transuranic Waste for the Waste Isolation Pilot Plant,” WIPP-DOE-157, Rev. 2, January 1989.



Cross-sectional views of the second-generation assay chamber show the layout and relative positions of both shielded and bare ³He detector packages.

Figure 2
Schematic PAN System Layout

Figure 5.2-2—Schematic PAN System Layout

- (b) optimize counting statistics depending on the actual relative neutron sources encountered.

For low count-rate waste containers, all counts detected by the neutron detector packages are summed to yield the lowest assay limit of detection possible. All detector count rates (acquired by both bare and shielded detectors) are summed electronically to obtain a "System Totals" neutron detection efficiency of approximately 12%.

For waste containers with higher Pu loadings (e.g., 100 g or more) coupled with strong (alpha, n) backgrounds, the Cd-shielded detectors are summed independently, and the "Shielded Totals" count rate is formed with a resulting neutron detection efficiency of 2.9%. However, this detection package possesses a much faster "die-away" or "neutron-collection" time, approximately six times faster than that of the slower "Systems Totals", which is approximately 15 microseconds. At low count rates, the slower collection time is of no consequence [i.e., accidental coincidences due to (alpha, n) reactions are small] and, thus, the Systems Totals provides not only a more sensitive but also statistically more precise passive assay measurement.

At higher count rates the faster die-away time of the Shielded Totals gains a higher precision than the less specific count rate (Systems Totals). As a consequence, at high neutron count rates the Shielded Totals Coincidence rate is used to obtain the more precise passive assay measurement value.

The cross-over count rate (i.e., the count rate at which the assay measurement value obtained by the Shielded Totals supplants the Systems Totals) has been experimentally determined to be approximately 2000 counts per second (cps) (Systems Total count rate), and this value is used in the assay algorithm. There is a substantial range in which either Systems Coincidence or Shielded Coincidence rates both provide precise assay values. Many data comparisons have been performed in this cross-over region to verify the self-consistency between the two coincidence measurements.¹⁷

Active Assay Portion

The active portion of PAN systems performs a high-sensitivity, pulsed thermal neutron interrogation assay of waste drums. As shown schematically in Figure 5.2-2, a small 14-MeV neutron generator placed within the assay chamber between the waste drum and moderating walls provides short pulses (5-10 microseconds [ms] of high-energy interrogating neutrons. In approximately 0.5 ms, all original fast neutrons in this interrogating pulse have been thermalized by multiple collisions with the graphite and polyethylene walls and moderating materials within the waste drum. This "thermalized interrogating pulse" persists ($T^{1/2}$ about 400 ms) for some time, during which induced fissions within the waste drum are produced, primarily in Pu-239 or other fissile isotopes. These events, in turn, result in prompt-fission, spectrum neutrons being emitted by each fissioning nucleus.

The cadmium-shielded detection packages have been designed to reject an external thermal neutron flux to 1 part in 10^7 , but to respond sensitively to fission spectrum neutrons. The

summed shielded detector packages shown in Figure 5.2-2 detect about 3% of all induced fission events that are produced within typical waste drums.

An additional measurement feature not shown in Figure 5.2-2, but discussed at length in Caldwell, et al., 1986,¹² is the set of thermal flux monitors, one Cd-shielded and collimated and the other bare, that are also positioned inside the assay chamber between the waste drum and the moderating walls. As discussed at length in Caldwell, et al., 1986,¹² the ratio of these flux monitors is highly sensitive to the neutron absorption characteristics of the waste drum contents. This ratio is used to form a drum "Absorption Index" (AI) (see Section 5.2.3.5.3).

5.2.3.5.3 PAN Assay Matrix Corrections

Two types of matrix effects can interfere with the active neutron measurements: absorption and moderation.¹² The absorption effects occur almost entirely as an attenuation of the interrogating thermal neutrons, caused by the presence of various neutron poisons within the waste matrix (e.g., boron, cadmium, chlorine, etc.).

Moderation effects occur at two stages of the measurement. The original burst of 14-MeV neutrons can be moderated to a considerable extent during passage through the waste matrix. Generally, this results in a larger thermal neutron interrogation flux than would have been produced in the absence of matrix. After the interrogation flux has produced fission reactions within the waste matrix, the same moderating materials can attenuate the prompt-fission signal neutrons resulting in a decrease in observed response relative to the no-matrix case. This attenuation of signal fission-neutrons also is the primary matrix effect for the passive measurement.

The approach to matrix corrections has been to base corrections on measured quantities determined as adjuncts to the primary active and passive TRU assay measurements. The systematic matrix correction algorithm is based on an analytic fit to assay measurements obtained for different positions of the source within a matrix drum. These analytic fits then provide estimates of uncertainty for the active and passive assay data.

The absorption matrix correction approach used by the PAN systems employs a ratio of an unshielded in-chamber flux monitor to a cadmium-collimated, in-chamber flux monitor (designated the barrel flux monitor). This ratio is termed the AI. The barrel flux monitor detects those neutrons that have undergone drum matrix interactions. The ratio of the monitors strongly reflects the neutronic properties of the matrix.

$$\text{AI} = \frac{[\text{flux monitor response (0.7-4.7 ms)}]}{[\text{barrel flux monitor response (0.7-4.7 ms)}]} \quad (1)$$

The MI depends upon the responses of the two detection systems (Cd-shielded and bare) to moderated neutrons. The shielded detectors are insensitive to thermal neutrons, while the bare detectors are very sensitive to the thermal neutron flux. In turn, the thermalized fraction depends very strongly on the moderator density of the matrix. To use this relationship in obtaining matrix correction factors, the ratio is normalized so that a value of zero is obtained when no moderator is present and, in addition, a small correction is made to account for self-absorption effects.

The general equation for a moderator index is given in Equation (2).

$$MI = \{1 - [(shielded\ totals)/(system\ totals)]/A_0\} \times \{A_1 + A_2 \times \ln(AI)\} \quad (2)$$

The term within the first set of brackets is the basic raw spectral data, and the term within the second set of brackets is the correction term for matrix absorption effects. The same MI values are used for both active and passive matrix corrections.

In order to obtain data to construct analytical models of matrix correction factors, 19 simulated waste matrices were fabricated,¹² and active and passive calibration standards were placed in known locations throughout the waste matrix drums. Both active and passive assay matrix response measurements were obtained as a function of location (radius, r, and height, z) of the standards. The resulting matrix response values varied smoothly as a function of r and z. These studies determined that the systematic effects are due only to gross neutron absorber and moderator amounts and are independent of the actual nature of the materials themselves. That is, a drum filled with Raschig rings (borated glass) produces the same responses as a drum filled with vermiculite mixed with an equally absorbing amount of borax.

Most of the observed distributions have been found to fit a power law as given in Equation (3):

$$y = A + Br^N \quad (3)$$

where A, B, and N are the fit parameters and r is the drum radius.

Volume-weighted average values were calculated using this equation, representing the most probable measurement result for either a totally uniform or a totally random distribution of source material within the matrix.

The matrix correction factor (MCFA) for an active assay measurement is a function of the AI and MI.

$$MCFA = MCFA(AI) \times MCFA(MI) \quad (4)$$

The MCFA values were fit to the power law (equation 3) as a function of their AI values for the 19 simulated waste matrices. The following set of equations describing the absorption portion of the active assay matrix correction factor were obtained for one PAN system:

$$MCFA(AI) = 1.00 \quad (5)$$

for the AI less than or equal to 2.272, and

$$\text{MCFA}(\text{AI}) = 0.54x(\text{AI})^{0.612} \quad (6)$$

for the AI greater than 2.72.

The moderator portion, MCFA(MI), of the active assay matrix correction factor is obtained by dividing the total measured MCFA values by the calculated MCFA(AI) values obtained in equations (5) or (6).

The analytic representation of these data is thus of the form

$$\text{MCFA}(\text{MI}) = 1.00, \quad (7)$$

for the MI less than or equal to 0.40,

$$\text{MCFA}(\text{MI}) = 0.483\exp[1.817(\text{MI})] \quad (8)$$

for the MI greater than 0.40.

The passive neutron matrix corrections are determined by systematic drum matrix measurements in a manner similar to the active measurements discussed previously. The passive matrix correction factors, MCFP, are a strong function of the MI.

The MCFP analytic fits to the four independent quantities measured during a passive assay scan are given below.

$$\text{MCFP}(\text{system totals}) = 1.00, \quad (9)$$

for the MI less than or equal to 0.355,

$$\text{MCFP}(\text{system totals}) = -0.16 + 3.28(\text{MI}), \quad (10)$$

for the MI greater than 0.355,

$$\text{MCFP}(\text{shielded totals}) = 1/[1 - \text{MI}], \quad (11)$$

$$\text{MCFP}(\text{system coincidence}) = [(0.5967)/(1 - \text{MI}) + 0.4187]^2, \quad (12)$$

$$\text{MCFP}(\text{shielded coincidence}) = [(0.8902)/(1 - \text{MI}) + 0.2337]^2. \quad (13)$$

The matrix correction equations given above or variations thereof are contained in the present PAN assay systems algorithms used throughout the DOE. Some sites perform additional matrix-dependent corrections to the assay results as discussed in Section 5.2.3.5.9.

Figure 5.2-3 shows the "Moderator Index" (see Caldwell, et al., 1986¹² for detailed discussion of the MI) obtained with mock matrix drums containing various hydrogen densities spanning the region of interest for general CH-TRU wastes. As can be seen, the MI varies smoothly with

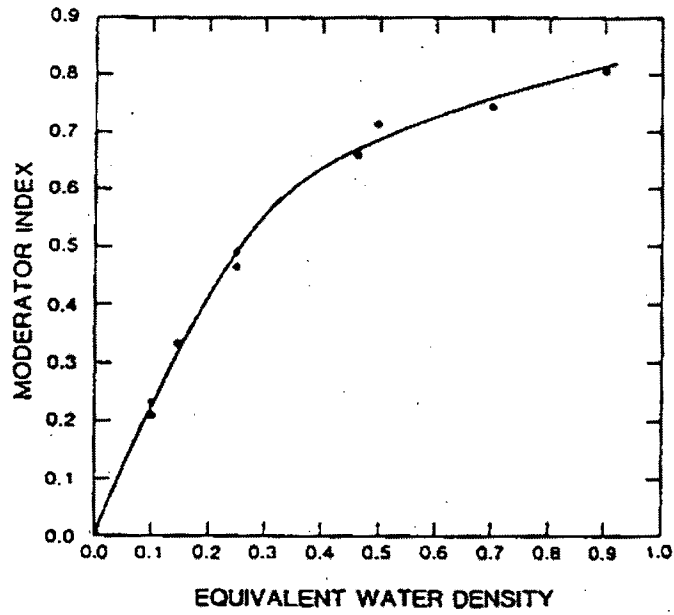


Figure 5.2-3—Moderator Index Measures for PAN Systems Using the Detector Ratio Method

average hydrogen density within a 208-L drum. Sludges display one of the higher average hydrogen densities of any CH-TRU waste form, with correspondingly high MIs (0.4 to 0.8). Lightly moderating matrices, such as combustibles, have MIs falling typically in the 0.1 to 0.3 region, and miscellaneous metals matrices, which generally contain no moderating materials, have measured MIs near 0.0.

Figure 5.2-4 shows the actual moderator correction factor (MCF) data¹² for the PNCC portion of the PAN systems as implemented at INEEL, Hanford, and SRS. The MCF value is the multiplicative factor required to normalize a given matrix measurement to the empty drum level of PNCC sensitivity. As can be seen, the MCF value varies smoothly as a function of the MI; Figure 5.2-4 can be used to estimate typical MCF values. For example,

- (a) Miscellaneous metals, MCF = 1.0 (i.e., same sensitivity as with empty drum),
- (b) Combustibles matrix, MCF = 1.35, and
- (c) Sludges, MCF = 3.6.

The MCF range observed for a 3,000 CH-TRU drum sludge assay campaign at INEEL was 1.8 to 10.0.

When performing PNCC assays of highly moderating matrices, such as sludges, measurement of a MCF value is essential for accurate assay results to be obtained. A "calibration" based on a "typical" sludge drum would result in assay errors of hundreds of percent for some drums because of the large hydrogen density variations observed.

Figures 5.2-5a and 5.2-5b show plots of the systematic active assay correction factors. As can be seen in Figures 5.2-5a and 5.2-5b, some waste materials require no matrix correction (relative to a standard response measured in an empty drum). Examples of these waste matrices are cellulose-based combustibles, graphite molds and scarfings, aluminum scrap, dry-to-moderately-wet dirt, and silica.

5.2.3.5.4 Assay Algorithm and Data Acquisition System

All PAN units utilize a similar assay algorithm. At present, all drum-size units are equipped with IBM/PC-based data acquisition systems as described in Kuckertz, et al, 1987.²¹ The system operating program (NEUT) controls all data acquisition and contains the assay algorithm.

Each data acquisition consists of sequential active and passive neutron assays, preceded by a user interactive initialization stage in which drum identification, content code information, drum weight, etc., can be entered from the PC keyboard, from a bar code reader, or from an RS-232 port by direct interaction with a site's data management computer. The weight of the drum's contents is used in calculating the nanocuries per gram (nCi/g) assay value that differentiates between TRU and non-TRU wastes. The content code input is used to flag difficult-to-assay

²¹ T. H. Kuckertz et al., "Making Transuranics Assay Measurements Using Modern Controllers," Proceedings 9th ESARDA Symposium on Safeguards and Nuclear Material Management, London UK, pages 389-393, May 1987.

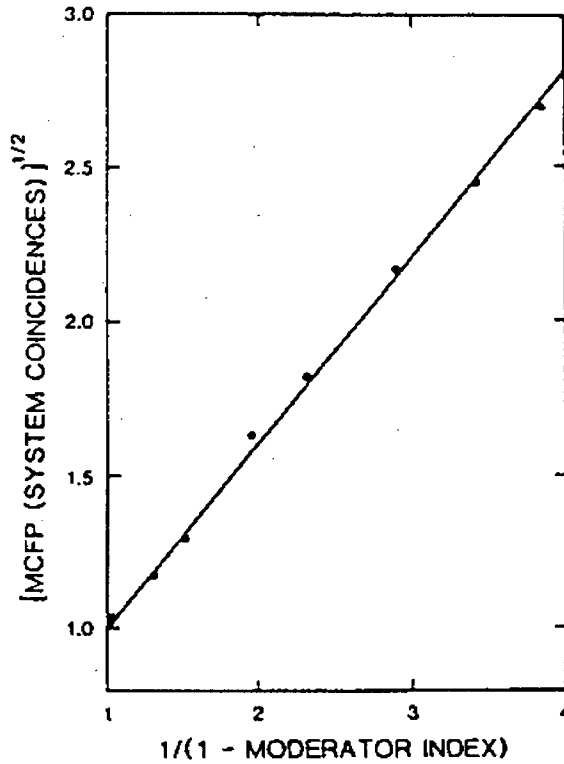


Figure 5.2-4—Use of the Moderator Index to Determine Passive Neutron Coincidence Matrix Correction Factors for a PAN System

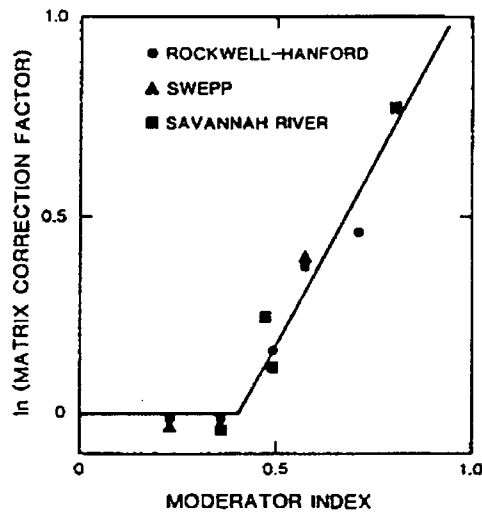
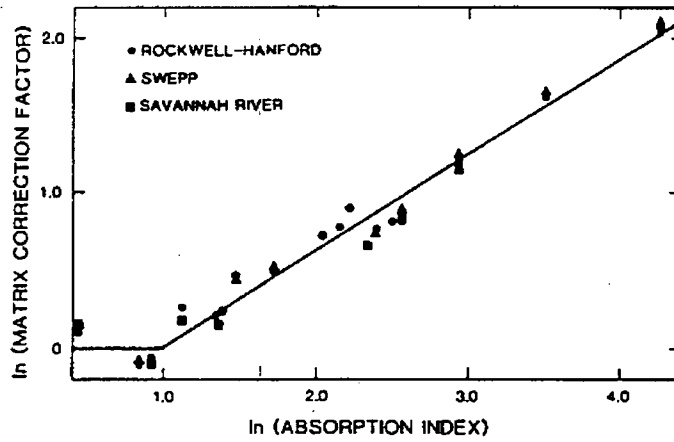


Figure 5.2-5—PAN System Active Assay Matrix Correction Factors Measured at Hanford, INEEL, and SRS with a Set of 20 Standard Matrix Drums

matrices or "special case" drums (see Section 5.2.3.5.11). All data input modes are in current use at the various sites. However obtained, that information becomes part of the permanent record stored with the TRU assay and matrix measurement data.

Modifications and upgrades have been performed at various times since the original algorithm was written in 1982. The development and upgrade of hardware and software has continued.^{12,22,23,24} The software revisions can be readily accomplished within the Fortran software framework of NEUT.

Measured data as well as all initialization information, date and time stamp from the internal PC clock/calendar, and final analyzed results are archived. An on-line hard copy printout of the assay parameters and results is also generated. All background and calibration measurements are routinely recorded and archived in the same fashion as normal assays. Thus, a continuous and traceable record of all data is maintained. Most sites, in fact, are maintaining this complete set of data in interactive databases (e.g., Lotus 1,2,3 or dBASE III), wherein all single-run assay data occupies one row in a single spreadsheet or database record. In some cases, 10,000 such records exist at a site (e.g., INEEL). This data archiving technique is an extremely important development as such extensive waste drum assay databases have not been developed previously in the NDA field, much less put into such readily accessible form. This greatly facilitates internal consistency checks and comparisons of large numbers of individual drum assays results obtained with different assay techniques.

RG Pu (i.e., Pu containing high Pu-240 content) is accommodated within the same PAN algorithm as is used for WG Pu. The PAN operator is queried before each assay as to whether the drum contains WG Pu and, if not, what is the correct Pu-240 percentage for that waste drum. Once the Pu-240 percentage is entered, the algorithm automatically corrects both passive and active assays for the different Pu isotopics.

The basic Pu algorithm cannot, however, directly accommodate Pu-238 or HSG Pu. Those sites assaying HSG Pu waste exercise a special algorithm option in their Main Menu that allows for analysis of the basic passive and active data in terms of HSG Pu. If selected this option:

- (a) Interprets the active assay results in terms of a Pu isotopic mix consisting of 18% Pu-239 and 82% Pu-238. Since only the Pu-239 fraction is fissile, total Pu mass is obtained by dividing the active assay result by the factor 0.18.

²² J. T. Caldwell, J.M. Bieri, and A.P. Colarusso, "The Los Alamos Second-Generation Passive-Active Neutron Assay System--FY86 Operations Record and System Evaluation", Los Alamos Technical Report LA-Q2TN-86-106, September 1986.

²³ A. P. Colarusso, et al., "Mobile Nondestructive Assay System," Proceedings of 28th Annual INMM Meeting, Newport Beach, Ca, July 12-15, 1987.

²⁴ K. L. Coop, J. T. Caldwell, and C. A. Goulding, "Assay of Fissile Materials Using a Combined Thermal/Epithermal Neutron Interrogation Technique," Third International Conference on Facility Operations-Safeguards Interface, San Diego, CA, November 29 - December 4, 1987.

- (b) Interprets the passive assay data similarly. Pu-238 undergoes spontaneous fission at a rate of 2600 neutrons per second per gram (n/s/g) (for comparison, the Pu-240 rate is 990 n/s/g). Thus, passive coincidence counts can be used to obtain an estimate of Pu-238 mass.
- (c) As in all cases the Systems Totals Passive Singles rate can be used, assuming oxide as the dominant chemical form, to estimate a total alpha particle emission rate. This estimate can then be used to calculate the Pu-238 mass.

The SRS possesses most of the DOE's Pu-238 waste, and is currently evaluating their Pu-238 algorithm.

5.2.3.5.5 Applicability to CH-TRU Wastes

The PAN systematic matrix correction factors discussed in Caldwell, et al., 1986¹², and Section 5.2.3.5.3, and now implemented in all drum-size PAN units enables the quantitative assay of virtually all DOE wastes presently packaged in 208-L drums. At present, these six implemented PAN units have been used to assay, collectively, about 20,000 CH-TRU waste drums at the various sites, including 2,000 drum assays performed with the mobile drum unit at the Nevada Test Site (NTS) and Lawrence Livermore National Laboratory (LLNL).

5.2.3.5.6 Instrument Calibration, Standards Preparation, and Implementation

Calibration of PAN units includes a thorough initial calibration after fabrication and routine calibrations using secondary standards.

Caldwell, et al., 1986¹², lists the standards used in all the present PAN units, for which all passive and active calibration standards have National Bureau of Standards (NBS)-traceable or NBS-referenceable origins. Absolute and matrix standards calibrations were conducted of the PAN unit. The PAN units were then each provided a set of secondary standards (placed in "Pink Drums" for conspicuous identification) consisting of standard, NBS-referenceable Cf-252 passive assay and U-235 active assay materials. A baseline reference data set for both passive and active assays was obtained for each PAN unit with these unique "Pink Drum" standards, and each unit has subsequently performed standard Pink Drum assays prior to each set of PAN waste drum assays.

A typical set of these standards measurements performed with the INEEL PAN unit and extending for almost a three-year period is shown in Figure 5.2-6. The individual passive and active standards measurements fall well within a +/- 5% window, with no measurable systematic drift during the three-year operational history. Caldwell, et al., 1986¹², lists the corresponding Pink Drum measurements for Hanford, SRS, and the mobile drum unit. All display the same basic stability of response.

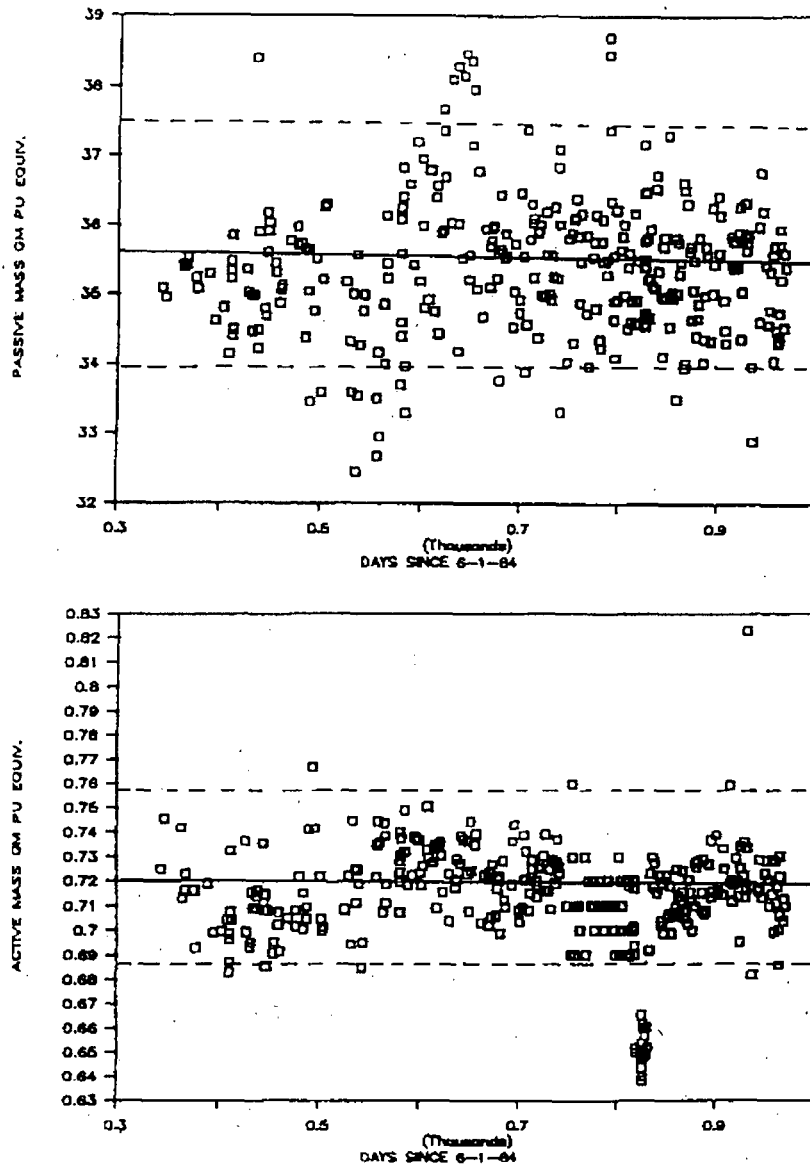


Figure 5.2-6—INEEL PAN Standards Measurements (Pink Drum) Performed Over a Three-Year Period.
 (Top Graph Shows Passive Standard and Bottom Graph Shows Active Standard. Dashed Lines Indicate a +/-5% Measurement Error Band About Expected Standards Assay Values.)

5.2.3.5.7 Operator Training Requirements and Practices

The present generation of PAN units are highly-automated, computer-based systems. The instruments are computer-controlled using relatively interactive (“user-friendly”) software. Only trained personnel are allowed to operate the assay equipment. Personnel are qualified according to DOE Order 5480.5.¹⁵

Standardized training requirements and guidelines for all DOE assay operators are based upon such already-existing industry standard training requirements, such as SNT-TC-1A. Each site provides a specialized training program for NDA instrument operators. The operators are directed and/or assisted by a designated site NDA expert. Expertise is attained by education and experience.

5.2.3.5.8 Assay Procedures

As of 1989, the PAN assay systems were comparatively recent additions (approximately six years) to NDA instrumentation and, as a consequence, ASTM and ANSI standards have not been developed for PAN assay systems. Active assay techniques have been used for approximately 18 years, but the 14-MeV thermalized neutron assay (active portion of PAN) is comparatively recent. Of course, the passive coincidence portion of PAN is similar to the PNCC assay technique and, therefore, PNCC ASTM, ANSI, and NRC standard practices and guidelines are followed for that portion of the PAN system.

All PAN standard operating procedures instruct operators to acquire a background and a “Pink Drum” data set before any assays on waste containers are performed. These data sets are checked for consistency and, if the results fall outside a predetermined (e.g., +/-10%) acceptance window, remedial action is taken. The remedial action can include a repetition of the background and/or standards measurements. If the second measurement is successful, general assays can resume. If the problem persists qualified personnel are contacted to “debug” the system. No CH-TRU waste drum assays can resume until the problem is satisfactorily resolved. If the background or standards measurement is outside the acceptance window, the diagnostic generally assumed is that a hardware problem exists.

The assay procedure for PAN units equipped with the IBM/PC data acquisition system is relatively straightforward. An operator inserts a waste drum into the PAN unit and enters all drum identification information via an interactive dialogue (PAN assay system software, NEUT, prompts the operator for the specific information). Once NEUT has checked the information for correct format, the assay record and programmable electronics hardware are properly indexed, gates set, etc., NEUT then sends a message to the operator (via the CRT screen) that the system is ready to begin an assay.

At this point the operator presses one button, the start sequence button on the MA165C neutron generator controller unit. This initiates the PAN active assay. At the conclusion of the active assay, NEUT automatically records all data and initiates the PAN passive assay. At the conclusion of the PAN passive assay, all data is recorded, analyzed and printed out for

immediate inspection. The operator is then informed (via the CRT Screen) that the system is ready to perform another assay.

5.2.3.5.9 Assay Precision, Bias, and Limit of Detection

The PAN assay algorithm contains a calculation of the measurement uncertainty¹² that combines statistical uncertainties and estimated systematic biases based on the measured matrix correction factor. For a generally heterogeneous matrix and TRU materials distribution, the larger the indicated matrix correction, the larger the expected assay uncertainty. These values are reported with the actual assay values, for both passive and active neutron assays. For many well-characterized waste streams a typical value for the estimated uncertainty (not including the statistical contribution to the error) is 20%.

When a systematic matrix correction formalism is used, the corresponding systematic uncertainty in the passive assay measurement can be decreased to 5% or less. This low an uncertainty is valid for dry, combustible, low-hydrogen content waste, such as general laboratory waste. The passive assay value uncertainty is calculated as for PNCC. The algorithm used in the passive coincidence portion of the PAN units calculates a composite assay uncertainty based on combining all the effects discussed above, which becomes part of the permanent archived assay record.

The active assay value uncertainty estimate includes a systematic bias contribution, which is a function of the MCF (AI and MI). For reasonably uniform TRU isotope distributions (such as are found in sludges), AI measurements indicate assay uncertainties of +/- 10%. For nonuniform TRU isotope distributions, the uncertainty is a function of the magnitude of the MCF.¹² That is, the larger the MCF, the larger is the associated assay uncertainty. The effects on the assay measurement of concentrated TRU activity in different drum locations have been calculated and plotted as a function of the total MCF. For example, a matrix correction factor of approximately five yields a corresponding uncertainty of 50% in the assay measurement.

Extensive comparisons have been performed for passive and active neutron assays of the same drum, for a great variety of matrix types (e.g., four types of sludges, job-control wastes, combustibles, graphite scarfings, miscellaneous metals, tantalum crucibles, glassware, molten salts, filter media, dirt, and others.) Some of these comparisons are shown in the figures of this document and are discussed in Fleissner, et al., 1986, and Schultz and Caldwell, 1988.^{16,17} It should be noted that the matrix corrections applied to passive and active assays for a given type of matrix (except where no matrix corrections are necessary) are quite distinct. Thus, there is a very low probability of obtaining agreement by accident between active and passive neutron assays for wastes with significant moderator and absorber amounts. If one obtains agreement, both independent PAN assay techniques are considered to yield unbiased assay measurement values.

The assay limit of detection for the active neutron portion of the PAN unit can be as low as a few milligrams of Pu-239 placed anywhere within a typical 208-L waste drum.

5.2.3.5.10 PAN Assay Results Comparisons

Comparisons of PAN assay results with SGS or radiochemical assay methods have been performed. The PAN assays, both passive and active, have been compared with SGS and radiochemistry assay results for (a) matrices requiring little or no matrix corrections, such as graphite molds and general laboratory wastes, and (b) homogeneous matrices (e.g., sludges).

Two papers^{13,17} detail several comparisons of PAN and SGS assay measurements. Caldwell, et al.¹³ includes a total database of some 5,000 assays performed at NTS, LLNL, Hanford, INEEL, LANL, and SRS. The drum assay and matrix correction formalism presented in Caldwell et al., 1986¹² was extensively evaluated for all types of waste matrices and waste content codes being generated within the DOE complex. Schultz and Caldwell 1988¹⁷ encompasses an even larger database, but is confined to INEEL PAN assays and comparisons with RFETS SGS assays.

Figures 5.2-7a, 5.2-7b, and 5.2-7c show a recent PAN/SGS comparison performed by LANL personnel¹¹ using a mobile PAN drum-sized unit. The data was acquired at LLNL from assays of a set of some 200, 208-L, WG Pu waste drums consisting of general laboratory wastes (e.g., glassware, cellulose, plastics, etc.) that had been assayed using the LLNL SGS unit.

Figures 5.2-7a, 5.2-7b, and 5.2-7c show the PAN passive neutron, PAN active neutron, and SGS assay measurements comparisons. A statistical analysis of this data set indicates systematic agreement between both PAN neutron data sets and the SGS assay results at the 5% level (95% confidence level). Figure 5.2-8 shows a plot of similar waste stream assays performed with the Hanford PAN system, comparing passive and active neutron assay values for a set of 300 waste drums.

Figures 5.2-9a and 5.2-9b show a set of over 300 "graphite molds" matrix waste drums (RG Pu) assayed with the PAN unit at INEEL and also with an SGS unit located at the RFETS. A statistical analysis of this data set indicates systematic agreement of all three independent assay methods to within 10% on the average, at the 95% confidence level.

Quantitative comparisons between radiochemical Pu (WG) and Am-241 determinations and active PAN have been performed at the INEEL facility (SWEPP).¹³ These comparison studies of approximately 1,300 drums of RFETS aqueous sludges comprise more than 100 individual sludge batches. These sludges contain low Pu and relatively high Am concentrations. The results of these comparisons are shown in Figure 5.2-10.

The batch-average drum Pu assay as determined at RFETS was compared to the same quantity as measured with the INEEL PAN unit. The indicated straight line shows the relationship RFETS Pu Mass = PAN Pu Mass. A statistical analysis of this same data indicates a best straight-line fit relationship of

$$\text{RFETS Pu Mass} = -0.06 + 0.85 * \text{PAN Pu Mass},$$

with a correlation factor of 0.51. The calculated correlation factor indicates that 51% of the variance does fit a straight line. The 0.85 constant indicates an approximately 15% average measurement bias between the two assay techniques.

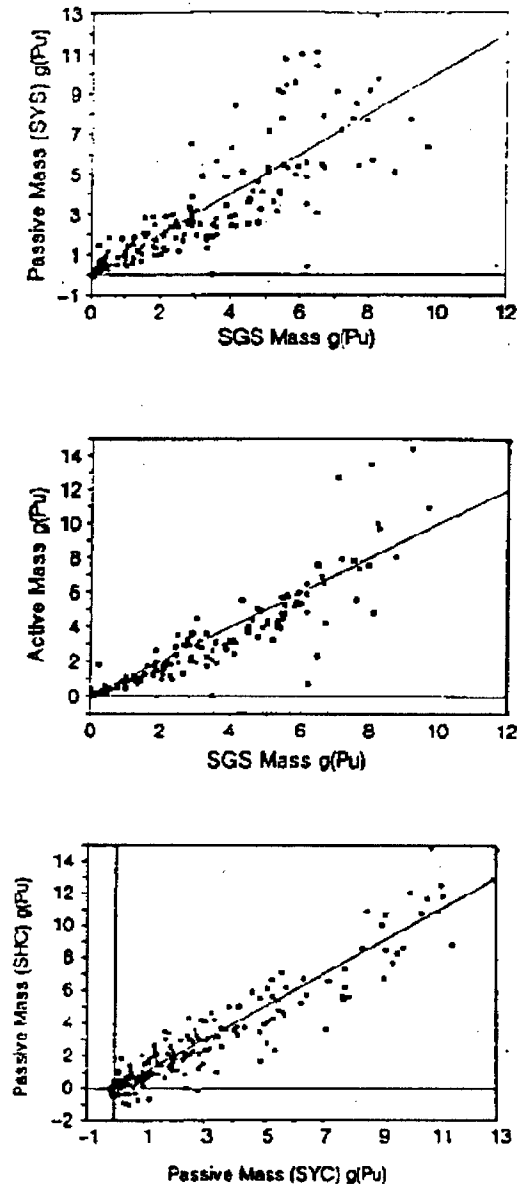


Figure 5.2-7—Comparison of Assay Data Sets of 200 LLNL CH-TRU Waste Drums.

Waste Matrix in Non-Segregated General Laboratory Waste.

Top Graph Shows Passive Neutron (PAN) Compared to SGS. Middle Graph Shows Active Neutron (PAN) Compared to SGS. Bottom Graph Shows Comparison of the Two Independent PAN Passive Neutron Assay Systems. Straight Line (X=Y) Depicts Ideal Case, Where Assay Techniques Shown Yield Identical Assay Measurement Results.

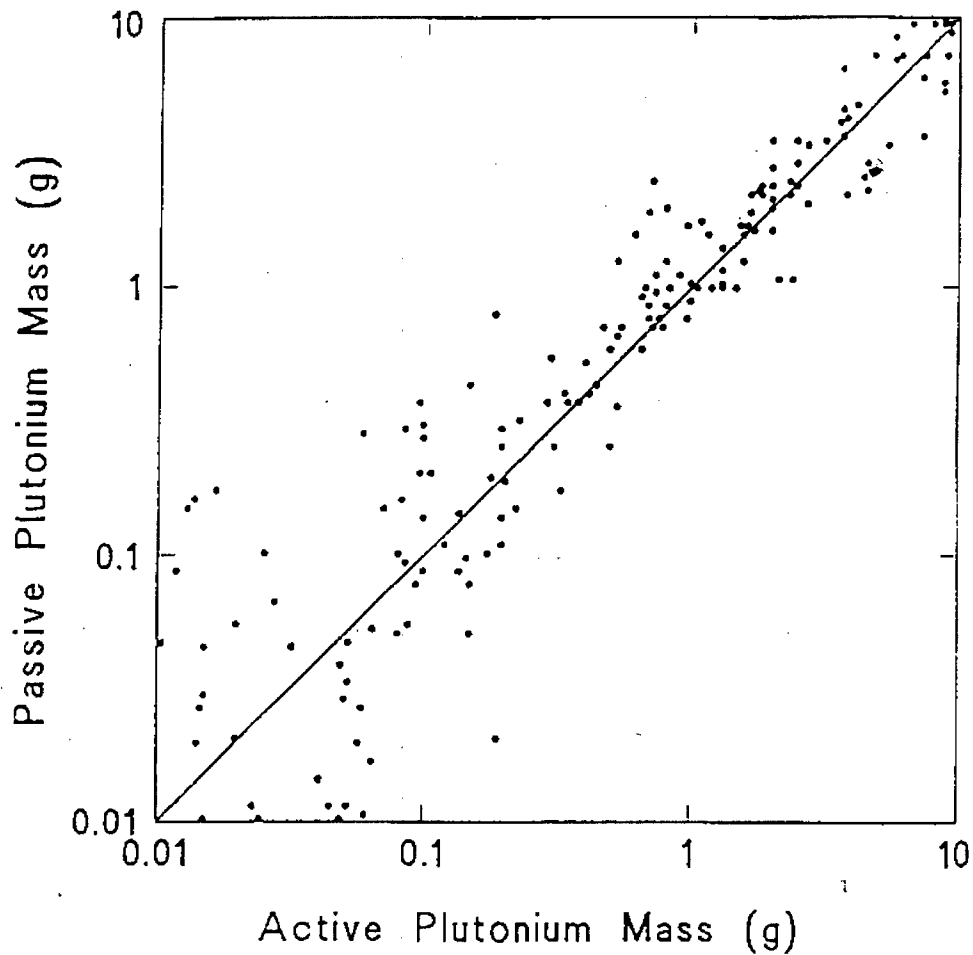


Figure 5.2-8—Comparison of 300 Hanford CH-TRU Waste Drum Assays Performed with the PAN System, Passive Neutron Compared to Active Neutron.

Straight Line ($X=Y$) Depicts Ideal Case, Where Assay Techniques Shown Yield Identical Assay Measurement Results.

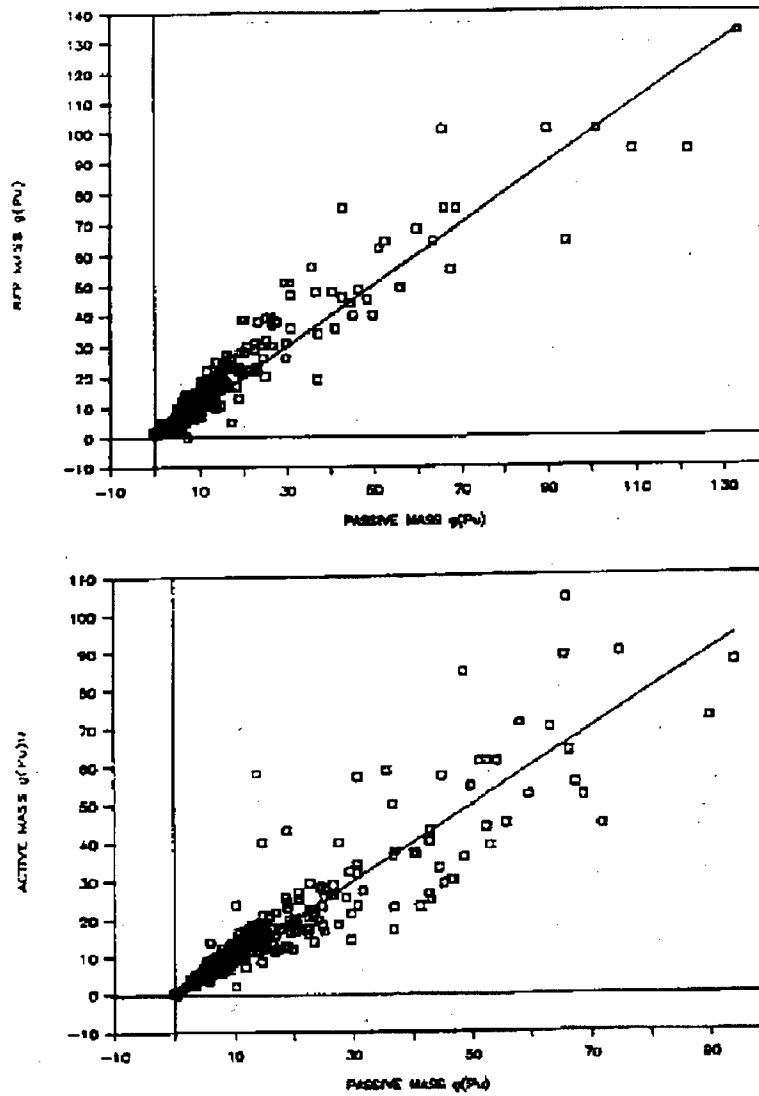


Figure 5.2-9—Assay Comparisons of a Set of 300 RFETS CH-TRU Waste Drums (Graphite Molds Matrix) Showing RFETS SGS System Assays Compared to INEEL PAN Unit Passive Neutron Assays (Top) and INEEL PAN Active Neutron and Passive Neutron Comparisons (Bottom).

Straight Lines (X=Y) Depict Ideal Case, Where Assay Techniques Shown Yield Identical Assay Measurement Results.

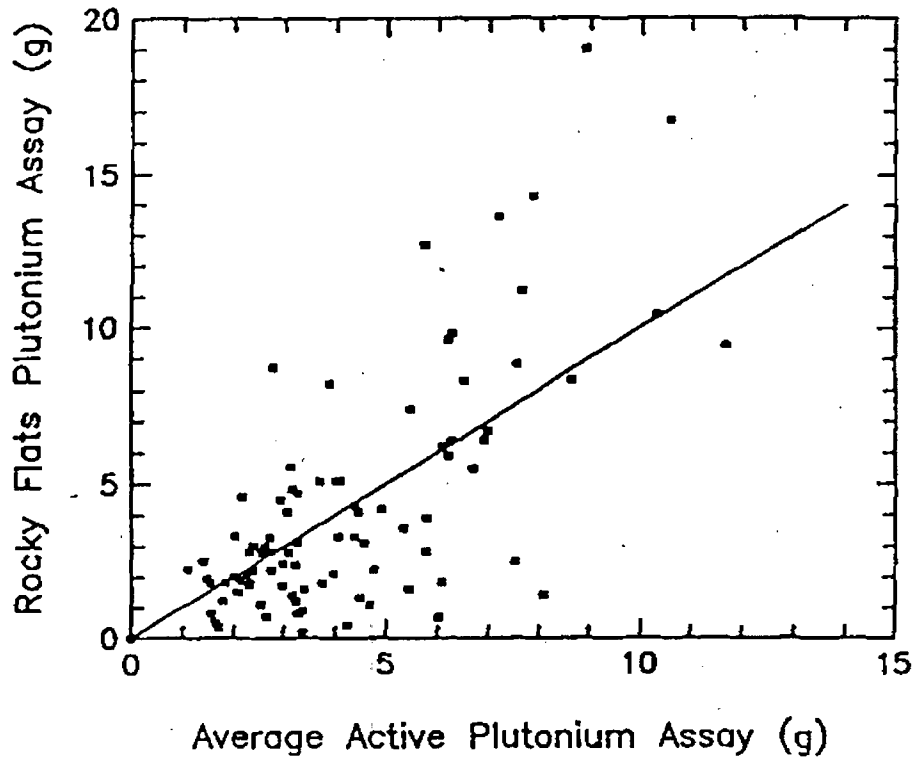


Figure 5.2-10—Batch Average Pu Assays of 1300 Sludge Drums Performed at RFETS Compared to PAN Assays of the Same Drums Done at INEEL.

Straight Line is a Linear Least Squares Fit to Data.

The individual PAN systematic measurement error (discussed in detail in Caldwell, et al., 1986¹²) for a typical sludge drum measurement is approximately 10% on average, due primarily to possible systematic errors in the matrix correction formalism. That error estimate is based on the observed standard deviation found for mockup sludge drum calibrations. PAN systems are able to measure the total uncorrelated neutrons, but cannot measure the individual contributions from mixed, uncorrelated sources of neutrons [e.g., (alpha, n) reactions due to Cm-244 and Am-241]. The contributions from Am-241, for example, can be calculated (obtained from passive single neutron rate) if no other (alpha, n) sources are present in the waste.

The two assay measurement techniques appear to agree within probable systematic errors associated with each technique (assuming a +/- 10% systematic error for both techniques). Other similar individual sludge drum NDA comparisons (passive and active PAN neutron assays of high-Pu, low-Am activity sludge drums¹³ verify the basic PAN matrix corrections at the +/-10% level.

Schultz and Caldwell, 1988¹⁷ details additional such comparisons for a great variety of matrix types, including heterogeneous matrices and highly neutron-absorbing matrices. In all cases the PAN assays are highly correlated with SGS assays and with each other. Comparison studies reported in Schultz and Caldwell, 1988¹⁷ indicate a slightly better agreement between PAN and radiochemistry assay methods than the 10-15% discussed above.

5.2.3.5.11 Choice of Passive or Active Assay Value

Two assay values, a "passive" mass and an "active" mass, are obtained with each PAN assay. A choice of the values to be reported as the PAN assay value is performed within the assay algorithm by an analytical evaluation of assay conditions. Content-code-specific algorithm options are developed by a site based upon an evaluation by the assay data reviewer or expert of the individual site's waste content codes.

When specific content code or matrix information is available that indicates, for example, that passive assay results are more reliable than active assay results for that content code, then the algorithm selects the passive assay results when that content code is entered via the PAN operating software, NEUT. Similar overrides involve the statistical accuracy of a measurement. For example, if the passive measurement has a large error associated with it, then the active measurement is selected.

The default PAN assay algorithm is known to underestimate the absorption correction factor for various waste streams (e.g., tantalum crucibles). This phenomenon is due to neutron tunneling effects caused by the stacked arrangement of the crucibles. A correction factor based on the RFETS SGS assay value is used to adjust the PAN assay values.

A similar method is used at INEEL to modify the MI obtained during the assay of sludge drums. For sludge drums having low Pu content, an average MI is used in the assay value calculations. The average MI value used was obtained from previous assays of the same waste stream containing higher Pu loadings and, thus, higher count rates and improved counting statistics.

One algorithm option that is used by Hanford is based on experimental results indicating that fissile self-absorbing effects in several of their content codes were small for Pu mass loadings of 10 g or less, but increasingly probable for successively higher Pu mass loadings. It also took into account the experimental fact that Pu loadings in excess of 10 g led to statistically more precise passive assay measurements. Of course, the exact "cross-over" point between using the PAN active or passive assay measurement depends on several experimental factors such as waste form, (alpha, n) source strength, isotopics, etc.

INEEL has modified their PAN algorithm option to reflect the phenomenon that sufficiently strong (alpha, n) sources cause experimental measurement problems for the PAN passive assay measurement, rendering it biased high. If the passive assay error bar exceeds 40 g Pu, then the option selects the self-absorption corrected active assay value. This algorithm option also reflects the development of a fissile self-absorption model that is applied to all PAN active assays. This model is purely empirical and assumes that the probability of fissile self-absorption is a monotonically increasing function of the total fissile loading in a waste drum. The function is determined from evaluations of large sets of actual CH-TRU waste drum assays employing PAN active and passive neutron and SGS measurements.¹² The derived functions, however, produce large error bars at the higher fissile mass values. In the "near 200 g Pu" regime, for example, the self-absorption corrected active assays may have relative errors of 40%.

PAN assay results may also be evaluated by the site NDA expert when special-case waste drums are encountered. The various factors that determine what is a "special case" drum include nominal assay values for CH-TRU waste drums near or in excess of the 200 g criticality limit and a lack of tag isotopics information (e.g., Pu-240 content). Both of these situations preclude proper interpretation of PAN assay measurement data.

Approximately one out of 500 RFP CH-TRU waste drums assayed with the INEEL PAN system are assigned an assay value near or in excess of the 200 g criticality limit. Typically, these drums contain very high (alpha, n) radioisotopic sources, which due to the high numbers of neutrons present, results in poor passive PAN coincidence measurements. The large numbers of neutrons (approximately 10^4 neutrons per second or greater) decrease the signal to noise ratio to below acceptable limits. Content codes 409 and 411 display this characteristic and also contain "lumps" of Pu that invalidates the active neutron assay. A panel of 3 or 4 INEEL experts examines and compares all assay and RTR information available, including a critical evaluation of the "tag" assay values. After a consensus of the expert panel is achieved a suitable resolution is proposed and the appropriate action taken. This action may include acceptance of the less than 200 g tag value or the waste drum is returned to the waste generator for repackaging. Both of these actions have occurred.

Hanford waste drum tag values obtained by using an SGS and the certification or check of the SGS assays with a PAN unit indicate assay values near or in excess of the 200 g criticality limit. The approach used at Hanford is basically the same one employed at INEEL, but a two-expert panel is used to evaluate the available data. The return-to-generator option is used frequently with drums having assay values near the 200 g limit.

Invalid or unavailable isotopics information occurred when a small set of Pacific Nuclear Laboratory (PNL) waste drums were assayed at Hanford using a PAN unit. These drums contained Cm-244, but this isotope was not originally listed on the accompanying data sheets. The PAN assay results indicated very high passive coincidence assay values. Many of the assay values were well in excess of the nominal 200 g limit. Experts resolved the problem through direct dialogues with the waste generator who, subsequently, agreed to provide the proper isotopic information that would then allow these drums to be properly assayed.

5.2.4 Fissile Material Content and Decay Heat Value Calculations

The fissile or fissionable isotope content for CH-TRU waste containers is expressed in terms of Pu-239 fissile gram equivalents (FGE), as defined in ANSI/ANS-8.1²⁵ and ANSI/ANS-8.15.²⁶ The standards list the maximum subcritical mass limits for fissile and non-fissile actinide nuclides. The fissile material (e.g., Pu-239, U-235, etc.) or fissionable content of a CH-TRU waste container may be obtained by using any of the previously described assay techniques. However, to obtain the number of Pu-239 FGE present, the isotopic composition contained in the waste form must be known.

The PNCC assay method detects the coincident neutrons emitted by the even-number TRU isotopes (e.g., Pu-240 and Cm-244). (See Section 5.2.3.4 for a detailed discussion of the PNCC assay technique.) Once the coincident neutron (spontaneous fission) emitters have been quantified and the proper correction factors applied (e.g., self-multiplication, system dead-time, etc.), one can calculate the fissile material content by applying the known isotopic ratios.

After the mass of each TRU isotope present has been determined, the decay heat can be calculated by multiplying the mass of each isotope by the decay heat per gram of the isotope. For the general case of alpha and beta decay, the decay heat per gram can be calculated by using Eq. 10 in ANSI-N15.22.^{8,20}

The original PAN system algorithm used a very conservative means to estimate a waste drum's decay heat. First, it was assumed that only the drum's alpha particle inventory was responsible for the waste drum's decay heating. Second, the conservative assumption was made that all neutrons detected were produced by (alpha, n) reactions within the drum's waste matrix. In the original algorithm this assumption led to the value of 98,000,000 MeV of alpha decay heat energy being associated with each neutron emitted. This estimate is conservative for two reasons:

- (1) In all cases of WG Pu, a fraction of the neutrons detected are produced by Pu-240 or other spontaneous fission reactions, with a much lower decay-heat-per-neutron factor. Typically each spontaneous fission neutron is associated with approximately 100 MeV of decay heat energy.

²⁵ ANSI/ANS-8.1, "Nuclear Criticality Safety in Operations with Fissionable Materials Outside Reactors."

²⁶ ANSI/ANS-8.15, "Nuclear Criticality Control of Special Actinide Elements."

- (2) In many waste packages the actual (alpha, n) production factor is higher than the conservative value (2 n/s/mCi-alpha) used in the PAN algorithm. Production factors as high as 14 n/s/mCi-alpha were observed for RFETS CH-TRU waste drums when assayed with the INEEL PAN system.²⁷ For the various fluoride, magnesium (Mg), aluminum (Al) salt, and typical sludge matrices values as high as 100 n/s/mCi-alpha are observed.

To obtain more realistic estimates of the decay heat value for sludge wastes and those containing fluorides, INEEL has used an experimentally determined (alpha, n) production factor. For example, an experimentally determined production factor is being used for RFETS aqueous sludges.²⁶ This derived production factor has been incorporated into the PAN assay algorithm.

Hanford and SRS use an (alpha, n) production factor based on given Pu isotopes contained in the waste drum. The modified PAN assay algorithm assumes that the entire 241 mass (i.e., sum of Pu-241 and Am-241) is in the form of Am-241. This assumption is very conservative since Am-241 produces approximately 35 times the decay heating associated with Pu-241.

ORNL uses a PAN decay heat calculation algorithm based upon the subtraction of the spontaneous fission neutron portion (passive neutron coincidence) from the observed total neutron count rate.

Error bars associated with the decay heat calculation propagate in the same fashion as that described for PAN Pu mass calculation (see Section 5.2.3.5.9).

The administrative classification of 200 millirem per hour (mrem/h) for container surface dose rate imposed for CH-TRU waste automatically limits the decay heat contributions from beta- and gamma-emitting radioisotopes.

To calculate the fission product inventories required to generate a surface dose rate of 200 mr/h one can assume the total external surface dose rate is produced by fission products (the beta- and gamma-emitters). Any TRU radioisotopes present are conservatively assumed not to contribute to the observed external dose rate. One also assumes that the short-lived fission products have decayed sufficiently to be of no concern. This is a conservative assumption since most waste drums are more than one year old. Consequently, only a small number of "pure" beta-emitters would then be present (e.g., strontium [Sr]-90). The remaining predominant radioisotopes producing the heat-generating radiation other than Sr-90 would then be cesium (Cs)-137 and cobalt (Co)-60.

Consider a CH-TRU waste drum containing 100 kilograms (kg) of medium atomic number wastes. Assume the maximum allowable container external dose rate of 200 mrem/h and that this rate is attributable solely to beta- and gamma-emitters (conservative assumption). Also, assume that the radioisotope inventory of this waste drum is a mixture of the dominant long-lived fission product species Sr-90 and Cs-137. For long-term decay 6.5% Cs-137 and 2.2% Sr-

²⁷ C. E. Moss and J. T. Caldwell, "Assay of TRU Wastes Containing (alpha, n) Sources," LA UR 86-2220, June 22, 1986.

90 are produced by reactor fissions.²⁸ This fission product mixture produces a decay heating of 0.91 MeV, 50% derived from beta emission and 50% derived from gamma-ray emission.²⁹

If one also makes the following conservative assumptions: (1) that only the Cs-137 0.67 MeV gamma ray exits the waste drum, (2) the Cs-137 is located in the center of the waste drum, and (3) the mass attenuation factor is very conservative (i.e., $0.74 \text{ cm}^2/\text{g}$), one can calculate the curies required to produce an container external dose rate of 200 mrem/h. These assumptions and calculations yield an estimate of 0.25 Ci of Cs-137 present in the example waste drum. Using the isotopic ratio discussed earlier, one calculates a beta and gamma decay heating of 0.001 watt. This decay heating value is equivalent to that produced by the alpha emissions of 0.4 g WG Pu.

Detailed gamma-ray spectral studies of ORNL and RFETS CH-TRU waste drums^{19,26,30} indicate that the detected gamma rays were attributable to TRU isotopes and not to fission products. Consequently, from the calculations above and the small quantities of observed fission products the contributions to the waste drum decay heat from beta- and gamma-emitters is negligible.

5.2.5 New Assay Developments

In keeping with the DOE's general policy of upgrading NDA hardware, software and procedures, the DOE continues to support a vigorous NDA development program, with specific support of TRU waste assay-related instrumentation. One recent example of this development is a significantly improved digital processing unit (upgraded shift register) for use with PNCC units that greatly reduces basic dead-time limitations associated with older PNCC units. The improvement considerably lowers processing errors. These newer processors are now either installed or in the process of being installed in all DOE facilities using PNCC assay techniques.

Another development nearing the implementation phase in support of the PAN assay method is "neutron imaging" of 208 L waste drums.³¹ With very little change in the basic PAN hardware, 208 L waste drum assay data may be acquired in a fashion that allows it to be processed with existing imaging software similar to that used in medical CAT scans. Neutron imaging has already been demonstrated using an upgraded DOE PAN unit,³⁰ the Mobile Drum System. Improved matrix and self-absorption corrections to the basic assay data will then be possible using the neutron imaging technique. Accurate determination of the TRU material distribution should result in considerably improved assay accuracies since it is known that incomplete matrix and self-absorption corrections are a major source of assay errors.

PAN box assay systems have been used in the DOE complex for several years. The earlier versions are discussed in several of the references^{13,21,22} that include assay campaigns at NTS and RFETS. Recently, some improvements in the box PAN systems have been made and

²⁸ "Chart of the Nuclides," Knolls Atomic Power Laboratory.

²⁹ David C. Kocher, "Radioactive Decay Data Tables," DOE/TIC-11026, 1981.

³⁰ F. J. Schultz, et al., "Neutron and Gamma-Ray Nondestructive Examination of Contact-Handled Transuranic Waste at the ORNL TRU Waste Drum Assay Facility," ORNL-6103, March 1985.

³¹ San Horton, "Neutron Imaging," U. S. Army, Ph.D. thesis, 1988.

implemented at some sites. The new box assay unit at INEEL and the Mobile System box assay unit are examples of this implemented PAN technology. The improvements have been in four areas:

- (a) Improved matrix corrections made possible by development and deployment of a "moving" shielded flux monitor that samples the emergent interrogating flux along the entire length of a box.
- (b) Improved detection uniformity throughout the box volume made possible by a better detector layout.
- (c) Smaller matrix inhomogeneity assay errors, achieved by implementation of a source location algorithm, which effects matrix corrections correlated with the location of the TRU material is based on crude neutron imaging, and
- (d) Implementation of IBM/PC data acquisition/controller hardware and software.

Improvement (a) is similar to the shielded flux monitor described in Section 5.2.3.5 that is used in the drum-size PAN. These new developments are being implemented simultaneously with the institution of the standard waste box.

5.2.6 QA and QC Practices

QA and QC are important functions at all DOE facilities, especially in special nuclear materials (SNM) accounting areas. The 18 elements of NQA-1 are being implemented throughout the DOE.¹⁵ TRU waste assay QA and QC practices adhere to the guidelines established in NQA-1. Some of these practices have been discussed previously in relationship to other subjects. A brief listing of some of these QA/QC practices in common use to assay newly generated and stored CH-TRU waste throughout the DOE complex are:

- (1) Expert NDA personnel check of NDA records before assay values assigned to the waste package (NQA-1 Elements 1. Organization and 10. Inspection). (The functions of these site NDA reviewers or experts have been discussed previously in Sections 5.2.3.2, 5.2.3.4, and 5.2.3.5),
- (2) Assay standards used before and after waste assays (NQA-1 Element 12. Control of Measuring and Test Equipment). Detailed discussions of the instrument calibration and calibrations standards preparation and implementation have been discussed in detail for each assay method in Sections 5.2.3.2.1.3, 5.2.3.4.3, and 5.2.3.5.6),
- (3) Automatic electronic system gain stabilization. (Element 3. Design Control). For each assay method manufacturer's system instructions and site operating procedures suggest to the assay system operators the correct settings for proper system gain and stabilization,
- (4) Automatic software flagging and tagging for special-case waste containers (NQA-1 Element 5. Instructions, Procedures, and Drawings). For example, less than 0.5%

transmission segments are flagged for SGS assay measurements and special-case waste matrices are flagged by the computer algorithm in PAN assay measurements,

- (5) Administrative tagging of failed segment assays as "LOWER LIMITS" (NQA-1 Element 15. Control of Nonconforming Items). This procedure is performed for those SGS waste drums that qualify.
- (6) Original segment assay and calibration data archived for future reference (NQA-1 Elements 6. Document Control and 17. Quality Assurance Records). PAN assay algorithm automatically archives all calibration data acquired (see Section 5.2.3.5.6),
- (7) Detailed data sheets are prepared for each drum and accompany the drum through all NDA, RTR, etc. stations. Some sites (e.g., INEEL) use automated, computerized data sheets and bar codes (NQA-1 Element 9. Control of Processes),
- (8) Most sites' SGS assays verified by one or two other independent NDA measurements (at the certification facility). For example, RFETS SGS assays are verified by the INEEL PAN passive and active assay measurements (NQA-1 Elements 9. Control of Processes and 18. Audits),
- (9) Nonconforming drums returned for repackaging (NQA-1 Element 15. Control of Nonconforming Items). When a drum is found to contain non-conforming items after RTR inspection or to contain, for example, greater than the acceptable nuclear criticality limit, it is returned to the waste generator for repackaging,
- (10) RTR inspection is used in appraisal of NDA "Special-Case" waste containers to aid in the evaluation of matrix problems (NQA-1 Element 16. Corrective Action). For example, special-case waste drums (e.g., INEEL. tantalum crucible content code) are flagged by the PAN assay algorithm through previous evaluation and identification of the content code by the site NDA reviewer (expert). See Section 5.2.3.5.11 for a more detailed discussion of the special-case waste drums,
- (11) RTR inspection is used routinely to verify or evaluate waste form or content code of all waste drums (NQA-1 Element 8. Identification and Control of Items). RTR inspections are used to confirm the proper identification of waste content codes.
- (12) General practice of upgrading NDA hardware, software, and procedures whenever available and fiscally possible is pursued (NQA-1 Elements 2. Quality Assurance Program and 3. Design Control). See Section 5.2.5 for a discussion of new NDA developments.

It is DOE policy to conduct periodic audits of all Waste Isolation Pilot Plant certification activities at each site.³² The audit teams consist of technical NDA (and nondestructive

³² WIPP-DOE 120, Quality Assurance.

examination [NDE]) and administrative personnel knowledgeable in several of the NDA technologies discussed in Section 5.2.3. The purpose of these audits is to provide independent monitoring and evaluation of each site's NDA and NDE activities on a regular basis and to foster compliance with certification plans. These in-depth evaluations take place on site, and a detailed audit team report, including recommendations for improvements in areas judged deficient, follow each such audit. In addition, each site conducts independent internal audits on at least an annual basis, covering the same overall procedures as performed in the DOE external audits. The effect of these audits is to provide considerable independent oversight of each DOE site's NDA and NDE operations, as overlays to each site's routine operations activities.